THE 8TH INTERNATIONAL CONFERENCE ON FOOD AND APPLIED BIOSCIENCE

February 5-6, 2026

PROCEEDING
FAB 2026

THE FOOD SINGULARITY: CONVERGING SUSTAINABLE AGRITECH TO FRONTIER FOOD ERA

International Conference on Food and Applied Bioscience

February 5-6, 2026

The Empress Hotel, Chiang Mai, Thailand

Proceeding

Organizer

Faculty of Agro-Industry, Chiang Mai University

Co-Hosts

Preface

It is a great honor and privilege to welcome you to the 8th International Conference on Food and Applied Bioscience (FAB 2026), held under the theme "The Food Singularity: Converging Sustainable AgriTech to the Frontier Food Era." The conference was held from 5 to 6 February 2026 at The Empress Hotel, Chiang Mai, Thailand, and was organized by the Faculty of Agro-Industry, Chiang Mai University, in collaboration with an extensive network of esteemed national and international partner institutions.

The agro-industry is a vital pillar of national development and a key engine of economic growth under the National Economic and Social Development Plan. In today's rapidly evolving global landscape, research and development play a critical role in driving industrial progress. Whether originating from academia, research institutions, or the private sector, the generation of new knowledge is essential for fostering innovation, enhancing competitiveness, and ensuring sustainable development.

Aligned with Chiang Mai University's strategic vision as a research-led institution, FAB 2026 provides an international platform to disseminate academic excellence and facilitate the exchange of research advances and innovative insights among faculty members, scholars, researchers, students, and industry representatives. Through meaningful discussions and knowledge exchange, the conference aims to foster the holistic development of knowledge and innovation within the agro-industrial and food bioscience sectors.

FAB 2026 brought together participants from multiple continents, including Asia, Europe, Africa, the Americas, Oceania, and other parts of the global research community, highlighting the truly international scope of the conference. The scientific program was the main focus of the event and included keynote lectures, invited talks, oral presentations, and poster sessions covering a wide range of topics in food science, applied bioscience, sustainable agritech, and frontier food innovation. The scope, depth, and quality of the contributions showcased both current research frontiers and emerging challenges within agro-industrial and food systems.

In addition to the academic sessions, the conference featured the CNX Food and Applied Science Invention & Exhibition (CNX FINEX), held for the first time alongside FAB 2026. This innovation exhibition offered a lively platform for students, researchers, and emerging entrepreneurs to showcase inventions and solutions related to sustainability, technology convergence, and future food systems. CNX FINEX further strengthened the link between research findings and practical applications while fostering collaboration among academia, industry, and other stakeholders.

The success of FAB 2026 was made possible through the robust collaboration and support of our distinguished co-hosting partners:

- Agro-Industry Academic Council Association (AIAC), Thailand
- College of Food Science and Nutritional Engineering, China Agricultural University, China
- Department of Marine Food Science and Technology, Gangneung-Wonju National University, Korea
- Department of Packaging & Logistics, Yonsei University, Korea
- Faculty of Agricultural Technology, Universitas Brawijaya, Indonesia
- Faculty of Agriculture, Yamagata University, Japan

- Food Science and Technology Association of Thailand (FoSTAT), Thailand
- Guangzhou Institute of Energy Conversion, Chinese Academy of Sciences, China
- Institute for Advanced Study, Gifu University, Japan
- Qingdao Institute of Bioenergy and Bioprocess Technology, Chinese Academy of Sciences, China
- SAFE-Network, Indonesia
- School of Food and Biological Engineering, Hezhou University, China
- School of Food Science and Biotechnology, Kyungpook National University, Korea

We would like to extend our deepest gratitude to all keynote and invited speakers, participants, reviewers, judges, and members of the organizing committee for their dedication and valuable contributions.

We sincerely hope that the 8th International Conference on Food and Applied Bioscience (FAB 2026) will act as a catalyst for new collaborations and inspire sustainable breakthroughs, making a meaningful contribution to the advancement of food and applied bioscience in this frontier food era.

(Associate Professor Yuthana Phimolsiripol, Ph.D.)
Chairman of the Organizing Committee
The 8th International Conference on Food and Applied Bioscience (FAB 2026)

Faculty of Agro-Industry, Chiang Mai University
February 2026

Table of Contents

	Page
Preface	i
Table of Contents	iii
Conference Committee	iv
Contents of Proceeding	vi
Proceeding of Oral Presentation	1
Proceeding of Poster Presentation	166
Sponsors	448

Conference Committee

Academic Advisory Committee:

Associate Professor Dr. Yuthana Phimolsiripol	Chiang Mai University

Administrative Chairperson:

Associate Professor Dr. Niramon Utama-ang	Chiang Mai University

Scientific Committee

Professor Dr. Alain Le Bail	ONIRIS, Nantes
Professor Dr. Anet Režek Jambrak	University of Zagreb
Professor Dr. Fabiano André Narciso Fernandes	Federal University of Ceará
Professor Dr. Faridah Abas	Universiti Putra Malaysia
Professor Dr. Francisco J. Barba	University of Valencia
Professor Dr. Fuli Li	Chinese Academy of Sciences
Professor Dr. Houda Berrada	University of Valencia
Professor Dr. Hui Hong	China Agricultural University
Professor Dr. Joe M. Regenstein	Cornell University
Professor Dr. Masahiro Ogawa	Kagawa University
Professor Dr. Masanori Watanabe	Gifu University
Professor Dr. Nathdanai Harnkarnsujarit	Kasetsart University
Professor Dr. Noma Seiji	Saga University
Professor Dr. Ozlem Tokusoglu	Celal Bayar University
Professor Dr. Sangguan You	Gangneung-Wonju National University
Professor Dr. Somesh Sharma	Shoolini University
Professor Dr. Sunghwan Kim	Kyungpook National University
Professor Dr. Sunyoung Lim	Korean Maritime & Ocean University
Professor Dr. Tomoaki Hagiwara	Tokyo University of Marine Science and Technology
Professor Dr. Uday S. Annapure	Institute of Chemical Technology (ICT) Nathalal Parekh Marg
Professor Dr. Weon-Sun Shin	Hanyang University
Professor Dr. Wei Qi	Chinese Academy of Sciences
Professor Dr. Witoon Prinyawiwatkul	Louisiana State University Agricultural Center Baton Rouge
Professor Dr. Wouter Saeys	KU Leuven
Associate Professor Dr. Kitipong Assatarakul	Chulalongkorn University
Associate Professor Dr. Massalin Nakphaichit	Kasetsart University
Associate Professor Dr. Mohsen Gavahian	National Pingtung University of Science and Technology
Associate Professor Dr. Ravi Jadeja	Oklahoma State University
Associate Professor Dr. Sajid Maqsood Maqsood Ahmed	United Arab Emirates University
Dr. Mahsa Majzoobi	RMIT University STEM College

Organizer

Faculty of Agro-Industry, Chiang Mai University

Co-hosts Organizations

Agro-Industry Academic Council Association (AIAC)	Thailand
College of Food Science and Nutritional Engineering, China Agricultural University	China
Faculty of Agriculture, Yamagata University	Japan
School of Food and Biological Engineering, Hezhou University	China
School of Food Science and Biotechnology, Kyungpook National University	Korea
Institute for Advanced Study, Gifu University	Japan
Department of Marine Food Science and Technology, Gangneung-Wonju National University	Korea
Department of Packaging & Logistics, Yonsei University	Korea
Qingdao Institute of Bioenergy and Bioprocess Technology, Chinese Academy of Sciences	China
Faculty of Agricultural Technology, Universitas Brawijaya	Indonesia
SAFE-Network	Indonesia
Food Science and Technology Association of Thailand (FoSTAT)	Thailand
Guangzhou Institute of Energy Conversion, Chinese Academy of Sciences	China

Contents of Proceeding

Oral Presentation

No.	Ref.	Title	Page
1	O-211	Ultrasound-Assisted Extraction of Anthocyanins from Doi Saket Black Rice Husk	1
2	O-224	Physicochemical, Phytochemical, Volatile Compounds, and Taste Profiles of *Apis mellifera* Honey from Longan (*Dimocarpus longan*) Flower	12
3	O-236	Effect of Maltodextrin Concentration on Stability and Physicochemical Properties of Concentrated Mahachanok Mango Smoothie	24
4	O-241	Effect of Tamarind Kernel Powder on Texture Formation of High-Moisture Extruded Soy Protein Meat Analogs	33
5	O-270	Machine Learning-Aided Optimization of Phenolic Extraction from Longan Processing Byproducts	41
6	O-285	Effect of Salt Concentration and Fermentation Temperature on the Microbiological and Chemical Properties of Watermelon Rind Fermentation	50
7	O-291	Characterization of γ-Oryzanol Extracted Using Medium-Chain Triglyceride Oil for Enhanced Stability and Bioactive Delivery	62
8	O-310	Comparative Effects of Drying Techniques on Bioactive Composition and Techno-Functional Properties of Kai (*Cladophora glomerata*)	73
9	O-311	Optimization of Pectinase-Assisted Aqueous Extraction for Anthocyanin Recovery from Black Goji Berries	86
10	O-340	Effect of Heat Treatment on Color, Proximate Composition, and Bioactive Compounds of Three Selected Mushrooms	96
11	O-344	Comparative Impact of Synthetic (polysorbate 80) and Protein-Based (α-lactalbumin) Emulsifiers on Intestinal Barrier Integrity and the Trans-Epithelial Transport of Polychlorinated Biphenyls	107
12	O-351	Optimized Procedure for Volatile Aroma Profiling in Chrysanthemum Leaf Tea	121
13	O-353	Development of Whole Green Banana (*Musa Sapientum* Linn, ABB Group, cv. Kluai Namwa) Flour Using Spray Drying with Focus on Resistant Starch Retention	131
14	O-362	Effect of Soaking Temperature on γ-Aminobutyric Acid (GABA) Content and Germination Rate of Ultrasonic-Assisted Germinated Brown Rice: KDML 105 and Riceberry	141
15	O-397	Salicylic Acid Alleviates Chilling Injury and Enhances Antioxidant Capacity in 'Nam Dok Mai' Mango during Cold Storage	153

Poster Presentation

No.	Ref.	Title	Page
1	P-183	Determination of Bioactive Compounds and Antioxidant Activities from Bitter Melon (*Momordica charantia* L.) Fruit Extracts Using Ultrasound-Assisted Extraction	166
2	P-184	Pasting Properties, Antioxidant Activities, Anthocyanins of Indigenous Pigmented Rice Flour and Its Correlation using Principal Component Analysis	175
3	P-185	Sustainable Valorization of Pectin from Guava Pulp using Ultrasound-Assisted Extraction	186
4	P-190	Analysis of Physicochemical Properties and Functional Properties of Six Banana (*Musa* sp.) Varieties and their Application as Ingredient for Energy Gel	199
5	P-191	Phytochemical Composition, Phenolic Profiling, and Bioactive Activities from Ethanolic Extraction of Different Parts of Mulberry (*Morus alba* L.)	211
6	P-201	Good Manufacturing Practices of Chili Paste Producing Community Enterprises in Songkhla, Thailand: Major Defect Criteria Outlook	221
7	P-204	Preparation and Characterization of Mulberry Leaf (*Morus alba* Linn.) Hydrogel Microparticles via Extrusion Microencapsulation	231
8	P-209	Optimization of Protein Hydrolysate Preparation and Nitric Oxide Scavenging Activity from Kam Kung Alga (*Chara corallina*) Using Response Surface Methodology	242
9	P-221	Packaging Effects on Freezing Rates and Quality of Roasted Chicken Drumettes	251
10	P-230	Efficiency of Extract from Jackfruit rags to Support Probiotic Growth	259
11	P-231	Investigation of Functional Carbohydrate Components from Indigenous Plants in Thailand	267
12	P-243	Effect of Thermo-Sonication Combined with Essential Oils on Bioactive Compounds and Antioxidant Activity in *Carissa carandas* L. Fruit Juice	274
13	P-288	Bioactive Compounds and Antioxidant Activities of *Ardisia polycephala* Wall. ex A. DC. Fruit Extract	287
14	P-299	Comparative Study on Ultrasonic and Pulsed Electric Field Extraction of Phrayawan (*Curcuma phrayawan* Boonma & sansouk) Rhizomes and Evaluation of Bioactive	298
15	P-317	Optimization and Characterization of Soluble Dietary Fiber Extracted from Edamame (*Glycine max L.)* Hulls by Plasma-Activated Water Technology	307

No.	Ref.	Title	Page
16	P-327	Comparative Effects of Finasteride and Minoxidil on Sperm Quality and Histological Changes in the Reproductive Organs of Male Mice with Testosterone-Induced Alopecia	321
17	P-330	Production of Alcoholic Beverage from Glutinous Rice	334
18	P-338	Effect of Heat Pump Drying Conditions on the Physicochemical Properties of King Oyster Mushroom (*Pleurotus eryngii*) Powder	340
19	P-352	Growth Stimulation of *Lachancea thermotolerans* and *Saccharomyces cerevisiae* Using Pulsed Electric Field	352
20	P-374	Development of Composite Film using Chitosan from Mantis Shrimp Shell and Gelatin as Bioactive carrier for Active packaging	357
21	P-403	Effect of Tween 20 and Tween 80 on Characteristics of the Water-in-Oil-in-Water Emulsion of *Centella asiatica* Beads	374
22	P-405	Development of Soy Protein-Based Meat Substitute using Freezing Process Combined with Transglutaminase and Alginate	384
23	P-407	Comparative Nutritional and Functional Attributes of Thai Underutilized Legumes	399
24	P-419	Efficiency of Pectin Extracted from Nam Wa Banana Peels in Encapsulation of *Centella asiatica* Extracts	410
25	P-431	Determination of Co-Flocculation Ability Between Distinct Cyanobacterial Genera and the Fungal Penicillium under the Antibiotic Stress by Erythromycin	419
26	P-433	Bioactive Compounds and Antioxidant Activity of Germinated Thai Indigenous Upland and Lowland Rice	427
27	P-439	Preliminary Study on the Development of a High-Fiber Wolffia-Enriched Snack Using Pineapple Pomace	438

O - 211

Ultrasound-Assisted Extraction of Anthocyanins from Doi Saket Black Rice Husk

Inthira Watthanaworawit, Thanyaporn Siriwoharn and Wachira Jirarattanarangsri*

Department of Food Science and Technology, Faculty of Agro-Industry, Chiang Mai University, Thailand

**Corresponding author E-mail: wachira.j@cmu.ac.th*

Abstract: Black rice husk is an abundant agro-industrial by-product with potential as a source of anthocyanins, yet it remains largely underutilized. This study optimized ultrasound-assisted extraction (UAE) of anthocyanins from Doi Saket black rice husk using response surface methodology based on a Box–Behnken design (BBD). Ethanol concentration (60–80%, v/v), extraction time (20–40 min), and ultrasonic amplitude (20–60%) were evaluated at a liquid-to-solid ratio of 20:1 (v/w), while maintaining the extraction temperature below 30 °C. Quadratic models adequately described most responses (adjusted R^2 = 0.809–0.855, $p < 0.05$), with extraction time and ultrasonic amplitude showing significant positive effects. Multi-response optimization identified optimal conditions at 60% ethanol, 29–30 min extraction time, and ~45% ultrasonic amplitude. Under these conditions, total anthocyanin content (TAC) reached 21.98 ± 1.34 mg cyanidin-3-O-glucoside (C3G)/100 g DW, and HPLC analysis confirmed C3G as the predominant anthocyanin. Predicted and experimental values showed deviations below 13%, indicating good model agreement. TAC was strongly correlated with antioxidant activities (DPPH, ABTS, and FRAP). The extract also exhibited α-glucosidase inhibitory activity under the tested conditions, along with moderate α-amylase inhibition. These findings indicate that optimized UAE provides an effective approach for valorizing black rice husk into anthocyanin-rich extracts.

Keywords: Black rice husk; Ultrasound-assisted extraction; Anthocyanin; Antioxidant activity; Cyanidin-3-O-glucoside

1. Introduction

Pigmented rice varieties, particularly black rice (*Oryza sativa L. var. indica*), are cultivated in northern Thailand and possess phytochemical compositions distinct from those of conventional white rice cultivars [(1)]. During milling, large quantities of rice husk are generated as an agro-industrial by-product. Rice husk accounts for approximately 20–22% of the total weight of paddy rice. This low-value residue is commonly used as fuel or discarded [(2)]. Despite its limited direct utilization, rice husk represents an abundant and inexpensive biomass resource that contains various phytochemicals. Previous studies have reported that black rice husk contains phenolic compounds, including anthocyanins, with cyanidin- and peonidin-based derivatives identified as predominant pigments [(3,4)]. These compounds exhibit antioxidant activity and have been associated with various health-promoting effects, including anti-diabetic and anti-inflammatory properties [(5,6)]. Anthocyanins may exert anti-diabetic effects partly via antioxidant mechanisms and inhibition of carbohydrate-hydrolyzing enzymes such as α-glucosidase and α-amylase [(7,8)]. Although the anthocyanin content in rice husk is generally lower than that in rice bran or pigmented rice grains, its large availability and low cost make it a promising alternative raw material for the recovery of bioactive compounds. Nevertheless, studies specifically targeting anthocyanin recovery from rice husk remain limited. Thus, valorization of black rice husk through

anthocyanin extraction represents a potential strategy for producing value-added bioactive ingredients [4].

Ultrasound-assisted extraction (UAE) is widely recognized as a green and efficient technique for recovering secondary metabolites from plant by-products, primarily by enhancing mass transfer through acoustic cavitation and cellular disruption [9]. Compared with conventional methods, UAE generally improves extraction efficiency and reduces processing time [4]. This process enhances solvent penetration and accelerates compound diffusion into the extraction medium [9–10]. However, anthocyanins are sensitive to thermal, mechanical stresses, and excessive ultrasonic energy or prolonged sonication may induce structural degradation and loss of bioactivity [4,6]. Consequently, optimization of UAE operating conditions is required to maximize anthocyanin recovery while preserving compound stability, for which response surface methodology (RSM) based on a Box–Behnken design (BBD) represents an effective statistical approach [11].

Therefore, the objective of this study was to investigate the extraction of anthocyanins from black rice husk using UAE combined with a BBD. The effects of key extraction parameters on total anthocyanin content (TAC), antioxidant activities (DPPH, ABTS, and FRAP), individual anthocyanin profiles (cyanidin-3-O-glucoside, C3G), and inhibitory activities against α-glucosidase and α-amylase were evaluated to identify optimal extraction conditions using a multi-response optimization approach.

2. Materials and Methods

2.1 Raw materials

Black rice husk was obtained from local farmers in Doi Saket District, Chiang Mai Province, Thailand, in October 2024. The husk was dried at 60 °C for 3 h, ground, and sieved through a 40-mesh screen. The moisture content of the processed sample was 4.44%. The initial TAC of the raw husk was 28.86 ± 1.27 mg C3G/100 g DW. The prepared husk was stored in opaque containers at −20 °C until extraction.

2.2 Chemicals and reagents

2,4,6-Tris(2-pyridyl)-s-triazine (TPTZ), 6-hydroxy-2,5,7,8-tetramethylchromane-2-carboxylic acid (Trolox), 2,2-diphenyl-1-picrylhydrazyl (DPPH), 2,2′-azinobis(3-ethylbenzothiazoline-6-sulfonic acid) (ABTS), and sodium carbonate (Na_2CO_3) were purchased from Sigma-Aldrich (St. Louis, MO, USA). Ethanol, methanol, acetonitrile, hydrochloric acid, phosphoric acid, ethyl acetate, and chemicals for buffer preparation were obtained from RCI Scientific (Thailand). α-Amylase and α-glucosidase were purchased from Megazyme (Wicklow, Ireland). 2-Chloro-4-nitrophenyl-α-D-maltotrioside (CNPG3) was obtained from Toronto Research Chemicals (Toronto, Canada), and p-Nitrophenyl-α-D-glucopyranoside (pNPG) from Macklin Biochemical (Shanghai, China). Cyanidin-3-O-glucoside chloride (C3G) standard was purchased from ChemFaces (Wuhan, China). C18 Sep-Pak cartridges (360 mg) were obtained from Waters Associates (Milford, MA, USA). Deionized water was used throughout the experiments.

2.3 Experimental design

UAE of anthocyanins from black rice husk was optimized using a BBD. Three independent variables were evaluated: ethanol concentration (60–80%, v/v), ultrasound amplitude (20–60%), and extraction time (20–40 min). Experimental runs, including replicated center points for estimation of experimental errors, are presented in Table 1. The evaluated responses included TAC, individual anthocyanin profiles, antioxidant activities, and enzyme inhibitory activities. All experimental runs in the BBD were performed in triplicate to ensure reproducibility, and the mean values were used for statistical analysis and model development [11].

2.4 UAE and purification of anthocyanins

Black rice husk (10 g) was extracted with 200 mL of acidified ethanol (0.1% HCl, v/v) using UAE under the conditions described in Table 1. A probe-type ultrasonic processor (13 mm probe, SONIC 3, SONIC Corporation, USA; 750 W) operating at a frequency of approximately 20 kHz was used, with amplitude adjusted according to the experimental design (20–60%). The extraction temperature was maintained below 30 °C using an ice-water bath. The extract was filtered and concentrated using rotary evaporation at 40 °C, reconstituted in acidified water, and subjected to purification using C18 Sep-Pak cartridges (360 mg). An aliquot (1 mL) was loaded onto a preconditioned cartridge, washed with acidified distilled water (0.01% HCl), air-dried using a syringe, and rinsed with ethyl acetate to remove non-anthocyanin compounds. Anthocyanins were eluted with acidified 95% ethanol (0.01% HCl), concentrated, reconstituted in acidified water, and stored at −20 °C until analysis [9,4].

2.5 Determination of TAC

TAC was determined using the pH differential method. Samples were diluted with pH 1.0 buffer (0.025 M potassium chloride) and pH 4.5 buffer (0.4 M sodium acetate). Absorbance was measured at 520 and 700 nm using a microplate reader [12].

$$A = (A_{520} - A_{700})_{pH\ 1.0} - (A_{520} - A_{700})_{pH\ 4.5}$$

TAC was expressed as mg C3G/100 g DW and calculated as:

$$TAC = \frac{A \times MW \times DF \times V}{\varepsilon \times L \times M}$$

where MW is the molecular weight of C3G (449.2 g/mol), ε is the molar absorptivity (26,900 $L \cdot mol^{-1} \cdot cm^{-1}$), DF is the dilution factor, V is the extract volume (mL), L is the path length (cm), and M is the sample mass (g). The same method was applied to determine the initial TAC of the raw husk.

Table 1. Experimental design with actual (uncoded) factor levels used in the BBD.

run	factors		
	ethanol (%)	time (min)	amplitude (%)
1	60	20	40
2	60	30	20
3	60	30	60
4	60	40	40
5	70	20	20
6	70	20	60
7	70	30	40
8	70	30	40
9	70	30	40
10	70	40	20
11	70	40	60
12	80	20	40
13	80	30	20
14	80	30	60
15	80	40	40

2.6 HPLC analysis of C3G

Samples were filtered through a 0.22 µm membrane prior to injection. Chromatographic separation was carried out on a ZORBAX Eclipse Plus C18 column (150 × 4.6 mm, 5 µm; Agilent Technologies, Santa Clara, CA, USA) at 30 °C with a flow rate of 1.0 mL/min and an injection volume of 10 µL. The mobile phase consisted of solvent A (deionized water with 1% phosphoric acid) and solvent B (acetonitrile). The gradient program was: 0–6 min, 98% A; 6–10 min, 80% A; 10–12 min, 60% A; 12 min, 98% A, followed by re-equilibration. Detection was performed at 520 nm using a diode array detector [13].

2.7 Antioxidant activity assays

2.7.1 DPPH radical scavenging activity

Diluted sample (10 µL) was mixed with 10 µL of acidified distilled water and 180 µL of 0.2 mM DPPH solution prepared in 70% methanol. The mixture was incubated in the dark at room temperature for 30 min, and absorbance was measured at 517 nm. Results were expressed as Trolox equivalent antioxidant capacity (µmol TE/g DW) [14].

2.7.2 ABTS radical cation scavenging activity

The ABTS•+ stock solution was prepared by mixing 7.4 mM ABTS with 2.45 mM potassium persulfate (1:1, v/v) and incubating in the dark for 16 h. The solution was diluted to an absorbance of 0.7 ± 0.2 at 734 nm. Sample (20 µL) was mixed with 180 µL of working solution and incubated for 6 min before measurement at 734 nm. Results were expressed as µmol TE/g DW [14].

2.7.3 Ferric reducing antioxidant power (FRAP)

The FRAP reagent was freshly prepared by mixing 10 mM TPTZ in 40 mM HCl, 20 mM $FeCl_3 \cdot 6H_2O$, and acetate buffer (pH 3.6) at a ratio of 1:1:10 (v/v/v). Sample (20 µL) was mixed with 180 µL of reagent, incubated at 37 °C for 30 min, and absorbance was measured at 593 nm. Results were expressed as µmol TE/g DW [14].

2.8 Enzyme inhibitory activity assays

2.8.1 α-Amylase inhibitory activity

α-Amylase inhibition was evaluated using CNPG3 as the substrate in sodium phosphate buffer (20 mM, pH 6.7) containing 6.7 mM NaCl. The reaction mixture consisted of buffer (20 µL), CNPG3 (100 µL), and sample extract (5 µL), pre-incubated at 37 °C for 5 min. The reaction was initiated by adding α-amylase (10 µL), incubated for 10 min, terminated with 0.5 M Na_2CO_3, and the absorbance was measured at 405 nm [8].

Enzyme inhibition (%) was calculated as:

$$Inhibition\ (\%) = \left[\frac{A_{sample} - A_{sample\ blank}}{A_{control} - A_{control\ blank}}\right] \times 100$$

2.8.2 α-Glucosidase inhibitory activity

α-Glucosidase inhibition was determined using pNPG in potassium phosphate buffer (0.1 M, pH 6.5). Buffer (40 µL), pNPG (100 µL), and sample extract (10 µL) were pre-incubated at 37 °C for 3 min. The reaction was initiated by adding α-glucosidase (20 µL), incubated for 5 min, terminated with 0.5 M Na_2CO_3, and the absorbance was measured at 405 nm [8]. Enzyme inhibition (%) was calculated using the same equation as that applied for the α-amylase inhibitory activity assay (Section 2.8.1).

2.9 Statistical analysis

All extraction experiments and analytical measurements were performed in triplicate, and the results were expressed as mean ± standard deviation. Data from the BBD were analyzed using Minitab software (version 16). Model significance was evaluated by analysis of variance (ANOVA) at $p < 0.05$. Model adequacy was assessed using the coefficient of determination (R^2 and adjusted R^2), the lack-of-fit test, and the agreement between predicted and experimental values. A non-significant lack-of-fit ($p > 0.05$) indicated that the model adequately described the experimental data [11].

Experimental data were fitted to a second-order polynomial model:

$$Y = \beta_0 + \beta_1 X_1 + \beta_2 X_2 + \beta_3 X_3 + \beta_{11} X_1^2 + \beta_{22} X_2^2 + \beta_{33} X_3^2$$

where Y is the response variable; β_0 is the intercept; and $\beta_1 - \beta_3$ and $\beta_{11} - \beta_{33}$ are the linear and quadratic coefficients of the independent variables X_1, X_2, and X_3.

3. Results and Discussion

3.1 Model performance and optimization of UAE

The BBD (Table 1) was used to evaluate the effects of ethanol concentration, extraction time, and ultrasonic amplitude on anthocyanin extraction from black rice husk. Quadratic polynomial models fitted to the experimental data (Table 2) showed that models for TAC, C3G, antioxidant activities (DPPH, ABTS, and FRAP), and α-glucosidase inhibitory activity were statistically significant ($p < 0.05$), with adjusted R^2 values ranging from 0.809 to 0.855, indicating adequate model performance. In contrast, the model for α-amylase inhibition exhibited a lower adjusted R^2 (0.716; $p < 0.05$), reflecting more limited explanatory capability. The adequacy of the developed models was further supported by a non-significant lack-of-fit ($p > 0.05$) for all response variables, indicating that the models adequately described the experimental data within the studied range and were suitable for process optimization.

Table 2. Fitted quadratic polynomial models, adjusted R^2 values, and regression significance levels for all response variables.

Response	Quadratic polynomial model	Adj.R^2	P value
TAC	−2.916 − 0.757×Ethanol + 3.274×Time + 0.636×Amp + 0.003×Ethanol² − 0.056×Time² − 0.007×Amp²	0.851	0.001
C3G	−16.284 + 0.074×Ethanol + 1.093×Time + 0.437×Amp − 0.001×Ethanol² − 0.019×Time² − 0.005×Amp²	0.809	0.002
DPPH	−93.132 + 2.019×Ethanol + 4.513×Time + 0.900×Amp − 0.018×Ethanol² − 0.079×Time² − 0.009×Amp²	0.814	0.002
ABTS	−4.318 − 0.570×Ethanol + 2.442×Time + 0.783×Amp + 0.003×Ethanol² − 0.042×Time² − 0.009×Amp²	0.850	0.001
FRAP	23.080 − 0.901×Ethanol + 3.055×Time + 0.508×Amp + 0.003×Ethanol² − 0.053×Time² − 0.005×Amp²	0.822	0.001

All models are quadratic polynomial equations using uncoded factors. Significant models were identified at $p < 0.05$; "ns" indicates non-significant regression. Abbreviations: TAC, total anthocyanin content; C3G, cyanidin-3-O-glucoside; DPPH, DPPH radical scavenging activity; ABTS, ABTS radical cation scavenging activity; FRAP, ferric reducing antioxidant power; Amp, ultrasonic amplitude.

Pearson correlation analysis revealed significant positive correlations between TAC, C3G, and antioxidant activities determined by DPPH, ABTS, and FRAP ($r = 0.92–0.96$, $p < 0.01$), showing that conditions favoring anthocyanin recovery were associated with enhanced antioxidant responses. This relationship was consistent with the antioxidant properties of anthocyanins, particularly C3G, which scavenge reactive oxygen species through electron or hydrogen donation mechanisms [(2)]. TAC and C3G also showed significant positive correlations with α-glucosidase inhibition ($p < 0.01$) and weaker but positive associations with α-amylase inhibition, supporting the potential role of black rice husk extracts in modulating carbohydrate digestion [(8)]. Extraction time and ultrasonic amplitude exerted positive linear effects on most responses, reflecting the contribution of ultrasonic energy to mass transfer through acoustic cavitation and cell wall disruption [(9)]. However, negative quadratic terms (Time² and Amplitude²) indicated the presence of optimal extraction regions, beyond which response values decreased, consistent with anthocyanin degradation caused by localized heating and mechanical stress during prolonged or high-intensity processing [(4,6)]. Although ethanol concentration was not statistically significant in the models, this most likely reflects the selection of an ethanol range already suitable for anthocyanin solubilization. Consequently, physical parameters played a more dominant role in controlling mass transfer efficiency under UAE.

Multi-response desirability analysis identified optimal extraction conditions at 60% ethanol, 29–30 minute extraction time, and approximately 45% ultrasonic amplitude. Deviations between experimental and predicted values ranged from 2.7% to 12.3% (Table 3), confirming the reliability of the models for process optimization.

Table 3. Predicted and experimental values of response variables at the optimum UAE conditions (TAC and C3G, mg C3G/100 g DW; DPPH, μmol TE/g DW; α-glucosidase inhibition, %).

Response	Predicted value	Experimental value (mean ± SD)	Deviation (%)
TAC	23.9103	21.9767 ± 1.3375	8.1
C3G	9.6069	8.4281 ± 0.3480	12.3
DPPH	50.3217	48.9745 ± 1.9645	2.7
α-Glucosidase	85.7681	83.0852 ± 2.1441	3.1

Values are expressed as mean ± standard deviation (n = 3). Deviation (%) was calculated as the percentage difference between the predicted and experimental values. Abbreviations: TAC, total anthocyanin content; C3G, cyanidin-3-O-glucoside; DPPH, DPPH radical scavenging activity.

3.2 Anthocyanin properties

The TAC of black rice husk extracts obtained from the BBD experiments ranged from 9.3 to 22.3 mg C3G/100 g DW (Table 4), demonstrating the influence of UAE conditions on anthocyanin release from the rigid husk matrix. Under optimized UAE conditions determined by multi-response desirability analysis, the extract achieved a TAC of 21.98 ± 1.34 mg C3G/100 g DW (Table 3), corresponding to an extraction recovery of approximately 76.2% based on the initial TAC of the raw husk (28.86 ± 1.27 mg C3G/100 g DW). Higher TAC values were associated with moderate extraction times and moderate to relatively high ultrasonic amplitudes, whereas

excessive intensity reduced TAC, likely due to anthocyanin degradation [6]. Compared with previous studies on rice husk, the TAC obtained in this work was substantially higher than the approximately 3 mg C3G/100 g DW reported for microwave–UAE [4], representing a 7.3-fold increase and indicating improved extraction efficiency. In contrast, rice bran consistently exhibits higher anthocyanin content, with reported values of 113–256 mg C3G/100 g DW for maceration [15] and 618 mg C3G/100 g DW for acidified solvent extraction [12]. Although different extraction techniques were used, this comparison reflects anthocyanin distribution across rice matrices, with significantly higher accumulation in the bran layer than in the husk, with values approximately 5–12 and 28 times higher than those obtained for rice husk under optimized conditions in this study, respectively. Rice husk can serve as an alternative anthocyanin source; however, its relatively low anthocyanin content compared to rice bran remains a key limitation, although its abundance and low cost support its potential for value-added applications if extraction efficiency can be further improved.

Table 4. Experimental values of anthocyanin content (mg C3G/100 g DW) and antioxidant activities (µmol TE/g DW) for different experimental runs.

Run	TAC	C3G	DPPH	ABTS	FRAP
1	19.61 ± 0.72^{b}	7.35 ± 0.34^{d}	43.86 ± 1.61^{bc}	20.52 ± 0.23^{abc}	34.17 ± 1.36^{b}
2	20.59 ± 1.05^{b}	6.83 ± 0.18^{e}	46.59 ± 0.80^{ab}	21.43 ± 0.73^{ab}	34.76 ± 1.52^{b}
3	22.32 ± 0.85^{a}	8.05 ± 0.30^{bc}	48.23 ± 1.44^{a}	21.60 ± 1.13^{ab}	38.95 ± 0.85^{a}
4	15.49 ± 0.98^{c}	8.02 ± 0.21^{b}	36.71 ± 0.90^{ef}	18.92 ± 0.83^{bcd}	29.34 ± 1.38^{cde}
5	9.86 ± 0.83^{ef}	4.64 ± 0.07^{h}	33.96 ± 1.61^{f}	13.14 ± 1.16^{f}	25.43 ± 1.15^{fg}
6	11.91 ± 0.96^{de}	5.92 ± 0.07^{f}	38.06 ± 0.92^{de}	16.21 ± 0.44^{de}	27.42 ± 0.93^{ef}
7	18.52 ± 0.72^{b}	7.73 ± 0.06^{cd}	44.76 ± 0.54^{b}	21.10 ± 0.22^{ab}	31.52 ± 1.23^{bcd}
8	19.47 ± 1.03^{b}	9.08 ± 0.37^{a}	45.89 ± 1.41^{ab}	22.26 ± 1.34^{a}	33.23 ± 1.77^{b}
9	21.23 ± 0.87^{ab}	9.29 ± 0.03^{a}	48.52 ± 0.95^{a}	23.42 ± 0.94^{a}	34.74 ± 1.20^{b}
10	10.54 ± 0.63^{ef}	3.75 ± 0.10^{i}	30.71 ± 1.10^{g}	11.89 ± 1.54^{f}	22.91 ± 1.89^{gh}
11	13.20 ± 0.77^{d}	5.17 ± 0.02^{g}	37.77 ± 1.74^{e}	17.20 ± 1.70^{d}	28.35 ± 0.59^{def}
12	12.44 ± 0.82^{d}	6.60 ± 0.09^{e}	36.92 ± 1.91^{ef}	18.05 ± 1.48^{cd}	26.32 ± 1.35^{ef}
13	9.39 ± 0.88^{f}	4.01 ± 0.27^{i}	29.06 ± 0.55^{g}	14.18 ± 0.75^{ef}	20.92 ± 1.04^{h}
14	15.48 ± 0.80^{c}	7.58 ± 0.03^{d}	41.00 ± 1.06^{cd}	18.93 ± 1.24^{bcd}	31.95 ± 1.14^{bc}
15	9.30 ± 0.93^{f}	4.85 ± 0.03^{h}	30.81 ± 0.62^{g}	16.04 ± 0.61^{de}	22.94 ± 1.13^{gh}

Values are mean ± SD (n = 3). Different superscript letters within a column indicate significant differences (Tukey's test, $p < 0.05$). Abbreviations: TAC, total anthocyanin content; C3G, cyanidin-3-O-glucoside; DPPH, DPPH radical scavenging activity; ABTS, ABTS radical cation scavenging activity; FRAP, ferric reducing antioxidant power.

Antioxidant activities measured by DPPH, ABTS, and FRAP followed trends consistent with TAC values. Pearson correlation coefficients between TAC and antioxidant activities ranged from 0.92 to 0.96 ($p < 0.01$), indicating that anthocyanins were major contributors to the antioxidant properties of the extracts. Similar strong correlations ($r = 0.92–0.98$) have been reported in pigmented rice systems [13, 16]. ABTS values in the present study (approximately 12–23 µmol TE/g DW) were slightly lower but comparable to 25.76 µmol TE/g DW reported for black rice bran, while DPPH values (approximately 29–49 µmol TE/g DW) were comparable to or slightly higher than 29.02 µmol TE/g DW [12]. FRAP values in the present study (approximately 20–38 µmol TE/g DW) were lower than 140.57 µmol TE/g DW reported for rice bran, likely due to the lower phenolic and anthocyanin contents in the husk matrix as well as differences in other reducing compounds present in the extracts.

HPLC analysis (Table 4) confirmed C3G as the predominant anthocyanin, with peonidin-3-O-glucoside (P3G) detected as a minor component. Under the optimized conditions, the C3G content reached 8.43 ± 0.35 mg/100 g DW, accounting for the majority of the detected anthocyanins. These findings are consistent with previous studies identifying C3G as the major anthocyanin across different rice fractions, including whole grain, bran, and husk [16,4]. The lower C3G content compared to TAC is attributable to differences in analytical methods, as TAC represents total anthocyanins, whereas HPLC quantifies individual compounds. The predominance of C3G and its association with TAC and antioxidant activities further support its major contribution to the antioxidant capacity of pigmented rice extracts. In addition, previous studies have shown that anthocyanins are more abundantly accumulated in rice bran than in husk, although advanced extraction techniques can enhance anthocyanin recovery from husk matrices.

3.3 α-Amylase and α-glucosidase inhibitory activities

The inhibitory activities of black rice husk extracts against α-amylase and α-glucosidase were evaluated separately using acarbose (0.1 mg/mL) as a positive control under identical conditions for each assay (Table 5). Due to differences in substrates and reaction conditions, comparisons were performed within each enzyme system. At a concentration corresponding to 0.12 g raw material equivalents/mL, inhibitory activities varied across experimental runs. For α-glucosidase, inhibition ranged from approximately 47.8% to 85.2%, with several runs exhibiting higher apparent inhibitory activity than acarbose at the tested concentration (64.08 ± 1.53%), while others showed comparable or lower activity. In contrast, α-amylase inhibition ranged from approximately 36.4% to 57.4%, with most values overlapping that of acarbose (48.10 ± 1.69%), although certain runs displayed higher apparent inhibitory activity under the same assay conditions. This inhibition levels are within the range reported for anthocyanin-rich rice extracts in previous studies [17,13] . Overall, the extracts consistently showed stronger inhibitory activity against α-glucosidase than α-amylase.

The differential inhibitory responses between the two enzymes are attributable to differences in their structures, substrate specificities, and inhibitor–enzyme interactions [5]. Anthocyanins and associated phenolic compounds possess glycosylated and polyhydroxylated structures that resemble carbohydrate moieties [13], enabling more effective accommodation and stabilizing interactions, including hydrogen bonding, within the relatively narrow and substrate-specific catalytic pocket of α-glucosidase. In contrast, the broader active-site cleft of α-amylase, adapted for polymeric starch substrates, may reduce interaction specificity [5,7]. Correlation analysis further supported this enzyme-specific behavior, revealing significant positive correlations between TAC and C3G with α-glucosidase inhibitory activity ($p < 0.01$), but no

significant correlations with α-amylase inhibition ($p > 0.05$). These findings suggest that α-glucosidase inhibition is associated with anthocyanin content, while α-amylase inhibition may be governed by additional factors beyond anthocyanins alone [17]. Consistent with previous reports of mixed-type inhibition by anthocyanin-rich rice extracts, both direct enzyme binding and substrate-level interference through the formation of starch–anthocyanin complexes likely contribute to the stronger and more consistent inhibition of α-glucosidase [5,17]. Because inhibitory activities were assessed at a single concentration, the results reflect inhibitory potential under the specified conditions rather than intrinsic inhibitory potency [17].

Table 5. Experimental values of α-glucosidase and α-amylase inhibitory activities (%inhibition) for different experimental runs.

Run	α-glucosidase	α-amylase
1	74.10 ± 0.24^{cd}	44.42 ± 0.61^{defg}
2	73.73 ± 0.30^{cde}	41.70 ± 0.78^{fg}
3	76.74 ± 0.66^{bc}	51.31 ± 0.84^{g}
4	72.50 ± 1.38^{cde}	36.40 ± 1.10^{h}
5	60.13 ± 0.40^{gh}	45.59 ± 1.20^{cdef}
6	69.97 ± 2.09^{cdef}	57.10 ± 1.77^{a}
7	77.74 ± 2.46^{bc}	56.12 ± 1.53^{ab}
8	82.41 ± 0.67^{ab}	57.43 ± 1.47^{a}
9	85.19 ± 1.92^{a}	53.30 ± 0.87^{b}
10	47.78 ± 1.08^{i}	42.60 ± 1.55^{efg}
11	60.65 ± 0.83^{gh}	46.21 ± 1.95^{cde}
12	62.78 ± 0.95^{fgh}	42.03 ± 1.71^{fg}
13	66.42 ± 1.27^{efg}	48.78 ± 1.94^{c}
14	67.26 ± 1.86^{defg}	54.42 ± 2.04^{ab}
15	58.72 ± 0.45^{h}	42.41 ± 0.70^{efg}
Acarbose	64.08 ± 1.53^{fgh}	48.10 ± 1.69^{cd}

Values are mean ± SD (n = 3). Different superscript letters within a column indicate significant differences (Tukey's test, $p < 0.05$). Acarbose (0.1 mg/mL) was used as a positive control for comparison of enzyme inhibitory activities.

4. Conclusion

This study demonstrated that UAE combined with a BBD is an effective approach for recovering anthocyanins from black rice husk, an underutilized agro-industrial by-product. The developed quadratic models adequately described the effects of ethanol concentration, extraction time, and ultrasonic amplitude on TAC, antioxidant activities, individual anthocyanins, and enzyme inhibitory activities. Optimal extraction conditions were identified at 60% (v/v) ethanol,

approximately 29–30 min extraction time, and ~45% ultrasonic amplitude. Under these conditions, the extract achieved a TAC of 21.98 ± 1.34 mg C3G/100 g DW and showed antioxidant activities. The extraction process achieved an estimated recovery of approximately 76% of the initial anthocyanin content of the raw husk. The extract also exhibited α-glucosidase inhibitory activity (83.09 ± 2.14%) under the tested conditions, while moderate α-amylase inhibition was observed. HPLC analysis confirmed C3G as the predominant anthocyanin, and its content showed strong correlations with antioxidant capacity and α-glucosidase inhibitory activity. Overall, these findings highlight the potential of black rice husk as a sustainable source of anthocyanins and support the application of optimized UAE for producing anthocyanin-rich extracts with antioxidant properties and enzyme inhibitory potential.

Acknowledgements

The authors gratefully acknowledge Chiang Mai University for providing research facilities and laboratory support. Appreciation is also extended to colleagues and staff for their assistance during the experimental work.

References

1. Yamuangmorn S, Prom-u-Thai C. The potential of high-anthocyanin purple rice as a functional ingredient in human health. *Antioxidants*. 2021;10(6):833.
2. Goufo P, Trindade H. Rice antioxidants: phenolic acids, flavonoids, anthocyanins, proanthocyanidins, tocopherols, tocotrienols, γ-oryzanol, and phytic acid. *Food Science & Nutrition*. 2014;2(2):75–104.
3. Chariyakornkul A, Punvittayagul C, Taya S, Wongpoomchai R. Inhibitory effect of purple rice husk extract on AFB1-induced micronucleus formation in rat liver through modulation of xenobiotic metabolizing enzymes. *BMC Complementary and Alternative Medicine*. 2019;19(1):237.
4. Jha P, Das AJ, Deka SC. Optimization of ultrasound and microwave assisted extractions of polyphenols from black rice (*Oryza sativa* cv. Poireton) husk. *Journal of Food Science and Technology*. 2017;54(12):3847–58.
5. Miao L, Xu Y, Jia C, Zhang B, Niu M, Zhao S. Structural changes of rice starch and activity inhibition of starch digestive enzymes by anthocyanins retarded starch digestibility. *Carbohydrate Polymers*. 2021;261:117841.
6. Patras A, Brunton NP, O'Donnell C, Tiwari BK. Effect of thermal processing on anthocyanin stability in foods: mechanisms and kinetics of degradation. *Trends in Food Science & Technology*. 2010;21(1):3–11.
7. Oteiza PI, Cremonini E, Fraga CG. Anthocyanin actions at the gastrointestinal tract: relevance to their health benefits. *Molecular Aspects of Medicine*. 2023;89:101156.
8. Akkarachiyasit S, Charoenlertkul P, Yibchok-anun S, Adisakwattana S. Inhibitory activities of cyanidin and its glycosides and synergistic effect with acarbose against intestinal α-glucosidase and pancreatic α-amylase. *International Journal of Molecular Sciences*. 2010;11(9):3387–96.
9. Chemat F, Rombaut N, Sicaire AG, Meullemiestre A, Fabiano-Tixier AS, Abert-Vian M. Ultrasound assisted extraction of food and natural products: mechanisms, techniques, combinations, protocols and applications. A review. *Ultrasonics Sonochemistry*. 2017;34:540–60.
10. Chemat F, E-Huma Z, Khan MK. Applications of ultrasound in food technology: processing, preservation and extraction. *Ultrasonics Sonochemistry*. 2011;18(4):813–35.
11. Ferreira SLC, Bruns RE, Ferreira HS, Matos GD, David JM, Brandão GC, et al. Box-Behnken design: an alternative for the optimization of analytical methods. *Analytica Chimica Acta*. 2007;597(2):179–86.

12. Halee, A. Effects of solvent types and citric acid concentrations on the extraction of antioxidants from black rice bran of *Oryza sativa* L. cv. Hom Nin. *Journal of Microbiology, Biotechnology and Food Sciences*. 2018;8(2):765–769.
13. Noviasari S, Kusnandar F, Setiyono A, Budijanto S. Antioxidant activity and inhibition of α-amylase and α-glucosidase in fermented black rice bran-based analog rice. *AIMS Agriculture and Food*. 2022;7(1):61–72.
14. Prior RL, Wu X, Schaich K. Standardized methods for the determination of antioxidant capacity and phenolics in foods and dietary supplements. *Journal of Agricultural and Food Chemistry*. 2005;53(10):4290–302.
15. Laokuldilok, T.; Shoemaker, C. F.; Jongkaewwattana, S.; Tulyathan, V. Antioxidants and antioxidant activity of several pigmented rice brans. *Journal of Agricultural and Food Chemistry*. 2011;59(1):193–199.
16. Iswanti W, Budijanto S, Abdullah M. Flavonoid and antioxidant activity analysis of anthocyanin black rice bran extract (ABRIBE) cv. Cempo Ireng origin from Indonesia. *Journal of Microbiology, Biotechnology and Food Sciences*. 2024;14(2):e10203.
17. Sansenya S, Nanok K. α-Glucosidase and α-amylase inhibitory potential and antioxidant activity of fragrant black rice (Thai coloured rice). *Flavour and Fragrance Journal*. 2020;35(4):376–86.

O - 224

Physicochemical, Phytochemical, Volatile Compounds, and Taste Profiles of *Apis mellifera* Honey from Longan (*Dimocarpus longan*) Flower

Gerry Renaldi[1,2], Arriya Tadtan[2,3], Napatsawan Chaimahawan[2,3], Terd Disayathanoowat[4,5], Rajnibhas Sukeaw Samakradhamrongthai[2,5,6]*

[1]*Department of Food Science and Technology, Faculty of Agro-Industry, Chiang Mai University, Chiang Mai 50100, Thailand*
[2]*Interdisciplinary and Food product development for wellness Research Unit, Faculty of Agro-Industry, Chiang Mai University, Chiang Mai 50100, Thailand*
[3]*Department of Food Science and Technology, Division of Food Innovation Design and Development, Faculty of Agro-Industry, Chiang Mai University, Chiang Mai 50100, Thailand*
[4]*Department of Biology, Faculty of Science, Chiang Mai University, Chiang Mai 50200, Thailand*
[5]*Research Center of Deep Technology in Beekeeping and Bee Products for Sustainable Development Goals (SMART BEE SDGs), Chiang Mai University, Chiang Mai 50200, Thailand*
[6]*Division of Product Development Technology, Faculty of Agro-Industry, Chiang Mai University, Chiang Mai 50100, Thailand*

**Corresponding author E-mail: rajnibhas.s@cmu.ac.th*

Abstract: Honey is a sweet, viscous substance produced by *Apis mellifera* L. from floral nectar, with monofloral varieties characterized by a predominance of pollen from a single plant species. In northern Thailand, longan (*Dimocarpus longan*) blossoms represent the main natural nectar source for honeybees. This study was conducted to analyze the physicochemical and phytochemical properties of longan honey (LH) collected from Chiang Mai, Thailand in February–March 2025. In addition, the aroma-active volatile organic compounds (VOC) and taste profiles were investigated using electronic nose (E-nose) and electronic tongue (E-tongue) respectively. The analysis showed the properties of the LH samples significantly ($p < 0.05$) varied with each other: moisture content (19.16–19.68%), color (2.02–50.98 mm Pfund, water white to light amber), pH (4.06–4.50), acidity (5.96–18.16 meq/kg), total phenolic content (22.56–46.99 mg GAE/100 g sample), total flavonoid content (0.66–24.01 mg CE/100 g sample), IC_{50} DPPH (81.57–496.53 mg/mL), IC_{50} ABTS (213.58–523.18 mg/mL), and FRAP (9.53–28.69 mg TE/100 g sample). VOC investigation identified esters, alcohols, aldehydes, and ketones as the major VOC group, with all samples contained 3-Nonanone (24.24–337.77 µg/kg) that provides floral aroma, followed by acetic acid (3.41–45.31 µg/kg), ethyl 3-(methylthio)propanoate (9.24–127.06 µg/kg), methyl cinnamate (0.66–3.07 µg/kg), and propan-2-one (205.75–355.44 µg/kg) in the majority of the samples. Based on taste profiling, honey samples exhibit distinct taste profiles, ranging from those dominated by high sweetness and low bitterness to those exhibiting elevated bitterness or complex savory notes. The principal component analysis (PCA) of the LH based on physicochemical properties, volatile compounds, and taste profile explained 99.4%, 95.4%, and 99.0%, of the total variance, respectively, indicating a strong and reliable representation of the data structure within two principal components. Based on the results, within the same floral origin, honey possessed differences in its composition. These findings highlight the unique characteristics and chemical diversity of longan honey produced in northern Thailand. The results also emphasize the potential of longan honey as a valuable natural product with distinct sensory qualities and significant antioxidant properties, making it promising for applications in functional foods formulations.

Keywords: Longan honey; Physicochemical properties; Volatile compound; Taste profile; Instrumental sensory analysis.

1. Introduction

Honey is a natural food produced by bees through the transformation of floral nectar, combined with bee-derived substances, and subsequently stored and matured in honeycombs.[1] Its use by human societies dates back to prehistoric times, with historical evidence indicating that honey has been consumed for approximately 8,000 years.[2] While honey was traditionally valued primarily as a natural sweetener, contemporary research has highlighted its distinctive nutritional composition, sensory attributes, and bioactive properties, leading to its widespread application in the food, cosmetic, and health-related sectors.[3] Importantly, the chemical composition and functional properties of honey are not uniform but vary considerably depending on factors such as botanical origin, geographical location, and environmental conditions, which form the basis for its classification and differentiation into distinct honey types.[4] Among these factors, botanical origin is particularly critical, as it underpins the classification of honey into monofloral and multifloral categories.

According to its botanical origin, honey is classified into monofloral and multifloral types. Monofloral/unifloral honey is derived predominantly from a single floral nectar source, whereas multifloral/polyfloral honey originates from multiple nectar sources collected simultaneously.[5] More than 300 monofloral honey varieties have been identified worldwide, including acacia, alfalfa, blueberry, eucalyptus, orange blossom, and pine honey, each characterized by distinct physicochemical, sensory, and bioactive properties.[3] Within this diversity, longan honey represents one of the most prominent monofloral honeys in Asia due to its distinctive characteristics and widespread production. Its prominence is strongly shaped by regional apicultural practices and the availability of longan floral resources across major honey-producing areas in Asia.

The prominence of longan honey is closely linked to regional apicultural practices and floral availability in Asia, which is the world's largest honey-producing and honey-consuming region.[3,6] In northern Thailand, *Apis mellifera* constitutes approximately 89% of the colonies used in commercial beekeeping, and the region is a major cultivation area for longan (*Dimocarpus longan*), a tropical fruit native to Southeast Asia. Longan plantations in northern Thailand cover approximately 160,000 hectares with an annual production exceeding 642,192 tons,[7] providing an abundant and stable nectar source that facilitates the large-scale production of monofloral longan honey.

The composition of honey varies depending on its botanical origin, bee species, geographical location, and environmental conditions.[8] These factors strongly influence the characteristics and functionality of honey, collectively determine its quality. In particular, *Apis mellifera* honey derived from longan flower is expected to exhibit distinctive composition reflecting the unique nectar source and regional growing conditions. However, comprehensive information linking these compositional attributes to the properties of longan honey remains limited. Thus, this study was done to investigate the physicochemical, phytochemical, volatile compounds, and taste profiles of *Apis mellifera* longan honey.

2. Materials and Methods

2.1 Raw material and chemicals

Five longan honey (LH) samples used in this study were obtained commercially from different brands in Chiang Mai, Thailand. All samples were labelled as 100% longan honey and were reported to be harvested from longan plantations in Chiang Mai during the flowering season (February–March 2025). After the arrival at the Division of Product Development Technology, Faculty of Agro-Industry, Chiang Mai University, the samples were kept in a dark place at room temperature (27±2 °C) until further analysis. All chemicals used in this study were analytical grade.

2.3 Physicochemical properties

2.3.1 Moisture content

The moisture content of the honey samples was determined with an indirect refractometric method using a digital refractometer at 20 °C and calculated using the Wedmore conversion table in triplicate.[9]

2.3.2 Color

Honey color was calculated by using Pfund scale and correlating it with the value of optical density obtained after measurement at 560 nm using a microplate reader (Tecan Infinite 200 Pro, Tecan Group Ltd., Männedorf, Switzerland) with glycerol as the blank.[10] The measurement was done in triplicate.

2.3.3 pH and free acidity

The pH and free acidity of the honey samples were determined according to AOAC Official Method 962.19.[10] For pH determination, 10 g of honey was dissolved in 75 mL of distilled water, and the pH was measured using a pH meter (model S220, Mettler Toledo AG, Greifensee, Switzerland). Free acidity was measured by titration method using a 0.05 M NaOH (Sigma-Aldrich Co., St. Louis, MO, USA) added to the honey solution, with ultrapure water prepared using a Milli-Q water purification system (Millipore, Paris, France) serving as the blank. The measurement was done in triplicate and expressed as milliequivalents (meq) of acid per kilogram of honey.

2.3.4 5-hydroxymethylfurfural

HMF was determined according to the White method, official method 980.23.[10] A clarified solution of 5 g of honey in a 25 mL volumetric flask was prepared using 0.50 mL Carrez I (a solution containing 21.90 g zinc acetate dihydrate (Sigma Aldrich) and 3 g glacial acetic acid (Sigma Aldrich) dissolved to a final volume of 100 mL with distilled water) and 0.50 mL Carrez II (a solution containing 10.60 g potassium ferrocyanide (Sigma Aldrich) dissolved to a final volume of 100 mL with distilled water). The absorbance of this solution was measured at 284 and 336 nm (model: Lambda 25, PerkinElmer, Inc., Waltham, MA, U.S.). The honey sample was replaced with sodium bisulfite (Sigma Aldrich) and used as a blank. The HMF was calculated using the following equation (1):

$$\text{HMF}\ (mg/kg) = (Abs_{284nm} - Abs_{336nm}) x\ 149.7\ x\ 5\ (\frac{\text{dilution factor}}{\text{sample weight (g)}})\ (1)$$

Where Abs_{284nm} and Abs_{336nm} correspond to the absorbance at 284 and 336 nm, respectively, while 149.7 is the standard calculation factor, and 5 represents the nominal sample mass (g) for the White method.

2.4 Phytochemical properties

2.4.1 Total phenolic content

The total phenolic content (TPC) of the honey extracts was determined using a modified Folin–Ciocalteu method.[9] Briefly, 20 µL of a 50% (w/v) honey solution was transferred into a well in a 96-well microplate and mixed with 100 µL of Folin–Ciocalteu reagent, then allowed to stand for 5 min at room temperature (25±2 °C). Subsequently, 80 µL of 7.5% Na_2CO_3 solution was added, and the mixture was incubated in the dark for 45 min at room temperature (25±2 °C). The absorbance was measured at 760 nm using a microplate reader (Tecan Infinite 200 Pro, Tecan Group Ltd., Männedorf, Switzerland) against a distilled water blank in triplicate. Gallic acid was used as the calibration standard, and results were expressed as milligrams of gallic acid equivalents per 100 g of honey (mg GAE/100 g).

2.4.2 Total flavonoid content

The total flavonoid content (TFC) of the honey samples was measured according to the modified $AlCl_3$ method.[11] A 50% (w/v) honey sample (20 µL) was mixed with 20 µL $NaNO_2$. After 5 min, 20 µL of 10% (w/v) $AlCl_3$ was transferred into the mixture, stirred for 6 min before 40 µL of 1 M NaOH were added. Distilled water (100 µL) was added before the mixture was shaken. The absorbance was measured at 510 nm using a microplate reader (Tecan Infinite 200 Pro, Tecan Group Ltd., Männedorf, Switzerland) in triplicate. Total flavonoids were expressed as mg catechin equivalent per 100 g sample (mg CE/100 g).

2.4.3 Antioxidant activity

Three antioxidant assays: DPPH, ABTS, and FRAP, were employed in this study with slight modification.[12] A 50% (w/v) honey solution was used as the sample. The absorbance of each assay was measured in triplicate using a microplate reader (Tecan Infinite 200 Pro, Tecan Group Ltd., Switzerland).

For the DPPH assay, 20 µL of sample was mixed with 180 µL of 0.5 mM DPPH methanolic solution and allowed to stand in the dark for 30 min. The absorbance of the sample was measured at 517 nm. The result was expressed as IC_{50} DPPH (mg/mL).

For the ABTS assay, 7 mM ABTS in water and 2.45 mM potassium persulfate (1:1) was combined to create a working solution and kept in the dark for 12–16 h. The mixture was diluted with distilled water until the absorbance at 734 nm reached approx. 0.7. The sample (20 µL) and the $ABTS^{\cdot+}$ solution (180 µL) was combined and its absorbance was measured. The result was expressed as IC_{50} ABTS (mg/mL).

For the ferric reducing antioxidant power (FRAP)assay, working solution was created by mixing 300 mM acetate buffer, 10 mM TPTZ in 40 mM HCl, and 20 mM $FeCl_3 \cdot 6H_2O$ (10:1:1) and heated at 37 °C for 30 min. The FRAP reagent (180 µL) was combined with the sample (20 µL). After 30 min of incubation at 37 °C in a water bath (Memmert, Schwabach, Germany), the absorbance value was measured at 593 nm. The result was expressed as mg Trolox equivalent (TE)/ 100 g sample.

2.5 Aroma-active volatile compounds identification using Gas Chromatograph–Electronic Nose (GC-E-Nose)

The aroma-active volatile organic compounds (VOCs) were identified using a Heracles II E-Nose (Alpha M.O.S., Toulouse, France) equipped with an MXT-5 column (280 µm × 0.5 µm). Flame ionization detectors (FID) were used for detection. Samples were incubated at 60 °C for 5 min prior to injection. A 5 mL volume of headspace gas was injected at a rate of 125 µL/s, with an injection temperature of 200 °C. The trap temperature was maintained at 40 °C, with a split flow rate of 10 mL/min. The initial column temperature was set to 50 °C, then increased to 80 °C at a rate of 1 °C/s, followed by a further increase to 250 °C at 3 °C/s and maintained at 250 °C for 21 sec. The detector temperature was set at 260 °C. The VOCs were identified using AroChemBase sensory analysis software module. Compounds with a pertinence index ≥ 80% were selected and subjected to further screening based on their sensory descriptors in published research articles. After the screenings, the selected compounds were quantified based on the information obtained from the identification (e.g. area) and their quantity was calculated against standard curve of hexanal generated from different concentration (0.001–100 µL/mL).

2.6 Taste profiling using Electronic Tongue (E-Tongue)

Taste profile was analyzed using an Astree Electronic Tongue (E-Tongue, Alpha M.O.S., Toulouse, France) equipped with a #6 sensor array consisting of seven sensors. AHS, CTS, NMS, ANS, and SCS correspond to basic human taste perceptions of sourness, saltiness, umami, sweetness, and bitterness, respectively, while PKS and CPS contribute to the comprehensive taste profile. A 1% (w/v) honey solution was prepared by dissolving the honey sample in distilled water at room temperature (25 ± 2 °C). The acquisition duration was set to 140 s, with an acquisition period of 1 s. The sensors were rinsed with deionized water immediately after analyzing each sample. The average response signal between the 120th and 140th s, when the signal was stable and representative, was used as the output value. Each sample was analyzed in triplicate.

2.7 Statistical analysis

All experimental data are presented as mean ± SD, and analyzed using SPSS version 16.0 (SPSS Inc., Chicago, IL, USA). The differences between means and the significance of mean differences were assessed by Duncan's Multiple Range Test with p-values < 0.05 considered statistically significant. The Pearson correlation analysis (CA) was done to investigate the correlation between physicochemical and phytochemical properties of the honey samples, while Principal Component Analysis (PCA) was used to analyze the correlation between honey samples with measured properties, both visualized using MetaboAnalyst 6.0.

3. Results & Discussion

3.1 Physicochemical properties

The physicochemical properties of the longan honey (LH) samples showed statistically significant differences ($p < 0.05$) among samples for all measured parameters, indicating variability likely associated with differences in botanical micro-origin and processing conditions (Table 1). The moisture content of LH samples ranged from 19.00 to 19.68%, remaining below the Codex Alimentarius maximum limit of 20 g/100 g.[13] These relatively low moisture levels suggest favorable shelf stability, as honeys with moisture contents below 20% are less susceptible to fermentation and microbial spoilage during storage. In addition to moisture, honey color is a key quality attribute influencing consumer perception and is often associated with floral origin and compositional characteristics. The color values of LH samples ranged from 2.02 to 50.98 mm on the Pfund scale (Table 1), corresponding to classifications from water white to light amber.[1] Honey color is known to be influenced by various factors, including nectar sources and environmental and post-harvest factors such as temperature, storage duration, and handling practices during extraction and bottling.[12]

Beyond visual quality attributes such as color, the chemical environment of honey plays a critical role in determining its stability and safety during storage. One of the key parameters reflecting this chemical environment is pH. Honey is characteristically acidic, with pH values typically ranging between 3.5 and 5.5, a property that contributes to its natural protection against microbial contamination.[5,14] Variations in pH among LH samples are influenced by the organic acid profile of the nectar, floral characteristics, edaphoclimatic conditions, and the chemical composition of longan blossoms. Another important indicator of honey quality is hydroxymethylfurfural (HMF), which accumulates as a result of excessive heating or prolonged storage and therefore serves as a marker of honey deterioration.[1] The HMF content of LH samples ranged from 28.50 to 31.20 mg/kg (Table 1), with all values well below the Codex

Alimentarius maximum limit of 80 mg/kg established for honeys produced in tropical regions.[13] These results indicate that the LH samples analyzed were fresh and of high quality, with minimal thermal or storage-related degradation.

Table 1. Physicochemical properties of LH samples

Sample	Moisture content (%)	Color (mm Pfund)		pH	Free acidity (meq/kg)	HMF (mg/kg)
LH-1	19.68 ± 0.30^{a}	13.84 ± 0.47^{d}	Extra White	4.50 ± 0.03^{a}	11.92 ± 0.09^{b}	28.50 ± 0.04^{c}
LH-2	19.16 ± 0.29^{ab}	46.60 ± 1.18^{b}	Extra Light Amber	4.07 ± 0.01^{c}	13.27 ± 1.32^{b}	29.72 ± 0.34^{b}
LH-3	19.00 ± 0.29^{b}	50.98 ± 1.45^{a}	Light Amber	4.06 ± 0.02^{c}	18.16 ± 1.63^{a}	30.92 ± 0.64^{a}
LH-4	19.50 ± 0.30^{ab}	2.02 ± 0.24^{e}	Water white	4.31 ± 0.06^{b}	5.96 ± 0.08^{c}	28.73 ± 0.47^{c}
LH-5	19.50 ± 0.30^{ab}	31.63 ± 1.37^{c}	White	4.32 ± 0.07^{b}	12.62 ± 1.02^{b}	31.20 ± 0.25^{a}

Remarks: Data was presented as mean ± SD; HMF = 5-hydroxymethylfurfural; different superscript letter within column means significant ($p < 0.05$) difference between sample.

3.2 Phytochemical properties

Based on the results in Table 2, the TPC and TFC of the LH samples were in the range of 22.56–46.99 mg GAE/100 g sample and 0.66–24.01 mg CE/g sample, respectively. The TPC of the LH samples in this study was higher than *Rubus* sp. honey from Romania (19.9 mg GAE/100 g)[15] and *Castanea sativa* honey from Turkey (5.49–8.01 mg GAE/100 g),[16] similar to orange (*Citrus sinensis*) honey from Portugal (32.10 mg GAE/100 g),[17] while lower than black locust (*Robinia pseudocacia*) honey from Poland (142.8 mg GAE/100 g).[18] In addition, other researcher found the TFC of orange blossom, lavender, eucalyptus, and heather honey from Portugal was in the range of 4.85–7.87 mg CE/100 g,[19] showing higher results with some of the LH samples (LH-1, LH-2, and LH-4), while also showed lower results compared to other samples (LH-3 and LH-5). This study also measured the antioxidant activity of honey by employing three different assays: DPPH, ABTS, and FRAP. As can be seen from the results, higher TPC and TFC provided higher IC_{50} DPPH (99.67–496.53 mg/mL), IC_{50} ABTS (213.58–523.18 mg/mL), and FRAP (9.53–28.69 mg TE/100 g sample) value. Polyphenols play a major role in contributing to the antioxidant properties of honey. The variation in the antioxidant activity values, including the TPC and TFC results, might be attributed to differences in the composition of the floral source.[20]

Table 2. Phytochemical properties of LH samples

Sample	TPC (mg GAE/ 100 g sample)	TFC (mg CE/100 g sample)	Antioxidant activity		
			DPPH (IC_{50} mg/mL)	ABTS (IC_{50} mg/mL)	FRAP (mg TE/100 g sample)
LH-1	26.27 ± 0.78^{d}	3.93 ± 0.14^{c}	496.53 ± 2.57^{a}	413.72 ± 13.99^{b}	9.53 ± 0.44^{e}
LH-2	37.52 ± 0.56^{c}	0.66 ± 0.09^{d}	249.18 ± 26.12^{b}	213.58 ± 6.16^{d}	22.90 ± 0.46^{c}
LH-3	46.99 ± 0.81^{a}	24.01 ± 1.48^{a}	99.67 ± 1.34^{d}	230.35 ± 0.70^{d}	27.06 ± 0.88^{b}
LH-4	22.56 ± 0.61^{e}	2.71 ± 0.06^{c}	191.65 ± 10.47^{c}	523.18 ± 29.37^{a}	15.04 ± 0.35^{d}
LH-5	40.48 ± 1.03^{b}	12.25 ± 0.55^{b}	81.57 ± 6.29^{d}	258.77 ± 6.99^{c}	28.69 ± 0.25^{a}

Remarks: Data was presented as mean ± SD; TPC = total phenolic content; TFC = total flavonoid content; GAE = gallic acid equivalent; CE = catechin equivalent; TE = Trolox equivalent; different superscript letter within column means significant ($p < 0.05$) difference between sample.

3.4 Correlation analysis

Pearson correlation analysis was done between the measured physicochemical and phytochemical properties of the LH samples (Figure 1). Based on the figure, color was shown to exhibited positive correlation with TPC (r = 0.93, $p < 0.001$). Darker honey exhibited higher polyphenols (Wu et al., 2023), contributing to higher antioxidant activity, showed by negative correlations with IC_{50} values of DPPH (r = -0.64, $p < 0.001$) and ABTS (r = -0.91, $p < 0.001$), along with positive correlation with FRAP value (r = 0.90, $p < 0.001$). Other studies also suggested that the total phenolic and flavonoid contents correlate with antioxidant activity of honey.[21] Polyphenols are known to have strong *in vitro* and *in vivo* antioxidant effects as they are reducing agents (i.e., reduction of Folin-Ciocalteu's phenol reagent and FRAP) and able to donate hydrogen or electrons to free radicals (i.e., DPPH).[21,22] In addition, HMF, products of Maillard reaction at intermediate stage, was found to also had influence on the properties of the LH samples, showing strong positive correlation with FRAP (r = 0.99, $p < 0.001$). HMF demonstrates reducing ability in antioxidant assays due to its aldehyde functionality.[23,24] Another study also found that HMF showed positive correlation with FRAP and showed negative correlation to MC.[25]

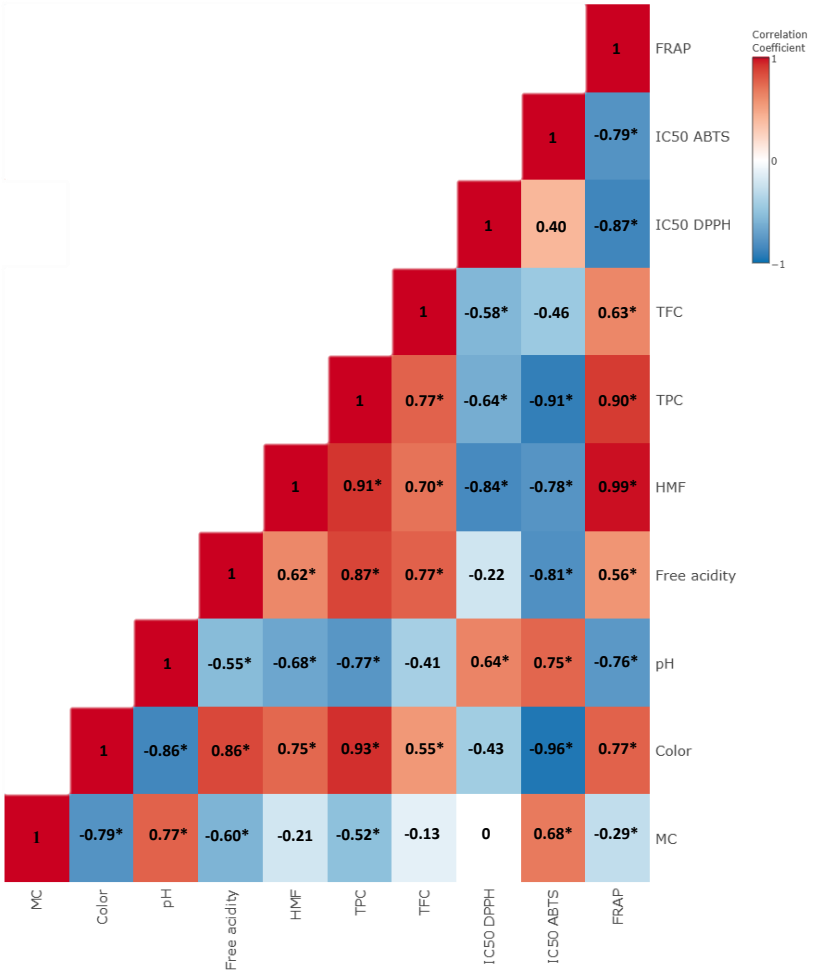

Figure 1. Correlation heatmap on the properties of LH samples. * = significant at 0.05

3.3 Aroma-active volatile compounds identification using GC-E-Nose

There were 89 identified aroma-active VOCs: 13 alcohols (14.61%), 13 aldehydes (14.61%), 3 alkanes (3.37%), 6 terpenes (6.74%), 1 aromatic hydrocarbon (1.12%), 2 carboxylic acids (2.25%), 25 esters (28.09%), 4 ethers (4.49%), 12 ketones (13.48%), 2 lactones (2.25), 1 nitrogen heterocycle (1.12%), 4 phenols (4.49%), 1 sulfide (1.12%), 1 thiazole (1.12%), and 1 thiol (1.12%), as shown in Figure 2. Among the identified group, esters represented the dominant group, followed by alcohols, aldehydes, and ketones.

The predominance of esters suggests their major contribution to the characteristics of longan honey, which is typical of nectar-derived volatiles. Esters are distinguished by delectable fruity, sweet, and honey characteristics.[26,27] Alcohol, aldehyde, and ketone were found to be high in number after esters. Alcohol is mainly associated with fermentation processes and thermal degradation reactions that promote the formation of alcohols from sugars and amino acid precursors,[28] while aldehydes are commonly generated through lipid oxidation, the Maillard reaction, or sugar degradation.[29] In addition, ketones were found to also be responsible for honey aroma.[2] A ketone, 3-Nonanone, was found in all LH sample (24.24–337.77 µg/kg), providing fruity-floral notes.[30] S(-)2-methyl-1-butanol (fruity, 1.89–7.72 µg/kg), acetic acid (vinegar-like, 3.41–45.31 µg/kg), ethyl 3-(methylthio)propanoate (fruity, 9.24–127.06 µg/kg), methyl cinnamate (sweet, 0.66–3.07 µg/kg), and propan-2-one (pungent, sweet, 205.75–355.44 µg/kg) was also found in the majority of the samples, providing fruity, pungent, and sweet aroma to the samples.[31,32]

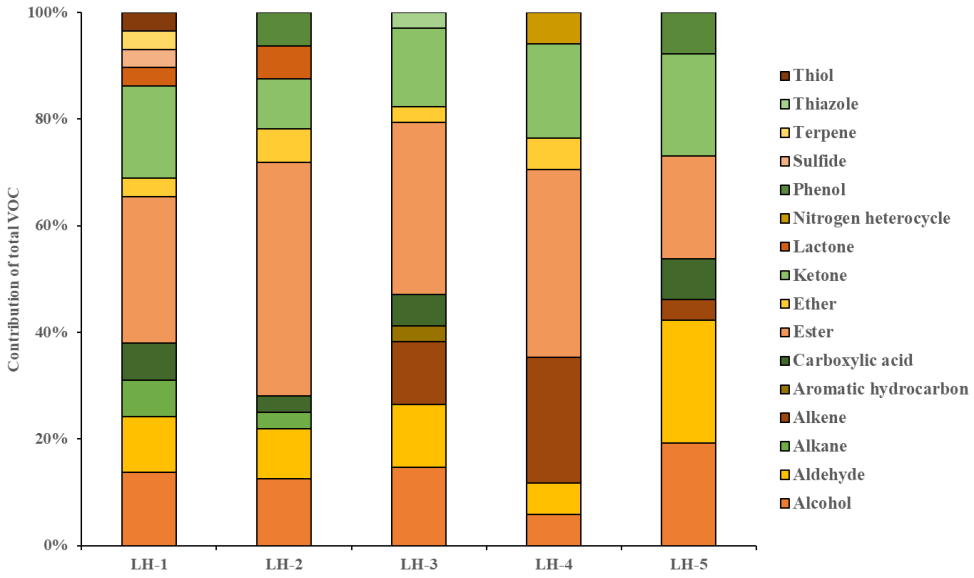

Figure 2. Contribution of each group to the total VOC of LH samples

3.4 Taste profiling using E-Tongue

The taste profile of the LH samples was identified using E-Tongue instrument, and the result was shown in Figure 3. Based on the figure, the taste profiles of the five LH samples reveal distinct taste profiles. Sample LH-2 exhibited the most pronounced flavor intensity, showing the highest scores for both sourness and sweetness, suggesting a strong sweet-sour profile. In contrast, LH-4 displays a divergent profile characterized by dominant bitterness and exhibited the lowest sourness intensity. The remaining samples, LH-1, LH-3, and LH-5, generally showed more moderate intensities across the spectrum. In correlation with the e-nose results, the sourness of the LH samples might be contributed to the presence of acetic acid, as it provides sourness to food products,[33] showing LH-2 exhibited the highest acetic acid content (45.31 µg/kg), followed by LH-3, LH-1, and LH-5 (3.41–35.70 µg/kg), with the absence of the compound in LH-4. In

terms of the sweetness, it showed the opposite trend compared to the bitterness results. Honey is sweet in nature, and sweetness can effectively mask bitterness,[34] shown by the results in this study.

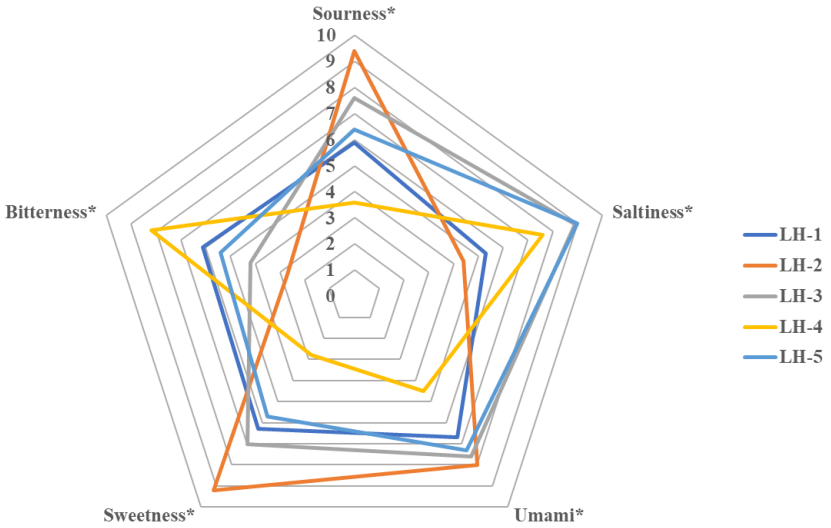

Figure 3. Taste profile of LH samples

3.5 Principal component analysis

To further explore the relationships between LH samples with the physicochemical properties, top 50% VOCs, and taste profile, principal component analysis (PCA) was applied, and the results were depicted in Figure 4. The PCA between LH samples and physicochemical properties (Figure 4a) showed PC1 (97.1) and PC2 (2.2%) collectively explaining 99.3% of the total variance, indicating a highly robust model for sample differentiation. The PCA biplot on top 50% of identified VOCs (Figure 4b) accounted for 95.4% (81.4% of PC1 and 14% of PC2). Top 50% compounds were selected in the generation of PCA biplot of the LH samples and the VOCs due to the top 50% compounds already provided sensory descriptors of honey aroma stated by sensory panels, which are sweet, acid, pungent, waxy, and plant-based notes.[35] Sample LH-2 is characterized by a high concentration of specific aldehydes and ketones, notably acetaldehyde and 3-nonanone, which dominate the upper-right quadrant of the biplot. In the lower-right quadrant, Samples LH-3 and LH-5 show a strong association with compounds such as homofuraneol. Conversely, Sample LH-4 is positioned toward the upper-left quadrant, where it is defined by the presence of some ester found exclusively in the sample, including ethyl (methylthio)acetate. The wide distribution of these VOC vectors across the biplot confirms that each sample in the LH samples is chemically unique in terms of their composition of VOCs. In terms of the taste profile, Figure 4c depicted the PCA biplot of LH samples and their taste profiles, showing 99.0% of total variance (80.1% of PC1 and 18.9% of PC2). Sample LH-4 is distinctly characterized by its high "Bitterness" score, positioning it in the upper-left quadrant away from other taste attributes. In contrast, samples LH-2 and LH-3 are associated with the right side of the biplot, where "Sweetness" and "Sourness" cluster. Overall, the PCA results demonstrate clear differentiation among LH samples based on physicochemical properties, volatile composition, and taste attributes, highlighting the pronounced influence of source-dependent variation on the chemical and sensory profiles of longan blossom honey.

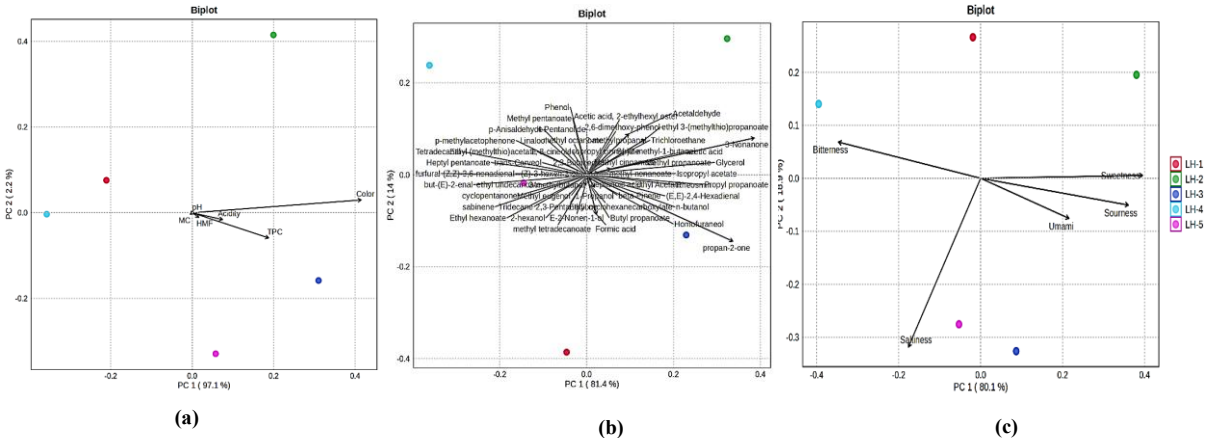

Figure 4. PCA biplot between LH samples and physicochemical/phytochemical properties (a); top 50% VOCs (b); and taste profile(c)

4. Conclusion

This study demonstrated that longan honey (LH) samples from northern region of Thailand are of high quality and freshness, characterized by moisture contents below 20% and HMF levels well within international safety standards. The phytochemical analysis revealed a significant correlation between measured properties. Volatile and taste profiling using electronic nose and electronic tongue further differentiated the samples, identifying 89 aroma-active compounds, dominated by esters, that contribute to the fruity and sweet notes of longan honey, and variety of taste profiles of each LH samples. The integration of the results and PCA confirmed unique characteristics for each sample, such as the sweet-sour profile of LH-2 linked to acetic acid and the distinct bitterness of LH-4 due to the low sweet profile. Ultimately, the robust PCA models (explaining over 90% of total variance) indicate that the interplay between properties effectively discriminates each LH sample from each other.

Nevertheless, while instrumental sensory techniques provide objective discrimination of honey samples, the inclusion of human sensory evaluation is essential to fully validate and interpret these findings. Sensory analysis using trained or consumer panels would enable direct correlation between instruments outputs and human perception. Such integration would strengthen the sensory relevance of instrumental data and provide a more comprehensive understanding of how compositional and volatile differences translate into perceived sensory attributes. Therefore, future studies should incorporate human sensory evaluation alongside instrumental approaches, particularly for honeys derived from longan blossoms, to achieve a holistic characterization of LH samples from different sources.

Acknowledgements

The author would like to thank the Faculty of Agro-Industry, Chiang Mai University, for supporting the instrument for this study. The first author (Gerry Renaldi) was a student in the Ph.D. Degree Program in the Department of Food Science and Technology, Faculty of Agro-Industry, Chiang Mai University, under the CMU Presidential Scholarship.

References

1. Pereira JR, Campos ANR, de Oliveira FC, Silva VRO, David GF, Da Silva JG, Nascimento WWG, Silva MHL, Denadai ÂML. Physical-chemical characterization of commercial honeys from Minas Gerais, Brazil. Food Biosci. 2020;36:100644.

2. Rahman MM, Alam MN, Fatima N, Shahjalal HM, Gan SH, Khalil MI. Chemical composition and biological properties of aromatic compounds in honey. J Food Biochem. 2017;41(4):e12405.
3. Kanbur ED, Yuksek T, Atamov V, Ozcelik AE. Comparison of physicochemical properties of chestnut and highland honey from Senoz Valley, Turkey. Food Chem. 2021;345:128864.
4. Machado AM, Miguel MG, Vilas-Boas M, Figueiredo AC. Honey volatiles as a fingerprint for botanical origin: a review on their occurrence in monofloral honeys. Molecules. 2020;25(2):374.
5. Koyuncu G. Determination of volatile compounds of Turkish commercial monofloral honeys by HS-SPME/GC–MS and sensory evaluation. Int J Food Sci Technol. 2025;60(2):vvaf151.
6. Food and Agriculture Organization of the United Nations. FAO infographics on honey. 2019. Available from: http://www.fao.org/resources/infographics/infographics-details/en/c/1202954/
7. Lertlakkanawat P, Sommano SR, Danmek K, Hongsibsong S, Jung C, Namin SM, Wongkaew M, Chuttong B. The phytochemical properties of low-grade longan syrup and its potential use as a dietary supplement for honey bees. Insects. 2024;15:946.
8. Wang X, Chen Y, Hu Y, Zhou J, Chen L, Lu X. Systematic review of characteristic markers in honey of various botanical, geographic and entomological origins. ACS Food Sci Technol. 2022;2(2):206–220.
9. Rababah T, Al-U'datt M, Naqresh A, Gammoh S, Almajwal A, Saleh M, Yücel S, AL-Rayyan Y, AL-Rayyan N. Effect of temperature and time on the physicochemical and sensory properties of crystallized honey. ACS Omega. 2024;9(18):20243–20252. doi:10.1021/acsomega.4c00570
10. AOAC International. Official methods of analysis of AOAC International. 21st ed. Gaithersburg (MD): AOAC International; 2021.
11. Chaikham P, Prangthip P. Alteration of antioxidative properties of longan flower honey after high-pressure, ultrasonic, and thermal processing. Food Biosci. 2015;10:1–7.
12. Bratosin ED, Tit DM, Purza AL, Pasca MB, Bungau GS, Marin RC, Radu AF, Gitea D. Exploratory analysis of phenolic profiles and antioxidant capacity in selected Romanian monofloral honeys. Antioxidants. 2025;14:1248.
13. Codex Alimentarius Commission. Revised Codex standard for honey (Draft). Rome: Food and Agriculture Organization of the United Nations; 2000.
14. Gürbüz S, Çakici N, Mehmetoğlu S, Atmaca H, Demir T, Apan MA, Atmaca OF, Güney F. Physicochemical quality characteristics of Southeastern Anatolia honey, Turkey. Int J Anal Chem. 2020;2020:8810029.
15. Pauliuc D, Dranca F, Oroian M. Antioxidant activity and phenolic composition for Romanian honey authentication. Foods. 2020;9:306.
16. Can Z, Yildiz O, Sahin H, Turumtay EA, Silici S, Kolayli S. Physicochemical properties and phenolic profiles of Turkish honeys. Food Chem. 2015;180:133–141.
17. Aazza S, Lyoussi B, Antunes D, Miguel MG. Physicochemical characterization and antioxidant activity of Portuguese honeys. J Food Sci. 2013;78:C1159–C1165.
18. Dimitrova B, Gevrenova R, Anklam E. Analysis of phenolic acids in honeys by SPE-HPLC. Phytochem Anal. 2007;18:24–32.

19. Gonçalves J, Ribeiro I, Marçalo J, Rijo P, Faustino C, Pinheiro L. Physicochemical, antioxidant and antimicrobial properties of Portuguese monofloral honeys. J Food Nutr Res. 2018;6(10):645–654.
20. Wu J, Zhao S, Chen X, Jiu Y, Liu J, Gao J, Wang S. Physicochemical and antioxidant properties of unifloral honeys from Apis cerana cerana. Food Sci Biotechnol. 2023;32:1821–1829.
21. Nascimento KS, Sattler JAG, Macedo LFL, González CVS, Melo ILP, Araújo ES, Granato D, Sattler A, Almeida-Muradian LB. Phenolic compounds and antioxidant capacity of Brazilian Apis mellifera honeys. LWT Food Sci Technol. 2018;91:85–94.
22. Granato D, Santos JS, Maciel LG, Nunes DS. Chemical perspective and criticism on analytical methods to estimate total phenolic content in foods. Trends Anal Chem. 2016;80:266–279.
23. Choudhary A, Kumar V, Kumar S, Majid I, Aggarwal P, Suri S. 5-Hydroxymethylfurfural formation and health concerns. Toxin Rev. 2020.
24. Kliuev FS, Runikhina SA, Afanasyev OI, Chusov D. Aldehydes as reducing agents in reductive alkylation of ketones. J Catal. 2026;453:116495.
25. Tang Y, Huang Y, Li M, Zhu W, Zhang W, Luo S, Zhang Y, Ma J, Jiang Y. Balancing Maillard reaction products and antioxidant activity in pan-baked buns. Food Res Int. 2024;195:114984.
26. Tian H, Shen Y, Yu H, Chen C. Aroma features of honey evaluated by sensory analysis, GC–MS and electronic nose. Int J Food Prop. 2018;21(1):1755–1768.
27. Samakradhamrongthai RS, Jannu T, Tongboonchu T, Sangpimpa W, Srichan P, Renaldi G, Detarun P, Siripongvutikorn S, Utaipan T, Wittaya T, Chansuwan W. Physicochemical and sensory properties of Southern Thai curry pastes. Int J Food Prop. 2025;28(1):2545527.
28. Yao L, Cai R, Wang H, Yu C, Tong C, He Z, Feng T, Sun M. Volatile composition and antioxidant capacity of Astragalus sinicus monofloral honey. LWT Food Sci Technol. 2024;205:116565.
29. Zhu M, Sun J, Zhao H, Wu F, Xue X, Wu L, et al. Volatile compounds of unifloral honeys from Northwest China by HS-SPME/GC–MS. Food Chem. 2022;384:132461.
30. Fischer E, Cachon R, Cayot N. Impact of ageing on pea protein volatile compounds and odor correlation. Molecules. 2022;27:852.
31. Štefániková J, Martišová P, Árvay J, Jankura E, Kačániová M, Gálová J, Vietoris V. Comparison of electronic systems with sensory analysis for cheese quality evaluation. Czech J Food Sci. 2020;38(5):273–279.
32. Zhang X, Chen Y, Liu J, Lan Y, Qian X, Zhu B. Chemical and sensory profiles of hawthorn wines from China. Food Chem X. 2025;26:102277.
33. Chen C, Wu S, Li Y, Huang Y, Yang X. Effects of acetic acid bacteria on bioactive and volatile compounds of black tea vinegar. LWT. 2022;171:114131.
34. Mennella JA, Bobowski NK. The sweetness and bitterness of childhood: insights from basic research on taste preferences. Physiol Behav. 2015;152(Pt B):502–507.
35. Starowicz M, Hanus P, Lamparski G, Sawicki T. Characterizing the colatile and sensory profiles, and sugar content of beeswax, beebread, bee pollen, and honey. Molecules. 2021;26;11.

O - 236

Effect of Maltodextrin Concentration on Stability and Physicochemical Properties of Concentrated Mahachanok Mango Smoothie

Niroth Oomnog, Lamphung Phumjan, Woatthichai Narkrugsa, Pongsert Sriprom*

School of Food Industry, King Mongkut's Institute of Technology Ladkrabang, Bangkok, 10520, Thailand

**Corresponding author E-mail: Pongsert.sr@kmitl.ac.th*

Abstract: This study aimed to develop a concentrated mango smoothie using Mahachanok mango as a main material and investigate the effect of maltodextrin addition on its stability and physicochemical properties. Smoothie formulations were prepared with maltodextrin concentrations of 0, 2, 4, 6, 8, and 10%, with 0% as the control. Stability was evaluated by measuring storage modulus (G′), loss modulus (G″), and loss tangent (tan δ). Other physicochemical properties, including total phenolic content (TPC), antioxidant activity (DPPH assay), color (L*, a*, b*), pH, and total soluble solids (TSS) were measured and analyzed using one-way ANOVA. Among the formulations, the smoothie containing 4% maltodextrin demonstrated the most favorable overall characteristics. The concentrated mango smoothie behaved as a non-Newtonian fluid with a solid-like behavior (G′>G″). Rheological analysis conditions of at 1% strain over a frequency range of 0.1-100 rad/s at 25 °C revealed a damping factor (tan δ) of 0.20, indicating a balanced viscoelastic behavior suitable for a concentrated beverage. This formulation also exhibited the highest TPC (534.19 mg GAE per liter of sample) and a strong antioxidant activity, as indicated by DPPH % inhibition of 50%, highlighting its enhanced functional potential. Color evaluation showed an acceptable brightness and slightly yellow-red hue, while pH (4.01) and TSS (24.10 °Brix) were within desirable ranges for taste and stability. These results suggest that 4% maltodextrin effectively optimizes the textural quality of concentrated mango smoothies, improving phenolic content survivability while providing a smooth, stable texture. Incorporation of maltodextrin at this concentration offers a promising approach for producing high-quality fruit beverages that balance sensory appeal and health benefits.

Keywords: Mahachanok; Maltodextrin; Mango; Smoothie; Stability.

1. Introduction

Mango (*Mangifera indica* L.) is a tropical evergreen fruit tree with a large canopy. In Thailand, more than 20 mango cultivars are commercially cultivated, with cultivar selection varying among orchards and regions according to production objectives. These objectives include fresh or immature fruit consumption, ripe fruit consumption, industrial processing, and export. Each cultivar exhibits specific characteristics that determine its suitability for uses. Mango cultivars commonly consumed within Thailand include ‘Ok Rong,’ ‘Lin Ngu Hao,’ ‘Yai Kla,’ ‘Sri Siam,’ ‘Man Duean Kao,’ ‘Bang Khun Sri,’ ‘Phet Ban Lat,’ ‘Khiao Morakot,’ ‘Nam Dok Mai,’ and ‘Rad’ [1]. According to the Office of Agricultural Economics (2023), Thailand has approximately 15,000–20,000 rai under ‘Mahachanok’ mango cultivation, producing an estimated 80,000–100,000 tons in 2023. Nevertheless, only about 10% of total production was exported, corresponding to 8,000–10,000 tons.

Mahachanok mango is a fruit with high nutritional value, particularly rich in carbohydrates, dietary fiber, vitamins—especially vitamin A in the form of β-carotene—and essential minerals such as calcium and potassium [2]. It provides notable health benefits,

including antioxidant activity. The mango flesh exhibits distinctive quality attributes in terms of color, aroma, and flavor, characterized by a deep yellow color, a strong and fragrant aroma at full ripeness, and a sweet taste. The fruit has a total soluble solids content of approximately 15–18 °Brix, thick flesh, and an average fruit weight of 350–500 g [3]. Mahachanok mango can be consumed at both immature and ripe stages; however, ripe fruit generally expresses its characteristic flavor more distinctly. Due to the short postharvest shelf life of ripe mangoes, they must be consumed within a limited period. Therefore, fruit processing into alternative products that allow longer storage while preserving the characteristic sensory qualities represents an effective approach to extending the shelf life of Mahachanok mango.

At present, the fruit juice beverage market has received widespread acceptance from consumers. Smoothies represent a highly popular form of fruit processing, particularly during hot weather. However, periods of excessive fresh fruit production that exceed market demand often led to a decline in the economic value of Mahachanok mango. In addition, strict quality grading results in a substantial proportion of fruit being rejected from the fresh market. To address problems related to market oversupply, low prices, and the short shelf life of fresh mangoes, various technologies have been applied to process mangoes into diversified products, thereby increasing market opportunities. These products include dried mango, candied dried mango, frozen mango, and mango-based beverages. Nevertheless, when mango is processed into blended beverages, challenges arise due to melting and phase separation between liquid and solid components. This separation adversely affects the flavor, texture, and color of the mango smoothie, leading to deterioration in overall product quality.

Phase separation occurs when a uniform dispersion becomes unstable and separates into two distinct layers. In liquid food systems, this is often observed as serum separation, where a clear liquid layer forms above a sedimented pulp or solid phase during storage. Particle aggregation happens when small dispersed particles stick together due to interparticle forces such as van der Waals attraction or polymer bridging. These changes affect important physical properties, including particle size, turbidity, density differences, and viscosity. As particles aggregate and grow larger, they settle faster under gravity, leading to sedimentation. In beverages, this results in visible layering and reduced cloud stability. In fruit juices and smoothies, phase separation can negatively impact texture, appearance, and mouthfeel. Processing methods such as homogenization and enzymatic treatments can modify particle interactions and improve stability. Stabilizers like hydrocolloids are often added to increase viscosity and slow down particle movement. Therefore, understanding and controlling these mechanisms is essential for maintaining the quality and stability of drinks [4–6].

Maltodextrin is a hydrolyzed starch derivative with stabilizing and structuring properties. The dextrose equivalent (DE) reflects the degree of hydrolysis; a DE range of 10–12 corresponds to relatively higher molecular weight fractions compared with high-DE maltodextrins, resulting in greater solution viscosity and lower sweetness. In smoothie systems, this moderate DE level contributes to increased continuous-phase viscosity, which reduces particle mobility and slows gravitational separation according to Stokes' law. By enhancing the viscosity of the serum phase, maltodextrin (DE 10–12) can limit sedimentation of pulp particles and improve suspension stability. Additionally, it can form a weak protective matrix around bioactive compounds such as phenolics and pigments, helping reduce oxidative and processing-related degradation. Compared with lower molecular weight carbohydrates, DE 10–12 maltodextrin provides a balance between solubility and thickening ability without imparting excessive sweetness. Therefore, its functional role in this formulation is not only as a carrier, but also as a viscosity modifier and physical stabilizer that enhances the structural stability and storage performance of smoothies and other fruit-based liquid products.[5]

Despite the growing popularity of fruit-based smoothies, maintaining physical stability remains a major challenge due to phase separation, sedimentation, and particle aggregation

during storage. These phenomena can negatively affect the appearance, texture, and overall quality of the beverage. Various stabilizing agents have been applied in beverage systems to improve suspension stability and reduce separation. Among them, maltodextrin is a promising candidate due to its good solubility, neutral flavor, and ability to increase the viscosity of the continuous phase, which may help reduce particle movement and enhance product stability. However, limited information is available regarding the application of maltodextrin in mango smoothie formulations, particularly in relation to its effect on stability and physicochemical properties. In addition, the appropriate concentration of maltodextrin required to achieve effective stabilization in mango smoothies has not yet been clearly established. Therefore, this study aimed to develop a smoothie product from Mahachanok mango and to evaluate the effect of maltodextrin incorporation on its stability and physicochemical characteristics. Specifically, this research determined the appropriate proportion of maltodextrin in mango smoothies and assessed its influence on product stability and quality attributes. The findings of this study are expected to provide useful information for improving the formulation and stability of mango-based smoothie beverages.

2. Materials and Methods

2.1 Materials

Mahachanok mango (16 - 18 °Brix) was obtained from Community Enterprise of Mahachanok Mango Growers and Processors, Ban Nong Bua Chum (Kalasin, Thailand). Syrup was supplied from Mitrphol Group Co., Ltd. (Bangkok, Thailand). Citric acid was acquired from Krungthepchemi company limited Co., Ltd. (Bangkok, Thailand). Rock salt was procured from Banphue salt Co., Ltd. (Udonthani, Thailand). Maltodextrin (MD) was supplied from Krungthepchemi company limited Co., Ltd. (Bangkok, Thailand). Folin-Ciocalteu Reagent was purchased from M&P Impex Co., Ltd. (Bangkok, Thailand). Sodium Carbonate was obtained from Krungthepchemi company limited Co., Ltd. (Bangkok, Thailand). DPPH (2,2-diphenyl-1-picrylhydrazyl) was procured from NP Chemical Supply Co., Ltd. (Bangkok, Thailand). Methanol was procured from Chemipan Corporation Co., Ltd. (Bangkok, Thailand).

2.2 Preparation of Mango Smoothie

Ripe Mahachanok mangoes were selected, peeled, and the flesh was sliced from the seed. The mango flesh was then blended using a Shimono EVO-950 PRO (Shimono (Thailand) Co., Ltd) and filtered through a stainless-steel sieve (60 mesh, 250 μm aperture) to remove fibrous residues, yielding pure mango pulp (MP) for smoothie preparation. The mango smoothie formulation consisted of mango pulp, syrup, citric acid, and salt in a total of 100%. MD (DE 10-12) was added and blended afterwards in 2%, 4%, 6%, 8%, and 10% W/V at a nominal operating speed of ≈28,000 rpm. at room temperature for 10 seconds. The prepared mango smoothie was subsequently subjected to physicochemical analysis in the following steps.

2.3 Color Evaluation

The color properties of Mahachanok mango smoothie were evaluated using a Konica Minolta Chroma Meter CR-400 (Konica Minolta Co., Chiyoda, Japan). Samples were placed in Petri dishes and covered with transparent plastic film prior to measurement. Color measurements were performed in triplicate.

2.4 Rheology Behavior

The rheology behavior of Mahachanok mango smoothie was investigated using an Anton Paar Modular Compact Rheometer 302 (Anton Paar GmbH, Graz, Austria). A smoothie sample with a volume of 30 mL was used for analysis. The measurements were performed using a PP50/TG parallel plate with a 1 mm gap, conducted at 1% strain over a frequency range of 0.1-

100 rad/s at 25 °C. The rheological properties, including storage modulus (G′), loss modulus (G″), and loss tangent (tan δ), were measured in triplicate.

2.5 Acidity Analysis (pH)

The acidity of Mahachanok mango smoothie was determined using a pH meter (inoLab® pH 7110, WTW). A smoothie sample volume of 50 mL was used for pH measurement. All measurements were performed in triplicate for each sample.

2.6 Total Soluble Solid (TSS)

The total soluble solids content of Mahachanok mango smoothie was measured using an ATAGO N1 and N2 hand-held refractometer (ATAGO Co., Ltd., Tokyo, Japan). Measurements were performed in triplicate for each sample.

2.7 Total Phenolic Content (TPC)

The total phenolic content was determined using the Folin–Ciocalteu method. A standard calibration curve for total phenolic content was prepared using gallic acid as the standard compound. Gallic acid standard solutions were prepared at concentrations of 0, 50, 100, and 150 mg/L. An aliquot of each standard solution was reacted with Folin–Ciocalteu reagent. Briefly, the standard solution was mixed with diluted Folin–Ciocalteu reagent and allowed to react for a specified time before the addition of sodium carbonate solution. The mixture was incubated at room temperature for the designated reaction period, and the absorbance was measured at 765 nm using a spectrophotometer. A calibration curve was constructed by plotting absorbance against gallic acid concentration.

An aliquot 0.2 mL of the sample was mixed with 0.8 mL of distilled water and 5.0 mL of Folin–Ciocalteu reagent (0.1 M) in a test tube. The mixture was vortexed for 2 min, after which 4.0 mL of sodium carbonate solution (75 g/L) was added. The reaction mixture was then incubated in the dark at room temperature for 1 h. and the absorbance was measured at 765 nm using a Shimadzu UV-1900i spectrophotometer (Shimadzu Europa GmbH, Kyoto, Japan). All measurements were performed in triplicate.

2.8 Antioxidant Properties (DPPH Assay)

The antioxidant activity of Mahachanok mango smoothie was evaluated using the DPPH radical scavenging assay. A DPPH solution (0.3 mM) was prepared by dissolving 6 mg of DPPH in 50 mL of methanol. For sample preparation, 1 g of smoothie sample was dissolved in 19 mL of methanol and stirred using a magnetic stirrer at 100 rpm for 20 min. The mixture was then filtered through filter paper (Whatman No. 41) to obtain the sample extract. An aliquot of 1.0 mL of the sample extract was mixed with 1.9 mL of the DPPH solution and incubated in the dark at room temperature for 30 min. Absorbance was measured at a wavelength of 517 nm using a Shimadzu UV-1900i spectrophotometer (Shimadzu Europa GmbH, Kyoto, Japan). The % inhibition was calculated as described by Brand-Williams W et al. using the equation:

$$\text{DPPH inhibition (\%)} = \frac{A_{Control} - A_{Sample}}{A_{Control}} \times 100$$

Where: $A_{Control}$ = Absorbance of the DPPH solution without sample
A_{Sample} = Absorbance of the DPPH solution with sample

2.9 Statistical Analysis

The date from this study were statistically analyzed using One-way Analysis of Variance (ANOVA) with SPSS Statistics 27.0.1 software (SPSS Inc., Chicago, IL). Difference in each group were assessed using Duncan's post-hoc test, with a significance level set at P>0.05.

3. Results & Discussion

3.1 Color Evaluation

The color of beverages such as smoothies influences consumer acceptability; therefore, evaluating color differences between the control and maltodextrin (MD)-incorporated samples is important. Samples containing 2%, 4%, 6%, 8%, and 10% MD showed ΔE values of 0.22, 0.36, 0.49, 0.60, and 0.81, respectively, compared with the control. These values are considered almost imperceptible to the human eye. Although the ΔE values increased slightly with increasing MD concentration, the overall color differences remained minimal, suggesting that MD addition at these levels does not noticeably affect the visual appearance of the smoothie.

3.2 Rheology Behavior

Mango smoothie samples used for rheological analysis showed a similar onset of structural breakdown at approximately 1.83 rad/s, indicated by a continual decrease in viscosity, storage modulus (G′), loss modulus (G″), and damping factor, followed by unstable readings. Therefore, rheological parameters were compared at 1.83 rad/s within the linear viscoelastic region. Results showed that the storage modulus increased in samples containing 2% and 4% maltodextrin (MD), then gradually decreased at 6%, 8%, and 10% MD. In contrast, the loss modulus decreased progressively with increasing MD concentration. Since the storage modulus reflects the elasticity and strength of the internal structure, and the damping factor represents the balance between viscous and elastic components, lower damping factor values indicate a more elastic system. Among the samples, the 4% MD mango smoothie exhibited the lowest damping factor, suggesting the most structured viscoelastic network.

Table 1. Rheology behavior data of Mahachanok mango smoothie on viscosity, storage modulus, loss modulus, and damping factor.

Samples	Parameters			
	Viscosity (Pa·s)	Storage Modulus (Pa)	Loss Modulus (Pa)	Damping Factor
Control	120 ± 1.47^{b}	211 ± 6.04^{c}	62.70 ± 1.13^{e}	0.30 ± 0.020^{c}
2% MD	129 ± 1.35^{c}	230 ± 1.05^{d}	57.50 ± 0.82^{d}	0.25 ± 0.015^{b}
4% MD	144 ± 1.00^{e}	260 ± 0.72^{f}	52.00 ± 0.85^{c}	0.20 ± 0.025^{a}
6% MD	135 ± 1.43^{d}	242 ± 1.25^{e}	52.00 ± 1.25^{c}	0.22 ± 0.025^{ab}
8% MD	104 ± 0.95^{a}	186 ± 0.58^{b}	45.90 ± 0.70^{b}	0.25 ± 0.025^{b}
10% MD	105 ± 1.19^{a}	126 ± 1.31^{a}	42.90 ± 1.21^{a}	0.34 ± 0.051^{c}

Different lowercase letters within a column indicate significant differences among treatments ($P < 0.05$) according to Duncan's test.

3.3 Acidity Analysis (pH)

The acidity of mango smoothies influences both sensory perception and several physicochemical properties related to product stability and quality. The control sample had a pH of 3.99, while the addition of maltodextrin (MD) at concentrations of 2%, 4%, 6%, 8%, and 10% resulted in slight increases to 4.01, 4.01, 4.02, 4.03, and 4.04, respectively. Although the change was small, the consistent increase suggests that MD slightly reduced the overall acidity of the smoothie. This effect may be attributed to the dilution of organic acids naturally present in mango pulp, since maltodextrin is a neutral carbohydrate with minimal inherent acidity. The increase in total soluble solids associated with MD incorporation may also contribute to the minor rise in pH.

Nevertheless, all samples remained within the typical acidic range for fruit-based beverages, indicating that MD addition did not substantially alter the fundamental acidity of the mango smoothie.

3.4 Total Soluble Solid (TSS)

Total soluble solids (TSS) are an important parameter reflecting the concentration of dissolved sugars, organic acids, and other soluble components in mango smoothies. TSS in mango pulp typically increases with fruit ripeness due to the enzymatic conversion of starch into simple sugars during maturation. In this study, the control sample exhibited a TSS value of 21.50 °Brix, while the addition of maltodextrin (MD) at concentrations of 2%, 4%, 6%, 8%, and 10% increased TSS to 22.80, 24.10, 25.20, 25.90, and 26.40 °Brix, respectively. This trend indicates that MD significantly contributed to the overall soluble solids content of the formulation. As a starch-derived polysaccharide with high solubility, MD readily dissolves in aqueous systems and increases dissolved solids without imparting strong sweetness or flavor. Consequently, increasing MD levels raised the °Brix values. These results suggest that MD addition modifies the formulation and increases soluble solids, which may influence the viscosity and physical characteristics of the smoothie.

3.5 Total Phenolic Content (TPC)

The total phenolic content (TPC) of the control and mango smoothie samples containing 2%, 4%, 6%, 8%, and 10% maltodextrin (MD) were 370.91, 371.16, 534.19, 533.89, 382.85, and 366.46 mg GAE/L, respectively. Although MD does not contain phenolic compounds, its incorporation may influence the stability and retention of phenolics naturally present in mango pulp. TPC increased markedly at moderate MD concentrations, reaching the highest value at 4% MD, followed by a decline at higher levels. This trend suggests that moderate MD concentrations may help preserve phenolic compounds by forming a stabilizing matrix that limits their exposure to degradative factors such as oxidation, heat, and enzymatic activity. The matrix may also restrict molecular mobility, creating a protective microenvironment that supports phenolic stability.

However, when MD concentration exceeded the optimal level, TPC values gradually decreased, consistent with the findings of Siacor et al. (2020). This reduction may result from a dilution effect, where larger amounts of MD increase the overall mass and volume of the sample without contributing additional phenolic compounds. In addition, excessive MD may reduce extraction efficiency during analysis. Higher MD concentrations can increase viscosity and form a more extensive carbohydrate matrix, which may hinder solvent penetration and limit the release of bound phenolics into the extraction medium. Overall, these results suggest that moderate MD levels may enhance phenolic retention in mango smoothies, whereas excessive concentrations may lower the measured TPC due to dilution and extraction limitations.

Table 2. Results on acidity analysis (pH), total soluble solid (TSS), and total phenolic content (TPC) of Mahachanok mango smoothie samples.

Samples	Parameters		
	pH level	Total Soluble Solid (°Brix)	Total Phenolic Content (mg GAE/L of sample)
Control	3.99 ± 0.021^{a}	21.50 ± 1.21^{a}	370.91 ± 2.31^{a}
2% MD	4.01 ± 0.040^{a}	22.80 ± 1.25^{ab}	371.16 ± 2.25^{a}
4% MD	4.01 ± 0.036^{a}	24.10 ± 1.35^{bc}	534.19 ± 1.70^{c}
6% MD	4.02 ± 0.025^{a}	25.20 ± 0.90^{cd}	533.89 ± 3.05^{c}
8% MD	4.03 ± 0.030^{a}	25.90 ± 1.15^{cd}	382.85 ± 3.40^{b}
10% MD	4.04 ± 0.029^{a}	26.40 ± 0.85^{d}	366.46 ± 2.65^{a}

Different lowercase letters within a column indicate significant differences among treatments ($P < 0.05$) according to Duncan's test.

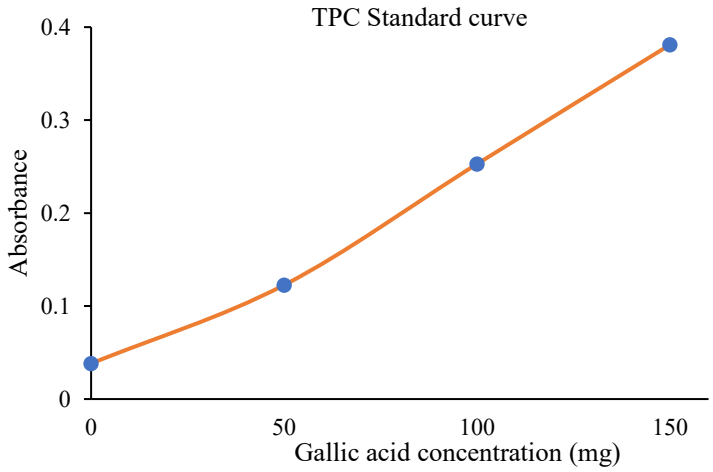

Figure 1. Standard curve of Gallic acid between concentration of Gallic acid and absorbance at 765 nm.

3.6 Antioxidant Properties (DPPH Assay)

The antioxidant activity of the control sample and mango smoothies containing 2%, 4%, 6%, 8%, and 10% maltodextrin (MD) showed DPPH inhibition values of 55%, 64%, 50%, 43%, 55%, and 57%, respectively. Although total phenolic content (TPC) peaked at 4% MD, the highest DPPH scavenging activity was observed at 2% MD. This suggests that overall antioxidant activity is influenced by multiple compounds, including phenolics, ascorbic acid, tocopherols, carotenoids, and other antioxidants that may be more reactive at lower MD levels. The slight increase in DPPH scavenging activity at 10% MD may indicate that higher MD concentrations help stabilize certain antioxidants, partially compensating for dilution effects. Therefore, while TPC and DPPH activity are related, they do not show a perfectly correlated trend.

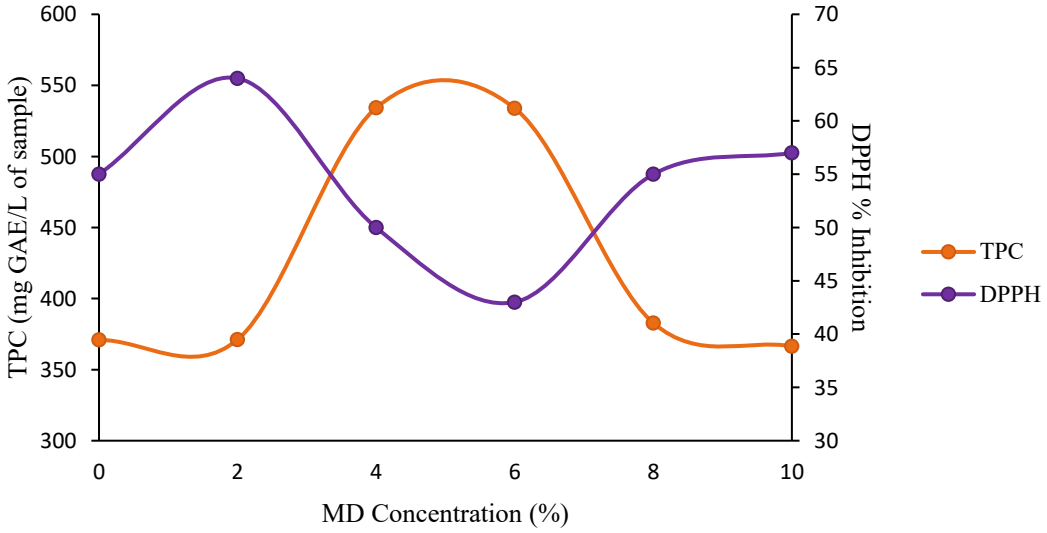

Figure 2. Correlation between the effect of maltodextrin concentration on TPC and DPPH scavenging activity on concentrated Mahachanok mango smoothie.

4. Conclusion

This study evaluated the effect of maltodextrin (MD) concentration (0–10%) on the rheological behavior and physicochemical properties of concentrated Mahachanok mango smoothie. Rheological parameters including viscosity, storage modulus (G′), loss modulus (G″), and damping factor were measured to characterize changes in the viscoelastic properties of the system. One-way ANOVA indicated significant differences ($p < 0.05$) among MD concentrations for viscosity, G′, G″, damping factor, total soluble solids (TSS), and total phenolic content (TPC), suggesting that the addition of MD influenced the structural and physicochemical characteristics of the smoothie matrix.

TPC increased as MD concentration increased from 0% to 4%, reaching the highest value at 4% MD, followed by a decrease at higher concentrations (8–10%). Although TPC decreased at higher maltodextrin concentrations, the DPPH radical scavenging activity did not follow the same trend. This discrepancy may be attributed to matrix effects during extraction and analysis. Phenolic compounds encapsulated or associated with the maltodextrin matrix may be less extractable in the Folin–Ciocalteu assay, resulting in lower measured TPC, while still contributing to radical scavenging activity in the DPPH assay. In addition, other antioxidant compounds naturally present in mango, such as ascorbic acid and carotenoids, may also contribute to DPPH inhibition but are not fully quantified by the TPC method.

Overall, the results indicate that maltodextrin concentration influences the rheological behavior and phenolic-related antioxidant characteristics of Mahachanok mango smoothie. Increased viscosity and viscoelastic moduli suggest the formation of a more structured matrix, which may contribute to improved physical stability of the beverage system.

References

1. Wongkhamchan S. Mango classification. Mango: Production and Postharvest Technology, Bangkok, Thailand: Postharvest Technology Innovation Center (PHTIC), Office of the Higher Education Commission; n.d., p. 3–14.
2. U.S. Department of Agriculture (USDA), Agricultural Research Service (ARS). What's in the Foods You Eat: Search Tool 2021–2023 2024.
3. Prempree N, Sretthapakdi R. Mahachanok: mango for export-oriented and processing industries. Kehakarn Kaset 1999;23:64–8, 70.
4. Patil BS, Mastiholimath V, Kulkarni AR. Novel wound dressing material derived from crosslinked tamarind seed polysaccharide: In vitro characterization and wound healing activity. Trends in Biomaterials & Artificial Organs 2011;25:149–53.
5. Chavan RS, Khedkar CD, Bhatt S. Fat Replacer. In: Caballero B, Finglas PM, Toldrá F, editors. Encyclopedia of Food and Health, Oxford: Academic Press; 2016, p. 589–95. https://doi.org/https://doi.org/10.1016/B978-0-12-384947-2.00271-3.
6. Ye G, Li G, Wang C, Ling B, Yang R, Huang S. Extraction and characterization of dextran from Leuconostoc pseudomesenteroides YB-2 isolated from mango juice. Carbohydrate Polymers 2019;207:218–23. https://doi.org/10.1016/j.carbpol.2018.11.092.
7. Brand-Williams W, Cuvelier ME, Berset C. Use of a free radical method to evaluate antioxidant activity. LWT - Food Science and Technology 1995;28:25–30. https://doi.org/10.1016/S0023-6438(95)80008-5.
8. Cui Y, Liu J, Han S, Li P, Luo D, Guo J. Physical Stability of Chestnut Lily Beverages (CLB): Effects of Shear Homogenization on Beverage Rheological Behavior, Particle Size, and Sensory Properties. Foods 2022;11. https://doi.org/10.3390/foods11203188.
9. Harris PJ, Smith BG. Plant cell walls and cell-wall polysaccharides: structures, properties and uses in food products. International Journal of Food Science and Technology 2006;41:129–43. https://doi.org/10.1111/j.1365-2621.2006.01470.x.

10. Lepaus BM, Santos AKP de O, Spaviero AF, Daud PS, de São José JFB. Stability parameters during refrigerated storage and changes on the microstructure of orange-carrot blend juice processed by high-power ultrasound. Frontiers in Sustainable Food Systems 2022;Volume 6-2022.
11. Marathe RM, Annapure US, Singhal RS, Kulkarni PR. Gelling behaviour of polyose from tamarind kernel polysaccharide. Food Hydrocolloids 2002;16:423–6. https://doi.org/10.1016/S0268-005X(01)00118-7.
12. Nisbet DR, Crompton KE, Hamilton SD, Shirakawa S, Prankerd RJ, Finkelstein DI, Horne MK, Forsythe JS. Morphology and gelation of thermosensitive xyloglucan hydrogels. Biophysical Chemistry 2006;121:14–20. https://doi.org/10.1016/j.bpc.2005.12.005.
13. Nishinari K, Takemasa M, Zhang H, Takahashi R. 2.19 - Storage Plant Polysaccharides: Xyloglucans, Galactomannans, Glucomannans. In: Kamerling H, editor. Comprehensive Glycoscience, Oxford: Elsevier; 2007, p. 613–52. https://doi.org/10.1016/B978-044451967-2/00146-X.
14. Pongsawatmanit R, Temsiripong T, Ikeda S, Nishinari K. Influence of tamarind seed xyloglucan on rheological properties and thermal stability of tapioca starch. Journal of Food Engineering 2006;77:41–50. https://doi.org/10.1016/j.jfoodeng.2005.06.017.
15. Sahoo S, Sahoo R, Nayak PL. Tamarind seed polysaccharide: a versatile biopolymer for mucoadhesive application. Journal of Pharmaceutical and Biomedical Sciences 2011;8:1–12.
16. Shirakawa M, Yamatoya K, Nishinari K. Tailoring of xyloglucan properties using an enzyme. Food Hydrocolloids 1998;12:25–8. https://doi.org/10.1016/S0268-005X(98)00052-6.
17. Siacor FDC, Lim KJA, Cabajar AA, Lobarbio CFY, Lacks DJ, Taboada EB. Physicochemical properties of spray-dried mango phenolic compounds extracts. Journal of Agriculture and Food Research 2020;2:100048.
18. Yamanaka S, Yuguchi Y, Urakawa H, Kajiwara K, Shirakawa M, Yamatoya K. Gelation of tamarind seed polysaccharide xyloglucan in the presence of ethanol. Food Hydrocolloids 2000;14.
19. York WS, van Halbeek H, Darvill AG, Albersheim P. Structural analysis of xyloglucan oligosaccharides by 1H-n.m.r. spectroscopy and fast-atom-bombardment mass spectrometry. Carbohydrate Research 1990;200:9–31. https://doi.org/10.1016/0008-6215(90)84179-X.
20. Zhu D, Kou C, Shen Y, Xi P, Cao X, Liu H, Li J. Effects of different processing steps on the flavor and colloidal properties of cloudy apple juice. J Sci Food Agric 2021;101:3819–26. https://doi.org/10.1002/jsfa.11016.

O - 241

Effect of Tamarind Kernel Powder on Texture Formation of High-Moisture Extruded Soy Protein Meat Analogs

Phimchanok Saisuwan, Lamphung Phumjan, Woatthichai Narkrugsa, Pongsert Sriprom*

School of Food Industry, King Mongkut's Institute of Technology Ladkrabang, Bangkok 10520

**Corresponding author E-mail: Pongsert.sr@kmitl.ac.th*

Abstract: This study investigated the effect of tamarind kernel powder (TKP) addition on the structural and textural properties of soy protein isolate (SPI) extrudates produced by twin-screw high-moisture extrusion. Formulations were prepared by incorporating TKP at different levels (0%, 2.5%, 5%, and 7.5%) with varying moisture contents (50%, 60%, and 70%) and screw speeds (150, 200, and 250 rpm). The mechanical and morphological characteristics of the extrudates were evaluated to determine the influence of TKP on the fibrous texture formation. Results indicated that increasing TKP content up to 5% significantly enhanced the tensile strength of the extrudates, reaching 118,551 Pa at 50% moisture and 150 rpm. However, excessive TKP (7.5%) slightly reduced texture uniformity. Increasing the moisture content from 50% to 70% decreased tensile strength but improved elongation, suggesting a more flexible structure. Screw speed at 200 rpm provided the most balanced texture, exhibiting both strength and elasticity. Overall, the addition of 5% TKP at 50–60% moisture and 200 rpm screw speed produced extrudates with structural integrity and fibrous characteristics closely resembling those of meat. These findings highlight the potential of TKP as a natural hydrocolloid modifier for improving the mechanical and sensory attributes of soy protein-based meat analogs.

Keywords: High-moisture extrusion; Soy protein isolate; Tamarind kernel powder; Fibrous structure; Meat analogs.

1. Introduction

In recent years, increasing awareness of health and environmental issues has led to a continuous rise in the demand for alternative protein products. Among these, textured vegetable protein (TVP) has attracted considerable attention and popularity. TVP is produced from protein sources such as soy protein isolate or wheat gluten through an extrusion process, yielding a product with a meat-like structure, high nutritional value, and broad applicability in various alternative protein-based foods. The extrusion process can be classified into low-moisture and high-moisture techniques. Notably, the high-moisture extrusion process is employed to enhance the textural properties of plant proteins, producing products with a fibrous structure analogous to meat. Moisture content plays a critical role in extrusion processing as it acts as a plasticizer, reducing melt viscosity and weakening intermolecular interactions between proteins. Higher moisture levels generally decrease mechanical shear and may lead to less aligned fibrous structures in high-moisture extruded products [5,7,8]. In addition, screw speed influences the shear forces and mechanical energy input during extrusion. Higher screw speeds increase shear stress and mixing intensity, which can promote protein unfolding and alignment, thereby affecting fiber formation and textural properties of the final product [7,8,11]. This technique is generally considered superior to low-moisture extrusion, often utilizing an extended cooling die, thereby generating plant proteins with a fibrous texture closely resembling that of real meat [1,2]. A common challenge in producing high-moisture vegetable protein is the suboptimal development of fibrous

properties resembling those of real meat. This issue is particularly pronounced when using vegetable protein alone, often resulting in dry, hard, and brittle products. Previous studies have demonstrated that incorporating reactive molecules or plasticizers, such as polysaccharides, into plant proteins can significantly enhance intermolecular interactions within the protein matrix, thereby improving both structural integrity and textural characteristics [5]. Several studies have reported that the incorporation of polysaccharides or hydrocolloids can significantly influence the structural and textural properties of plant protein extrudates under high-moisture extrusion conditions. These biopolymers may modify protein–water interactions, rheological properties, and molecular aggregation, thereby promoting the formation of fibrous structures in plant-based meat analogs. The addition of polysaccharides such as sodium alginate, xanthan gum, and maltodextrin significantly enhanced protein aggregation behavior and promoted the formation of fibrous structures during high-moisture extrusion. [6]. Tamarind kernel powder is rich in xyloglucan, a branched hemicellulosic polysaccharide known for its high water-binding capacity and rheological functionality. Unlike other hydrocolloids such as guar gum or β-glucan, the unique molecular structure of xyloglucan may facilitate specific interactions with soy proteins during extrusion, potentially influencing fiber formation and texture development. [9,12,13]

One strategy that has received considerable attention for enhancing the properties of textured vegetable protein (TVP) is the incorporation of polysaccharides, such as beta-glucan, a natural compound recognized for its water-holding capacity, viscosity-enhancing effect, and ability to promote fibrous structures. Consequently, beta-glucan has been highlighted for its potential to improve the fibrous characteristics of high-moisture plant protein products [3]. In addition, it exhibits beneficial nutritional effects, including reductions in cholesterol and blood sugar, and can function as a texturizing agent in food applications [4]. Recently, there has been growing interest in using indigenous Thai plant extracts, such as tamarind kernel powder (TKP), which contains various polysaccharides, including beta-glucan, as a potential functional ingredient, particularly in extrusion for TVP production [3].

While several studies have explored the incorporation of beta-glucan derived from oats or mushrooms into plant protein products, no research has specifically investigated the effects of beta-glucan from tamarind seed powder on the properties of plant proteins produced through the high-moisture extrusion process, particularly regarding physical attributes such as fiber content.

Therefore, the present study aimed to investigate the effects of incorporating tamarind seed powder beta-glucan on the physical properties of high-moisture plant protein. This approach not only adds value to agricultural by-products, such as tamarind seeds, but also promotes Thailand's circular economy and bio-circular-green (BCG) economy initiatives. Additionally, the findings are intended to inform the development of high-quality, sustainable alternative protein products.

2. Materials and Methods

2.1 Materials

Soybean Protein Isolate (SPI) was sourced from Krungthepchemi Company Limited, Co., Ltd. (Bangkok, Thailand). Wheat gluten (WG) was procured from Anhui Ante Food Co., Ltd. (Anhui, China). Tamarind kernel powder (TKP) was sourced from Pin Petch Global Co., Ltd. (Pathum Thani, Thailand). Rice bran oil was obtained from King Rice Oil Group Co., Ltd. (Samut Prakan, Thailand). Calcium Carbonate was obtained from Krungthepchemi company limited Co., Ltd. (Bangkok, Thailand). Sodium methyl cellulose was obtained from Krungthepchemi company limited Co., Ltd. (Bangkok, Thailand).

2.2 Preparation of SPI-TKP extrudates by extrusion

The extrusion experiment was conducted using the CTE-D22L32 twin-screw extruder (Chareontut Co., Ltd., Samut Prakan, Thailand). The extruder contained a co-rotating intermeshed screw with a diameter of 21.5 mm and a length-to-diameter ratio of 30:1. The cooling die

dimensions were 10 x 20 x 400 mm (H x W x L), and the screw speed was set to 150, 200, and 250 rpm. The extrusion feedstock was prepared by mixing soybean protein isolate (SPI), Wheat gluten (WG), Rice bran oil, Calcium Carbonate and Sodium methyl cellulose for total based proteins 100% and added Tamarind kernel powder (TKP) in varying ratios (w/w): 100:0 (0%), 100:2.5 (2.5%), 100:5 (5%), and 100:7.5 (7.5%)

The high-moisture experimental process was divided into eight zones: feeding zone, mixing zone I, cooking zone I, cooking zone II, melting zone I, melting zone II, die, and cooling. Each zone's temperature was independently controlled via a designated control panel. The temperature for these zones was set at 50ºC, 90ºC, 100ºC, 110ºC, 120ºC, 110ºC, 100ºC, and 55ºC,respectively. After cooling to room temperature, the extruded samples were vacuum sealed for subsequent analyses and stored at a constant temperature of 4ºC

2.3 Textural properties

The textural properties of the extruded samples, including tensile strength and elongation, were assessed using a texture analyzer (TA.XT2i Plus, Stable Micro Systems, UK), with a week following extrusion. The extruded samples were cut into 10 x 20 x 50 mm (H x W x L) by hand and tested using an A-TG texture analyzer probe. The test parameters were set as follows: test speed of 0.5 mm/s; distance of 30mm; trigger force of 3g. All measurements were conducted in triplicate for accuracy.

2.4 Statistical Analysis

The date from this study were statistically analyzed using Three-way Analysis of Variance (ANOVA) with SPSS Statistics 27.0.1 software (SPSS Inc., Chicago, IL). Difference in each group were assessed using Duncan's post-hoc test, with a significance level set at $P>0.05$.

3. Results & Discussion

3.1 TKP supplement level effects on textural properties of SPI-TKP extrudates.

Based on results from varying TKP supplementation levels, the effects of moisture content and screw speed on tensile strength showed a clear trend. As the moisture content increased from 50% to 70%, the tensile strength decreased significantly across all formulations. This could be due to higher moisture, which causes protein structures to expand and form weaker intermolecular bonds, resulting in reduced tensile strength and less compact fibrous structures. Moisture content is a critical factor in extrusion processing, as it acts as a plasticizer that reduces melt viscosity and weakens intermolecular interactions between protein molecules. At higher moisture levels, the shear forces within the extruder are reduced, which may lead to less aligned fibrous structures in high-moisture extruded products [5,7,8]. Excess moisture may hinder proper alignment of protein molecules during extrusion, leading to looser, less oriented fiber formation. Additionally, when the screw speed increased from 150 to 250 rpm, the tensile strength generally decreased or remained constant, which may be attributed to the increased shear force at higher screw speeds, leading to uneven or disrupted protein structure and thereby weakening fiber formation. Comparing among formulations, those containing 5% and 7.5% TKP exhibited higher tensile strength than the control (SPI only) at 50% moisture content. The incorporation of TKP may contribute to improved structural integrity of the extrudates. This effect could be associated with interactions between soy proteins and polysaccharides present in TKP, which may influence the organization and continuity of fibrous structures formed during high-moisture extrusion [7,8,9].

Table 1. Texture analysis data of HM-TVP on tensile strength.

Formulas	Moisture levels	Screw speeds	Tensile strength (Pa) (N.mm)
Control	50	150	63738.89 ± 2941.47^{aC1}
		200	72144.44 ± 5555.73^{aC2}
		250	80052.22 ± 3621.26^{aC2}
	60	150	5795.56 ± 1194.23^{aB1}
		200	16298.89 ± 2613.92^{aB2}
		250	36006.67 ± 2782.95^{aB2}
	70	150	2997.78 ± 329.39^{aA1}
		200	3510.00 ± 364.06^{aA2}
		250	4326.67 ± 914.79^{aA2}
TKP 2.5%	50	150	44526.67 ± 2055.41^{bC1}
		200	61850.00 ± 1094.41^{bC2}
		250	56206.67 ± 3213.67^{bC2}
	60	150	36996.67 ± 398.17^{bB1}
		200	40760.00 ± 1151.26^{bB2}
		250	51537.78 ± 5583.19^{bB2}
	70	150	3674.44 ± 326.36^{bA1}
		200	3597.78 ± 443.53^{bA2}
		250	5206.67 ± 346.66^{bA2}
TKP 5%	50	150	118551.11 ± 8059.67^{cC1}
		200	112204.44 ± 1932.34^{cC2}
		250	86863.33 ± 1159.02^{cC2}
	60	150	44276.67 ± 808.46^{cB1}
		200	45401.11 ± 3340.03^{cB2}
		250	36626.67 ± 2930.66^{cB2}
	70	150	2012.22 ± 413.87^{cA1}
		200	3818.89 ± 386.92^{cA2}
		250	4052.22 ± 191.08^{cA2}
TKP 7.5%	50	150	72361.11 ± 1637.46^{dC1}
		200	74924.44 ± 734.90^{dC2}
		250	67003.33 ± 4600.32^{dC2}
	60	150	35192.22 ± 3708.92^{dB1}
		200	34623.33 ± 2454.56^{dB2}
		250	39876.67 ± 2249.86^{dB2}
	70	150	4321.11 ± 361.05^{dA1}
		200	4352.22 ± 608.88^{dA2}
		250	4264.44± 244.04^{dA2}

Statistical significance at $P \leq 0.05$
Lower superscript letters (a, b, c, d) within the same column indicates different formulas.
Upper superscript letters (A, B, C) within the same column indicates different moisture levels.
Numbers (1, 2, 3) within the same column indicates different screw speeds.

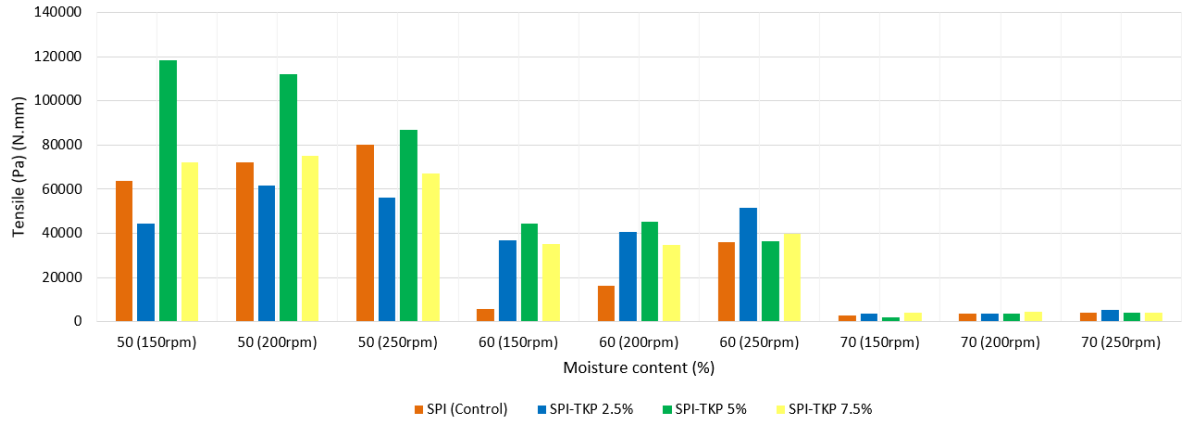

Fig 1. Influence of TKP level, moisture content, and screw speed on SPI-TKP extrudate texture and tensile strength.

When comparing the effects of moisture content and screw speed on elongation, the overall trend showed that elongation values did not vary as clearly with moisture content as tensile strength did. At a moderate moisture content (60%), the samples exhibited the highest elongation, likely because sufficient water enabled the protein matrix to become more flexible and extensible. Among the formulations, those containing 5% and 7.5% TKP generally showed higher elongation values than the control. This may be attributed to the viscous nature of TKP, which enhances the flexibility of the protein structure and improves the overall elasticity of the extrudates. These improvements in elongation were also reflected in the fiber structure: formulations with moderate TKP content exhibited more continuous, well-aligned fibrous strands, indicating that enhanced protein-TKP interactions promoted a more organized, extensible fiber network. Consequently, the combination of optimal moisture and moderate TKP facilitated the formation of fibrous structures that could stretch more before breaking, linking elongation directly to the quality of the fibers in the extrudates.

Table 2. Texture analysis data of HM-TVP on elongation.

Formulas	Moisture levels	Screw speeds	Elongation (%)
Control	50	150	14.33 ± 1.31^{aA1}
		200	21.56 ± 1.44^{aA2}
		250	20.19 ± 2.17^{aA2}
	60	150	8.87 ± 1.87^{aB1}
		200	13.90 ± 1.38^{aB2}
		250	24.39 ± 3.05^{aB2}
	70	150	22.62 ± 1.37^{aC1}
		200	30.58 ± 1.94^{aC2}
		250	26.33 ± 2.13^{aC2}
TKP 2.5%	50	150	19.25 ± 0.57^{bA1}
		200	21.23 ± 0.17^{bA2}
		250	18.12 ± 0.54^{bA2}
	60	150	30.98 ± 1.32^{bB1}
		200	26.14 ± 1.84^{bB2}
		250	29.91 ± 2.11^{bB2}
	70	150	19.50 ± 3.29^{bC1}
		200	19.86 ± 3.23^{bC2}
		250	22.32 ± 0.53^{bC2}
TKP 5%	50	150	22.75 ± 0.64^{aA1}
		200	21.50 ± 0.82^{aA2}
		250	17.83 ± 2.04^{aA2}
	60	150	25.09 ± 2.97^{aB1}
		200	26.51 ± 1.76^{aB2}
		250	22.71 ± 2.53^{aB2}
	70	150	14.57 ± 1.09^{aC1}
		200	18.24 ± 1.08^{aC2}
		250	18.90 ± 0.23^{aC2}
TKP 7.5%	50	150	20.11 ± 5.00^{bA1}
		200	18.22 ± 2.28^{bA2}
		250	19.22 ± 0.56^{bA2}
	60	150	23.22 ± 2.59^{bB1}
		200	29.04 ± 0.34^{bB2}
		250	24.38 ± 2.53^{bB2}
	70	150	23.98 ± 1.84^{bC1}
		200	29.05 ± 2.38^{bC2}
		250	21.34 ± 1.33^{bC2}

Statistical significance at $P \leq 0.05$
Lower superscript letters (a, b, c, d) within the same column indicates different formulas.
Upper superscript letters (A, B, C) within the same column indicates different moisture levels.
Numbers (1, 2, 3) within the same column indicates different screw speeds.

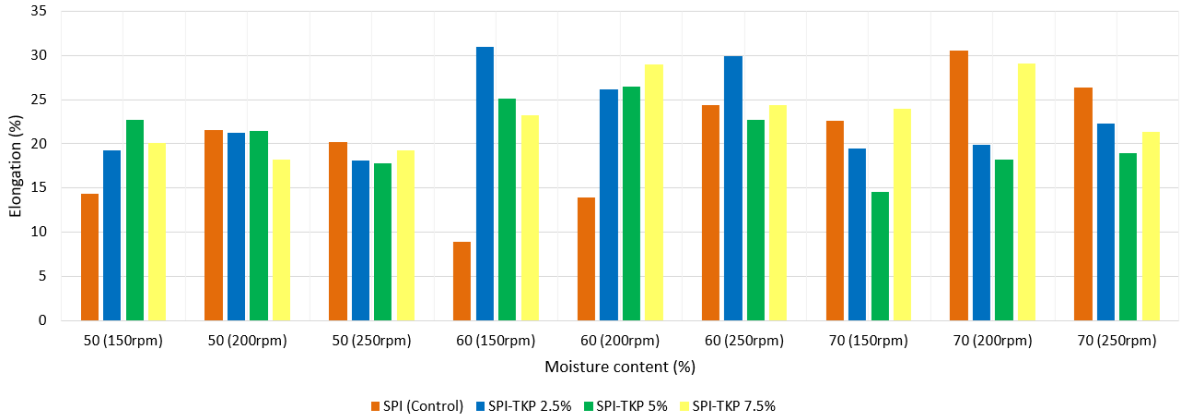

Fig 2. Influence of TKP level, moisture content, and screw speed on SPI-TKP extrudate texture and elongation.

From the comparison of the correlation values, it was observed that the relationship between moisture content and tensile strength was consistently negative across all formulas. As the moisture content increased, the tensile strength decreased significantly, indicating that higher moisture levels clearly reduced the material's strength. This reduction in tensile strength may also be associated with a weaker and less organized fibrous structure, as excess moisture can interfere with protein–protein interactions during extrusion, leading to poorer fiber alignment. In contrast, the elongation varied by formula, showing no distinct or consistent trend. This variation may be attributed to the differing effects of moisture content on the formation and flexibility of the fibrous network under various formulations or processing conditions. Regarding the influence of screw speed on tensile strength, the correlations were found to be very weak or almost negligible in all formulas, suggesting that screw speed had no apparent effect on tensile strength or the degree of fiber formation. Similarly, the correlations between screw speed and elongation were also very weak, indicating that screw speed did not exert a significant influence on the extensibility or integrity of the fibrous structure.

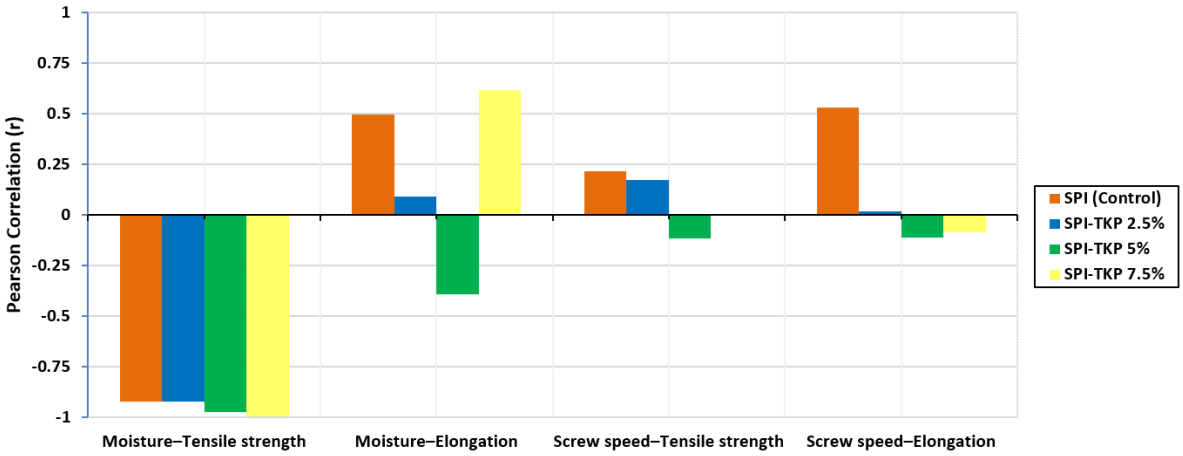

Fig 3. Comparison of All Variable Correlations Across Formulas of SPI-TKP extrudate

4. Conclusion

This study examined the effects of tamarind kernel powder (TKP) concentration, moisture content, and screw speed on the fibrous properties of high-moisture soy protein isolate (SPI) meat analogs. Increasing moisture content reduced tensile strength, while the 5% TKP formulation showed the highest strength. Excessive screw speed also decreased strength. Elongation was highest at 60% moisture, and adding 5–7.5% TKP improved flexibility, though very high screw speeds slightly reduced it. These trends indicate that moderate TKP levels and lower moisture promote a well-aligned fibrous network through stronger protein–polysaccharide interactions, whereas excessive moisture or shear disrupts structure formation. Overall, moisture content was the key factor affecting mechanical and fibrous properties, significantly reducing tensile strength as it increased, while screw speed had no significant effect.

The findings of this study provide useful insights into the role of tamarind kernel powder in modifying the texture and fibrous structure of high-moisture extruded soy protein. The incorporation of TKP may offer a promising strategy for improving the structural integrity and textural quality of plant-based meat analogs. [7,8,10] These results could contribute to the formulation optimization of commercial plant-based meat products and provide a basis for further investigation of protein–polysaccharide interactions in extrusion systems.

References

1. Lin S, Huff HE, Hsieh F. Texture and chemical characteristics of soy protein meat analog extruded at high moisture. *J Food Sci*. 2000;65(2):264–9.
2. Samard S, Ryu G-H. A comparison of physicochemical characteristics, texture, and structure of meat analogue and meats. *J Sci Food Agric*. 2019;99(6):2708–15.
3. Julapuk P, Nakharaksa W. Comparison of pasting characteristics, flow behavior and some physical properties of tamarind kernel powder from sweet and sour tamarind varieties of Thailand. *J Res Dev Walailak Univ Sci Technol*. 2019;16(2):1–12.
4. Zhang J, Liu L, Li L, Jiang Y, Wang Y, Chen L. Low moisture extrusion of soybean protein isolate: Effect of β-glucan on the physicochemical properties of the product. *Food Hydrocoll*. 2020;107:105949.
5. Zhang J, Liu L, Jiang Y, Wang Y, Li L, Chen L. The effects of maltodextrin/starch in soy protein isolate–wheat gluten on the thermal stability of high-moisture extrudates. *Food Hydrocoll*. 2021;118:106754.
6. Wang F, Lian W, Gu X, et al. Effect of polysaccharides on the rheological behaviour of soy–wheat protein aggregation and conformational changes during high-moisture extrusion. *Journal of the Science of Food and Agriculture*. 2023.
7. Osen R, Toelstede S, Eisner P, Schweiggert-Weisz U. High-moisture extrusion cooking of plant proteins: A review. *Trends in Food Science & Technology*. 2014;41:79–88.
8. Dekkers BL, Boom RM, van der Goot AJ. Structuring processes for meat analogues. *Trends in Food Science & Technology*. 2018;81:25–36.
9. Nishinari K, Fang Y, Guo S, Phillips GO. Soy proteins: A review on composition, aggregation and emulsification. *Food Hydrocolloids*. 2014;39:301–318.
10. Zhang J, Liu L, Jiang Y, Chen L. Research advances in plant protein-based products: Protein sources, processing technology and food applications. *Critical Reviews in Food Science and Nutrition*. 2022.
11. Kyriakopoulou K, Dekkers B, van der Goot AJ. Plant-based meat analogues. *Trends in Food Science & Technology*. 2019;81:92–103.
12. Gidley MJ, Lillford PJ, Rowlands DW. Tamarind seed polysaccharide: structure and rheological properties. *Food Hydrocolloids*. 1991.
13. Saha D, Bhattacharya S. Hydrocolloids as thickening and gelling agents in food: a critical review. *Journal of Food Science and Technology*. 2010;47:587–597.

O - 270

Machine Learning-Aided Optimization of Phenolic Extraction from Longan Processing Byproducts

Idris Kaida Zubairu*, Yuthana Phimolsiripol

Faculty of Agro-Industry, Chiang Mai, 50100, Thailand

**Corresponding author E-mail: idriskaida_z@cmu.ac.th*

Abstract: The extensive processing of longan produces nearly 1 million tons of byproducts each year, leading to waste management challenges and potentially hindering the achievement of SDGs 9, 12, and 13. These byproducts are recognized as valuable in traditional medicine for their bioactive content and have potential applications in functional foods, pharmaceuticals, and cosmeceuticals. Among bioactive compounds, polyphenolics are of particular interest; however, the most suitable extraction conditions for their effective utilization using machine learning (ML) models have not been previously studied. This study applied ML approaches to optimize extraction conditions for higher recovery and bioactivity. A dataset of 53 experimental observations from published studies was analyzed, including variables such as time, temperature, solvent type, and solvent ratio, to evaluate their predictive accuracy and performance. The RFR has a higher coefficient of determination (R^2) (0.96) than the other models. Furthermore, based on the predictions, temperature, aqueous ethanol concentration, and amplitude were used to extract longan byproducts. The optimized UAE conditions were within the median for all the factors: temperature (X1, 40-80 °C), amplitude (X2, 40-100%), and aqueous ethanol concentration (X3, 20-60%). They significantly improved polyphenol recovery and functional properties compared to conventional methods. These findings on the extraction of bioactive compounds from longan processing byproducts support the use of ML models to select conditions and optimize bioactive compound extraction, thereby paving the way for sustainable valorization of industrially generated longan waste streams.

Keywords: AI-aided extraction; Smart extraction; AI optimization; Longan byproducts; Sustainability.

1. Introduction

Machine learning (ML) is now a prevalent tool in food and bioprocess engineering for modeling and optimizing processes. ML algorithms such as RFR and ANN can identify nonlinear relationships among multiple variables (e.g., time, temperature, solvent ratio) and predict optimal conditions for maximizing extraction yield and compound stability, which might not be achieved using most conventional trial-and-error methods (Alsaedi et al., 2023; Chy et al., 2025). ML enhances precision, reduces costs, and delivers environmental benefits (Alsabt et al., 2024), making it a suitable innovative pathway for identifying the optimal conditions for recovering functional ingredients from fruit byproducts, including longan byproducts.

Chy et al. (2025) and Subramani et al. (2025) compared the effectiveness of ANN and response surface methodology (RSM) for optimizing and modeling the extraction of bioactive compounds from fruits, medicinal plants, vegetables, and their byproducts. Their findings provide updated details on the sustainable valorization of longan byproducts, with emphasis on advanced green extraction techniques and machine-learning-assisted optimization for the efficient recovery of functional ingredients. For instance, ultrasound-assisted extraction (UAE) (Fikry et al., 2024) and microwave-assisted extraction (MAE) (Fuangchoom et al., 2024) have been used to recover

polyphenols from longan seeds, whereas subcritical water extraction has been shown to efficiently extract flavonoids from longan peels (Liu et al., 2015). Machine learning models, particularly ANNs (De Vries et al., 2021; Shekhar et al., 2023), have also been used to optimize bioactive recovery from Allium sativum leaves, demonstrating higher predictive accuracy than conventional RSM (Subramani et al., 2025). These highlighted the versatility of bioactive compound-rich extracts for diverse applications and emphasized the role of eco-innovative technologies in promoting resource-efficient, scalable solutions, while underscoring the translational potential of integrating green technologies with ML optimization to enhance the economic and environmental value of fruit and agro-industrial byproducts.

Despite the growing number of publications on ML applications, the valorization of longan byproducts enabled by engineering tools, such as ML, has been studied only to a limited extent. Therefore, this study aims to review recent developments in the sustainable extraction of longan byproducts, focusing on green extraction technologies combined with Artificial Intelligence (AI) through ML models for optimization.

2. Materials and Methods

2.1 Materials and sample preparation

Chemicals and reagents, including 2,2-diphenyl-1-picrylhydrazyl (DPPH), gallic acid, and ascorbic acid, were obtained from Sigma (St. Louis, MO, USA). Ethanol (99.8%) was supplied by a liquor distillery in Bangkok, Thailand. FC-reagent. The seeds, including pomace and peel, were obtained in a mixed form from longan processors (PM 80 Ltd., Lamphun, Thailand). The mixed byproducts were ground using a vertical grinder (Heavybao, HLB-JGY-AB, China) and then passed through a 60-mesh sieve to produce a fine powder (Tan et al., 2023). The powder was sealed in polyethylene bags and stored at 25 °C until further analysis.

2.2 Experimental design

The experimental flowchart is shown in Figure 1. The figure illustrates an integrated experimental workflow for optimizing polyphenol extraction from longan byproducts using a machine learning-guided approach. Experimental data comprising 53 observations were compiled from multiple published studies, incorporating key input parameters such as extraction time, temperature, solvent type, solvent ratio, and amplitude, with extraction yield as the target response. These data were analyzed using ANN and RFR models implemented in Python to evaluate predictive performance and identify influential variables. Guided by the model outcomes, critical factors including temperature, amplitude, and aqueous ethanol were selected for ultrasound-assisted extraction of longan byproducts. Finally, RSM was applied to determine the optimal extraction conditions.

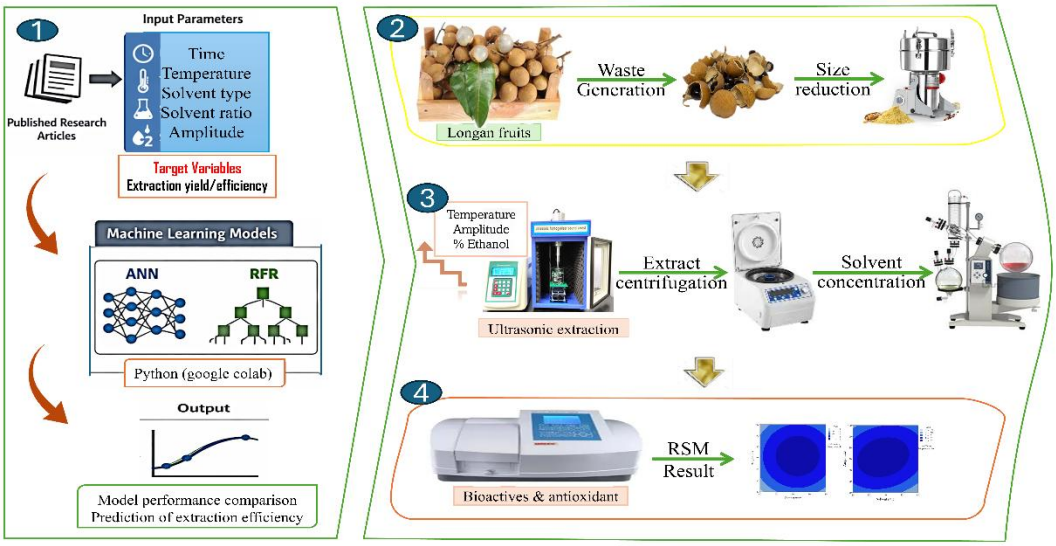

Figure 1. Experimental framework

2.2 Machine Learning Application in Optimization of Longan Byproducts' Extraction

ANN and RFR machine learning models were employed to predict the extraction efficiency of various bioactive compound extraction techniques. The data were obtained from published research articles, and the extracted parameters include time, temperature, yield, solvent type, and solvent ratio. The models are well-suited for modeling relationships between variable sets using Python on Google *Colab*.

2.3 Data Training and Validation

The data were trained using the model's default and adjusted hyperparameter settings (Table 1). For the Random Forest model, n_estimators is the number of decision trees; it affects performance, stability, and computational time. The random state is often used to control the randomness of bootstrapping, thereby ensuring reproducibility of results. *obb_score* describes "to use out-of-bag (OBB)" in estimating the generalization score (R^2), it is also a form of internal cross-validation and is very useful in obtaining unbiased estimation. The *max_depth* parameter was used to limit the maximum tree depth; in this research, the model was allowed to grow to the maximum purity. The *max_feature*s parameter introduces randomness and diversity into the trees when selecting the best split. The MLP Regressor for ANN was trained on the data by adjusting hyperparameters, thereby achieving optimal performance given our small dataset.

Table 1: Model hyperparameters for data training.

Artificial Neural Network		Random Forest	
Hyperparameter	Set Value	Hyperparameter	Set Value
hidden_layer_size	10	*n-estimator*	100
Activation	Relu	*Random_state*	42
Solver	Adam	*Obb_score*	True
Alpha	0.1	*max_depth*	Default
max_iter	2000	*min_samples_split*	2
random_state	42	*min_samples_leaf*	1
n_inter_no_change	30	*max_feature*	Auto
early_stopping	True	-	-
Tol	$1x10^{-4}$	-	-
learning_rate_init	0.001	-	-

The selection of all hyperparameters for both models was based on experimental observations, considering dataset size and limitations to avoid underfitting or overfitting, and was guided by Shekhar et al. (2023) and Chy et al. (2025). The *hidden_layer_sizes* hyperparameter specifies the number of neurons in each hidden layer, thereby describing the model's network capacity. The '*activation*' parameter was set to 'relu' (Rectified Linear Unit) to define the activation function for the hidden layer. The Adam solver was used to optimize the weights. The alpha value (0.1) was used for regularization to avoid overfitting by shrinking larger weights toward zero. A maximum of 2000 epochs (max_iter) was used. The *random state* parameter controls the random initialization of the weights and biases to ensure reproducibility, while early_stopping was set to terminate training when the validation score stopped, to avoid overfitting.

2.4 Extraction of phenolic compounds

Extraction of longan byproduct phenolics was conducted following the method of Sai-Ut et al. (2023). Dried longan byproducts comprising seeds, pericarps, and pomace (approximately 30% of longan fruit dry weight) were ground using a vertical grinder (Heavybao HLB-JGY-AB, China) and passed through 60 mesh sieves to obtain the fine powder. Consequently, extraction was done using a probe-type ultrasonic processor (VCX750, Sonics & Materials Inc., Newtown, CT, USA) for 25 min per run. Three independent variables: temperature (X_1, 40-80 °C), amplitude (X_2, 40-100%), and aqueous ethanol concentration (X_3, 20-60%) were investigated at three levels using a Box-Behnken RSM design. The extract was centrifuged at 8644 × g at 25 °C (Rotina 380R, Hettich Zentrifugen, Tuttlingen, Germany) for 15 min, filtered, and concentrated under reduced pressure at 40 °C (BUCHI, Rotavapor® R-300, Thailand Ltd). The final samples were stored at -20 °C. The selected process variables and their corresponding coded and actual levels are presented in Table 1. Model coefficients were estimated using multiple linear regression with a quadratic polynomial (Eq. 1), while optimal extraction conditions were identified using the desirability function approach implemented in Minitab® (version 21.1.1; Minitab LLC, Chicago, USA).

$$Y = \beta_0 + \sum_{i=1}^{3} \beta_i X_i + \sum_{i=1}^{3} \beta_{ii} X_i^2 + \sum_{i=1}^{2} \sum_{j=2}^{3} \beta_{ij} X_i X_j \ldots\ldots\ldots\ldots\ldots\ldots (1)$$

2.5 Total phenolic and DPPH assays

Total phenolic content (TPC) was determined based on the methods described by Chailangka et al. (2023). TPC was measured using the colorimetric Folin-Ciocalteu method. Gallic acid (0-100 µg/mL) was used as a standard. Absorbance read at 765 nm and results expressed as mg gallic acid equivalents (GAE)/g sample. A 100 µL solution of DPPH (0.08 mg/mL in 70% aqueous ethanol) was mixed with 25 µL of the standard or sample, and the mixture was incubated at 30 °C in the dark for 30 min, as described by Chaiwong et al. (2025). Ascorbic acid (50-3.12 µg/mL) was used as the standard, and absorbance was measured at 517 nm. Both (TPC and DPPH) measurements were taken using a spectrophotometer (Ultrospec 200UV/V Visible Spectrophotometer, Pharmacia Biotech, Piscataway Township, NJ, USA).

3. Results & Discussion

3.1 Model selection

The R^2, RMSE, and MSE values from the training, validation, and test sets were used to assess each model's performance, as presented in Table 2. A high R^2 value and a low RMSE indicate optimal model performance. The feature importance remains constant, highlighting the importance of flags in the extraction methods, temperature, and time. Although artificial neural networks exhibit less stable performance than RFR, they have demonstrated the potential to

capture more complex interactions. The random forest feature distribution of extract yield across the extraction solvents is shown in Figure 2.

Table 2: The R^2, RMSE, and MSE values determined by the training for ANN and RFR models.

Models	R^2	MSE	RMSE
Artificial Neural Network (ANN)	0.7413	0.4625	0.6801
Random Forest Regression (RFR)	0.9621	0.1422	0.3770

R^2=coefficient of determination; MSE=Mean Squared Error; RMSE=Root Mean Squared Error.

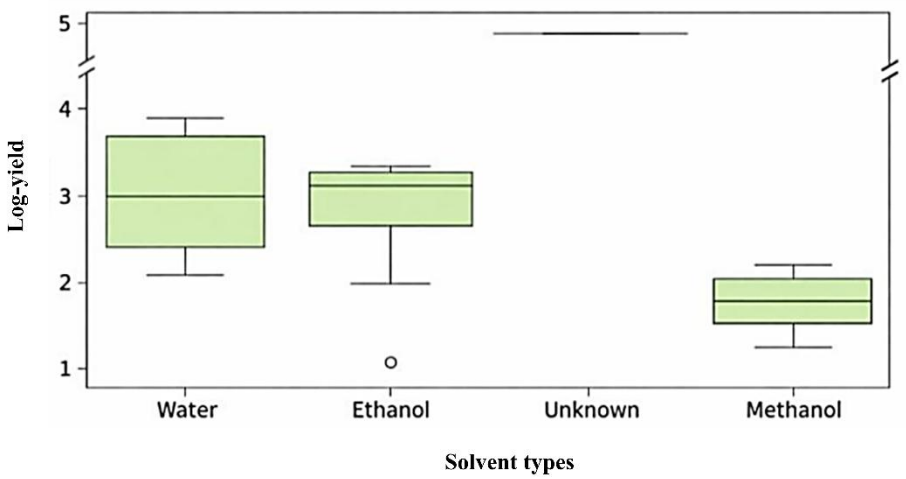

Figure 2. The plot of log-yield versus solvent type is commonly used in the extraction of longan byproducts.

3.2 Correlation analysis

The correlation matrix reveals a moderate positive correlation between temperature (r = 0.48) and a weaker negative correlation with time (r = 0.30). Temperature and extraction time are positively correlated (r = 0.43), indicating a relationship between extraction duration and temperature (Figure 3). Extraction time, solvent portions, and temperature influence the bioactive compounds produced from longan products. Although the temperature and solvent portions are negatively correlated, with coefficients of 0.15 and -0.09, respectively, extraction experiments at higher solvent ratios require lower temperatures and shorter times; therefore, optimization of bioactive compound extraction should focus on the combination of time, temperature, and solvent ratio.

The training results demonstrate a clear difference in predictive performance between the models. The RFR achieved a higher coefficient of determination (R^2 = 0.9621) than the ANN (R^2 = 0.7413), along with lower MSE (0.1422) and RMSE (0.3770), indicating a better fit to the data. This advantage likely reflects the robustness of the ensemble of three methods and their suitability for the dataset, rather than universal model superiority.

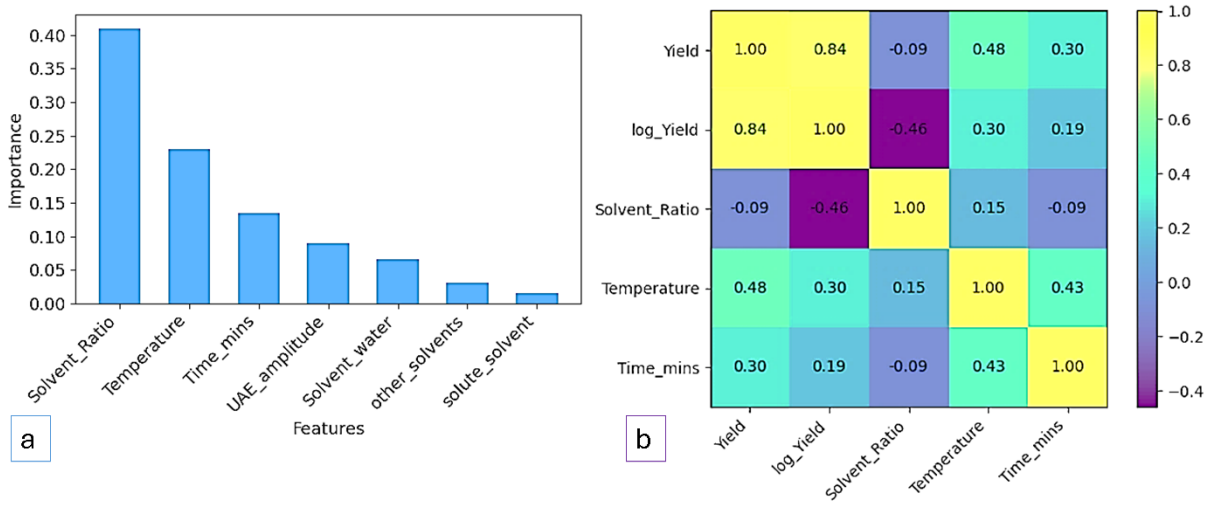

Figure 3. Model response for the variables involved in the extraction of longan byproducts: (a) features of importance and (b) correlation matrix.

The developed ANN and RFR models offer valuable tools for optimizing extraction conditions to valorize longan byproducts. These models can inform decisions regarding key process parameters, such as temperature, time, and solvent ratios, to enhance the yield and bioactive content of extracts (Shekhar et al., 2023). The RFR model demonstrated stronger predictive performance under the current data constraints, making it more reliable for immediate application in pilot-scale operations (Sai-Ut et al., 2023). Integrating these models into industrial workflows can accelerate process development, reduce material and energy waste, and support scalable, cost-effective valorization strategies. Ultimately, they aid experimental planning by identifying key variables and reducing trial-and-error experimentation, thereby supporting the sustainable utilization of agro-industrial byproducts and aligning with the principles of SDGs 9, 12, and 13 (Fuangchoom et al., 2024). The weaker ANN performance may stem from limited hyperparameter tuning or insufficient sample size, as neural networks typically require careful tuning to achieve optimal performance. Therefore, while RFR more accurately captures the training data, definitive conclusions should be based on out-of-sample validation and improved ANN optimization to ensure a balanced comparison.

3.3 RSM optimization of yield, TPC, and DPPH

The experimental matrix and responses generated by the Box-Behnken design are described in the method sections (2.4). The design included 15 runs, with three center points to assess the effects of temperature (X_1), ethanol concentration (X_2), and ultrasonic amplitude (X_3) on extraction yield, TPC, and DPPH. The second-order equations (Table 4), incorporating linear, quadratic, and interaction terms, enabled reliable prediction of responses across extraction conditions. Temperature (X_1) had the strongest linear effect on yield and TPC, whereas the $X_1 \times X_3$ interaction significantly influenced FRAP, underscoring the interdependence of these variables. These validated models were used to construct response surfaces and determine optimal conditions via the desirability function. Figure 3 illustrates the 2-dimensional contour plots generated from the Box-Behnken design, showing the interactive effects of temperature (X_1), solvent ratio (X_2), and ultrasonic amplitude (X_3) on the extraction yield, total phenolic content (TPC), and DPPH. Each subfigure (a-i) represents the interaction between two independent variables, while the third is kept constant at its center level. The plots exhibit clear curvature patterns, confirming the quadratic nature of the fitted models. Yield and TPC reached maximum values at intermediate temperature (around 64 °C) and amplitude (69%), whereas both low and high extremes yielded lower responses, likely due to incomplete extraction or phenolic degradation. DPPH followed

similar trends, indicating that moderate extraction conditions offered the best compromise between efficiency and compound stability. These tendencies are consistent with an earlier study on longan seeds (Fikry et al., 2024), which also reported that moderate temperatures and a 1:1 solvent ratio maximize polyphenol recovery and antioxidant potential. The contour plots of the interactions among the variables for each response parameter are shown in Figure 4, and the regression models relating the independent variables to the measured responses are presented in Table 3.

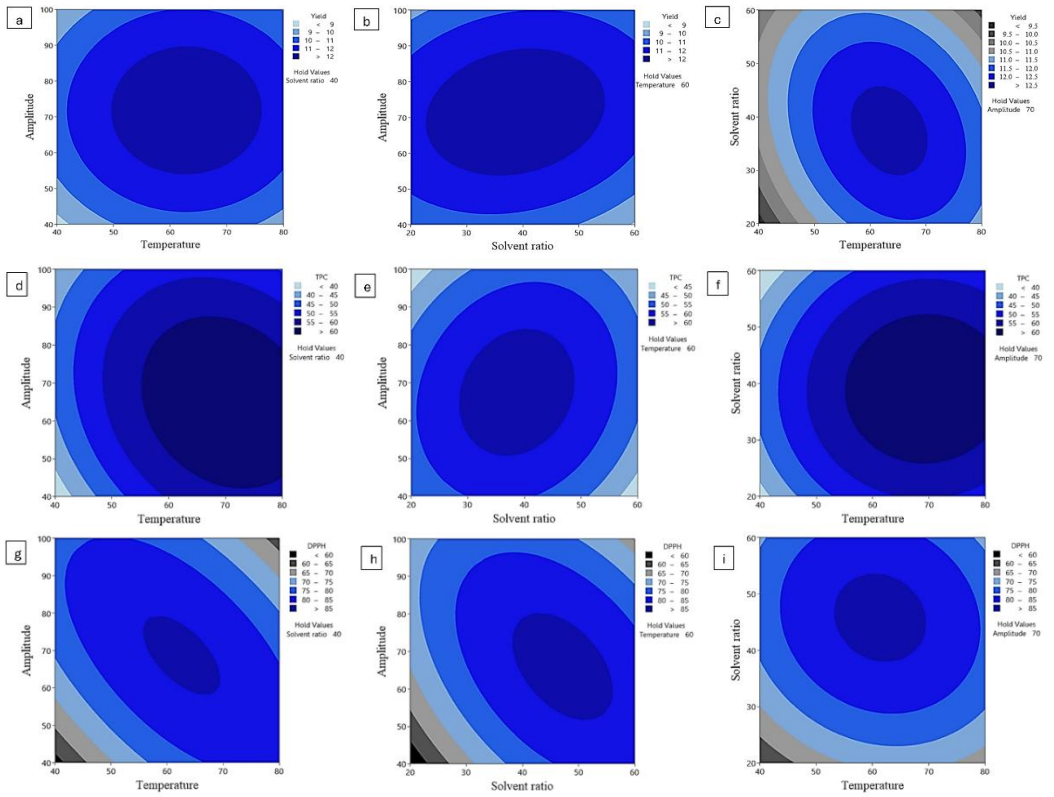

Figure 4. Contour plots illustrate the interactive effects of extraction parameters on response variables. Panels (a–c) depict the influence of temperature, solvent ratio, and amplitude on extraction yield; (d–f) represent their effects on DPPH radical scavenging activity; and (g–i) show the variation in total phenolic content (TPC). The elliptical contour patterns indicate significant interaction among the variables, with darker regions corresponding to higher response values. The hold values for the non-varied factors are shown in each panel, highlighting the combined effect of process parameters on maximizing extraction efficiency and antioxidant properties.

Table 3. Regression equations for the RSM model.

Responses	Equations
Yield	$-17.70+0.5269X_1+0.2284X_2+0.2631X_{32}-0.003734X_1\times X_1-0.002541X_2\times X_2-0.002063X_3\times X_3-0.001475X_1\times X_2+0.000025X_1\times X_3+0.000788X_2\times X_3$
TPC	$-119.8+3.211X_1+1.484X_2+1.337X_3-0.02065X_1\times X_1-0.02440X_2\times X_2-0.00901X_3\times X_3+0.00088X_1\times X_2-0.00533X_1\times X_3+0.00517X_2\times X_3$
DPPH	$-197.3+3.841X_1+3.226X_2+2.701X_3-0.02028X_1\times X_1-0.02217X_2\times X_2-0.00869X_3\times X_3-0.00507X_1\times X_2-0.01598X_1\times X_3-0.01263X_2\times X_3$

TPC*:* total phenolic content; DPPH*: 2,2-diphenyl 1-picrylhydrazyl.*

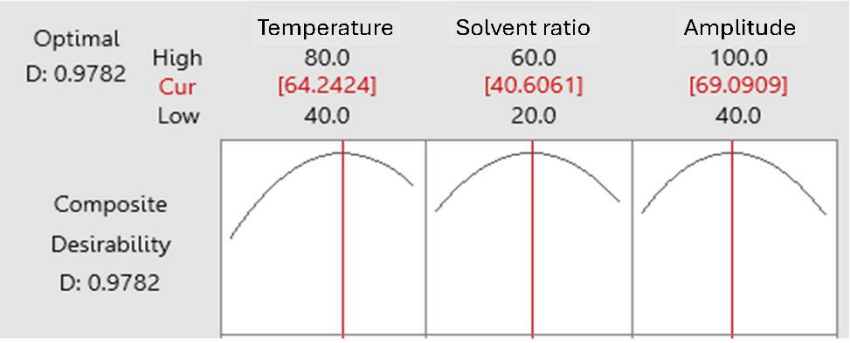

Figure 5. Plot depicting the variables' curves and composite desirability for the three variables used for the optimization. The optimal conditions were identified at 64.24 °C, 40.61% solvent concentration, and 69.09% amplitude, yielding a high overall desirability (D = 0.9782).

3.4 Validation for the RSM model

The reliability of the developed model was confirmed through validation (Table 4), which demonstrates strong agreement between predicted and experimental values for yield, TPC, and DPPH. The minimal deviations between predicted and observed results suggest high predictive accuracy and validate the adequacy of the optimization approach. This is further supported by the high coefficients of determination (R^2 = 0.979-0.983) and adjusted R^2 values (0.942-0.952), indicating that a substantial proportion of the variability in the responses is explained by the model, given the number of predictors. The statistically significant p-values ($p < 0.001$) confirm the overall model significance, and the non-significant lack-of-fit values ($p > 0.05$) indicate that the models sufficiently capture the experimental data without systematic errors. Thus, these statistical indicators highlight the robustness, goodness-of-fit, and suitability of the regression models for predicting extraction performance and antioxidant properties under the optimized conditions.

Table 4. Validation and model fitting.

Parameter(s)	Responses					
	Predicted	Experiment	R^2	Adj. R^2	p-value	Lack of fit
Yield (%)	12.65	12.56±0.23	0.982	0.951	0.001	0.194
TPC (mg GAE/g)	63.27	62.55±0.61	0.979	0.942	0.001	0.358
DPPH (mg AAE/g)	85.72	85.81±0.32	0.983	0.952	0.001	0.256

TPC: total phenolic content; DPPH: *2,2-diphenyl 1-picrylhydrazyl*

4. Conclusion

The application of ML in this study (the RFR model, which outperformed the ANN model) proved highly effective in providing key information on optimal extraction strategies for longan byproducts. Extraction conditions, including solvent ratio, amplitude, and temperature, were determined to be optimal using the UAE-assisted method to fully recover bioactive phenolic compounds from longan byproducts, as experimentally validated by an RSM model. However, for ML adoption, emphasis should be placed on expanding the dataset to improve model stability and reduce predictive variance across experimental conditions. Future research should focus on integrating larger, more diverse datasets and exploring hybrid modeling approaches that combine ML with mechanistic understanding, while also incorporating additional antioxidant assays and advanced profiling techniques to enable a more comprehensive evaluation of bioactive properties,

as well as extending the framework to predict bioactivity outcomes and assess scale-up feasibility for industrial applications.

Acknowledgments

The authors appreciate the Agro-Industry and FAB organizers for providing the research facilities and technical support. Gratitude is also extended to Abubakar Ibrahim Garba for valuable guidance and commitment in supporting the application of the modeling approaches.

References

1. Alsaedi AWM, Al-Mousawi AJ, Al-Hilphy AR, Gavahian M. Non-thermal pasteurization of milk by an innovative energy-saving moderate electrical field equipped with elongated electrodes and process optimization. Innovative Food Science & Emerging Technologies. 2023;88:103445.
2. Chy MdWR, Ahmed T, Sarkar R, Islam MdZ, Rana MdR. Artificial Neural Network and response surface methodology modeling-based optimization approach for the ultrasonication-assisted extraction of phenolics from mustard (BARI Sharisa-18) seed meal. Applied Food Research. 2025;5(1):101016.
3. Alsabt R, Alkhaldi W, Adenle YA, Alshuwaikhat HM. Optimizing waste management strategies through artificial intelligence and machine learning - An economic and environmental impact study. Cleaner Waste Systems. 2024;8:100158.
4. Subramani V, Tomer V, Balamurali G, Mansingh P. Artificial neural network in optimization of bioactive compound extraction: recent trends and performance comparison with response surface methodology. Analytical Sciences. 2024;41(2):101–17.
5. Fikry M, Jafari S, Shiekh KA, Kijpatanasilp I, Khongtongsang S, Khojah E, et al. Ultrasound-assisted extraction of bioactive compounds from longan seeds powder: Kinetic modelling and process optimization. Ultrasonics Sonochemistry. 2024;108:106949.
6. Fuangchoom V, Narkprasom N, Jaturonglumlert S, Varith J, Unpaprom Y, Narkprasom K. Sustainability-driven optimization of microwave-assisted extraction for enhanced corilagin and total phenolic compound yield from *Dimocarpus longan*. Environmental Quality Management. 2024;34(1).
7. De Vries L, Guevara-Rozo S, Cho M, Liu LY, Renneckar S, Mansfield SD. Tailoring renewable materials via plant biotechnology. Biotechnology for Biofuels. 2021;14(1):167.
8. Shekhar S, Prakash P, Singha P, Prasad K, Singh S. Modeling and optimization of ultrasound-assisted extraction of bioactive compounds from *Allium sativum* leaves using response surface methodology and artificial neural network coupled with genetic algorithm. Foods. 2023;12(9):1925.
9. Tan S, Ke Z, Zhou C, Luo Y, Ding X, Luo G, et al. Polyphenol profile, antioxidant activity, and hypolipidemic effect of longan byproducts. Molecules. 2023;28(5):2083.
10. Sai-Ut S, Kingwascharapong P, Mazumder MdAR, Rawdkuen S. Optimization of ethanolic extraction of phenolic antioxidants from lychee and longan seeds using response surface methodology. Foods. 2023;12(15):2827.
11. Chaiwong N, Gavahian M, Tridtitanakiat PC, Therdtatha P, Moukamnerd C, Leksawasdi N, et al. Ultrasound–accelerated maillard reaction to improve functional and antioxidant properties of hemp protein–carboxymethyl chitosan conjugates as a future food ingredient. Innovative Food Science & Emerging Technologies. 2025;104:104118.
12. Chailangka A, Autsavapromporn N, Karnjanapratum S, Leksawasdi N, Castagnini JM, Barba FJ, et al. Kinetic stability, gastrointestinal fate, and cytotoxicity of vitamin D3 emulsion incorporated with cricket protein-fructooligosaccharide conjugate. Food Hydrocolloids. 2023;146:109288.
13. Zubairu IK, Rakariyatham K, Bai-Ngew S, Leksawasdi N, Regenstein JM, Lao F, et al. Nutritional and therapeutic potential of longan fruit by-products for liver diseases: Pathway to functional foods. Current Nutrition Reports. 2025;14(1):28.
14. Liu H, Wang H, Liang Y. Microwave-assisted extraction of flavonoids from longan pericarp and its antioxidant activity study. Natural Product Research and Development. 2015;27(3):438-41.

O - 285

Effect of Salt Concentration and Fermentation Temperature on the Microbiological and Chemical Properties of Watermelon Rind Fermentation

Shankar Neupane[1], Yonn Pwint Phyu[1], Nattaya Konsue[1,2]*

[1]*Food Science and Technology Program, School of Agro-Industry, Mae Fah Luang University, Chiang Rai, 57100, Thailand*
[2]*Research Center of Innovative Food Packaging and Biomaterials, Mae Fah Luang University, Chiang Rai, 57100, Thailand*

**Corresponding author E-mail: nattaya.kon@mfu.ac.th*

Abstract: Watermelon rind, a major agricultural by-product of watermelon processing, is often discarded as waste despite its edibility. Fermentation offers a sustainable approach to turning such underutilized materials into the food value chain by enhancing preservation and safety. As a part of the effort to valorize through fermentation, this study investigated the effects of salt concentration (2%, 4%, 6%) and fermentation temperature (25, 30, 35, 40°C) on the microbiological and chemical properties of naturally fermented watermelon rind over 10 days. Lactic acid bacteria (LAB) growth, yeast and mold, Enterobacteriaceae counts, pH, and titratable acidity were monitored. Results indicated that both temperature and salt concentration significantly influenced microbial dynamics and acidification. The highest LAB growth (8.80 ± 0.01 log CFU/g) was observed at 40°C with 6% salt on day 2, although LAB populations declined rapidly thereafter, causing lower acidification. At lower temperatures (25–35°C), LAB growth was more stable, with 6% salt consistently supporting robust LAB growth. Maximum counts at 25°C (8.40 ± 0.03 log CFU/g) and 30°C (8.35 ± 0.05 log CFU/g) were not significantly different, highlighting sustained LAB activity at moderate temperatures. Yeast and mold were eliminated most rapidly at higher salt concentrations and temperatures, disappearing within 2 days in 6% salt samples at 30-40°C. Enterobacteriaceae, initially present at high levels (7.72-7.35 log CFU/g), were undetectable in all samples by day 5. The pH drop was most rapid and pronounced at 30°C with 6% salt, achieving the lowest final pH of 3.23±0.01. Acidity increased correspondingly with LAB activity, with lower salt concentrations (2%) generally yielding higher final acidity at most temperatures, except at 40°C where acid production was suboptimal. The study concludes that fermenting watermelon rind at 30°C with 6% salt provides optimal conditions for stable LAB growth, complete acidification, and efficient elimination of undesirable microorganisms.

Keywords: Watermelon rind, Fermentation, Lactic acid bacteria, Salt, Temperature

1. Introduction

Watermelon (*Citrullus lanatus*) is world's second largest produced fruit ranking after banana. The total worldwide production of this fruit accounts for about 105 million tons, with a significant portion of its production, around 80% concentrated in Asia as of 2023 data (1). Thailand ranks 44th place in watermelon production worldwide with its annual production about 166 thousand tons. Watermelon is majorly celebrated worldwide for its juicy flesh as thirst quenching and heat reliever drink especially in tropical regions (2). However, the rind, which makes up approximately 30% of the fruit's total weight, is often discarded. According to 2023 figures, the rind alone constitutes almost 30 billion tons (1, 3). This results in significant urban waste and lost possibilities for sustainable food utilization. The United Nations Sustainable Development Goals

(SDG) for 2030 emphasize reducing food waste as a critical step towards eradicating hunger and promoting sustainability (4). Researches indicate that watermelon rind is edible and a valuable source of nutrients including minerals, dietary fibers, phenolic compounds and other phytochemicals that contribute to its therapeutic properties, such as antioxidant (5), antidiabetic (6), antihypertensive (7), carcinogenic (8) and anti-inflammatory effects (5). However, lack of the flavor and its perishability hinders its potential applications.

On the other hand, lactic acid bacteria (LAB) fermentation has been attached to the livelihood of people since prehistoric times for food preservation, processing, and flavor enhancement (9). Fermented products such as kimchi, sauerkraut, miso, soy sauce, and fermented cucumber are widely accepted by consumers. Moreover, scientific evidence indicates that LAB provide direct health benefits as probiotics by colonizing the intestinal tract, thereby supporting gut health and influencing both the immune and nervous system (10). They also exhibit anti-carcinogenic properties by stimulating natural killer (NK) cells, modulating immune responses, and suppressing the activity of certain carcinogenic enzymes (11). In addition, LAB contribute to food safety through their roles as natural bio-preservatives, inhibitors of foodborne pathogens, and reducers of anti-nutritional factors in foods (12, 13). More recent articles even highlight that fermented vegetables were associated with the lowering the mortality rate during COVID-19 in some areas (14). Salt and temperature are very important extrinsic factors to manipulate LAB growth (15). Despite the global recognition of LAB fermentation, there remains a significant research gap in the valorization of underutilized agricultural by-products such as watermelon rind through natural fermentation. Existing studies have primarily focused on proximate composition and LAB identification, with little emphasis on understanding how fermentation conditions influence the microbial dynamics and subsequent acidification in such substrates (16).

It was hypothesized that salt concentration and fermentation temperature influence microbial succession and acidification during watermelon rind fermentation, thereby affecting the dominance of lactic acid bacteria and the suppression of undesirable microorganisms. Therefore, this study investigated the effects of salt concentration and fermentation temperature on the microbiological and chemical characteristics, specifically LAB, yeast and mold, and Enterobacteriaceae counts, as well as pH and titratable acidity during the course of fermentation of watermelon rind with the aim is to identify suitable fermentation conditions for producing a microbiologically safe and stable fermented watermelon rind with high LAB counts.

2. Materials and Methods

2.1 Materials

Watermelon (*Citrullus lanatus*) rind of *Kinnaree* variety was received from Triple J Food and Beverage Co., Ltd., Chiang Rai. The rind, a byproduct during preparation of the crispy watermelon processing, was collected from the company. The rind was transported in sterile plastic bags to the university, maintaining the cold chain and stored in the chilling room. The processing of the watermelon rind started within 24 h of storage at low temperature. All the media, including MRS agar, Potato dextrose agar, VRBGA, Peptone were purchased from Himedia Laboratories Pvt. Ltd., India and chemicals; Sodium Hydroxide, Phenolphthalein from the RCI Labscan Ltd, Thailand.

2.2 Methods

2.2.1 Natural Fermentation

Watermelon rind was fermented according to the method mentioned by Dahal et.al. (2005) with some modifications (17). In brief, watermelon rind was washed with tap water to remove visible dirt and surface debris, and no disinfectant or antimicrobial agent was applied, in order to preserve the naturally occurring microbiota responsible for spontaneous fermentation. The clean sample was peeled and cut into pieces (1 cm long). It was then mixed with salt at

different concentrations (2%, 4 % and 6 %) and pressed in the glass bottles to minimize oxygen inside and kept for fermentation *in situ* up to 10 days at different temperatures (25, 30, 35 and 40°C). Samples of each temperature and salt concentration were taken every day for the analysis of the pH and acidity (as lactic acid) and microbial enumeration in terms of LAB, yeast and mold and Enterobacteriaceae count.

2.2.2 Microbial Enumeration

For microbial analysis, LAB, yeast and mold and Enterobacteriaceae count were performed. Enumeration of LAB, yeast and mold and Enterobacteriaceae was carried out according to Tamang & Tamang, (2010) (18). Samples (10 g) were mixed with 90 ml of 0.10 % (w/v) sterile peptone water and homogenized in a Stomacher at 200 rpm for 2 min. A serial dilution up to appropriate dilution in the same diluents was made.

For LAB count, one milliliter of appropriately diluted sample was transferred into a sterile Petri dish, followed by the addition of approximately 15 to 20 ml of molten MRS agar. The plates were then incubated at 35°C for 48 h. Confirmation of LAB was done by microscopic observation, Gram's reaction and catalase test. Yeast and mold count was examined on potato dextrose agar (PDA) acidified with tartaric acid. Exactly 0.1 ml of diluted sample was put on the plated petri dish and was spread by the glass spreader. The plate was incubated at 25°C for 5 days. Isolated colonies based on colony morphology were counted from the highest diluted plates. Purity of the isolates was checked by streaking again and sub-culturing on fresh agar plates of the isolation media. For the Enterobacteriaceae count, diluted 1 ml sample was pipetted on the sterile petri plate. Molten VRBG agar was poured over the sample, mixed well and allowed to set. The media plate was then incubated in inverted position at 37°C for 24 h. After incubation, plates containing colonies between 25-250 in number were selected for enumeration. In each case, the microbial count is expressed as:

$$\text{Count (CFU/g)} = \frac{Average\ number\ of\ colonies\ from\ duplicate\ plates}{Dilution\ factor \times Volume\ taken}$$

Count is expressed in $\log_{10}$ scale.

2.2.3 pH and Acidity

pH and acidity were assessed as described in AOAC, (2005) (19). Briefly, 50 g of rind sample was removed in triplicate from each glass jar. Samples were ground using a table blender (Problend Crush, Philips, Indonesia), and pH levels were measured using a pH meter (Mettler Toledo™, F20 FiveEasy™, Switzerland) in triplicate. The flat surface pH probe (Mettler Toledo™, LE438, Switzerland) was carefully cleaned between samples with distilled water and was calibrated with pH 4.01 and 7.00 and 10.01 buffer solutions before use. The probe was placed directly into the pureed fermented samples until consistent reading was obtained. The readings were duplicated for each sample and pH values were averaged. These samples were retained for titratable acidity.

For acidity measurement, about 10 g of sample was taken and diluted to the appropriate dilution with distilled water and titrated against 0.05 N NaOH with phenolphthalein indicator. The acidity was calculated by following the formula.

$$\text{Acidity as lactic acid(\%)} = \frac{Titer \times Strength\ of\ NaOH \times Vol\ make\ up \times Eq.\ wt\ .of\ lactic\ acid\ (90.08) \times 100}{Wt.\ of\ sample\ taken \times Aliquot\ taken \times 1000}$$

2.2.4 Statistical Analysis

Full factorial design was used to design the experiment. Statistical significance was assessed by ANOVA using IBM SPSS Statistics 27 software. The graph and bar diagram were obtained from Microsoft excel 365.

3. Results and Discussion

3.1 Microbiological change during the fermentation

Lactic acid bacteria

The lactic acid bacteria count was observed for 10 days in three salt concentrations (2 %, 4 % and 6 %) at different fermentation temperatures (25°C, 30°C. 35°C and 40°C). The LAB count at 2 %, 4 % and 6 % salt concentration watermelon at day 0 was 6.50±0.07, 6.37±0.05 and 6.30±0.07 log CFU/g respectively (Figure 1). On this day, LAB count at 6 % salt concentration was significantly lower ($p \leq 0.05$) than that of the 2 % salt concentration sample, however it is not significantly different when compared to the 4 % salt sample. As expected, the higher salt concentration provides the osmotic shock to the surface lactic acid bacteria (20).

Salt concentration, fermentation temperature, and their interaction (T × S) all had significant effects on LAB count ($p<0.05$). At 25°C, the highest LAB growth at 2% salt was observed on the 5th day of fermentation (7.64 ± 0.09 log CFU/g), after which it remained stable. At 4% salt, the maximum growth occurred one day earlier. For the 6% salt sample, the highest count (8.40 ± 0.03 log CFU/g) was recorded on day 3, which was significantly higher than those at 2% and 4% salt. With increase in fermentation temperature at 30°C, LAB growth was also highest at 6% salt, reaching its peak (8.35 ± 0.05 log CFU/g) on day 3, staying stable until day 4, and then gradually declining. At 35°C, the 6% salt sample again showed the highest count, with maximum growth on the 2nd day, stability until the 4th day, and a decline thereafter. A comparable trend was observed at 40 °C, where all salt levels peaked on day 2 but the 6% salt sample still showed the highest count (8.80 ± 0.01 log CFU/g). However, after the second day, LAB growth decreased sharply, which can be attributed to the simultaneous stress of high temperature and rapid acidification. At 40°C, the elevated temperature accelerated LAB metabolism, resulting in a faster and more intense accumulation of lactic acid compared to lower temperatures. This rapid acid production caused an abrupt decline in pH. Concurrently, at temperatures above the optimal growth range, LAB commonly experiences excessive increase in cell membrane fluidity, as the lipid bilayer loses its structural integrity under heat stress. This loss of membrane integrity increases its permeability to protons, disrupting the transmembrane pH gradient that is essential for energy generation and ion homeostasis (21). When this occurs alongside a low external pH, the already high extracellular proton concentration drives accelerated proton influx into the cytoplasm, causing intracellular acidification. This in turn leads to denaturation of key metabolic enzymes and ribosomal structures, inhibition of DNA replication, and energy-generating mechanism of the cell (22). The convergence of these two stresses, auto-acidification and thermal, membrane disruption likely caused the decline of LAB count and thus ultimate pH at 40°C observed after day 2.

Across all tested temperatures, the highest microbial growth was observed at 6% salt concentration. Temperature shown to have significant effect on the growth kinetics. While compared between temperatures, maximum count at 40°C was found significantly higher ($p<0.05$) than other lower temperatures. Maximum count was not found significantly different between 25 and 30°C (Table 1). However, the stability period, growth and death kinetics differed between temperatures.

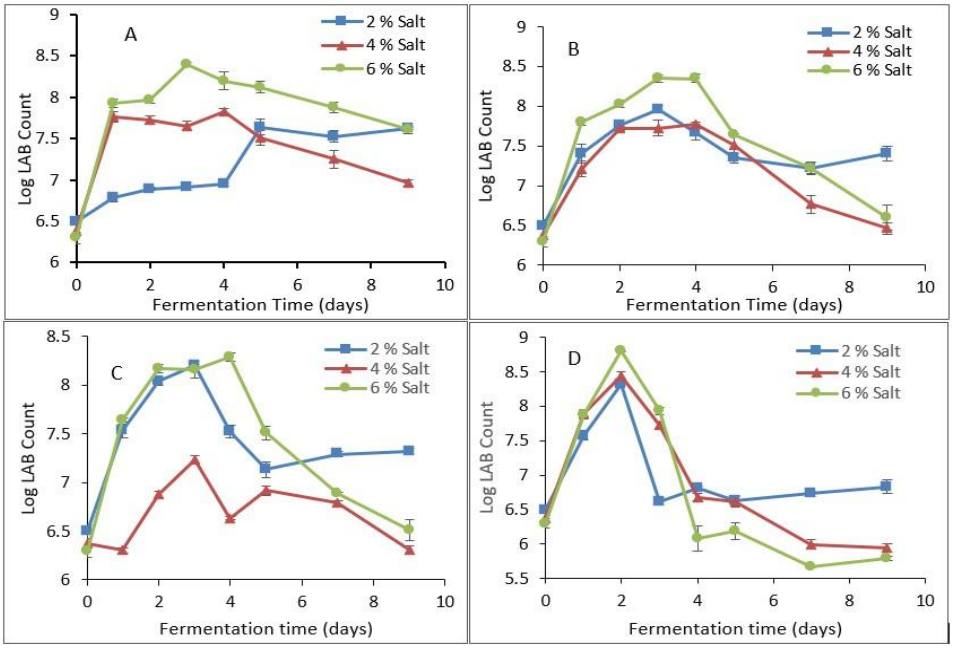

Figure 1. Effect of fermentation time and salt concentration on LAB count (log CFU/g) at different temperatures (A) 25°C, (B) 30°C, (C) 35°C, and (D) 40°C

Generally, LAB can withstand relatively high levels of salt. In commercial fermentations, the salt level typically exceeds 2%, depending on the product; cucumbers are fermented at 6–10%, olives at 5–8%, and cabbage (sauerkraut) at 2–3% (23). Another study reported a similar trend to our results, observing that during the natural fermentation of black olives with 4%, 6%, and 10% salt, the greatest LAB growth occurred at 6% under both high and low temperatures (24). Likewise, in Suancai fermentation conducted with 0%, 3%, 6%, and 9% salt, a 6% concentration yielded the highest abundance of *Lactobacillus* and lactic acid production (25). Conversely, previous research reported that salt concentration (2.5%, 5%, and 10%) did not significantly affect LAB counts during natural cucumber fermentation (26). In contrast, Paocai (Chinese radish) fermentation showed that the lowest salt concentration (1%) resulted in the highest microbial counts among the treatments tested (1%, 3%, 5%, and 7%) (27). These findings suggest that LAB responses to salt concentration vary across different food matrices. Nonetheless, LAB are known to tolerate high salinity through mechanisms such as Osmo-protectant accumulation, membrane remodeling, ion transport regulation, protective protein synthesis, and metabolic reprogramming. All of which support their survival and activity under salt-stressed fermentation conditions (28).

Table 1: Maximum LAB count observed at different fermentation temperatures

No.	Fermentation Temperature (°C)	Maximum count observed (log CFU/g)	Respective salt concentration (%)
1	25	8.40 ± 0.03^{b}	6
2	30	8.35 ± 0.05^{bc}	6
3	35	8.29 ± 0.04^{c}	6
4	40	8.80 ± 0.01^{a}	6

Values are presented as mean ± standard deviation (SD). Different subscript letters within the same column indicate statistically significant differences between the treatments ($p\leq0.05$).

Furthermore, higher salt content might have destroyed harmful undesirable microorganisms, leaving the nutrients for LAB only. Some studies reported that for some strains, salt promotes the growth of LAB (29). In addition, the sample with higher salt concentration likely

promoted greater extraction of sugars into the fermentation medium (15), which could have provided more readily available substrates for LAB metabolism, allowing them to grow and ferment more actively than in samples with lower salt concentrations.

Yeast and Mold

At day 0, yeast and mold counts were 5.68 ± 0.03, 5.54 ± 0.14, and 5.41 ± 0.16 log CFU/g for samples containing 2%, 4%, and 6% salt, respectively (Figure 2). The count observed at 2% salt concentration was significantly higher than that of 6%, but not significantly different from the 4% sample. The reduction in microbial load at higher salt concentrations may be attributed to the osmotic stress or cell lysis induced by salt, which could have inactivated or destroyed some surface yeast and mold cells (30). At 25 °C of fermentation, complete elimination of yeast and mold occurred after 6 days in the 2% salt sample, 4 days in the 4% sample, and 2 days in the 6% salt sample. At higher fermentation temperatures, only the 2% salt sample required 6 days for elimination, while yeast and mold disappeared within 2 days in all other treatments. The rapid decline of fungal populations in the high-salt and higher-temperature fermentations can be attributed to the enhanced growth of lactic acid bacteria, particularly in the 6% salt sample, which significantly reduced pH and created a more anaerobic environment unfavorable for fungal survival. The accelerating effect of temperature aligns with reports that the optimal growth range of most mesophilic fungi is 25–30 °C, beyond which their activity declines (31). The initial yeast and mold counts in this study were within the general range reported for raw vegetables (5–7 log CFU/g) (32), but higher than those observed in cucumber fermentation (3.39 ± 0.42 log CFU/g) (33) and raw cabbage used for sauerkraut fermentation (3.75–4.00 log CFU/g) (34). The comparatively higher fungal counts in samples may be attributed to the use of an industrial byproduct as the fermentation substrate. Similar patterns of fungal reduction

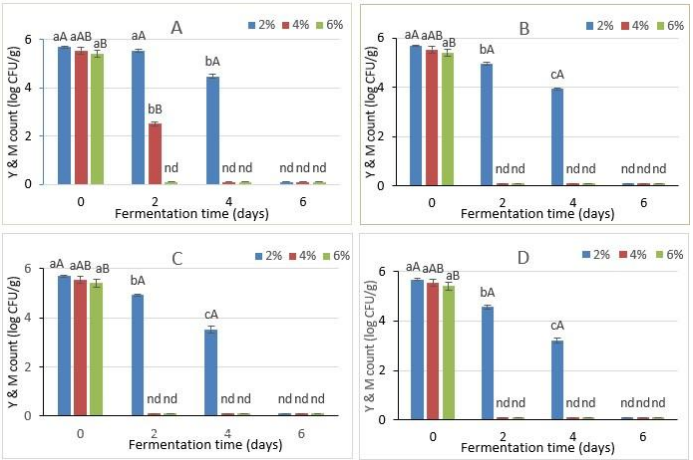

Figure 2. Effect of fermentation time and salt concentration on yeast and mold count (log CFU/g) at different temperatures (A) 25°C, (B) 30°C, (C) 35°C, (D) 40°C (Different lowercase letters indicate a significant difference among fermentation days within the same salt concentration. Different uppercase letters indicate a significant difference among salt concentrations (2%, 4%, 6%) on the same day. nd = not detected.)

have been documented in vegetable fermentations such as sauerkraut, where yeast and mold inhibition occurred after 96 h in 5% brine or 108 h in 2% brine (34), supporting the present observation that both higher salt concentration and fermentation temperature effectively suppress fungal growth. Some researchers have reported that a yeast and mold count of 10^3 CFU/g is the maximum acceptable limit for fermented pickles(35). Accordingly, our samples containing 4%

and 6% salt reached values within the acceptable standard by the second day of fermentation, whereas the 2% salt sample required 6 days to fall within the standard range.

Enterobacteriaceae

Enterobacteriaceae represent a large group of Gram-negative bacteria commonly associated with human diseases. They are predominantly found in the intestinal tract and include genera such as *Salmonella*, *Escherichia*, *Klebsiella*, and *Shigella*. Therefore, monitoring Enterobacteriaceae is a key indicator of food safety (36). In this study, the initial Enterobacteriaceae counts at day 0 were 7.72 ± 0.07, 7.61 ± 0.03, and 7.35 ± 0.09 log CFU/g for samples containing 2%, 4%, and 6% salt, respectively. The significantly lower ($p \leq 0.05$) counts observed on this day at higher salt (6%) concentrations could be attributed to the inhibitory effect of salt on surface microflora (37, 38). By the 5th day of fermentation, Enterobacteriaceae were no longer detected in any of the samples, regardless of salt concentration or fermentation temperature, indicating effective microbial suppression during fermentation. The initial Enterobacteriaceae counts observed in this study were somewhat higher than those reported in other fermented vegetables, which may be related to the use of an industrial byproduct as the substrate. For instance, one study reported counts of 5.0 ± 0.9 log CFU/g in cucumber fermentation (39), while another research observed 6.62 ± 0.07 log CFU/ml (40). In Chinese *Paocai* (fermented radish), study reported 4 log CFU/ml, with complete disappearance of Enterobacteriaceae by day 6 (34). Similarly, in traditional Nepali fermented vegetables such as *gundruk* and *khalpi*, reported that Enterobacteriaceae became undetectable after 8 days and 18 hours of fermentation, respectively (18).

3.2 Effect of fermentation on chemical parameters

pH

During fermentation, the pH showed a declining trend across all salt concentrations and fermentation temperatures. The initial pH of sample was 5.17±0.03, 5.19±0.03 and 5.05±0.02 for 2 %, 4 % and 6 % salt concentration sample, respectively. As fermentation progressed, the rate of pH decline was more pronounced at higher temperature compared to low temperature. Across all temperatures range, 6 % salt sample had the lowest pH. It might be due to higher LAB growth at this salt concentration (Figure 1) and subsequent acidification in high salt concentration sample. The influence of salt concentration and fermentation temperature on pH is displayed in Figure 3.

Salt concentration, fermentation temperature, and their interaction (T × S) all had significant effects on pH ($p<0.05$). At 25 °C, the pH gradually decreased throughout fermentation and stabilized around day 7, irrespective of salt concentration, reaching final values between 3.31 and 3.56. This slower decline can be attributed to the sustained activity of LAB over a longer period. In contrast, at 30 °C and 35 °C, the pH dropped more rapidly and became relatively stable after day 4, coinciding with the peak LAB population. At 30 °C, the minimum pH values recorded for 2%, 4%, and 6% salt concentrations were 3.67 ± 0.02, 3.33 ± 0.02, and 3.23 ± 0.01, respectively, while at 35 °C, the corresponding values were 3.71 ± 0.03, 3.42 ± 0.00, and 3.28 ± 0.01. A rapid pH drop was also observed at 40 °C up to day 2; however, the final pH remained higher than at lower temperatures. This pattern corresponds well with the sharp initial increase in LAB count followed by a rapid decline at 40 °C, indicating thermal and acidic stress on microbial survival. At this temperature, the minimum pH for the 6% salt sample was 3.65 ± 0.02, compared to 4.01 ± 0.02 for the 2% salt sample. The comparison of minimum pH values across different fermentation temperatures revealed that the sample fermented at 40°C exhibited the highest

minimum pH, followed by those fermented at 25°C and 35°C, between which no significant difference was observed (Table 2). In contrast, fermentation at 30°C produced the lowest minimum pH among all conditions tested, suggesting optimal conditions for acidification. Except at 25 °C, all treatments reached pH < 4 within the first three days of fermentation, whereas at 25 °C, this level was attained by day 4. Similar trends have been reported in vegetable fermentation; for example, Xiong et.al. (2016) observed a pH drop to 4 up to 3.5 days in sauerkraut (34), while Liang et.al. (2020) reported a minimum pH in 6% salt *Suancai* after up to days, with pH falling below 4 within 5 days (25). These observations align closely with the acidification pattern observed in the present study.

Table 2: Effect of fermentation temperature on minimum pH value and maximum acidity

No.	Temperature (°C)	Minimum pH observed	Maximum acidity observed (% as Lactic acid)
1.	25	3.31 ± 0.03^{b}	1.14 ± 0.03^{a}
2.	30	3.23 ± 0.01^{c}	1.07 ± 0.04^{a}
3.	35	3.28 ± 0.01^{b}	1.08 ± 0.07^{a}
4.	40	3.65 ± 0.02^{a}	0.80 ± 0.03^{b}

Values are presented as mean ± standard deviation (SD). Different subscript letters within the same column indicate statistically significant difference between the treatments ($p\leq0.05$).

Acidity

Overall, titratable acidity showed an increasing trend and eventually stabilized, indicating an inverse pattern to pH, which decreased and reached a stable point. The stabilization period of acidity closely corresponded to the point at which the pH value became stable (Figure 3). The initial acidity values were 0.06 ± 0.01%, 0.05 ± 0.00%, and 0.06 ± 0.02% as lactic acid at 2 %, 4 % and 6% salt, respectively. Except at 40 °C, all fermentation temperatures showed acidity levels exceeding 1%. When comparing the maximum acidity values obtained at different fermentation temperatures, no significant differences were observed among samples fermented at 25°C, 30°C, and 35°C (Table 2). In contrast, fermentation at 40°C produced a significantly lower acidity value (0.80 ± 0.03%). This reduction in acidity at 40°C is likely attributed to reduced acid production caused by the rapid decline of LAB, which also corresponded with the highest pH values. Regarding salt concentration, at 25 °C, samples with 2% salt consistently showed the highest acidity throughout fermentation. At 30 °C and 35 °C, the 2% salt samples also had higher acidity up to the 4th day compared to other salt levels. On the 4th day, the acidity values for the 2% salt samples were 0.97 ± 0.05% at 30 °C and 0.94 ± 0.02% at 35 °C. Even at 40 °C, the highest acidity was observed on the 4th day with 2% salt, though the overall acidity was lower than at other temperatures.

Mi et.al. (2022) reported a lower range of acidity in radish *paocai* compared to the present study (27). However, similar to our findings, they observed that lower salt concentrations resulted in higher acidity, with a maximum of about 3.75 g/L as lactic acid. However, in their study, acidity continued to increase throughout the 20-day fermentation period. Likewise, a study on fermentation of sauerkraut found that at a low salt concentration (0.5%), both pH and acidity values were the highest in most of their observations, supporting our results (40). Similarly, another recent study investigated the fermentation of *Brassica napus* at salt concentrations ranging from 4% to 9% and found the highest total acidity (2.01 ± 0.01%) at 8% salt, followed by 6% (1.59 ± 0.24%), with the lowest acidity (0.35 ± 0.01%) recorded at 7% (41). A study on table olive fermentation reported that both temperature and salt concentration significantly affected the pH and acidity during fermentation. At 4% salt, the titratable acidity reached 1.2 g at 22°C but only

0.59 g at 30°C. Nevertheless, the final acidity was found to be strongly influenced by the salt concentration (42).

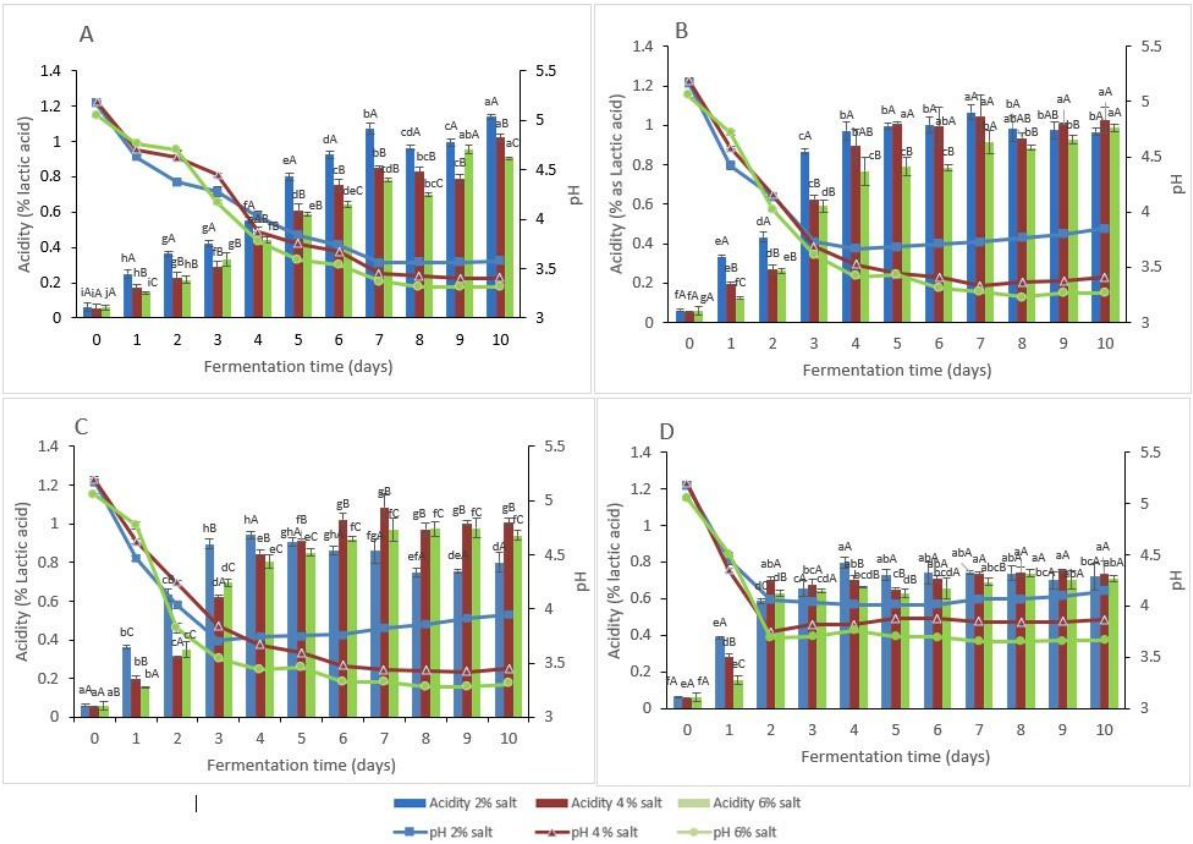

Figure 3: Effect of fermentation time and salt concentration on titratable acidity and pH at different temperatures (A) 25°C, (B) 30°C, (C) 35°C, (D) 40°C (Different lower-case letters indicate a significant difference among different days of fermentation and different capital letters indicate a significant difference between three salt concentration (2 %, 4%, 6%) on the same day. nd=not detected.)

4. Conclusion

This study successfully demonstrates the feasibility of valorizing watermelon rind, a major agricultural by-product, through natural lactic acid fermentation. The findings clearly showed that both salt concentration and fermentation temperature are critical factors governing the microbiological and chemical profile of the final product. A 6% salt concentration was found to be highly favorable for promoting vigorous LAB growth and rapid acidification, particularly at a fermentation temperature of 30°C, which yielded the lowest final pH. All tested fermentation conditions effectively ensured food safety by eliminating Enterobacteriaceae within five days and suppressing yeast and mold populations, with higher temperatures and salt concentrations accelerating their reduction. While the highest LAB count was recorded at 40°C, the subsequent rapid decline led to higher final pH and lower acidity. Relatively lower temperature of fermentation showed a sustained LAB growth, low pH, higher acidity and were found effective in controlling enteric bacteria. This research helps to pave the way for its potential use as a functional food ingredient, contributing to waste reduction and the creation of sustainable food systems in line with the UN Sustainable Development Goals.

Acknowledgement

The authors express their sincere appreciation to Mae Fah Luang University for the provision of laboratory facilities and research support. Appreciation is also extended to Triple J Food and Beverage Co., Ltd., Chiang Rai, Thailand, for kindly providing the samples utilized in this study.

References

1. FAO of United Nations . FAOSTAT: Crop and Livestock Products Rome, Italy: FAO; 2024 [10]. Available from: https://www.fao.org/faostat/en/#data/QCL.
2. Paris HS. Origin and emergence of the sweet dessert watermelon, Citrullus lanatus. Annals of botany. 2015;116(2):133–48.
3. Zia S, Khan MR, Shabbir MA, Aadil RM. An update on functional, nutraceutical and industrial applications of watermelon by-products: A comprehensive review. Trends in Food Science & Technology. 2021;114:275–91.
4. Prokić D, Ćurčić L, Stepanov J, Stojić N, Pucarević M. The role of circular economy in food waste management in fulfilling the United Nations' sustainable development goals. Acta Universitatis Sapientiae, Alimentaria. 2022;15:51–66.
5. Saiharini N and Padmaja A. Studies on nutrient and phytochemical composition and assessment of in vitro antioxidant and enzyme inhibitory properties of watermelon fruit by-products. Annals of Phytomedicine. 2022;11(1):419–25.
6. Asari H and Sugiyanta S. Influence of administering watermelon rind water extract (Citrullus vulgaris Schard) on glucose level of male white rats (Rattus norvegicus) induced with streptozotosin. Folia Medica Indonesiana. 2020;56(3):174–7.
7. Abu-Hiamed H. Hypocholesterolemic effects of watermelon fruit rind on rats. Nutrition & Food Science. 2018;48(5):836–45.
8. Reddy CS, Natarajan P, Nimmakayala P, Hankins GR, Reddy UK. From fruit waste to medical insight: the comprehensive role of watermelon rind extract on renal adenocarcinoma cellular and transcriptomic dynamics. International Journal of Molecular Sciences. 2023;24(21):15615.
9. Sionek B, Szydłowska A, Küçükgöz K, Kołożyn-Krajewska D. Traditional and new microorganisms in lactic acid fermentation of food. Fermentation. 2023;9(12):1019.
10. Akpoghelie PO, Edo GI, Mafe AN, Isoje EF, Igbuku UA, Ali AB, Yousif E, Owheruo JO, Oberhiri Oberhiri S, Essaghah AE. Food, health, and environmental impact of lactic acid bacteria: The superbacteria for posterity. Probiotics and Antimicrobial Proteins. 2025;17(5):2819–55.
11. Nowak A, Śliżewska K, Błasiak J, Libudzisz Z. The influence of Lactobacillus casei DN 114 001 on the activity of faecal enzymes and genotoxicity of faecal water in the presence of heterocyclic aromatic amines. Anaerobe. 2014;30:129–36.
12. Ibrahim SA, Ayivi RD, Zimmerman T, Siddiqui SA, Altemimi AB, Fidan H, Esatbeyoglu T, Bakhshayesh RV. Lactic acid bacteria as antimicrobial agents: Food safety and microbial food spoilage prevention. Foods. 2021;10(12):3131.
13. Vieco-Saiz N, Belguesmia Y, Raspoet R, Auclair E, Gancel F, Kempf I, Drider D. Benefits and inputs from lactic acid bacteria and their bacteriocins as alternatives to antibiotic growth promoters during food-animal production. Frontiers in Microbiology. 2019;10:57.
14. Bousquet J, Anto JM, Czarlewski W, Haahtela T, Fonseca SC, Iaccarino G, Blain H, Vidal A, Sheikh A, Akdis, CA. Cabbage and fermented vegetables: from death rate heterogeneity in countries to candidates for mitigation strategies of severe COVID-19. Allergy. 2021;76(3):735–50.
15. Battcock M, Azam-Ali S. Fermented fruits and vegetables: a global perspective: Food & Agriculture Org.; 1998.

16. Ao O, Es O. Effect of Fermentation on the Proximate Composition of the Epicarp of Watermelon (Citrullus lanatus). International Journal of Swarm Intelligence and Evolutionary Computation. 2016;05(03).
17. Dahal NR, Karki TB, Swamylingappa B, Li Q, Gu G. Traditional foods and beverages of Nepal—a review. Food Reviews International. 2005;21(1):1–25.
18. Tamang B, Tamang JP. In situ fermentation dynamics during production of gundruk and khalpi, ethnic fermented vegetable products of the Himalayas. Indian Journal of Microbiology. 2010;50(Suppl 1):93–8.
19. AOAC. Official Methods of Analysis. 18 ed. Horwitz WL, G.W., editor: AOAC International; 2005.
20. Wierzbicka A, Janiszewska-Turak E. Influence of the salt addition during the fermentation process on the physical and chemical properties of dried yellow beetroot. Applied Sciences. 2024;14(2):524.
21. Fonseca F, Pénicaud C, Tymczyszyn EE, Gómez-Zavaglia A, Passot S. Factors influencing the membrane fluidity and the impact on production of lactic acid bacteria starters. Applied Microbiology & Biotechnology. 2019;103(17):6867–83.
22. Papadimitriou K, Alegría Á, Bron PA, de Angelis M, Gobbetti M, Kleerebezem M, Lemos JA, Linares DM, Ross P, Stanton C, Turroni F, van Sinderen D, Varmanen P, Ventura M, Zúñiga M, Tsakalidou E, Kok J. Stress Physiology of Lactic Acid Bacteria. Microbiol and Molecular Biology Review. 2016;80(3):837–90.
23. Peréz-Dıaz I, Breidt F, Buescher R, Arroyo-López F, Jiménez-Dıaz R, Garrido-Fernández A, Johanningsmeire S. Fermented and acidified vegetables. Compendium of methods for the microbiological examination of foods. 2013:521–32.
24. Tassou C, Panagou E, Katsaboxakis K. Microbiological and physicochemical changes of naturally black olives fermented at different temperatures and NaCl levels in the brines. Food microbiology. 2002;19(6):605–15.
25. Liang H, He Z, Wang X, Song G, Chen H, Lin X, Ji C, Li S. Effects of salt concentration on microbial diversity and volatile compounds during suancai fermentation. Food Microbiology. 2020;91:103537.
26. Stoll DA, Müller A, Meinhardt A-K, Dötsch A, Greiner R, Kulling SE, Huch M. Influence of salt concentration and iodized table salt on the microbiota of fermented cucumbers. Food Microbiology. 2020;92:103552.
27. Mi T, Wang D, Yao S, Yang H, Che Y, Wu C. Effects of salt concentration on the quality and microbial diversity of spontaneously fermented radish paocai. Food Research International. 2022;160:111622.
28. He X, Cui Y, Jia Q, Zhuang Y, Gu Y, Fan X, Ding Y. Response mechanisms of lactic acid bacteria under environmental stress and their application in the food industry. Food Bioscience. 2025;64:105938.
29. Sionek B, Szydłowska A, Trząskowska M, Kołożyn-Krajewska D. The impact of physicochemical conditions on lactic acid bacteria survival in food products. Fermentation. 2024;10(6):298.
30. Serrazanetti DI, Gottardi D, Montanari C, Gianotti A. Dynamic stresses of lactic acid bacteria associated to fermentation processes. Lactic acid bacteria-R & D for food, health and livestock purposes: IntechOpen; 2013.
31. Awuchi CG, Ondari EN, Eseoghene IJ, Twinomuhwezi H, Amagwula IO, Morya S. Fungal growth and mycotoxins production: Types, toxicities, control strategies, and detoxification. Fungal reproduction and growth: IntechOpen; 2021.
32. Di Cagno R, Coda R. Fermented foods: Fermented vegetable products. Encyclopedia of food microbiology: Elsevier Academic Press; 2014. p. 875–83.

33. Swider O, Wojcicki M, Bujak M, Juszczuk-Kubiak E, Szczepanska M, Roszko ML. Time Evolution of Microbial Composition and Metabolic Profile for Biogenic Amines and Free Amino Acids in a Model Cucumber Fermentation System Brined with 0.5% to 5.0% Sodium Chloride. Molecules. 2021;26(19).
34. Xiong T, Li J, Liang F, Wang Y, Guan Q, Xie M. Effects of salt concentration on Chinese sauerkraut fermentation. LWT-Food Science and Technology. 2016;69:169–74.
35. Lozer PE, Leal RMP, de São José JFB. Microbiological and Physical–Chemical Quality of Pickled Vegetables Produced by Rural Family Agribusinesses. Microbiology Research. 2025;16(12):257.
36. Kang E, Crouse A, Chevallier L, Pontier SM, Alzahrani A, Silué N, Campbell-Valois, FX, Montagutelli X, Gruenheid S, Malo D. Enterobacteria and host resistance to infection. Mammalian genome. 2018;29(7):558–76.
37. Bautista-Gallego J, Rantsiou K, Garrido-Fernández A, Cocolin L, Arroyo-López F. Salt reduction in vegetable fermentation: reality or desire? Journal of Food Science. 2013;78(8):R1095–R100.
38. Osaili TM, Alaboudi AR, Al-Quran HN, Al-Nabulsi AA. Decontamination and survival of Enterobacteriaceae on shredded iceberg lettuce during storage. Food Microbiology. 2018;73:129–36.
39. Pérez-Díaz IM, Hayes JS, Medina E, Webber AM, Butz N, Dickey AN, Lu Z, & Azcarate-Peril MA. Assessment of the non-lactic acid bacteria microbiota in fresh cucumbers and commercially fermented cucumber pickles brined with 6% NaCl. Food microbiology. 2019;77:10–20.
40. Yang X, Hu W, Xiu Z, Jiang A, Yang X, Saren G, Ji Y, Guan Y, Feng K. Effect of salt concentration on microbial communities, physicochemical properties and metabolite profile during spontaneous fermentation of Chinese northeast sauerkraut. Journal of Applied Microbiology. 2020;129(6):1458–71.
41. Zhang S, Li C, Wu J, Peng S, Mao H, Wu W, Liao L. Effect of Salt Concentration on Flavor Characteristics and Physicochemical Quality of Pickled Brassica napus. Fermentation. 2023;9(3).
42. Issaoui KE, Senhaji NS, Bouhdid S, Amajoud N, Abrini J, Khay EO. Effects of Lactiplantibacillus plantarum 11 and Chloride Sodium on Biochemical and Microbiological Quality of Table Olives during Fermentation. Journal of Food Quality and Hazards Control. 2022.

O - 291

Characterization of γ-Oryzanol Extracted Using Medium-Chain Triglyceride Oil for Enhanced Stability and Bioactive Delivery

Pinthunicha Premkamon[1], Carol Hutchinson[1], Sakunta Manakla[2], Supathra Lilitchan[1]*

[1]*Department of Nutrition, Faculty of Public Health, Mahidol University, Rachathewi, Bangkok 10400, Thailand*
[2]*Department of Nutrition and Dietetics, Faculty of Science and Technology, Valaya Alongkorn Rajabhat University under the Royal Patronage, Pathumthani, 13180, Thailand*

**Corresponding author E-mail: supathra.lil@mahidol.ac.th*

Abstract: This study investigated the extraction of γ-oryzanol from rice bran (KDML 105) using medium-chain triglyceride (MCT) oil as an edible and environmentally friendly solvent and the subsequent development of the extract into an oleogel as a potential functional ingredient. Extraction of γ-oryzanol from rice bran was performed under various conditions (30–50 °C for 1–9 min), revealing that extraction at 40 °C for 1 min yielded the highest γ-oryzanol content of 4,333.54 µg/g ($p < 0.05$), demonstrating the suitability of MCT oil for rapid extraction of bioactive compounds. The peroxide values (PV) showed that the oleogel phase consistently exhibited lower PV than the liquid oil phase, indicating improved oxidative stability due to the formation of a three-dimensional gel network. Rheological analysis revealed that the structural strength of the oleogels increased with policosanol concentrations (1–9% w/w), confirming the formation of a more reinforced and stable gel network. The oleogels exhibited semi-solid behavior with notable elasticity, supporting their potential as delivery matrices for bioactive compounds. Antioxidant activity measured by the DPPH radical scavenging assay was 88.7–91.0% for the MCT oil and 75.7–78.9% for the oleogel, demonstrating substantial free radical-scavenging potential in both systems. Thus, it has promising potential for various practical applications, either as a cooking oil or as a fat-replacement spread with antioxidant properties. These findings suggest that MCT oil is a promising green solvent for bioactive compound extraction, and the resulting oleogel may serve as a functional ingredient or delivery matrix in food applications.

Keywords: γ-Oryzanol; Medium-Chain Triglyceride; Oleogel; Partial extraction; Delivery matrix

1. Introduction

From a cohort study conducted by the Global Cardiovascular Risk Consortium, the incidence of cardiovascular diseases was reported to be 57.2% in women and 52.6% in men, with a substantial proportion of cases associated with non-HDL cholesterol levels [1]. Oxidative modification of cholesterol has been widely recognized as a key factor contributing to the development of cardiovascular diseases.

Gamma-oryzanol (γ-oryzanol) is an important bioactive compound found in rice bran and has been reported to exhibit antioxidant activity, including the inhibition of cholesterol oxidation [2]. In addition to γ-oryzanol, rice bran contains various antioxidant and bioactive compounds that contribute to health-promoting effects. Saji et al. demonstrated that phenolic extracts from rice bran exhibit significant antioxidant and anti-inflammatory activities [3]. Furthermore, Thoopkrajae et al. reported that rice bran from different rice cultivars possesses high antioxidant capacity and substantial levels of bioactive compounds, highlighting its potential as a functional food ingredient [4]. Rice bran, a by-product of rice milling, accounts for approximately 8–12% of the grain weight, depending on the degree of milling and rice variety [5]. And represents a valuable source of bioactive compounds, particularly γ-oryzanol, which is predominantly concentrated in

the bran layer [6]. Owing to its antioxidant and hypocholesterolemic properties, γ-oryzanol has been reported to play an important role in reducing cardiovascular disease risk [7]. While rice bran bioactive compounds have been reported to support immune-related functions [3,4]. Therefore, effective utilization of rice bran is of considerable importance from both nutritional and economic perspectives.

Currently, the extraction of γ-oryzanol commonly relies on organic solvents such as hexane, petroleum ether, and methanol [8,9]. However, these solvents present several limitations, including toxicity, prolonged extraction times, and the potential presence of residual solvents in the extracts. Previous studies have demonstrated the feasibility of using edible oils as alternative solvents for γ-oryzanol extraction, with extraction efficiency depending on the type of oil employed [10]. To overcome these limitations, the present study investigates the use of MCT oil as an alternative solvent. MCT oil exhibits favorable physicochemical properties, including low viscosity, good oxidative stability, and high solubility for lipophilic compounds, while being safe for consumption [11]. Compared with long-chain triglycerides, MCTs show higher solubilization capacity due to their shorter carbon chain length and greater molecular mobility in lipid systems [12]. In contrast, short-chain fatty acids (SCFAs) are more volatile and less stable, making them less suitable as lipid carriers. Therefore, MCT oil represents a promising green solvent for replacing conventional organic solvents. Furthermore, incorporation of γ-oryzanol extracts into oleogel systems, which are structured lipid systems, may enhance the stability of bioactive compounds and enable controlled release, thereby facilitating their application as functional ingredients in food products [13].

Therefore, this study aims to investigate the extraction of γ-oryzanol from rice bran using MCT oil as an edible and environmentally friendly solvent, as well as to develop the extract into an oleogel system to support its potential application as a functional ingredient in future food products.

2. Materials and Methods

2.1 General

Rice bran samples of the Khao Dawk Mali 105 (KDML105) variety were obtained from the Pathum Thani Rice Research Center, Rice Department, Thailand. Gamma-oryzanol (purity 99%) used as a reference standard was purchased from Tokyo Chemical Industry Co., Ltd. (Tokyo, Japan). Commercial medium-chain triglyceride (MCT) oil was purchased from Bangkok Chemical Company (Thailand), the MCT oil mainly consisted of caprylic acid (C8:0) and capric acid (C10:0), with minor amounts of caproic acid (C6:0) and lauric acid (C12:0). Policosanol was purchased from Xi'an Biof Bio-Technology Co., Ltd. (Shaanxi, China). Monoglyceride (MG) and fully hydrogenated triglyceride (TG), used as stabilizers, were kindly provided by DPO (Thailand) Co., Ltd. (Bangkok, Thailand).

Analytical-grade chemicals and reagents, including ethyl acetate (≥99.5%, AR grade) and glacial acetic acid, were purchased from QReC (New Zealand). Chloroform was purchased from RCI Labscan (Thailand), while potassium iodide and sodium thiosulfate were purchased from Ajax Finechem (Australia). Soluble starch was purchased from KEMAUS (Australia). These chemicals were used for peroxide value determination. DL-α-tocopherol (analytical grade) was used as a reference antioxidant (Brenntag, Germany), while 2,2-diphenyl-1-picrylhydrazyl (DPPH) was purchased from Sigma-Aldrich (St. Louis, MO, USA) and used for antioxidant activity analysis.

2.2 Preparation of oleogel from MCT oil

Oleogels were prepared according to the method described by Prakansamut et al. [14], with slight modifications. Briefly, policosanol (1–9g), monoglycerides (2 g), and triglycerides (3 g) were added to 90–95 g of MCT oil in a 250 mL beaker. The mixture was then heated to 85 °C

under continuous stirring at a speed of 200 rpm for 5 min. After heating, the sample was rapidly cooled using an ice-water bath. Subsequently, the oleogel was stored in a freezer for 1 h and then kept at -20 °C until testing.

2.3 Sample preparation for accelerated thermal oxidation testing

MCT oil and oleogel samples containing γ-oryzanol were subjected to accelerated thermal treatment prior to analysis. The thermal treatment was carried out using a temperature-controlled water bath (LAUDA, model LAUDA Hydro H 20 SW / LAUDA Hydro H 20 SOW). Briefly, 100 mL of each sample was transferred into a 250 mL glass beaker and heated at 80 °C in the water bath to accelerate oxidative reactions. At predetermined heating times (0, 1, 2, 3, and 4 h), approximately 20 mL of the sample was withdrawn and transferred into screw-capped glass bottles. After heating, the samples were cooled to room temperature and stored at −20 °C until further analysis.

2.4 Analysis of γ-oryzanol in rice bran by partial extraction (PE)

Gamma-oryzanol in rice bran was extracted by using the PE method as previously described by Lilitchan et al. [15], with slight modifications. KDML105 Rice bran (1.0 g) was accurately weighed and divided into two test tubes. MCT oil (4 mL and 8 mL) was added to test tubes 1 and 2, respectively. The tubes were tightly sealed, vortex-mixed for 1 min at room temperature, and subsequently placed in a water bath at 30–50 °C for 1–9 min. The mixtures were then centrifuged at 4,000–8,000 rpm for 5 min to remove suspended particles and sediment. The clear supernatant was collected and analyzed for γ-oryzanol content using a UV-visible spectrophotometer at a wavelength of 320 nm, with MCT oil used as the blank. The γ-oryzanol concentration was quantified by comparison with a standard calibration curve prepared from γ-oryzanol dissolved in MCT oil.

2.5 Peroxide value analysis (PV)

Peroxide value (PV) was determined according to the AOCS Official Method Cd 8-53 (2003), with a scaled-down modification based on AOAC (2001). Approximately 2 g of oil sample was accurately weighed and transferred into a 125 mL conical flask. For oleogel samples, the samples were gently heated in a water bath at 60 °C until completely melted and homogenized prior to weighing to ensure accurate measurement. A blank sample without oil was prepared in parallel. A solvent mixture of glacial acetic acid and chloroform (3:2, v/v; 20 mL) was added to the flask, and the mixture was shaken for 1 min. Subsequently, 0.2 mL of saturated potassium iodide (KI) solution was added, and the reaction mixture was kept in the dark for 1 min. Distilled water (30 mL) was then added, and the liberated iodine was titrated with 0.01 N sodium thiosulfate solution until the solution became pale yellow. Starch solution (0.5 mL) was added as an indicator, and titration was continued until the blue color disappeared completely, indicating the endpoint.

2.6 Rheological measurement

Rheological measurements for MCT oil were performed according to the method described by Yalcin et al. [16]. Briefly, steady shear measurements were conducted using a cone-and-plate geometry at a constant temperature of 25 °C. Approximately 12 mL of oil sample was placed between the cone and plate, and the shear rate was increased from 0.1 to 100 s^{-1}. The flow behavior was analyzed using the Newtonian model.

Rheological properties of oleogel samples were determined according to previously reported methods [17,18] using a rheometer (MCR 302e, Anton Paar, Austria). Oscillatory measurements were performed using a parallel-plate geometry (40 mm diameter, 2 mm gap). Prior to rheological measurements, the flow point of the samples was determined to establish an appropriate stress range. Subsequently, the linear viscoelastic region (LVR) was identified by an

amplitude sweep test conducted under strain-controlled conditions over a shear strain range of 0.01–10% at 20 °C. All rheological measurements were performed within the LVR.

2.7 Antioxidant activity analysis (DPPH (2,2-diphenyl-1-picrylhydrazyl) radical scavenging assay)

The free radical-scavenging activity of liquid oil and oleogel samples was evaluated using the DPPH assay was determined according to Gao et al. [19], with slight modifications. Samples (0.5 g) were extracted with ethyl acetate (5 mL) and mixed thoroughly to obtain homogeneous solutions. An aliquot of the extract was then reacted with a 1 mM DPPH solution prepared in ethyl acetate and vortex-mixed to ensure complete interaction. The reaction mixtures were incubated in the dark at room temperature (25 °C) for 2 h to allow radical scavenging to occur.

Absorbance values were measured at 517 nm using a UV-visible spectrophotometer, with ethyl acetate used as the blank. The antioxidant activity was quantified using a calibration curve constructed from DL-α-tocopherol standard solutions prepared in ethyl acetate at concentrations of 1.1, 1.375, 2.2, 2.75, and 5.5 µmol/L. Results were expressed as micromoles of DL-α-tocopherol equivalents per kilogram of sample (µmol TE/kg).

The DPPH radical scavenging activity (%) was calculated according to the following equation:

$$R\ (\%) = [1 - (A_2 - A_3) / A_1] \times 100 \qquad (1)$$

where A_1 is the absorbance of the DPPH solution with solvent, A_2 is the absorbance of the DPPH solution mixed with the sample extract, and A_3 is the absorbance of the sample extract without DPPH.

2.8 Statistical analysis

Results were expressed as mean ± standard deviation of triplicate determinations. All experiments were performed in triplicate. Statistical analyses were performed using one-way analysis of variance (one-way ANOVA) followed by Tukey's honestly significant difference (HSD) test for multiple comparisons. Two-way ANOVA was applied to evaluate the effects of independent variables and their interactions, where appropriate. Regression analysis was conducted to assess the relationships between variables. Differences were considered statistically significant at $P < 0.05$. All statistical analyses were performed using IBM SPSS Statistics version 30 (IBM Corp., Armonk, NY, USA) for Windows.

3. Results & Discussion

3.1 Quantification of γ-oryzanol in rice bran using the partial extraction method

The effect of extraction temperature at a fixed extraction time of 3 min is presented in Table 1. The results showed that γ-oryzanol contents obtained at 30 and 40°C were higher than that at 50°C. However, one-way ANOVA indicated no statistically significant difference among temperatures ($p > 0.05$), suggesting that temperature alone was not a dominant factor under the short extraction time.

Table 1. γ-Oryzanol content in rice bran extracted with MCT oil at different extraction temperatures for 3 min

Temperature (°C)	γ-oryzanol (µg/g)
30	3,668.06 ± 1,370.02
40	3,324.40 ± 599.15
50	1,674.86 ± 692.91

Values are expressed as mean ± SD (n = 3). No significant difference was observed ($p > 0.05$).

When the effect of extraction time was evaluated at 40°C (Figure 1), the highest γ-oryzanol content was observed at an extraction time of 1 min, followed by a decreasing trend with increasing extraction time. Although no statistically significant difference was detected among extraction times ($p > 0.05$), linear regression analysis revealed a negative relationship between extraction time and γ-oryzanol content, indicating that prolonging the extraction time did not enhance extraction efficiency.

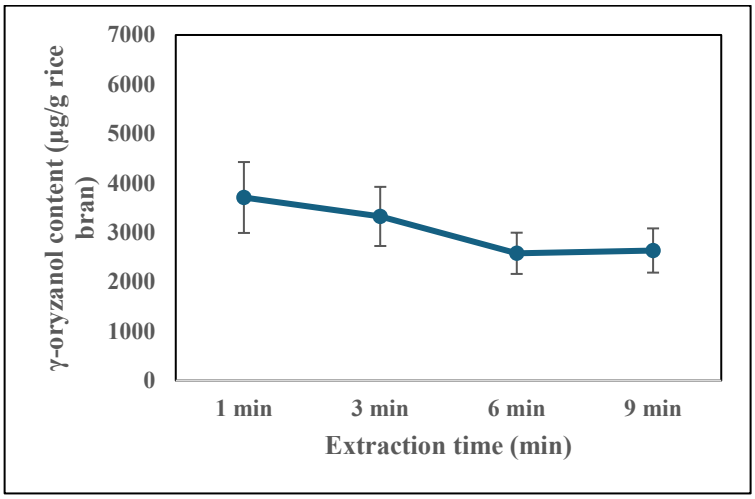

Fig. 1. Effect of extraction time on γ-oryzanol content at 40°C.

To confirm the optimal extraction condition, a confirmatory experiment was conducted at a fixed extraction time of 1 min by comparing extraction temperatures of 30, 40, and 50°C (Table 2). The results demonstrated that temperature significantly affected γ-oryzanol content ($p < 0.05$), with the highest γ-oryzanol yield obtained at 40°C (4,333.54 µg/g). These findings indicate that a moderate extraction temperature combined with a short extraction time is a key factor for enhancing extraction efficiency when MCT oil is used as the solvent.

Table 2. γ-Oryzanol content in rice bran extracted with MCT oil at different extraction temperatures for 1 min

Temperature (°C)	γ-oryzanol (µg/g)
30	1,292.70 ± 536.89[b]
40	4,333.54 ± 1,584.38[a]
50	950.25 ± 267.98[b]

Values are expressed as mean ± SD (n = 3).
Different superscript letters indicate significant differences ($p < 0.05$).

Overall, the results demonstrate that MCT oil is a suitable green solvent for the rapid and efficient extraction of γ-oryzanol from rice bran. The extraction efficiency achieved using MCT oil under mild conditions was comparable to those reported for conventional organic solvents [15]. reported that γ-oryzanol could be effectively extracted from rice bran using organic solvents such as hexane in a partial extraction approach for rapid analysis. The comparable recovery observed in the present study suggests that MCT oil can achieve similar extraction performance while avoiding the use of volatile and potentially hazardous organic solvents. Moreover, the use of an edible solvent such as MCT oil offers advantages for direct incorporation of the extract into structured lipid systems, such as oleogels, enabling further development of functional food ingredients and delivery matrices for bioactive compounds.

3.2 Peroxide Value (PV) of MCT Oil and MCT-Based Oleogel

The peroxide values (PV) of MCT oil and MCT-based oleogel structured with rice bran-derived policosanol (PC) and monoglyceride (MG) at different heating times are presented in Table 3. Under accelerated heating conditions, the PVs of both systems remained relatively low throughout the heating period (0 – 4 h). At all heating times, the oleogel phase consistently exhibited lower PV values than the corresponding MCT oil phase. For example, at 0 h, the PV of MCT oil was 2.31 ± 1.19 meq O_2/kg oil, whereas the oleogel showed a markedly lower PV of 0.37 ± 0.17 meq O_2/kg oil. A similar trend was observed at 1–4 h, where the oleogel maintained lower PV values (0.16 – 0.74 meq O_2/kg oil) compared to MCT oil (0.86 – 2.31 meq O_2/kg oil). And at 4 h, the peroxide value of the oleogel was not detected.

Table 3. Peroxide value (PV) of MCT oil and MCT-based oleogel during heating at 80 °C

Heating time (h)	MCT oil (meq O_2/kg oil)	Oleogel (meq O_2/kg oil)
0	2.31 ± 1.19	0.37 ± 0.17
1	1.25 ± 1.41	0.13 ± 0.18
2	1.60 ± 1.56	0.37 ± 0.18
3	0.86 ± 1.22	0.74 ± 0.21
4	1.47 ± 1.03	0.74 ± 0.01

Values are expressed as mean ± SD (n = 3)

The consistently lower PV observed in the oleogel suggests that oleogelation using PC and MG contributed to improved oxidative stability relative to the liquid oil. This finding is in agreement with previous reports showing that oleogels prepared with PC and MG in triacylglycerol-based oil systems exhibited only slight increases in peroxide value during storage, indicating good oxidative quality of such structured lipid systems [14]. The enhanced oxidative stability of the oleogel can be attributed to the formation of a three-dimensional crystalline network formed by PC and MG molecules, which may restrict oxygen diffusion and reduce the mobility of lipid radicals, thereby retarding the initiation and propagation of lipid oxidation reactions.

In addition, the relatively low PV values observed in both systems are consistent with the inherent oxidative stability of MCT oil, which is mainly composed of saturated medium-chain fatty acids and therefore exhibits lower susceptibility to lipid peroxidation compared with more unsaturated oils [20]. Nevertheless, the consistently lower PV values measured in the oleogel throughout the heating period indicate that the structured network provided by the PC-MG oleogel offered an additional protective effect against peroxide formation under the applied accelerated conditions. It should be noted that the present results are based on descriptive analysis with a limited number of replicates (n = 3) and should therefore be considered preliminary.

3.3 Rheological Properties of MCT Oil and MCT-Based Oleogel

The rheological behavior of liquid MCT oil was first investigated to establish a baseline for comparison. As shown in Figure 2, liquid MCT oil exhibited nearly Newtonian flow behavior, characterized by a linear relationship between shear stress and shear rate and a relatively constant viscosity over the tested shear rate range. This behavior is typical of triglyceride oils lacking a three-dimensional structural network and reflects the low resistance to deformation of the liquid oil (21,22).

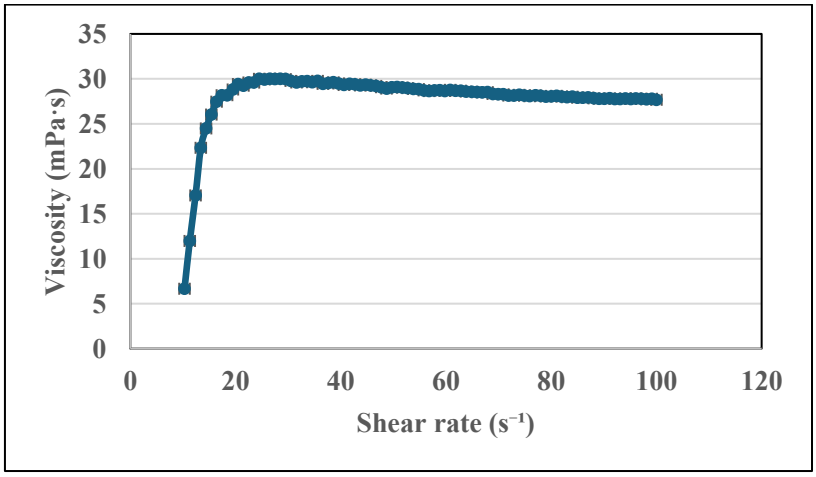

Fig. 2. Apparent viscosity of MCT oil as a function of shear rate measured using a rheometer

In contrast, MCT-based oleogels exhibited pronounced viscoelastic behavior, as evidenced by the dominance of storage modulus (G′) over loss modulus (G″) within the linear viscoelastic region (LVR). Amplitude sweep measurements demonstrated that all oleogel formulations containing different policosanol concentrations (1–9% w/w) displayed elastic-dominated, gel-like behavior, confirming the successful transformation of MCT oil into a semi-solid system through oleogelation (22,23).

Table 4. Storage modulus (G′) of MCT-based oleogels containing different policosanol concentrations

Policosanol (% w/w)	Storage modulus, G′ (Pa)
1%	4,264.83 ± 552.32[a]
3%	5,149.47 ± 554.74[a]
5%	6,505.27 ± 1,247.79[a]
7%	10,481.27 ± 1,507.31[b]
9%	20,878.33 ± 828.27[c]

Values are expressed as mean ± standard deviation (n = 3).
Different superscript letters indicate significant differences according to Tukey's test ($p < 0.05$).
Storage modulus values were obtained from the linear viscoelastic region determined by amplitude sweep measurements.

The rheological results obtained in this study are consistent with previous reports on oleogels structured by crystalline gelators, in which the formation of a three-dimensional network enhances elasticity and mechanical stability compared with liquid oils (21–24). The storage modulus (G′) increased significantly with increasing policosanol concentration (Table 4), confirming the critical role of gelator content in determining oleogel strength (22,24). Statistical

analysis revealed a significant effect of policosanol concentration on G′ ($p < 0.001$), with oleogels containing 7% and 9% policosanol exhibiting significantly higher storage moduli than those formulated with lower concentrations. Overall, the rheological findings agree with the oxidative stability results and support the potential application of MCT-based oleogels as functional semi-solid lipid systems for the delivery of bioactive compounds (23,25).

3.4 Antioxidant capacity assays

Table 5. DPPH radical scavenging activity of liquid MCT oil and MCT-based oleogel during heating at 80 °C

Heating time (h)	MCT oil (%R)	Oleogel (%R)
0	90.85 ± 0.79^{a}	76.70 ± 4.85^{b}
1	90.14 ± 0.17^{a}	75.73 ± 3.64^{b}
2	88.80 ± 2.46^{a}	78.93 ± 3.25^{b}
3	91.00 ± 2.84^{a}	78.54 ± 4.39^{b}
4	88.69 ± 0.44^{a}	75.71 ± 5.94^{b}

Values are expressed as mean ± SD (n = 3).
Different superscript letters within the same row indicate significant differences between sample types at the same heating time ($p < 0.05$).

The antioxidant capacity of MCT oil and MCT-based oleogel subjected to accelerated thermal treatment (0–4 h) was evaluated using the DPPH radical scavenging assay. Two-way ANOVA revealed that the type of lipid system had a significant effect on antioxidant activity ($p < 0.001$), whereas heating time and the interaction between the type of lipid system and heating time had no significant effects ($p > 0.05$), indicating that the antioxidant capacity of both systems remained stable throughout the tested heating period (Table 5).

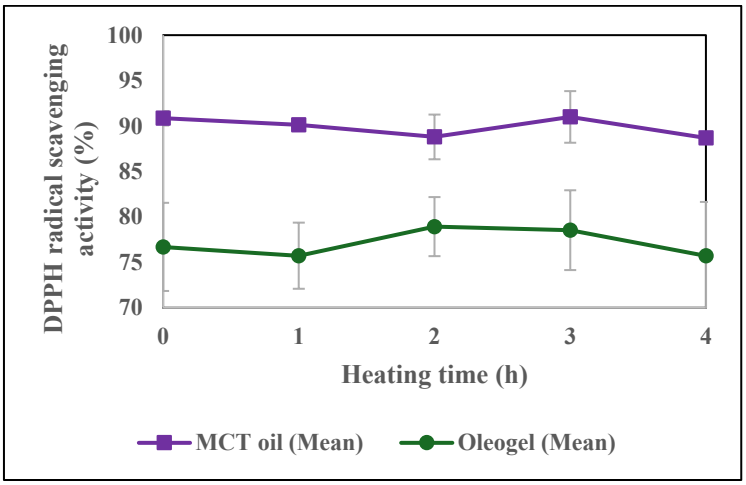

Fig. 3. DPPH radical scavenging activity of MCT oil and MCT-based oleogel during heating at 80 °C

Overall, MCT oil exhibited higher DPPH radical scavenging activity than the MCT-based oleogel, with values ranging from 88.7–91.0% and 75.7–78.9%, respectively (Fig. 3.) . Nevertheless, the oleogel system retained a high level of antioxidant activity, demonstrating that the oleogelation process did not compromise the antioxidant properties of MCT oil. Furthermore, no significant reduction in antioxidant capacity was observed after thermal exposure for up to 4 h,

reflecting the thermal stability of antioxidant compounds within the structured lipid system. Similar observations have been reported in previous studies, where structuring edible oils into oleogel was shown to enhance oxidative stability by limiting molecular mobility and oxygen diffusion within the lipid matrix (26,27).

The absence of a significant heating time effect is consistent with the rheological results, which indicated the formation of an elastic-dominated structure in the MCT-based oleogels. The development of a three-dimensional gel network may restrict molecular mobility within the oil matrix, thereby contributing to the preservation of antioxidant activity during thermal treatment. Overall, these findings support the potential application of MCT-based oleogels as functional semi-solid lipid systems with antioxidant properties, such as cooking oils or fat-replacement spreads, and highlight their suitability as delivery matrices for bioactive compounds.

4. Conclusion

This study demonstrated that medium-chain triglyceride (MCT) oil is an effective green solvent for the extraction of γ-oryzanol from rice bran (KDML 105). Extraction at 40 °C for 1 min yielded the highest γ-oryzanol content (4,333.54 μg/g, $p < 0.05$), indicating that mild extraction conditions are sufficient for efficient bioactive compound recovery. The extracted γ-oryzanol was successfully developed into oleogels using MCT oil in combination with policosanol, monoglycerides, and triglycerides. Rheological analysis confirmed the formation of semi-solid oleogels with pronounced elastic behavior, as evidenced by a significant increase in storage modulus (G′) when policosanol concentration increased from 1% to 9% (w/w) ($p < 0.001$). Under accelerated thermal conditions, the oleogels exhibited lower peroxide values than MCT oil, reflecting improved oxidative stability. In addition, DPPH radical scavenging activity of both MCT oil (88.7–91.0%) and oleogels (75.7–78.9%) remained stable throughout the heating period, with no significant effect of heating time ($p > 0.05$). These findings highlight the potential of MCT-based oleogels as functional lipid systems for delivery matrix and food applications.

Acknowledgements

This research project was financially supported by Mahidol University under the Fundamental Fund: Fiscal year 2024, funded by National Science Research and Innovation Fund (NSRF), Thailand (Project No. FF-138/2567). In addition, the presentation of this work was supported by the Faculty of Graduate Studies, Mahidol University.

References

1. Global Cardiovascular Risk Consortium. Global effect of modifiable risk factors on cardiovascular disease and mortality. N Engl J Med. 2023;389(14):1273–1285.
2. Xu Z, Hua N, Godber JS. Antioxidant activity of tocopherols, tocotrienols, and γ-oryzanol components from rice bran against cholesterol oxidation accelerated by 2,2′-azobis-(2-methylpropionamidine) dihydrochloride. J Agric Food Chem. 2001;49:2077–2081.
3. Saji N, Francis N, Schwarz LJ, Blanchard CL, Santhakumar AB. The antioxidant and anti-inflammatory properties of rice bran phenolic extracts. Foods. 2020;9(6):829.
4. Thoopkrajae S, Wisetkomolmat W, Wongsingha N, et al. Comparative analysis of nutritional components and antioxidant capacity of rice bran from different cultivars. Front Nutr. 2022;9:833730.
5. Zhang Y, Li X, Wang Q, Chen J, Liu H. Fermentation of rice milling by-products can completely replace soybean meal in the diet of *Oreochromis niloticus* fingerlings. Front Mar Sci. 2025;12:1718289.
6. Moongngarm A, Daomukda N, Khumpika S. Chemical compositions, phytochemicals, and antioxidant capacity of rice bran, rice bran layer, and rice germ. APCBEE Procedia. 2012;2:73–79.

7. Rong N, Ausman LM, Nicolosi RJ. Rice bran oil decreases total and LDL cholesterol in humans with hypercholesterolemia. J Nutr. 1997;127(3):509–514.
8. Gopala Krishna AG, Khatoon S, Shiela PM, Sarmandal CV, Indira TN, Mishra A. Effect of refining of crude rice bran oil on the retention of oryzanol in the refined oil. J Am Oil Chem Soc. 2001;78(2):127–131.
9. Lerma-García MJ, Herrero-Martínez JM, Simó-Alfonso EF. Composition, industrial processing and applications of rice bran γ-oryzanol. Food Chem. 2009;115(2):389–404.
10. Yi B, Kim MJ. Extraction of γ-oryzanol from rice bran using diverse edible oils: enhancement in oxidative stability of oils. Food Sci Biotechnol. 2020;29:393–399.
11. Duranova H, Kuzelova L, Fialkova V, et al. Coconut-sourced MCT oil: its potential health benefits beyond traditional coconut oil. Phytochem Rev. 2025;24:659–700.
12. Zulfakar MH, Pubadi H, Ibrahim SI, Hairul NM. Medium-chain triacylglycerols (MCTs) and their fractions in drug delivery systems: a systematic review. J Oleo Sci. 2024;73(3):293–310.
13. Pandolsook S, Kupongsak S. Storage stability of bleached rice bran wax organogels and water-in-oil emulsions. Food Meas. 2019;13:431–443.
14. Prakansamut N, Adulpadungsak K, Sonwai S, Aryusuk K, Lilitchan S. Application of functional oil blend-based oleogels as novel structured oil alternatives in chocolate spread. LWT Food Sci Technol. 2024;203:116322.
15. Lilitchan S, Tangprawat C, Aryusuk K, Krisnangkura S, Chokmoh S, Krisnangkura K. Partial extraction method for the rapid analysis of total lipids and c-oryzanol contents in rice bran. Food Chem. 2008;106:752–759.
16. Yalcin H, Toker OS, Dogan M. Effect of oil type and fatty acid composition on dynamic and steady shear rheology of vegetable oils. J Oleo Sci. 2012;61(4):181–187.
17. Fayaz G, Polenghi O, Giardina A, Cerne V, Calligaris S. Structural and rheological properties of medium-chain triacylglyceride oleogels. Int J Food Sci Technol. 2021;56(2):1040–1047.
18. Jadhav HB, Pratap AP, Gogate PR, Annapure US. Ultrasound-assisted synthesis of highly stable MCT-based oleogel and evaluation of its baking performance. Appl Food Res. 2022;2:100156.
19. Gao P, Liu Y, Wang S, Huang C, Zhong W, Yin J, et al. Effects of different oleogelators on the structural properties and composition of iron walnut-oil oleogels. Ultrason Sonochem. 2024;102:106729.
20. Amft J, Bauer JL, Rostek J, Spielvogel S, Döring F, Schwarz K. Use of medium-chain triglycerides as low-oxidizable lipid systems. Eur J Lipid Sci Technol. 2020;122:1900350.
21. Hwang HS, Kim S, Singh M, Winkler-Moser JK, Liu SX. Organogelation of edible oils with long-chain fatty alcohols. Food Res Int. 2012;48(1):305–311.
22. Dassanayake LSK, Kodali DR, Ueno S, Sato K. Physical properties of rice bran wax in bulk and organogels. J Am Oil Chem Soc. 2009;86(12):1163–1173.
23. Lim J, Jeong S, Oh IK, Lee S. Rheological, structural, and thermal properties of medium-chain triglyceride oil oleogels structured with natural waxes. Food Struct. 2017;12:1–9.
24. Toro-Vazquez JF, Morales-Rueda JA, Dibildox-Alvarado E, Charó-Alonso MA, Alonzo-Macias M, González-Chávez MM. Thermal and textural properties of organogels developed by candelilla wax in safflower oil. J Am Oil Chem Soc. 2007;84(11):989–1000.

25. Ogutcu M, Yilmaz E. Oleogels of virgin olive oil with carnauba wax and monoglyceride as spreadable products. Food Chem. 2014;165:329–336.
26. Calligaris S, Manzocco L, Anese M, Nicoli MC. Effect of oil structure on oxidation kinetics of sunflower oil. Food Chem. 2013;141(4):3940–3947.
27. Panagiotopoulou E, Moschakis T, Katsanidis E. Sunflower oil organogels and their oxidative stability. LWT Food Sci Technol. 2016;73:653–660.

O - 310

Comparative Effects of Drying Techniques on Bioactive Composition and Techno-Functional Properties of Kai (*Cladophora glomerata*)

Yonn Pwint Phyu[1], Shankar Neupane[1], Nattaya Konsue[1,2]*

[1]*Food Science and Technology Program, School of Agro-Industry, Mae Fah Luang University, Chiang Rai 57100, Thailand*
[2]*Research Centre of Innovative Food Packing and Biomaterials, Mae Fah Luang University, Chiang Rai 57100, Thailand*

**Corresponding author E-mail: nattaya.kon@mfu.ac.th*

Abstract: The freshwater macroalga Kai (*Cladophora glomerata*) is a nutrient-rich, sustainable source of bioactive compounds with potential as a functional food ingredient. This study systematically evaluated the effects of freeze-drying (FD), tray drying (TD), and sun drying (SuD) on the bioactive composition, microstructure, and functional properties of Kai powder for future food applications. Drying method significantly ($p < 0.05$) influenced powder characteristics. TD yielded the highest chlorophyll (4.41 mg·g^{-1}) and total flavonoids (6.60 mg QE·g^{-1}) content, as well as antioxidant activity (FRAP: 20.86 mmol Fe^{2+}·g^{-1}), whereas SuD had the highest total phenolic content (1.13 mg GAE·g^{-1}). Mineral analysis demonstrated that all powders were rich in essential elements, with heavy metal concentrations below safety limits. Techno-functional properties varied with drying method: SuD exhibited the highest water holding capacity (14.95 g water·g^{-1} powder), whereas TD had the greatest swelling capacity (25.50 mL·g^{-1}); nonetheless, all powders displayed poor flowability (Carr's index >30%). The highest initial foaming capacity (44.6%) was observed in TD samples, but the foam collapsed rapidly, whereas FD (42.9%) and SuD powders (27.4%) maintained foam more effectively over time. FD showed structural integrity, as evidenced by SEM and FTIR analyses, resulting in superior emulsifying capacity (63.33%) and emulsion stability (86.61%). In conclusion, drying method can strategically modulate Kai algae functionality: FD is optimal for structure-sensitive and emulsification applications, TD enhances color and flavonoid-based antioxidant content, and SuD maximizes phenolic-related functionality. This study provides a clear framework for developing Kai algae powders as natural, nutrient- and bioactive-rich ingredients for functional foods and nutraceuticals, supporting the sustainable utilization of freshwater macroalgae in the food industry.

Keywords: Kai Algae; Drying Methods; Bioactive Compounds; Techno-functional Properties

1. Introduction

Global food demand is projected to rise to 60% by 2050, while climate change is expected to limit the cultivation of traditional crops. This drives the need for efficient, nutrient-rich ingredients for food and supplements (1, 2). Freshwater algae are promising candidates because they offer high nutritional and bioactive density with low land and input requirements. Nonetheless, most research and commercialization have focused on marine algae and microalgae, so freshwater macroalgae remain comparatively underutilized (3, 4).

Cladophora glomerata, a filamentous green macroalga (Chlorophyta) forming dense riverine mats, is traditionally consumed in northern Thailand as "Kai," as well as Laos, France and Hawaii (5). It is rich in minerals and fiber, with moderate protein and carbohydrates that vary with environmental conditions and analytical methods (6). Kai also contains polyunsaturated fatty acids

and exhibits antioxidants, gastroprotective, and other bioactivities, indicating potential as a multifunctional food ingredient (7, 8).

Due to its high initial moisture content, Kai must be dehydrated to ensure microbial stability, extend its shelf life, and enable its incorporation as a powder. Drying not only preserves the biomass but also restructures it, influencing pigment, phenolic, lipid, and protein retention, as well as microstructural features controlling hydration, rheology, and interfacial behavior (9, 10, 11). Sun drying, tray drying, and freeze drying are widely applied to algal and plant materials, yet studies in other matrices show diverse and contrasting effects on bioactive retention, color, and techno-functional performance, depending on species, composition, and process conditions (12, 13, 14).

Although several studies have described the nutritional composition of Kai, the impacts of different drying techniques on its nutritional quality, microstructure, and techno-functional properties are still poorly characterized. This study therefore evaluated the effects of sun drying, tray drying, and freeze drying on the bioactive composition, mineral safety, microstructural features, and functional performance of Kai powder, with the aim of identifying drying conditions that can be strategically selected for different food applications.

2. Materials and Methods

2.1 Materials preparation and drying procedure

Fresh Kai algae harvested from the Nan River were transported to the laboratory within 24 h under controlled temperature (5 °C). Upon arrival, visible impurities, including sand, stones, and foreign materials were removed. The samples were washed twice with tap water, drained, and cut into uniform pieces (~10 cm) to ensure consistent drying behavior. Clean, size-standardized Kai samples were subjected to three drying methods: sun drying (SuD), tray drying (TD), and freeze-drying (FD). For SuD, Kai strands were arranged in a single layer on mesh trays and dried under direct sunlight to a constant weight. For TD, samples were spread as a 1 cm-thick layer on stainless-steel trays and dried in a hot-air tray dryer (Kluay Nam Thai Towop, Thailand) at 50 °C for 6 h. For FD, samples were frozen at −18 °C for 24 h and subsequently lyophilized in a freeze dryer (Alpha 3–4 LSC basic, Germany) at 0.1 mbar for 90 h, with the condenser temperature maintained at −70 °C. Dried samples were ground, passed through a 100-mesh sieve, vacuum-packed, and stored at −18 °C until further analysis.

2.2 Sample extraction

Extractions were carried out following Konsue et al. (15) with minor modifications. One gram of sample was mixed with 10 mL of 80% methanol in a 50 mL centrifuge tube, sonicated for 30 min at room temperature, and centrifuged at 14,000 rpm for 15 min at 4 °C. The supernatant was collected, and the residue was re-extracted under the same conditions. The combined supernatants were filtered through Whatman No. 1 filter paper, adjusted to 40 mL with 80% methanol, and used for the determination of phytochemical and antioxidant activities.

2.3 Chemical characteristics

2.3.1 Proximate composition

The proximate composition was determined according to AOAC methods. Moisture content was measured by oven drying (AOAC 950.46), ash by dry ashing at 550 °C (AOAC 920.15), crude protein by the Kjeldahl method using a nitrogen conversion factor of 6.25 (AOAC 954.01), crude fat by Soxhlet extraction with petroleum ether (AOAC 960.39), crude fiber by acid–alkali digestion (AOAC 991.43) and carbohydrate by calculating difference which may reflect cumulative errors from other components.

2.3.2 Mineral content

Mineral composition was analyzed following Nandang et al. (16) with slight modifications. 0.3 g sample was digested with concentrated HNO_3 and H_2O_2 using a microwave digestion system, diluted to 50 mL with double-distilled water, and analyzed alongside a blank prepared by same conditions. Macro- and micro-minerals and selected heavy metals were quantified by ICP-MS/MS, and results were expressed as $mg \cdot kg^{-1}$ dry weight.

2.3.3 Chlorophyll content

Chlorophyll a and b contents were determined according to Nandang et al. (16) with modifications. Samples (100 mg) were mixed with 10 mL acetone, stored at 4 °C for 30 min, then centrifuged (3000 rpm, 10 min, 4 °C). Absorbance of supernatants was measured at 663 nm and 646 nm. Chlorophyll contents were calculated using Equations (1) and (2) and contents were expressed as $mg \cdot g^{-1}$ sample after volume and weight corrections.

$$\text{Chl a } (mg \cdot L^{-1}) = (12.25 \times Abs_{663}) - (2.79 \times Abs_{646}) \quad (1)$$

$$\text{Chl b } (mg \cdot L^{-1}) = (21.5 \times Abs_{646}) - (5.10 \times Abs_{663}) \quad (2)$$

2.4 Phytochemical and antioxidant activities

2.4.1 Total phenolic content

Total phenolic content (TPC) was determined using the Folin–Ciocalteu method (ISO 14502-1, 2005). Extract (25 µL) was mixed with 125 µL of 10% (v/v) Folin–Ciocalteu reagent and 100 µL of 7.5% (w/v) Na_2CO_3, incubated 60 min in the dark and absorbance was measured at 765 nm. Gallic acid was used for calibration, and results were expressed as mg gallic acid equivalents (GAE) per g dry weight.

2.4.2 Total flavonoid content

TFC was measured following the colorimetric method of Christ–Müller, as described by Hu et al (17) and Korzeniowska et al (18), with slight modifications. Briefly, 0.5 mL of extract was mixed with 150 µL of 5% $NaNO_2$ and 2.2ml of DI water. After 5 min, 150 µL of 10% $AlCl_3$ was added, and the mixture was kept in the dark for 5 min and then 0.5 mL of 1 M NaOH was added. After 10 min, absorbance was measured at 415 nm. Quercetin was used as the standard, and results were expressed as mg quercetin equivalents (QE) per g dry weight.

2.4.3 DPPH radical scavenging activity

DPPH (2,2-diphenyl-1-picrylhydrazyl) radical-scavenging activity was determined using a modified ISO 14502-1:2005 method. A 50 µL aliquot of extract was mixed with 1.95 mL of 0.06 mM DPPH solution in methanol and incubated for 30 min in the dark at room temperature. Absorbance was measured at 517 nm using methanol as the blank, with Trolox as the standard, and results were expressed as mg Trolox equivalents (TE) per g dry weight.

2.4.4 ABTS radical scavenging activity

ABTS radical-scavenging activity was determined following Re et al. (19) with minor modifications. The $ABTS^+$ working solution was prepared by reacting 7 mM ABTS with 2.45 mM $K_2S_2O_8$ and incubating the mixture in the dark at room temperature for ≥16 h, then diluted with ethanol to an absorbance of 0.70 ± 0.02 at 734 nm. For the assay, 60 µL of extract was mixed with 240 µL of the diluted $ABTS^+$ solution, reacted for 6 min, and the absorbance was measured at 734 nm. Trolox was used as the standard, and results were expressed as mg Trolox equivalents (TE) per g dry weight.

2.4.5 Ferric reducing antioxidant potential

The ferric reducing antioxidant potential (FRAP) was quantified according to the standardized methodology developed by Benzie & Strain (20). A volume of 400 µL extract was mixed with 2.6 mL of freshly prepared FRAP reagent (300 mM acetate buffer pH 3.6, 10 mM TPTZ in 40 mM HCl, and 20 mM $FeCl_3 \cdot 6H_2O$ in a 10:1:1 ratio). After incubation at 37 °C for 30 min in the dark, absorbance was measured at 595 nm. A standard curve was prepared using $FeSO_4 \cdot 7H_2O$, and results were expressed as mmol Fe^{2+} equivalents per g dry weight.

2.5 Physical properties determination

2.5.1 Color

The surface color of Kai powders was measured using a HunterLab colorimeter in the CIE L*ab** system, calibrated with a standard white tile (L* = 93.80, a* = −0.82, b* = 0.91). Measurements were performed under D65 illumination with a 10° standard observer. The instrument recorded L* (lightness), a* (green [−] to red [+]), and b* (blue [−] to yellow [+]) values. Chroma (C*), hue angle (h°), and total color difference (ΔE) were calculated from these coordinates according to Armesto et al. (21) by Equations (3, 4 and 5).

$$H° = 180° + \text{ArcTan}\left(\frac{b^*}{a^*}\right) \quad \text{(for a*<0 and b*>0)} \quad (3)$$

$$C^* = \sqrt{a^{*2} + b^{*2}} \quad (4)$$

$$\Delta E^*_{AB} = \sqrt{(L^*_2 - L^*_1)^2 + (a^*_2 - a^*_1)^2 + (b^*_2 - b^*_1)^2} \quad (5)$$

Where, L1*, a1*, and b1* are control (FD) values, L2*, a2*, and b2* are the values of the samples subjected to different treatments.

2.5.2 Water activity

Water activity (aw) was measured using a water activity meter (2108018, Novasina AG, Lachen, Switzerland). After calibration, an appropriate amount of sample was placed in the sample cup, inserted into the measurement chamber, and the reading was recorded.

2.6 Techno-functional properties determination

2.6.1 Water holding capacity (WHC) and Oil Holding Capacity (OHC)

Water-holding capacity and oil-holding capacity were determined according to Zhao et al. (22) with minor modifications. Briefly, 0.10 g of Kai sample was mixed with 10 mL of distilled water (WHC) or 5 g of corn oil (OHC), vortexed at high speed for 30 s, and allowed to stand at room temperature for 1 h. The mixtures were then centrifuged at 10,000 rpm for 10 min, the supernatants decanted by inverting the tubes for 2 min, and the tubes reweighed. WHC and OHC were calculated as grams of water or oil retained per gram of dry sample ($g \cdot g^{-1}$) using Equations (6) and (7).

$$\text{WHC}\left(\frac{g}{g\ DW}\right) = \frac{\text{Sample weight after Holding Water} - \text{Dry Weight of Sample}}{\text{Dry weight of Sample}} \quad (6)$$

$$\text{OHC}\left(\frac{g}{g\ DW}\right) = \frac{\text{Sample weight after holding oil} - \text{Dry weight of Sample}}{\text{Dry weight of Sample}} \quad (7)$$

2.6.2 Swelling capacity (SC)

Swelling capacity was determined according to Zhao et al. (22). Briefly, 0.2 g of sample was placed in a 15 mL graduated cylinder, mixed with 10 mL of distilled water, stirred, and incubated at room temperature for 24 h. SC was calculated using Equation (8).

$$\text{SC}\left(\frac{mL}{gDW}\right) = \frac{\text{Final Volume of Sample} - \text{Initial Volume of Sample}}{\text{Dry Weight of Sample}} \quad (8)$$

2.6.3 Foaming capacity (FC) and foam stability (FS)

Foaming capacity and foam stability were determined following Lamsal et al. (23) with minor modifications. Briefly, 100 mg of Kai powder was dispersed in 10 mL of distilled water and homogenized at maximum speed using an IKA RW 20 digital homogenizer for 5 min. The dispersion was immediately transferred to a 100 mL graduated cylinder, and the total volume (liquid + foam) was recorded to calculate foaming capacity (FC) using Equation (9).

$$\text{FC}\ (\%) = \frac{\text{Volume After Whipping}}{\text{Volume Before Whipping}} \times 100 \qquad (9)$$

Foam stability (FS) was evaluated by recording the foam volume at 10, 20, 30, 40, 50, 60, 70, 80, and 90 min after homogenization. The remaining foam was expressed as a percentage of the initial foam volume and calculated using Equation (10).

$$\text{FS}\ (\%) = \frac{\text{Volume After Standing} - \text{Volume Before Whipping}}{\text{Volume Before Whipping}} \times 100 \qquad (10)$$

2.6.4 Emulsifying capacity (EC) and stability (ES)

Emulsifying capacity (EC) and emulsion stability (ES) were determined according to Lamsal et al. (23) with minor modifications. Briefly, 200 mg of sample was suspended in 10 mL of distilled water and 10 mL of soybean oil, homogenized at 10,000 rpm for 1 min, and the height of the emulsion layer was recorded. The mixture was then centrifuged at 1300 rcf for 5 min, and EC was calculated using Equation (11).

$$\text{EC}\ (\%) = \frac{\text{Height of Emulsified Layer after Centrifugation(cm)}}{\text{Initial Emulsion Height}}\ \text{x}100 \qquad (11)$$

Emulsion stability (ES) was determined by heating the emulsion at 80 °C for 30 min in a water bath, followed by cooling under running water for 30 min and centrifugation under the same conditions as described above. ES was calculated using Equation (12).

$$\text{ES}\ (\%) = \frac{\text{Height of Emulsified Layer after Heating}}{\text{Height of Emulsified Layer before Heating}}\ \text{x}100 \qquad (12)$$

2.6.5 Loose and tapped bulk density, Carr's index and Hausner ratio

Loose and tapped bulk densities of samples were determined using a modified method based on Pugliese et al. (24). A known mass of powder was gently poured into a pre-weighed graduated cylinder without vibration to obtain the unsettled volume, which was used to calculate loose bulk density ($g \cdot cm^{-3}$). The cylinder was then repeatedly tapped until no further volume change occurred, and the final volume was recorded to calculate tapped bulk density ($g \cdot cm^{-3}$). Carr's compressibility index (CI) and Hausner ratio (HR) were calculated from loose and tapped densities to assess powder flowability using Equations (13) and (14).

$$\text{CI} = \frac{\text{Tapped Density} - \text{Loose Density}}{\text{Tapped Density}} \times 100 \qquad (13)$$

$$\text{HR} = \frac{\text{Tapped Density}}{\text{Loose Density}} \qquad (14)$$

2.7 Determination of microstructure (SEM)

Microstructural analysis was conducted using a scanning electron microscope (SEM; TESCAN MIRA, TESCAN ORSAY HOLDING, Brno, Czech Republic). Samples were cut into small pieces (~5 mm^2), mounted on aluminum stubs with double-sided conductive carbon tape, and sputter-coated with gold for 45 s (Quorum SC7620, Quorum Technologies Ltd., East Sussex, UK) to improve conductivity. Imaging was performed at magnifications of 150×, 300×, and 1000× using an accelerating voltage of 5 kV.

2.8 Fourier transform infrared spectroscopy

Dried Kai powders were homogenized with spectroscopic-grade KBr using a mortar and pestle and pressed into translucent pellets (~1 mm thick). FTIR spectra were recorded at room temperature over the range of 4000–400 cm^{-1}.

2.9 Statistical analysis

All experiments were conducted in triplicate using independent samples. Data were expressed as mean ± standard deviation. Statistical differences were analyzed using one-way analysis of variance followed by Duncan's Multiple Range Test to determine significant differences between drying methods. All analyses were performed using SPSS software, with significance defined at $p < 0.05$.

3. Results & Discussion

3.1 Composition and nutritional characteristics

Drying method significantly affected the proximate and mineral composition of Kai (Table 1). Moisture was lowest in FD and TD and highest in SuD, indicating less efficient dehydration under ambient conditions, while ash was the dominant component in all samples and was slightly higher in FD and TD than in SuD, consistent with reports for *Cladophora* from other regions (25). Protein content was highest in TD samples (13.95%), while FD and SuD showed comparable levels (11.21–11.46%). This trend is consistent with reports on *Kappaphycus alvarezii* and *Sargassum polycystum*, in which convective drying resulted in higher apparent protein levels due to solid-phase concentration and enhanced nitrogen accessibility after thermal denaturation (26). FD retained the highest crude fiber content (25.95%), whereas SuD and TD showed slightly lower values, suggesting that low-temperature sublimation better preserves structural polysaccharides (9). Fat and carbohydrate contents were relatively low in all samples; SuD exhibited the highest fat (2.95%) and carbohydrate (18.58%), while TD had the lowest carbohydrate, which may reflect partial thermal and oxidative degradation of labile carbohydrates at tray-drying conditions, combined with a concentration effect on protein and ash (9, 26).

Minerals were abundant across treatments; SuD exhibited higher Na and Fe contents, likely due to concentration effects from prolonged moisture loss and possible deposition of environmental particulates during open-air drying, while TD showed the highest Ca and Mg. Mn levels were high in all samples, comparable with values reported for *Cladophora* from other regions where these elements predominate (27). For micro-minerals, FD preserved the highest Zn , TD the highest Cu, while SuD generally increased Co, Ni, Cr and V, indicating that each drying method slightly shifts the trace-element pattern while maintaining overall abundance (12, 26). Heavy metals remained below EU limits (As ≤1.68, Cd ≤0.027, Pb ≤0.339, Hg ≤0.021 $mg \cdot kg^{-1}$), confirming safety (28).

Table 1. Composition and nutritional characteristics of Kai samples

Component	FD	SuD	TD
Proximate composition (%)			
Moisture	5.20 ± 0.08[b]	6.65 ± 0.17[a]	5.40 ± 0.13[b]
Ash	38.26 ± 0.06[a]	35.75 ± 0.05[b]	38.34 ± 0.16[a]
Protein	11.21 ± 0.20[b]	11.46 ± 0.08[b]	13.95 ± 0.27[a]
Fiber	25.95 ± 0.89[a]	24.61 ± 0.07[b]	24.76 ± 0.02[b]
Fat	2.23 ± 0.09[b]	2.95 ± 0.15[a]	2.30 ± 0.11[b]
Carbohydrate	17.15 ± 0.73[b]	18.58 ± 0.24[a]	15.26 ± 0.46[c]
Macro-minerals			
Na	777.55 ± 73.02[b]	1401.32 ± 31.22[a]	792.92 ± 25.74[b]
Ca	1806.80 ± 152.86[b]	1880.33 ± 58.68[ab]	2017.73 ± 62.38[a]
Mg	762.75 ± 87.39[b]	861.44 ± 35.98[ab]	939.89 ± 17.34[a]
Fe	123.87 ± 15.11[b]	208.05 ± 6.39[a]	133.73 ± 5.40[b]
Mn	1105.84 ± 100.08[a]	1184.91 ± 19.08[a]	819.98 ± 31.37[b]
Micro-minerals			
Zn	13.97 ± 1.30[a]	8.75 ± 0.49[c]	11.66 ± 0.55[b]
Cu	1.60 ± 0.16[b]	1.47 ± 0.05[b]	2.21 ± 0.09[a]
Co	0.59 ± 0.05[b]	0.87 ± 0.01[a]	0.59 ± 0.02[b]
Ni	0.09 ± 0.01[b]	0.15 ± 0.02[a]	0.14 ± 0.018[a]
Cr	0.27 ± 0.03[c]	0.80 ± 0.04[a]	0.43 ± 0.04[b]
V	1.44 ± 0.04[b]	3.47 ± 0.35[a]	1.33 ± 0.05[b]
Heavy Metal			
As	0.868 ± 0.082[b]	1.676 ± 0.597[a]	0.651 ± 0.020[b]
Cd	0.027 ± 0.003[a]	0.026 ± 0.001[a]	0.023 ± 0.001[a]
Pb	0.149 ± 0.013[b]	0.339 ± 0.005[a]	0.157 ± 0.007[b]
Hg	0.021 ± 0.003[b]	0.016 ± 0.002[b]	0.011 ± 0.003[a]

Values are presented as mean ± standard deviation (SD). Different superscript letters within the same row indicate statistically significant differences between treatments ($p < 0.05$). Carbohydrate calculated by difference; values may reflect cumulative errors from other proximate components. Mineral contents are expressed as $mg \cdot kg^{-1}$ dry weight

3.2 Phytochemical composition and antioxidant properties

The drying method significantly affected the phytochemical composition and antioxidant activity of Kai powder ($p < 0.05$) (Figure1). TPC was highest in SuD (1.13 mg GAE.g^{-1}), followed by FD and TD, possibly due to improved extractability during prolonged drying, although oxidative and concentration effects may also occur, whereas the lower TPC in TD likely reflects partial degradation of heat-labile compounds (12, 29). Conversely, TFC was highest in TD (6.60 mg QE$\cdot g^{-1}$), followed by SuD and FD, indicating greater thermal stability of flavonoids and improved extractability under controlled convective drying (29). These compositional shifts were reflected in antioxidant assays: SuD showed the highest DPPH radical-scavenging activity (3.12 mg TEg^{-1}), in line with its elevated TPC, while TD exhibited the greatest FRAP and ABTS values (20.86 mmol $Fe^{2+} \cdot g^{-1}$ and 1.56 mg TE$\cdot g^{-1}$ respectively), indicating that its flavonoid-rich profile favored reducing and electron-transfer mechanisms (11). FD generally produced intermediate values across assays, representing a more conservatively processed baseline with minimal modification of the native antioxidant profile. Overall, the results highlight a trade-off between

preserving total phenolics and enhancing flavonoid extractability, with SuD favoring phenolic-rich, DPPH-active powders, and TD promoting flavonoid-driven reducing capacity.

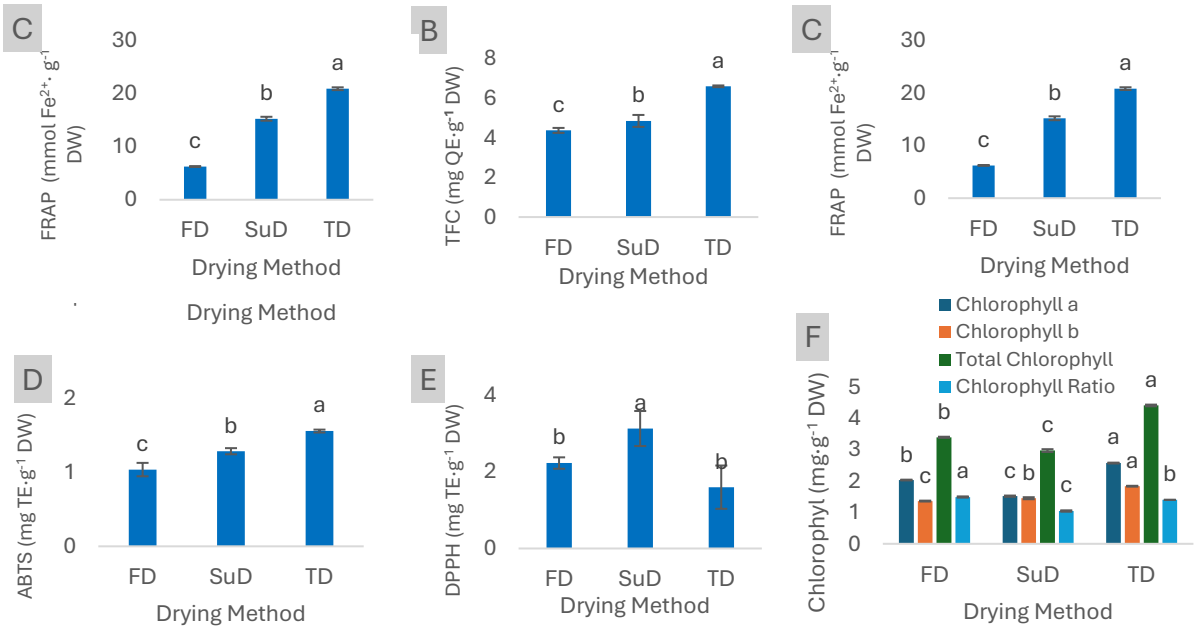

Figure 1. Phytochemical composition and antioxidant properties of Kai from different drying methods. (A) TPC; (B) TFC; (C) FRAP; (D) ABTS; (E) DPPH; (F) chlorophyll content and ratio. Different superscript letters above the bar indicate statistically significant differences between treatments ($p < 0.05$).

3.3 Physical properties

3.3.1 Chlorophyll content and color attributes

Drying treatments significantly influenced chlorophyll a, chlorophyll b, and total chlorophyll contents of Kai samples (Figure 1). TD exhibited the highest chlorophyll a (2.57 mg·g^{-1}), chlorophyll b (1.84 mg·g^{-1}), and total chlorophyll (4.41 mg·g^{-1}), followed by FD, whereas SuD showed the lowest pigment indicating that controlled convective drying was the most effective for pigment retention. This can be attributed to the intermediate temperature and short drying time, which promote enzyme inactivation and limit oxidative degradation while enhancing pigment extractability (30). In contrast, prolonged exposure to light and oxygen during SuD likely enhanced photooxidation and chlorophyllase activity, leading to pigment degradation (12). The chlorophyll ratio ranged from 1.05 to 1.49, with FD > TD > SuD, reflecting the greater susceptibility of chlorophyll a to heat- and light-induced degradation relative to chlorophyll b.

All Kai samples were located within the green–yellow region of the CIELAB color space (h° 103–111°), confirming overall retention of algal pigmentation after drying (Table 2). TD samples exhibited a darker yet more saturated green color (L* 58.88, a* −7.45, C* 21.38), matching its superior chlorophyll retention. FD showed a balanced green hue (L* 60.95, a* -5.73), while SuD yielded the lightest, least green powder (L* 61.11, a* -3.87) shifting toward yellow (h° 103.4°), reflecting chlorophyll degradation, pheophytin formation, and photo-oxidative reactions during prolonged solar exposure (12). The overall color difference remained within an acceptable visual range, indicating that all three methods produced visually acceptable powders, with TD showing the highest green color preservation.

3.3.2 Water activity

Water activity was also significantly influenced by drying method (Table 2). Water activity followed the order FD (0.42) < TD (0.46) < SuD (0.54), reflecting drying efficiency. Freeze-drying's sublimation removed water most completely, while sun drying's uncontrolled conditions

left higher residual moisture (31). TD provided intermediate aw by combining moderate temperature with forced airflow (32). The low aw of FD and medium TD powders indicates good shelf-stability, whereas the higher aw of SuD may require more careful packaging and storage to avoid quality deterioration.

Table 2. Chlorophyl content and color attributes of Kai samples

Parameter	FD	SuD	TD
Appearance			
L*	60.95 ± 0.25[a]	61.11 ± 0.19[a]	58.88 ± 0.06[b]
a*	−5.73 ± 0.24[b]	−3.87 ± 0.10[a]	−7.45 ± 0.04[c]
b*	15.02 ± 0.08[c]	16.26 ± 0.19[b]	20.04 ± 0.01[a]
C*	16.08 ± 0.16[c]	16.71 ± 0.19[b]	21.38 ± 0.00[a]
h°	110.88 ± 0.69[a]	103.39 ± 0.36[b]	110.38 ± 0.11[a]
ΔE		2.25 ± 0.13[b]	5.70 ± 0.02[a]
aw	0.42 ± 0.01[c]	0.54 ± 0.01[a]	0.46 ± 0.00[b]

Values are presented as mean ±standard deviation (SD). Different superscript letters within the same row indicate statistically significant differences between treatments ($p < 0.05$).

3.4 Technofunctional properties

3.4.1 Water holding, oil holding and swelling capacity

SuD exhibited the highest WHC(14.95 $g \cdot g^{-1}$), followed by FD and TD, suggesting that partial structural collapse during sun drying increased exposure of hydrophilic sites and favored water binding (9, 30) (Figure 2). OHC was similar among treatments, indicating that hydrophobic binding sites were largely maintained irrespective of drying conditions. SC was highest in TD (26.41 $mL \cdot g^{-1}$), followed by SuD and FD, implying that moderate thermal treatment promotes matrix relaxation and swelling, whereas the more rigid structure preserved by freeze drying limits volumetric expansion despite comparable OHC (30).

3.4.2 Foam formation and stability

Foam formation and stability were clearly decoupled by the different drying methods (Figure 2). TD generated the highest initial foaming capacity 44.55%, FD showed slightly lower values, and the lowest observed in SuD 27.39%, indicating that moderate heating may enhance air incorporation through partial unfolding of proteins and structural modification of polysaccharides (33). However, TD foam collapsed rapidly during storage while FD and SuD retained substantially higher foam volumes over 90 min. These patterns suggest that the structural changes induced by TD favor foam formation but yield less stable interfacial films that are susceptible to coalescence (9, 30). FD and SuD better preserve interactions that support cohesive, more stable foams. Meanwhile, FD preserves intermolecular interactions, such as hydrogen bonds and hydrophobic interactions, while SuD induces mild oxidative cross-linking, both of which favor cohesive and viscoelastic interfacial layers that slow liquid drainage and maintain foam volume (9). FD and SuD powders are more suitable for applications requiring stable foams, whereas TD is better suited for systems where rapid foam collapse is desirable.

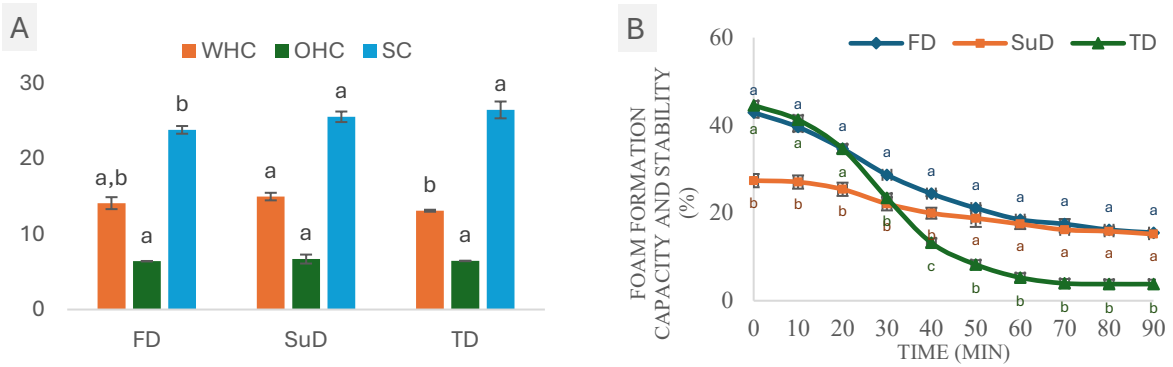

Figure 2. Technofunctional properties of FD,SuD and TD Kai. (A) water holding, oil holding and swelling capacity; (B) foam formation capacity and stability. Values are presented as mean ±standard deviation (SD). Different superscript letters indicate statistically significant differences between treatments ($p < 0.05$).

3.4.3 Powder flow and emulsifying properties

Flow properties showed only minor variation among drying methods (Table 3). Loose and tapped bulk densities were slightly higher in TD, but all samples exhibited Carr's index values above 30% and Hausner ratios around 1.5, corresponding to "poor to very poor" flowability according to European Pharmacopoeia classifications (24). In contrast, emulsifying properties were more sensitive to drying conditions (Table 3). FD powders exhibited the highest emulsifying capacity (63.33%) and stability (86.61%), followed by SuD and TD. FD's preserved microstructure forms superior interfacial films, whereas thermal and environmental stresses associated with SuD and TD slightly impair interfacial performance.

Table 3. Powder flow and emulsifying properties of Kai samples

Analysis	Abbreviation	FD	SuD	TD
Loose Density ($g \cdot cm^{-3}$)		0.112 ± 0.003^{ab}	0.108 ± 0.002^{b}	0.116 ± 0.002^{a}
Tapped Density ($g \cdot cm^{-3}$)		0.170 ± 0.007^{ab}	0.161 ± 0.004^{b}	0.179 ± 0.002^{a}
Carr's Index (%)		34.33 ± 4.51^{a}	32.67 ± 1.15^{a}	35.33 ± 0.58^{a}
Hausner Ratio		1.53 ± 0.11^{a}	1.49 ± 0.03^{a}	1.55 ± 0.01^{a}
Emulsifying Capacity	EC	63.33 ± 0.42^{a}	61.81 ± 1.05^{b}	60.97 ± 0.24^{b}
Emulsifying Stability	ES	86.61 ± 2.74^{a}	77.51 ± 1.71^{b}	76.99 ± 2.17^{b}

Values are presented as mean ±standard deviation (SD). Different superscript letters within the same row indicate statistically significant differences between treatments ($p < 0.05$).

3.5 Microstructure (SEM)

Scanning electron microscopy (SEM) analysis (Figure 3) revealed distinct morphological alterations in Kai filaments that provide structural validation for the techno-functional properties reported in Section 3.4. FD samples exhibited long, smooth filaments with well-defined contours and minimal cellular disruption, confirming preservation of the native polysaccharide-protein matrix responsible for superior emulsifying capacity and stability. In contrast, SuD produced highly convoluted and shrunken filaments indicative of cell wall collapse under uncontrolled ambient conditions, corroborating the exposure of hydrophilic sites that underpin the highest observed water holding capacity. TD displayed uniformly twisted filaments reflecting controlled thermal deformation of the matrix, validating the enhanced swelling capacity measured experimentally. These SEM observations provide direct microstructural evidence supporting the structure-function relationships established through physicochemical analyses.

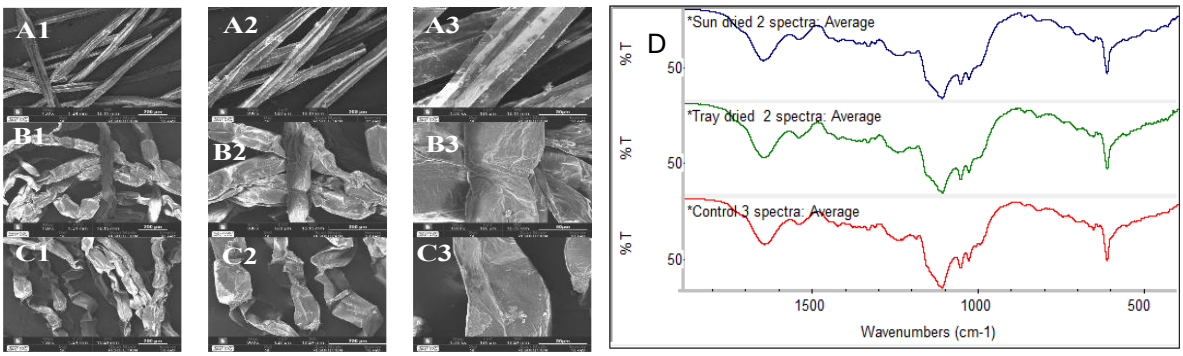

Figure 3. Microstructural and molecular characteristics of Kai samples subjected to different drying methods. A–C show representative images of FD, SuD, and TD samples, respectively: (A1–C1) 150×, (A2–C2) 300×, and (A3–C3) 1000×micrographs (SEM) of FD, SuD and TD Kai at different magnifications; (D) FTIR spectra of FD, SuD, and TD Kai

3.6 Fourier transform infrared spectroscopy (FTIR)

FTIR spectra of Kai samples showed the typical bands of polysaccharides and proteins, indicating that the main chemical groups were preserved across all drying methods (Figure 3). All samples exhibited characteristic bands near 1640 cm^{-1} and 1540 cm^{-1}, assigned to amide I and amide II vibrations of proteins, confirming proteinaceous components in the powders (34, 35). The absence of marked peak shifts among drying methods suggests that protein secondary structures were largely preserved, with only slight broadening of the amide I band in TD indicating minor thermally induced rearrangement. In the carbohydrate dominated region (approximately 1200–900 cm^{-1}), FD powders generally exhibited slightly sharper or more defined peaks, suggesting a more ordered polysaccharide structure, whereas TD and SuD samples showed broader, less resolved bands consistent with partial structural rearrangement under thermal or environmental stress (9, 34, 36).

4. Conclusion

This study demonstrated that drying method markedly modulates the nutritional, phytochemical, microstructural, and techno-functional properties of Kai. All drying techniques produced mineral-dense powders with heavy metal levels below EU regulatory limits, indicating that Kai from the studied source is safe for use as a food ingredient.

FD best preserved structural integrity, as reflected in SEM and FTIR, and showed balanced hydration with the highest emulsifying capacity and stability, making it particularly suited for structure-sensitive systems and emulsion-type products. TD at 50 °C enhanced reducing antioxidant capacity (FRAP, ABTS), flavonoids, protein, Ca, and chlorophyll, as well as high swelling ability, supporting its use in applications where color, antioxidant activity, and swelling are desirable. SuD maximized total phenolic content, DPPH activity, WHC, and some energy-related components, suggesting potential in high-fiber or water-binding applications, despite higher residual moisture and pronounced structural collapse.

These findings indicate that drying can be strategically selected to tailor Kai functionality to specific product requirements; FD for stable emulsions and aerated systems, TD for pigment- and antioxidant-rich powders, and SuD for formulations where high WHC and phenolic content are advantageous. These results support the development of Kai-based functional foods and nutraceuticals and highlight freshwater macroalgae as promising, sustainable ingredients for the food industry.

Acknowledgement

This research was supported by the National Science, Research and Innovation Fund 2025 (NSRF, Grant#692A04028) and Mae Fah Luang University.

References

1. Wheeler T, Von Braun J. Climate Change Impacts on Global Food Security. Vol. 341, Science. 2013.
2. Alexandratos N, Fao JB. World Agriculture Towards 2030 / 2050 The 2012 Revision ESA Working Paper Rome. Fao. 2012;(October 2012).
3. Selvaraj S, Bains A, Sharma M, Chawla P, Sridhar K. Freshwater Edible Algae Polysaccharides: A Recent Overview of Novel Extraction Technologies, Characterization, and Future Food Applications. J Polym Environ. 2023;
4. Costa JAV, Lucas BF, Alvarenga AGP, Moreira JB, de Morais MG. Microalgae Polysaccharides: An Overview of Production, Characterization, and Potential Applications. Vol. 2, Polysaccharides. 2021.
5. Khuantrairong T, Traichaiyaporn S. The nutritional value of edible freshwater Alga Cladophora sp. (Chlorophyta) grown under different phosphorus concentrations. Int J Agric Biol. 2011;13(2).
6. Surayot U, Lee JH, Kanongnuch C, Peerapornpisal Y, Park WJ, You SG. Structural characterization of sulfated arabinans extracted from Cladophora glomerata Kützing and their macrophage activation. Biosci Biotechnol Biochem. 2016;80(5).
7. Munir M, Qureshi R, Bibi M, Khan AM. Pharmaceutical aptitude of Cladophora: A comprehensive review. Vol. 39, Algal Research. 2019.
8. Srimaroeng C, Ontawong A, Saowakon N, Vivithanaporn P, Pongchaidecha A, Amornlerdpison D, et al. Antidiabetic and renoprotective effects of cladophora glomerata kützing extract in experimental type 2 diabetic rats: A potential nutraceutical product for diabetic nephropathy. J Diabetes Res. 2015;2015.
9. Tagliapietra BL, Salvador-Reyes R, Pinto CC, de Souza SM, Pallone JAL, de Araújo Bezerra J, et al. Nutritional and techno-functional properties of the brown seaweed Sargassum filipendula. Food Research International. 2024;191:114728.
10. Aljabri H, Cherif M, Siddiqui SA, Bounnit T, Saadaoui I. Evidence of the drying technique's impact on the biomass quality of Tetraselmis subcordiformis (Chlorophyceae). Biotechnology for Biofuels and Bioproducts. 2023;16(1).
11. Nunes A, Dutra F de S, Brito S de NS, Pereira-Vasques MS, Azevedo GZ, Schneider AR, et al. Effect of Biomass Drying Protocols on Bioactive Compounds and Antioxidant and Enzymatic Activities of Red Macroalga Kappaphycus alvarezii. Methods Protoc. 2024;7(6):88.
12. Mu Y, Zhang B, Zeng C, Zhu T, Hu S. Mechanistic and Multi-Parametric Insights into Preserving Nutritional, Bioactive, and Flavor Attributes of Daylily (Hemerocallis citrina): A Comparative Evaluation of Freeze-Drying, Hot-Air Drying, and Sun Drying. LWT. 2025;117510.
13. Zhao T, Dong Q, Zhou H, Yang H. Drying kinetics, physicochemical properties, antioxidant activity and antidiabetic potential of Sargassum fusiforme processed under four drying techniques. LWT. 2022;163.
14. Kim GM, Kim YK. Drying Techniques of Microalgal Biomass: A Review. Vol. 33, Applied Chemistry for Engineering. 2022.
15. Konsue N, Bunyameen N, Donlao N. Utilization of young jackfruit (Artocarpus heterophyllus Lam.) as a plant-based food ingredient: Influence of maturity on chemical attributes and changes during in vitro digestion. LWT. 2023;180.
16. Nandang SA, Setiawan PB, Purnomo EH, Qin S, Ketnawa S, Wongsa P, et al. Comparative effects of high-pressure and thermal processing on the nutritional and functional properties of duckweed. Food Chemistry Advances. 2025;9.

17. Hu Z, Fang Y, Yi Z, Tian X, Li J, Jin Y, et al. Determining the nutritional value and antioxidant capacity of duckweed (Wolffia arrhiza) under artificial conditions. LWT. 2022;153.
18. Korzeniowska K, Łęska B, Wieczorek PP. Isolation and determination of phenolic compounds from freshwater Cladophora glomerata. Algal Res. 2020;48.
19. Re R, Pellegrini N, Proteggente A, Pannala A, Yang M, Rice-Evans C. Antioxidant activity applying an improved ABTS radical cation decolorization assay. Free Radic Biol Med. 1999;26(9–10).
20. Benzie IFF, Strain JJ. The ferric reducing ability of plasma (FRAP) as a measure of "antioxidant power": The FRAP assay. Anal Biochem. 1996;239(1).
21. Armesto J, Gómez-Limia L, Carballo J, Martínez S. Effects of different cooking methods on some chemical and sensory properties of Galega kale. Int J Food Sci Technol. 2016;51(9).
22. Zhao S, Pan Z, Azarakhsh N, Ramaswamy HS, Duan H, Wang C. Effects of high-pressure processing on the physicochemical and adsorption properties, structural characteristics, and dietary fiber content of kelp (Laminaria japonica). Curr Res Food Sci. 2024;8.
23. Lamsal BP, Koegel RG, Gunasekaran S. Some physicochemical and functional properties of alfalfa soluble leaf proteins. LWT. 2007;40(9).
24. Pugliese A, Cabassi G, Chiavaro E, Paciulli M, Carini E, Mucchetti G. Physical characterization of whole and skim dried milk powders. J Food Sci Technol. 2017;54(11).
25. Michalak I, Messyasz B. Concise review of Cladophora spp.: macroalgae of commercial interest. Vol. 33, Journal of Applied Phycology. 2021.
26. Nurshahida MSF, Aini MAN, Faizal WIWM, Hamimi IA, Nazikussabah Z. Effect of drying methods on nutrient composition and physicochemical properties of Malaysian seaweeds. In: AIP Conference Proceedings. 2018.
27. Prazukin A V., Anufriieva E V., Shadrin N V. Biomass of Cladophora (Chlorophyta, Cladophorales) is a promising resource for agriculture with high benefits for economics and the environment. Vol. 32, Aquaculture International. 2024.
28. Vitor Verdelho. Food safety regulation and recommendations involving Algae and Algae based products Chemical and microbiological contaminants in Algae for food. 2023 Nov.
29. Babaei Rad S, Mumivand H, Mollaei S, Khadivi A. Effect of drying methods on phenolic compounds and antioxidant activity of Capparis spinosa L. fruits. BMC Plant Biol. 2025;25(1).
30. Stévant P, Indergård E, Ólafsdóttir A, Marfaing H, Larssen WE, Fleurence J, et al. Effects of drying on the nutrient content and physico-chemical and sensory characteristics of the edible kelp Saccharina latissima. J Appl Phycol. 2018;30(4).
31. Bhatta S, Janezic TS, Ratti C. Freeze-drying of plant-based foods. Vol. 9, Foods. 2020.
32. Bin Hameed O, Ahsan H, H. Rather A, Z. Hussain S, R. Naik H. Influence of Pretreatments and Drying methods on Water Activity, Dehydration and Rehydration ratio of Dried Tomato. Biosci Biotechnol Res Asia. 2016;13(4).
33. Li C, Tian Y, Liu C, Dou Z, Diao J. Effects of Heat Treatment on the Structural and Functional Properties of Phaseolus vulgaris L. Protein. Foods. 2023;12(15).
34. Kačuráková M, Wilson RH. Developments in mid-infrared FT-IR spectroscopy of selected carbohydrates. Carbohydr Polym. 2001;44(4).
35. Fleury N, Lahaye M. Chemical and physico-chemical characterisation of fibres from Laminaria digitata (kombu breton): A physiological approach. J Sci Food Agric. 1991;55(3).
36. Zhang Q, Wu S, Dai Q, Hu P, Chen G. Effects of Different Drying Methods on the Structural Characteristics and Multiple Bioactivities of Rosa roxburghii Tratt Fruit Polysaccharides. Foods. 2024;13(15).

O - 311

Optimization of Pectinase-Assisted Aqueous Extraction for Anthocyanin Recovery from Black Goji Berries

Feng Jiao, Pongsert Sriprom*

[1]*School of Food Industry, King Mongkut's Institute of Technology Ladkrabang, Bangkok, Thailand, 10520*

**Corresponding author E-mail: pongsert.sr@kmitl.ac.th*

Abstract: This study aimed to optimize a pectinase-assisted aqueous extraction process to enhance anthocyanin recovery from black goji berries (*Lycium ruthenicum*), in which pigment release is often limited by the pectin-rich cell wall matrix. Briefly, dried black goji berries were milled into powder and subjected to enzymatic hydrolysis using pectinase during aqueous extraction, followed by filtration and anthocyanin quantification. A three-factor, three-level response surface methodology (RSM) based on a Box–Behnken design was employed to systematically evaluate the effects of extraction temperature, enzyme dosage, and enzymatic hydrolysis time on anthocyanin yield. The optimal extraction conditions were determined to be 49.1 °C, 280 U/g, and 49.9 min, resulting in an anthocyanin concentration of 2003.70 ± 35 mg/L, corresponding to an extraction yield of 20.04 ± 0.35 mg/g (based on dry weight of black goji berries). Pectinase treatment effectively disrupted the pectin-dominated cell wall structure, significantly improving anthocyanin release compared with conventional aqueous extraction. Overall, this study demonstrates the critical role of pectinase in facilitating anthocyanin extraction and provides a simplified, food-grade, and scalable strategy for the utilization of black goji berry pigments in functional foods, anti-aging products, and smart packaging applications.

Keywords: Black goji berry; Anthocyanins; Enzyme-assisted extraction; Response surface methodology.

1. Introduction

Black goji berry (*Lycium ruthenicum* Murr.) is a wild medicinal and edible plant mainly distributed in the arid regions of northwestern China. It is renowned for its exceptionally high anthocyanin content, particularly petunidin- and malvidin-based derivatives, which exhibit strong antioxidant, anti-inflammatory, and anti-aging properties. Compared with the commonly consumed red goji (*Lycium barbarum*), black goji possesses considerably greater potential as a natural source of functional bioactive compounds.

Anthocyanins are a class of water-soluble flavonoid pigments responsible for the red, purple, and blue coloration of many fruits, flowers, and roots. This group includes anthocyanidins and their glycosylated derivatives, among which delphinidin, cyanidin, petunidin, pelargonidin, paeonidin, and malvidin are the most widely distributed. To date, at least 23 anthocyanin types have been identified. Owing to their strong antioxidant capacity and color-forming properties, anthocyanins have attracted increasing interest for applications in functional foods, nutraceuticals, cosmetics, and intelligent packaging (1).

Enzyme-assisted extraction (EAE) is an efficient and environmentally friendly technique that uses cell wall–degrading enzymes such as pectinase to hydrolyze plant tissue matrices and enhance the release of intracellular compounds (2, 3). Compared with conventional solvent extraction, EAE operates under mild conditions, requires fewer organic solvents, shortens extraction time, and better preserves heat-sensitive pigments such as anthocyanins (4). As a result, EAE has become a major research focus for improving anthocyanin recovery, with recent studies

emphasizing optimal enzyme combinations, process intensification, integration with ultrasound or microwave technologies, and strategies to enhance pigment stability (5, 6). Despite these advances, challenges remain, including limited enzyme reusability, complex parameter interactions, and the instability of anthocyanins during extraction (7, 8). Therefore, systematic optimization of extraction parameters is essential to maximize pigment recovery while maintaining structural integrity.

In this study, pectinase assisted aqueous extraction was employed to enhance the release of anthocyanins from black goji berries under mild processing conditions. A three-factor, three-level response surface methodology (RSM) was used to optimize extraction temperature, enzyme dosage, and enzyme hydrolysis time. The findings aim to establish an efficient, gentle, and scalable extraction method that supports the utilization of black goji anthocyanins in functional foods, nutraceutical applications, and smart packaging technologies.

2. Materials and Methods

2.1 Materials

Black goji berries (*Lycium ruthenicum*) were sourced from the Qaidam (Tsaidam) Basin, Mongolia. Pectinase (30,000 U/g) was obtained from Shanghai Shifeng Biotechnology Co. (Shanghai, China). Potassium chloride (KCl), hydrochloric acid (HCl), sodium acetate, and other analytical-grade chemicals were purchased from standard suppliers. Cyanidin-3-glucoside (C3G) was used as the analytical standard. All solutions were prepared with distilled water

2.2 Sample preparation

Fresh fruits were cleaned, destemmed, and dried at 45 °C for 24 h in a hot-air oven. The dried materials were milled and sieved through a 100-mesh sieve. The resulting black goji berry powder was vacuum-packed and stored at room temperature in the dark until use. For each extraction, 1.0 g of powder (dry basis) was weighed.

2.3 Enzyme-assisted aqueous extraction

Enzyme-assisted extraction was performed using the pectinase activity ratio. The powdered sample (1.0 g) was dispersed in distilled water at a solid-to-liquid ratio of 1:10 (w/v). The mixture was incubated at the designated temperature, enzyme dosage (U/g), and enzyme hydrolysis time according to the experimental design. After enzymatic hydrolysis, the mixture was filtered and the filtrate was collected for analysis.

2.4 Experimental design

The experimental design for enzyme-assisted extraction was carried out using Response Surface Methodology (RSM) based on a Box-Behnken design (BBD) created in MINITAB version 18.1. Three independent variables were temperature (°C), time (min), and Enzyme addition (U/g) were tested. The response measured was the anthocyanin concentration (mg/L). The coded and actual factor levels are shown in Table 1.

Table 1. The coded and actual factor levels used in RSM design

Factors	Coded	Level		
		-1	0	1
Temperature (°C)	X_1	20	40	60
Time (min)	X_2	20	40	60
Enzyme addition (U/g)	X_3	150	300	450

2.5 Determination of total anthocyanin content (TAC)

TAC was determined using the pH differential method. Each sample (100 µL) was diluted to a final volume of 10 mL using either 0.025 mol/L KCl–HCl buffer (pH 1.0) or 0.4 mol/L NaAc–HCl buffer (pH 4.5). The diluted solutions were mixed thoroughly and equilibrated in a constant-temperature water bath at 40 °C. The equilibration time was 30 min for pH 1.0 and 20 min for pH 4.5. After equilibration, the absorbance of each solution was measured at 525 nm and 700 nm. TAC was calculated according to equation (1). All measurements were performed in triplicate, and the average values were reported.

$$M = (A \cdot Mw \cdot DF \times 10^3) / (\varepsilon \cdot L) \quad (1)$$

where M is the total anthocyanin content (mg/L), A is the absorbance calculated as ($A_{525} - A_{700}$) at pH 1.0 minus ($A_{525} - A_{700}$) at pH 4.5, MW is the molecular weight of C3G (449.2 g/mol), DF is the dilution factor, ε is the molar extinction coefficient of C3G (26,900 L/(mol·cm)), and L is the path length of the cuvette (1 cm). The final anthocyanin content (mg/L) was converted to mg/g for reporting purposes as

$$\text{Extraction yield (mg/g dry weight)} = (C \times V) / m \quad (2)$$

where C is the anthocyanin concentration (mg/L), V is the extraction volume (L), and m is the mass of dried raw material (g).

3. Results & Discussion

3.1 Regression model

Table 2 presents the complete set of experimental runs and corresponding anthocyanin concentrations obtained from the Box–Behnken design. Anthocyanin concentration (mg/L) was used as the response variable, while temperature (X_1), extraction time (X_2), and enzyme addition (X_3) served as the independent factors. The experimental data were fitted to a second-order polynomial model using Minitab 21. The resulting regression model is shown in equation (2).

$$\text{Anthocyanin (mg/L)} = -2.6818 + 115.7\,X_1 + 30.8\,X_2 + 6.06\,X_3 - 0.87\,X_1^2 - 0.322\,X_2^2 - 0.00501\,X_3^2 - 0.102\,X_1X_2 + 0.0243\,X_1X_3 - 0.0889\,X_2X_3 \quad (3)$$

Table 2. The experimental results of enzyme-assisted extraction

Temperature (°C) X_1	Time (min) X_2	Enzyme addition (u/g) X_3	Anthocyanin concentration (mg/L)
60	40	150	1747.37
20	60	300	1234.05
20	40	150	559.75
60	60	300	1726.16
40	20	450	1277.46
60	20	300	1437.61
40	40	300	1799.81
20	40	450	1371.48
40	60	150	1637.33
40	60	300	1682.68
40	20	150	1417.40
60	40	450	1492.21
20	20	300	782.68
40	20	300	1511.08
40	60	450	1789.45

The regression model was statistically significant (P = 0.004), indicating that the fitted equation reliably represents the experimental data. The coefficient of determination (R^2 = 96.64%) demonstrates excellent agreement between the fitted and observed values. The adjusted R^2 (90.60%) confirms that the model accounts for more than 90% of the variability in anthocyanin concentration after adjusting for non-significant terms. Although the predicted R^2 (65.66%) is lower, it still indicates acceptable predictive ability for process interpretation and optimization.

Analysis of Variance (ANOVA) results showed that temperature (X_1) had a highly significant effect on anthocyanin yield (P = 0.001) and was the most influential factor. Extraction time (X_2) was also significant (P = 0.005), while enzyme addition (X_3) did not show a significant main effect (P = 0.128). Among the quadratic terms, X_1^2 was highly significant (P = 0.003), indicating a nonlinear temperature–response relationship and suggesting the existence of an optimal temperature window. The interaction between temperature and enzyme addition (X_1X_3) was also significant (P = 0.005), implying joint effects of thermal conditions and enzyme activity on anthocyanin release. Other quadratic and interaction terms (X_2^2, X_3^2, X_1X_2 and X_2X_3) were not significant (P > 0.1), suggesting that they exert relatively minor influence under the tested conditions.

Table 3. Analysis of Variance

Source	DF	Adj SS	Adj MS	F-Value	P-Value
Model	9	1752460	194718	15.99	0.004
Linear	3	1064151	354717	29.14	0.001
X_1	1	753626	753626	61.9	0.001
X_2	1	270089	270089	22.19	0.005
X_3	1	40437	40437	3.32	0.128
Square	3	375792	125264	10.29	0.014
X_1^2	1	363415	363415	29.85	0.003
X_2^2	1	38318	38318	3.15	0.136
X_3^2	1	38146	38146	3.13	0.137
2-Way Interaction	3	312517	104172	8.56	0.021
X_1X_2	1	6627	6627	0.54	0.494
X_1X_3	1	284565	284565	23.37	0.005
X_2X_3	1	21325	21325	1.75	0.243

* R^2 = 96.64%, R^2 (adj.) = 90.60%, and R^2 (pred.) = 95.66%

3.2 Residual analysis

Residual diagnostics were carried out to evaluate the adequacy of the fitted regression model (Fig.1). The normal probability plot showed that most residuals aligned closely with the reference line, indicating that the residuals followed an approximately normal distribution with only slight deviations near the tails. The plot of residuals versus fitted values exhibited a random scatter around zero without discernible patterns, confirming that the assumption of linearity was met, although a slight increase in variance at higher fitted values suggested mild heteroscedasticity. The histogram of residuals showed a nearly symmetric distribution centered near zero, further supporting the assumption of normality. Additionally, the residuals versus observation order plot revealed no increasing or decreasing trend, indicating that the residuals were independent and not influenced by the experimental run order. Overall, the residual analysis confirms that the regression model is appropriate and statistically robust. The residuals were normally distributed, independent, and randomly scattered, with only minor heteroscedasticity observed at higher fitted values.

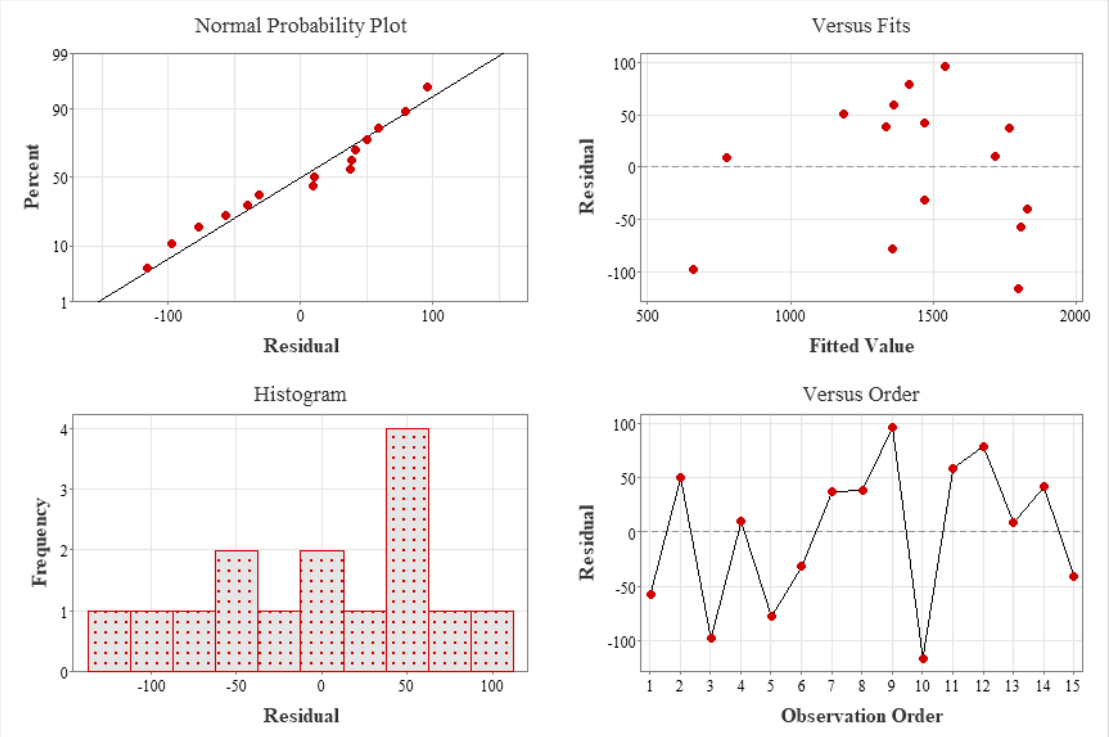

Fig.1 Residual plots for enzyme-assisted extraction of anthocyanin concentration.

3.3 Main effect

The main effects of temperature, extraction time, and enzyme addition on anthocyanin extraction were evaluated at the 95% confidence level, as illustrated in Fig.2. The corresponding P-values confirmed that temperature and extraction time had significant influences on anthocyanin concentration, whereas enzyme addition did not exhibit a statistically significant effect within the tested range.

Temperature showed a pronounced parabolic trend, where anthocyanin concentration increased sharply with rising temperature and reached a maximum near the optimal point before declining at higher temperatures. This behavior suggests that moderate heating enhances pigment solubility, disrupts cellular structures, and improves mass transfer, thereby promoting anthocyanin release. However, temperatures beyond the optimal range likely accelerate thermal degradation, polymerization, or structural breakdown of anthocyanins due to their heat sensitivity. This observation is consistent with the highly significant P-value ($P = 0.001$), confirming temperature as the most influential factor in the extraction process.

Extraction time also displayed a similar curvilinear pattern. Anthocyanin yield increased steadily with time until reaching a plateau and slightly decreased with prolonged extraction. The decline may be attributed to oxidation or hydrolytic degradation during extended exposure. The significant P-value ($P = 0.005$) indicates that extraction time had a considerable effect on extraction efficiency, emphasizing the need for an optimal duration to maximize pigment release while minimizing degradation.

In contrast, enzyme addition exhibited a moderate increasing trend at lower concentrations but showed a slight reduction at higher levels. Although enzyme-assisted extraction can enhance cell wall disruption and facilitate pigment diffusion, excessive enzyme levels may lead to reduced catalytic efficiency or undesirable secondary reactions (9). Although enzyme addition did not show a statistically significant effect ($p > 0.05$), an increasing trend in anthocyanin yield was observed, suggesting a potential contribution under optimized conditions.

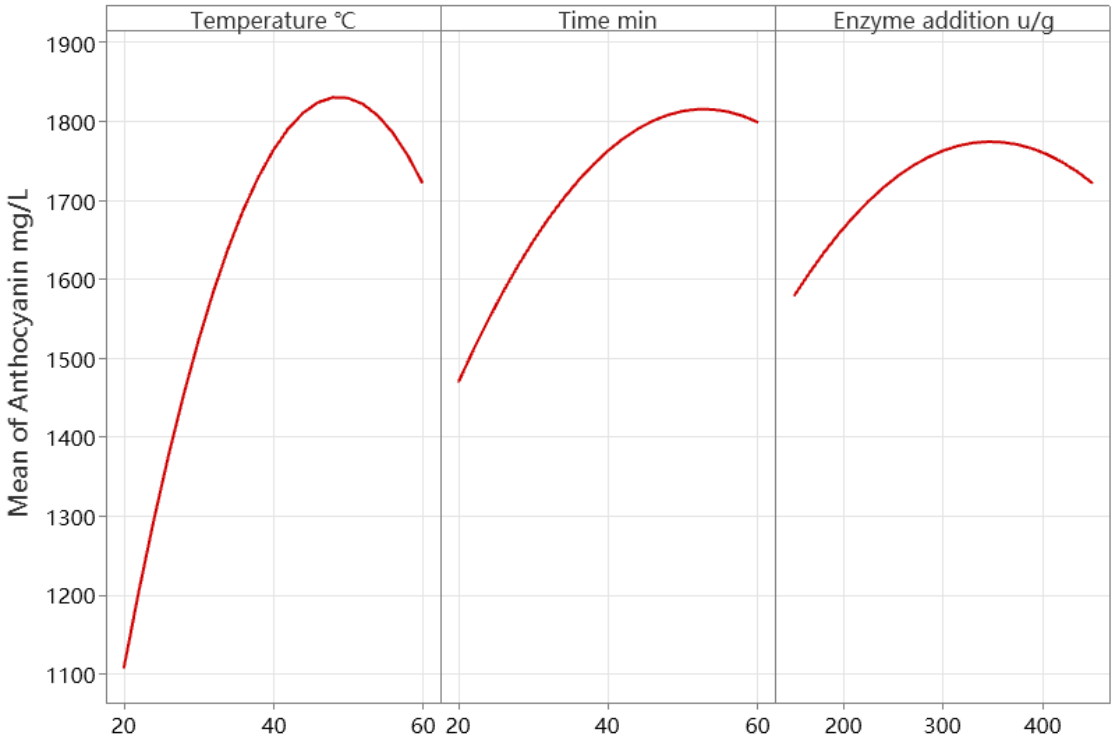

Fig.2 Main effect for enzyme-assisted extraction of anthocyanin concentration.

3.4 Interaction effect

The interaction effects among temperature, extraction time, and enzyme addition on anthocyanin yield were evaluated using contour plots generated from the fitted response surface model (Fig. 3). These contour plots illustrate how the combined influence of two variables affects anthocyanin concentration while keeping the third variable at its central level. The interaction between temperature and extraction time. Anthocyanin concentration increased as both temperature and time increased, reaching higher yields at approximately 50–55 °C and 45–55 min. Beyond this temperature range, the yield tended to plateau or slightly decline, which may be attributed to thermal degradation of anthocyanins at elevated temperatures. The contour lines in this plot appear nearly circular, indicating a weak interaction between the two variables. This observation is consistent with the non-significant interaction term ($P = 0.494$), suggesting that temperature and extraction time mainly exert independent effects within the studied range.

The interaction between temperature and enzyme addition. Anthocyanin yield increased substantially with increases in both temperature and enzyme dosage. The highest yield (>1800 mg/L) was observed near 50 °C combined with enzyme levels of approximately 350–400 U/g. The contour plot displays elongated and tilted elliptical patterns, indicating a strong interaction between the two factors. This visual trend aligns with the significant interaction term ($P = 0.005$), demonstrating that temperature strongly modulated the effect of enzyme concentration on anthocyanin release. This is likely due to the temperature-dependent catalytic activity of the enzyme, which enhances the breakdown of cell wall structures and promotes pigment diffusion under optimal thermal conditions.

The interaction between enzyme addition and extraction time. Anthocyanin concentration increased with increases in both variables, and the highest yields occurred at higher enzyme dosages and longer extraction times. However, the contour lines are relatively broad and rounded, indicating a weak interaction. This is supported by the non-significant interaction term ($P = 0.243$), suggesting that enzyme dosage and extraction time acted independently and did not substantially reinforce each other's effects under the experimental conditions. These findings indicate that only

the interaction between temperature and enzyme addition exhibited a statistically significant effect on anthocyanin extraction. This reinforces the key role of temperature-dependent enzymatic activity in facilitating pigment release, while the other factor pairs influenced anthocyanin yield primarily through their individual main effects rather than through interaction.

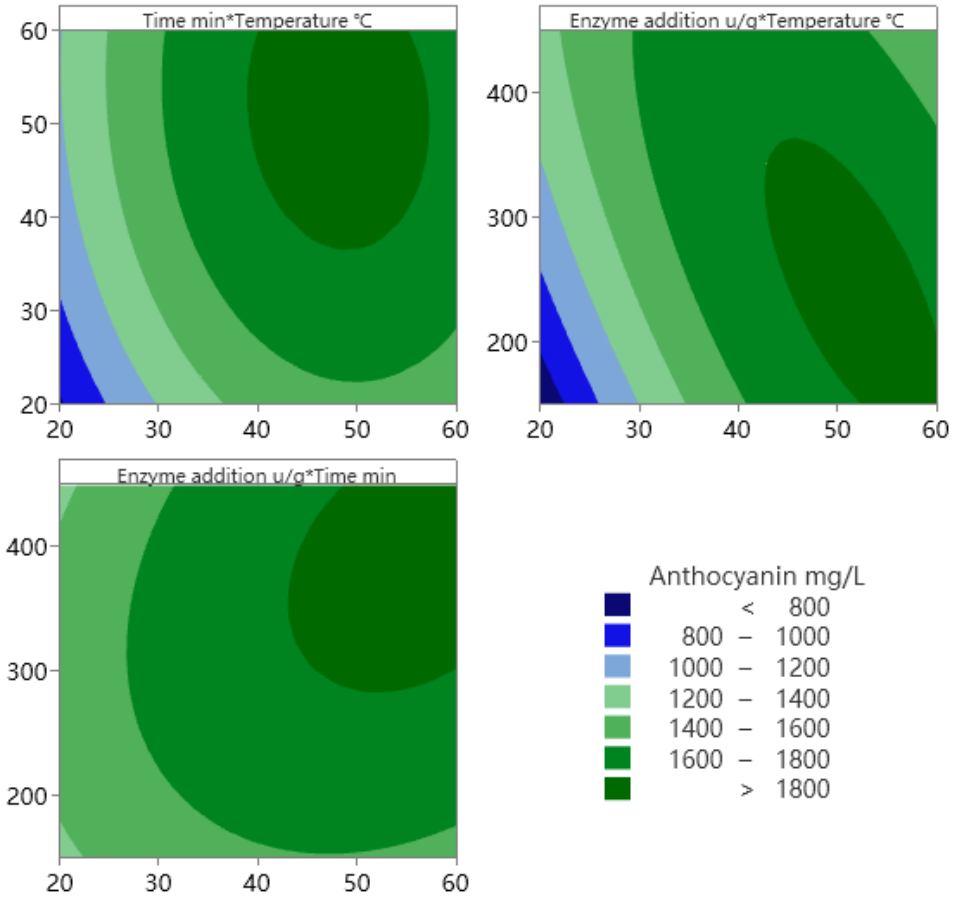

Fig.3 Contour plots for enzyme-assisted extraction of anthocyanin concentration.

3.5 Optimization

The response surface model was used to determine the optimal conditions for anthocyanin extraction. The predicted optimum was a temperature of 49.1 °C, an enzyme addition of 280 U/g, and an extraction time of 49.9 min. Under these conditions, the model estimated an anthocyanin yield of 1870.88 mg/L within the 95% confidence interval.

To verify the prediction, the extraction was carried out in triplicate under the same optimal conditions. The experimental results showed an anthocyanin concentration of 2003.70 ± 35 mg/L, corresponding to an extraction yield of 20.04 ± 0.35 mg/g (based on dry weight of black goji berries), which was consistent with the model prediction and significantly higher than those obtained using various conventional extraction methods.(10) This result confirms that the regression model provides reliable predictions and is suitable for optimizing enzyme-assisted anthocyanin extraction.

4. Conclusion

In this study, pectinase assisted aqueous Extraction of anthocyanins from black goji berries was optimized under mild and environmentally friendly conditions. Response surface methodology was used to evaluate the effects of temperature, enzyme addition, and extraction time on anthocyanin yield. The optimized conditions were 49.1 °C, 280 U/g, and 49.9 min, which produced an experimental anthocyanin concentration of 2003.70 ± 35 mg/L, corresponding to an extraction yield of 20.04 ± 0.35 mg/g (based on dry weight of black goji berries), in close agreement with the model prediction.

The results showed that temperature and extraction time were the most influential factors, while the interaction between temperature and enzyme addition was the only significant interaction effect. This highlights the necessity of jointly optimizing enzyme dosage and temperature to maximize extraction efficiency. Overall, the regression model demonstrated good predictive performance and offers a reliable basis for tuning enzyme-assisted extraction systems. Importantly, the mild temperature and moderate enzyme dosage required for optimal performance emphasize the potential of this approach as a green, energy-efficient, and sustainable extraction method for anthocyanins. This makes the process attractive for future applications in food, nutraceutical, and natural pigment industries seeking eco-friendly technologies.

Acknowledgements

This work was supported by School of Food Industry from King Mongkut's Institute of Technology Ladkrabang, Bangkok.

References

1. Veberic R, Slatnar A, Bizjak J, Stampar F, Mikulic-Petkovsek M. Anthocyanin composition of different wild and cultivated berry species. LWT - Food Science and Technology. 2015;60(1):509-17.
2. Yun D, Wu Y, Yong H, Tang C, Chen D, Kan J, et al. Recent Advances in Purple Sweet Potato Anthocyanins: Extraction, Isolation, Functional Properties and Applications in Biopolymer-Based Smart Packaging. Foods. 2024;13(21):3485.
3. Costa JR, Tonon RV, Cabral L, Gottschalk L, Pastrana L, Pintado ME. Valorization of Agricultural Lignocellulosic Plant Byproducts through Enzymatic and Enzyme-Assisted Extraction of High-Value-Added Compounds: A Review. ACS Sustainable Chemistry & Engineering. 2020;8(35):13112-25.
4. Tena N, Asuero AG. Up-To-Date Analysis of the Extraction Methods for Anthocyanins: Principles of the Techniques, Optimization, Technical Progress, and Industrial Application. Antioxidants. 2022;11(2):286.
5. Kim J, Lee Y, Suh H-J, Lee H-S, Lee C. Enzymatic extraction of anthocyanins from the pomace of aronia (Aronia melanocarpa). Bioscience, Biotechnology, and Biochemistry. 2024;88(6):639-47.
6. Li Y, Tao F, Wang Y, Cui K, Cao J, Cui C, et al. Process optimization for enzymatic assisted extraction of anthocyanins from the mulberry wine residue. IOP Conference Series: Earth and Environmental Science. 2020;559(1):012011.
7. Wang F, Zhang S, Deng G, Xu K, Xu H, Liu J. Extracting Total Anthocyanin from Purple Sweet Potato Using an Effective Ultrasound-Assisted Compound Enzymatic Extraction Technology. Molecules. 2022;27(14):4344.
8. Li J, Guo X, Wang R, Geng Z, Jia J, Pang S, et al. Ultrasonic assisted extraction of anthocyanins from rose flower petal in DES system and enzymatic acylation. LWT. 2023;180:114693.

9. Leonarski E, Cesca K, de Oliveira D, Zielinski AAF. A review on enzymatic acylation as a promising opportunity to stabilizing anthocyanins. Critical Reviews in Food Science and Nutrition. 2023;63(24):6777-96.
10. Vidana Gamage G, Choo W. Effect of hot water, ultrasound, microwave, and pectinase-assisted extraction of anthocyanins from black goji berry for food application Heliyon, 2023; 9

O - 340

Effect of Heat Treatment on Color, Proximate Composition, and Bioactive Compounds of Three Selected Mushrooms

Pakjira Yawong, Nattaya Konsue, Chutamat Niwat*

School of Agro-Industry, Mae Fah Luang University, Thailand

**Corresponding author E-mail: chutamat@mfu.ac.th*

Abstract: Heat treatments are widely used as post-harvest processes and can strongly influence the nutritional and functional properties of mushrooms. This study aimed to evaluate the effects of three heat treatments including boiling, steaming, and grilling on color, protein content, and bioactive compounds in three edible mushroom species: King Oyster mushroom (*Pleurotus eryngii*), Shimeji mushroom (*Hypsizygus commune*), and Split Gill mushroom (*Schizophyllum commune*). For the boiling process, samples were treated in reverse osmosis water at 100°C for 20 minutes with a 1:10 mushroom-to-water ratio, while steaming was conducted at 100°C for 20 minutes. Grilling was carried out at 180°C for 3 minutes. The analytical assessments covered color measurement, proximate composition analysis, evaluation of total phenolic content, and quantification of beta-glucan. The results demonstrated that all heat treatments induced significant alterations in mushroom nutritional composition compared with fresh samples. Steaming provided the greatest color preservation in Shimeji and Split Gill mushrooms, whereas in King Oyster, steaming produced the lowest lightness (L^*) value. Among the heat treatments, steaming was the most effective overall, as it best preserved color quality and maintained high protein levels, yielding 13.61, 15.52, and 18.79 g/100 g dry weight in King Oyster, Shimeji, and Split Gill mushrooms, respectively. In contrast, boiling better retained carbohydrate content, while grilling resulted in the lowest moisture levels among the treatments ($P < 0.05$). Steaming also produced significantly higher levels of total phenolics and beta glucans content compared with boiling and grilling ($P < 0.05$). Overall, the findings highlight the suitability of steaming as a post-harvest treatment for retaining key nutritional components and valuable bioactive compounds in the examined mushroom species, providing meaningful insights into quality preservation and health-related benefits.

Keywords: Bioactive compounds; Edible mushroom; Heat treatment; Beta glucan content; Nutritional composition.

1. Introduction

In recent years, global demand for alternative protein sources has significantly increased, driven by health concerns associated with the excessive intake of animal proteins, including hypertension and cardiovascular diseases[1]. Mushrooms have emerged as a promising alternative protein source due to their high nutritional value, including substantial protein content, essential amino acids, dietary fiber, and numerous bioactive compounds beneficial for human health[2,3]. The global production and consumption of edible mushrooms have markedly increased. Notably, *Agaricus bisporus*, *Lentinus edodes*, and *Pleurotus spp*. are among the most extensively consumed mushrooms globally due to their well-established nutritional profiles and ease of cultivation[2]. Additionally, mushrooms are abundant in diverse bioactive compounds, including antioxidants, antiviral, antibacterial, anti-inflammatory, and anti-aging agents[3]. Recent comparative studies have highlighted significant differences in nutritional and bioactive profiles among various mushroom species and their responses to processing methods[1,5]. Processing techniques such as heat treatments

(boiling, steaming, roasting, microwaving) are essential to extend mushroom shelf-life, improve food safety, and enhance sensory properties[6]. However, these processes can negatively influence the nutritional and bioactive qualities of mushrooms due to the sensitivity of certain compounds to heat-induced degradation[7,8]. Recent literature underscores the critical need to assess these changes systematically, as findings vary widely based on mushroom species and heat treatment methods[1]. Despite extensive research on mushroom nutrition, limited comparative data exist on how different heat treatments simultaneously affect multiple nutritional and bioactive parameters across various mushroom species. Addressing this gap, the novelty of this study lies in providing an integrated analysis of color, proximate composition, bioactive compounds, and antioxidant activities in three edible mushroom species (*Schizophyllum commune*, *Pleurotus eryngii*, and *Hypsizygus tessellatus*) subjected to three distinct heat treatments: boiling, steaming, and grilling. Understanding these effects holds practical implications for food processing industries, dietary recommendations, and consumer practices aimed at maximizing nutritional benefits.

2. Materials and Methods

2.1 Chemicals

Deionized water was prepared using a Milli-Q water purification system (Millipore, Billerica, MA, USA). Methanol was purchased from RCI Labscan (Bangkok, Thailand). Beta-Glucan Assay Kit (K-BGLU) was obtained from Megazyme International (Wicklow, Ireland). Folin-Ciocalteu's phenol reagent were from Loba Chemie (Mumbai, India). Gallic acid monohydrate was from Sigma-Aldrich (St. Louis, MO, USA). Sodium carbonate, sodium acetate, and potassium chloride were purchased from Ajax Finechem (Wellington, New Zealand). Hydrochloric acid was obtained from Merck (Kenilworth, NJ, USA).

2.2 Samples

Fresh fruiting bodies of King Oyster (*Pleurotus eryngii*), Shimeji (*Hypsizygus commune*), and Split Gill mushrooms (*Schizophyllum commune*) were selected without defects. King Oyster and Shimeji mushrooms were purchased from local supermarkets in Chiang Rai, Thailand, while Split Gill mushrooms were obtained from mushroom Villa Farm Project Co. Ltd. in Krabi, Thailand. All samples were stored at 4°C before use.

2.3 Heat treatment and sample preparation

Mushrooms underwent boiling, steaming, or grilling. Samples were sliced vertically to 2 mm thickness. For boiling, samples were treated in reverse osmosis water at 100°C for 20 minutes using a 1:10 mushroom-to-water ratio, whereas steaming was performed at 100°C for 20 minutes. Grilling was performed at 180°C for 3 minutes. Then, the samples were cooled at room temperature (25±2°C) before analysis[9]. Fresh mushrooms (without heat treatment) were included as controls.

2.4 Color

Measurement surface color was evaluated using a HunterLab LabScan Colorimeter. Measurements followed the CIELAB system (L* for lightness, a* for redness-greenness, and b* for yellowness-blueness), conducted under standard illuminant D65 and observer angle of 10°. Analyses were performed in triplicate. Total color differences (ΔE) were calculated using the equation: (1):

$$\Delta E = \sqrt{(\Delta L)^2 + (\Delta a)^2 + (\Delta b)^2} \quad (1)$$

2.5 Proximate analysis

Proximate analysis was completed in agreement with the AOAC methods to quantify moisture, ash, and fat. A conversion factor of 4.38 was employed to determine protein content[10]. This equation (2) was used to determine the total carbohydrates content (g/100 g dry weight basis) by calculating the difference:

$$\text{Total carbohydrates (\%)} = 100\text{-(\%moisture +\%ash+\%fat+\% protein)} \quad (2)$$

2.6 Bioactive compounds

Beta-glucan content determination

Beta-glucan was quantified using the Megazyme assay kit. Samples dried at 60°C for 16-18 hours were ground and sieved (Retsch AS200-Control, 500 µm mesh). Total glucan extraction involved acid hydrolysis with sulfuric acid and neutralization. Alpha-glucan was extracted with NaOH. Enzymatic treatments with glucan-specific enzymes followed. Absorbance was measured at 510 nm with a UV–VIS spectrophotometer (Thermo Fisher Scientific, Waltham, MA, USA). Beta-glucan content (%) was calculated by subtracting alpha-glucan from total glucan. The alpha glucan content was expressed as alpha glucan, unit %weight by weight. The beta-glucan content was calculated using the following equation (3):

$$\text{Beta glucan content} = \text{Total glucan content} - \text{Alpha glucan content} \quad (3)$$

Total polyphenol content (TPC) determination

Total phenolic content (TPC) was determined by ISO method (2005) using Folin-Ciocalteu reagent and expressed as gallic acid equivalents (GAE, g/100 g dry weight). Absorbance was measured at 765 nm (Thermo Fisher Scientific).

2.7 Statistical analysis

All experiments were conducted in triplicate (n=3), and data are reported as mean ± standard deviation. One-way ANOVA and Duncan's multiple range tests were performed using SPSS version 20.0 (IBM Corporation, NY, USA). Pearson correlation analysis was conducted to identify relationships among measured parameters. A significance level was set at $P<0.05$.

3. Results

3.1 The impact of heat treatment on color

The color characteristics on the CIELab scale: L^* value represents lightness, a^* value represents red-green color, and b^* value represents yellow-blue color. Fresh and cooked of King Oyster mushroom, Shimeji mushroom, and Split Gill mushroom using different heat treatments are presented in Table 1. The overall L^* value of fresh King Oyster, Shimeji, and Split Gill mushroom samples were 96.19, 99.53 and 68.03, respectively. The L* values of all heat treatments were significantly decreased compared with fresh samples ($P<0.05$). The lowest L^* value of King Oyster mushroom was observed in steaming process, whereas grilling process was showed the lowest L^* value in Shimeji mushroom. The decrease in L^* value and increase in Browning Index (BI) of cooked mushrooms, especially when grilled, are likely a consequence of forming Maillard reaction products[10]. Further, the thermal process might also induce non-enzymatic oxidative changes in polyphenol levels, resulting in the development of dark compounds that reduce luminosity[12]. However, the fresh Split Gill mushroom was nonsignificant different in L^* value compared with heat treatments ($P>0.05$), indicating that lightness was relatively stable across the applied heat treatments. This stability may reflect the inherent color characteristics and tissue structure of Split Gill mushroom, which make its surface lightness less sensitive to the thermal conditions used in this study[47]. Value of a^* in three fresh mushrooms varied from -0.90 to 7.12. The decrease of a^* value in fresh King Oyster mushroom was significantly decreased ($P<0.05$) in boiling and steaming process when compared with fresh sample and other heat treatments. The highest a^* value of Shimeji mushroom was observed in grilling process, while the boiling and steaming process was significantly decreased ($P<0.05$). The a^* value of Split Gill mushrooms was significantly increased in steaming and grilling process, which was found in the range 9.29-10.25. In contrast the boiling process was showed nonsignificant different ($P>0.05$) in a^* value. The overall b^* value of fresh King Oyster, Shimeji, and Split Gill mushroom samples were 7.37,5.30, 25.82, respectively**.** When compared with fresh King Oyster mushroom, boiling and steaming was indicated nonsignificant different ($P>0.05$), whereas the grilling was significantly increased ($P<0.05$) from 7.37 to 16.34.

According to the heat treatments, the highest observe value in Shimeji mushroom was presented in grilling process. While, steaming process was showed significantly lower value ($P<0.05$) than grilling process. However, the boiling process were nonsignificant different in the *b** value of King Oyster and Shimeji mushroom when compared with their fresh sample ($P>0.05$). In contrast, the *b** value of Split Gill mushroom after the boiling process was showed significantly decreased compared with fresh sample ($P<0.05$). This may be due to the high temperature and prolonged drying which may have caused the proteins or amino acids in the mushrooms to react with the reducing sugars in the Maillard reaction, resulting in a darker and yellower color[13]. The brownish color could be enhanced by reddish pigments developed during cooking. The increase in carotenoids concentration in mushrooms during cooking, due to loss of water, could also contribute to the color changes observed[31]. The high temperatures used in roasting and grilling treatments contributed to reaching the activation energy necessary to develop the Maillard reaction and the formation of yellowish-reddish compounds[14].

Table 1. Impact of heat treatments on color parameters in mushroom samples.

Mushroom	Treatments	Color value		
		L*	a*	b*
King oyster	Fresh	96.19±0.22^{a}	-0.90±0.22^{a}	7.37±0.68^{b}
	Boiling	72.68±2.51^{c}	-2.10±0.30^{b}	5.73±0.52^{b}
	Steaming	67.33±0.57^{d}	-1.94±0.66^{b}	6.86±2.51^{b}
	Grilling	76.02±1.05^{b}	-0.71±0.73^{a}	16.34±1.76^{a}
Shimeji	Fresh	99.53±0.77^{a}	-0.93±0.23^{b}	5.30±0.50^{c}
	Boiling	69.38±0.94^{c}	-3.37±0.14^{c}	3.81±0.92^{c}
	Steaming	77.33±2.20^{b}	-1.64±0.73^{c}	11.41±1.38^{b}
	Grilling	54.65±1.48^{d}	8.18±1.74^{a}	29.88±2.58^{a}
Split Gill	Fresh	68.03±2.60^{a}	7.12±1.83b^{c}	25.82±3.09^{a}
	Boiling	61.65±2.23^{a}	4.96±0.59^{c}	19.72±1.08^{b}
	Steaming	58.34±4.01^{a}	10.25±0.74^{a}	27.06±1.57^{a}
	Grilling	65.37±3.99^{a}	9.29±1.72^{ab}	27.08±1.85^{a}

*Values are expressed as mean ± SD. Different letters in each sample in the same column indicate significant differences ($P< 0.05$).

3.2 Impact on proximate composition in response to heat treatments

The proximate analysis of fresh and cooked mushroom by the heat treatments are shown in Table 2.

Table 2. Proximate analysis of mushroom samples using different heat treatments.

Mushroom	Treatment	Moisture content (%)	Ash content*ns	Fat*	Protein*	Carbohydrate*
King Oyster	Fresh	90.18±0.10^{b}	1.12±0.05	1.72±0.40^{a}	15.12±0.01^{a}	72.22±0.48^{b}
	Boiling	92.87±0.08^{a}	1.24±0.02	1.68±0.23^{a}	11.76±0.02^{c}	78.19±0.14^{a}
	Steaming	89.24±0.09^{c}	1.33±0.03	0.52±0.13^{b}	13.61±0.17^{b}	73.79±0.19^{b}
	Grilling	67.07±0.28^{d}	1.30±0.15	0.46±0.07^{b}	10.69±0.06^{d}	54.62±0.43^{c}
Shimeji	Fresh	91.63±0.17^{b}	2.26±0.02	1.77±0.41^{a}	17.12±1.02^{a}	70.48±1.47^{b}
	Boiling	93.99±0.09^{a}	2.34±0.11	1.73±0.47^{a}	14.71±0.03^{b}	75.20±0.33^{a}
	Steaming	90.36±0.07^{c}	2.31±0.03	0.21±0.08^{b}	15.52±1.07^{b}	72.33±1.15^{b}
	Grilling	75.43±0.89^{d}	2.25±0.18	0.49±0.03^{b}	11.29±0.00^{c}	61.41±1.08^{c}
Split Gill	Fresh	76.75±0.13^{b}	1.50±0.14	0.63±0.14^{a}	21.31±0.31^{a}	53.31±0.06^{b}
	Boiling	87.35±0.15^{a}	1.53±0.01	0.45±0.24^{a}	15.94±0.52^{d}	69.44±0.68^{a}
	Steaming	75.11±0.13^{c}	1.54±0.02	0.71±0.12^{a}	18.79±0.19^{b}	54.08±0.13^{b}
	Grilling	41.35±0.39^{d}	1.51±0.02	0.74±0.04^{a}	17.59±1.01^{c}	21.51±1.32^{c}

*Values are mean ± SD and expressed as g/100 g dry weight basis of mushroom sample. Different letters in each sample in the same column indicate significant differences ($P< 0.05$). NS indicates non-significant differences among treatments ($P > 0.05$).

The moisture content of fresh mushroom ranged from 76.75%-91.63%. The moisture content was significantly decreased in steaming and grilling samples compared to the fresh samples, which may be attributed to increased water evaporation and tissue shrinkage caused by direct heat exposure. Heat promotes moisture migration from the intracellular matrix toward the surface, leading to substantial water loss under high-temperature conditions[45]. However, the moisture content was higher after boiling process ($P<0.05$), likely due to the immersion of mushrooms in hot water, which reduces evaporative loss and may facilitate partial water absorption into the porous tissue structure. Similar trends, where boiling limits moisture loss while dry-heat methods enhance dehydration, have been reported in previous studies on edible mushrooms[45, 46]. This finding aligns with previous reports by Ulziijargal and Mau [15] and Crisan and Sands [16], who indicated that most fresh mushrooms contain approximately 85–93% moisture. In the present study, fresh King Oyster mushrooms exhibited a moisture content of 86.60% [17], which falls within this typical range, whereas fresh Split Gill mushrooms showed a lower moisture level of 75.83% [18].

The ash content of three fresh mushroom samples ranged between 1.12-2.34 g/100g dry weight basis. These values were lower than those previously reported by Md.A.R. Mazumder et al.[19] The ash content of the three fresh mushroom species ranged from 1.12 to 2.34 g/100 g dry weight. Across all heat treatments, the ash content was nonsignificant different ($P > 0.05$), indicating that heating had little effect on the mineral components of the mushrooms. This result shows that the minerals remained stable during boiling, steaming, and grilling and were not easily lost during processing. The stable ash values observed here are consistent with previous reports that mushroom ash rich in phosphorus and potassium with smaller amounts of magnesium and sulfur is generally resistant to typical cooking conditions. Differences in ash content reported in earlier studies are more often linked to soil mineral composition and growing environments rather than to processing methods, as described by Kalač[20].

The fat content of fresh mushrooms was 1.72 g/100g dry weight basis (King Oyster mushroom), 1.77 g/100g dry weight basis (Shimeji mushroom) and 0.63 g/100g dry weight basis (Split Gill mushroom). The fat content of steamed and boiled King Oyster and Shimeji mushroom

showed significantly decreased compared to fresh samples ($P<0.05$). In addition, the fat content of all Split Gill mushroom sample was nonsignificant different ($P>0.05$). Fong-in et al.[9] reported that the fat content of cooked mushrooms was in the range of 0.96–1.07% dry weight basis. Normally, the fat content in mushrooms is very low due to low lipid content and unsaturated fatty acids[9,10,21]. In addition, boiled and grilled samples, which were significantly lower than that of fresh mushrooms. This is due to the lipid, which may have been denatured and broken down into glycerol and fatty acids during these culinary heat treatment procedures, resulting in a lower fat content[9].

The protein content of fresh King Oyster, Shimeji, and Split Gill mushroom was 15.12, 17.12, 21.31 g/100g dry weight basis, respectively. The protein content of all heat samples was significantly decreased ($P<0.05$) compared to fresh samples. Under boiling conditions, Shimeji mushrooms exhibited the smallest percentage change in protein content when compared with King Oyster and Split Gill mushrooms. In contrast, grilling resulted in the greatest percentage loss of protein in both Shimeji and King Oyster mushrooms, with reductions of 34.05% and 29.30%, respectively. By comparison, the steaming process produced the lowest percentage change in protein loss among all treatments. The steaming process indicated significantly higher protein content compared to the other heat treatments. This might be attributed to the nitrogenous substances that were solubilized and leached out during the boiling process[22]. The finding in this study was in agreement with Liu et al.[23], who demonstrated that the rate of amino acid loss of Rooting Shank mushrooms in boiling was higher than in steaming[9]. Normally, mushrooms have high protein content. On average, mushroom contains 19%−35% protein by dry weight[19]. The results of this study show that Split Gill mushroom is rich in protein content 21.31%, which agreed with other studies which found that usually, the mushroom fruiting bodies, contain about 39.9% carbohydrate, 17.5% protein, and 2.9% fats on a dry weight basis[24]. The King Oyster mushroom contained 15.12% protein content and 1.72% fats which similar to the study of Bakratsas et al.[25] that reported the protein and fat content in Oyster mushrooms was 24.30% and 1.60%, respectively.

Table 2 demonstrates the carbohydrate content of three different fresh mushrooms was approximately 72.22, 70.48, and 53.31 g/100g dry weight basis for King Oyster, Shimeji, and Split Gill mushroom, respectively. Carbohydrate levels in fresh samples considerably increased ($P<0.05$) after boiling compared to other heat treatments. The increase in carbohydrate content with cooking might be due to the destruction of mushroom cell walls that causes an increase in solubility of carbohydrates in water. A smaller increase of carbohydrates in boiled sample might be due to the fact that when the cell walls are destroyed, the carbohydrates might have leached into the boiling water before the extraction for analysis[26]. Grilling showed the lowest carbohydrate amount compared to other cooking methods and fresh samples. Normally, the fruiting bodies of mushrooms generally have approximately 90% moisture, except for the hard, bare fruiting body of Reishi mushroom. Their dry matter is rich in carbohydrates (50–65%) and proteins (19–35%) with small amounts of fats (2–6%)[3].

3.3 The impact of heat treatment on bioactive compounds

3.3.1 Beta glucan content

The beta-glucan contents of King Oyster mushroom, Shimeji mushroom, and Split Gill mushroom fresh and cooked using different heat treatments are shown in Table 3.

Table 3. Glucan content in mushroom samples.

Mushroom	Treatments	Total glucan (% w/w)	Alpha-glucan (% w/w)	Beta-glucan (% w/w)
King Oyster	Fresh	72.42±2.51^{a}	40.12±2.73^{a}	32.32±3.11^{a}
	Boiling	46.35±3.21^{d}	19.95±1.62^{c}	26.40±2.15^{b}
	Steaming	64.10±0.84^{b}	41.77±1.05^{a}	22.33±1.31^{b}
	Grilling	52.00±0.46^{c}	29.07±1.63^{b}	22.92±1.17^{b}
Shimeji	Fresh	64.10±1.45^{b}	28.54±3.00^{c}	35.57±4.20^{a}
	Boiling	45.98±0.56^{d}	33.77±2.24^{b}	12.21±2.24^{c}
	Steaming	71.61±0.26^{a}	39.62±0.31^{a}	31.99±0.16^{a}
	Grilling	52.89±2.66^{c}	33.66±2.31^{b}	19.22±1.88^{b}
Split Gill	Fresh	50.81±1.24^{a}	1.91±0.48^{b}	48.90±1.49^{a}
	Boiling	46.64±1.74^{b}	1.81±0.14^{b}	44.84±1.61^{c}
	Steaming	49.55±2.36^{b}	1.68±0.27^{b}	47.86±2.12^{a}
	Grilling	45.31±1.10^{c}	6.41±1.47^{a}	38.91±0.53^{b}

*Values are mean ± SD. Different letters in each sample in the same column indicate significant differences ($P< 0.05$).

The total glucan content of fresh King Oyster, Shimeji, and Split Gill mushrooms were 72.42%, 64.10%, and 50.81% (w/w), respectively. Heat treatments influenced glucan composition differently across the mushroom species[44]. Total glucan content generally decreased after heating, except in steamed Shimeji mushrooms, which maintained levels comparable to the fresh samples[43]. In King Oyster mushrooms, α-glucan content significantly declined during boiling and grilling, whereas steaming preserved α-glucan without significant loss, indicating that steaming minimized thermal degradation of glucan polymers[43]. Interestingly, all heat-treated Shimeji samples exhibited a significant increase in α-glucan compared to the fresh sample, suggesting that heat exposure may enhance glucan extractability through cell-wall softening or structural disruption[43]. For Split Gill mushrooms, only grilling resulted in a significant increase in α-glucan content, possibly due to moisture loss and subsequent concentration effects[44]. The beta-glucan content of King Oyster mushroom samples significantly decreased during heat treatments compared to fresh samples ($P<0.05$). On the other hand, the beta glucan of fresh Shimeji and Slit Gill mushroom was nonsignificant change during the steaming process ($P<0.05$). This finding shows that steaming process could maintain the beta-glucan in these mushroom species. Mushroom-derived polysaccharides are primarily linear and branched glucans with different glycosidic linkages such (1→3), (1→6)-beta-glucans, and (1→3)-alpha-glucans[27]. Beta-glucan is the primary polysaccharide present in mushrooms, located in the cell walls of fungi and yeast. Mushroom glucans are part of both soluble and insoluble dietary fibers. The rise in insoluble carbohydrates in boiled mushrooms may be due to the leaching of soluble molecules during boiling, as shown by Roncero-Ramos et al.[28]. The cooking process involves the evaporation of water from the raw sample, leading to a decrease in water content and an increase in nutrient concentration. Interactions among different chemicals, chemical reactions, and thermal degradation can also lead to a reduction in nutrient contents[17]. Several factors influence the concentration and efficacy of bioactive substances, such as the mushroom type, substrate, fruiting habitat, developmental stage, mushroom age, storage conditions, and cooking techniques[29]. King Oyster mushroom contains 19.24% glucan, 3.92% alpha-glucan, and 15.32% beta-glucan[41]. Roncero-Ramos et al.[28] studied the impact of several processing methods on Oyster mushroom.

They discovered that temperature and time of heating are crucial factors. The culinary processing led to a decrease in both the amount and effectiveness of polysaccharides.

3.3.2 Total phenolic content (TPC)

The total phenolic content (TPC) of the King Oyster mushroom, Shimeji mushroom, and Split Gill mushroom samples subjected to different heat treatments are shown in Figure 2. Fresh three mushroom samples were 46.59, 51.64, and 19.98 mg GAE/100g, respectively. The TPC all heat mushroom samples were significantly decreased compared to fresh samples ($P<0.05$). Furthermore, this study demonstrated that steaming provided the highest TPC, while grilling resulted in the lowest TPC ($P<0.05$). The variation in this fact can be attributed to the inherent compositional traits of each species and the different growing conditions such as wild or cultivated mushroom[31]. TPC losses in the grilled samples may have occurred due to exposure to high temperatures (180 °C), which caused the compounds to become unstable to heat. Heat treatment contributes to the denaturation of membrane proteins by increasing permeability and causing a change in the structure of the tissue due to softening of the cells, with the consequent loss of water and water-soluble phenolic compounds[32]. Furthermore, heat contributes to the development of non-enzymatic browning reactions in which some compounds that might be quantified as phenolic compounds are generated[33]. The decline in TPC with cooking treatments might be due to their thermal decomposition[9]. Additionally, excessive losses observed in the moist heat methods including boiling, microwaving, and steaming could possibly be due to the leaching loss and degradation of polyphenols. One possibility is that thermal heating has destroyed the polyphenol oxidase (PPO) enzymes that employ phenols as their substrates for browning reaction. For example, steam treatments in *Hericium erinaceus* mushrooms, compared to boiling, effectively decreased the PPO activity[34]. The degradation of phenolic compounds in the boiling treatment, a moist heat process, may be explained by the fact these compounds are water soluble substances[35].

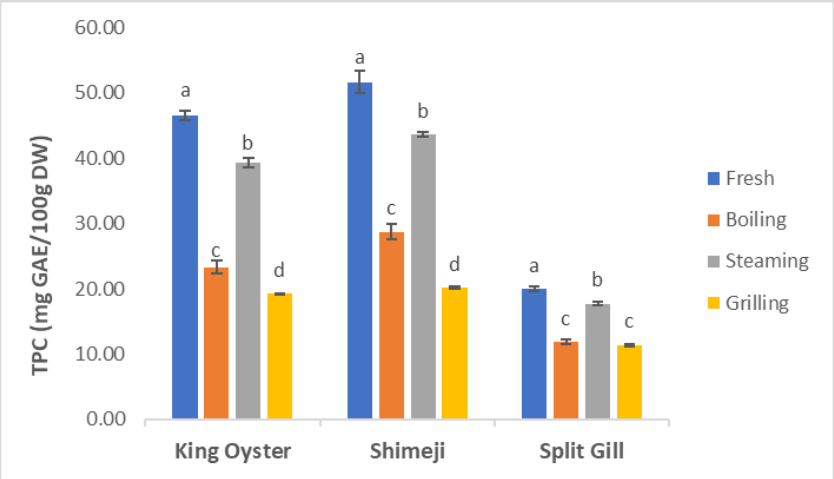

Figure 2. Total polyphenol content (TPC) in Three mushroom samples.

*Error bars represent SD. Different letters in same sample indicate significant differences ($P< 0.05$).

4. Conclusions

Heating led to notable color alterations, reflected by decreased lightness (L^*) and increased redness (a^*) and yellowness (b^*). Heat treatments affected the proximate composition of the three mushroom species in different ways. Grilling led to the most substantial reduction in moisture content because the dry heat caused strong water loss. Ash content showed no significant variation among treatments, suggesting that the mineral components remained stable during heating. Fat content decreased after steaming and grilling in both King Oyster and Shimeji mushrooms, likely

due to heat-related lipid loss. Steaming was the most effective method for retaining protein compared with both boiling and grilling, while boiling produced the highest carbohydrate levels, indicating that moist-heat cooking helped preserve carbohydrates better than dry-heat methods. Steaming emerged as the superior heat treatment method, effectively preserving nutritional quality, total phenolic content, and beta-glucan content compared to boiling and grilling. These findings offer practical guidance for selecting appropriate post-harvest heat treatments to maximize nutritional retention and bioactive compounds potential in mushrooms, beneficial for food industries and community-based food initiatives. Future research should investigate the impacts of these heat treatments on the bioaccessibility of nutrients using *in vitro* digestion models, thereby enriching the understanding of their nutritional implications.

Conflicts of Interest: The author declares no conflict of interest.

References

1. Wang T, Kaur L, Furuhata Y, Aoyama H, Singh J. 3D printing of textured soft hybrid meat analogues. *Foods*. 2022;11(3):478.
2. González A, Cruz M, Losoya C, Nobre C, Loredo A, Rodríguez R. Edible mushrooms as a novel protein source for functional foods. *Food Funct.* 2020;11(9):7400–7414.
3. Rathore H, Sehwag S, Prasad S, Sharma S. Technological, nutritional, functional and sensorial attributes of the cookies fortified with *Calocybe indica* mushroom. *J Food Meas Charact.* 2019;13:976–987.
4. Food and Agriculture Organization of the United Nations (FAO). FAOSTAT [Internet]. Rome (Italy): FAO; 2020 [cited 2025 Nov 13]. Available from: https://www.fao.org/faostat/
5. Manan S, Ullah MW, Ul-Islam M, Atta OM, Yang G. Synthesis and applications of fungal mycelium-based advanced functional materials. *J Bioresour Bioprod.* 2021;6(1):1–10.
6. Tian Q, Liu N, Bai W, Li L, Chen J, Reich PB. A novel soil manganese mechanism drives plant species loss with increased nitrogen deposition in a temperate steppe. *Ecology*. 2016;97(1):65–74.
7. Essien E, Udoh I, Peter N-U. Proximate composition and anti-nutritive factors in some wild edible medicinal macrofungi. *J Nat Prod Plant Resour.* 2013;3:29–33.
8. Ariza MT, Reboredo-Rodríguez P, Cervantes L, Soria C, Martínez-Ferri E, González-Barreiro C, et al. Bioaccessibility and potential bioavailability of phenolic compounds from achenes as a new target for strawberry breeding programs. *Food Chem.* 2018;248:155–165.
9. Fong-in S, Khwanchai P, Prommajak T, Boonsom S. Physicochemical, nutritional, phytochemical properties and antioxidant activity of edible *Astraeus odoratus* mushrooms: Effects of different cooking methods. *Int J Gastron Food Sci.* 2023;33:100743.
10. Kała K, Krakowska A, Szewczyk A, Ostachowicz B, Szczurek K, Fijałkowska A. Determining the amount of potentially bioavailable phenolic compounds and bioelements in edible mushroom mycelia of Agaricus bisporus, Cantharellus cibarius, and Lentinula edodes. *Food Chem.* 2021;352:129456.
11. Yen G-C, Chen H-Y. Antioxidant activity of various tea extracts in relation to their antimutagenicity. *J Agric Food Chem.* 1995;43(1):27–32.
12. Zivanovic S, Büscher R, Kim SK. Mushroom texture, cell wall composition, color, and ultrastructure as affected by pH and temperature. *J Food Sci.* 2006;68:1860–1865.
13. He J-Z, Ru Q-M, Dong D-D, Sun P-L. Chemical characteristics and antioxidant properties of crude water soluble polysaccharides from four common edible mushrooms. *Molecules.* 2012;17(4):4373–4387.
14. Jiménez-Zamora A, Delgado-Andrade C, Rufián-Henares JA. Antioxidant capacity, total phenols and color profile during the storage of selected plants used for infusion. *Food Chem.* 2016;199:339–346.

15. Ulziijargal E, Mau J-L. Nutrient compositions of culinary-medicinal mushroom fruiting bodies and mycelia. *Int J Med Mushrooms.* 2011;13(4):343–349.
16. Crisan E, Sands A. Nutritional value. In: Chang ST, Hayes WA, editors. *The biology and cultivation of edible mushrooms*. New York: Academic Press; 1978. pp. 137–168.
17. Manzi P, Marconi S, Aguzzi A, Pizzoferrato L. Commercial mushrooms: nutritional quality and effect of cooking. *Food Chem.* 2004;84(2):201–206.
18. He Z, Shen Q, Wang L, Fan X, Zhuang Y. Effects of different drying methods on the physical characteristics and non-volatile taste components of *Schizophyllum commune*. *J Food Compos Anal.* 2023;123:105632.
19. Mazumder MAR, Sangsomboon M, Ketnawa S, Rawdkuen S. Mushroom-based Northern Thai style sausages: Physico-chemical, nutritional profile and *in vitro* digestibility. *J Agric Food Res.* 2024;16:101103.
20. Kalač P. Chemical composition and nutritional value of European species of wild growing mushrooms: A review. *Food Chem.* 2009;113(1):9–16.
21. Tang J, Resurreccion FP. Electromagnetic basis of microwave heating. In: Lorence MW, Pesheck PS, editors. *Development of packaging and products for use in microwave ovens*. Cambridge: Woodhead Publishing; 2009. pp. 3–38e.
22. Reis FS, Martins A, Vasconcelos MH, Morales P, Ferreira ICFR. Functional foods based on extracts or compounds derived from mushrooms. *Trends Food Sci Technol.* 2017;66:48–62.
23. Liu Y, Duan X, Zhang M, Li C, Zhang Z, Liu A. Cooking methods effect on the nutrients, bioaccessibility and antioxidant activity of *Craterellus cornucopioides*. *LWT*. 2020;131:109768.
24. Ikechukwu O, Ikechukwuka C, Nwosu CP, Johnpaul O. Pharmaceutical and nutritional prospects of two wild macro-fungi found in Nigeria. *Biotechnology*. 2007;6(4):567–572.
25. Bakratsas G, Polydera A, Katapodis P, Stamatis H. Recent trends in submerged cultivation of mushrooms and their application as a source of nutraceuticals and food additives. *Future Foods*. 2021;4:100086.
26. Reid T, Munyanyi M, Mduluza T. Effect of cooking and preservation on nutritional and phytochemical composition of the mushroom *Amanita zambiana*. *Food Sci Nutr.* 2017;5(3):538–544.
27. Wunjuntuk K, Ahmad M, Techakriengkrai T, Chunhom R, Jaraspermsuk E, Chaisri A, et al. Proximate composition, dietary fibre, beta-glucan content, and inhibition of key enzymes linked to diabetes and obesity in cultivated and wild mushrooms. *J Food Compos Anal.* 2022;105:104226.
28. Roncero-Ramos I, Mendiola-Lanao M, Pérez-Clavijo M, Delgado-Andrade C. Effect of different cooking methods on nutritional value and antioxidant activity of cultivated mushrooms. *Int J Food Sci Nutr.* 2017;68(3):287–297.
29. Guillamón E, García-Lafuente A, Lozano M, Rostagno MA, Villares A, Martínez JA. Edible mushrooms: role in the prevention of cardiovascular diseases. *Fitoterapia*. 2010;81(7):715–723.
30. Sari M, Prange A, Lelley JI, Hambitzer R. Screening of beta-glucan contents in commercially cultivated and wild growing mushrooms. *Food Chem.* 2017;216:45–51.
31. Mena García M, Paula VB, Olloqui ND, García DF, Combarros-Fuertes P, Estevinho LM. Effect of different cooking methods on the total phenolic content, antioxidant activity and sensory properties of wild *Boletus edulis* mushroom. *Int J Gastron Food Sci.* 2021;26:100416.
32. Nimrat S, Soodsaweang P, Vuthiphandchai V. Chemical composition and antibacterial activity of ethanol extract of lemon grass (*Cymbopogon citratus*) on pathogenic bacteria: a review. *Journal of Science and Technology, Ubon Ratchathani University*. 2019;20(3):20–28..

33. Bork LV, Rohn S, Kanzler C. Characterization of colorants formed by non-enzymatic browning reactions of hydroxycinnamic acid derivatives. *Molecules.* 2022;27(21):7564.
34. Kim S. Antioxidant compounds for the inhibition of enzymatic browning by polyphenol oxidases in the fruiting body extract of the edible mushroom *Hericium erinaceus*. *Foods.* 2020;9(7):951.
35. Mashiane P, Mashitoa FM, Slabbert RM, Sivakumar D. Impact of household cooking techniques on colour, antioxidant and sensory properties of African pumpkin and pumpkin leaves. *Int J Gastron Food Sci.* 2021;23:100307.
36. Ng ZX, Tan WC. Impact of optimised cooking on the antioxidant activity in edible mushrooms. *J Food Sci Technol.* 2017;54(12):4100–4111.
37. Palermo M, Pellegrini N, Fogliano V. The effect of cooking on the phytochemical content of vegetables. *J Sci Food Agric.* 2014;94(6):1057–1070.
38. Pogoń K, Jaworska G, Duda-Chodak A, Maciejaszek I. Influence of the culinary treatment on the quality of *Lactarius deliciosus*. *Foods.* 2013;2(2):238–253.
39. Choudhary A, Kumar V, Kumar S, Majid I, Aggarwal P, Suri S. 5-Hydroxymethylfurfural (HMF) formation, occurrence and potential health concerns: recent developments. *Toxin Rev.* 2021;40(4):545–561.
40. Liu Y, Zheng W, Ibrahim SA, Yang H, Huang W. Chemical properties of vacuum-fried *Pleurotus eryngii* during storage and characterization of brown pigment. *Int J Food Prop.* 2017;20(suppl 3):S2349–S2358.
41. Liu Y. Effect of heat treatment on the color and bioactive compounds of mushrooms. *Food Bioprocess Technol*. 2023;6(1.2):155-162.
42. Lee K, Lee H, Choi Y, Kim Y, Jeong HS, Lee J. Effect of different cooking methods on the true retention of vitamins, minerals, and bioactive compounds in shiitake mushrooms (*Lentinula edodes*). *Food Sci Technol Res.* 2019;25(1):115–122.
43. Kiss A, Grünvald P, Ladányi M, Papp V, Papp I, Némedi E, Mirmazloum I. Heat treatment of Reishi medicinal mushroom (*Ganoderma lingzhi*) basidiocarp enhanced its β-glucan solubility, antioxidant capacity and lactogenic properties. *Foods*. 2021;10(9):2015.
44. Morales D, Bal MA, Figueredo S, Soler-Rivas C, Ruiz-Rodríguez A. Effect of household cooking treatments on the stability of β-glucans, ergosterol and phenolic compounds in mushrooms. *Food Bioprocess Technol*. 2024.
45. Yao F, Sun B, Zhang C, Xu X, Hao J, Liu J, et al. Effect of different cooking methods on the physicochemical and sensory properties of shiitake mushroom (*Lentinula edodes*). *Foods*. 2023;12(5):1035.
46. Fong-in S, Nopharatana M, Rattanapan C. Physicochemical, nutritional, and phytochemical properties of edible mushrooms after thermal processing. *J Food Meas Charact*. 2023;17:2141–2154.
47. Prabsangob N, Sittiketgorn S. Profile of taste-related compounds and bioactivity of split gill mushroom (*Schizophyllum commune*) as affected by blanching and drying. *International Journal of Food Properties*. 2023 Sep 22;26(1):2078-90.

O - 344

Comparative Impact of Synthetic (polysorbate 80) and Protein-Based (α-lactalbumin) Emulsifiers on Intestinal Barrier Integrity and the Trans-Epithelial Transport of Polychlorinated Biphenyls

Banjara Vivek and Thaiudom Siwatt*

Institute of Agricultural Technology, Suranaree University of Technology, Thailand

**Corresponding author E-mail: thaiudom@g.sut.ac.th*

Abstract: Food emulsifiers are integral components of processed food matrices that stabilize formulations but may concurrently modulate intestinal barrier function and xenobiotic bioavailability. Given the rising consumer demand for natural "clean-label" ingredients, this study systematically evaluated the comparative effects of the synthetic emulsifier Polysorbate 80 (P80) and the natural protein-based emulsifier a-lactalbumin (a-LA) on epithelial integrity. Using a validated *in vitro* Caco-2 cell monolayer model, differentiated cells were exposed to non-cytotoxic concentrations of P80 or a-LA (0.05–0.1%) in the presence or absence of polychlorinated biphenyl (PCB) congeners 138 and 153 (1mM) for 4 h. Barrier functionality was assessed via transepithelial electrical resistance (*TEER*) and Lucifer Yellow (LY) paracellular flux, while tight junction (*TJ*) gene expression were analyzed through RT-qPCR (*TJP-1, OCLN, CLDN-1)*. PCB transport was quantified using GC-MS/MS. The results indicated that while TEER remained stable across all treatments, P80 (0.1%) significantly increased LY permeability ($Papp = (2.9 \pm 0.5) \times 10^{-7}$ cm/s) compared to the buffer control ($(1.2 \pm 0.1) \times 10^{-7}$ cm/s), representing a 2.5-fold increase in paracellular leakage. This effect was exacerbated by co-exposure with PCBs (3.8-fold increase), whereas a-LA maintained barrier function with no significant change in *Papp*. Molecular analysis revealed that P80 (0.1%) selectively downregulated *CLDN* mRNA, suggesting *TJ*-specific perturbation. Furthermore, P80 facilitated a dose-dependent increase in PCB transport, with basolateral concentrations of PCB-153 and PCB-138 reaching 144.6 ± 9.2 nM and 141.7 ± 15.6 nM, respectively—over 4-fold higher than PCB-only controls. Conversely, a-LA significantly attenuated PCB transport. These findings demonstrate that P80 compromises the intestinal interface and enhances xenobiotic absorption, whereas a-LA preserves epithelial barrier function. This study highlights the importance of emulsifier selection in food formulation to safeguard consumer health and mitigate the uptake of environmental contaminants.

Keywords: Emulsifiers; Polysorbate-80; α-Lactalbumin, Intestinal barrier; Polychlorinated biphenyls.

1. Introduction

Food emulsions represent an omnipresent structural motif in the human diet, underpinning the matrix of various dairy products, beverages, sauces, and ultra-processed foods. These systems, primarily oil-in-water (O/W) dispersions, are stabilized by amphiphilic emulsifiers that adsorb at the oil–water interface to lower interfacial tension and inhibit droplet coalescence [(1)]. Beyond their role in ensuring physicochemical stability, emulsifiers are pivotal in modulating the bio-accessibility and bioavailability of lipophilic constituents, such as essential vitamins, carotenoids, and various nutraceuticals [(2, 3)]. Emerging research underscores that the interfacial architecture of an emulsion directly dictates the intestinal absorption kinetics of hydrophobic molecules, a phenomenon well-documented for bioactives such as curcumin and b-carotene [(4, 5)].

The selection of emulsifying agents is therefore a critical determinant of both a product's techno-functional performance and its subsequent interaction with intestinal physiology and xenobiotic uptake. While synthetic, low-molecular-weight emulsifier like P80 are industrially favored for their robust emulsifying efficiency, a paradigm shift toward clean-label and natural ingredients has intensified interest in milk-derived proteins[6]. However, the role of emulsifiers extends beyond simple stabilization; they are increasingly recognized as active modulators of intestinal homeostasis [7]. P80 is extensively utilized across baked goods, dairy, beverages and infant formulas [8]. Despite its regulatory approval, evidence suggests that P80 may contribute to deleterious health outcomes, including compromised intestinal permeability [9], exacerbated inflammation [10], gut microbiota dysbiosis [11], and metabolic dysfunction [12]. Mechanistically, these effects are linked to the downregulation of mucosal proteins and tight junction (*TJ*) components [13], potentially facilitating the systemic translocation of allergens and environmental contaminants [14, 15].

Conversely, a-lactalbumin (a-LA)—a primary whey protein constituting approximately 13% of bovine whey and 2% of total milk protein—offers a promising natural alternative due to its inherent amphiphilicity [16]. Beyond its industrial utility, a-LA exhibits significant bioactivity, including anti-inflammatory properties [17], gastroprotective effects in ulcer models [18], and the ability to mitigate intestinal inflammation [19]. Crucially, a-LA has been shown to reinforce the intestinal barrier, suppressing disruptions induced by various toxins [20].

Concurrently with the intake of food additives, the diet serves as a primary exposure route for persistent organic pollutants (POPs), specifically polychlorinated biphenyls (PCBs) [21]. These synthetic organochlorine compounds, characterized by biphenyl rings with variable chlorination patterns, comprise 209 congeners with distinct toxicological profiles [22]. Despite their 2004 global ban under the Stockholm Convention, their lipophilicity and environmental persistence drive continued bioaccumulation within the food chain, resulting in detectable concentrations in human tissues [22, 23]. Dietary intake remains the dominant exposure pathway [21], with chronic exposure linked to carcinogenic, genotoxic, endocrine, and immunological disorders [24]. Animal-derived lipids, such as those found in milk and meat, act as significant dietary reservoirs for these lipophilic contaminants [23, 25].

The intestinal epithelium serves a dual, albeit conflicting, role: facilitating the absorption of vital nutrients while maintaining a rigorous defense against pathogens and xenobiotics [26]. Compromised barrier integrity is a hallmark of gastrointestinal pathologies, including inflammatory bowel disease (IBD) and celiac disease, as well as systemic conditions like obesity and neurodegeneration [27]. Food additives, particularly emulsifiers present in modern day diets, have been associated with perturbations in gut microbiota, inflammation, and barrier permeability [10].

Despite the prevalence of both emulsifiers and PCBs in the modern food supply, there is a conspicuous lack of comparative data regarding how natural versus synthetic emulsifiers affect contaminant transport. This study addresses this knowledge gap by systematically evaluating the influence of P80 and a-LA on intestinal barrier function and the trans-epithelial transport of PCB congeners 138 and 153 using a validated *in vitro* Caco-2 cell model. Furthermore, this research explores the mechanistic contribution of emulsifier properties to PCB flux. These findings aim to clarify the biological impact of dietary emulsifiers on food safety and xenobiotic exposure, ultimately informing safer food formulation strategies and more comprehensive risk assessments.

2. Materials and methods

2.1 Chemicals and reagents

The human colorectal adenocarcinoma cell line, Caco-2, was sourced from the Laboratory of Cell-Based Assays and Innovation (Suranaree University of Technology, Thailand). Cell culture media and supplements, including Dulbecco's Modified Eagle Medium (DMEM; 4.5 g/L D-

glucose), fetal bovine serum (FBS), penicillin-streptomycin (10,000 units/mL), non-essential amino acids (NEAA), 0.25% trypsin, phenol red-free Hank's Balanced Salt Solution (HBSS) with Ca^{2+} and Mg^{2+}, 7.5% sodium bicarbonate, and 1 M HEPES buffer, were procured from Gibco (Grand Island, NY, USA).

Polyester Transwell inserts (24 mm diameter, 0.4 mm pore size) were obtained from Corning Inc. (Lowell, MA, USA). Analytical reagents, including the PureLink RNA Mini Purification Kit and MTT (3-(4,5-dimethylthiazol-2-yl)-2,5-diphenyltetrazolium bromide), were from Invitrogen (Thermo Fisher Scientific, USA). Molecular biology reagents, specifically ReverTra ACE qPCR Master Mix with gDNA Remover and qPCRBIO SYGreen Mix Lo-Rox, were purchased from Toyobo (Osaka, Japan) and PCR Biosystems (Texas, USA), respectively.

The emulsifiers a-LA and P80, along with Lucifer Yellow (LY) CH dipotassium salt and dimethyl sulfoxide (DMSO), were obtained from Sigma-Aldrich (St. Louis, MO, USA). High-purity reference standards for PCB 153 (2,2',4,4',5,5'-hexachlorobiphenyl) and PCB 138 (2,2',3,4,4',5'-hexachlorobiphenyl) were purchased from Dr. Ehrenstorfer (Augsburg, Germany). All solvents (n-hexane and acetone) were of HPLC grade; all other reagents were of analytical grade. Apical dosing solutions were sterilized using 0.22 mm filters prior to application.

2.2 Caco-2 cell culture and subculture

Caco-2 cells were maintained in T-75 cm^2 tissue culture flasks using complete DMEM (supplemented with 10 % FBS, 1% penicillin-streptomycin, and 1% NEAA). Cultures were incubated in a humidified environment at 37°C with 5% CO_2, adhering to established protocols described by Putt et. al.[28].

2.3 Preparation of emulsifier and PCB solutions

Stock solutions of P80 and a-LA (5% w/v) were prepared in sterile PBS, vortexed, and solubilized in a 60°C water bath for 30 min. Solutions were then hydrated overnight at 4°C. Working concentrations were freshly prepared in complete DMEM or transport buffer (HBSS supplemented with 20 mM HEPES, 0.35g/L $NaHCO_3$, pH 7.4). PCB congeners 138 and 153 were dissolved in DMSO to create 10 mg/500 mL stock solutions. Equimolar solutions of PCB 138 and 153 mix were prepared by combining equal volume of stocks in the respective treatment media or buffer containing final DMSO concentration ≤0.1% (v/v).

2.4 MTT cytotoxicity assay

Cells were seeded at density of 20×10^4 cells/well into 96-well plates and allowed to adhere for 24 h. Monolayers were then exposed to treatment media containing varying concentrations of P80 or a-LA (0.01-2% v/v), PCBs (0.5-100 mM), or their combinations for 24 h. Post-exposure, 100 mL of MTT reagent (0.5 mg/mL in PBS) was added and incubated for 3 h at 37°C. The resulting formazan crystals were solubilized in 100 mL DMSO. Absorbance was recorded at 570 nm using a SPECTROstar Nano reader (BMG LABTECH, Germany). Cell viability was calculated as a percentage relative to the untreated control [29].

$$\% \text{ Viability} = \frac{\text{Mean Optical density of sample} - \text{Mean optical desnity of background}}{\text{Mean optical density of control} - \text{mean optical density of backround}} X100 \quad (1)$$

2.5 Caco-2 monolayer formation and TEER measurement

Cells were seeded onto Transwell inserts (4.67 cm^2 surface area) at a density of $2.6\text{x}10^5$ cells/cm^2. The apical and basolateral chambers were filled with 1.5 mL and 2.5 mL of complete DMEM, respectively. Transepithelial electrical resistance (TEER) was monitored using a Millicell ERS-2 (Merck, USA) with STX01 Ag–AgCl electrodes at 37°C as described by Hubatsch et. al.[30]. The final TEER values, expressed as Ωcm^2 were calculated based on the following equation:

$$TEER = (R–Rb) \times A \quad (2)$$

where R is the resistance of filter insert with Caco-2 cells, Rb is the background resistance of the filter alone, A is the surface area

Monolayers with TEER values above 450Ωcm^2 were only selected for subsequent experiments. TEER was recorded immediately before treatment (t=0) and after 4 h exposure and TEER changes were expressed relative to initial values.

2.6 Paracellular permeability assay (LY)

Paracellular flux was evaluated using 100 mM LY in the apical chamber. Basolateral samples (200 mL) were collected at 0, 0.5, 1, 2, 3, and 4 h and replaced with fresh buffer to maintain sink conditions. Fluorescence was quantified (Ex: 428 nm, Em: 540 nm) using a Varioskan LUX reader (Thermo Fisher Scientific, USA). The apparent permeability coefficient (P_{app}) was calculated using:

$$P(app)\left(\frac{cm}{s}\right) = \frac{dQ/dt}{A*Co} \quad (3)$$

where dQ/dt is the steady-state rate of LY appearance in the basolateral compartment (µmol/s), A is the membrane area (cm²), and C_0 is the initial apical LY concentration (µM).

When LY data were expressed as concentration in the basolateral compartment, dQ/dt was obtained from the slope of concentration versus time multiplied by basolateral volume; sampling-volume corrections were applied when needed. LY P_{app} values ≤ 1 × 10^{-6} cm/s and paracellular flux ≤ 0.5–0.7% were considered to indicate intact monolayers, consistent with commonly used acceptance criteria. [31].

2.7 RT-qPCR Analysis

After 4h exposure to P80/α-LA (0.05% and 0.1% v/v) and 1µM PCB (equimolar 138 and 153) congener mix, monolayers were washed three times with transport buffer and mRNA extracted using PureLink RNA Mini Kit (Invitrogen, USA) following the manufacturer's instructions. RNA concentration and purity were determined by NanoDrop spectrophotometer (Thermo Fisher Scientific, USA), and samples with A_{260}/A_{280} between 1.9 and 2.2 and A_{260}/A_{230} > 1.8 were used for cDNA synthesis. 100 ng of RNA was added for the 20 µL transcription reaction using ReverTra Ace qPCR Master Mix with gDNA Remover (Toyobo Co. Ltd., Japan) following manufacturer's instructions. Primers for tight junction proteins (*TJP-1, CLDN-1, OCLN*) designed using NCBI Primer-BLAST and validated against published sequences, described in table 1 [15, 28]. qPCR was performed using qPCRBIO SyGreen Mix Lo-Rox (PCR Biosystems, USA) on a QuantStudio 3 Real-Time PCR System (Applied Biosystems, USA). Cycling conditions: initial denaturation (95°C, 2min), followed by 35 cycles of denaturation (95°C, 5s), annealing (60°C, 15s), extension (72°C, 20s) with fluorescence acquisition at the end of extension 72°C step; a melt curve (65–95 °C) was run at the end of each reaction to verify specificity. Non-template controls (NTC) and no-RT controls (NRT) were included for each primer pair to confirm absence of contamination and genomic DNA amplification. Ct values were exported, and relative gene expression was calculated using the $2^{-\Delta\Delta Ct}$ method, normalizing target genes to GAPDH and comparing treated samples to the relevant control group. All reactions were performed in technical duplicates, and at least three independent experiments (biological replicates) were analyzed for each condition [15, 32].

Table 1 List of primers used in real-time RT-qPCR assay

Gene	Forward (5'-3')	Reverse (5'-3')	Reference
TJP-1	CAAGATAGTTTGGCAGCAAGAGATG	ATCAGGGACATTCAATAGCGTAGC	(15, 28)
CLDN-1	TGGTGGTTGGCATCCTCCTG	AATTCGTACCTGGCATTGACTGG	
OCLN	CCAATGTCGAGGAGTGGG	CGCTGCTGTAACGAGGCT	
GADPH	GCACCGTCAAGGCTGAGAAC	TGGTGAAGACGCCAGTGGA	

2.8 Transepithelial transport of PCB

For the PCB transport assays, monolayers were pre-equilibrated in transport buffer for 30 min in an orbital shaker at 150 rpm. The apical compartment was loaded with 1.5 mL of transport buffer containing equimolar concentration of 1 µM PCB mixture (PCB-138 and PCB-153), 100 µM LY, and either 0.05% or 0.1% P80/α-LA. To simulate physiological protein binding and maintain sink conditions, the basolateral compartment was filled with 2.5 mL of transport buffer supplemented with 4% (v/v) bovine serum albumin (BSA). The plates were then incubated at 37°C for 4 h on an orbital shaker (150 rpm). To monitor barrier integrity, transepithelial electrical resistance (TEER) was measured at the onset (t = 0 h) and the conclusion (t = 4 h) of the incubation period. Following the 4 h incubation, apical and basolateral aliquots were collected for PCB and LY quantification. Paracellular permeability was evaluated based on basolateral LY fluorescence, while transepithelial transport was determined by assessing PCB distribution within the basolateral receiver compartment. [33, 34].

2.8.1 Sample preparation for PCB quantification

PCB extraction from basolateral transport buffers was carried out by a modified liquid–liquid extraction protocol based on Ghosh et. al.[35] with slight modification. Briefly, 1 mL of the basolateral sample was transferred to a glass tube and mixed with 0.5 g of NaCl and 0.5 mL of acetone. Following vertexing, 0.5 mL of hexane was added, and the mixture was vortexed for an additional 2 min. The samples were then centrifuged at 15,000 x g for 10 min at room temperature. The resulting organic phase was transferred to amber autosampler vials and stored at −20 °C prior to GC–MS/MS analysis. To ensure analytical rigorousness, matrix blanks and spiked recovery samples were processed alongside each experimental batch.

2.8.2 Quantification of PCBs

PCB concentrations were determined using gas chromatography-tandem mass spectrometry (GC–MS/MS), following the protocol described by Garcia-Bermejo et. al.[36], with minor modifications. Analysis was performed on an Agilent 7890A GC system coupled to a 7000B triple quadrupole MS operating in electron ionization (EI) mode at 70 eV. Samples (2 µL) were introduced via spitless injection at an inlet temperature of 290°C. The auxiliary and ion source temperatures were maintained at 280°C and 230°C, respectively. High-purity helium served as the carrier gas at a constant flow rate of 1 mL/min, while nitrogen was utilized as the collision gas. Chromatographic separation was performed on an HP-5ms capillary column (30 m x 250 µm x 0.25 µm film thickness). The oven temperature program was initiated at 90°C (held for 2 min), followed by a ramp of 10°C/min to 280°C (held for 3 min), resulting in a total run time of 24 min. The MS was operated in multiple reaction monitoring (MRM) mode. For each PCB congener, two specific precursor-to-product ion transitions (quantifier and qualifier) were optimized using AutoSRM. Quantification was performed using external calibration curves generated from equimolar PCB-138 and PCB-153 standards in hexane, ranging from 0.01nM to 500nM. All curves exhibited excellent linearity (R^2 = 0.996). Extraction recoveries were determined using matrix-matched spiked controls. The limits of detection (LOD) and quantification (LOQ) were established using low-level standards and blanks. Analyte identity was confirmed based on retention time and qualifier/quantifier ion ratios within established tolerances.

2.9 Statistical Analysis

Data are expressed as mean ± SEM from at least three biological replicates. Statistical significance was determined using one-way or two-way ANOVA followed by Dunnett's post-hoc test ($p < 0.05$) via GraphPad Prism v10.4.2 (GraphPad Software, San Diego, CA, USA).

3. Results and discussion

3.1 Establishing experimental dosage of emulsifiers and PCB

3.1.1 Cytotoxicity of PCBs

An equimolar mixture of PCB 138 and PCB 153 was evaluated over an expanded concentration range (0.5–100 µM) for 24 h and 48 h. As illustrated in Fig. 3.1, no significant cytotoxicity was observed at concentrations up to 50 µM after 24 h. However, a 48-h exposure to 50 µM resulted in a statistically significant reduction in cell viability. A more pronounced cytotoxic effect was recorded at 100 µM, with viability decreasing to 73.9 ± 5.0% at 24 h and 57.4 ± 1.3% at 48 h. Collectively, these results indicate a time- and concentration-dependent cytotoxic profile for the PCB mixture.

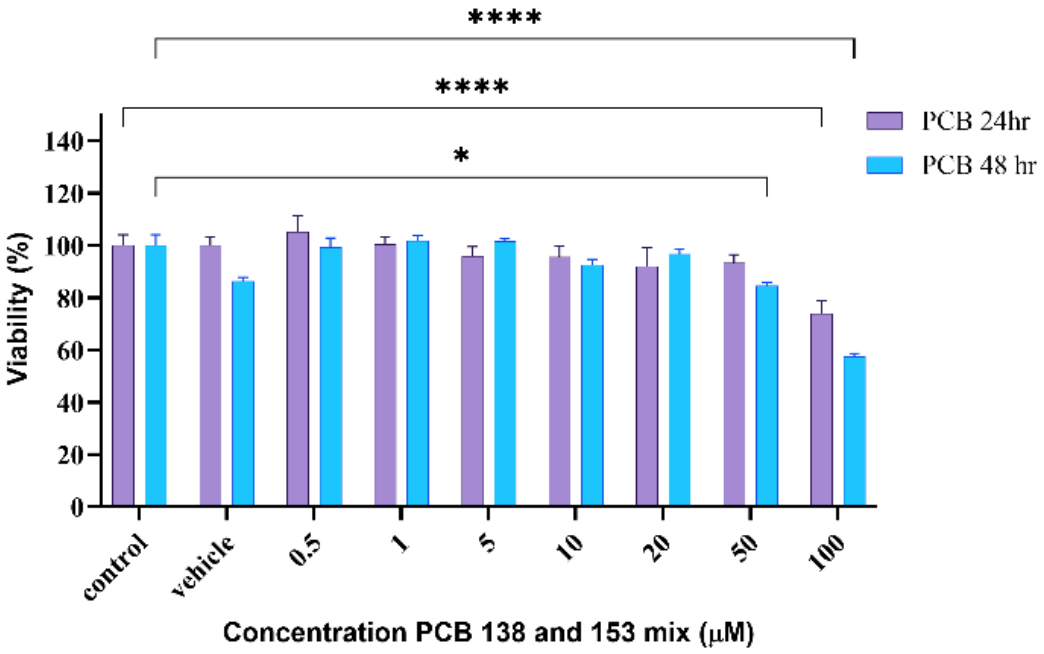

Fig. 3.1 Cell viability (%) to various concentrations of PCB mix after 24 h and 48 h exposure. Values are expressed as mean ± SEM (n=3). Asterisks denote significant differences vs control (**p<0.001; *p<0.05, ***p<0.0001)

An equimolar mixture of PCB 138 and PCB 153 at a total concentration of 1 µM was selected for all subsequent experiments, as this concentration did not show cytotoxic effects while remained analytically quantifiable in transepithelial transport study. Furthermore, comparable concentrations have been extensively documented in previous *in vitro* studies on PCB uptake and toxicity without adverse effects on cell viability [35, 37].

3.1.2 Cytotoxicity of P80 and α-LA with PCBs

MTT analysis in Caco-2 cells (24 h exposure) showed that P80 was non-cytotoxic up to 0.2% but exhibited marked, dose-dependent cytotoxicity at ≥0.5% (10.8 ± 1.5% viability) and near-complete cell death at 1–2%, whereas α-LA (0.01–2%) showed no significant cytotoxicity

and maintained cell viability across all tested concentrations (supplementary S1). The combined cytotoxic effects of a 1 µM PCB mixture (comprising equimolar concentrations of congeners 138 and 153) and non-cytotoxic concentrations of P80 and α-LA (0.05–0.2%) were evaluated in Caco-2 cells using the MTT assay. Co-administration of α-LA with the PCB mixture, across all tested concentrations up to 0.2%, did not result in a significant reduction in cell viability, indicating a favorable safety profile and negligible cytotoxic interaction (Fig. 3.2 B).

In contrast, 0.2% P80 in combination with 1 µM PCB significantly decreased cell viability to 66.7 ± 0.2%, suggesting a synergistic cytotoxic interaction (Fig. 3.2 A). Notably, while 0.2% P80 alone reduced viability to 82.4 ± 1.3% (Supplementary S1), its combination with the PCB mixture led to a significantly more pronounced reduction, further supporting the hypothesis of enhanced toxicity through interaction. Consequently, concentrations of 0.05% and 0.1% for both P80 and α-LA were selected for subsequent analyses.

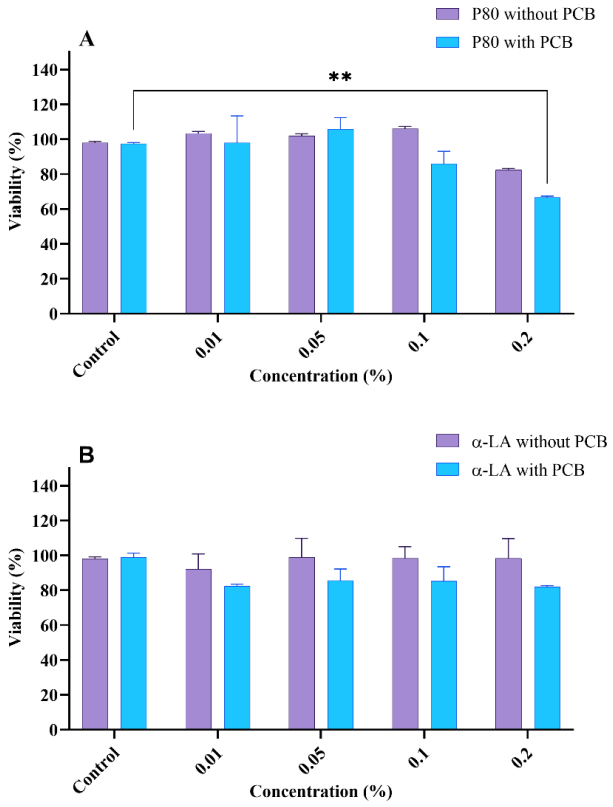

Fig. 3.2 Cell viability (%) to various concentrations of **(A)** P80, **(B)** α-LA with or without 1µM PCB mix after 24h exposure. Values are expressed as mean ± SEM (n=3). Asterisks denote significant differences vs control (**p<0.001)

3.2 Effect of emulsifiers and PCBs on barrier properties

Caco-2 monolayers cultured for 21 days achieved stable transepithelial electrical resistance (TEER) values exceeding 450 Ω·cm² consistent with established benchmarks for intestinal barrier integrity [30]. During the 4 h exposure period, TEER remained stable across all treatment groups, including individual applications of P80, α-LA, and the PCB mixture (supplementary information S2), as well as combinations of P80/α-LA with the 1 µM PCB mixture.

These observations suggest that acute exposure to these treatments did not induce gross disruptions of the tight junctional complexes detectable by electrical resistance. However, TEER stability may not fully reflect subtle alterations in paracellular permeability, as resistance can remain constant even in instances of increased solute flux [38].

To further evaluate monolayer integrity, the paracellular permeability of LY—a hydrophilic marker [39] was quantified. Treatment with 0.1% P80 induced a significant, time-dependent increase in basolateral LY concentrations, rising from 0.93 ± 0.07 µM at 2 h to 1.2 ± 0.07 µM at 4 h. In comparison, values for the HBSS control were 0.32 ± 0.03 µM and 0.45 ± 0.06 µM at 2 h and 4 h, respectively. Conversely, 0.05% P80, α-LA (0.05 and 0.1%), and PCBs alone elicited only marginal, non-significant deviations from the control (supplementary information S3).

The apparent permeability coefficient (P_{app}) for LY following 0.1% P80 treatment was (2.9 ± 0.5) × 10^{-7} cm/s, representing a 2.5-fold elevation compared to the HBSS control (1.2± 0.1) × 10^{-7} cm/s (Fig. 3.3 A). Although statistically significant, this value remained below the established threshold for a compromised barrier (1 × 10^{-6} cm/s) [40]. Ujhelyi et. al.[41], who demonstrated that even 0.01% P80 enhances the paracellular permeability of LY within 2 h of exposure.

In contrast, α-LA (0.05 or 0.1%) did not significantly alter the P_{app}, indicating a negligible effect on paracellular diffusion in its native form. This is consistent with previous reports suggesting that while intact α-LA supports intestinal cell growth and survival, it does not significantly disrupt epithelial barrier function [42]. Similarly, PCBs alone did not alter the apparent permeability of LY. Collectively, these observations suggest that P80 functions as a modest paracellular enhancer, whereas native α-LA is largely barrier-neutral (Fig. 3.3A).

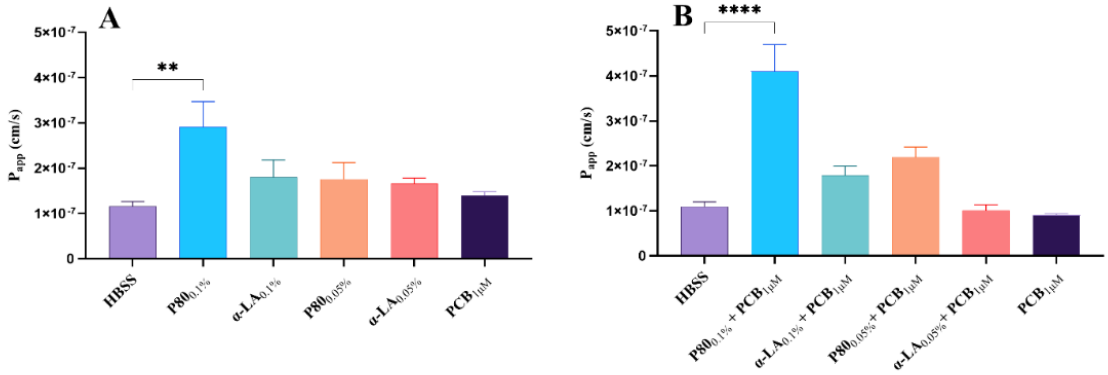

Fig. 3.3 Lucifer Yellow apparent permeability (P_{app} cm/s) across differentiated Caco-2 monolayers after 4 h exposure **(A)** P80/α-LA and PCB alone, **(B)** Co-exposure of P80/α-LA with PCB. Values are expressed as mean ± SEM (n=3). Asterisks denote significant differences vs HBSS (**p<0.001, ****p<0.0001)

In contrast, co-exposure to P80 and PCBs significantly enhanced LY permeability compared to the HBSS control. The P_{app} for LY reached (4.1 ± 0.6) × 10^{-7} cm/s in the 0.1% P80 + 1 µM PCBs, compared to (1.1 ± 0.1) × 10^{-7} cm/s in the control (HBSS), representing a significant 3.8-fold enhancement. Notably, 0.1% P80 alone produced only a 2.5-fold enhancement, indicating that the addition of PCBs potentiates the permeabilizing effect of P80 (Fig. 3.3 B). A similar trend was observed for 0.05% P80, where the combination with PCBs yielded a 2-fold increase in P_{app} compared to the 1.5-fold increase observed with the emulsifier alone. These findings resonate with the growing body of literature indicating that P80 can enhance the transepithelial passage of co-ingested contaminants or pharmaceuticals by modulating barrier fluidity and the micellar solubilization of lipophilic compounds [14, 43]. Furthermore, Wu et. al.[15] reported that emulsifiers can intensify the cytotoxicity of food-borne contaminants in gastrointestinal models without necessarily inducing a dramatic loss of TEER.

Interestingly, the α-LA + PCB combination produced fold-changes in LY P_{app} similar to those of α-LA alone, both of which were substantially lower than the P80 + PCB results. This

suggests a subtle interaction that may reflect shifts in micellar structure or protein–PCB binding rather than direct tight-junction disassembly. Previous research indicates that milk proteins, including α-LA, can form complexes with fatty acids [44], flavoring compounds [45] and hydrophobic micronutrients [46], thereby modulating their solubility and transport. The modest P_{app} increase observed here may therefore represent a small shift in paracellular leakage or transcellular trafficking under co-exposure, but the effect is clearly weaker than that of P80 (Fig 3.3 B).

Overall, these data indicate that P80 exacerbates the paracellular permeability of monolayer in the presence of PCBs, whereas α-LA maintains near-baseline barrier function. These findings are broadly consistent with *in vivo* and *in vitro* studies showing that P80 promotes the intestinal absorption of xenobiotics, such as phthalates [13], while α-LA is generally characterized as barrier-supportive [20]. While PCBs have been shown to disrupt intestinal integrity via NADPH oxidase-induced alterations of tight junction protein expression [47] our study highlights that P80 can specifically potentiate these effects. Thus, P80 functions as a potent intestinal permeability enhancer, whereas α-LA exhibits a neutral effect on barrier function under these conditions.

3.3 Effect of emulsifiers on tight junction gene expression

The paracellular permeability assays using LY indicated significant variations in solute flux, suggesting that the treatments may modulate the expression of tight junction proteins *(TJPs*), such as *TJP-1* (zonula occludens-1), *OCLN* (occludin), and *CLDN-1* (claudin-1), which are essential for maintaining epithelial barrier integrity [48]. To investigate these molecular changes, RT-qPCR performed following a 4 h exposure to P80 and α-LA at concentrations of 0.05 and 0.1%.

The results revealed that *CLDN1* expression was significantly downregulated in cells treated with 0.1% P80 compared to the control group (Fig 3.4 C). Conversely, P80 did not induce statistically significant alterations in the transcript levels of *TJP-1* or *OCLN*. Notably, treatment with α-LA or PCBs, either alone or in combination, failed to elicit significant changes in the expression of any of the target tight junction-associated genes (Fig. 3.4).

These findings underscore the differential impact of food emulsifiers on the molecular architecture of tight junctions. Specifically, the observed downregulation of *CLDN1* in P80-treated cells correlates with the previously noted increase in paracellular permeability. This aligns with prior studies suggesting that certain emulsifiers may impair barrier function via the selective modulation of gene expression in the absence of overt cytotoxicity, highlighting a nuanced relationship between emulsifier exposure and epithelial integrity [14, 15].

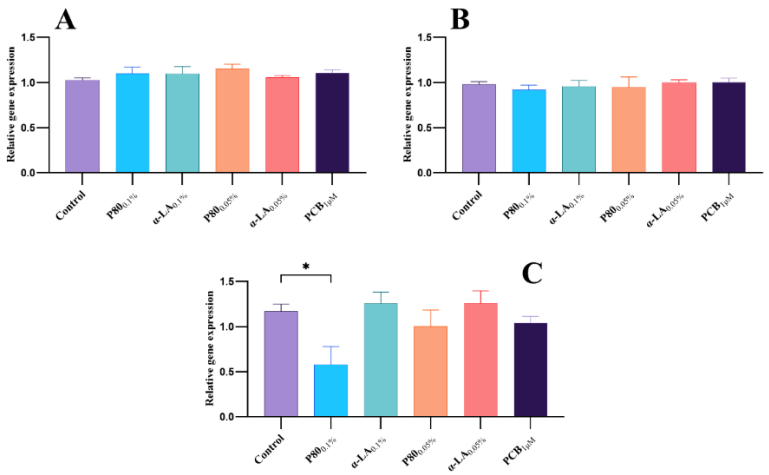

Fig. 3.4 Relative gene expression ($2^{-\Delta\Delta CT}$) of **(A)** *TJP-1*; **(B)** *OCLN*; and **(C)** *CLDN-1* in differentiated Caco-2 cells exposed to P80, α-LA and PCBs for 4 h. Values are expressed as mean ± SEM (n=3). Asterisks denote significant differences vs control(*p<0.05)

3.4 Effect of α-LA and P80 on transport of PCB

The transepithelial transport of PCB congeners across the Caco-2 monolayer exhibited a distinct dependence on both the PCB congener subtype and the concentration of P80 administered. In the presence of 0.1% P80, the basolateral accumulation of PCB-153 reached 144.6 ± 9.2 nM, representing a substantial increase compared to the 33.5 ± 3.6 nM observed in the PCB-only control group. Similarly, PCB-138 transport was significantly enhanced, reaching 141.7 ± 15.6 nM. Notably, the lower P80 concentration (0.05%) also facilitated a significant increase in transport, with recorded values of 93.8 ± 15.3 nM for PCB-153 and 80.6 ± 6.7 nM for PCB-138.

In contrast, treatment with α-LA resulted in significantly lower transport levels relative to the P80-treated groups, with values remaining near or below the control levels. This suggests that while P80 functions as a potent transport enhancer for these contaminants, α-LA does not exhibit similar facilitative properties (Fig. 3.5). These findings corroborate existing literature highlighting the role of food emulsifiers in augmenting the intestinal absorption of lipophilic xenobiotics [43], likely by enhancing micellar solubilization and modulating epithelial barrier properties [49].

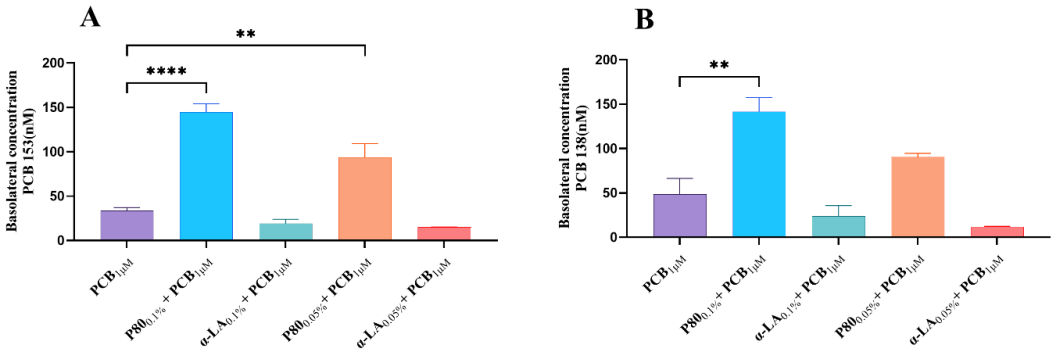

Fig. 3.5 Dose dependent effect of P80 and α-LA on **(A)** PCB 153 and **(B)** PCB 138 transported after exposure to 4 h. Values are expressed as mean ± SEM (n=3). Asterisks denote significant differences vs PCB only (**p<0.001, ****p<0.00001)

4. Conclusion

The present study provides insights into the differential impact of emulsifiers on the transepithelial transport of PCBs within a Caco-2 cell model. Our findings demonstrate that P80 modulates paracellular permeability through the modulation of TJ function. In contrast, native α-LA maintained barrier integrity and exhibited a protective or neutral effect. These results suggest that dietary emulsifiers at permitted levels promote the intestinal absorption of POPs by compromising barrier function. Dietary components can also influence the bioaccessibility and bioavailability of xenobiotics [50]. Future research exploring the mechanisms of intestinal barrier function modulation under physiologically relevant conditions could motivate to assess the potential risks associated with the use of synthetic emulsifiers in diet.

References

1. McClements D. Food emulsions: principles, practices, and techniques. 2015.
2. Tan C, McClements DJ. Application of Advanced Emulsion Technology in the Food Industry: A Review and Critical Evaluation. Foods. 2021;10(4).
3. Zhang R, Wu W, Zhang Z, Lv S, Xing B, McClements DJ. Impact of food emulsions on the bioaccessibility of hydrophobic pesticide residues in co-ingested natural products: Influence of emulsifier and dietary fiber type. Journal of agricultural and food chemistry. 2019;67(21):6032-40.

4. Gulseren I, Guri A, Corredig M. Effect of interfacial composition on uptake of curcumin-piperine mixtures in oil in water emulsions by Caco-2 cells. Food Funct. 2014;5(6):1218-23.
5. Lu W, Kelly AL, Maguire P, Zhang H, Stanton C, Miao S. Correlation of emulsion structure with cellular uptake behavior of encapsulated bioactive nutrients: Influence of droplet size and interfacial structure. Journal of Agricultural and Food Chemistry. 2016;64(45):8659-66.
6. Arancibia C, Riquelme N, Zúñiga R, Matiacevich S. Comparing the effectiveness of natural and synthetic emulsifiers on oxidative and physical stability of avocado oil-based nanoemulsions. Innovative Food Science & Emerging Technologies. 2017;44:159-66.
7. Chassaing B, Van de Wiele T, De Bodt J, Marzorati M, Gewirtz AT. Dietary emulsifiers directly alter human microbiota composition and gene expression ex vivo potentiating intestinal inflammation. Gut. 2017;66(8):1414-27.
8. Sandall A, Smith L, Svensen E, Whelan K. Emulsifiers in ultra-processed foods in the UK food supply. Public Health Nutr. 2023;26(11):2256-70.
9. Oscarsson E, Lindberg T, Zeller KS, Lindstedt M, Agardh D, Håkansson Å, et al. Changes in intestinal permeability ex vivo and immune cell activation by three commonly used emulsifiers. Molecules. 2020;25(24):5943.
10. Bancil AS, Sandall AM, Rossi M, Chassaing B, Lindsay JO, Whelan K. Food additive emulsifiers and their impact on gut microbiome, permeability, and inflammation: mechanistic insights in inflammatory bowel disease. Journal of Crohn's and Colitis. 2021;15(6):1068-79.
11. Chassaing B, Koren O, Goodrich JK, Poole AC, Srinivasan S, Ley RE, et al. Dietary emulsifiers impact the mouse gut microbiota promoting colitis and metabolic syndrome. Nature. 2015;519(7541):92-6.
12. De Siena M, Raoul P, Costantini L, Scarpellini E, Cintoni M, Gasbarrini A, et al. Food emulsifiers and metabolic syndrome: the role of the gut microbiota. Foods. 2022;11(15):2205.
13. Zhu YT, Yuan YZ, Feng QP, Hu MY, Li WJ, Wu X, et al. Food emulsifier polysorbate 80 promotes the intestinal absorption of mono-2-ethylhexyl phthalate by disturbing intestinal barrier. Toxicol Appl Pharmacol. 2021;414:115411.
14. Khuda SE, Nguyen AV, Sharma GM, Alam MS, Balan KV, Williams KM. Effects of emulsifiers on an in vitro model of intestinal epithelial tight junctions and the transport of food allergens. Molecular Nutrition & Food Research. 2022;66(4):2100576.
15. Wu MM, Liao B, Xia IF, Luk PK, Wong KH, Kwok KW. Food emulsifiers increase toxicity of food contaminants in three human GI tract cell lines. Food Chem Toxicol. 2024;185:114499.
16. Kilara A, Vaghela MN. Whey proteins. Proteins in Food Processing2018. p. 93-126.
17. Ohashi Y, Ushida K. Health-beneficial effects of probiotics: Its mode of action. Anim Sci J. 2009;80(4):361-71.
18. Mezzaroba LFH, Carvalho JE, Ponezi AN, Antônio MA, Monteiro KM, Possenti A, et al. Antiulcerative properties of bovine α-lactalbumin. International Dairy Journal. 2006;16(9):1005-12.
19. Yamaguchi M, Takai S, Hosono A, Seki T. Bovine milk-derived α-lactalbumin inhibits colon inflammation and carcinogenesis in azoxymethane and dextran sodium sulfate-treated mice. Bioscience, biotechnology, and biochemistry. 2014;78(4):672-9.
20. Fukawa A, Baba S, Iwasawa K, Yamaguchi M, Hosono A. Dietary α-Lactalbumin protects against thioacetamide-induced liver cirrhosis by maintaining gut-liver axis function in rats. Bioscience, Biotechnology, and Biochemistry. 2020;84(1):171-7.

21. EFSA. Update of the monitoring of levels of dioxins and PCBs in food and feed. EFSA Journal. 2012;10(7).
22. IARC. Polychlorinated Biphenyls and Polybrominated Biphenyls. 2016.
23. Malisch R, Schächtele A, Lippold R, Hardebusch B, Krätschmer K, Van Leeuwen FR, et al. Overall conclusions and key messages of the WHO/UNEP-coordinated human milk studies on persistent organic pollutants. Persistent Organic Pollutants in Human Milk: Springer; 2023. p. 615-75.
24. JECFA. Safety evaluation of certain food additives and contaminants. 2016.
25. Yaminifar S, Aeenehvand S, Ghelichkhani G, Ahmadloo M, Arabameri M, Moazzen M, et al. The measurement and health risk assessment of polychlorinated biphenyls in butter samples using the QuEChERS/GC-MS method. International Journal of Dairy Technology. 2021;74(4):737-46.
26. Schoultz I, Keita AV. The Intestinal Barrier and Current Techniques for the Assessment of Gut Permeability. Cells. 2020;9(8).
27. Di Tommaso N, Gasbarrini A, Ponziani FR. Intestinal Barrier in Human Health and Disease. Int J Environ Res Public Health. 2021;18(23).
28. Putt KK, Pei R, White HM, Bolling BW. Yogurt inhibits intestinal barrier dysfunction in Caco-2 cells by increasing tight junctions. Food & function. 2017;8(1):406-14.
29. Kowapradit J, Opanasopit P, Ngawhirunpat T, Apirakaramwong A, Rojanarata T, Ruktanonchai U, et al. In vitro permeability enhancement in intestinal epithelial cells (Caco-2) monolayer of water soluble quaternary ammonium chitosan derivatives. Aaps Pharmscitech. 2010;11:497-508.
30. Hubatsch I, Ragnarsson EG, Artursson P. Determination of drug permeability and prediction of drug absorption in Caco-2 monolayers. Nature protocols. 2007;2(9):2111-9.
31. Faralli A, Shekarforoush E, Ajalloueian F, Mendes AC, Chronakis IS. In vitro permeability enhancement of curcumin across Caco-2 cells monolayers using electrospun xanthan-chitosan nanofibers. Carbohydrate polymers. 2019;206:38-47.
32. Wagner EM. Monitoring gene expression: quantitative real-time rt-PCR. Methods Mol Biol. 2013;1027:19-45.
33. Shi A, Wang J, Guo R, Feng X, Ge Y, Liu H, et al. Improving resveratrol bioavailability using water-in-oil-in-water (W/O/W) emulsion: Physicochemical stability, in vitro digestion resistivity and transport properties. Journal of Functional Foods. 2021;87:104717.
34. Ma J-J, Huang X-N, Yin S-W, Yu Y-G, Yang X-Q. Bioavailability of quercetin in zein-based colloidal particles-stabilized Pickering emulsions investigated by the in vitro digestion coupled with Caco-2 cell monolayer model. Food Chemistry. 2021;360:130152.
35. Ghosh S, De S, Chen Y, Sutton DC, Ayorinde FO, Dutta SK. Polychlorinated biphenyls (PCB-153) and (PCB-77) absorption in human liver (HepG2) and kidney (HK2) cells in vitro: PCB levels and cell death. Environ Int. 2010;36(8):893-900.
36. Garcia-Bermejo A, Abalos M, Saulo J, Abad E, Gonzalez MJ, Gomara B. Triple quadrupole tandem mass spectrometry: A real alternative to high resolution magnetic sector instrument for the analysis of polychlorinated dibenzo-p-dioxins, furans and dioxin-like polychlorinated biphenyls. Anal Chim Acta. 2015;889:156-65.
37. Hamers T, Kamstra JH, Cenijn PH, Pencikova K, Palkova L, Simeckova P, et al. In vitro toxicity profiling of ultrapure non-dioxin-like polychlorinated biphenyl congeners and their relative toxic contribution to PCB mixtures in humans. Toxicol Sci. 2011;121(1):88-100.
38. Van Itallie CM, Fanning AS, Bridges A, Anderson JM. ZO-1 Stabilizes the Tight Junction Solute Barrier through Coupling to the Perijunctional Cytoskeleton. Molecular Biology of the Cell. 2009;20(17):3930-40.
39. Angelis ID, Turco L. Caco-2 cells as a model for intestinal absorption. Curr Protoc Toxicol. 2011;Chapter 20:Unit20 6.

40. Kus M, Ibragimow I, Piotrowska-Kempisty H. Caco-2 cell line standardization with pharmaceutical requirements and in vitro model suitability for permeability assays. Pharmaceutics. 2023;15(11):2523.
41. Ujhelyi Z, Fenyvesi F, Váradi J, Fehér P, Kiss T, Veszelka S, et al. Evaluation of cytotoxicity of surfactants used in self-micro emulsifying drug delivery systems and their effects on paracellular transport in Caco-2 cell monolayer. European Journal of Pharmaceutical Sciences. 2012;47(3):564-73.
42. Dupont C, Rivero M, Grillon C, Belaroussi N, Kalindjian A, Marin V. α-Lactalbumin-enriched and probiotic-supplemented infant formula in infants with colic: growth and gastrointestinal tolerance. European journal of clinical nutrition. 2010;64(7):765-7.
43. Lu Y, Wang YY, Yang N, Zhang D, Zhang FY, Gao HT, et al. Food emulsifier polysorbate 80 increases intestinal absorption of di-(2-ethylhexyl) phthalate in rats. Toxicol Sci. 2014;139(2):317-27.
44. Brinkmann C, Thiel S, Larsen M, Petersen T, Jensenius JC, Heegaard C. Preparation and comparison of cytotoxic complexes formed between oleic acid and either bovine or human α-lactalbumin. Journal of dairy science. 2011;94(5):2159-70.
45. Andiç S, Boran G. Milk Proteins: Functionality and Use in Food Industry. Functional Polymers in Food Science2015. p. 159-80.
46. Chen W, Yu H, Shi R, Ma C, Gantumur M-A, Qayum A, et al. Comparison of carrying mechanism between three fat-soluble vitamins and alpha-lactalbumin: Effects on structure and physicochemical properties of alpha-lactalbumin. Food Hydrocolloids. 2021;116:106662.
47. Choi YJ, Seelbach MJ, Pu H, Eum SY, Chen L, Zhang B, et al. Polychlorinated biphenyls disrupt intestinal integrity via NADPH oxidase-induced alterations of tight junction protein expression. Environmental health perspectives. 2010;118(7):976-81.
48. Vancamelbeke M, Vermeire S. The intestinal barrier: a fundamental role in health and disease. Expert Rev Gastroenterol Hepatol. 2017;11(9):821-34.
49. Ogulur I, Yazici D, Pat Y, Bingol EN, Babayev H, Ardicli S, et al. Mechanisms of gut epithelial barrier impairment caused by food emulsifiers polysorbate 20 and polysorbate 80. Allergy. 2023;78(9):2441-55.
50. Zhang R, Zhang Z, Li R, Tan Y, Lv S, McClements DJ. Impact of pesticide polarity and lipid phase dimensions on the bioaccessibility of pesticides in agricultural produce consumed with model fatty foods. Food & function. 2020;11(7):6028-37.

Supplementry Information

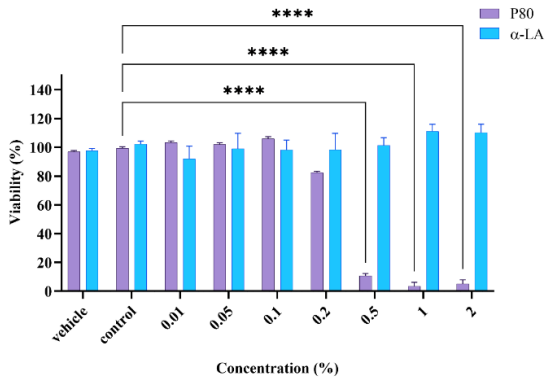

S 1 Cell viability (%) to various concentrations of P80 and α-LA after 24 h exposure. Values are expressed as mean ± SEM (n=3). Asterisks denote significant differences vs control (****p<0.00001)

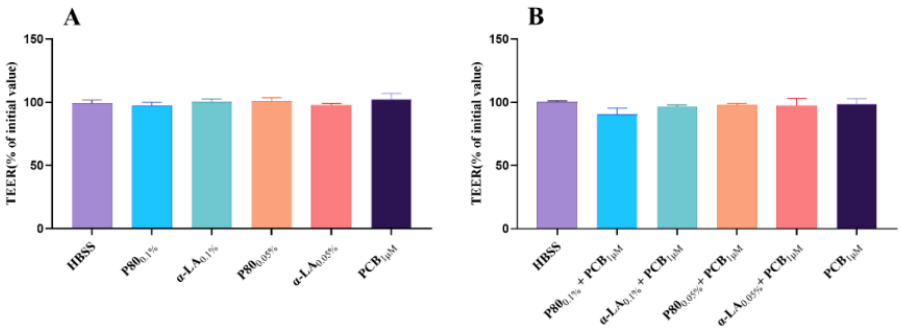

S 2 TEER values (relative % of initial values) across differentiated Caco-2 monolayers after 4 h exposure (A) P80/α-LA and PCB alone, (B) Co-exposure of P80/α-LA with PCB. Values are expressed as mean ± SEM (n=3).

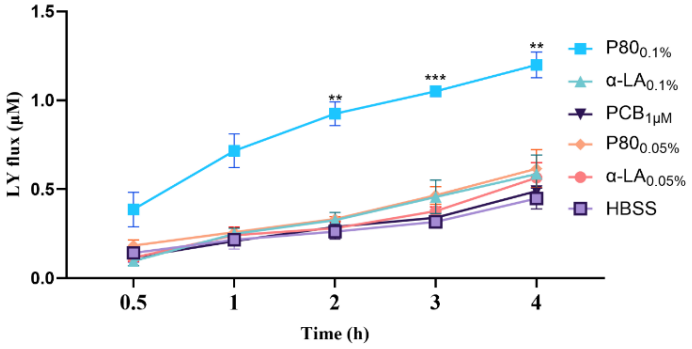

S 3 Lucifer Yellow flux (μM) across differentiated Caco-2 monolayers with treatments during 4 h exposure. Values are expressed as mean ± SEM (n=3). Asterisks denote significant differences vs HBSS (**p<0.001, ***p<0.0001)

O - 351

Optimized Procedure for Volatile Aroma Profiling in Chrysanthemum Leaf Tea

Charintip Niemphol, Pitiya Kamonpatana, Yaowapa Lorjaroenphon*

Department of Food Science and Technology, University of Kasetsart, Bangkok, Thailand

**Corresponding author E-mail: yaowapa.l@ku.ac.th*

Abstract: Flavor is a key determinant of the quality and consumer preference of food and beverage. The chrysanthemum leaf is an agricultural waste that has the potential to produce tea. This study aimed to establish a robust and practical analytical approach for volatile aroma profiling of chrysanthemum leaf tea using headspace solid-phase microextraction (HS-SPME) coupled with gas chromatography-mass spectrometry (GC-MS). The optimal sample incubation and extraction temperature for volatile in tea prepared via filtration (filtered tea) was identified as 60 °C. This moderate temperature produced a balanced volatile aroma profile and more closely resembled the beverage as it is commonly consumed, while incubation and extraction at 80 °C resulted in a higher-yield but woody-dominated profile especially from 5,6,7,7a-tetrahydro-4,4-7a-trimethyl-2(4*H*)-benzofuranone, β-caryophyllene, and germacrene D. However, the aroma concentrations in the 60 °C treatment were relatively low compared to those in the tea leaf itself, and the tea leaf aroma did not reflect the typical sensory characteristics of the beverage. Therefore, a tea sample prepared by direct leaf steeping (loose-steeped tea) was used to enhance the analytical signal intensities. This sample preparation effectively represented the tea aroma profile and importantly, yielded exactly the same aroma-active compounds with odor activity values (OAVs) greater than one. It was also crucial for quantifying low-abundance aroma compounds. These findings emphasize the significant influence of both incubation and extraction temperature as well as the sample matrix on aroma composition, and they provide a practical framework for quality evaluation of chrysanthemum leaf tea.

Keywords: Chrysanthemum; Tea; Flavor; Volatile aroma compound; Headspace solid-phase microextraction (HS-SPME)

1. Introduction

Tea is the second most consumed beverage worldwide (1). It is well recognized for its rich phytochemical composition and associated health benefits, particularly its antioxidant potential. Tea consumption has also been associated with enhanced metabolism, stress reduction, and improved cognitive function, contributing to its increasing global popularity (1, 2). In recent years, rising public awareness of health and wellness has led to growing demand for natural and functional beverages. Chrysanthemum leaves are typically discarded as agricultural waste after flower cutting; however, they are edible and have potential applications in food and beverage (3-5). In China, chrysanthemum leaves are traditionally consumed as herbal tea due to its richness in bioactive compounds with potential health benefits, including anti-inflammatory, antimicrobial, antioxidant, and anticancer properties (5-7). In addition to its functional properties, chrysanthemum leaf tea as a functional beverage exhibits a distinct pleasant aroma that enhances consumer preference. These characteristics highlight the potential of chrysanthemum leaves to support a sustainable strategy for valorizing agricultural waste.

Aroma is a key factor influencing consumer acceptance of tea. The distinctive flavor of tea arises from a complex mixture of volatile compounds generated during processing and brewing

(8, 9). These compounds collectively determine the sensory characteristics and overall quality of the beverage. Consequently, aroma analysis plays an essential role in evaluating tea quality, optimizing processing conditions, and guiding the development of products with desirable sensory attributes. In recent years, instrumental analytical techniques have been increasingly employed to achieve more objective and precise assessments of aroma characteristics. Among these, headspace solid-phase microextraction (HS-SPME) coupled with gas chromatography-mass spectrometry (GC-MS) is widely used for volatile aroma identification in food and beverage due to its versatility and strong qualitative and quantitative capabilities. Therefore, the present study aimed to establish a practical analytical approach for aroma quality evaluation of chrysanthemum leaf tea by optimizing of the SPME extraction temperature and modifying of the sample matrix.

2. Materials and Methods

2.1 Preparation of chrysanthemum tea leaf

Chrysanthemum morifolium leaf was obtained from organic cultivation in Ratchaburi Province, Thailand. The tea was prepared using a green tea processing method (10) with some modifications. Fresh chrysanthemum leaf (200 g) was initially steamed for 2.5 min. The leaf was then rolled for 10 cycles using a 700-gram spherical stone before oven drying at 50 °C for 10 h. The resulting dried tea leaf was subsequently stored in light-protective vacuum bag at room temperature until further analysis.

2.2 Optimization of incubation and extraction temperature for volatile aroma analysis

Sample preparation was carried out according to the published methods (11, 12) with slight modifications. The filtered tea was prepared using a 1:50 (w/v) leaf-to-hot distilled water (80 °C) ratio for 2.5 min. After infusion, the tea was filtered and accurately weighed (~5 g) into a 20-mL headspace vial. Twenty microliters of an internal standard solution (0.130 mg of 2-methyl-3-heptanone (Sigma-Aldrich, St. Louis, MO, USA) in 1 mL of methanol (HPLC grade; Thermo Fisher Scientific, Waltham, MA, USA)) was then added, followed by 1 g of sodium chloride (NaCl; KemAus™, New South Wales, Australia). A 30-mm stir bar was inserted, and the vial was sealed with screw cap equipped with a PTFE/silicone septa. The sample was incubated at two different temperatures, 60 °C and 80 °C, using an agitator-stirrer (Gerstel GmbH & Co. KG, Mülheim an der Ruhr, Germany) at 250 rpm for 10 min, followed by volatile aroma extraction using a 50/30 µm DVB/CAR/PDMS SPME fiber (PAL System; CTC Analytics, Zwingen, Switzerland) at the same temperature for 30 min prior to GC-MS analysis.

Volatiles absorbed on the SPME fiber were desorbed at the GC inlet in splitless mode (Gerstel TDU & CIS 4 (Gerstel GmbH & Co. KG, Mülheim an der Ruhr, Germany) coupled with a GC-8890 and MS-5977C (Agilent Technologies, Inc., MA, USA)) at 250 °C for 4 min, following a modified method of reference (13). Ultra-high purity helium was used as the carrier gas at a constant flow rate of 1 mL/min through a Stabilwax® column (30 m × 250 µm × 0.25 µm; Restek Ltd., PA, USA). The oven temperature program was initially held at 35 °C for 5 min, increased at 4 °C/min to 225 °C, and was held for 10 min.

Aroma compounds were tentatively identified by comparing their mass spectra with the National Institute of Standards and Technology (NIST) Mass Spectral Library (version 20, 2020) and their calculated retention indices (RI) with the literature values. The RI were determined using the retention times (RT) of the analytes relative to those of a homologous series of *n*-alkane standards (C7-C30; Sigma-Aldrich; MO, USA) analyzed under the same GC-MS conditions, as shown in eq 1. Tentative identification was confirmed by comparison with the authentic standard compounds (hexanal, heptanal, gamma-terpinene, *p*-cymene, octanal, 6-methyl-5-hepten-2-one, nonanal, linalool, terpene-4-ol, beta-caryophyllene (Sigma-Aldrich; MO, USA); benzaldehyde (Fluka; Buch, Switzerland)).

$$RI = 100N + 100n\left[\frac{RT_a - RT_N}{RT_{N+n} - RT_N}\right] \quad (1)$$

Here N = carbon no. of lower alkane, n = difference in carbon no. (bracket the analyte), a = analyte, and RT = retention time.

The relative concentrations of the volatile aroma compounds were determined by calculating the ratio of the analyte peak area to the internal standard peak area, according to eq 2.

$$relative\ concentration_a = \frac{concentration_i \times volumn_i \times area_a \times R_f}{mass\ of\ sample \times area_i} \quad (2)$$

Here i = internal standard, a = analyte, and R_f = response factor (equal to 1).

All samples were prepared and analyzed in triplicate. Comparisons between two treatment means were performed using a paired samples *t*-test (two-tailed) in SPSS software (version 22; IBM Corp., Armonk, USA) at a significance level of 0.05.

2.3 Modification of the sample matrix to enhance GC-MS signal intensities

The loose-steeped tea sample was prepared by accurately weighing 0.25 g of tea leaf into a 20-mL HS vial, followed by the addition of 5 mL of odorless distilled water prior to the analysis of volatile aroma compounds. All three samples, including loose-steeped tea, filtered tea (section 2.2), and tea leaf (~0.25 g) were analyzed following the previously described procedure using an incubation and extraction temperature at 60 °C.

The odor activity value (OAV) of each volatile aroma compound was calculated as the ratio of its relative concentration to its corresponding odor threshold value in water, as reported in the literatures. Volatile with an OAV equal to or greater than one was classified as odor-active compound and considered likely contributor to the overall tea aroma profile. A heat map was generated using OriginPro software (version 2025; OriginLab Corp., Northampton, USA) to visualize the distribution patterns of volatile aroma profiles across treatments.

3. Results & Discussion

3.1 Optimal incubation and extraction temperature for volatile aroma analysis

The volatile aroma composition of the filtered chrysanthemum leaf tea was analyzed using an HS-SPME and GC-MS approach. The sample incubation and SPME extraction temperatures were selected based on conventional brewing practices and consumer relevance for herbal teas, with 80 °C reflecting typical brewing temperatures of herbal teas (14, 15) and 60 °C representing typical consumption conditions (16). The results indicated that the incubation and extraction temperatures did not alter the qualitative profile, with a total of 49 aroma compounds consistently detected (Table 1). These comprised 18 terpenes, 11 aldehydes, 9 ketones, 9 alcohols, and 2 hydrocarbons. The dominance of the terpene group, specifically of monoterpenes and sesquiterpenes, is highly consistent with the chrysanthemum phytochemical characteristics, as widely reported in aroma profiling studies on *Chrysanthemum morifolium* flower (17, 18). The studies (19, 20) also identified terpenes as the predominant volatile components in its leaf.

Table 1. Volatile aroma compounds identified in filtered chrysanthemum leaf tea incubated and extracted at different temperatures

no.	compound[a]	RI[b]	Odor[c]	relative concentration[d] (ng/g)	
				60 °C	80 °C
1	hexanal*	1077	grassy	87.64 ± 1.00	70.04 ± 4.01
2	heptanal*	1188	citrus, rancid	55.73 ± 0.56	53.74 ± 0.33
3	β-thujene*	1196	spice	31.62 ± 2.34	47.44 ± 3.97
4	(*E*)-2-hexenal*	1212	green	1.92 ± 0.14	3.68 ± 0.09
5	(3*E*)-2,6-dimethyl-1,3,5-heptatriene[ns]	1236	floral	23.08 ± 6.36	210.13 ± 10.07
6	γ-terpinene*	1260	turpentine	39.37 ± 2.54	93.82 ± 9.99
7	*p*-cymene[ns]	1273	citrus, fruity	10.25 ± 0.77	36.49 ± 1.20
8	3-ethyltoluene*	1278	fragrant	23.31 ± 0.26	74.60 ± 1.57
9	octanal*	1289	orange-like	6.05 ± 0.18	12.15 ± 0.01
10	6-methyl-5-hepten-2-one*	1332	green bean	659.21 ± 49.57	787.49 ± 26.62
11	2,6-dimethyl-5-heptenal*	1349	citrus, melon	13.78 ± 0.27	45.16 ± 2.13
12	nonanal*	1391	citrus, green	45.16 ± 1.54	102.50 ± 11.69
13	(*E*)-2-octenal*	1417	fatty, green	37.48 ± 6.31	71.91 ± 3.13
14	*p*-cymenene*	1427	petrol	43.00 ± 3.42	73.09 ± 5.21
15	1-octen-3-ol*	1435	mushroom	21.27 ± 2.30	30.43 ± 2.21
16	(*E*)-linalool oxide*	1455	floral	14.77 ± 1.16	21.72 ± 1.48
17	*cis*-chrysanthenol*	1461	sweet, floral	118.75 ± 3.30	278.35 ± 12.66
18	(*E,E*)-2,4-heptadienal*	1474	fatty, floral	69.58 ± 5.66	85.79 ± 6.13
19	benzaldehyde*	1496	almond, sugar	128.15 ± 10.95	220.07 ± 11.75
20	3,5-ocatadien-2-one*	1501	fruity	170.60 ± 17.62	229.78 ± 13.70
21	*trans*-chrysanthenyl acetate[ns]	1520	floral	33.35 ± 0.72	127.55 ± 80.66
22	α-copaene*	1528	woody	21.40 ± 2.07	23.39 ± 1.61
23	linalool*	1531	floral	52.75 ± 3.96	81.83 ± 1.15
24	2-bornene*	1537	green	42.12 ± 2.36	73.09 ± 4.38
25	(*E,E*)-3,5-octadien-2-one*	1548	fruity	99.88 ± 9.86	147.46 ± 10.39
26	6-methyl-3,5-heptadiene-2-one*	1571	cinnamon	193.24 ± 20.39	263.26 ± 21.01
27	terpinen-4-ol*	1580	minty	83.71 ± 9.42	187.96 ± 10.35
28	3,7-dimethyl-1,5,7-octatrien-3-ol*	1588	floral	45.27 ± 4.57	136.14 ± 9.38
29, 30	[β-cyclocitral + *cis*-β-copaene]*	1596	citrus, lemon/ fennel, fruity	91.81 ± 4.03	139.45 ± 3.06
31	β-caryophyllene*	1616	woody	112.73 ± 0.02	237.14 ± 7.06
32	borneol*	1670	camphor	78.69 ± 7.97	50.75 ± 1.56
33	*trans*-verbenol*	1692	herb	195.46 ± 8.76	405.50 ± 10.98
34, 35	[2,5-dimethylbenzaldehyde + γ-muurolene]*	1698	tea-like, mint/ woody	67.05 ± 4.06	171.95 ± 7.98
36	geranial[ns]	1707	citrus, floral	20.14 ± 1.08	79.69 ± 0.74
37	germacrene D*	1716	woody	52.01 ± 5.08	142.37 ± 6.00
38	*p*-acetyltoluene*	1741	sweet, floral	48.08 ± 3.27	128.05 ± 6.13
39	*p*-isopropylbenzaldehyde*	1747	pungent, herb	34.20 ± 1.15	92.56 ± 3.35
40	α-curcumene[ns]	1769	herb	14.25 ± 1.45	77.57 ± 9.19
41	β-sesquiphellandrene[ns]	1775	sweet, woody	21.14 ± 1.98	79.58 ± 1.77
42	*trans*-calamenene[ns]	1823	herb, spice	12.20 ± 0.89	58.05 ± 5.23
43	*trans*-geranylacetone*	1834	floral, green	54.45 ± 4.03	179.75 ± 0.40
44	cubebol*	1864	spicy, minty	19.40 ± 0.01	61.22 ± 3.33
45	β-ionone*	1906	violet, woody	266.43 ± 15.45	696.63 ± 12.22
46	caryophyllene oxide*	1954	herb, sweet	1,795.94 ± 88.22	5,045.03 ± 69.68
47	(+)-spathulenol*	2078	herb, fruity	1,653.03 ± 159.29	5,428.95 ± 169.58
48	5,6,7,7a-tetrahydro-4,4-7a-trimethyl-2(4*H*)-benzofuranone*	>2100	woody	77.83 ± 11.34	509.53 ± 57.67
49	benzophenone[ns]	>2100	rose-like	103.55 ± 14.76	541.12 ± 68.95

[a]Compound name followed by * indicates a significant difference whereas [ns] indicates no significant difference ($\alpha = 0.05$).
[b]Identified from a Stabilwax® column.
[c]Obtained from published literature sources (1, 18, 20-36).
[d]2-Methyl-3-heptanone as an internal standard.

Although the overall volatile composition was conserved across temperatures, notable quantitative differences were observed. The majority of compounds exhibiting statistically significant differences in relative concentration were present at higher levels when using incubation and extraction at 80 °C (Table 1). This elevated temperature resulted in significantly greater extraction efficiency for the entire volatile suite, especially low-volatility aroma compounds including α-curcumene, 5,6,7,7a-tetrahydro-4,4-7a-trimethyl-2(4*H*) benzofuranone, and benzophenone, when compared to the lower extraction temperature. This finding strongly suggests that aroma compounds are more efficiently released at higher temperatures due to increased thermal energy.

The preliminary assessment of overall aroma characteristic was conducted via self-examination, and the research team described the tea extracted at 80 °C as predominantly woody and lacking complexity. In contrast, extraction at 60 °C produced a more balanced aroma that closely resembled the characteristic aroma of the consumed tea. This corresponded with the comparison of the ten most abundant volatiles. The aroma profile of the 60 °C treatment, dominated by caryophyllene oxide, (+)-spathulenol, 6-methyl-5-hepten-2-one, β-ionone, *trans*-verbenol, 6-methyl-3,5-heptadiene-2-one, 3,5-ocatadien-2-one, benzaldehyde, *cis*-chrysanthenol, and β-caryophyllene, exhibited a more diverse and balanced range of odor notes, including woody, floral, fruity, cinnamon-like, and sweet characteristics. This complex aroma profile is consistent with previous descriptions of tea aroma, which typically encompasses grassy, floral, woody, fruity, roasted, cinnamon, burnt, and slightly metallic notes (1, 2, 17, 21, 37, 38). On the other hand, the volatile profile at the 80 °C treatment, dominated by (+)-spathulenol, caryophyllene oxide, 6-methyl-5-hepten-2-one, β-ionone, benzophenone, 5,6,7,7a-tetrahydro-4,4-7a-trimethyl-2(4*H*)-benzofuranone, *trans*-verbenol, *cis*-chrysanthenol, 6-methyl-3,5-heptadiene-2-one, and β-caryophyllen, was characterized mainly by woody notes, complemented by a persistent floral undertone. This difference can be attributed to the higher abundance of sesquiterpenes, which typically impart woody aroma (39) and possess higher boiling points than monoterpenes. Thus, 60 °C was selected as the optimal SPME extraction temperature parameter for aroma analysis of chrysanthemum leaf tea.

3.2 Modified sample matrix to enhance GC-MS signal intensities

The filtered tea exhibited a balanced aroma profile characterized by floral, woody, greeny, and citrus notes, which closely to the typical sensory characteristics of a tea beverage. However, its aroma concentration was relatively low (Table 1), making compound identification more challenging and potentially reducing the accuracy of detecting slight differences in trace aroma compounds. Therefore, further development of sample preparation is needed to establish a robust and practical analytical approach for aroma quality evaluation of chrysanthemum leaf tea, aimed at improving the detection and characterization of its aroma compounds. Thus, the tea leaf was evaluated to serve as an alternative sample for assessing the quality of the filtered tea. The results revealed that the volatile concentrations in the tea leaf were greater than those in the filtered tea. However, the tea leaf aroma did not reflect the typical sensory characteristics of the beverage. It was more intense in woody and greeny notes. The different in aroma perception was supported by the OAVs. OAVs were estimated to investigate the impact of aroma-active compounds on the overall aroma quality. It should be emphasized that some compounds were excluded from this calculation because their odor threshold values were not reported in any published medium.

β-Ionone contributed most significantly to the violet and woody notes in both tea leaf and filtered tea samples (Figure 1) due to its very low odor detection threshold. It is generated through carotenoid degradation (40) during the tea drying process. However, the compound with the second highest OAV in the filtered tea, linalool (floral note), was absent from the tea leaf. This might be due to its existence in a bound form. Liu *et al*. (41) reported that linalool in fresh black tea (*Camellia sinensis* var. Yinghong No. 9) leaf is primarily exists as non-volatile glycosides which are odorless. Thermal hydrolysis during the chrysanthemum tea brewing process effectively

cleaves the glycosidic bonds, releasing free linalool (Figure 1). Another clear difference between these two samples is highlighted by the absence of citrus note odorants, including heptanal, octanal, and geranial in the tea leaf (Figure 1). These four volatiles are recognized as key aroma compounds in oolong tea and black tea (1, 32). Heptanal and octanal have been reported as the significant aroma compounds, imparting freshness and dimensionality to black tea (32). Their formation is driven primarily by lipid degradation of unsaturated fatty acids, specifically linoleic and linolenic acids, through the lipoxygenase pathway. In addition, the tea leaf aroma was moderately influenced by β-caryophyllene, which is described as a woody note.

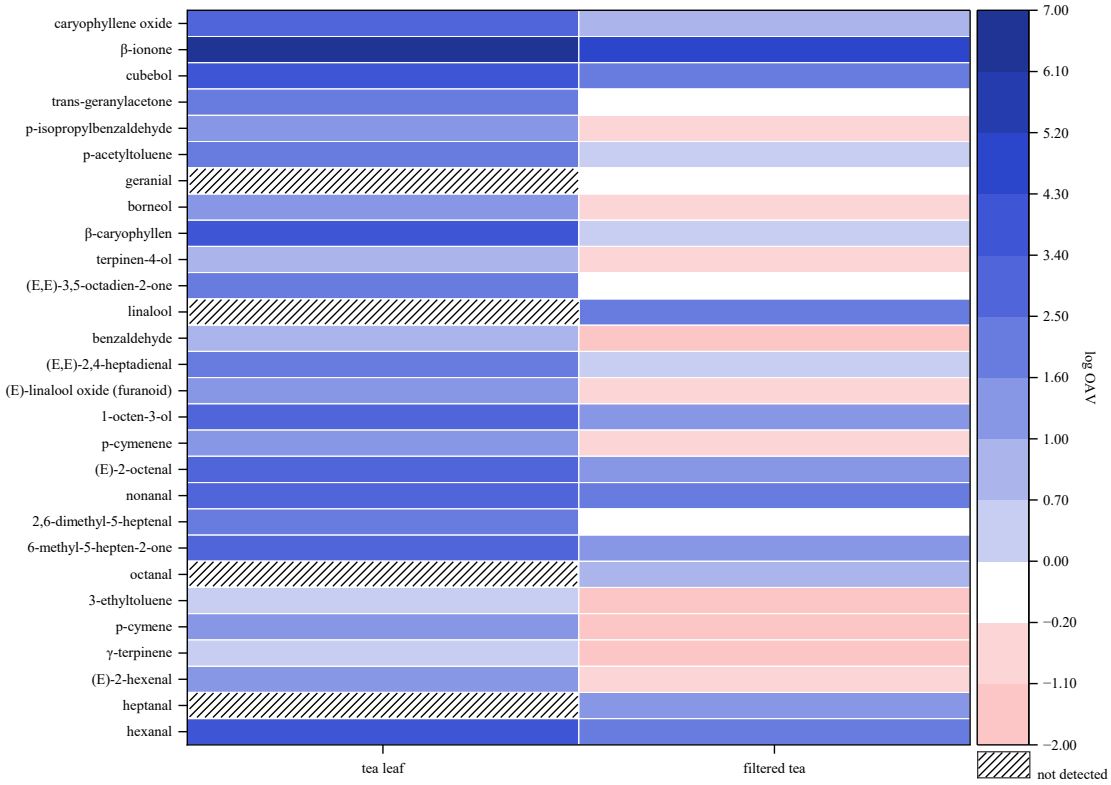

Figure 1. Heat map illustrating the OAVs of aroma compounds in chrysanthemum tea leaf and its filtered tea

The challenges encountered in achieving both high sensitivity detection and a balanced aroma profile prompted the development of an improved sample preparation method. The sample preparation procedure was modified from filtration to direct leaf steeping. Total aroma concentrations in the loose-steeped tea were almost 20 times higher than those in the filtered tea, and both samples exhibited an aroma aligning closely with the typical tea aroma characteristics. These results coincide with the aroma-active compounds shown in Table 2.

Table 2. Aroma-active compounds (odor active value; OAV ≥ 1) in filtered and loose-steeped chrysanthemum leaf tea

no.	compound	threshold[a] (ng/g)	OAV	
			filtered tea	loose-steeped tea
45	β-ionone	0.007	38,061	697,612
23	linalool	0.22	240	26,938
1	hexanal	1	88	4,992
12	nonanal	1	45	4,160
44	cubebol	0.461	42	4,917
15	1-octen-3-ol	1	21	2,188
2	heptanal	3	19	619
10	6-methyl-5-hepten-2-one	50	13	933
13	(*E*)-2-octenal	3	12	963
46	caryophyllene oxide	200	9	285
9	octanal	0.7	9	606
38	*p*-acetyltoluene	19	3	145
31	β-caryophyllene	64	2	955
18	(*E,E*)-2,4-heptadienal	45	2	120
43	*trans*-geranylacetone	60	<1	42
11	2,6-dimethyl-5-heptenal	16	<1	98
36	geranial	28	<1	34
25	(*E,E*)-3,5-octadien-2-one	150	<1	43
39	*p*-isopropylbenzaldehyde	60	<1	31
32	borneol	140	<1	28
14	*p*-cymenene	85	<1	43
27	terpinen-4-ol	340	<1	8
16	(*E*)-linalool oxide	60	<1	26
4	(*E*)-2-hexenal	17	<1	30
7	*p*-cymene	150	<1	13
19	benzaldehyde	3,500	<1	3
8	3-ethyltoluene	800	<1	3

[a]Compound number corresponding to Table 1.
[b]Odor detection thresholds in water obtained from the literature (42).

The 14 aroma-active compounds identified in filtered tea significantly contributed to the overall aroma of loose-steeped tea (Table 2). All of them, except caryophyllene oxide and β-caryophyllene, are largely in agreement with previously reported key aroma-active compounds in yellow tea, oolong tea, and black tea (1, 2, 29, 38). The results indicated that direct leaf steeping effectively enhanced the detection of aroma compounds without altering the overall aroma profile. Moreover, it yielded exactly the same order of the top three aromas with the highest OAVs, including β-ionone, linalool, and hexanal. This analytical procedure serves as a reliable aroma analysis approach to support quality assessment of chrysanthemum leaf tea and facilitate its application in research and industry.

4. Conclusion

The HS-SPME temperature conditions and sample matrix significantly influence the volatile aroma profile of chrysanthemum leaf tea. Incubation and extraction by SPME fiber at 60 °C yielded a sensorially superior and balanced aroma compared to 80 °C. Dried tea leaf did not reflect typical tea characteristics, whereas direct leaf steeping enhanced the detection limit of trace aromas and produce an aroma perception closely resembling the tea beverage.

References

1. Yang P, Yu M, Song H, Xu Y, Lin Y, Granvogl M. Characterization of Key Aroma-Active Compounds in Rough and Moderate Fire Rougui Wuyi Rock Tea (*Camellia sinensis*) by Sensory-Directed Flavor Analysis and Elucidation of the Influences of Roasting on Aroma. J Agric Food Chem. 2022;70(1):267-278.
2. Lin Y, Wang Y, Huang Y, Song H, Yang P. Aroma Identification and Classification in 18 Kinds of Teas (Camellia sinensis) by Sensory Evaluation, HS-SPME-GC-IMS/GC x GC-MS, and Chemometrics. Foods. 2023;12(13):1-15.
3. Marchyshyn S, Polonets O, Savych A, Nakonechna S. Determination of carbohydrates of *Chrysanthemum morifolium* l. Leaves and flowers by gc-ms. Pharmakeftiki. 2020;32(4):202-212.
4. Yan H, Liu Y, Xu Y, Fang Y, Guo L, Liu D. Analysis and evaluation of mineral elements of *Chrysanthemum morifolium* for medicinal and tea use of different germplasm resources. China Journal of Chinese Materia Medica. 2021;46(2):272-280.
5. Li Y, Yang P, Luo Y, Gao B, Sun J, Lu W, et al. Chemical compositions of chrysanthemum teas and their anti-inflammatory and antioxidant properties. Food Chemistry. 2019;286:8-16.
6. Hassan HMA, Aljidaemi FF, Salem GM, Bannur ZM, Aljeaday H, Aldaba LNE, et al. Utilization of *Chrysanthemum* Leaf and Stem Extracts as Antioxidants, Anticancer, Anti-inflammatory, and Phytochemical Agents. Green Chemistry. 2026;10(1):84-100.
7. Shahrajabian MH, Sun W, Zandi P, Cheng Q. A Review of Chrysanthemum, the Eastern Queen in Traditional Chinese Medicine with Healing Power in Modern Pharmaceutical Sciences. Applied Ecology and Environmental Research. 2019;17(6):1-15.
8. Wang W, Feng Z, Min R, Yin J, Jiang H. The Effect of Temperature and Humidity on Yellow Tea Volatile Compounds during Yellowing Process. Foods. 2024;13(20):3283-3293.
9. Wang Z, Han B, Jing W, Yi Z, Zhang Y, Ren D, et al. Effects of Different Steeping Temperatures on the Leaching of Aroma Components in Black Tea by SPME-GC-MS Coupled with Chemometric Method. J AOAC Int. 2019;102(6):1834-1844.
10. Yan Z, Zhou Z, Jiao Y, Huang J, Yu Z, Zhang D, et al. Hot-air drying significantly improves the quality and functional activity of orange black tea compared with traditional sunlight drying. Foods. 2023;12(9).
11. Lorjaroenphon Y, Cadwallader KR. Identification of character-impact odorants in a cola-flavored carbonated beverage by quantitative analysis and omission studies of aroma reconstitution models. J Agric Food Chem. 2015;63(3):776-786.
12. An H, Liu J, Chen Y, Huang Y, Chen J, Liu Z, et al. Characterization of key volatile compounds in jasmine tea infusion with different amount of flowers. Food Chemistry: X. 2023;19:1-10.
13. Kullananant N, Chaiseri S, Lorjaroenphon Y. The superiority of ultrapasteurization over conventional heat treatments regarding Riceberry beverage aroma. Food Science. 2020;0(0):1-8.
14. Chong YK, Nyam KL. Effect of brewing time and temperature on the physical properties, antioxidant activities and sensory of the kenaf leaves tea. J Food Sci Technol. 2022;59(2):510-517.
15. Jiang B, Luo X, Yan J, Liu K, Wang C, Jiao W, et al. Investigation of the Effect of Fragrance-Enhancing Temperature on the Taste and Aroma of Black Tea from the Cultivar Camellia sinensis (L.) O. Kuntze cv. Huangjinya Using Metabolomics and Sensory Histology Techniques. Fermentation. 2024;10(10):520-543.
16. Luo H, Ge H. Hot Tea Consumption and Esophageal Cancer Risk: A Meta-Analysis of Observational Studies. Front Nutr. 2022;9:1-10.

17. Gao Y, Wang J, Li M, Wang J, Qiao L, Zhang N, et al. Aroma profiling of Chinese Chrysanthemum (Chrysanthemum morifolium Ramat.) using flavoromics analysis. Journal of Food Composition and Analysis. 2025;138:1-10.
18. Xiao Z, Fan B, Niu Y, Wu M, Liu J, Ma S. Characterization of odor-active compounds of various Chrysanthemum essential oils by gas chromatography–olfactometry, gas chromatography–mass spectrometry and their correlation with sensory attributes. Journal of Chromatography B. 2016;1009-1010:152-162.
19. Xue H, Jiang Y, Zhao H, Köllner TG, Chen S, Chen F, et al. Characterization of composition and antifungal properties of leaf secondary metabolites from thirteen cultivars of *Chrysanthemum morifolium* Ramat. Molecules. 2019;24(23):1-11.
20. Usami A, Ono T, Marumoto S, Miyazawa M. Comparison of Volatile Compounds with Characteristic Odor in Flowers and Leaves of Nojigiku (*Chrysanthemum japonense*). Journal of Oleo Science. 2013;62(8):631-636.
21. Kaneko S, Chen J, Wu J, Suzuki Y, Ma L, Kumazawa K. Potent Odorants of Characteristic Floral/Sweet Odor in Chinese Chrysanthemum Flower Tea Infusion. J Agric Food Chem. 2017;65(46):10058-10063.
22. Kumazawa K, Masuda H. Identification of Potent Odorants in Different Green Tea Varieties Using Flavor Dilution Technique. Journal of Agricultural and Food Chemistry. 2002;50(20):5660-5663.
23. Asfaw N, Storesund HJ, Aasen AJ, Skattebol L. Constituents of the Essential Oil ofLaggera tomentosaSch. Bip. ex Oliv. et Hiern Endemic to Ethiopia. Journal of Essential Oil Research. 2003;15(2):102-105.
24. Chang K-M, Kim G-H. Volatile aroma constituents of gukhwa (*Chrysanthemum morifolium* R.). Food Science and Biotechnology. 2013;22(3):659-663.
25. Chen C, Yu F, Wen X, Chen S, Wang K, Wang F, et al. Characterization of a new (Z)-3:(E)-2-hexenal isomerase from tea (Camellia sinensis) involved in the conversion of (Z)-3-hexenal to (E)-2-hexenal. Food Chemistry. 2022;383:1-9.
26. Chen X, Yang D, Huang L, Li M, Gao J, Liu C, et al. Comparison and identification of aroma components in 21 kinds of frankincense with variety and region based on the odor intensity characteristic spectrum constructed by HS-SPME-GC-MS combined with E-nose. Food Research International. 2024;195:1-16.
27. Cheng H, Liu F, Zhang Y, Ye Z, Chen J, Chen S, et al. The Flavor Characterization of 'Huyou' (*Citrus changshanensis*) Essential Oils Extracted by Conventional and Novel Methods. Agriculture. 2024;14(1):131-149.
28. Fan F, Wang Z, Chen X, Yu Q, Yang X, Su X, et al. Impact of oxygen scavenger, temperature, and packaging materials on freshness quality of packaged green teas during storage. Food Frontiers. 2024;5(5):2275-2289.
29. Fang QT, Luo WW, Zheng YN, Ye Y, Hu MJ, Zheng XQ, et al. Identification of Key Aroma Compounds Responsible for the Floral Ascents of Green and Black Teas from Different Tea Cultivars. Molecules. 2022;27(9):2809-2824.
30. Iwasa M, Nakaya S, Maki Y, Marumoto S, Usami A, Miyazawa M. Identification of Aroma-active Compounds in Essential Oil from Uncaria Hook by Gas Chromatography-Mass Spectrometry and Gas Chromatography-Olfactometry. Journal Oleo Science. 2015;64(8):825-833.
31. Jiang K, Xu K, Wang J, Meng F, Wang B. Based on HS-SPME-GC-MS combined with GC-O-MS to analyze the changes of aroma compounds in the aging process of Citri Reticulatae Pericarpium. Food Bioscience. 2023;54:1-12.
32. Jiang R, Ouyang J, Chen H, Zhang X, Xu H, Wang K, et al. Characterization of key aroma in Huangjincha black tea processed from four different cultivars. Food Chemistry: X. 2025;27:1-11.

33. Jordan MJ, Margaria CA, Shaw PE, Goodner KL. Volatile components and aroma active compounds in aqueous essence and fresh pink guava fruit puree (*Psidium guajava* L.) by GC-MS and multidimensional GC/GC-O. Agricultural and Food Chemistry. 2003;51(5):1421-1426.
34. Kesen S. Characterization of aroma and aroma-active compounds
35. of Turkish turmeric (*Curcuma longa*) extract Journal of Raw Materials to Processed Foods. 2020;1:13-21.
36. Laokuldilok N, Utama-ang N, Kopermsub P, Thakeow P. Characterization of odor active compounds of fresh and dried turmeric by gas chromatography-mass spectrometry, gas chromatography olfactometry and sensory evaluation. Food and Applied Bioscience. 2015;3(3):216-230.
37. Xiao Z, Wu Q, Niu Y, Wu M, Zhu J, Zhou X, et al. Characterization of the Key Aroma Compounds in Five Varieties of Mandarins by Gas Chromatography-Olfactometry, Odor Activity Values, Aroma Recombination, and Omission Analysis. Agricultural and Food Chemistry. 2017;65(38):8392-8401.
38. Yang Y, Zhu H, Chen J, Xie J, Shen S, Deng Y, et al. Characterization of the key aroma compounds in black teas with different aroma types by using gas chromatography electronic nose, gas chromatography-ion mobility spectrometry, and odor activity value analysis. Lwt. 2022;163:1-10.
39. Hong X, Wang C, Jiang R, Hu T, Zheng X, Huang J, et al. Characterization of the Key Aroma Compounds in Different Aroma Types of Chinese Yellow Tea. Foods. 2022;12(1):27-42.
40. Li Z, Howell K, Fang Z, Zhang P. Sesquiterpenes in grapes and wines: Occurrence, biosynthesis, functionality, and influence of winemaking processes. Compr Rev Food Sci Food Saf. 2019;19(1):247-281.
41. Paparella A, Shaltiel-Harpaza L, Ibdah M. beta-Ionone: Its Occurrence and Biological Function and Metabolic Engineering. Plants. 2021;10(4):754-766.
42. Liu C, Li J, Wang M, Jian G, Zhu C, Li H, et al. (R)-Linalool is a key indicator of aroma quality levels of a distinctive black tea (Camellia sinensis var. Yinghong No. 9). Industrial Crops and Products. 2025;225:1-12.
43. Gemert van LJ. ODOUR THRESHOLDS: Compilations of odour threshold values in air, water and other media. 2011 ed. 2, editor. Utrecht, Netherlands: Oliemans Punter & Partners BV; 2011.

O - 353

Development of Whole Green Banana (*Musa Sapientum* Linn, ABB Group, cv. Kluai Namwa) Flour Using Spray Drying with Focus on Resistant Starch Retention

Trinh K. Nguyen, Nattira On-Nom, Rungtiwa Wongsagonsup, Warangkana Srichamnong*

Institute of Nutrition, Mahidol University, Nakhon Pathom, Salaya, Thailand

**Corresponding author E-mail: warangkana.sri@mahidol.ac.th*

Abstract: Whole green banana flour (WGBF) is an emerging functional food ingredient owing to its exceptionally high resistant starch (RS) content. Conventional processing by low-temperature oven drying (50–60 °C) effectively preserves RS but yields a poorly soluble flour, limiting its applicability across diverse food systems. This study evaluated spray drying (SD) as a scalable alternative processing strategy to enhance the functional properties of WGBF while maintaining RS integrity. WGBF was produced from whole stage-1 green bananas (°Brix 2–5), using an optimized feed suspension at a banana-to-water ratio of 1:2. Spray drying was conducted at an inlet temperature of 130 ± 5 °C, outlet temperature of 70 ± 5 °C, and a feed rate of 0.6 L h^{-1}, with atomization and airflow parameters held constant. Compared with oven drying, SD yielded WGBF with a significantly higher RS content (62.87 vs. 53.56 g/100 g, dry basis; $P < 0.05$), indicating superior preservation of starch crystallinity under the selected conditions. However, unmodified SD powders exhibited lower solubility than oven-dried counterparts. Incorporation of gum arabic (10% w/w) as a carrier during SD substantially improved solubility, but this was accompanied by a pronounced reduction in RS content (17.17 g/100 g; $P < 0.05$). These findings highlight a critical trade-off between RS retention and hydration functionality, emphasizing the need for systematic optimization of spray-drying parameters, including thermal input, feed composition, and carrier selection. With further refinement, spray drying represents a promising and industrially viable approach for producing WGBF with tailored functional and nutritional attributes for use in functional food applications.

Keywords: Green banana flour; Resistant starch; Spray drying optimization; Hydration properties; Functional food ingredient

1. Introduction

Resistant starch (RS) has attracted a lot of attention recently because of its health benefit potential. RS resists the digestion in the small intestine of healthy people and reaches the large intestine (1), assisting in the prevention of diabetes, obesity, colon cancer and cardiovascular diseases by reducing glycemic response, reducing low-density lipoprotein cholesterol and improving gut health (2). There are five categories of RS, including RS present in whole grains and seeds (RS1), raw starchy plants (RS2), retrograded starch (RS3), chemical modified starch (RS4) and in amylose-lipid complexes (RS5) (3).

Banana is the world's fourth most important crop. Its global production reached 19.7 million tonnes in 2024 (4). Unripe (green) banana is superior in RS2 and total dietary fiber (TDF) (5). Beside the banana pulp, the fruit peel is also rich in bioactive compounds and TDF such as pectin cellulose and lignin (6). According to Khoozani et al. (7), in whole green banana, RS and TDF accounts for 40.14% and 22.91% of dry weight, respectively. However, RS in raw green

banana rapidly decreases during ripening (8), thereby necessitating the production of banana flour at its first ripening stage for RS retention.

Different drying methods has been used to produce green banana flour (GBF) and whole green banana flour (WGBF), including oven air-drying (9) (10), spouted-bed drying (11), and freeze drying (7). Drying does effects on the interior cellular structure of starches and thus influencing the flour properties and RS content. Hot air drying (OD) and freeze drying (FD) currently have their limitations in large-scale industrial production as prolonged operational time, batch-mode, and high instrument cost (12). From that point, an alternative drying method, such as spray drying, needs to be investigated for banana flour production.

Spray drying (SD) is a popular and cost-effective method to produce food powders. The process involves atomizing fluid, followed by dehydrating atomized fluid droplets in a hot convective medium into fine dried powder (13). Moreover, SD can enhance physical properties of food powder such as solubility while preserve nutritional values by controlling process conditions and application of carrier materials, for example, gum arabic (GA) (14). Oil et al. (15) has reported the feasibility of using spray dryer for green banana production; nevertheless, the study of characteristics of spray-dried WGBF was limited.

Hence, this research aims to (1) develop WGBF retaining RS by using spray drying technique, and (2) elucidate the physicochemical, structural and functional properties of spray-dried WGBF for their utilization in food development and applications.

2. Materials and Methods

2.1 Materials

Fresh whole full-green bananas (*Musa sapientum* Linn, ABB group, cv. Kluai Namwa) with no maturation treatments, were purchased at Makro supermarket, Nakhon Pathom province, Thailand between October and November 2025. Soluble solids (°Brix) of all batches of bananas were measured to assure the consistency in the ripening status and processed on arrival maintained ° Brix at 2–5 (7). All chemical reagents used in this study were analytical grade and obtained from Sigma-Aldrich (St. Louis, Missouri, U.S.A.).

2.2 Production of whole green banana flour

The whole green banana slurry was prepared as described by Carolina Vieira et al. (11) and Oil et al. (15) with some modifications. The fruits were rinsed with 1.0% (w/v) sodium chloride solution to remove impurities and cut into pieces. After that, the lot was dipped in 0.5% (w/v) citric acid solution for 10 min and drained to reduce the enzymatic browning. The banana was divided into three portions for: (1) conventional oven drying, (2) spray drying without carrier, and (3) spray drying with carrier gum Arabic.

Oven drying was carried out at 55 ± 5 °C for 21 hours. As for spray drying, pre-treated bananas were crushed in a blender until obtaining a homogenous slurry, banana and water ratio used was 1:2 (w/w) before filtered through sieve of 35 Mesh (500 microns). Carrier agent GA was added into the slurry at 10 % w/w.

The operation of spray drying technique is referenced from the work of Rosalyn et al. (16) with modifications. Spray drying of whole green banana slurry was accomplished using a pilot-scale spray dryer (Niro Mobile Minor Spray Dryer, Denmark) with curved-vane rotary atomizer. Peristaltic pump was employed for pumping feed slurry to the dryer while the dehumidified air was supplied via air inlet nozzle on the top of the drying chamber for atomization. The drying chamber was supplied with heated dehumidified air to evaporate the moisture content in the atomized feed once it is sprayed into the chamber. Spray drying was carried out at the inlet temperature 130 ± 5 °C. Outlet temperature (70 ± 5 °C), feed flow rate (0.6 L/h), atomizer disc speed (15000 rpm), air drying flow rate (400 L/h) and air pressure (4 bar) were kept constant during the drying process. The collected powers in stored in a desiccator for further analysis.

2.3 Moisture content analysis

Moisture content (g/100g) analysis was performed by the Analytical Services of Institute of Nutrition, Mahidol University – accredited laboratory complying with the ISO/IEC 17025/2017.

2.4 Starch analysis of the whole green banana flour

Resistant starch content was determined based on AOAC Official Method 2002.02, using the Megazyme Rapid Resistant Starch (K-RAPRS) assay kit (Megazyme International Ireland Ltd, Bray, Ireland), as in the previous study (17).The samples were incubated in a shaking water bath with two enzymes, pancreatic α-amylase (PAA) and amyloglucosidase (AMG) for 4 h at 37 °C, in which digestible starch (DS) was hydrolyzed to D-glucose. After centrifugation, the pellet was washed with ethanol (50% v/v) and supernatant was removed by decantation. The resistant starch in the pellet was dissolved in 1.7 M NaOH by vigorously stirring in an ice-water bath for 20 min. The starch is then quantitatively hydrolyzed to D-glucose with AMG. D-glucose was measured with a glucose oxidase/peroxidase reagent (GOPOD) and RS content was calculated as mg of glucose × 0.9 (conversion factor). The DS was determined by the original supernatant, adjusting the volume to 100 mL and measuring D-glucose concentration with GOPOD reagent. Total starch (TS) was calculated as the sum of RS and DS.

2.5 Starch crystallinity

An X-ray diffractometer (D2 Phaser, Bruker, Germany) operating at 30kV and 10mA with CuKa radiation (λ=1.5418 °A) was used to observe the starch crystallinity (18). The measurement range was selected from 5° to 40° of the diffraction angle 2θ, step size of 0.02° and measuring time of 8 s.

2.6 Particle morphology analysis by SEM

The morphology of the flours and gum Arabic were scanned through a JCM-7000 NeoScope™ Benchtop SEM (JEOL, Tokyo, Japan) (18). Each sample was covered with gold in a sputter coater prior to scanning and photographing at 1000× magnification. An accelerating potential voltage of 15kV was applied during the capturing of image.

2.7 Chemical functional group

The functional groups of WGBF was analyzed using an infrared spectrometer (Nicolet™ iS50 FTIR Spectrometer, Thermo Fisher Scientific, USA) equipped with a DTGS detector and a single reflectance ATR cell with a ZnSe crystal (19). All flour measurements were recorded at ambient temperature in a wavenumber range of 600–4000 cm^{-1}. OMNIC Paradigm software was used to analyze the data.

2.8 Statistical analysis

All analyses were carried out in triplicates, and the results were presented as the mean value with standard deviation. One-way Analysis of Variance (ANOVA) and respective interactions were determined using Tukey's test at a 0.05 probability level were employed for statistical analysis using SPSS software (SPSS Statistics for Windows Version 18.0, IBM, Armonk, New York, U.S.A.).

3. Results & Discussion

3.1 Starch analysis

Whole green banana flour dried by different drying conditions with and without carrier were measured for resistant starch (RS), digestible starch (DS), and total starch (TS) as showed in Table 1.

Table 1. Starch analysis of whole green banana flours (WGBF)

Samples	Moisture content (g/100g)	RS (g/100g WGBF d.b.)	DS (g/100g WGBF d.b.)	TS (g/100g WGBF d.b.)	RS (g/100g TS d.b.)
OD55	6.48 ± 0.04 ^{b}	53.56 ± 1.75 ^{b}	2.86 ± 0.67 ^{a}	56.42 ± 1.79 ^{b}	94.93 ± 1.14 ^{b}
SDNO130	6.61 ± 0.17 ^{b}	62.87 ± 1.70 ^{a}	2.08 ± 0.20 ^{b}	64.95 ± 1.50 ^{a}	96.79 ± 0.39 ^{a}
SDGA10-130	8.34 ± 0.08 ^{a}	17.17 ± 0.41 ^{c}	0.72 ± 0.02 ^{c}	17.89 ± 0.43 ^{c}	95.96 ± 0.06 ^{ab}

Data followed by the different superscripts in the same column are significantly different ($p < 0.05$).
OD55, OD at 55 °C; SDNO130, SD without carrier at 130 °C; SDGA10-130, SD with GA 10% at 130 °C

Starch is broadly classified according to its digestibility into digestible starch and resistant starch (RS) (20). Green banana is a particularly rich source of RS and total dietary fiber (TDF), with RS predominantly present as RS2, which corresponds to native, ungelatinized starch characterized by B- or C-type crystalline polymorphs (21). Previous studies have reported that green banana flour contains a wide range of RS, from 33.86 to 58.5 g/100 g dry basis (d.b.), along with approximately 7.2 g/100 g d.b. of non-starch dietary fiber (7) (9). In addition, banana peel, which accounts for approximately 30–40% of the total fruit weight, has been identified as a notable source of RS (17.89 ± 0.40 g/100 g d.b.) (22). These findings highlight the importance of including the peel in green banana flour production to enhance both RS and TDF contents, as also reported by Carolina Vieira et al. (11).

The RS content of whole green banana flour (WGBF) is influenced by multiple processing factors, particularly drying method and temperature. Freeze drying (FD) and oven drying (OD) at moderate temperatures (50–60 °C) have been shown to preserve RS more effectively (35–60 g/100 g d.b.) than OD at elevated temperatures (≥80 °C), where partial starch gelatinization and disruption of RS2 crystalline structures occur (9). The present findings (Table 1) further emphasize that drying mode, in addition to temperature, plays a critical role in RS preservation. Spray-dried WGBF exhibited a significantly higher RS content (62.87 g/100 g d.b.) than oven-dried samples processed at 55 °C (53.56 g/100 g d.b.; $p < 0.05$), which is consistent with values reported for oven-dried “Namwa” green banana flour by Vatanasuchart et al. (10). Despite the higher inlet air temperature applied during spray drying, the residence time of the material in contact with hot air is markedly shorter (approximately 30–40 s) compared with oven drying. This is attributable to rapid moisture evaporation resulting from atomization of the feed into fine droplets (10–150 μm), which increases the effective surface area for heat and mass transfer (23). In contrast, the lower RS and higher digestible starch content observed in oven-dried WGBF can be attributed to prolonged thermal exposure, leading to greater disorganization of starch crystalline structures (9).

Gum arabic (GA) is widely used as a carrier agent in the food industry due to its neutral sensory profile, strong film-forming ability, and low viscosity. In the present study, GA was incorporated during spray drying to improve the solubility of inherently poorly water-soluble WGBF by reducing particle aggregation and enhancing dispersibility (24). Moreover, because GA is classified as a dietary fiber, its inclusion was expected to contribute to an increase in total dietary fiber content (25). The observed reduction in RS content in spray-dried WGBF containing GA, relative to samples without a carrier, can be attributed to dilution of the total starch (TS) fraction in the composite powder. When RS content was normalized to the TS fraction, the RS levels in the GA-containing spray-dried sample (SDGA10-130) were comparable to those of both oven-dried and spray-dried samples without GA. This indicates that incorporation of GA during spray

drying does not intrinsically alter the RS content of WGBF but rather affects its proportional representation within the overall matrix.

3.2 Starch crystallinity

Starch crystalline structures are commonly classified into three polymorphic types—A, B, and C—based on their X-ray diffraction (XRD) patterns. A-type starches, such as those derived from wheat and maize, possess surface pores and channels and are relatively susceptible to enzymatic digestion, whereas C-type starches are structurally less stable and readily disrupted during thermal processing, including boiling, cooking, and baking, resulting in partial or complete starch gelatinization. In contrast, the B-type crystalline structure characteristic of green banana starch exhibits high resistance to digestion in the small intestine, owing to its compact molecular organization and densely packed starch granules (21).

As shown in Figure 1, WGBF samples in the present study displayed XRD patterns consistent with B-type crystallinity, characterized by distinct diffraction peaks at 15°, 17°, and 23° (2θ) (7) (18). Spray drying at an inlet temperature of 130 °C did not alter the fundamental crystalline pattern of green banana starch in WGBF when compared with conventional oven drying, indicating that spray drying can serve as an effective alternative processing method for WGBF production without compromising RS-associated crystalline integrity.

In contrast, the SDGA10-130 sample exhibited a broadened diffraction peak at 17° and the disappearance of the peak at 23° (2θ), indicative of an increased amorphous fraction relative to the other samples (26). While a higher degree of amorphization is generally associated with enhanced starch digestibility and potential disruption of RS structures due to increased enzyme accessibility (27), the RS content of the SDGA10-130 sample (95.96 ± 0.06 g/100 g d.b.) was not significantly different from that of the SDNO130 sample (96.79 ± 0.39 g/100 g d.b.; $p > 0.05$). This observation can be explained by the emergence of a diffraction peak at approximately 20° (2θ), corresponding to V-type crystallinity associated with amylose–lipid complexes, which are known to be resistant to enzymatic digestion (28). The inclusion of GA as a carrier during spray drying likely contributed to the preservation of these amylose–lipid complexes by forming a protective film that limits oxidation of lipids and fatty acids, such as oleic and linoleic acids, thereby stabilizing RS5 structures (29).

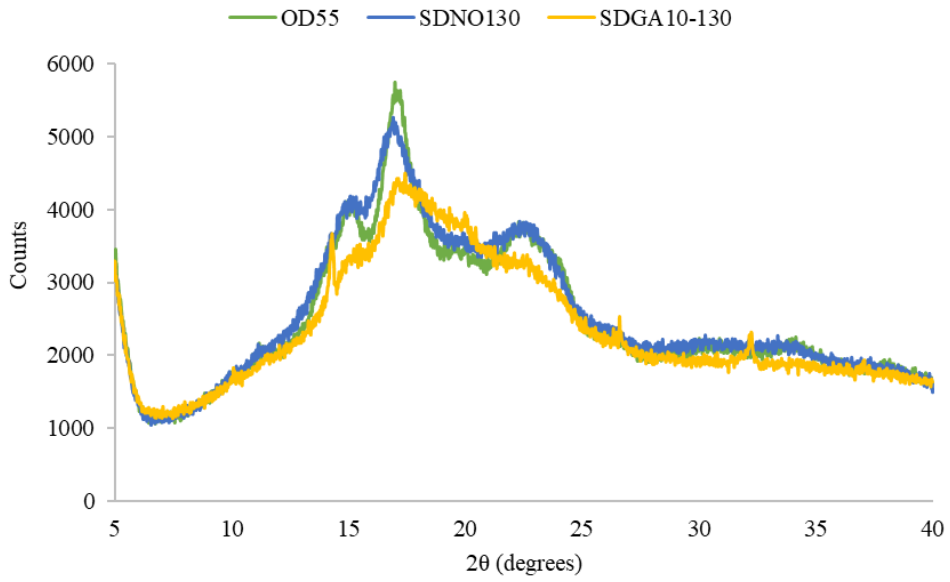

Figure 1. X-ray diffraction patterns of WGBF samples obtained by OD and SD

3.3 Chemical functional group

Fourier-transform infrared (FTIR) spectroscopy (Figure 2) was employed to assess short-range molecular order within starch granules, providing insight into processing-induced changes in starch behavior and the chemical properties of WGBF following thermal treatment and encapsulation. The FTIR spectra of all WGBF samples displayed a broad absorption band centered at approximately 3302 cm^{-1}, corresponding to O–H stretching vibrations associated with hydroxyl and carboxylic acid groups, along with characteristic C–H stretching vibrations of methyl and methylene groups at 2925 cm^{-1}. These spectral features are consistent with previous reports on WGBF and green banana peel flour produced by oven drying and freeze drying (19) (30). A band near 1630 cm^{-1}, attributed to the amide I region, was observed in all WGBF samples, indicating the presence of protein-associated functional groups (19).

Notably, the SDGA10-130 sample exhibited a slight peak shift toward the 1560–1500 cm^{-1} region, corresponding to the amide II band, which suggests molecular interactions between GA and the starch–protein matrix. In addition, a shift in absorption from 1360 to 1420 cm^{-1} was detected exclusively in the SDGA10-130 sample, indicative of C=O stretching vibrations of carboxylic acid and carboxylate groups originating from GA, thereby confirming successful encapsulation (31). Within the carbohydrate fingerprint region (1200–600 cm^{-1}), all samples exhibited characteristic C–O stretching and glycosidic C–O–C vibrations in the range of approximately 995–1100 cm^{-1}. However, the disappearance of the absorption band at 1045 cm^{-1} in the encapsulated sample reflects a reduction in starch crystallinity (32), which is in agreement with the structural changes observed in the corresponding XRD analysis.

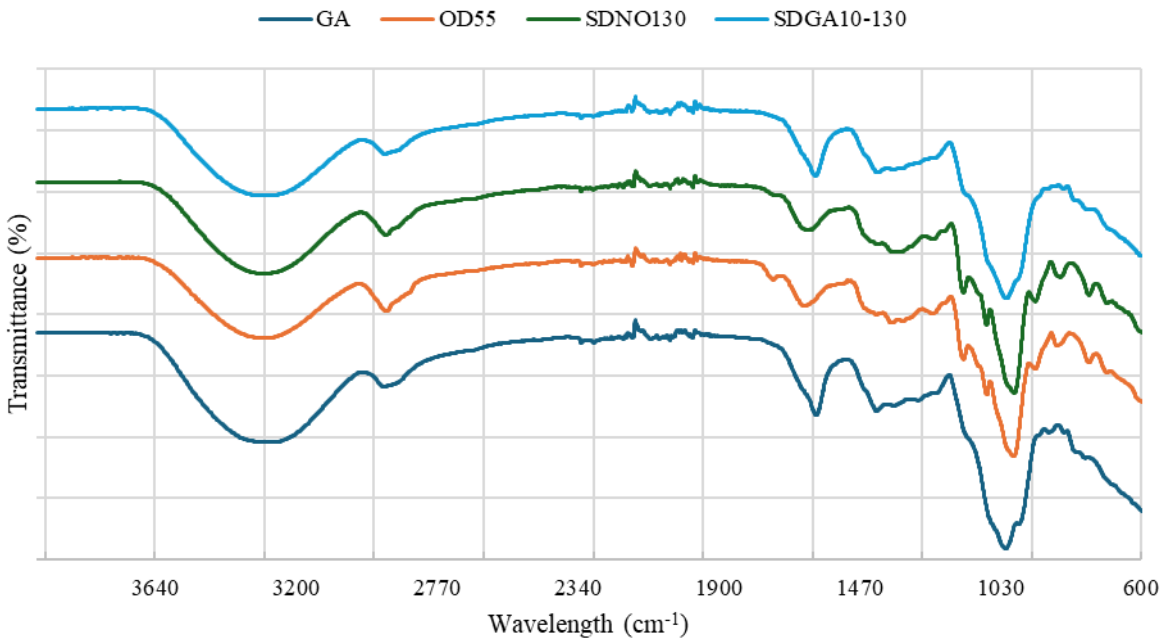

Figure 2. FTIR spectrum of WGBF samples and GA

3.4 Particle morphology

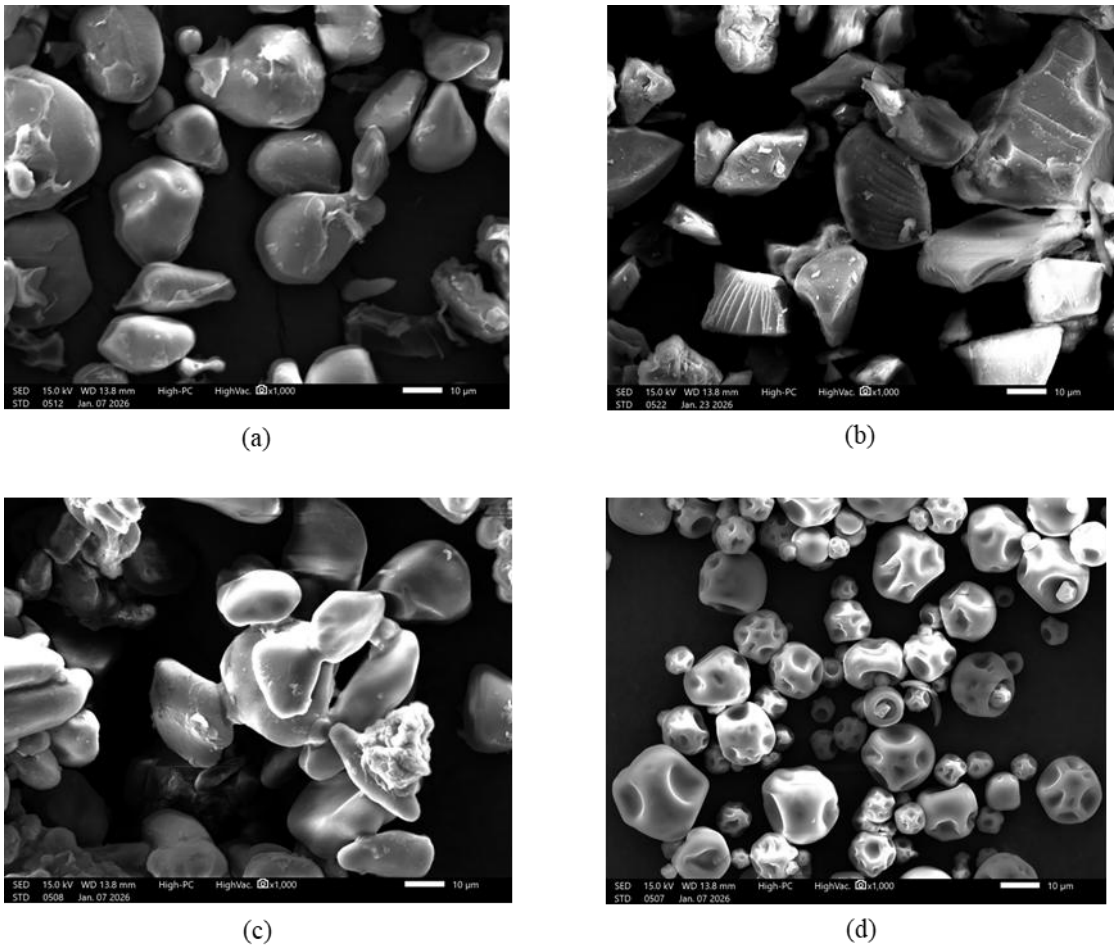

Figure 3. Scanning electron micrographs (1000× magnification) of WGBF samples and GA. (a) OD55, (b) GA, (c) SDNO130 and (d) SDGA10-130

Scanning electron microscopy (SEM) micrographs (Figure 3) provide detailed information on starch granule size, structure, and surface morphology, all of which are markedly influenced by processing conditions. Beyond crystalline organization, starch granule morphology plays a critical role in determining enzymatic accessibility and, consequently, the resistant starch (RS) content of WGBF. The OD55 WGBF sample exhibited well-separated starch granules with oblong, ellipsoidal, and elongated morphologies and relatively smooth, compact surfaces, consistent with previous observations reported by Jasim et al. (18).

In contrast, the SDNO130 WGBF sample displayed pronounced granule aggregation, with particles appearing flattened and irregular in shape, similar to the morphological characteristics described by Jasim et al. (18). The addition of water during spray-dryer feed preparation likely enhanced the structural stability of parenchyma tissues in both banana pulp and peel, promoting intergranular adhesion and subsequent agglomeration in spray-dried WGBF (30). Aggregation may also arise from particle–particle collisions during drying, particularly when particles are in a sticky, partially dehydrated state as moisture evaporates (33). Such aggregate formation increases the effective particle size and reduces the available surface area for enzymatic hydrolysis, thereby providing a plausible mechanistic explanation for the higher RS content observed in spray-dried WGBF relative to oven-dried samples (Table 1).

The SDGA10-130 WGBF sample exhibited a distinct microstructure characterized by hollow spherical particles with porous surfaces. Incorporation of GA as a carrier promoted particle

segregation by forming a surface coating that inhibited interparticle adhesion Moreover, the presence of hollow spheres, which differ from the crystalline morphology of pure GA, suggests that complete encapsulation of starch components was achieved (24). This encapsulating structure likely contributes to reduced enzymatic accessibility and enhanced protection of starch fractions, thereby inherently limiting starch digestibility and supporting RS preservation in the encapsulated WGBF.

4. Conclusion

The present findings showed the feasibility of spray drying as an alternative drying method for WGBF production, considering the increasing demand of the inclusion of green banana in food formulations as a source of TDF, especially RS. The utilization of banana peel can add nutritional and economic value while contribute to the reduction of food waste. Spray drying with and without GA carrier yielded dominant resistant starch content in whole green banana flour compared to the conventional oven drying. The inclusion of GA (10% w/w) during spray drying did not affect the RS content of WGBF; however, it altered total starch levels, thereby changing the proportion of RS within the overall flour matrix. Furthermore, spray drying at 130 ^{o}C without carrier preserved the RS2 (B-type) crystallinity in WGBF as oven drying. Whereas the formation of the RS5 (V-type) crystalline pattern was observed in WGBF with GA, partially compensating for the amorphization of RS. FTIR spectrum confirmed the success of the encapsulation of whole green banana using GA by showing the C=O stretching vibrations of carboxylic acid and carboxylate groups derived from GA. The distinction in the granule morphology of WGBF samples suggested the difference in physicochemical and functional properties, in which aggregates in spray-dried WGBF without GA exhibited the higher resistance to enzyme digestion.

This study suggests the need of future work on hydration, rheological properties, starch digestibility and food applications of the WGBF to understand their potential behavior in food processing and nutrition.

Acknowledgements

This research was conducted with the support of the Institute of Nutrition, Mahidol University, Thailand.

References

1. Englyst HN, Kingman SM, Hudson GJ, Cummings JH. Measurement of resistant starch *in vitro* and *in vivo*. Br J Nutr. 1996 May;75(5):749–55.
2. Bojarczuk A, Skąpska S, Mousavi Khaneghah A, Marszałek K. Health benefits of resistant starch: A review of the literature. Journal of Functional Foods. 2022 June;93:105094.
3. Birt DF, Boylston T, Hendrich S, Jane JL, Hollis J, Li L, et al. Resistant Starch: Promise for Improving Human Health. Advances in Nutrition. 2013 Nov;4(6):587–601.
4. FAO. Banana Market Review 2024. 2025 Aug.
5. Campuzano A, Rosell CM, Cornejo F. Physicochemical and nutritional characteristics of banana flour during ripening. Food Chemistry. 2018 Aug;256:11–7.
6. Zhu X, Li Q, Li J, Luo J, Chen W, Li X. Comparative Study of Volatile Compounds in the Fruit of Two Banana Cultivars at Different Ripening Stages. Molecules. 2018 Sept 25;23(10):2456.
7. Khoozani AA, Bekhit AEDA, Birch J. Effects of different drying conditions on the starch content, thermal properties and some of the physicochemical parameters of whole green banana flour. International Journal of Biological Macromolecules. 2019 June;130:938–46.
8. Soares CA, Peroni-Okita FHG, Cardoso MB, Shitakubo R, Lajolo FM, Cordenunsi BR. Plantain and Banana Starches: Granule Structural Characteristics Explain the Differences in Their Starch Degradation Patterns. J Agric Food Chem. 2011 June 22;59(12):6672–81.

9. Tribess TB, Hernández-Uribe JP, Méndez-Montealvo MGC, Menezes EW, Bello-Perez LA, Tadini CC. Thermal properties and resistant starch content of green banana flour (Musa cavendishii) produced at different drying conditions. LWT - Food Science and Technology. 2009 June;42(5):1022–5.
10. Nednapis Vatanasuchart, Boonma Niyomwit, Wongkrajang K. Resistant starch content, in vitro starch digestibility and physico-chemical properties of flour and starch from Thai bananas. 2. 2012;6:Maejo International Journal of Science and Technology.
11. Bezerra CV, Amante ER, De Oliveira DC, Rodrigues AMC, Da Silva LHM. Green banana (Musa cavendishii) flour obtained in spouted bed – Effect of drying on physico-chemical, functional and morphological characteristics of the starch. Industrial Crops and Products. 2013 Jan;41:241–9.
12. Barbosa J, Borges S, Amorim M, Pereira MJ, Oliveira A, Pintado ME, et al. Comparison of spray drying, freeze drying and convective hot air drying for the production of a probiotic orange powder. Journal of Functional Foods. 2015 Aug;17:340–51.
13. 13. Woo MW, Bhandari B. Spray drying for food powder production. In: Handbook of Food Powders [Internet]. Elsevier; 2013 [cited 2025 Aug 10]. p. 29–56. Available from: https://linkinghub.elsevier.com/retrieve/pii/B9780857095138500029
14. Pujapanda R, Hamid, Bashir O, Shams R, Dash KK, Goksen G, et al. Influence of carrier agents on nutritional, chemical, and antioxidant profiles of fruit juices during drying processes: a comprehensive review. Discov Food. 2025 July 17;5(1):228.
15. Ricardo Oi, Jose Carlos Curvelo Santana, Elias Basile Tambourgi, Deovaldo Moraes Junior. Feasibility study for production of green banana flour in spray dryer. Chemical Engineering Transactions. 2013 May;32:1825–30.
16. Izidoro DR, Sierakowski MR, Haminiuk CWI, De Souza CF, Scheer ADP. Physical and chemical properties of ultrasonically, spray-dried green banana (Musa cavendish) starch. Journal of Food Engineering. 2011 June;104(4):639–48.
17. Srichamnong W, Lasukhang W. Structural and chemical analysis of resistant starch effected by pre-treatments, cooking methods, reheating and storage condition in parboiled germinated brown rice (*Oryza sativa*). Int J of Food Sci Tech. 2022 Apr;57(4):2060–8.
18. Ahmed J, Thomas L, Khashawi R. Influence of hot-air drying and freeze-drying on functional, rheological, structural and dielectric properties of green banana flour and dispersions. Food Hydrocolloids. 2020 Feb;99:105331.
19. Amini Khoozani A, Birch J, Bekhit AEDA. Textural properties and characteristics of whole green banana flour produced by air-oven and freeze-drying processing. Food Measure. 2020 June;14(3):1533–42.
20. Englyst HN, Cummings JH. Digestion of polysaccharides of potato in the small intestine of man. The American Journal of Clinical Nutrition. 1987 Feb;45(2):423–31.
21. Van Hung P, Lan Phi NT, Vy Vy TT. Effect of debranching and storage condition on crystallinity and functional properties of cassava and potato starches. Starch Stärke. 2012 Dec;64(12):964–71.
22. Viana LM, Rodrigues FSR, Santos MCB, Lima ADS, Nabeshima EH, Leite MDO, et al. Green banana (Musa ssp.) mixed pulp and peel flour: A new ingredient with interesting bioactive, nutritional, and technological properties for food applications. Food Chemistry. 2024 Sept;451:139506.
23. Masters K. Spray drying handbook. 5th ed. [Harlow] New York: Longman scientific and technical J. Wiley and sons; 1991.
24. Bucurescu A, Blaga AC, Estevinho BN, Rocha F. Microencapsulation of Curcumin by a Spray-Drying Technique Using Gum Arabic as Encapsulating Agent and Release Studies. Food Bioprocess Technol. 2018 Oct;11(10):1795–806.

25. Khalid SA, Musa AM, Saeed AM, Abugroun EA, Sid Ahmed EO, Ghalib MB, et al. Manipulating dietary fibre: Gum Arabic making friends of the colon and the kidney. Bioactive Carbohydrates and Dietary Fibre. 2014 Apr;3(2):71–6.
26. Dome K, Podgorbunskikh E, Bychkov A, Lomovsky O. Changes in the Crystallinity Degree of Starch Having Different Types of Crystal Structure after Mechanical Pretreatment. Polymers. 2020 Mar 12;12(3):641.
27. Rodríguez-Ambriz SL, Islas-Hernández JJ, Agama-Acevedo E, Tovar J, Bello-Pérez LA. Characterization of a fibre-rich powder prepared by liquefaction of unripe banana flour. Food Chemistry. 2008 Apr;107(4):1515–21.
28. Zhu J, Zhuang J, Liu H, Chen Z, Li C. Recent understanding of resistant starch type 5 (RS5) and its role in modulating gut microbiota. Food Chemistry. 2025 Sept;487:144685.
29. Fang X, Shima M, Adachi S. Effects of Drying Conditions on the Oxidation of Linoleic Acid Encapsulated with Gum Arabic by Spray-drying. FSTR. 2005;11(4):380–4.
30. Castañeda-Niño JP, Mina-Hernández JH, Solanilla-Duque JF. Extraction and Characterization of Starches from the Pulp and Peel of Native Plantain (Musa AAB Simmonds) from Two Colombian Departments. Polysaccharides. 2025 Apr 14;6(2):34.
31. Vuillemin ME, Michaux F, Adam AA, Linder M, Muniglia L, Jasniewski J. Physicochemical characterizations of gum Arabic modified with oxidation products of ferulic acid. Food Hydrocolloids. 2020 Oct;107:105919.
32. Dhull SB, Chandak A, Chawla P, Goksen G, Rose PK, Rani J. Modifications of native lotus (Nelumbo nucifera G.) rhizome starch and its overall characterization: A review. International Journal of Biological Macromolecules. 2023 Dec;253:127543.
33. Gianfrancesco A, Turchiuli C, Dumoulin E, Palzer S. Prediction of Powder Stickiness along Spray Drying Process in Relation to Agglomeration. Particulate Science and Technology. 2009 Sept 3;27(5):415–27.

O - 362

Effect of Soaking Temperature on γ-Aminobutyric Acid (GABA) Content and Germination Rate of Ultrasonic-Assisted Germinated Brown Rice: KDML 105 and Riceberry

Wahyu Atmaja Kharisma Jati[1], Natthakan Rungraeng[1,2]*

[1]*Food Science and Technology Program, School of Agro-Industry, Mae Fah Luang University, Chiang Rai, 57100, Thailand*
[2]*Research Center of Innovative Food Packaging and Biomaterials Unit, Mae Fah Luang University, Chiang Rai 57100, Thailand*

**Corresponding author E-mail: natthakan.run@mfu.ac.th*

Abstract: Ultrasonication (US) is an innovative and efficient physical stimulation technology for assisting grain germination. This study investigated ultrasonic-assisted germination of two Thai brown rice cultivars (KDML 105 and Riceberry), focusing on the effect of the initial soaking temperature on γ-aminobutyric acid (GABA) content and germination rate. Brown rice grains were soaked at different temperatures (30, 35, and 40°C) for 6 h, followed by US treatment using a probe system (20 kHz, 35% amplitude, 35°C, 5 min) and then incubated at 30°C for 36 h (89% RH). A control treatment employed conventional soaking at room temperature (28°C) without US. The highest GABA content for both cultivars was achieved with a 30°C soaking temperature. For KDML 105, the GABA content was 6.60 ± 1.98 mg/100 g DW, compared to 5.89 ± 0.98 mg/100 g DW in the control. Riceberry showed a more marked increase, reaching 16.78 ± 0.88 mg/100 g DW compared with 11.11 ± 4.57 mg/100 g DW in its control. However, while the control groups soaked at room temperature exhibited high germination rates (44.71 ± 2.78% for KDML 105 and 29.47 ± 1.32% for Riceberry), the application of US treatment after initial soaking at 30°C did not significantly alter these rates (42.43 ± 2.46% and 27.46 ± 1.76%, respectively). Furthermore, textural analysis revealed that ultrasonic-assisted germination reduced the hardness of KDML 105 compared to ungerminated brown rice, indicating structural softening of the grain matrix in the cooked rice. In contrast, Riceberry exhibited only minimal textural changes. Color parameters were also affected, with uncooked germinated samples showing increased redness (a*) and yellowness (b*) without significant changes in lightness (L*). After cooking, cultivar-dependent color changes were observed, which may be attributed to mild Maillard browning and pigment transformation. These findings suggest that US treatment is an effective strategy for enriching GABA in germinated brown rice without adversely affecting the germination rate, with the optimal response for both cultivars observed at the 30°C soaking temperature.

Keywords: GABA; Germination; Soaking; Ultrasound; Germinated Brown Rice

1. Introduction

Germination is a natural biochemical process recognized as an economical and effective method for enhancing the nutritional and functional quality of cereals. Germinated brown rice (GBR), in particular, has gained prominence in the food industry as a functional ingredient due to its superior nutritional profile and elevated levels of beneficial bioactive compounds compared to non-germinated brown rice (BR) [(1,2)]. The germination process activates endogenous enzymes, such as amylases, xylanases, phytases, proteases, and lipases, facilitates the breakdown of macromolecules and anti-nutritional factors, thereby improving the sensory properties and digestibility of brown rice [(3)]. In parallel, this enzymatic activity promotes the synthesis and accumulation of bioactive compounds. A key bioactive component in GBR is γ-aminobutyric acid

(GABA), which is associated with multiple health benefits such as inhibiting cancer cell proliferation, inducing apoptosis, regulating blood pressure and cholesterol, and alleviating pain and anxiety [3,4]. Although GABA content in brown rice is naturally low, it increases substantially during germination [4]. Recent research has focused on optimizing germination conditions to enhance GABA and other nutrients in brown rice, as GABA accumulation is strongly influenced by both cultivar selection and germination parameters [4,5].

The germination procedure typically involves surface sterilization, soaking, and sprouting. Pre-germination soaking is critical for seed rehydration and the initiation of metabolic activity [6]. Key soaking parameters such as temperature, duration, and the seed-to-water ratio should be adjusted according to seed size, coat thickness, and water absorption capacity. Soaking is generally conducted at room temperature for 6–24 hours with a seed-to-water ratio ranging from 1:1.5 to 1:20 [7]. Previous studies have reported that modifying soaking and germination conditions including duration, temperature, and pH of soaking water can significantly increase GABA production in brown rice. The optimal temperature for GABA accumulation is reported to range from 30 to 40 °C [8-11].

Ultrasonication (US) is an efficient and environmentally friendly processing technology used to physically stimulate seed germination. US treatment enhances the germination rate and sprout growth while promoting the accumulation of health-promoting compounds [2]. The technology employs low-frequency acoustic energy, generating rapid pressure fluctuations in the liquid media, resulting in the formation, growth, and collapse of cavities (bubbles) where the pressure is relatively low. The collapse of cavitation bubbles produces high pressure, local heat, shock waves, and microjets, exerting mechanical and chemical effects on seed tissue while forming pores or fissures in the seed coat and pericarp [2,12].

Ding et al. reported that US stress treatment during soaking and germination significantly increased GABA content in germinated red rice [13]. Zhang et al. found that brown rice treated with an ultrasonic bath (40 kHz) for 30 min after soaking for 12 h, followed by germination for 36 h at 28±1 °C, exhibited an increase in the germination rate of brown rice of up to approximately 28% at 30 h compared to the non-sonicated control [14]. Collectively, these findings indicate that US is considered an established technique with significant potential in food processing and holds promise for developing novel GBR-based products [2]. Both bath and probe US systems have been applied to stimulate seed germination, with probe systems offering greater versatility, customization, and scalability [12]. However, little is known about the effect of power ultrasound using a probe sonication system on GABA accumulation and germination rate during brown rice germination. Therefore, this study aimed to determine the optimal soaking temperature and evaluate the effect of US treatment on GABA content and germination rate in two Thai brown rice cultivars (KDML 105 and Riceberry). In addition, the color and texture profiles of both brown rice and GBR were investigated.

2. Materials and Methods

2.1 Materials

Brown rice (*Oryza sativa* L.) of the non-pigmented Thai Jasmine rice variety (Khao Dawk Mali 105 (KDML 105)), approximately 8 months after harvesting, was purchased from Nam Om Community Enterprise Network (Kwannam-Om), Yasothon, Thailand in July 2025. The pigmented rice variety (Riceberry), produced by Unigrain Marketing (1999) Co., Ltd. (manufacturing date: 20 August 2025), was obtained from a local grocery store located in Mueang Chiang Rai district, Chiang Rai, Thailand. All samples were purchased in vacuum-sealed packaging and stored at room temperature prior to experiments.

γ-Aminobutyric acid (GABA) analytical standard was procured from Sigma-Aldrich (St. Louis, MO, USA); acetonitrile (HPLC grade) was obtained from RCI Labscan Limited; hydrogen peroxide (standard grade) was sourced from Nippon Intertrade Co., Ltd.

2.2 Germination Procedure

The germination of brown rice was performed according to the method described by Chatchavanthatri et al. [11] with modifications. To initiate the process, 50 g of brown rice was first washed with distilled water and then surface-sterilized using 3% hydrogen peroxide (rice-to-solution ratio of 1:2.5 w/v) at room temperature for 30 min. The grains were subsequently rinsed three times with deionized (DI) water to ensure complete removal of the sterilizing agent. Subsequently, the sterilized grains were placed in tissue culture bottles with lids, to which 100 mL of water was added (a ratio of 1:2 w/v). The bottles were placed in separate water baths, and soaking was conducted for 6 hours at three different temperatures: 30, 35, and 40 °C. To assess the influence of sonication, a US treatment was applied after the 6 h soaking step. A 20 kHz ultrasonic processor (Vibra Cell VCX500, Sonics & Materials, Inc., USA) with a nominal power of 500 W and a 1-inch (25 mm) solid probe was used. The treatment was conducted at 35% amplitude for 5 min, with a pulse cycle of 5 s on and 5 s off, and the temperature setting was maintained at 35 °C, based on preliminary studies. US treatment was carried out in a 250 mL glass beaker (height = 9.5 cm, diameter = 7.0 cm) placed in an ice bath to prevent overheating. The soaked grains were dispersed in distilled water at a ratio of 1:2 w/v (rice-to-water). The probe was immersed to a depth of 2 cm below the liquid surface (total liquid height ~6 cm), positioning the tip approximately 1-1.5 cm above the grain samples. The average electrical input power measured during active pulses was ~50 W, resulting in a total energy input of approximately 15,200–15,500 J for the entire process. Specific energy input was calculated per treatment by dividing cumulative energy by total sample mass (soaked rice-water), incorporating cultivar-dependent water absorption, and was approximately 69-72 J/g. Control samples were drained immediately after soaking without undergoing US treatment.

Following the soaking and US treatment steps, all samples were drained and transferred to polypropylene (PP) bowls for sprouting. A double layer of cheesecloth was placed over the bowls, which were then covered with perforated lids. Germination occurred at 30 °C for 36 h in a constant temperature and humidity chamber (Memmert, model HPP1060eco, USA) set to 89% relative humidity. During germination, the kernels were rinsed with DI water every 12 h. Subsequently, GBR samples were dried in a hot-air oven at 50 °C for 9 h until the moisture content reached a maximum of 14%. A portion of the dried GBR was then ground and passed through a 60-mesh sieve to obtain GBR powder. The powder was stored in a dry chamber for subsequent analysis. All experiments were performed in triplicate for each rice variety and treatment condition.

2.3 Determination of germination rate

The brown rice grain was considered germinated when a white embryo protrusion was visible (0.5-1.0 mm in length). One hundred grains of rice were selected randomly after 36 h of germination, and grains which reached the standard of germination were counted [14]. The germination rate was calculated based on the total 100 grains using the following formula:

$$\text{Germination rate (\%)} = \frac{The\ number\ of\ germinated\ seeds}{Total\ number\ of\ seeds} \text{ x } 100$$

Additionally, GBR was then grouped into three categories after measuring its sprout length by direct observation and vernier caliper [4]. For record-keeping and subsequent verification, brown rice was photographed alongside a scale. These images were later analyzed using ImageJ software to confirm the manual length assessments and categorization.

2.4 Determination of GABA Content

The extraction method for GABA from the samples was adapted from the previous work conducted by Nacha et al. [15] with minor modification. From each rice flour powder, 0.5 g was extracted using DI water at a 1:15 w/v ratio. The solutions were boiled in a water bath

(MemmertWNB, Memmert, USA) maintained at 90°C for 5 min and centrifuged at 10000 g for 15 min at 25°C using a Thermo Scientific Sorvall Legend X1R centrifuge (Thermo Fisher Scientific, USA). After centrifugation, the supernatant was diluted with 50 % (v/v) acetonitrile and filtered through a nylon filter (0.45 µm) prior to further analysis. The extracted samples were used for GABA analysis.

GABA content analysis was performed according to the procedure described by Nacha et al [15]. A series of GABA standard solutions was prepared, with concentrations ranging from 0 to 50 ppm, to create a calibration standard curve. Subsequently, the GABA content in both standard compounds and extracted rice samples was measured using a liquid chromatography-mass spectrometry (LC-MS/MS) triple quadrupole system (Shimadzu, Nexera X2/LCMS-8060NX, Japan) with Infinity Lab Poroshell 120 HILIC-Z column (2.1×100mm, 2.7µm).

2.5 Texture Profile Analysis

The texture of the cooked rice was analyzed using a texture analyzer (Model TA.XTplus, Stable Micro Systems, UK), following the method of Li et al. [16] and Chin et al. [17] with some modifications. Rice grains (10 g) were rinsed twice and soaked for 10 min in DI water in 8 x 5 x 3.5 cm aluminum pleated cups. The rice was cooked by steaming using an electric cooker (NW-REP1010, Newwave, Thailand) for 25 min with a rice-to-water ratio of 1:1.6 w/v, after which it was allowed to stand in the closed cooker for 10 min. The cooked rice was then transferred to a plastic cup with a lid and cooled to room temperature. The experiments were performed in triplicate for each rice variety and treatment condition.

The texture profiles were determined using a texture analyzer with 75 mm diameter aluminum probe. Twenty cooked rice grains were arranged closely in a single layer on the platform below the probe. A two-cycle compression program (TPA) was run with pre-test, test, and post-test speeds of 1 mm/s. A compression platen probe (P/75) was used to achieve 80% strain, with a 5 s interval between the two compressions. The auto trigger force was set at 5.0 g.

2.6 Color Analysis

The color of uncooked and cooked rice samples was quantified using the CIE L*, a*, b* color scale, following the method by Devi and Badwaik [18]. Color measurements were performed with a UltraScan VIS colorimeter (HunterLab, Reston, VA, USA) on rice samples placed in clear, transparent plastic bags. In this system, L* represents lightness, ranging from 0 (black) to 100 (white). The a* value indicates redness (+) to greenness (-), while b* indicates yellowness (+) to blueness (-). Prior to analysis, the instrument was calibrated using standard white and black reference tiles. All measurements were conducted under illuminant D65 (medium daylight) with a 10° standard observer angle.

2.7 Statistical Analysis

All data were statistically analyzed using analysis of variance (ANOVA), and mean comparisons were conducted using Duncan's multiple range test to determine significant differences between samples at a 95% confidence level ($p < 0.05$). All statistical analyses were carried out using IBM SPSS Statistics version 27.0.0 for Windows software (IBM Corporation, NY, USA).

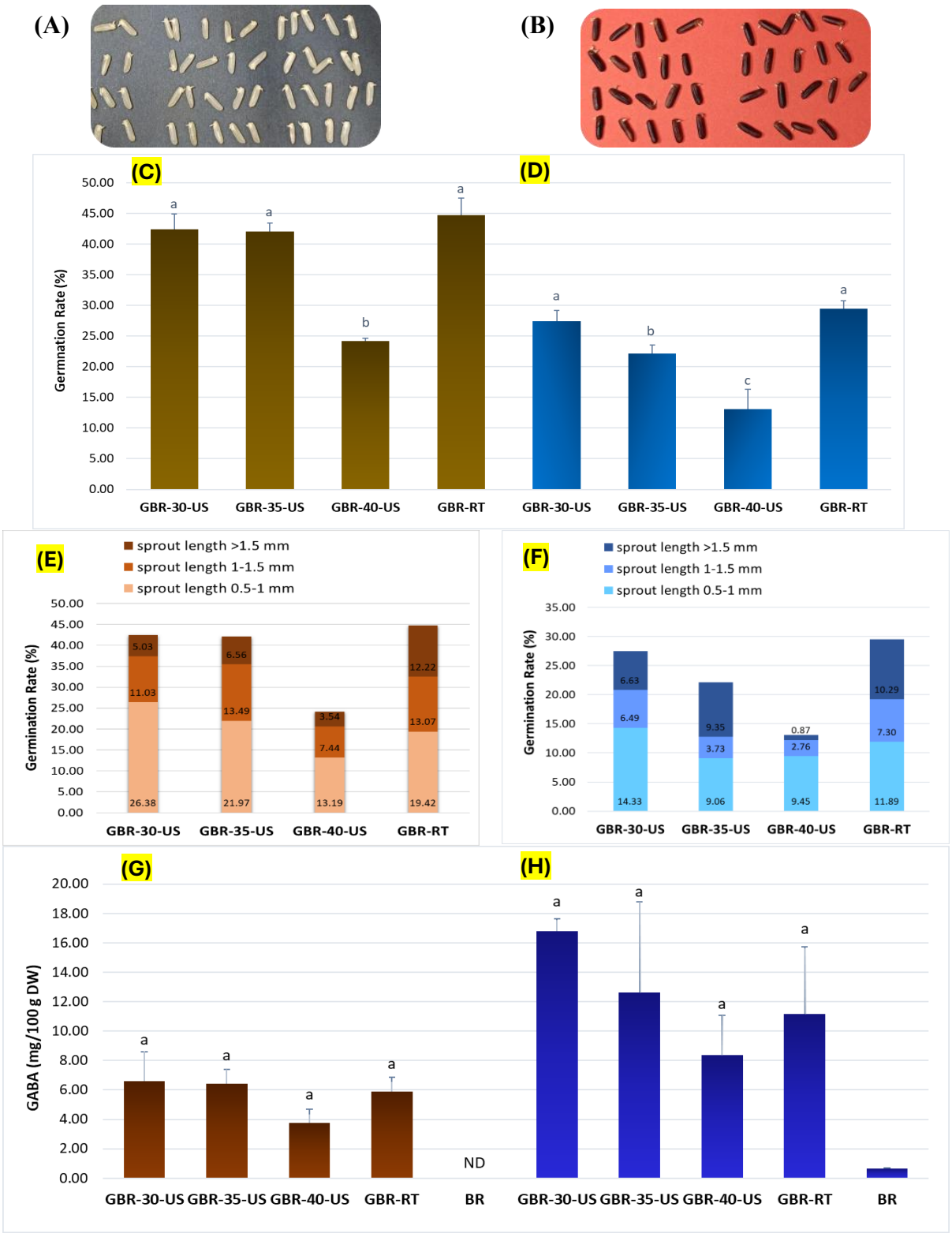

Figure 1. Effects of initial soaking temperature and US treatment on germination rate and GABA content of brown rice. (A-B) Germinated brown rice of KDML 105 (A) and Riceberry (B); (C-D) Germination Rate of KDML 105 (C) and Riceberry (D); (E-F) Sprout Length Distribution of KDML 105 (E) and Riceberry (F); (G-H) GABA Content of KDML 105 (G) and Riceberry (H). Ungerminated brown rice (control) was excluded from statistical analysis. Different superscript letters (a–c) indicate significant differences among treatments within each variety ($p \leq 0.05$, Duncan's multiple range test). No significant interaction between variety and treatment was observed.

3. Results & Discussion

The following treatment codes are used throughout this section to denote the experimental conditions: BR (ungerminated brown rice), GBR-RT (germinated brown rice soaked at room temperature, 28 °C, without ultrasound), GBR-30-US (germinated brown rice soaked at 30 °C with ultrasound), GBR-35-US (soaked at 35 °C with ultrasound), and GBR-40-US (soaked at 40 °C with ultrasound).

3.1 Effects of initial soaking temperature and ultrasound treatment on germination rate

The germination rate of both KDML 105 and Riceberry cultivars was significantly influenced by initial soaking temperature. In KDML 105, germination remained relatively stable (~42–45%) for GBR-RT, GBR-30-US, and GBR-35-US, but sharply decreased to 24.18% for GBR-40-US. Riceberry showed a similar trend with lower overall germination (~22–29% for GBR-RT through GBR-35-US) declining to 13.09% for GBR-40-US, demonstrating temperature sensitivity across both cultivars (Figure 1C, D). High temperature may accelerate metabolic rate and cause excessive consumption of dissolved oxygen in the soaking water, potentially damaging the seed embryo and suppressing sprout growth, ultimately reducing germination rate [19]. These results align with Chatchavanthatri et al. [6], who found that increasing soaking temperature from 30 °C to 40 °C caused a slight decrease in germination rate ($p > 0.05$), probably due to increased water content in paddy. They also reported that US treatment for 15 min after 8 h of soaking significantly increased germination rate at 24 h of germination, but showed no significant effect between 24 and 48 h. This plateau possibly reflects that the physiological capacity of the seeds has been reached, as ~95–99% of seeds germinated after 36 h. At that point, neither ultrasound treatment nor extended germination time meaningfully increased the germination rate [6].

In contrast, some studies have shown improved germination under optimized US conditions. Yaldagard et al. observed increased germination of barley seeds with controlled US (20–90% amplitude of 460 W for 5–15 min), with maximum germination achieved at 100% amplitude for 15 min, corresponding to an increase of 1.06 times [20]. Hassan et al. reported that US amplitude and duration influenced germination enhancement in sorghum sprouts [21]. The power and duration of US exposure are determining factors that can stimulate seed vitality, requiring clear dosage optimization to minimize negative changes [22].

Sprout length distribution further supported the conclusion that moderate temperatures promote more robust sprout elongation, whereas elevated temperature combined with US treatment reduces both total germination percentage and sprout development (Figure 1E, F). At moderate temperatures (GBR-30-US, GBR-35-US, and GBR-RT), a greater proportion of sprouts reached ≥1 mm, whereas GBR-40-US showed fewer elongated sprouts. However, He et al. proposed that a grain length of 0.5–1.0 mm represents an optimal range at which nutrient content and biological activity are maximized, with further elongation associated with nutritional decline [23].

Although US treatment can stimulate enzymatic activity and crop growth, high-intensity US treatment of seeds may cause cell rupture and enzyme inactivation [24]. Therefore, careful optimization of ultrasonic parameters is necessary for maximizing beneficial effects while preventing tissue damage, as ideal conditions vary depending on plant species [24].

3.2. Effect of initial soaking temperature and ultrasound treatment on GABA content

Germination for 36 h markedly increased GABA content in both KDML 105 and Riceberry compared with ungerminated brown rice (BR) (Figure 1G, H). In KDML 105, GABA was below the detection limit in BR, whereas Riceberry contained 0.60 ± 0.04 mg/100 g DW. After germination, all treatments enhanced GABA accumulation. Although the differences among germinated samples were not statistically significant ($p > 0.05$), initial soaking at 30 °C followed by ultrasonic treatment (GBR-30-US) produced the highest GABA content in both cultivars. In

KDML 105, GABA reached 6.60 ± 1.98 mg/100 g DW in GBR-30-US, followed by GBR-35-US (6.44 ± 0.95 mg/100 g DW), while GBR-RT showed 5.89 ± 0.98 mg/100 g DW. GBR-40-US exhibited the lowest value (3.76 ± 0.96 mg/100 g DW). In Riceberry, a similar pattern was observed at markedly higher levels. GBR-30-US showed the highest GABA content (16.78 ± 0.88 mg/100 g DW), followed by GBR-35-US (12.64 ± 6.15 mg/100 g DW) and GBR-RT (11.11 ± 4.57 mg/100 g DW), while GBR-40-US showed the lowest value (8.36 ± 2.72 mg/100 g DW). Thus, despite varietal differences in GABA accumulation, the same temperature ranking was maintained.

The soaking temperature significantly impacts the GABA accumulation in sprouted grain [19]. Zhang et al. [9] reported that soaking at 30 °C and germination at 35 °C for 36 h maximized GABA accumulation in japonica and indica rice, while Singh et al. [10] similarly demonstrated that soaking temperature significantly influences GABA formation in GBR. These findings support the superior performance of GBR-30-US observed in the present study. Conversely, the lower GABA content at 40 °C is consistent with the observation of Dong et al., who reported that elevated soaking temperature (40 °C) significantly decreased GABA accumulation due to inhibition of endogenous enzyme activities in germinated coix seed [19]. When soaking temperature exceeds the optimum range, glutamate decarboxylase (GAD), a key enzyme responsible for GABA synthesis, may decline in activity, limiting conversion of glutamate to GABA [19]. As noted by Hou et al. [5] and do Nascimento et al. [7], GABA accumulation during germination is highly dependent on enzymatic kinetics and stress-responsive metabolic activation.

US treatment further enhanced GABA accumulation, particularly under favorable temperature conditions. Compared with GBR-RT, GBR-30-US showed slightly higher GABA in both cultivars. This observation aligns with Ding et al. [13], who reported that ultrasonication significantly enhanced GABA and related metabolites in germinated red rice. Naumenko et al. also showed that US stimulated antioxidant activity and GABA production in germinated wheat, suggesting that ultrasonic stress may activate defense-related metabolic pathways [22]. The mechanism underlying US enhancement is attributed to cavitation effects, which increase cell membrane permeability and facilitate water and oxygen diffusion into the grain matrix [2, 6, 24]. According to Wang et al. [24] and Nogueira et al. [12], US can accelerate metabolic activation during seed germination by improving mass transfer and inducing mild stress responses. Consequently, US probe treatment used in this study likely promoted GAD activity and substrate availability, thereby enhancing GABA accumulation under optimal temperature conditions. However, US treatment could not overcome thermal stress at elevated temperatures. At 40 °C, the stimulatory effect of ultrasound was likely diminished due to enzyme inhibition caused by above-optimal temperature. These findings demonstrate that the combination of appropriate soaking temperature and US treatment is critical for maximizing GABA synthesis.

3.3 Effects of initial soaking temperature and ultrasound treatment on texture of cooked rice

Texture is a critical determinant of cooked rice eating quality and consumer acceptability [16,25,26]. The effects of different treatments on texture profile parameters of cooked brown rice are presented in Table 1. Significant differences among treatments ($p < 0.05$) were observed for hardness, adhesiveness, and cohesiveness in KDML 105, whereas no significant differences were detected in Riceberry ($p > 0.05$), indicating cultivar-dependent responsiveness to germination and US treatment.

Untreated brown rice (BR) exhibited the highest hardness (9781.96 ± 525.28 gf), indicating a firmer cooked texture. All GBR samples showed reduced hardness, particularly GBR-30-US (7526.07 ± 515.42 gf) and GBR-35-US (7669.66 ± 1645.98 gf) ($p < 0.05$). Adhesiveness (more negative values) was significantly greater in all germinated treatments (−340.96 to −432.56 g·s) compared with BR (−241.92 ± 21.66 g·s). Cohesiveness differed significantly in KDML 105, with BR lowest (0.41 ± 0.01) and GBR-40-US highest (0.45 ± 0.01). No consistent significant

differences were observed for springiness across treatments. Chewiness, mathematically derived from hardness, cohesiveness, and springiness, was highest in BR (2885.95 ± 392.39 g·s), corresponding with its greater hardness.

These textural changes arise from US-assisted germination. Germination activates hydrolytic enzymes (amylases and proteases) that partially degrade starch–protein matrices, weakening the compact endosperm structure [7,23,26]. Heberle et al. further suggested that enzymatic reduction of macromolecules creates internal voids and decreases fracture resistance, thereby affecting cooking time and grain hardness [27]. US treatment intensifies these effects through cavitation, generating mechanical vibrations and microjets, increasing surface porosity that deform the outer cell layers, disrupt cell walls, and induce cracks and fissures in the grain [2,25-27]. Bonto et al. observed by scanning electron microscopy (SEM) that US bath treatment caused loss of morphological integrity compared with non-sonicated controls, exposing parenchyma cell walls and the starch-rich sub-aleurone layer, with fragmented and loosened starch granule packing. These microstructural changes increased surface area and mass transfer into the surrounding water medium [28]. Similarly, Mudgal and Singh reported that US probe treatment during soaking increased α-amylase activity due to enhanced oxygen availability and water uptake associated with cavitation and microstreaming. Cracks formed on the outer grain layer increased permeability during germination, stimulating α-amylase production and reducing total starch. US also disrupted starch–protein and starch–lipid complexes, increasing substrate susceptibility to enzymatic hydrolysis, accelerating starch degradation [2]. Collectively, the combined enzymatic degradation and cavitation-induced structural disruption enhance hydration and starch gelatinization during cooking, leading to reduced hardness. The weakened structure also facilitates starch swelling and amylose leaching during cooking, increasing adhesiveness [25,26]. Cohesiveness, representing internal bonding strength of the rice gel network after compression, showed cultivar-dependent variation. Although germination weakens the rigid native matrix, US treatment combined with cooking may promote formation of a more homogeneous internal structure through improved hydration and uniform gelatinization [25]. The reduced hardness in germinated samples also explains their lower chewiness values, as chewiness is directly influenced by hardness [16].

In contrast to KDML 105, the pigmented Riceberry rice cultivar exhibited minimal textural changes after germination and US treatment. This resistance to softening can be attributed to several factors. First, the peripheral layer architecture and internal composition of pigmented cultivars influence their texture properties [27]. Additionally, anthocyanins and related polyphenols concentrated in the bran layer can form hydrogen bonds with starch chains and compete for available water, thereby restricting granule swelling during gelatinization [15,18,29]. These interactions stabilize amorphous and semi-crystalline regions of starch, limit amylose mobility, and constrain structural expansion during cooking [29]. Riceberry has been reported to contain relatively high amylose and protein contents, which further reinforce this resistance [18,30]. Elevated amylose accelerates reassociation during cooling, promoting rapid retrogradation and increasing gel stiffness, while protein–starch interactions strengthen the internal matrix [18]. Although germination and cooking may partially reduce anthocyanin levels, residual phenolic–starch–protein interactions probably remain sufficient to maintain matrix rigidity, effectively counterbalancing ultrasound-induced microstructural weakening [15].

Table 1. Texture profiles of cooked KDML 105 and Riceberry rice

Treatment	Hardness (gf)	Adhesiveness (g.s)	Springiness	Cohesiveness	Chewiness (g.s)
KDML 105					
GBR-30-US	7526.07 ± 515.42^{a}	-365.78 ± 48.64^{b}	0.66 ± 0.04^{a}	0.43 ± 0.01^{a,b}	2132.27 ± 263.34^{a}
GBR-35-US	7669.66 ± 1645.98^{a}	-387.59 ± 87.64^{b}	0.61 ± 0.05^{a}	0.43 ± 0.02^{a,b}	2079.67 ± 734.98^{a}
GBR-40-US	8727.07 ± 499.06^{a,b}	-340.96 ± 9.55^{b}	0.68 ± 0.06^{a}	0.45 ± 0.01^{a}	2702.11 ± 228.75^{a}
GBR-RT	8560.34 ± 243.64^{a,b}	-432.56 ± 37.95^{b}	0.63 ± 0.01^{a}	0.43 ± 0.01^{a}	2333.59 ± 34.16^{a}
BR	9781.96 ± 525.28^{b}	-241.92 ± 21.66^{a}	0.70 ± 0.03^{a}	0.41 ± 0.01^{b}	2885.95 ± 392.39^{a}
Riceberry					
GBR-30-US	7635.11 ± 595.83^{a}	-245.01 ± 30.60^{a}	0.68 ± 0.02^{a}	0.40 ± 0.02^{a}	2106.11 ± 305.32^{a}
GBR-35-US	8675.40 ± 335.78^{a}	-294.3 ± 53.01^{a}	0.67 ± 0.03^{a}	0.42 ± 0.005^{a}	2464.7 ± 187.81^{a}
GBR-40-US	8112.08 ± 359.75^{a}	-281.57 ± 135.72^{a}	0.66 ± 0.05^{a}	0.41 ± 0.01^{a}	2146.96 ± 56.62^{a}
GBR-RT	8131.96 ± 217.13^{a}	-296.96 ± 73.76^{a}	0.67 ± 0.05^{a}	0.41 ± 0.01^{a}	2257.04 ± 301.14^{a}
BR	8159.03 ± 712.94^{a}	-155.32 ± 35.67^{a}	0.69 ± 0.03^{a}	0.38 ± 0.02^{a}	2152.64 ± 347.90^{a}

Data are expressed as mean ± standard deviation (n = 3); different superscript letters (a-b) within the same column indicate significant differences ($p \leq 0.05$); comparisons were performed separately for each rice variety.

Table 2. Color profiles of uncooked and cooked KDML 105 and Riceberry rice

Treatment	uncooked rice			cooked rice		
	L*	a*	b*	L*	a*	b*
KDML 105						
GBR-30-US	64.53±1.02^{a}	2.98±0.27^{a}	17.64±0.46^{a,b}	61.98±0.42^{b}	-0.53±0.16^{a}	11.39±0.67^{a}
GBR-35-US	65.20±0.90^{a}	2.68±0.31^{a,b}	17.90±0.24^{a}	62.01±0.37^{b}	-0.86±0.38^{a}	10.74±1.05^{a}
GBR-40-US	65.20±1.08^{a}	2.14±0.30^{b}	16.89±0.46^{b}	60.08±1.31^{c}	-0.62±0.16^{a}	9.67±0.69^{a}
GBR-RT	64.48±0.52^{a}	3.10±0.56^{a}	17.69±0.53^{a,b}	60.51±1.43^{b,c}	-0.43±0.09^{a}	10.25±0.96^{a}
BR	64.24±1.14^{a}	2.19±0.16^{b}	15.32±0.64^{c}	63.88±0.27^{a}	-0.61±0.58^{a}	10.59±2.14^{a}
Riceberry						
GBR-30-US	39.05±0.22^{a}	2.82±0.23^{a}	0.76±0.21^{a}	30.92±2.83^{a,b}	6.55±0.93^{a}	3.04±0.46^{a}
GBR-35-US	38.79±0.17^{a}	3.56±0.16^{a}	1.22±0.06^{a}	32.92±1.63^{a}	6.04±0.26^{a,b}	3.02±0.42^{a}
GBR-40-US	38.69±0.26^{a}	2.95±0.23^{a}	0.70±0.28^{a,b}	32.11±2.26^{a}	5.93±0.88^{a,b}	2.12±0.25^{b}
GBR-RT	39.13±0.74^{a}	3.01±0.71^{a}	1.05±0.85^{a}	30.80±0.87^{a,b}	7.05±0.29^{a}	3.61±0.40^{a}
BR	38.82±0.12^{a}	1.62±0.73^{b}	-0.11±0.40^{b}	27.20±1.82^{b}	4.75±0.79^{b}	0.49±0.41^{c}

Data are expressed as mean ± standard deviation (n = 3). Different superscript letters (a–c) within the same column indicate significant differences ($p \leq 0.05$); comparisons were performed separately for each rice variety and condition.

3.4 Effects of initial soaking temperature and ultrasound treatment on color of uncooked and cooked rice

Color is a critical quality parameter as it reflects chemical reactions during germination and processing, including lipid oxidation, Maillard reactions, and pigment migration, while strongly influencing consumer acceptance [27,31]. Color parameters of uncooked and cooked rice are presented in Table 2. For uncooked rice, lightness (L*) values ranged from 64.24–65.20 in KDML 105, and 38.69–39.13 in Riceberry, with no significant differences among treatments within each cultivar. This indicates that germination and US treatment did not markedly affect the overall L* value of raw grains. The substantial cultivar difference in L* is expected, as Riceberry,

as a pigmented rice, naturally contains high anthocyanin concentrations in the bran layer, resulting in significantly lower lightness compared with non-pigmented KDML 105 [1,18]. However, increases in redness (a*) and yellowness (b*) were observed in GBR-30-US, GBR-35-US, and GBR-RT treatments, indicating enhanced color saturation.

Pigments located in the bran and outer endosperm may become more visually prominent after germination due to hydration and structural modification of outer layers [31]. Zhang et al. suggested that the drying process may initiate oxidation reactions in fats and proteins within rice grains, producing substances with a reddish hue, and this may increase a* values. Additionally, starch in rice grains may convert to reducing sugars under certain conditions, initiating Maillard reactions that form reddish-brown compounds [32].

After cooking, cultivar-dependent responses were observed. In KDML 105, germinated samples showed lower L* compared with ungerminated brown rice, while a* and b* showed no significant differences. This lightness decrease suggests mild browning reactions during cooking. In contrast, Riceberry germinated samples exhibited higher L*, a*, and b* value compared with ungerminated rice. This opposite behavior reflects the higher initial pigment content of Riceberry [15]. Cooked GBR may lose part of its soluble phenolic compounds during cooking due to leaching into water, which can increase lightness as pigmented compounds are partially removed [15,33]. Since cooking was performed using DI water, the pH remained near-neutral. Anthocyanins, the primary pigments in pigmented rice, are water-soluble and sensitive to processing conditions, particularly temperature and pH [15,29]. They are stable under acidic conditions but show reduced stability at near-neutral pH, as in the present study where cooking was performed with DI water [29]. Therefore, cooking likely promoted anthocyanin degradation and leaching, reducing pigment concentration in the rice grains and contributing to increased lightness (L*) [15,33]. Simultaneously, thermal processing promotes Maillard reactions between free amino acids, which are elevated after germination, and reducing sugars, forming brown melanoidins that may decrease L* and increase a* and b* [34].

4. Conclusion

Ultrasound-assisted germination effectively enhanced the nutraceutical and functional quality of Thai brown rice cultivars (KDML 105 and Riceberry). Optimal GABA accumulation was achieved with initial soaking at 30 °C for 6 h followed by US treatment, without significantly affecting germination rate. The treatment also reduced hardness in cooked KDML 105 rice and induced cultivar-dependent color modifications. These findings demonstrate that ultrasound acts as a physical stimulus promoting structural disruption and metabolic activation during germination, thereby improving both functional and quality attributes. Future research should explore optimizing specific ultrasonic parameters, including amplitude, treatment duration, and pulsed mode settings, across different rice cultivars to establish standardized protocols that maximize GABA accumulation without compromising germination performance at higher temperatures.

Acknowledgements

This research was financially supported by the Graduate School, Mae Fah Luang University, Chiang Rai, Thailand, and the Thailand International Cooperation Agency (TICA), Ministry of Foreign Affairs of Thailand, under the Thailand International Postgraduate Programme (TIPP) Scholarship.

References

1. Beaulieu JC, Boue SM, Goufo P. Health-promoting germinated rice and value-added foods: a comprehensive and systematic review of germination effects on brown rice. Crit Rev Food Sci Nutr. 2023 Dec 20;63(33):11570–603.

2. Mudgal S, Singh N. Impact of ultrasonication on the physicochemical, pasting, amino acid, mineral, phenolic, and sugar profile of germinated brown rice from various varieties. J Food Sci Technol. 2025 Mar 13;62(3):492–507.
3. Chen C, Tao Y, Han Y, Ding Y, Jian X, Li D. Preparation of germinated brown rice with high γ-aminobutyric acid content and short root by magnetic field treatment. J Cereal Sci. 2023 Jul;112:103720.
4. Munarko H, Sitanggang AB, Kusnandar F, Budijanto S. Effect of different soaking and germination methods on bioactive compounds of germinated brown rice. Int J Food Sci Technol. 2021 Sep 1;56(9):4540–8.
5. Hou D, Tang J, Feng Q, Niu Z, Shen Q, Wang L, Zhou S. Gamma-aminobutyric acid (GABA): a comprehensive review of dietary sources, enrichment technologies, processing effects, health benefits, and its applications. Crit Rev Food Sci Nutr. 2024;64(24):8852-8874.
6. Chatchavanthatri N, Junyusen T, Moolkaew P, Arjharn W, Junyusen P. Effect of soaking and sprouting treatment on germination rate of paddy. E3S Web of Conf. 2020 Sep 8;187:04016.
7. do Nascimento LÁ, Abhilasha A, Singh J, Elias MC, Colussi R. Rice germination and its impact on technological and nutritional properties: a review. Rice Sci. 2022;29(3):201–15.
8. Hassan S, Hussain MB, Waheed M, Ahmad K, Kassymov S, Shariati MA, et al. Effect of germination processing on bioactive compounds of cereals and legumes. In: Egbuna C, Tupas GD, editors. Functional foods and nutraceuticals: bioactive components, formulations and innovations. Cham: Springer International Publishing; 2020. p. 283–306.
9. Zhang Q, Xiang J, Zhang L, Zhu X, Evers J, van der Werf W, et al. Optimizing soaking and germination conditions to improve gamma-aminobutyric acid content in japonica and indica germinated brown rice. J Funct Foods. 2014;10:283–91.
10. Singh K, Simapisan P, Decharatanangkoon S, Utama-ang N. Effect of soaking temperature and time on GABA and total phenolic content of germinated brown rice (Phitsanulok 2). Curr Appl Sci Technol. 2017;17(2):224-32.
11. Patil SB, Khan MdK. Germinated brown rice as a value added rice product: A review. J Food Sci Technol. 2011;48(6):661–7. doi:10.1007/s13197-011-0232-4
12. Nogueira A, Teixeira A, Gerós H, Puga H. Ultrasound Prototype for Improving Germination and Seedling Growth in Tomato and Maize Seeds. J Plant Growth Regul. 2024;43(4):1216–29.
13. Ding J, Ulanov A V, Dong M, Yang T, Nemzer B V, Xiong S, et al. Enhancement of gama-aminobutyric acid (GABA) and other health-related metabolites in germinated red rice (*Oryza sativa* L.) by ultrasonication. Ultrason Sonochem. 2018;40:791–7.
14. Zhang G, Xu J, Wang Y, Sun X, Huang S, Huang L, et al. Combined transcriptome and metabolome analyses reveal the mechanisms of ultrasonication improvement of brown rice germination. Ultrason Sonochem. 2022;91:106239.
15. Nacha J, Soodpakdee K, Chamyuang S. Nutritional improvement of germinated riceberry rice (*Oryza sativa*) cultivated with *Pleurotus ostreatus* mycelium. Trends Sci. 2023;20(9):5574.
16. Li C, Yao S, Song B, Zhao L, Hou B, Zhang Y, et al. Evaluation of cooked rice for eating quality and its components in geng rice. Foods. 2023;12(17).
17. Chin L, Therdthai N, Ratphitagsanti W. Effect of microwave cooking on quality of riceberry rice (*Oryza sativa* L.). J Food Qual. 2020 Jan 1;2020(1):4350274.
18. Devi LM, Badwaik LS. Variety difference in physico-chemical, cooking, textural, pasting and phytochemical properties of pigmented rice. Food Chem Adv. 2022;1:100059.
19. Dong L, Yang Y, Zhao Y, Liu Z, Li C, He L, et al. Effect of different conditions on the germination of coix seed and its characteristics analysis. Food Chem X. 2024;22:101332.

20. Yaldagard M, Mortazavi SA, Tabatabaie F. Application of ultrasonic waves as a priming technique for accelerating and enhancing the germination of barley seed: optimization of method by the Taguchi Approach. J Inst Brew. 2008;114(1):14–21.
21. Hassan S, Imran M, Ahmad MH, Khan MI, XU C, Khan MK, Muhammad N. Phytochemical characterization of ultrasound-processed sorghum sprouts for the use in functional foods. Int J Food Prop. 2020;23(1):853–63.
22. Naumenko N, Potoroko I, Kalinina I. Stimulation of antioxidant activity and γ-aminobutyric acid synthesis in germinated wheat grain *Triticum aestivum* L. by ultrasound: Increasing the nutritional value of the product. Ultrason Sonochem. 2022;86:106000.
23. He LY, Yang Y, Ren LK, Bian X, Liu XF, Chen FL, et al. Effects of germination time on the structural, physicochemical and functional properties of brown rice. Int J Food Sci Technol. 2022 Apr;57(4):1902-10.
24. Wang J, Ma H, Wang S. Application of ultrasound, microwaves, and magnetic fields techniques in the germination of cereals. Food Sci Technol Res. 2019;25(4):489–97.
25. Liu X, Guo Y, Wang S, Wang X, Wang Z, Wang Z. Effects of ultrasound combined with hydrothermal treatment on the quality of brown rice. LWT. 2024;196:115874.
26. Bonto AP, Tiozon Jr RN, Sreenivasulu N, Camacho DH. Impact of ultrasonic treatment on rice starch and grain functional properties: A review. Ultrason Sonochem. 2021;71:105383.
27. Heberle T, Rondan FS, Gohlke G, Flores EMM, Ashokkumar M, Mesko MF. Ultrasound effect on the pre-germination soaking stage of pigmented rice: Impact on nutritional and technological aspects. Ultrason Sonochem. 2025;120:107421.
28. Bonto AP, Tiozon RN Jr, Rojviriya C, Sreenivasulu N, Camacho DH. Sonication increases the porosity of uncooked rice kernels affording softer textural properties, loss of intrinsic nutrients and increased uptake capacity during fortification. Ultrason Sonochem. 2020;68:105234.
29. Evangelista GC, Schönlechner R. Potential of pigmented rice in bread, bakery products, and snacks: a narrative review of current technological and nutritional developments. Appl Sci. 2025;15(12):6698.
30. Bani C, Cappa C, Restani P, Sala M, Colombo F, Mercogliano F, et al. Physicochemical and nutritional quality of pigmented rice and bran: Influence of milling and cooking. LWT. 2024;208:116653.
31. Liu Q, Kong Q, Li X, Lin J, Chen H, Bao Q, et al. Effect of mild-parboiling treatment on the structure, colour, pasting properties and rheology properties of germinated brown rice. LWT. 2020;130:109623.
32. Zhang P, Li B, Hu Z, Zhang Q, Zhu Y, Hao W. Effects of ultrasonic and microwave treatment on color, quality and drying characteristics of rice. J Cereal Sci. 2024;116:103856.
33. Sirisoontaralak P, Nakornpanom NN, Koakietdumrongkul K, Panumaswiwath C. Development of quick cooking germinated brown rice with convenient preparation and containing health benefits. LWT Food Sci Technol. 2015;61(1):138–44.
34. Toyoizumi T, Kosugi T, Toyama Y, Nakajima T. Effects of high-temperature cooking on the gamma-aminobutyric acid content and antioxidant capacity of germinated brown rice (*Oryza sativa* L.). CyTA J Food. 2021;19(1):360–9.

O - 397

Salicylic Acid Alleviates Chilling Injury and Enhances Antioxidant Capacity in 'Nam Dok Mai' Mango during Cold Storage

Rungdarunlak Charatsaengphaibun[1], Satoru Kondo[1,2], Ampa Kongsuwan[3], Phunsiri Suthiluk[1,3], Sutthiwal Setha[1,3]*

[1]*School of Agro-Industry, Mae Fah Luang University, Chiang Rai, Thailand*
[2]*Graduate School of Horticulture, Chiba University, Matsudo, Japan*
[3]*Research Group of Postharvest Technology, Mae Fah Luang University, Chiang Rai, Thailand*

**Corresponding author E-mail: sutthiwal.set@mfu.ac.th*

Abstract: Chilling injury (CI) is a major postharvest problem during prolonged low-temperature storage of mango fruit, resulting in surface pitting, uneven ripening, and deterioration of market quality. This study evaluated the effectiveness of salicylic acid (SA) treatment in reducing CI and preserving fruit quality and antioxidant capacity in 'Nam Dok Mai' mango. Mature fruits were immersed in a 2 mM SA solution for 10 minutes, with untreated fruits serving as controls, and stored at 10 °C for 28 days. The results showed that SA treatment significantly alleviated CI symptoms, reducing the CI index by approximately 40% compared to the control. Although SA-treated fruits exhibited slightly lower physiological weight loss, no significant differences were observed between treatments. SA application resulted in substantially higher total phenolic content (TPC) in both peel and pulp, increasing by about 20% and 54%, respectively, indicating a potent systemic signaling effect and high metabolic sensitivity of the pulp tissue to exogenous SA. SA-treated fruits further maintained significantly greater firmness and retained higher L* and hue angle values, while exhibiting lower total soluble solids (TSS) and higher titratable acidity (TA). This delay in biochemical changes indicates that SA treatment effectively retards the ripening process. Antioxidant activities assessed by DPPH and FRAP were consistently higher in the SA-treated group. A correlation analysis revealed a strong negative correlation ($r = -0.87$) between the CI index and DPPH activity in the pulp, alongside a positive correlation with TPC ($r = 0.53$), suggesting that while the fruit accumulates phenolics in response to stress, the depletion of free radical scavenging capacity is closely linked to the severity of chilling injury. Overall, the results demonstrate that postharvest SA treatment effectively reduces chilling-induced physiological damage, maintains tissue integrity, and enhances the antioxidant defense system of mangoes, consequently helping maintain fruit quality and marketability during cold storage.

Keywords: Antioxidant activity; Chilling injury; Mango; Salicylic acid

1. Introduction

Mango (*Mangifera indica L.*) is a widely cultivated tropical fruit of significant economic importance, valued globally for its consumption as fresh fruit and its export potential. Among commercial cultivars, 'Nam Dok Mai' is a premium Thai variety highly sought after in international markets due to its distinctive aroma, sweetness, and superior sensory qualities. However, postharvest management remains a critical challenge, as the fruit is climacteric and highly perishable, susceptible to rapid quality deterioration during long-distance transportation **(1).**

Low-temperature storage is the standard method employed to retard ripening, suppress respiration rate, and extend shelf life. As a climacteric fruit, mangoes undergo rapid ripening and senescence after harvest. While low-temperature storage is widely used to suppress the climacteric

respiratory peak, this very action often triggers a physiological disorder known as chilling injury (CI). This trade-off between ripening suppression and CI development creates a significant challenge in postharvest management, as the resulting symptoms such as surface pitting, peel discoloration, and pulp breakdown severely compromise fruit quality **(2)**. Therefore, necessitates the application of signaling molecules like Salicylic Acid (SA) to mitigate these adverse effects.

The development of CI involves complex cellular and metabolic dysfunctions, primarily driven by the cold stress-induced overproduction and accumulation of reactive oxygen species (ROS) **(3)**. Under chilling stress, this excessive ROS accumulation disrupts cellular homeostasis and leads to severe oxidative damage, which overwhelms the fruit's antioxidant defense system and accelerates senescence **(4).** Although fruits possess endogenous antioxidant defense mechanisms to scavenge these free radicals, they are often insufficient to counteract prolonged cold stress. Consequently, there is growing interest in utilizing natural elicitors to enhance the natural antioxidant capacity including elevating total phenolic compounds and radical scavenging activities to mitigate oxidative damage and improve chilling tolerance **(5).**

Salicylic acid (SA), a naturally occurring phenolic compound, acts as a pivotal signaling molecule regulating plant defense systems and stress responses. Extensive research indicates that exogenous SA application can mitigate CI by enhancing antioxidant system activity, reducing ROS accumulation, and maintaining membrane stability. Beneficial effects of SA have been demonstrated in various horticultural crops, including pomegranate, peach, banana, and papaya, where it successfully reduced CI severity and preserved total phenolic content and antioxidant capacity **(5).**

Despite these findings, while previous studies have explored SA applications in ‘Nam Dok Mai’ mangoes **(6),** the integrated relationship between the CI index and specific antioxidant capacities during extended cold storage remains not fully elucidated. Furthermore, the differential biochemical responses between the peel and pulp tissues under chilling stress have not been thoroughly compared. Therefore, to address this specific research gap, the present study aims to investigate the integrated physiological and biochemical responses of ‘Nam Dok Mai’ mango to SA treatment during cold storage, with a particular focus on the antioxidant defense mechanisms in both peel and pulp tissues.

Accordingly, this study aimed to evaluate the efficacy of postharvest SA treatment in alleviating chilling injury and maintaining the quality of ‘Nam Dok Mai’ mango during low-temperature storage. A wide range of physiological and biochemical parameters, including CI index, firmness, color, ripening index (TSS/TA ratio), total phenolic content, and antioxidant activities (by DPPH and FRAP assays), were monitored to elucidate the mechanisms of SA-induced chilling tolerance. The findings provide novel insights that contribute to the development of safe, cost-effective, and efficient postharvest strategies to extend the shelf life and enhance the marketability of mango fruit.

2. Materials and Methods

2.1 Plant materials

Mango fruit (Mangifera indica L. cv. Nam Dok Mai) at commercial maturity stage (110 days after full bloom) was obtained from a commercial orchard in Phrao district, Chiang Mai province, Thailand (19°21′57″N 99°12′8″E), and transported to the Postharvest Technology Research Laboratory at Mae Fah Luang University. Fruits were initially selected for uniformity in size, shape, color, and absence of visual defects. To confirm the initial uniformity before treatment, baseline quality parameters were recorded: the initial average fruit weight was approximately 350 g, initial peel color values were L = 77.45 and hue angle = 81.55, and the initial TSS was 14.14 °Brix. To ensure a standardized commercial maturity, fruits were subjected to specific gravity separation in a 2% NaCl solution, and the 'sinkers' (specific gravity ≥ 1.02) were selected for the

experiment **(7)**, followed by washing with tap water. To control postharvest decay, the fruits were dipped in 200 mg L^{-1}sodium hypochlorite solution for 1 min and air-dried at ambient temperature.

2.2 Postharvest treatments

The prepared fruits were randomly divided into two groups and immersed in either distilled water (serving as the control) or a 2 mM SA solution (pH 3.1, adjusted with 0.1 M NaOH) for 10 min. The concentration of 2 mM SA was selected based on established literature demonstrating its efficacy in alleviating chilling injury in mango fruit **(8),** as well as our recent findings which validated its practical application in preserving the quality of 'Nam Dok Mai' mangoes **(9)**. Following immersion, the fruits were air-dried at room temperature for approximately 1 hour, packed in corrugated cardboard boxes, and stored at 10±1 °C with 85±5% relative humidity (RH). For the evaluation, the experimental fruits were divided into two parallel sets: a non-destructive set and a destructive set. For the non-destructive parameters (such as weight loss and CI index), a specific set of three replicates (consisting of two fruits each per treatment) was continuously monitored throughout the entire storage period. For the destructive physico-chemical and biochemical analyses, a separate set of three replicates (two fruits each per treatment) was destructively sampled at each specific time point (0, 7, 14, 21, and 28 days), after which the sampled tissues were immediately frozen in liquid nitrogen and stored at −20 °C.

2.3 Determination of quality attributes

2.3.1 Chilling injury (CI) and weight loss

CI severity was evaluated visually using a 6-point scale ranging from 0 to 5. To reduce subjectivity and ensure reproducibility, the visual assessment was based on precise observational criteria, including the approximate percentage of the affected surface area, the extent of peel browning, and the severity of surface pitting. The scores were specifically defined as follows: 0 (No injury) = 0% of the surface area affected; normal peel color with complete absence of pitting or browning, 1 (Slight injury) = 1–10% of the surface area affected; characterized by faint, localized discoloration and superficial, very shallow pitting, 2 (Mild injury) = 11–25% of the surface area affected; distinct but mild brown spots with slightly deeper pitting scattered on the peel, 3 (Moderate injury) = 26–50% of the surface area affected; exhibiting moderate dark browning, distinct surface pitting, and early signs of coalescence among the pitted spots, 4 (Severe injury) = 51–75% of the surface area affected; characterized by severe dark browning, extensive deep pitting, and clear coalescence of lesions, severely impacting visual quality, 5 (Extremely severe injury) = >75% of the surface area affected; deep, widespread pitting with very dark brown to black discoloration over most of the fruit surface, resulting in a complete loss of marketability. The CI index was calculated according to **(6).** Photographs documenting the CI symptoms were captured using a camera at a fixed distance inside a controlled LED light box (5,500K daylight) to ensure consistent illumination and comparability

$$\text{CI index} = \frac{\sum (\text{CI scale} \times \text{number of fruit at that scale})}{(\text{Total number of fruits} \times \text{Highest scale})}$$

Weight loss was determined by monitoring changes in individual fruit weights and expressed as a percentage of the initial weight **(10)**.

Figure 1. Visual rating scale used for evaluating chilling injury (CI) severity in the pulp of 'Nam Dok Mai' mango fruit, ranging from score 0 (no injury) to score 5 (severe browning)

2.3.2 Determination of fruit firmness and color

Fruit firmness was measured using a texture analyzer (Model: GY-4) equipped with a 5-mm diameter stainless steel probe. The measurements were taken at two opposite sides of the fruit along the equatorial zone after peeling. The maximum force required for penetration was recorded and expressed in Newtons (N).

Peel and pulp color were measured using a colorimeter (Minolta CR-400). The color values were expressed as L^* (lightness) and the hue angle (h°). The hue angle was calculated as h °= arctan (b^*/a^*), where a* represents redness-greenness and b^* represents yellowness-blueness **(11)**.

2.3.3 Determination of total soluble solids (TSS) and titratable acidity (TA)

Total soluble solids (TSS) and titratable acidity (TA) were determined using a digital Brix-Acidity meter (Model ATAGO PAL-BX/Acid F5 Master Kit). The results were expressed as °Brix for TSS and as the percentage of citric acid equivalent for TA. The ripening index was calculated as the TSS/TA ratio.

2.3.4 Extract preparation and total phenolic content (TPC)

TPC was determined using the Folin–Ciocalteu method as described by **(12)**. with minor modifications. Fruit tissue (2 g of peel or pulp) was homogenized with 20 mL of 80% methanol. The homogenate was centrifuged at 10,000 × *g* for 15 min at 4°C, and the supernatant was collected for analysis. An aliquot of the extract (0.5 mL) was mixed with 10% Folin–Ciocalteu reagent and 7.5% Sodium Carbonate After incubation in the dark for 90 min, the absorbance was measured at 765 nm using a spectrophotometer (Multiskan GO, Thermo Scientific, Vantaa, Finland). The results were expressed as mg of gallic acid equivalents (GAE) per kg of fresh weight (FW).

2.3.5 Antioxidant capacities

The DPPH radical scavenging activity was assayed according to the method of **(13)**. with minor modifications. The extract was mixed with a methanolic solution of DPPH (2,2-diphenyl-1-picrylhydrazyl), and the solution was incubated in the dark for 30 min at room temperature. The absorbance was assayed at 517 nm with a spectrophotometer (Multiskan GO, Finland). The DPPH activity was expressed as µmol Trolox equivalents (TE) per kg FW.

FRAP assay was performed according to **(14)**. with minor modifications. The FRAP reagent consisted of acetate buffer (pH 3.6), TPTZ solution, and $FeCl_3$ solution. The mixture was incubated for 30 min at 37 °C. The absorbance was measured at 595 nm using a spectrophotometer (Multiskan GO, Finland). The results were expressed as µmol FeSO4 per kg FW.

2.4 Statistical analysis

Statistical analyses were performed using IBM SPSS Statistics for Windows, Version 22.0 (IBM Corp., Armonk, NY, USA). All data are presented as mean ± standard error (S.E.) of three replications. To evaluate the effect of the treatments, an independent samples *t*-test was used to compare the means between the control and SA-treated groups at each storage interval. Differences were considered statistically significant at $p < 0.05$.

3. Results & Discussion

3.1 Effect of SA on chilling injury (CI) and visual appearance

The effect of SA treatment on chilling injury (CI) symptoms in 'Nam Dok Mai' mango fruit stored at 10°C is illustrated in **Figure 2**. CI symptoms, visibly manifested as internal browning and discoloration of the pulp, were first observed in the control group on day 7, reaching a CI index of 1.67. In contrast, SA-treated fruits exhibited negligible symptoms (CI index < 0.2) at this stage. Throughout the storage period, the severity of chilling injury in control fruits increased rapidly. By day 28, control fruits showed severe damage with a maximum CI index of 4.67, characterized by extensive darkening of the flesh. However, the application of 2 mM SA significantly delayed and suppressed the development of these symptoms. Although CI indices increased in SA-treated fruits over time, they remained significantly lower than the control throughout storage, reaching a final index of 3.33 on day 28. Visually, the flesh of SA-treated fruits retained better color and showed less browning compared to the damaged appearance of control fruits.

These results demonstrated that dipping 'Nam Dok Mai' mangoes in 2 mM SA effectively alleviated chilling injury symptoms during cold storage. The reduction in CI symptoms, such as peel browning and internal flesh browning, suggests that SA treatment enhances the fruit's tolerance to low-temperature stress. This protective effect is likely attributed to the ability of SA to activate the antioxidant defense system and maintain membrane integrity, thereby preventing ion leakage and reducing oxidative damage **(6, 15)**. Similar reductions in CI severity following SA treatment have been reported in mango and other tropical fruits, indicating that the protective role of SA against chilling stress is a conserved response across species **(10, 16)**.

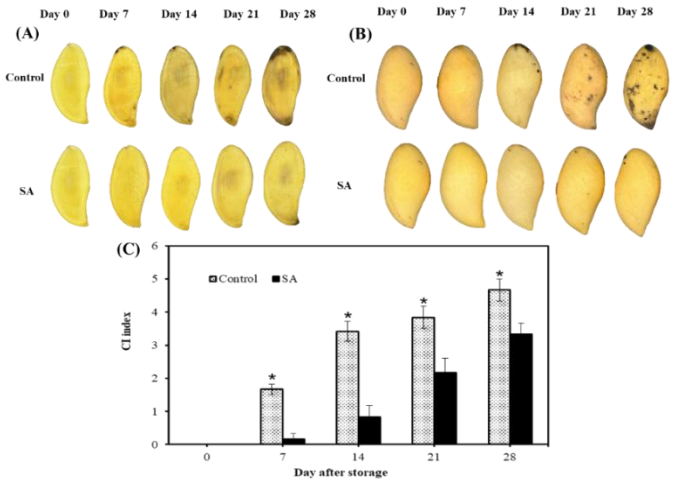

Figure 2. Chilling injury (CI) symptoms and CI index in 'Nam Dok Mai' mango fruit during storage at 10 °C for 28 days. (A) Internal CI symptoms (flesh browning) and (B) external CI symptoms (skin browning) in fruit treated with distilled water (Control) and 2 mM salicylic acid (SA). (C) Effects of SA treatment on CI index. Asterisks (*) indicate significant differences ($p \leq 0.05$) based on independent samples t-test. Data are means ± SE from three replicates.

3.2 Weight Loss, Firmness, and Color Changes

Physiological weight loss increased progressively in both treatment groups with prolonged storage **(Table 1).** Although SA-treated fruits generally showed slightly lower weight loss values compared to the control, no significant differences were observed between the treatments throughout the storage period. This suggests that the treatment had a minimal effect on water loss under these specific storage conditions. The lack of significant difference in weight loss may indicate that SA treatment at 2 mM did not substantially modify the physical barriers of the fruit, such as the cuticular wax structure or lenticel morphology **(17)**. Furthermore, the high relative humidity (RH) typically maintained during cold storage may have minimized the vapor pressure deficit, thereby masking any potential physiological influence of SA on the fruit's transpiration rate **(18)**. These findings suggest that the observed retention of firmness by SA was likely mediated through internal biochemical pathways rather than a significant reduction in water loss.

Regarding fruit texture, firmness decreased continuously over the storage period in all samples. Control fruits softened rapidly, with firmness values dropping from 58.05 N (day 0) to 6.17 N (day 28). The SA treatment significantly retarded the softening process, maintaining a firmness of 10.23 N on day 28, which was significantly higher than that of the control. Interestingly, while SA treatment effectively maintained fruit firmness, it did not significantly influence weight loss. This discrepancy suggests that in ‘Nam Dok Mai’ mangoes, SA acts predominantly through biochemical pathway regulation rather than physical barrier enhancement. The observed retention of firmness in SA-treated mangoes is consistent with the reported role of SA in inhibiting cell wall-degrading enzymes, such as polygalacturonase (PG) and pectin methylesterase (PME), as documented in various climacteric fruits **(3, 10, 15)**. Although the activities of these enzymes were not directly measured in the present study, the significant delay in softening suggests that SA may have suppressed the disassembly of cell wall polysaccharides, thereby preserving the middle lamella and maintaining the structural integrity of the fruit tissue.

Additionally, the suppression of ethylene production by SA likely contributed to the delayed disassembly of cell wall polymers. Notably, the retention of firmness in SA-treated fruits is closely associated with the reduced CI severity observed in this study, as chilling-induced membrane damage and cell wall disassembly are key contributors to textural deterioration **(19)**.

Table 1. Effect of salicylic acid (SA) treatment on physico-chemical quality attributes of 'Nam Dok Mai' mango fruit during storage at 10°C.

Day	Treatment	TSS (°Brix)	TA (%)	TSS/TA ratio	Firmness (N)	Weight loss (%)
0	Non treat	14.14±0.07	1.72±0.15	8.47±0.87	58.05±0.34	0±0
7	Control	15.82±0.28 a	1.25±0.05 a	13.85±0.59 a	55.77±0.41 b	7.47±0.87 a
	SA	13.50±0.87 b	1.64±0.2 a	11.09±0.54 b	58.37±0.03 a	4.05±1.92 a
14	Control	18.73±0.04 a	1.03±0.04 b	18.43±1.03 a	13.37±1.49 b	5.83±0.26 a
	SA	16.45±0.02 b	1.23±0.01 a	13.38±0.20 b	34.55±2.12 a	4.16±1.84 a
21	Control	20.08±0.11 a	0.93±0.01 b	21.61±0.33 a	14.12±0.31 b	7.58±2.10 a
	SA	17.70±0.04 b	1.20±0.05 a	14.86±0.86 b	23.13±1.82 a	5.94±0.97 a
28	Control	22.03±0.08 a	0.53±0.02 b	38.74±1.37 a	6.17±0.07 b	12.39±1.85 a
	SA	19.07±0.13 b	1.04±0.01 a	18.30±0.16 b	10.23±0.04 a	9.64±0.79 a

Note: Data are presented as mean ± standard error (S.E.) of three replications. Means followed by different letters within the same column for each storage interval are significantly different according to independent samples t-test ($p < 0.05$).

Color changes were assessed for both peel and pulp. The peel L* value, indicating lightness, decreased significantly in the control group from 77.45 to 47.46, reflecting severe browning. SA-treated fruits retained significantly higher peel L* values (61.49 at day 28) **(Table 2)**. A similar trend was observed in the pulp, where SA treatment maintained significantly higher pulp L* values (57.40) compared to the control (38.11) on day 28, indicating a reduction in internal browning **(Table 3)**. Additionally, the peel hue angle decreased in both groups. Typically, a hue angle around 120° represents green color, while a value descending towards 90° or lower indicates a shift to yellow **(11)**. In this study, the decrease in hue angle reflected the ripening progress. However, SA-treated fruits maintained significantly higher hue values compared to the control throughout the storage period, particularly at day 28 (81.40 vs 76.19). This suggests that while the control fruits had reached an advanced stage of yellowing (senescence), the SA treatment effectively delayed this color transition. The maintenance of higher L* values (in both peel and pulp) and hue angle in SA-treated fruits indicates a delay in senescence and enzymatic browning. SA effectively inhibited the degradation of chlorophyll and likely suppressed the activity of polyphenol oxidase (PPO), which is responsible for tissue browning **(6, 16)**.

Table 2. Effect of salicylic acid on peel color parameters of 'Nam Dok Mai' mango during cold storage.

Parameters	Treatments	Days after storage				
		0	7	14	21	28
L* values	Control	77.45±0.08	73.31±0.10 b	68.18±0.77 b	54.50±0.67 b	47.46±1.29 b
	SA		76.42±0.55 a	72.85±0.43 a	67.47±0.70 a	61.49±0.15 a
°Hue values	Control	81.55±0.35	78.83±0.23 b	75.88±0.54 b	73.96±0.08 b	71.77±0.3 b
	SA		80.04±0.02 a	79.10±0.26 a	77.64±0.16 a	78.87±0.09 a

Note: Data are presented as mean ± standard error (S.E.) of three replications. Means followed by different letters within the same column for each storage interval are significantly different according to independent samples t-test ($p < 0.05$).

Table 3. Effect of salicylic acid on pulp color parameters of 'Nam Dok Mai' mango during cold storage.

Parameters	Treatments	Days after storage				
		0	7	14	21	28
L* values	Control	76.27±0.11	67.07±0.69 b	59.45±1.48 b	42.51±1.12 b	38.11±0.97 b
	SA		73.71±0.26 a	72.53±0.23 a	68.40±0.92 a	57.40±0.92 a
°Hue values	Control	84.55±0.48	79.23±0.80 a	77.94±1.45 a	76.18±0.17 b	76.19±0.43 b
	SA		81.49±0.37 a	80.46±0.64 a	79.63±0.94 a	81.40±0.25 a

Note: Data are presented as mean ± standard error (S.E.) of three replications. Means followed by different letters within the same column for each storage interval are significantly different according to independent samples t-test ($p < 0.05$).

3.3 TSS, TA, and TSS/TA Ratio Changes

The changes in TSS, TA, and TSS/TA ratio are presented in **Table 1**. TSS content increased in all fruits during storage; however, the rate of increase was significantly slower in SA-treated fruits. At the end of storage, the TSS of control fruits was 22.03 °Brix, while that of SA-treated fruits was 19.07 °Brix. Conversely, TA values decreased during storage. The SA treatment effectively delayed the loss of acidity, retaining a TA of 1.04% on day 28 compared to 0.53% in the control. Consequently, the TSS/TA ratio, used as a ripening index, was significantly lower in the SA group (18.30) compared to the control (38.74) at the end of the experiment.

The slower increase in TSS and the higher retention of TA in SA-treated fruits confirm that salicylic acid effectively delays the ripening process **(2, 10)**. This delayed ripening behavior is particularly advantageous for cold-chain management. Although SA-treated fruits exhibited lower TSS and higher TA compared to the control, this profile signifies a preservation of freshness and a delay in senescence, rather than a reduction in quality. The maintained acidity contributes to a desirable balance of flavor and prevents the insipid taste often associated with over-ripe or chilling-injured fruit. Consequently, this treatment allows for extended storage while preserving the potential for normal flavor development upon subsequent ripening.

3.4 Total phenolic content (TPC) and antioxidant activity

The changes in TPC and antioxidant capacity, assessed by DPPH and FRAP assays, in the peel and pulp tissues are presented in **Figure 3** and **Figure 4**, respectively. In terms of TPC, the peel tissue **(Figure 3A)** generally exhibited an increase in phenolic content during storage, with the SA-treated fruit exhibiting significantly higher levels than the control group from day 7 onwards. A similar increasing pattern was observed in the pulp tissue **(Figure 4A)**, where SA treatment induced a significantly higher accumulation of phenolic compounds throughout the storage period (day 7 to 28) compared to the control. The enhanced retention of TPC in SA-treated fruits can be attributed to the role of SA as a signal molecule that activates the phenylpropanoid metabolic pathway, leading to the synthesis of secondary metabolites, including phenolics **(15)**. These compounds are crucial as they function as non-enzymatic antioxidants that neutralize reactive oxygen species (ROS), thereby mitigating oxidative stress **(15, 16)**. The induction of TPC by SA was more pronounced in the pulp (54% increase) than in the peel (20% increase) relative to their respective controls. This differential response suggests a potent systemic signaling effect, where the initial perception of SA at the fruit surface triggers a signal transduction cascade that deeply reaches the internal pulp tissue.The higher accumulation of TPC in the pulp may indicate a heightened metabolic sensitivity of 'Nam Dok Mai' flesh to exogenous SA, potentially resulting

from a more robust activation of enzymes like phenylalanine ammonia-lyase (PAL) in the pulp relative to the more structurally specialized peel **(16)**.

Regarding antioxidant capacity, SA treatment consistently maintained higher activity levels in both assays compared to the control. In the peel **(Figure 3B)**, SA-treated fruit showed significantly higher DPPH radical scavenging activity compared to the control from day 7 onwards, while in the pulp **(Figure 4B)**, although DPPH activity generally exhibited a declining trend indicative of senescence and stress progression, the SA-treated fruit maintained significantly higher scavenging capacity than the control at all sampled intervals. Similarly, the ferric reducing antioxidant power (FRAP) in the peel **(Figure 3C)** was significantly higher in SA-treated fruits, particularly on days 7, 21, and 28. In the pulp **(Figure 4C)**, FRAP activity tended to increase over time, yet SA treatment significantly further enhanced this activity compared to the control, especially on days 14, 21, and 28. In the pulp **(Figure 4C)**, FRAP activity tended to increase over time, yet SA treatment significantly further enhanced this activity compared to the control, especially on days 14, 21, and 28. The higher antioxidant activities observed in SA-treated mangoes correlate well with the elevated TPC levels, suggesting that phenolic compounds, acting as efficient hydrogen donors, directly contribute to the scavenging of ROS. By enhancing the non-enzymatic antioxidant system, SA treatment effectively limited ROS accumulation, thereby preventing lipid peroxidation, maintaining membrane integrity, and reducing the cellular damage associated with chilling injury **(15, 19)**

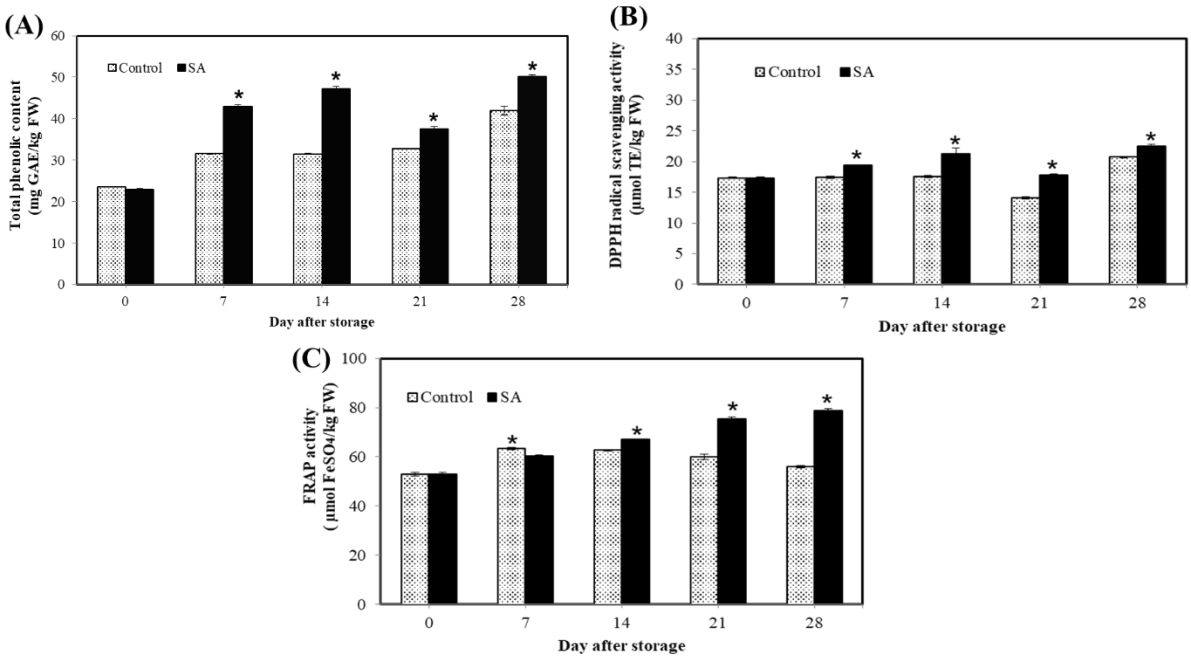

Figure 3. Total phenolic content and antioxidants in the **peel** of 'Nam Dok Mai' mango fruit treated with 2 mM salicylic acid (SA) and Control during storage at 10°C for 28 days: **(A)** TPC, **(B)** DPPH, and **(C)** FRAP. Asterisks (*) indicate significant differences ($p \leq 0.05$) based on independent samples t-test. Data are means ± SE from three replicates.

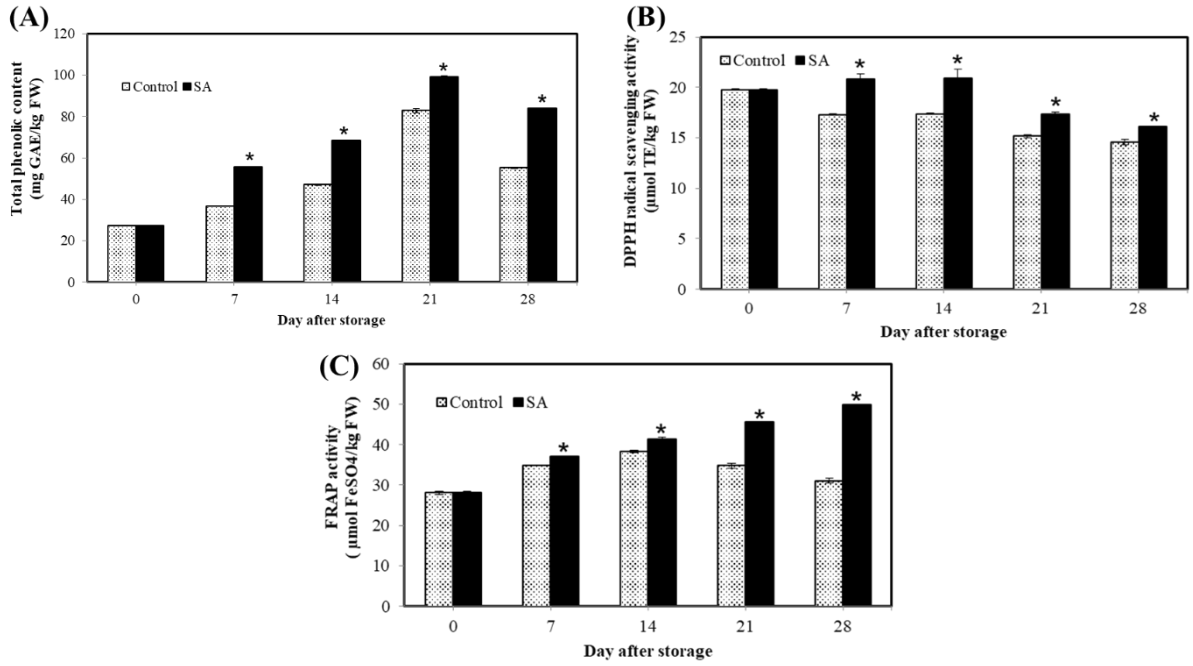

Figure 4. Total phenolic content and antioxidants in the **pulp** of 'Nam Dok Mai' mango fruit treated with 2 mM salicylic acid (SA) and Control during storage at 10°C for 28 days: **(A)** TPC, **(B)** DPPH, and **(C)** FRAP. Asterisks (*) indicate significant differences ($p \leq 0.05$) based on independent samples t-test. Data are means ± SE from three replicates.

3.5 Correlation Analysis

A Pearson correlation analysis was performed to investigate the relationships between the Chilling Injury (CI) index and the antioxidant parameters, specifically TPC, DPPH radical scavenging activity, and FRAP, in both the peel and pulp tissues of 'Nam Dok Mai' mango fruit. To ensure a comprehensive biological assessment, the correlation coefficients (r) were calculated using pooled data from all treatment groups across all sampling intervals (Day 0 to Day 28), as presented in **Table 4.** In the peel tissue, the statistical analysis revealed no significant correlations between the CI index and any of the measured antioxidant parameters. Specifically, the correlation coefficients (r) for TPC, DPPH, and FRAP were calculated as 0.270, 0.004, and 0.264, respectively, indicating that the progression of external chilling injury symptoms in the peel was not linearly associated with changes in these antioxidant levels during the storage period. This suggests that the development of external CI symptoms, such as surface pitting and browning, may be driven by mechanisms distinct from general antioxidant depletion. While the pulp shows a clear link between antioxidant capacity and damage, peel browning is likely more closely associated with localized enzymatic browning mediated by polyphenol oxidase (PPO) **(20)**. Chilling stress can trigger membrane leakage, allowing PPO to come into contact with its phenolic substrates, leading to rapid surface discoloration that does not necessarily correlate linearly with the overall radical scavenging activities measured by DPPH or FRAP **(21)**.

In contrast to the peel, the pulp tissue exhibited distinct and significant correlations between the development of chilling injury and specific antioxidant markers. A moderate but significant positive correlation was observed between the CI index and TPC ($r = 0.52$), suggesting that total phenolic compounds accumulated in the flesh as the severity of chilling injury increased. This accumulation is likely part of the fruit's physiological stress response to low temperatures, as

phenolic compounds are often synthesized to reinforce cellular structures or act as defense molecules under stress conditions **(15)**. Conversely, a strong and highly significant negative correlation was found between the CI index and DPPH radical scavenging activity (r = -0.86). This strong negative relationship implies a severe depletion of the pulp's antioxidant capacity to scavenge free radicals as chilling injury symptoms worsened. This finding highlights a state of oxidative stress where the consumption of antioxidants exceeded their regeneration, leading to membrane damage and cellular dysfunction characteristic of chilling injury **(15, 19)**. The stronger association between antioxidant depletion and CI in the pulp, compared to the peel, may be attributed to the different physiological roles and environmental exposure of these tissues. The pulp is a relatively more stable metabolic environment, where CI symptoms like internal browning result directly from systemic oxidative stress and the failure of the antioxidant defense system. Consequently, the decline in DPPH scavenging activity serves as a reliable biochemical indicator for internal damage. In contrast, the peel is the primary interface with the external environment and is subject to rapid localized triggers, such as surface dehydration and immediate enzymatic browning, which can initiate visible symptoms before a significant or linear decline in total antioxidant capacity is detected **(21)**. Meanwhile, the FRAP values in the pulp did not show a significant correlation with the CI index (r = 0.260), mirroring the lack of correlation observed in the peel for this specific parameter. These findings collectively suggest that while the fruit pulp attempts to respond to cold stress by accumulating phenolic compounds, the overall radical scavenging capacity is significantly compromised, which is a key factor in the development of chilling injury symptoms.

Table 4. Pearson correlation coefficients (r) between the Chilling Injury (CI) index and antioxidant parameters in the peel and pulp of 'Nam Dok Mai' mango fruit.

Parameters	Correlation coefficient (r)	
	Peel	Pulp
TPC	0.27	0.52*
DPPH	0.004	-0.87*
FRAP	0.25	0.25

Note: *The values represent Pearson correlation coefficients (r). Asterisks indicate statistical significance at * $p < 0.05$. Abbreviations: CI, chilling injury; TPC, total phenolic content; DPPH, DPPH radical scavenging activity; FRAP, ferric reducing antioxidant power.*

5. Conclusion

In conclusion, the postharvest application of 2 mM salicylic acid (SA) is an effective strategy for alleviating chilling injury (CI) in 'Nam Dok Mai' mangoes stored at 10 °C. The SA treatment significantly suppressed the visual development of CI symptoms and successfully retained fruit firmness, although it had a minimal impact on minimizing weight loss. The mitigation of CI was closely associated with the stimulation of the fruit's antioxidant defense system, as evidenced by the enhanced total phenolic content and DPPH radical scavenging activity, particularly within the pulp tissue. Overall, the results demonstrate that postharvest SA treatment effectively reduces chilling-induced physiological damage, maintains structural tissue integrity, and strengthens the overall antioxidant capacity, consequently helping maintain fruit quality during cold storage.

Acknowledgements

This research was financially supported by Mae Fah Luang University.

References

1. Mitra S. Postharvest physiology and storage of tropical and sub-tropical fruit CAB. TNT Nadia west Bengal India. 1997.
2. Nair S, Singh Z. Pre-storage ethrel dip reduces chilling injury, enhances respiration rate, ethylene production and improves fruit quality of 'Kensington'mango. J Food Agric Environ. 2003;1:93-7.
3. Huang T, Liu G, Zhu L, Liu J, Xiang Y, Xu X, et al. Mitigation of chilling injury in mango fruit by methyl jasmonate is associated with regulation of antioxidant capacity and energy homeostasis. Postharvest Biology and Technology. 2024;211:112801.
4. Sevillano L, Sanchez-Ballesta MT, Romojaro F, Flores FB. Physiological, hormonal and molecular mechanisms regulating chilling injury in horticultural species. Postharvest technologies applied to reduce its impact. Journal of the Science of Food and Agriculture. 2009;89(4):555-73.
5. Asghari M, Aghdam MS. Impact of salicylic acid on post-harvest physiology of horticultural crops. Trends in food science & technology. 2010;21(10):502-9.
6. Junmatong C, Faiyue B, Rotarayanont S, Uthaibutra J, Boonyakiat D, Saengnil K. Cold storage in salicylic acid increases enzymatic and non-enzymatic antioxidants of Nam Dok Mai No. 4 mango fruit. Sci Asia. 2015;41:12-21.
7. Kapse BM, Katrodia J, editors. Ripening behaviour of'Kesar'mangoes in relation to specific gravity. V International Mango Symposium 455; 1996.
8. Barman K, Asrey R. Salicylic acid pre-treatment alleviates chilling injury, preserves bioactive compounds and enhances shelf life of mango fruit during cold storage. J Sci Ind Res. 2014;73(11):713-8.
9. Ampa K, Naradisorn M, Suthiluk P, Kondo S, Wongsa P, Ketnawa S, et al. The impact of hot water and salicylic acid treatments on metabolomic changes and defense mechanisms against anthracnose caused by Colletotrichum gloeosporioides in mango fruit. Journal of Agriculture and Food Research. 2025:102586.
10. Srivastava MK, Dwivedi UN. Delayed ripening of banana fruit by salicylic acid. Plant science. 2000;158(1-2):87-96.
11. McGuire RG. Reporting of objective color measurements. 1992.
12. Vl S. Analysis of total phenols and other oxidation substrates and antioxidants by means of Folin-Ciocalteu reagent. Methods in Enzymology. 1999;299:152-78.
13. Brand-Williams W. Use of a free radical method to evaluate antioxidant activity. Food Sci Technol. 1999;28:1231-7.
14. Benzie IF, Strain JJ. The ferric reducing ability of plasma (FRAP) as a measure of "antioxidant power": the FRAP assay. Analytical biochemistry. 1996;239(1):70-6.
15. Ding ZS, Tian SP, Zheng XL, Zhou ZW, Xu Y. Responses of reactive oxygen metabolism and quality in mango fruit to exogenous oxalic acid or salicylic acid under chilling temperature stress. Physiologia Plantarum. 2007;130(1):112-21.
16. Lu X, Sun D, Li Y, Shi W, Sun G. Pre-and post-harvest salicylic acid treatments alleviate internal browning and maintain quality of winter pineapple fruit. Scientia Horticulturae. 2011;130(1):97-101.
17. Rymbai H, Srivastav M, Sharma R, Singh S. Lenticels on mango fruit: Origin, development, discoloration and prevention of their discoloration. Scientia horticulturae. 2012;135:164-70.
18. Paull R. Effect of temperature and relative humidity on fresh commodity quality. Postharvest biology and technology. 1999;15(3):263-77.

19. Jackman R, Yada R, Marangoni A, Parkin K, Stanley D. Chilling injury. A review of quality aspects. Journal of food quality. 1988;11(4):253-78.
20. Tangpao T, Phuangsaujai N, Kittiwachana S, George DR, Krutmuang P, Chuttong B, et al. Evaluation of markers associated with physiological and biochemical traits during storage of 'Nam Dok Mai Si Thong'mango fruits. Agriculture. 2022;12(9):1407.
21. Vega-Alvarez M, Salazar-Salas NY, López-Angulo G, Pineda-Hidalgo KV, López-López ME, Vega-García MO, et al. Metabolomic changes in mango fruit peel associated with chilling injury tolerance induced by quarantine hot water treatment. Postharvest Biology and Technology. 2020;169:111299.

P - 183

Determination of Bioactive Compounds and Antioxidant Activities from Bitter Melon (*Momordica charantia* L.) Fruit Extracts Using Ultrasound-Assisted Extraction

Daranporn Chumkaew[1,2] and Rajnibhas Sukeaw Samarkradhamrongthai[1,2,3]*

[1]*Department of Food Science and Technology, Faculty of Agro-Industry, Chiang Mai University, Thailand*
[2]*INterdisciplinary and Food product development for wellness Research unit (INFRU), Chiang Mai University, Thailand*
[3]*Division of Product Development Technology, Faculty of Agro-Industry, Chiang Mai University, Thailand*

**Corresponding author E-mail: rahjnibhas.s@cmu.ac.th*

Abstract: Bitter melon fruit (*Momordica charantia* L.) contains phenolic and flavonoid compounds with strong antioxidant properties. Efficient extraction of these bioactives is essential, and ultrasound-assisted extraction (UAE) is a promising green alternative to conventional maceration. In this study, dried bitter melon fruit was extracted using UAE under a 3^2 factorial design by varying amplitude (20, 40, and 60%) and extraction time (10, 20, and 30 min) at a constant power of 500 W, with maceration in 75% ethanol used as a control. The results showed that extraction performance depended on the response variable. The highest total phenolic content was 15.239 ± 1.030 mg GAE/g extract and the lowest DPPH IC_{50} value was 0.194 ± 0.015 mg/mL, both obtained at 20% amplitude for 10 min. The highest FRAP value was 17.838 ± 0.984 mg TE/g extract and the lowest ABTS IC_{50} value was 0.303 ± 0.011 mg/mL, both observed at 60% amplitude for 20 min. Notably, the condition of 60% amplitude for 30 min yielded the highest total flavonoid content of 112.997 ± 1.110 mg QE/g extract and showed relatively high FRAP values, along with moderate TPC and ABTS responses, suggesting balanced extraction performance. Correlation analysis indicated positive associations of phenolic and flavonoid contents with FRAP, whereas DPPH IC_{50} showed a negative relationship with phenolic compounds. PCA explained 69.07% of the total variance, confirming that extraction conditions influenced phytochemical composition and antioxidant activities. Compared with maceration, UAE improved extraction yield and bioactive properties, highlighting its potential for functional food and nutraceutical applications.

Keywords: Bitter melon fruit; Ultrasound-assisted extraction (UAE); Bioactive compounds; Antioxidant activities

1. Introduction

Momordica charantia L., commonly known as bitter melon, is a medicinal and edible plant belonging to the Cucurbitaceae family and is widely cultivated and consumed in many Asian countries, including Thailand. Bitter melon has long been utilized in traditional medicine for the management of diabetes and inflammatory-related disorders. Recent scientific studies have confirmed that bitter melon is a rich source of bioactive compounds, including phenolic compounds, flavonoids, saponins, cucurbitane-type triterpenoids, and bioactive peptides, which contribute to its antioxidant, anti-inflammatory, and antidiabetic activities [1,2,3].

Oxidative stress and chronic inflammation are closely associated with the progression of non-communicable diseases such as diabetes mellitus and cardiovascular diseases. Phenolic compounds and triterpenoids found in bitter melon have been reported to effectively scavenge free

radicals, inhibit inflammatory mediators, and regulate glucose metabolism through multiple biochemical pathways, including the inhibition of α-amylase and α-glucosidase enzymes [4,5]. However, the efficiency of recovering these bioactive compounds largely depends on the extraction method employed.

Conventional extraction techniques such as maceration, Soxhlet extraction, and reflux extraction are widely used for plant materials due to their simplicity; however, they present several limitations, including long extraction times, high solvent consumption, low extraction efficiency, and possible degradation of thermolabile compounds during prolonged heat exposure [6]. In addition, these conventional approaches often yield lower amounts of phenolic compounds and antioxidants, which makes them less suitable for obtaining bioactive-rich extracts for functional food and nutraceutical applications [7]. To address these drawbacks, ultrasound-assisted extraction (UAE) has emerged as an innovative and efficient alternative. UAE is based on acoustic cavitation, where the formation and collapse of microbubbles generated by ultrasonic waves disrupt plant cell walls, enhance solvent penetration, and improve mass transfer [8], thereby reducing extraction time and solvent use while increasing the yield and bioactivity of extracted compounds [9]. Accordingly, several studies have reported that UAE enhances the extraction efficiency of phenolic compounds and flavonoids and improves antioxidant activity from bitter melon and other medicinal plants compared with conventional extraction methods [10,11]. Moreover, UAE is considered a green extraction technology because of its lower energy requirements and reduced environmental impact, aligning with the principles of sustainable food processing.

Therefore, this study aimed to compare the extraction efficiency and bioactive compound content of bitter melon extracts obtained by maceration and ultrasound-assisted extraction, which contribute to high bioactive activity and the development of functional ingredients for health-promoting food products.

2. Materials and Methods

2.1 Plant material and chemicals

The fruits of *M. charantia* were obtained from MAKRO (CP Axtra Public Company Limited, Chiang Mai, Thailand). Ethanol (>95% v/v), Methanol, Hydrochloric acid 37%, Acetate buffer, Sodium nitrite, Aluminium chloride, Potassium persulfate Sodium hydroxide and Sodium Carbonate were purchased from UNION SCIENCE.CO.,Ltd. DPPH, ABTS, FRAP reagents (TPTZ, $FeCl_3$), Folin–Ciocalteu reagent, Trolox, Quercetin, Gallic acid, were obtained from Sigma Aldrich (St. Louis, MO, USA). All chemicals and reagents were of analytical grade.

2.2 Preparation of bitter melon extracts

Fresh bitter melon fruits were washed thoroughly with distilled water to remove adhering dirt and debris, and the seeds removed, then the edible portion was sliced into small pieces. The prepared samples were dried in a hot-air oven at 70 °C for 36 h, then ground and sieved through a 0.5 mm mesh sieve to obtain a uniform powder. The powdered sample was extracted using 75% (v/v) ethanol at a solid-to-solvent ratio of 1:10 (w/v). Maceration for 24 h under ambient conditions was performed as the control. For ultrasound-assisted extraction (UAE), an ultrasonic generator with a maximum power of 500 W was used and the experiment was arranged as a 3^2 factorial design to varying extraction amplitude (20%, 40%, and 60%) and extraction time (10, 20, and 30 min). After extraction, the mixtures were vacuum-filtered through Whatman No. 4 filter paper, and the filtrates were concentrated using a rotary evaporator under reduced pressure at 40 °C to obtain viscous crude extracts. The concentrates were subsequently freeze-dried, and the dried extracts were stored at −20 °C in light-protected containers until further analysis. For preparation of the extract stock solution, 1.0 g of the dried extract was accurately weighed and dissolved in 10 mL of 80% methanol (w/v) to obtain a stock solution; working solutions for antioxidant assays were prepared by serial dilution to give final test concentrations ranging from

0.30 to 0.004 mg/mL prior to analysis. The yield was calculated as a percentage for further analysis using the following Equation (1) :

$$\text{Yield (\%)} = \frac{Weight\ of\ extract\ (g)}{Weight\ of\ dried\ sample\ (g)} \times 100 \quad \text{(Eq.1)}$$

2.3 DPPH radical scavenging activity

The free radical scavenging activity of bitter melon extracts was determined using the DPPH assay according to Haideri *et al.* (2024), with slight modifications. A DPPH stock solution was prepared in methanol. In a 96-well microtiter plate, 180 µL of the DPPH solution was mixed with 20 µL of bitter melon extract. The reaction mixture was incubated in the dark for 30 min, after which the absorbance was measured at 517 nm using a Spark® microplate reader (Tecan, Männedorf, Switzerland). The radical scavenging activity was expressed as the 50% inhibitory concentration (IC_{50}), calculated from the relationship between percentage inhibition and sample concentration. The DPPH free radical scavenging activity was calculated as a percentage using the following Equation (2):

$$\%\ \text{scavenging activity} = \left[\frac{A_0 - A_1}{A_0}\right] \times 100\% \quad \text{(Eq. 2)}$$

where A_0 = absorbance of control and A_1 = absorbance of the extract with DPPH

2.4 ABTS radical scavenging activity

The antioxidant activity of bitter melon extracts was determined using the ABTS decolorization assay following Haideri *et al.* [12]. The ABTS radical cation solution was prepared by mixing 7 mM 2,2′-azino-bis (3-ethylbenzthiazoline-6-sulphonic acid) (ABTS) with 2.45 mM potassium persulfate ($K_2S_2O_8$) at a 1:1 (v/v) ratio. The mixture was incubated in the dark at room temperature for 12 h to generate the $ABTS^{\bullet+}$ radical. After incubation, the solution was diluted with 80% ethanol to obtain the working ABTS solution at the desired concentration. For the assay, 20 µL of bitter melon extract at various concentrations was added to a 96-well microtiter plate. A control was prepared in the same manner without the extract. The reaction mixtures were incubated in the dark for 30 min, and the absorbance was measured at 734 nm using a Spark® microplate reader (Tecan, Männedorf, Switzerland). The radical scavenging activity was expressed as the 50% inhibitory concentration (IC_{50}), calculated from the relationship between percentage inhibition and sample concentration. The inhibition percentage was calculated following Equation (3):

$$\text{ABTS radical scavenging activity (\%)} = \left[\frac{A_0 - A_1}{A_0}\right] \times 100\% \quad \text{(Eq. 3)}$$

where A_0 = absorbance of control and A_1 = absorbance of ABTS•+ with sample extract.

2.5 Ferric reducing antioxidant power (FRAP)

The ferric-reducing antioxidant power (FRAP) of the bitter melon extract was evaluated using a modified colorimetric method adapted from Haideri *et al.* [12]. The FRAP working reagent was freshly prepared by mixing 2.5 mL of 10 mM TPTZ (2,4,6-tripyridyl-s-triazine) dissolved in 40 mM HCl, 2.5 mL of 20 mM $FeCl_3$, and 25 mL of 300 mM acetate buffer (pH 3.6). The extract was diluted with 80% methanol, and 20 µL of the diluted sample was combined with 180 µL of FRAP reagent in a 96-well microtiter plate. After incubation in the dark for 30 min, absorbance was recorded at 593 nm using a Spark® microplate reader (Tecan, Männedorf, Switzerland).

FRAP activity was quantified against a Trolox standard curve (0–0.2 mg/mL) and reported as mg Trolox equivalent (TE) per g of extract.

2.6 Total phenolic content

Total phenolic content (TPC) was determined using a modified Folin–Ciocalteu colorimetric method from Jeytawan *et al*. [13], with slight modifications. Gallic acid prepared in 80% methanol was used as the reference standard. Briefly, 20 µL of bitter melon extract was mixed with 100 µL of Folin–Ciocalteu reagent previously diluted 10-fold with distilled water in a 96-well microplate. Then, 80 µL of 7% (w/v) sodium carbonate (Na_2CO_3) were added and the mixture was gently mixed; the wells were checked for turbidity prior to measurement. The absorbance was recorded at 760 nm using a Spark® microplate reader (Tecan, Männedorf, Switzerland). TPC was calculated from a gallic acid calibration curve (0–0.5 mg/mL) and expressed as mg gallic acid equivalents per g of extract (mg GAE/g extract).

2.7 Total flavonoid content

Total flavonoid content (TFC) was determined using the aluminum chloride colorimetric method from Jeytawan *et al.* [13], with slight modifications, using quercetin as the reference standard. Briefly, 120 µL of sample, blank, or quercetin standard solutions (0–0.2 mg/mL) was pipetted into a 96-well microplate, followed by 6 µL of 7% sodium nitrite ($NaNO_2$) solution; the mixture was incubated at room temperature for 5 min. Next, 12 µL of 10% aluminum chloride ($AlCl_3$) solution was added, mixed thoroughly, and kept at room temperature for another 6 min. Finally, 40 µL of 1 M sodium hydroxide (NaOH) and 22 µL of distilled water were added and incubated at room temperature for 5 min. Absorbance was measured at 510 nm against a water blank using a Spark® microplate reader (Tecan, Männedorf, Switzerland), and TFC was calculated from the quercetin calibration curve and expressed as mg quercetin equivalents per g of extract (mg QE/g extract).

2.8 Statistical analysis

The data were analyzed using a one-way analysis of variance (ANOVA), followed by Duncan's multiple range test to compare the mean values, using SPSS version 23. All the results are expressed as mean ± standard deviation. Principal component analysis was also conducted to evaluate the relationships between the phytochemical parameters (total phenolic contents and total flavonoid contents) and antioxidant activities (DPPH, ABTS, and FRAP).

3. Results & Discussion

3.1 Effect of extraction method on yield recovery of bitter melon (*Momordica charantia* L.) extracts

The extraction yield of bitter melon (*Momordica charantia* L.) fruit was significantly affected by the extraction method and ultrasound-assisted extraction (UAE) conditions, including amplitude and extraction time, as shown in Table 1 ($p < 0.001$). Under UAE, the yield recovery ranged from 24.506 ± 0.290% to 30.527 ± 0.261%, demonstrating that extraction efficiency varied depending on processing parameters. The highest yield, 30.527 ± 0.261%, was achieved at 60% amplitude for 30 min, followed by 29.513 ± 0.280% at 40% amplitude for 20 min and 28.915 ± 0.177% at 60% amplitude for 10 min. In contrast, the lowest yield was observed at 20% amplitude for 20 min, with a value of 24.506 ± 0.290%. Overall, increasing amplitude and extraction time tended to enhance yield recovery, likely due to more intense cavitation effects that promote plant cell disruption and improve mass transfer. When compared with the conventional maceration method, which provided a yield of 24.427 ± 0.261%, most UAE conditions resulted in higher extraction yields. This finding confirms that UAE improves extraction efficiency over traditional techniques. The enhanced performance of UAE can be attributed to acoustic cavitation, which

facilitates solvent penetration and accelerates the release of intracellular compounds. These results are consistent with previous studies reporting that UAE enhances extraction yield and bioactive compound recovery from plant materials, including bitter melon and other medicinal plants [8–10]. For example, ultrasound has been shown to improve the extraction of key phytochemicals such as charantin by optimizing amplitude and extraction time, leading to higher recovery efficiency [10]. Therefore, UAE represents an effective and promising approach for improving extraction yield and supporting the development of bioactive-rich extracts for functional food applications.

Table 1 Yield recovery percentage of bitter melon (*Momordica charantia* L.) extracts obtained from different extraction methods

Amplitude (%)	Time of extraction (Minute)	%Yield recovery
20	10	26.752 ± 0.405^{de}
	20	24.506 ± 0.290^{f}
	30	26.421 ± 0.270^{e}
40	10	26.020 ± 0.172^{e}
	20	29.513 ± 0.280^{b}
	30	27.248 ± 0.232^{cd}
60	10	28.915 ± 0.177^{b}
	20	27.856 ± 0.222^{c}
	30	30.527 ± 0.261^{a}
Maceration method		24.427 ± 0.261^{f}
***p*-value**		
Main effect (Amplitude)		<0.001
Main effect (Time)		<0.001
Interaction (Amplitude*Time)		<0.001

Note : Each values are expressed as mean ± SD (*n = 3*). Different superscript letters within the same column indicate significant differences ($p < 0.05$).
**The significant of main effect and interaction towards the responses

3.2 Antioxidant activities and phytochemical contents under different ultrasound-assisted extraction conditions

The effects of ultrasound-assisted extraction (UAE) conditions (amplitude and extraction time) on antioxidant activities and phytochemical contents of bitter melon extracts are summarized in Table 2. Overall, the responses differed across conditions, and a significant amplitude × time interaction was observed for all parameters ($p < 0.001$). The most suitable condition varied by indicator. The lowest DPPH IC_{50} and the highest TPC were obtained at 20% amplitude for 10 min (0.194 mg/mL; 15.239 mg GAE/g extract), suggesting that mild, short sonication favored phenolic recovery related to DPPH response, while prolonged treatment at 20% reduced FRAP and TPC. In contrast, 60% amplitude for 20 min produced the best ABTS IC_{50} and the highest FRAP (0.303 mg/mL and 17.838 mg TE/g extract, respectively), implying that stronger cavitation enhanced the extraction of compounds contributing to electron-transfer antioxidant capacity. TFC reached its maximum at 60% amplitude for 30 min (112.997 mg QE/g extract), indicating that higher amplitude with longer time improved flavonoid release. These results confirm that UAE parameter selection should be based on the targeted functional outcome at 20% amplitude for 10 min for maximizing TPC and DPPH, at 60% amplitude for 20 min for maximizing FRAP and ABTS, and at 60% amplitude for 30 min for maximizing TFC.

These response-dependent optima indicate that UAE selectively enriches different groups of antioxidant-related compounds depending on sonication intensity and extraction duration. This observation is consistent with metabolomics evidence demonstrating that bitter melon extracts contain a diverse range of antioxidant-associated metabolites [3]. The pronounced sensitivity of extraction outcomes to processing parameters also agrees with previous reports showing that solvent systems and extraction severity markedly affect the recovery of bioactive compounds and antioxidant activity in bitter melon [14,15]. Beyond phenolics and flavonoids, bitter melon is also rich in other antioxidant contributors, including polysaccharides [5], which help explain why the optimal extraction conditions differ among antioxidant assays.

Table 2 Antioxidant activities (DPPH, ABTS, FRAP), total phenolic content (TPC), and total flavonoid content (TFC) of bitter melon (*Momordica charantia* L.) extracts under different ultrasonic extraction conditions

Amplitude (%)	Time of extraction (Minute)	DPPH (IC_{50}, mg/ml)	ABTS (IC_{50}, mg/ml)	FRAP (mg TE/g extract)	TPC (mg GAE/g extract)	TFC (mg QE/g extract)
20	10	0.194 ± 0.015^{c}	0.479 ± 0.030^{cd}	16.361 ± 2.267^{a}	15.239 ± 1.030^{a}	104.409 ± 2.694^{b}
	20	0.401 ± 0.048^{a}	0.410 ± 0.018^{e}	7.278 ± 0.611^{c}	11.054 ± 0.651^{bc}	81.782 ± 3.638^{d}
	30	0.436 ± 0.010^{a}	0.531 ± 0.031^{bc}	5.250 ± 0.615^{de}	9.618 ± 0.613^{de}	106.913 ± 6.014^{b}
40	10	0.410 ± 0.032^{a}	0.488 ± 0.015^{c}	3.604 ± 0.308^{e}	6.963 ± 0.254^{g}	62.076 ± 2.308^{f}
	20	0.308 ± 0.011^{b}	0.427 ± 0.064^{de}	6.708 ± 1.337^{cd}	8.066 ± 0.231^{fg}	98.668 ± 1.817^{c}
	30	0.441 ± 0.074^{a}	0.590 ± 0.041^{a}	6.144 ± 0.124^{cd}	8.042 ± 0.503^{fg}	75.642 ± 0.839^{e}
60	10	0.360 ± 0.028^{ab}	0.567 ± 0.018^{ab}	15.983 ± 2.486^{a}	8.658 ± 0.755^{ef}	83.129 ± 2.281^{d}
	20	0.318 ± 0.005^{b}	0.303 ± 0.011^{f}	17.838 ± 0.984^{a}	10.072 ± 1.011^{cd}	82.965 ± 2.561^{d}
	30	0.441 ± 0.039^{a}	0.399 ± 0.014^{e}	16.462 ± 1.422^{a}	11.939 ± 1.037^{b}	112.997 ± 1.110^{a}
Maceration method		0.443 ± 0.098^{a}	0.402 ± 0.037^{e}	10.230 ± 0.849^{b}	7.756 ± 1.659^{fg}	83.110 ± 1.161^{d}
***p*-value**						
Main effect (Amplitude)		0.156	<0.001	<0.001	<0.001	<0.001
Main effect (Time)		<0.001	<0.001	<0.001	0.205	<0.001
Interaction (Amplitude*Time)		<0.001	<0.001	<0.001	<0.001	<0.001

Note : Each values are expressed as mean ± SD (*n = 3*). Different superscript letters within the same column indicate significant differences ($p < 0.05$). TE = Trolox equivalent; GAE = gallic acid equivalent; QE = quercetin equivalent.
**The significant of main effect and interaction towards the responses

3.3 Correlation coefficients between antioxidant activities and polyphenol content

Correlation analysis in Table 3 revealed that TPC and TFC were positively correlated with FRAP ($r = 0.583$ for FRAP–TPC; $r = 0.373$ for FRAP–TFC), suggesting that phenolic and flavonoid compounds contributed to the reducing power of the extracts. However, the relatively weak correlation between FRAP and TFC ($r = 0.373$, sig. = 0.144) indicates that flavonoids are not the predominant contributors to the reducing power as determined by the FRAP assay. This observation suggests that other constituents, particularly non-flavonoid phenolics and diverse bioactive compounds, exert a more significant influence on the reducing power of the extracts. TPC also showed a positive relationship with TFC ($r = 0.627$, sig. = 0.026), consistent with the co-extraction of these phytochemical groups. In contrast, DPPH exhibited negative correlations with TPC ($r = -0.581$, sig. = 0.039) and FRAP ($r = -0.462$, 0.089), as expected, because lower IC_{50} values indicate stronger antioxidant activity; therefore, extracts with higher phenolic levels and greater reducing capacity tend to exhibit lower DPPH IC_{50} values. ABTS showed weaker correlations with TPC and TFC, suggesting that ABTS radical-scavenging activity reflects

contributions from additional compound classes and/or different reaction sensitivities, consistent with reports of bitter melon's complex phytochemical composition and diverse antioxidant-related metabolites [1,3]. Overall, these results indicate that total phenolics and flavonoids explain FRAP well, whereas broader compositional factors influence radical-scavenging assays.

Table 3 Correlation coefficients between antioxidant activities from DPPH, ABTS, and FRAP assays, total flavonoid contents (TFC) and total phenolic content (TPC) in bitter melon (*Momordica charantia* L.) extracts

		DPPH	ABTS	FRAP	TFC	TPC
Correlation	**DPPH**	1.000				
	ABTS	0.167	1.000			
	FRAP	-0.462	-0.387	1.000		
	TFC	-0.236	-0.136	0.373	1.000	
	TPC	-0.581	-0.205	0.583	0.627	1.000
Sig. (1-tailed)	**DPPH**					
	ABTS	0.322				
	FRAP	0.089	0.141			
	TFC	0.256	0.354	0.144		
	TPC	0.039	0.285	0.038	0.026	

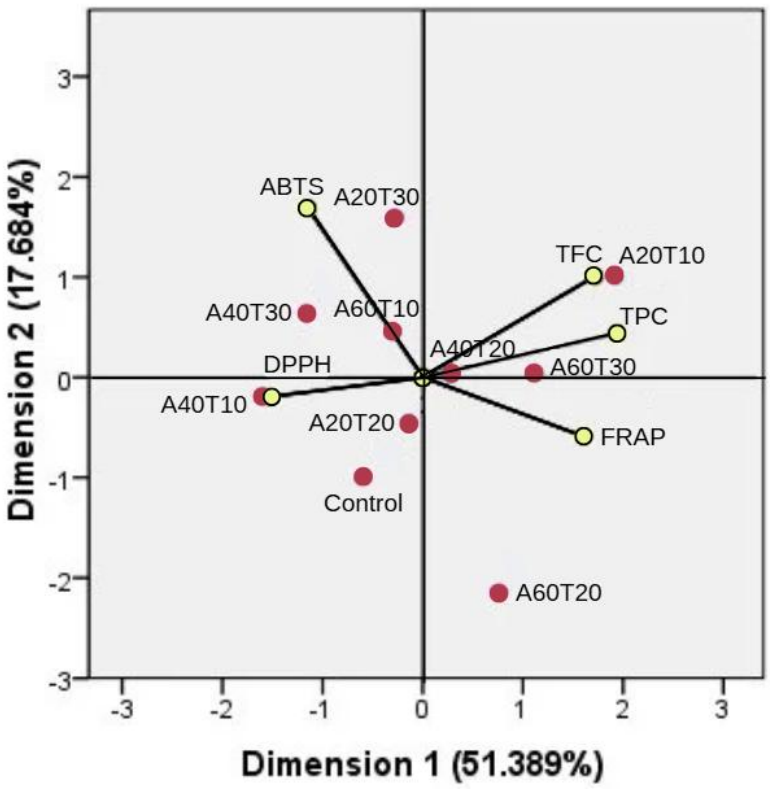

Fig.1 Biplot of PCA illustrating the relationship between phytochemical contents (TPC and TFC) and antioxidant activities of bitter melon (*Momordica charantia* L.) extracts

PCA supported the correlation analysis and confirmed that extraction conditions markedly influenced the overall "phytochemical–antioxidant" profile of bitter melon extracts. The PCA model explained 69.073% of the total variance (PC1 = 51.389%, PC2 = 17.684%) in Fig.1, indicating that most variability among samples was captured by the first two principal components. In the biplot, TPC and TFC were oriented close to FRAP, suggesting that extracts with higher phenolic and flavonoid levels tended to exhibit stronger reducing power. This association is mechanistically reasonable because the FRAP assay primarily reflects an electron-transfer process that many phenolics and flavonoids can donate electrons due to their hydroxyl groups and conjugated structures, thereby reducing Fe(III) to Fe(II) and increasing FRAP values [1,3].

Conversely, DPPH and ABTS were expressed as IC_{50}, where lower values indicate stronger radical scavenging; therefore, as phenolic and flavonoid concentration increases, the required concentration to reach 50% inhibition decreases, producing an apparent inverse relationship and often an opposite orientation to TPC and TFC in PCA space. The alignment of ABTS with TPC and TFC is weaker than FRAP because ABTS can respond to a broader range of antioxidants and is influenced by non-phenolic constituents and matrix effects. In bitter melon, antioxidants are not limited to polyphenols; for example, polysaccharides and their derivatives have also been reported to contribute to antioxidant activity [5], which can partially decouple ABTS behavior from total phenolics and flavonoids. Overall, the clustering and loading patterns in Fig. 1 indicate that changing UAE amplitude and time shifts the chemical composition of the extracts and, consequently, their measured antioxidant performance, consistent with the reported metabolite diversity of bitter melon [3].

4. Conclusion

This study confirmed that ultrasound-assisted extraction (UAE) improved the extraction performance of bitter melon (*Momordica charantia* L.) fruit compared with conventional maceration. UAE produced a higher extract yield (27.28%) than maceration (24.18%) and enhanced the recovery of bioactive compounds and antioxidant-related properties. Correlation analysis indicated that TPC and TFC were positively associated with FRAP, while DPPH showed negative relationships with phenolic compounds. PCA (69.073% total variance) further demonstrated that extraction conditions strongly influenced sample grouping and that higher phenolic and flavonoid contents were linked to stronger antioxidant activity. Overall, UAE is a promising green method for producing bitter melon extracts for potential use in functional foods, dietary supplements, and natural antioxidant ingredients.

Acknowledgements

The authors sincerely appreciate the Faculty of Agro-Industry, Chiang Mai University, Thailand, for supporting laboratory facilities and equipment for this research.

References

1. Mukherjee, S., & Karati, D. (2023). Exploring the phytochemistry and pharmacological activities of Momordica charantia. Pharmacological Research – Modern Chinese Medicine, 6, 100226. https://doi.org/10.1016/j.prmcm.2023.100226
2. Poovitha, S., & Parani, M. (2016). In vitro and in vivo α-amylase and α-glucosidase inhibition by bitter gourd proteins. BMC Complementary and Alternative Medicine, 16, 185. https://doi.org/10.1186/s12906-016-1085-1
3. Perumal, V. et al. (2021). Antioxidant profile of Momordica charantia fruit extract. Food Chemistry: Molecular Sciences, 2, 100012. https://doi.org/10.1016/j.fochms.2021.100012
4. Desai, S. et al. (2020). Isolation and quantitative analysis of charantin. Food Chemistry, 345, 128717. https://doi.org/10.1016/j.foodchem.2020.128717

5. Chen, F. et al. (2019). Antioxidant activity of bitter melon polysaccharides. International Journal of Biological Macromolecules, 138, 673–680. https://doi.org/10.1016/j.ijbiomac.2019.07.129
6. Azmir, J. et al. (2013). Techniques for extraction of bioactive compounds from plant materials. Journal of Food Engineering, 117, 426–436. https://doi.org/10.1016/j.jfoodeng.2013.01.014
7. Dai, J., & Mumper, R.J. (2010). Plant phenolics: Extraction, analysis and applications. Molecules, 15, 7313–7352. https://doi.org/10.3390/molecules15107313
8. Chemat, F. et al. (2017). Ultrasound assisted extraction of food and natural products. Ultrasonics Sonochemistry, 34, 540–560. https://doi.org/10.1016/j.ultsonch.2016.06.035
9. Vilkhu, K. et al. (2008). Applications and opportunities for ultrasound assisted extraction. Innovative Food Science & Emerging Technologies, 9, 161–169. https://doi.org/10.1016/j.ifset.2007.04.014
10. Mir, S.A. et al. (2015). Optimization of ultrasound-assisted extraction of charantin. Journal of Pharmacy and Bioallied Sciences, 7(4), 304–308. https://doi.org/10.4103/0975-7406.168032
11. Wang, L. et al. (2020). Ultrasound-assisted extraction of phenolics. Food Research International, 132, 109067. https://doi.org/10.1016/j.foodres.2020.109067
12. Haideri, M. H., Phanjaroen, T., Khiaolaongam, W., Boonchalaem, T., Laoung-On, J., Chaipoot, S., Hongsibsong, S., Boonyapranai, K., & Ounjaijean, S. (2024). Effect of Different Extraction Techniques on Phenolic Profile and Phytochemical Potential of Gymnema inodorum Leaf Extract. Molecules, 29(22), 5475. https://doi.org/10.3390/molecules29225475
13. Jeytawan, N., Yadoung, S., Jeeno, P., Yana, P., Sutan, K., Naksen, W., Wongkaew, M., Sommano, S., & Hongsibsong, S. (2022). Antioxidant and Phytochemical Potential and Phytochemicals in Gymnema inodorum (Lour.) Decne in Northern Thailand. Plants, 11(24), 3498. https://doi.org/10.3390/plants11243498
14. Solórzano-Zambrano, L. J., Bonilla-Loor, M. J., Pazmiño, A., Segovia-Cedeño, D., Pinargote, K. A., Moreira-Menendez, H. O., Laz-Mero, M., & González, C. (2025b). Effect of extraction solvent on the recovery of bioactive compounds and antioxidant activity in Momordica Charantia: Towards sustainable processes. Edelweiss Applied Science and Technology, 9(6), 180–190. https://doi.org/10.55214/25768484.v9i6.7779
15. Rahim, N. D. A., Yaakob, H., Hisam, R. H. @., Sarmidi, M. R., & Cheng, K. (2021b). Effect of extraction solvents on the phytochemical content and bioactivity of Momordica charantia Linn. fruits. Malaysian Journal of Fundamental and Applied Sciences, 17(1), 79–83. https://doi.org/10.11113/mjfas.v17n1.2170
16. Perez, J. L., Jayaprakasha, G., & Patil, B. S. (2019). Metabolite profiling and in vitro biological activities of two commercial bitter melon (Momordica charantia Linn.) cultivars. *Food Chemistry*, *288*, 178–186. https://doi.org/10.1016/j.foodchem.2019.02.120
17. Banpacha, N., Janpeng, H., Renaldi, G., & Samakradhamrongthai, R. S. (2025). Influence of semi-fermentation and drying on the phytochemical properties, antioxidant activity, and volatile compounds of Gymnema inodorum (Lour.) Decne leaves. *Applied Food Research*, *5*(2), 101523. https://doi.org/10.1016/j.afres.2025.101523

P - 184

Pasting Properties, Antioxidant Activities, Anthocyanins of Indigenous Pigmented Rice Flour and Its Correlation using Principal Component Analysis

Natnara Khasom[1,2], Rajnibhas Sukeaw Samarkradhamrongthai[1,2,3]*

[1]*Department of Food Science and Technology, Faculty of Agro-Industry, Chiang Mai University*
[2]*INterdisciplinary and Food product development for wellness Research unit (INFRU), Chiang Mai University, Thailand*
[3]*Division of Product Development Technology, Faculty of Agro-Industry, Chiang Mai University, Thailand*

**Corresponding author E-mail: rahjnibhas.s@cmu.ac.th*

Abstract: In Thailand, indigenous pigmented rice varieties are traditionally cultivated in upland and northern regions and are characterized by high concentrations of anthocyanins that contribute to antioxidant activity. This study aimed to evaluate the functional properties, antioxidant activities, and anthocyanin composition of indigenous pigmented rice flour. Five indigenous pigmented rice varieties from Thailand, including Khao Kam Jao CMU 107 (KCM), Red Jasmine Rice (KCT), Thapthim Chumphae Rice (KCH), Kam Doi Saket Glutinous Rice (KND), and Royal Project Kam Glutinous Rice (KNR), were processed into rice flour for analysis. Pasting properties, antioxidant activities, and anthocyanin content showed significant differences among rice varieties. KCM exhibited the highest peak viscosity (5,076.67 ± 90.52 cP), while glutinous rice KNR displayed a shorter peak time (~4.1 min) than non-glutinous varieties (~5.2 min), indicating faster pasting behavior. KNR also demonstrated the strongest antioxidant activity, with the lowest IC_{50} value for DPPH radical scavenging (0.774 ± 0.283 mg/mL). Anthocyanin profiling revealed substantial variation among varieties. KCM contained cyanidin-3-glucoside (C-3-G) at 8.32 ± 1.83 mg/L and peonidin-3-glucoside (P-3-G) at 738.23 ± 62.03 mg/L. Notably, KNR exhibited exceptionally high anthocyanin levels, with C-3-G (128.80 ± 7.16 mg/L) and P-3-G (11,431.65 ± 635.94 mg/L), far exceeding other varieties. Principal Component Analysis (PCA) effectively differentiated rice varieties based on functional properties and antioxidant activities. Anthocyanins (C-3-G and P-3-G) were strongly associated with glutinous rice varieties, whereas antioxidant parameters (DPPH, ABTS, and FRAP) clustered with non-glutinous types. The first two principal components explained 81.14% of pasting property variance and 88.06% of antioxidant and anthocyanin variation. These findings highlight the potential of indigenous pigmented rice flour for functional food and nutraceutical development.

Keywords: Indigenous pigmented rice; Pasting properties; Antioxidant activities; Anthocyanins; Principal component analysis

1. Introduction

Rice (*Oryza sativa L.*) is the staple food for more than half of the global population and represents a vital source of carbohydrates, proteins, and bioactive compounds [1]. Among rice types, pigmented varieties such as red, purple, and black rice are attracting increasing scientific and commercial interest due to their rich content of phytochemicals, particularly phenolics and anthocyanins, which contribute to health-promoting properties [2,3]

In Thailand, indigenous pigmented rice varieties are traditionally cultivated in upland and northern regions, where they play an important role in food culture, local economy, and agricultural biodiversity [4]. These varieties include black sticky rice (khao niao dam), red jasmine

rice (khao hom dang), and local purple rice landraces, which are often grown without intensive chemical inputs and are well adapted to diverse agro-ecological conditions. Indigenous pigmented rice is not only consumed as a staple but also incorporated into traditional desserts, beverages, and medicinal foods, reflecting its cultural and nutritional importance [5]. Compared with conventional white rice, Thai pigmented rice varieties are characterized by higher concentrations of dietary fiber, phenolic compounds, and anthocyanins, which contribute to antioxidant, anti-inflammatory, and anti-diabetic activities [3,6].

From a physicochemical perspective, the flour quality of rice strongly influences its cooking, processing, and end-use applications. Rapid Viscosity Analysis (RVA) is widely employed to characterize pasting behavior, which determines texture, stability, and consumer acceptability of rice-based products [7]. Meanwhile, antioxidant capacity, often measured by assays such as DPPH, ABTS, and FRAP, reflects the potential of pigmented rice to mitigate oxidative stress and associated chronic diseases [8]. Anthocyanins, particularly cyanidin-3-glucoside and peonidin-3-glucoside, are the major pigments in pigmented rice that contribute not only to antioxidant defense but also to anti-inflammatory and anti-carcinogenic activities [9]
However, rice quality traits are multidimensional, and their relationships cannot always be fully understood using univariate analyses alone. Principal component analysis (PCA) provides an effective statistical tool to visualize correlations among functional, antioxidant, and bioactive parameters, and to classify rice varieties according to their characteristic profiles [10]. Such integrative analysis helps reveal functional diversity and supports the strategic valorization of indigenous pigmented rice.

Therefore, this study aimed to evaluate the pasting properties, antioxidant capacity, and anthocyanin content of selected indigenous pigmented rice flour, and to apply PCA for multivariate differentiation. The findings are expected to provide insights into the nutritional and functional potential of indigenous rice varieties, supporting their utilization in the functional food and nutraceutical industries.

2. Materials and Methods

2.1 Materials and chemicals

Five indigenous pigmented rice varieties were used in this study: Khao Kam Jao CMU 107 (KCM), Red Jasmine Rice (KCT), Thapthim Chumphae Rice (KCH), Kam Doi Saket Glutinous Rice (KND), and Royal Project Kam Glutinous Rice (KNR). Khao Kam Jao CMU 107 was obtained from the Lanna Rice Research Center, Chiang Mai University, Thailand, while the other rice samples were sourced from local producers and highland cultivation areas in northern Thailand. DPPH, ABTS, potassium persulfate, TPTZ, ferric chloride, ferrous sulfate, and cyanidin-3-glucoside (Sigma–Aldrich, St. Louis, MO, USA). Ethanol and buffer reagents for the pH-differential method (pH 1.0 and pH 4.5) were of analytical grade and obtained from Merck (Darmstadt, Germany).

2.2 Sample preparation

Indigenous pigmented rice (KCM, KCT, KCH, KND, and KNR) were ground using a hammer mill (Model: Cyclotec™ 1093 Sample Mill, FOSS, Hillerød, Denmark)and sieved through a 16-mesh sieve to obtain uniform particle size. The prepared rice flour samples were stored in opaque aluminum foil bags at room temperature (25 ± 2 °C) until further analysis.

2.3 Pasting properties analysis

The pasting profiles were analyzed using a Rapid Visco Analyzer (RVA) (Newport, Warri wood, Australia). RVA refers to viscosity change of rice starch during heating. The operation process was based on the American Association of Cereal Chemists (AACC) operating procedures (16). About 4g of rice flour was mixed with 25 ml of water and then put in an aluminum can. The

RVA program first heated at 45°C for one minute, then heated to 90°C in 3.75 minutes, and then heated at 95°C for 2.5 min. It was then cooled to 45°C for 3.75 min and held for 1.4 min. Indicators of starch gelatinization included peak viscosity, hold viscosity, final viscosity, breakdown, setback, peak time, and pasting temperature.

2.4 Antioxidant activities

2.4.1 Sample extraction

Indigenous pigmented rice samples (KCM, KCT, KCH, KND, and KNR) were extracted using 95% (v/v) ethanol at a sample-to-solvent ratio of 1:10 (w/v). The extraction was performed by maceration at room temperature for 24 h. The extracts were then filtered through a syringe filter (0.45 µm nylon syringe filter, Whatman, GE Healthcare, UK) to obtain clear solutions. The filtered extracts were prepared at five different concentrations by two-fold serial dilution, resulting in final concentrations of 10, 5, 2.5, 1.25, and 0.625 mg/mL. Each concentration was subsequently used for antioxidant activity evaluation using DPPH, ABTS, and FRAP assays.

The use of 95% ethanol was selected to efficiently extract a broad range of phenolic compounds, including moderately polar and less polar antioxidant components such as phenolic acids, flavonoids, and anthocyanin derivatives. Although lower-concentration acidified ethanol is commonly used for anthocyanin extraction, high-concentration ethanol has been reported to improve the extraction of total antioxidant compounds and reduce co-extraction of sugars and other polar impurities, resulting in improved antioxidant assay sensitivity.

2.4.2 DPPH radical scavenging activity

The sample solution (20 µL) was mixed with 180 µL of 60 µmol/L DPPH solution. The mixed solution was kept in the dark at 30 °C for 30 min. The absorbance of the mixed solution was measured at 517 nm using a UV–Visible spectrophotometer (The Spark® multimode microplate reader; Tecan, Männedorf, Switzerland).The DPPH radical scavenging activity was calculated as the percentage of inhibition using the following equation1

$$\text{Radical scavenging (\%)} = \left[\frac{A_{\text{control}} - (A_{\text{control}} - A_{\text{sample}})}{A_{\text{control}}}\right] \times 100 \qquad \text{Eq.1}$$

where $A_{\text{control}}$is the absorbance of the DPPH solution without sample and $A_{\text{sample}}$is the absorbance in the presence of the sample.

For IC_{50} determination, the sample was prepared at different concentrations and analyzed under the same conditions. The percentage of DPPH radical scavenging activity was plotted against sample concentration, and the IC_{50} value (the concentration required to inhibit 50% of DPPH radicals) was calculated by nonlinear regression analysis.

2.4.3 ABTS radical scavenging activity

The sample solution was added to the ABTS radical solution with a ratio of 1:20. The mixed solution was incubated at 30 °C for 7 min. The absorbance was measured at 734 nm against a blank (distilled water instead of sample solution). The ABTS radical scavenging activity was calculated using the following equation2

$$\text{Radical scavenging (\%)} = \left[\frac{A_{\text{control}} - (A_{\text{control}} - A_{\text{sample}})}{A_{\text{control}}}\right] \times 100 \qquad \text{Eq.2}$$

where A_{control}represents the absorbance of the ABTS radical solution without sample and A_{sample}represents the absorbance after reaction with the sample.

To determine IC_{50} values, the sample was tested at various concentrations, and the percentage inhibition was plotted against concentration. The IC_{50} value was calculated from the dose–response curve using nonlinear regression analysis.

2.4.4 Ferric reducing antioxidant power (FRAP) assay

The ferric reducing antioxidant power (FRAP) assay was performed to evaluate the reducing capacity of the samples. The sample solution (20 µL) was mixed with 180 µL of freshly prepared FRAP reagent and incubated at room temperature for 30 min. The absorbance was then measured at 593 nm. A standard calibration curve was constructed using $FeSO_4 \cdot 7H_2O$ solutions at concentrations of 100, 200, 400, 600, 800, and 1000 µM. Each concentration level was prepared and analyzed under the same experimental conditions as the samples, and the absorbance values were plotted against the corresponding $FeSO_4 \cdot 7H_2O$ concentrations to generate the standard curve. The FRAP values of the samples were calculated from this calibration curve and expressed as micromoles of $FeSO_4 \cdot 7H_2O$ equivalents, representing the ferric reducing antioxidant capacity of the samples.

2.5 Determination of total anthocyanin content

The total anthocyanin content of the extracts from indigenous pigmented rice flour was determined using the pH-differential method as described by Wrolstad (1976). The extract was diluted with two buffer systems: KCl buffer (pH 1.0) and CH_3COONa buffer (pH 4.5) in a ratio of 1:100 (v/v). The absorbance was measured at 520 nm and 700 nm using a UV–Visible spectrophotometer (The Spark® multimode microplate reader; Tecan, Männedorf, Switzerland). The results were expressed as cyanidin-3-glucoside (C-3-G) and peonidin-3-glucoside (P-3-G) equivalents. The total anthocyanin content was calculated using the following equation3

$$\text{Anthocyanin} = \frac{\text{A} \times \text{MW} \times \text{DF} \times 1000}{\varepsilon \times \text{l}} \qquad \text{Eq.3}$$

$A = (A_{520} - A_{700})_{pH1.0} - (A_{520} - A_{700})_{pH4.5}$
= difference in absorbance between pH 1.0 and pH 4.5 buffers at 520 and 700 nm wavelengths.
MW = molecular weight of cyanidin-3-glucoside and peonidin-3-glucoside
ε = molar extinction coefficient of cyanidin-3-glucoside and peonidin-3-glucoside
DF= dilution factor
l =length of the microplate

2.6 Statistical Analysis

All experiments were performed in triplicate and results were expressed as mean ± standard deviation. Statistical analysis was conducted using SPSS (version 17.0). Significant differences among samples were evaluated by one-way analysis of variance (ANOVA), followed by Duncan's multiple range test (DMRT) at $p < 0.05$. Pearson's correlation analysis was used to determine relationships between antioxidant activities, anthocyanin contents, and pasting properties. Principal component analysis (PCA) was applied to visualize multivariate relationships after data standardization.

3. Results & Discussion

3.1 Pasting properties of indigenous pigmented rice flour

The pasting properties of indigenous pigmented rice flour exhibited significant varietal differences (Table 1). Peak viscosity ranged from 4,467.00 ± 64.21 cP (KNR) to 5,076.67 ± 90.52 cP (KCM), with KCM showing a significantly higher value ($p < 0.05$), indicating greater starch

granule swelling and water-binding capacity during heating. Similar varietal differences in pasting behavior have been attributed to starch molecular architecture and interactions with phenolic compounds [13,14]. Hold viscosity, which reflects paste stability under continuous heating and shear, was highest in KCT, indicating greater resistance to granule disintegration. Such stability is desirable for processed rice products requiring thermal endurance [7]. In contrast, KCM and KCH exhibited lower hold viscosity, suggesting weaker granular integrity.

Final and setback viscosities further differentiated the rice varieties. KCT showed the highest final and setback viscosities, indicating a strong tendency toward starch reassociation and retrogradation during cooling. High setback viscosity is commonly associated with enhanced amylose reassociation and firmer gel formation [17]. Conversely, KND exhibited the lowest final and setback viscosities, suggesting limited retrogradation and softer gel structure, characteristics favorable for instant and ready-to-eat products [18,19].The shorter peak time and lower pasting temperature observed in KND indicate earlier gelatinization and reduced energy requirements during processing, which are advantageous for pregelatinized or instant rice-based foods [14]. Overall, the observed RVA profiles highlight the functional diversity of indigenous pigmented rice flour and their potential for targeted food applications.

Table 1. Pasting properties of indigenous pigmented rice flour

	Peak Viscosity (cP)	Hold Viscosity (cP)	Final Viscosity (cP)	Setback (cP)	Peak Time (min) (ns)	Pasting Temperature (°C)
KCM	5076.67 ± 90.52 ^{a}	1998.00 ± 54.34 ^{c}	4015.67 ± 87.66 ^{c}	2017.67 ± 74.14 ^{c}	5.13 ± 0.06	74.98 ± 1.65 ^{b}
KCT	4472.67 ± 83.34 ^{d}	3025.00 ± 130.53 ^{a}	6085.00 ± 36.75 ^{a}	3060.00 ± 167.01 ^{a}	5.20 ± 0.11	80.37 ± 1.29 ^{a}
KCH	4733.33 ± 49.09 ^{c}	1916.00 ± 30.31 ^{c}	4139.33 ± 38.89 ^{b}	2223.33 ± 23.50 ^{b}	5.25 ± 0.04	73.68 ± 1.21 ^{b}
KND	4723.00 ± 35.04 ^{c}	2646.00 ± 160.68 ^{b}	3638.33 ± 93.06 ^{d}	775.67 ± 19.35 ^{d}	4.11 ± 0.11	69.40 ± 0.75 ^{c}
KNR	4467.00 ± 64.21 ^{d}	1963.67 ± 80.38 ^{c}	4096.00 ± 17.58 ^{bc}	2132.33 ± 97.65 ^{bc}	4.11 ± 1.77	78.77 ± 0.93 ^{a}

* Values are expressed as mean ± standard deviation (SD). Different superscript letters within the same column indicate significant differences among rice varieties ($p < 0.05$).
** Khao Kam Jao CMU 107; KCT, Red Jasmine Rice; KCH, Thapthim Chumphae Rice; KND, Kam Doi Saket Glutinous Rice; KNR,and Royal Project Kam Glutinous Rice.

3.2 Antioxidant activities and anthocyanin content

The in vitro antioxidant activity and anthocyanin content of indigenous pigmented rice flour are presented in Table 2. Significant differences ($p < 0.05$) were observed among rice varieties across all antioxidant assays and individual anthocyanin contents. For DPPH radical scavenging activity, KNR exhibited the lowest IC_{50} value (0.77 ± 0.28 mg/mL), indicating the strongest antioxidant activity, followed by KCH (1.50 ± 0.37 mg/mL) and KCT (1.86 ± 0.46 mg/mL). In contrast, KCM and KND showed significantly higher IC_{50} values (4.40 ± 0.64 and 4.38 ± 0.37 mg/mL, respectively), reflecting weaker radical scavenging capacity. A comparable pattern was observed in the ABTS assay, where KCT exhibited the lowest IC_{50} value (0.62 ± 0.32 mg/mL), indicating the strongest antioxidant activity, followed by KNR (0.72 ± 0.10 mg/mL) and KCH (0.88 ± 0.54 mg/mL). In contrast, KCM and KND exhibited significantly higher IC_{50} values (4.10 ± 0.44 and 4.08 ± 0.22 mg/mL, respectively), indicating weaker radical scavenging capacity. Ferric reducing antioxidant power (FRAP) values also differed significantly among the samples. KCH demonstrated the highest FRAP value (3.45 ± 0.46 mg Trolox/g), indicating superior

reducing power, while KNR and KCT showed the lowest FRAP values (0.27 ± 0.04 and 0.30 ± 0.09 mg Trolox/g, respectively). KCM and KND exhibited intermediate reducing capacities.

Total monomeric anthocyanin content differed significantly among rice varieties. KNR exhibited the highest anthocyanin content, followed by KCM and KND, while KCT showed the lowest anthocyanin concentration. Moderate anthocyanin contents were observed in KCM and KND, whereas KCT exhibited the lowest concentrations [3,6,15].

The extraction solvent plays an important role in determining antioxidant recovery and anthocyanin stability. Acidified polar solvents enhance anthocyanin solubility and stability by maintaining the flavylium cation structure. Therefore, differences in antioxidant activity among rice varieties may be influenced not only by anthocyanin concentration but also by solvent extraction efficiency. The observed varietal differences in antioxidant activity can be largely attributed to variations in anthocyanin concentration and composition. Lower IC_{50} values in DPPH and ABTS assays indicate higher hydrogen atom transfer and electron-donating capacities, which are characteristic features of anthocyanin-rich matrices [2,6,20]. The strong radical scavenging activity of KNR corresponds well with its high anthocyanin content. Interestingly, although KCH exhibited the highest FRAP value, its radical scavenging activity was lower than that of KNR. This discrepancy suggests that antioxidant capacity is not governed solely by total anthocyanin concentration but is also influenced by the dominant antioxidant mechanism involved. The FRAP assay primarily reflects electron-donating ability under acidic conditions, whereas DPPH and ABTS assays capture different radical quenching behaviors [8,21].

Additionally, solvent polarity influences the extraction of different phenolic compounds, which may contribute differently to antioxidant activity depending on assay conditions.

Moreover, interactions between anthocyanins and other phenolic compounds, proteins, or starch components within the rice matrix may influence antioxidant accessibility and responsiveness in vitro assays [22,23].

Table 2. Antioxidant activity and anthocyanin content of indigenous pigmented rice flour

	DPPH IC50 (mg/mL)	ABTS IC50 (mg/mL)	FRAP (mg Trolox/g)	C-3-G (mg/L)	P-3-G (mg/L)
KCM	4.40 ± 0.64 ^{a}	4.10 ± 0.44 ^{a}	1.00 ± 0.15 ^{b}	8.32 ± 1.82 ^{b}	738.23 ± 62.03 ^{b}
KCT	1.86 ± 0.46 ^{b}	0.62 ± 0.32 ^{b}	0.30 ± 0.09 ^{c}	1.57 ± 0.67 ^{c}	139.34 ± 43.19 ^{c}
KCH	1.50 ± 0.37 ^{bc}	0.88 ± 0.54 ^{b}	3.45 ± 0.46 ^{a}	5.02 ± 0.67 ^{bc}	445.21 ± 59.85 ^{bc}
KND	4.38 ± 0.37 ^{a}	4.08 ± 0.22 ^{a}	0.39 ± 0.07 ^{c}	7.16 ± 0.69 ^{bc}	635.94 ± 60.89 ^{bc}
KNR	0.77 ± 0.28 ^{c}	0.72 ± 0.10 ^{b}	0.27 ± 0.04 ^{c}	128.80 ± 7.16 ^{a}	11,431.65 ± 635.94 ^{a}

Values are expressed as mean ± standard deviation (SD). Different superscript letters within the same column indicate significant differences among rice varieties ($p < 0.05$).
** Khao Kam Jao CMU 107; KCT, Red Jasmine Rice; KCH, Thapthim Chumphae Rice; KND, Kam Doi Saket Glutinous Rice; KNR,and Royal Project Kam Glutinous Rice.

3.3 Correlation of indigenous pigmented rice flour and its antioxidant activities and pasting properties using principal component analysis (PCA)

Principal component analysis (PCA) was conducted to clarify the relationships among pasting properties of indigenous pigmented rice flour, including peak viscosity, hold viscosity, final viscosity, setback, peak time, and pasting temperature. The PCA was performed using mean values obtained from triplicate measurements for each rice variety. Prior to analysis, variables were standardized using mean-centering and unit variance scaling (z-score normalization) to

minimize the influence of different measurement units. PCA was performed using standardized variables, and biplots were constructed using the first two principal components. The axes intersect at zero (0,0), representing the origin of the dataset. Samples positioned closer to variable vectors indicate stronger associations, whereas those located near the center indicate weaker relationships. The first two principal components explained 81.14% of the total variance, with PC1 accounting for 52.27% and PC2 for 28.87%, indicating that these components captured most of the variability in starch pasting behavior among the rice varieties. PC1 appeared to be associated with viscosity development during heating and cooling, as evidenced by positive loadings for final viscosity, setback, and peak time. Rice varieties located on the positive side of PC1, particularly KCM, were suggestively associated with high final viscosity and setback values, suggesting a greater tendency toward starch retrogradation and gel firming during cooling. Elevated setback viscosity is widely associated with enhanced amylose reassociation and reduced paste stability during storage, which can negatively affect the textural quality of ready-to-eat products [25,26]. Therefore, while KCM may be less suitable for instant food applications, its strong gel-forming ability could be advantageous in products requiring firm or structured textures. PC2 appeared to be influenced by hold viscosity and pasting temperature, reflecting paste stability under continuous heating and the thermal resistance of starch granules. KND was positioned in the positive region of PC2 and showed an apparent association with hold viscosity, indicating superior resistance to granule breakdown during prolonged heating and shear stress. This behavior suggests stronger granular integrity and a more compact starch structure, which has been linked to enhanced crystalline organization and amylose–amylopectin interactions [27].

In contrast, KCT was located nearer to the pasting temperature vector, indicating a higher gelatinization temperature and greater thermal stability of starch granules. Such characteristics may be attributed to differences in amylose content, crystalline perfection, or the formation of amylose–lipid complexes, which have been reported to elevate gelatinization temperatures and restrict granule swelling [28,29].

KNR and KCH were positioned on the negative side of PC1 and were more closely associated with peak viscosity, indicating a higher swelling capacity of starch granules during heating. This behavior reflects greater water absorption ability and weaker internal bonding forces within the starch granules, which facilitate rapid viscosity development [30,31]. Such pasting characteristics are desirable for applications requiring fast thickening and smooth paste formation, such as instant porridges or beverage-type formulations. However, these relationships should be interpreted cautiously due to the limited number of rice varieties included in the analysis.

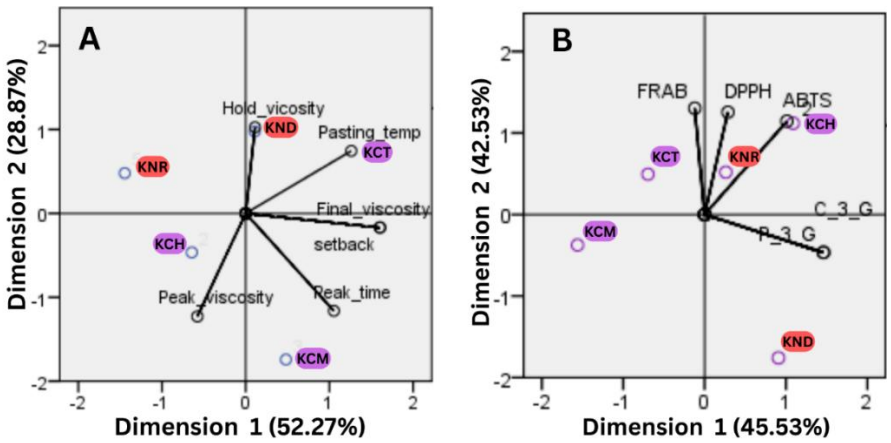

Figure 1. Biplot of principal component analysis (PCA) showing the relationships between (A) pasting properties and (B) antioxidant activities and anthocyanin compounds in indigenous pigmented rice flour (Khao Kam Jao CMU 107; KCT, Red Jasmine Rice; KCH, Thapthim Chumphae Rice; KND, Kam Doi Saket Glutinous Rice; KNR,and Royal Project Kam Glutinous Rice.)

Principal component analysis (PCA) was also applied to elucidate the relationships between antioxidant activities (DPPH, ABTS, and FRAP), total anthocyanin content, and indigenous pigmented rice varieties. The analysis was conducted using standardized mean values from triplicate measurements. The first two principal components explained 88.06% of the total variance, with PC1 and PC2 accounting for 45.53% and 42.53%, respectively, indicating good representation of antioxidant variability among the rice samples. PC appeared to be associated with radical scavenging activity and anthocyanin content, as reflected by the positive loadings of DPPH, ABTS, and total anthocyanin content. The alignment of anthocyanin vectors with DPPH and ABTS suggests that anthocyanins may contribute substantially to radical scavenging capacity in pigmented rice, consistent with previous studies highlighting the role of anthocyanins in hydrogen atom and electron donation mechanisms [21,31].

Rice varieties KCH and KNR were in the positive region of PC1, indicating relatively stronger radical scavenging activity. KNR showed an apparent association with anthocyanin content, which agrees with its higher antioxidant activity observed in DPPH and ABTS assays. In contrast, PC2 appeared to be influenced by FRAP, indicating that reducing power represents an antioxidant mechanism partially independent of free radical scavenging. KCT was more closely associated with FRAP, suggesting that its antioxidant activity may be contributed by non-anthocyanin phenolic compounds, such as phenolic acids or flavonoids, which are known to exhibit strong electron-donating capacity under acidic conditions [22].

Meanwhile, KCM and KND were separated from antioxidant-related vectors, reflecting comparatively lower antioxidant potential despite measurable anthocyanin contents. This behavior may be attributed to differences in anthocyanin composition, molecular structure, or interactions with starch and protein matrices that can limit antioxidant accessibility and efficiency [23]. Given the limited sample size, PCA and correlation results should be considered exploratory, and further studies with larger sample sets are recommended to confirm these observed relationships.

3.4 Relationship within antioxidant activities and withing pasting properties using heat map analysis

Color shading in Figure 2 indicates the strength and direction of correlations among variables. Red shades represent positive correlations, whereas blue shades indicate negative correlations. Darker colors reflect stronger correlations, while lighter colors indicate weaker relationships. Statistical significance was considered at $p < 0.05$. Correlation analysis of pasting properties revealed strong interrelationships among viscosity-related parameters of indigenous pigmented rice flour (Figure 2A). Peak viscosity showed a strong positive correlation with final viscosity ($r = 0.845$, $p < 0.01$) and setback viscosity ($r = 0.724$, $p < 0.01$), indicating that rice samples with greater starch granule swelling during gelatinization tended to develop stronger and more stable paste structures after cooling. Similar strong correlations between final viscosity and setback ($r = 0.823$, $p < 0.01$) further suggest that these parameters are closely associated with starch reassociation and retrogradation behavior, which are strongly governed by amylose content, molecular chain length distribution, and the reorganization of starch polymers during cooling [25,29]. Pasting temperature exhibited significant positive correlations with final viscosity and setback ($p < 0.01$), implying that rice varieties requiring higher gelatinization temperatures tend to form more rigid and stable paste networks. This behavior may be attributed to stronger crystalline regions, enhanced molecular ordering, or the presence of amylose–lipid complexes within starch granules, which delay gelatinization and promote structural stability after cooling [23,31]. In contrast, peak time showed weak and non-significant correlations with most viscosity parameters, indicating that the rate of gelatinization was not a primary determinant of paste strength or retrogradation behavior in these rice samples. Similar observations have been reported in recent studies on pigmented and non-pigmented rice flour, where paste stability was more closely linked to viscosity development rather than gelatinization rate [24].

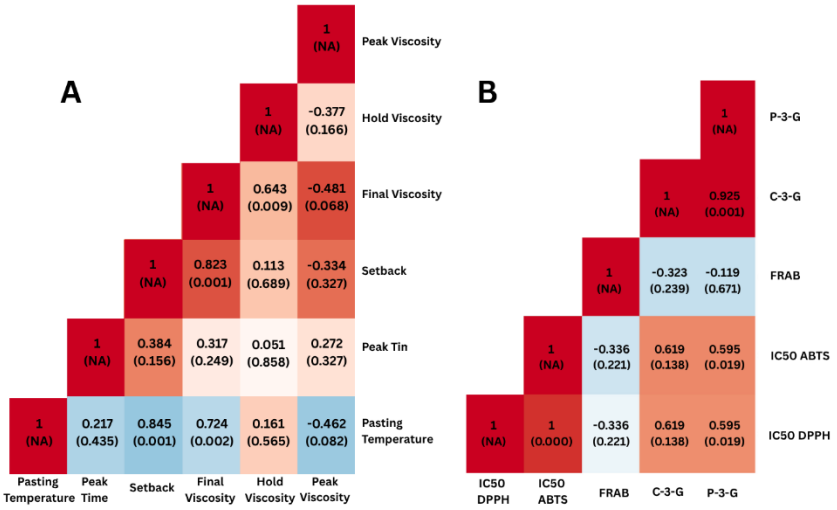

Figure 2. Correlation heatmaps of (A) pasting properties and (B) anthocyanin contents and antioxidant activities of indigenous pigmented rice flour. Values in each cell represent Pearson correlation coefficients (upper number) and p-values (lower number in parentheses).

Correlation analysis among anthocyanin contents and antioxidant activities is presented in Figure 2B. A very strong positive correlation was observed between cyanidin-3-glucoside (C-3-G) and peonidin-3-glucoside (P-3-G) ($r = 0.925$, $p < 0.01$), indicating that these major anthocyanins tend to co-occur in indigenous pigmented rice varieties. This finding suggests a shared biosynthetic pathway and genetic control over anthocyanin accumulation in rice grains.

FRAB values showed weak and non-significant negative correlations with both C-3-G and P-3-G, suggesting that ferric reducing antioxidant power may be influenced by other phenolic compounds or non-anthocyanin antioxidants present in rice, such as phenolic acids and flavonoids. In contrast, IC_{50} values of ABTS and DPPH assays exhibited moderate positive correlations with anthocyanin contents, with a statistically significant correlation observed between IC_{50} DPPH and C-3-G ($r = 0.595$, $p < 0.05$). Since lower IC50 values indicate stronger antioxidant activity, this relationship implies that higher anthocyanin concentrations are associated with enhanced radical scavenging capacity.

Notably, IC_{50} ABTS and IC_{50} DPPH were perfectly correlated ($r = 1.000$, $p < 0.001$), demonstrating strong consistency between the two radical scavenging assays in evaluating antioxidant activity of pigmented rice extracts. Overall, these results confirm that anthocyanins, particularly C-3-G, contribute significantly to the antioxidant potential of indigenous pigmented rice, although the magnitude of antioxidant activity is also affected by the assay type and the presence of other bioactive compounds.

4. Conclusion

This study demonstrated clear varietal differences in pasting properties, antioxidant capacity, and anthocyanin profiles among indigenous pigmented rice flour. The results revealed that starch pasting behavior was strongly influenced by varietal characteristics, with KCM exhibiting high peak viscosity and setbacks, indicating a strong tendency toward starch retrogradation, whereas KND showed lower final and setback viscosities, suggesting better suitability for instant or ready-to-eat products. Antioxidant analysis confirmed that radical scavenging activity was closely associated with anthocyanin content, particularly cyanidin-3-glucoside and peonidin-3-glucoside, with KNR and KCH showing superior antioxidant potential as reflected by low IC_{50} values in DPPH and ABTS assays. Multivariate analyses further highlight

distinct functional groupings among rice varieties based on their starch and bioactive characteristics. Overall, the findings emphasize the functional diversity of indigenous pigmented rice and support the targeted utilization of specific varieties for functional food and nutraceutical applications, depending on desired textural and antioxidant properties.

Acknowledgements

The authors sincerely appreciate the Faculty of Agro-Industry, Chiang Mai University, Thailand, for supporting laboratory facilities and equipment for this research.

References

1. FAO. Rice Market Monitor; Food and Agriculture Organization of the United Nations: Rome, Italy, 2022.https://www.fao.org/markets-and-trade/publications/rice-market-monitor
2. Zhang, M.; Zhang, R.; Wang, Y.; Guo, D.; Li, L. Phenolic compounds, antioxidant activity, and health benefits of pigmented rice: A review. Food Chemistry 2020, 332, 127372. https://doi.org/10.1016/j.foodchem.2020.127372
3. Sompong, R.; Siebenhandl-Ehn, S.; Linsberger-Martin, G.; Berghofer, E. Physicochemical and antioxidative properties of red and black rice varieties from Thailand, China and Sri Lanka. Food Chemistry 2011, 124, 132–140.https://doi.org/10.1016/j.foodchem. 2010.05.115
4. Department of Rice, Thailand. Indigenous Rice Varieties and Biodiversity Conservation in Thailand; Ministry of Agriculture and Cooperatives: Bangkok, Thailand, 2021.(Report; no DOI)
5. Laokuldilok, T.; Shoemaker, C.F.; Jongkaewwattana, S.; Tulyathan, V. Antioxidants and antioxidant activity of several pigmented rice brans. Journal of Agricultural and Food Chemistry 2011, 59, 193–199.https://doi.org/10.1021/jf103649q
6. Zhao, C.; Giusti, M.M. Anthocyanins in pigmented rice: Bioactivity and health benefits. Food Research International 2019, 116, 137–146.https://doi.org/10.1016/j .foodres.2018.12.061
7. Zhou, Z.; Robards, K.; Helliwell, S.; Blanchard, C. Composition and functional properties of rice. International Journal of Food Science & Technology 2010, 45, 9–17.https://doi.org /10.1111/j.1365-2621.2009.02112.x
8. Apak, R.; Özyürek, M.; Güçlü, K.; Çapanoğlu, E. Antioxidant activity/capacity measurement: Classification, physicochemical principles, mechanisms, and applications. Chemical Reviews 2016, 116, 997–1027.https://doi.org/10.1021/acs.chemrev.5b00510
9. He, J.; Giusti, M.M. Anthocyanins: Natural colorants with health-promoting properties. Annual Review of Food Science and Technology 2010, 1, 163–187.https://doi.org/10.1146/annurev.food.080708.100754
10. Granato, D.; Santos, J.S.; Escher, G.B.; Ferreira, B.L.; Maggio, R.M. Use of principal component analysis (PCA) and hierarchical cluster analysis (HCA) for multivariate association between bioactive compounds and functional properties. Food Chemistry 2018, 257, 160–169.https://doi.org/10.1016/j.foodchem.2018.02.100
11. AACC International. Approved Methods of Analysis, 11th ed.; Method 76-21.02; AACC International: St. Paul, MN, USA, 2010.(Official method; no DOI)
12. Brand-Williams, W.; Cuvelier, M.E.; Berset, C. Use of a free radical method to evaluate antioxidant activity. LWT – Food Science and Technology 1995, 28, 25–30.https://doi.org/10.1016/S0023-6438(95)80008-5
13. Zhu, F. Relationships between starch composition, structure and physicochemical properties of rice starch. Food Chemistry 2017, 232, 532–541.https://doi.org/10.1016/j.foodchem.2017.04.028
14. Li, H.; Fitzgerald, M.A.; Prakash, S.; Nicholson, T.M.; Gilbert, R.G. The molecular structural features controlling starch digestibility in cooked rice. Food Chemistry 2016, 203, 206–216.https://doi.org/10.1016/j.foodchem.2016.02.009

15. Yodmanee, S.; Karrila, T.T.; Pakdeechanuan, P. Physical, chemical and antioxidant properties of pigmented rice grown in Southern Thailand. International Food Research Journal 2011, 18, 901–906.
16. Tester, R.F.; Morrison, W.R. Swelling and gelatinization of cereal starches. I. Effects of amylopectin, amylose, and lipids. Cereal Chemistry 1990, 67, 551–557.
17. 17. Singh, N.; Singh, J.; Kaur, L.; Sodhi, N.S.; Gill, B.S. Morphological, thermal and rheological properties of starches from different botanical sources. Food Chemistry 2003, 81, 219–231.https://doi.org/10.1016/S0308-8146(02)00416-8
18. Patindol, J.; Wang, Y.J. Fine structures and physicochemical properties of starches from chalky and translucent rice kernels. Journal of Agricultural and Food Chemistry 2016, 64, 332–341.https://doi.org/10.1021/acs.jafc.5b05142
19. Luo, Z.; He, X.; Fu, X.; Peng, L.; Gao, Y. Effect of starch fine structure on pasting and retrogradation properties of rice flour. Food Hydrocolloids 2022, 124, 107291.https://doi.org/10.1016/j.foodhyd.2021.107291
20. Khoo, H.E.; Azlan, A.; Tang, S.T.; Lim, S.M. Anthocyanidins and anthocyanins: Colored pigments as food, pharmaceutical ingredients, and potential health benefits. Food & Nutrition Research 2017, 61, 1361779.https://doi.org/10.1080/16546628.2017.1361779
21. Wang, Y.; Zhang, Y.; Xu, L.; Li, X. Antioxidant mechanisms of anthocyanins and their interaction with other phenolic compounds. Trends in Food Science & Technology 2022, 121, 90–102.https://doi.org/10.1016/j.tifs.2022.01.008
22. Zhu, F.; Zhang, H.; Guo, X. Interaction of starch with phenolic compounds: Impact on structure, digestion and functionality. Food Hydrocolloids 2021, 118, 106789.https://doi.org/10.1016/j.foodhyd.2021.106789
23. Chen, Y.; Zhang, Y.; Wang, L.; Li, M. Effects of phenolic–starch interactions on physicochemical properties of rice flour. Carbohydrate Polymers 2022, 276, 118731.https://doi.org/10.1016/j.carbpol.2021.118731
24. Zhu, F. Impact of starch retrogradation on food quality and nutrition. Comprehensive Reviews in Food Science and Food Safety 2021, 20, 193–216.https://doi.org/10.1111/1541-4337.12651
25. Li, C.; Huang, J.; Chen, Y.; Liu, R. Amylose reassociation and gel firmness of rice starch during storage. Food Chemistry 2022, 372, 131258.https://doi.org/10.1016/j.foodchem.2021.131258
26. Zhang, B.; Li, X.; Li, E.; Shi, C. Structural characteristics of rice starch related to thermal and pasting properties. International Journal of Biological Macromolecules 2021, 183, 1005–1014.https://doi.org/10.1016/j.ijbiomac.2021.05.090
27. Li, Y.; Wang, S.; Zhang, J. Formation of amylose–lipid complexes and their effect on starch gelatinization. Food Hydrocolloids 2020, 105, 105756.https://doi.org/10.1016/j.foodhyd. 2020.105756
28. Wang, S.; Li, C.; Copeland, L.; Niu, Q.; Wang, S. Starch retrogradation: A comprehensive review. Food Chemistry 2023, 406, 135042.https://doi.org/10.1016/j.food chem.2022.135042
29. Zhou, Z.; Blanchard, C. Pasting and textural properties of rice flours and starches. Journal of Cereal Science 2020, 95, 103043.https://doi.org/10.1016/j.jcs.2020.103043
30. Wrolstad, R.E. Color and Pigment Analyses in Fruit Products; Agricultural Experiment Station Bulletin 624; Oregon State University: Corvallis, OR, USA, 1976.
31. Tian, Y.; Zhang, H.; Chen, L. Effect of crystalline structure on gelatinization and retrogradation behavior of rice starch. Food Chemistry 2023, 399, 133968.https://doi.org/10.1016/j.foodchem.2022.133968

P - 185

Sustainable Valorization of Pectin from Guava Pulp using Ultrasound-Assisted Extraction

Tem Sasiluksananukul[1,2] and Rajnibhas Sukeaw Samarkradhamrongthai[1,2,3]*

[1]*Department of Food Science and Technology, Faculty of Agro-Industry, Chiang Mai University, Thailand*
[2]*INterdisciplinary and Food product development for wellness Research Unit (INFRU), Chiang Mai University, Chiang Mai 50200 Thailand*
[3]*Division of Product Development Technology, Faculty of Agro-Industry, Chiang Mai University, Thailand*

**Corresponding author E-mail: rajnibhas.s@cmu.ac.th*

Abstract: Fruit and vegetable processing generates significant by-products, which are often discarded or degraded despite their potential bioactivity. Guava pulp (*Psidium guajava* L.) is rich in pectin, a soluble dietary fiber widely used in the food industry and possessing health-promoting properties. This study investigated the extraction of pectin from guava pulp using ultrasound-assisted extraction (UAE), considering different ultrasound amplitudes (20, 30, and 40%) and durations (10, 20, and 30 min). The commercial pectin was also analyzed for physicochemical properties compared to extracted pectin. The extraction was significantly affected by both parameters (amplitude and time). It was found that the extraction at 40% amplitude for 10 min was identified as the optimal condition, yield (6.51 ± 0.84%) was obtained. The obtained pectin showed an esterification value of 85.10 ± 1.72, a methoxyl content of 14.54 ± 0.28, and a galacturonic acid content of 28.29 ± 0.07%, indicating that it was of high purity and suitable for use as a concentrate in beverage products. Principal component analysis (PCA) revealed that the first two components (PC1 and PC2) explained 81.0% of the total variation. The optimal condition at 40% amplitude and 10 min explained 55.99% of the PC1 axis, indicating that the response values in this condition were close together and positively related, namely total dietary fiber (TDF), water holding capacity (WHC), methoxyl content (MeO), esterification value (DE), insoluble dietary fiber (IDF). Furthermore, this optimal extraction condition also explain 25.04% of the PC2 axis, which results indicated that the response values in this condition were close together and positively related along the axis, namely Soluble Dietary Fiber (SDF) and Galacturonic Acid Content (GA). Notably, the process at 40% amplitude for 10 min was strongly associated with water holding capacity (WHC), TDF, SDF, IDF, DE, and MeO, indicating that these functional properties were directly influenced by the extraction conditions. The results of this study demonstrate that UAE is a sustainable and efficient approach for valorizing guava by-products, as it improves both yield and quality while supporting waste reduction and resource sustainability in the food industry.

Keywords: Guava pulp by-products; Ultrasound-assisted extraction; Pectin; Sustainability; Valorization

1. Introduction

Thailand is a major exporter of processed fruits and vegetables, with fruit and processed product exports valued at approximately 84.235 billion baht in 2022. However, processing generates a considerable amount of by-products, many of which are either discarded or used as low-value animal feed. These residues represent an underutilized resource, as fruit and vegetable

peels are rich in nutrients, particularly dietary fiber and pectin, with reported pectin contents ranging from 2.95% to 28.98% (1). Among Thai fruits, guava (*Psidium guajava* L.) has the highest pectin content. Its by-products, primarily pulp and seeds, have been incorporated into fiber-enriched baked goods (2) and fermented to produce vitamin B12-enriched products (3). Moreover, previous studies have indicated that the water-soluble fraction of guava pulp may contain up to ~84% pectin (4), highlighting its potential as a valuable source of functional ingredients. Utilizing guava pulp by-products for pectin extraction therefore presents an opportunity to reduce waste, promote resource efficiency, and support a circular economy (5). Pectin is a versatile biopolymer widely used in the food industry as a gelling agent, stabilizer, and source of dietary fiber with functional health benefits. Ultrasound-assisted extraction (UAE) significantly improves efficiency over conventional methods. This process creates intense shear forces, bubbles that collapse, and localized high temperature/pressure zones, which rupture cell walls, increase mass transfer rates. UAE reduces extraction times from hours to minutes, reduces solvent consumption, lowers energy costs, and typically results in higher yields of high-quality, bioactive compounds (6). Accordingly, this study focused on extracting pectin from guava pulp using UAE, with particular attention to the effects of ultrasonic amplitude and extraction time on yield and pectin characteristics. The findings aim to provide insights into the sustainable utilization of guava by-products and propose practical guidelines for valorizing agricultural residues into value-added food ingredients.

2. Material and methods

2.1 Raw materials and chemicals

Fresh guava (*Psidium guajava L.*) pulp by-products were obtained from Lanna Products company limited, Chiang Mai, Thailand. All chemicals and solvents used in this study were of analytical grade. 2,2-Diphenyl-1-picrylhydrazyl (DPPH) (PubChem CID 57654141; Sigma-Aldrich, Darmstadt, Germany), aluminum chloride (PubChem CID 24564; KemAus, Australia), carbazole (PubChem CID 6854; Sigma-Aldrich, Darmstadt, Germany), commercial pectin powder (Chiangmai Bakermart, Chiang Mai, Thailand), D-galacturonic acid (PubChem CID 439215; Sigma-Aldrich, Darmstadt, Germany), ferric chloride hexahydrate (PubChem CID 16211236; KemAus, Australia), Folin–Ciocalteu reagent (Loba Chemie Pvt. Ltd., India), methanol (PubChem CID 887; Avantor Performance Materials, LLC., Poland), sodium carbonate (PubChem CID 10340; KemAus, Australia), sodium hydroxide (PubChem CID 14798; Loba Chemie Pvt. Ltd., India; RCI Labscan Limited, Bangkok, Thailand), sodium nitrite (PubChem CID 233668193; KemAus, Australia), sodium tetraborate (PubChem CID 10219853; KemAus, Australia), and sulfuric acid (PubChem CID 1118; RCI Labscan Limited, Bangkok, Thailand) were used in this study.

2.2 Guava pulp preparation

Fresh guava fruits were thoroughly washed, peeled, and trimmed prior to juice extraction using a juice extractor (Sharp EJ-150LP, Japan). The residual guava pulp was dried in a hot-air oven at 45 °C for 5 h (Binder GmbH, Germany). After drying, the pulp was milled and passed through a 40-mesh sieve. The obtained guava pulp powder was stored in airtight containers at 25 °C until further analysis.

2.3 Pectin extraction from guava pulp using ultrasound-assisted extraction (UAE)

Pectin was extracted from guava pulp by-products using ultrasound-assisted extraction (UAE) based on a 3^2 factorial design. The study investigated the effects of two primary extraction parameters ultrasonic amplitudes (20, 30, and 40%) and extraction times (10, 20, and 30 min). A solid-to-liquid ratio of 1:15 (w/v) was maintained, utilizing guava pulp powder and a solvent solution as the solid and liquid phases, respectively. Following sonication, the mixture was filtered through Whatman No. 4 filter paper to isolate the pectin-rich extract from the solid residue. The

resulting supernatant was precipitated with ethanol at a ratio of 1:2 (v/v) and stored at 4 °C for 24 h to ensure complete precipitation. The pectin precipitate was subsequently washed twice with ethanol to remove residual impurities. Finally, the extracted pectin was dried in a hot-air oven at 60 °C (Binder, Binder GmbH, Germany) until a constant weight was achieved. Yield recovery was calculated using the following equation 1 :

$$(\%)Yield\ recovery\ = \frac{Dried\ extracted\ pectin\ (g)}{Dried\ powder\ (g)} \times 100$$

2.4 Scanning electron microscopy of pectin from guava pulp

The morphology of the extracted pectin samples was investigated by a field emission scanning electron microscope (JEOLJSM-IT200 InTouchScope, Japan). The samples were sputter coated with gold palladium and investigated at an accelerating voltage of 15.00 kV at various magnifications.

2.5 Water holding capacity (WHC) of pectin from guava pulp

The water holding capacity of the extracted pectin was determined following the method described by Nguyen et al. (7). Briefly, 2 g of sample were weighed and mixed with 30 mL of distilled water. The mixture was allowed to stand at room temperature for 10 min and then centrifuged at 2,000 rpm for 15 min. The supernatant was removed, and the sediment was weighed. The water holding capacity was calculated using the following equation 2 :

$$WHC = \frac{W_2 - W_1}{W_1} \qquad \textbf{(Equation 2)}$$

where W_1 = weight of dietary fiber powder from the sample (g), and W_2 = weight of the water-holding sediment after centrifugation (g).

2.6 Determination of degree of esterification (DE) and methoxyl content of pectin from Guava Pulp

The degree of esterification (DE) of the extracted pectin was determined using the potentiometric titration method described by Pinheiro et al. (8) with slight modifications. Briefly, 0.5 g of dried pectin sample was transferred into a 250 mL flask and dissolved in 100 mL of distilled water. After complete dissolution, 25 mL of 95% ethanol was added to precipitate the pectin, and the mixture was kept under continuous stirring until the pectin was fully dissolved. The solution was titrated with 0.5 M NaOH in the presence of three drops of phenolphthalein, and the volume consumed was recorded as the initial titer (V_1). Subsequently, 10 mL of 0.5 M NaOH was added, and the mixture was shaken vigorously and left under continuous stirring for 15 min to saponify the ester groups of the polymer. Afterwards, 10 mL of 0.5 M HCl was added, and the solution was shaken until the pink color disappeared. Three additional drops of phenolphthalein were added, and the solution was titrated again with 0.5 M NaOH until a faint pink color persisted after vigorous shaking. This volume was recorded as the final titer (V_2).

The degree of esterification was calculated using the following equation 3 :

$$DE(\%) = \frac{V_1}{V_1 + V_2} \times 100 \qquad \textbf{(Equation 3)}$$

where V_1 is the initial titer (free carboxyl groups) and V_2 is the saponification titer (esterified carboxyl groups).

2.7 Determination of moisture content and water activity of pectin from guava Pulp

The moisture content of the pectin samples was determined using the gravimetric method according to AOAC Official Method 991.43 (AOAC, 2020) (9). Approximately 0.5 g of sample was weighed and dried in a hot-air oven at 105 °C until a constant weight was achieved, and the percentage of moisture was calculated from the weight loss during drying. Water activity was measured at 25 °C using a hygrometer (AQUA LAB PRE00061, TE, USA).

2.8 Determination of galacturonic acid (GalA) of pectin from guava pulp

The galacturonic acid (GalA) content was determined following the method of (10) with modifications. Briefly, 0.1 g of extracted pectin from guava pulp was dissolved in 0.05 M sodium hydroxide (NaOH) solution, and the volume was adjusted to 50 ml. The mixture was stirred with a glass rod for 15 min to ensure complete dissolution. A 10 mL aliquot of this solution was diluted to 100 mL with distilled water. From the diluted solution, 2 mL was transferred into a test tube, followed by the addition of 1 mL of 1% carbazole solution and 12 mL of 95% sulfuric acid (H_2SO_4). The mixture was shaken thoroughly and allowed to stand at room temperature for 25 min. Absorbance was measured at 525 nm using a spectrophotometer, and the GalA content was quantified based on a calibration curve prepared from galacturonic acid standards.

2.9 Dietary fiber of pectin from guava pulp

Total dietary fiber (TDF), insoluble dietary fiber (IDF), and soluble dietary fiber (SDF) contents were determined using the enzymatic gravimetric method according to AOAC (2019) (11). All measurements were performed in triplicate.

2.10 Statistical Analysis

All experiments were conducted in triplicate, and the results were expressed as mean ± standard deviation (SD). Statistical analyses were performed using SPSS software version 17 (SPSS Inc., Chicago, IL, USA). One-way analysis of variance (ANOVA) was used to determine significant differences among treatments, and mean comparisons were performed using Duncan's multiple range test. Statistical significance was set at a confidence level of 95% ($p < 0.05$). Multivariate analysis was performed to further elucidate the relationships among the studied variables. Principal component analysis (PCA), together with qualitative compound analysis, was conducted using SPSS to investigate underlying patterns and variations within the experimental dataset.

3. Results and discussion

3.1 Yield recovery of extracted pectin from guava pulp

The pectin yield obtained from guava pulp by-products ranged from 1.10 ± 0.14% to 7.46 ± 0.96%. The highest extraction yield was achieved at 30% amplitude for 30 min, demonstrating a significant synergistic interaction ($p = 0.001$) between ultrasonic intensity and extraction time. This finding indicates that moderate cavitation provides sufficient mechanical energy to disrupt the rigid guava cell wall without inducing macromolecular shearing. As reported by Mazurek-Hołys et al. (12), acoustic cavitation enhances solvent diffusivity, facilitating deeper penetration into the plant matrix. In this study, the moderate amplitude (30%) likely optimized the sponge effect a mechanism where ultrasonic waves create alternating compression and expansion, effectively pumping the solvent into the guava pulp tissues and washing out the pectin (13) . In contrast, the lower yields observed at 10 min across all amplitudes suggest a kinetic limitation, where insufficient exposure time restricts the complete release of pectin from the cell wall complex. Although higher amplitudes generally promote increased yield, excessive ultrasonic intensity may cause pectin degradation due to hydroxyl radical formation or localized thermal

effects (4). Overall, these results highlight the importance of optimizing UAE parameters to maximize recovery while maintaining the structural integrity of the biopolymer.

3.2 Morphology of extracted pectin from guava pulp

The morphological characteristics of extracted pectin from guava pulp by-products using ultrasound-assisted extraction (UAE) were examined by scanning electron microscopy (SEM) to elucidate structural changes induced by different ultrasonic amplitudes and extraction times. The control pectin obtained from commercial pectin (a) exhibited a relatively compact, plate-like morphology with a smooth and continuous surface, indicating minimal structural disruption during the extraction process, which is typical of conventionally extracted pectin (14). In contrast, pectin samples obtained by UAE exhibited pronounced morphological alterations, characterized by fragmented, irregular, and rough surfaces, consistent with ultrasound-induced mechanical disruption reported in previous studies.

At a lower ultrasonic amplitude of 20% (b–d), the pectin particles remained comparatively large but showed early signs of surface erosion and microcrack formation. These features indicate partial disruption of the cell wall matrix, which is consistent with moderate cavitation energy that is insufficient to completely disintegrate the plant structure (13). As the ultrasonic amplitude increased to 40%, the pectin structure became increasingly disintegrated into smaller fragments with a more porous and uneven surface, This transition in morphology is driven by micro-jetting and shock waves resulting from the asymmetrical collapse of cavitation bubbles near the solid surface of the guava pulp (15). These intense local shear forces not only strip away the outer layers of the cell wall but also increase the internal surface area, allowing for the liberation of tightly bound pectin fractions.

These morphological changes showed a strong correlation with the physicochemical properties of the extracted pectin. Higher ultrasonic amplitudes resulted in increased extraction yield and total dietary fiber content, reflecting more efficient breakdown of the guava pulp matrix and enhanced mass transfer, as previously reported for UAE-treated polysaccharides (15). Furthermore, samples extracted at 40% amplitude (h–j) exhibited significantly higher degrees of esterification and methoxyl content, suggesting that intense ultrasonication effectively liberated high-molecular-weight pectin polymers from the cell wall complex prior to extensive depolymerization. The increased porosity and surface roughness observed in these samples also contributed to a higher water-holding capacity (WHC). This is because the enlarged surface area and capillary-like structures created by cavitation provide more active sites for water molecule entrapment through hydrogen bonding with the hydroxyl groups of the pectin chains, in agreement with earlier findings on the relationship between pectin microstructure and hydration properties.

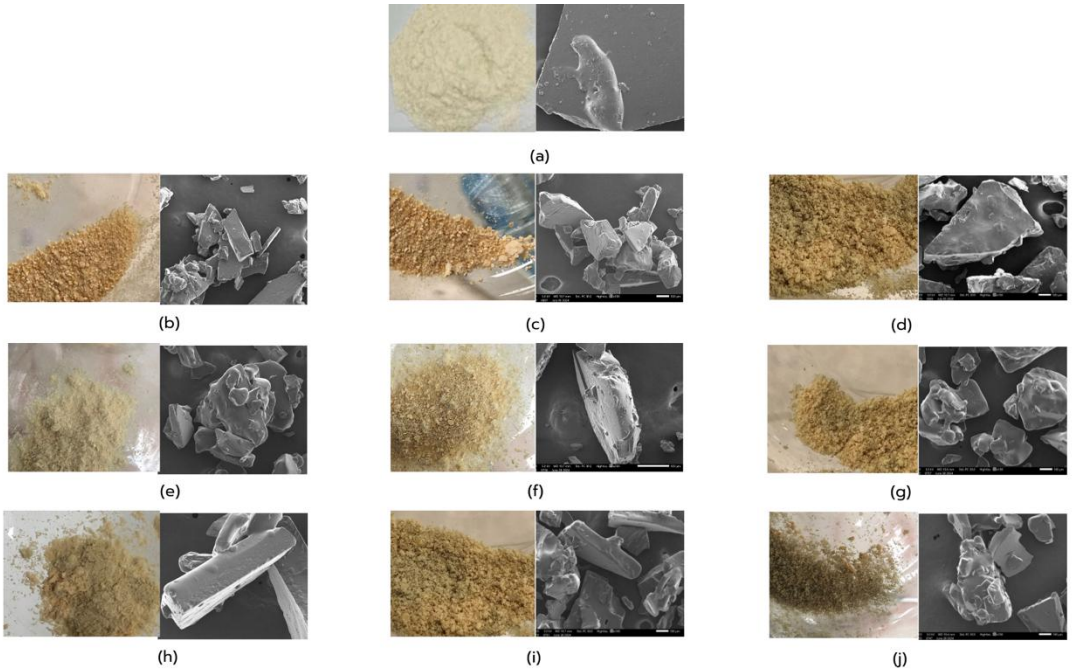

Figure 1. Physical appearance and SEM micrograph of extracted pectin from guava pulp using UAE : (a) commercial pectin (b) extracted pectin using UAE 10 min at amplitude 20% (c) extracted pectin using UAE 20 min at amplitude 20% (d) extracted pectin using UAE 30 min at amplitude 20% (e) extracted pectin using UAE 10 min at amplitude 30% (f) extracted pectin using UAE 20 min at amplitude 30% (g) extracted pectin using UAE 30 min at amplitude 30% (h) extracted pectin using UAE 10 min at amplitude 40% (i) extracted pectin using UAE 20 min at amplitude 40% (j) extracted pectin using UAE 30 min at amplitude 40%

3.3 Water holding capacity of extracted pectin from guava pulp

The WHC of guava pectin ranged from 3.31 to 4.85 g/g, with the highest value observed at 40% amplitude for 10 min. Statistical analysis confirmed that amplitude was the primary driver of WHC ($p < 0.001$), likely due to the intense mechanical effects of cavitation which increase the porosity of the pectin molecules. The physical structure and the availability of hydrophilic sites, such as carboxyl and hydroxyl groups, are critical for water binding. The high WHC at 40% amplitude suggests that stronger ultrasonic waves expose more of these functional groups, enhancing the pectin's ability to trap water within its fibrous network. This property is highly desirable in food applications for improving texture and preventing syneresis in gelled products (1)

3.4 Degree of esterification of extracted pectin from guava pulp

The DE values identified the extracted pectin as high-methoxyl (HM), with a peak of 85.10% at 40% amplitude and 10 min. Amplitude significantly influenced DE ($p < 0.001$), whereas extraction time did not, suggesting that the initial shock of cavitation is more decisive in releasing esterified pectin than prolonged exposure (16) state that pectin with a DE above 50% is categorized as HM pectin, which is valued for its rapid gelling properties in high-sugar and acidic conditions. The retention of a high DE despite the use of ultrasound indicates that the UAE conditions were mild enough to avoid significant de-esterification of the polygalacturonic acid chain. This makes guava pulp a premium source for industrial gelling agents (2).

3.5 Moisture content and water activity of extracted pectin from guava pulp

No significant differences ($p > 0.05$) were detected in moisture content or water activity among pectin samples extracted under different ultrasound-assisted extraction (UAE) conditions, indicating that variations in ultrasonic amplitude, extraction time, and their interaction had no measurable influence on moisture-related properties. This result suggests that the UAE process, together with the applied drying procedure, did not modify the intrinsic water-binding behavior of the pectin. The consistently low moisture content and water activity across all treatments are critical for ensuring product stability, as they limit microbial proliferation and reduce the likelihood of powder caking during storage (17). The lack of treatment effects further implies that any structural modifications induced by ultrasonic cavitation were insufficient to alter residual or free water retention within the pectin matrix (18). These findings demonstrate that UAE parameters within the investigated range did not compromise the moisture stability of the extracted pectin, supporting the reliability and reproducibility of the extraction process for producing shelf-stable pectin powders suitable for downstream applications.

3.6 Galacturonic acid content (GalA) of extracted pectin from guava pulp

Galacturonic acid (GalA) content is widely used as an indicator of pectin purity and is directly associated with its gelling capacity and functional performance in food systems (19). In this study, the highest GalA content was obtained at 20% ultrasonic amplitude for 30 min (29.16 mg/g). Although statistically significant differences among treatments were observed ($p < 0.001$), the overall variation in GalA content remained relatively narrow. This suggests that while higher ultrasonic amplitudes (40%) are effective in enhancing extraction yield and dietary fiber solubilization, lower amplitudes may be more selective in extracting the GalA rich homogalacturonan backbone, This selectivity at lower energy levels likely minimizes the concurrent cleavage of non-pectic cell wall polysaccharides (such as hemicellulose or cellulose fragments), which at higher intensities might dilute the GalA Concentration in the final extract (20). The relatively stable GalA content across UAE conditions further indicates that the ultrasonic treatment did not cause substantial degradation of the pectin backbone. This observation agrees with previous reports demonstrating that properly controlled ultrasound-assisted extraction enhances mass transfer without significantly disrupting the galacturonan chain structure . The preservation of GalA levels even at 40% amplitude suggests that the acoustic cavitation energy was primarily utilized for physical cell wall disruption rather than the hydrolytic cleavage of glycosidic bonds Withing the pectin polymer (21). Moreover, the GalA values obtained in this study fall within the range reported for functional pectin suitable for gel formation and stabilization applications . These findings confirm that the UAE process successfully isolated the pectin fraction from guava pulp by-products while preserving structural features essential for gelling behavior, thereby supporting its potential application as a functional food additive (16).

3.7 Dietary fiber of extracted pectin from guava pulp

Dietary fiber fractions (TDF, SDF, and IDF) were significantly influenced by the interaction of amplitude and time ($p < 0.001$) as shown in Table 1. The contents of total dietary fiber (TDF), soluble dietary fiber (SDF), and insoluble dietary fiber (IDF) in the extracted pectin were significantly influenced by ultrasonic amplitude, extraction time, and their interaction ($p < 0.001$), as shown in Table 1. The highest TDF (7.87 ± 0.12 g/100 g) and SDF (1.88 ± 0.009 g/100 g) were obtained at 40% amplitude for 20 min, while the lowest TDF (3.60 ± 0.02 g/100 g) was observed at 30% amplitude for 20 min. In contrast, IDF reached its maximum value (9.58 ± 0.11 g/100 g) at 40% amplitude for 30 min, This shift in fiber composition where SDF peaks at 20 min but IDF continues to increase at 30 min suggests a complex dynamic between solubilization and re-aggregation or over-extraction of rigid structural components. The peak in SDF at 20 min

indicates the optimal window for releasing pectin and other soluble polysaccharides from the cell wall matrix. However, prolonged exposure to high-intensity ultrasound (30 min) may trigger the release of more recalcitrant, insoluble lignocellulosic fragments that were previously bound, thereby increasing the IDF fraction at the expense of the overall purity of The soluble pectin extract (20). Overall, the increase in dietary fiber content at 40% amplitude highlights the efficiency of ultrasound-assisted extraction (UAE) in enhancing cell wall disruption and pectin solubilization, thereby improving fiber recovery and valorizing guava residues into a nutritionally dense ingredient that provides both functional soluble pectin and physiological insoluble fiber benefits (22).

Table 1. Physicochemical properties of extracted pectin from guava pulp

Amplitude	Time	Yield recovery (%)	Water holding capacity	Degree of esterification (DE)(%)	Methoxyl content (%)	Galacturonic acid content (mg/g)	Total dietary fiber (g/100g)	Soluble dietary fiber (g/100g)	Insoluble dietary fiber (g/100g)
20	10	3.94 ± 0.51^{c}	3.48±0.02^{a}	22.5±3.53^{a}	3.67±0.40^{a}	27.85±0.11^{d}	3.90±0.01^{b}	0.24±0.01^{b}	3.66±0.01^{b}
	20	3.32 ± 0.43^{bc}	3.48±0.06^{a}	27.5±3.53^{a}	4.48±0.40^{a}	27.36±0.02^{b}	5.26±0.05^{d}	0.68±0.01^{e}	4.58±0.05^{d}
	30	5.59 ± 0.72^{d}	3.72±0.08^{ab}	29.16±5.89^{a}	4.75±0.67^{a}	27.16±0.01^{a}	5.67±0.04^{e}	0.43±0.01^{d}	5.24±0.04^{e}
30	10	1.10 ± 0.14^{a}	3.60±0.09^{ab}	36.67±4.71^{a}	5.98±0.54^{a}	28.43±0.01^{g}	6.93±0.03^{f}	0.36±0.01^{c}	6.57±0.03^{h}
	20	1.92 ± 0.25^{ab}	3.35±0.03^{a}	16.67±23.57^{a}	2.71±2.71^{a}	28.33±0.04^{fg}	3.60±0.02^{a}	0.77±0.01^{g}	2.83±0.01^{a}
	30	7.46 ± 0.96^{e}	3.31±0.07^{a}	29.16±5.89^{a}	4.75±0.67^{a}	27.2±0.01^{a}	4.02±0.08^{bc}	0.12±0.01^{a}	3.90±0.08^{c}
40	10	6.51 ± 0.84^{de}	4.85±0.65^{c}	85.10±1.72^{b}	14.54±0.19^{b}	28.29±0.07^{fg}	7.07±0.03^{f}	0.73±0.01^{f}	6.34±0.03^{g}
	20	6.12 ± 0.79^{de}	4.18±0.33^{b}	79.51±2.45^{b}	12.97±0.28^{b}	27.25±0.01^{ab}	7.87±0.12^{g}	1.88±0.01^{h}	5.98±0.11^{f}
	30	6.70 ± 0.86^{de}	4.19±0.25^{b}	75.07±1.97^{b}	12.25±0.22^{b}	27.67±0.01^{c}	4.11±0.02^{c}	0.44±0.01^{d}	3.67±0.02^{b}
Main effect (Amplitude)		<0.001	<0.001	<0.001	<0.001	<0.001	<0.001	<0.001	<0.001
Main effect (Time)		<0.001	0.161	0.309	0.309	<0.001	<0.001	<0.001	<0.001
Interaction (Amplitude * Time)		0.001	0.276	0.28	<0.001	<0.001	<0.001	<0.001	<0.001

Note : The different superscript lowercase letters (a–d) within the same column indicated significant different ($p < .05$)

3.8 Correlation of extract pectin properties using principal component analysis (PCA)

Principal component analysis (PCA) effectively summarized the relationships among physicochemical properties of pectin samples, with the first two principal components explaining 81.0% of the total variance (PC1 = 55.9% and PC2 = 25.1%), indicating a strong representation of the dataset (Figure 2). Most treatments (TRT) were clustered closely, suggesting similar overall properties, whereas TRT5 and TRT6 were clearly separated from the main group, reflecting distinct physicochemical characteristics, which was consistent with the variations observed in Table 1.

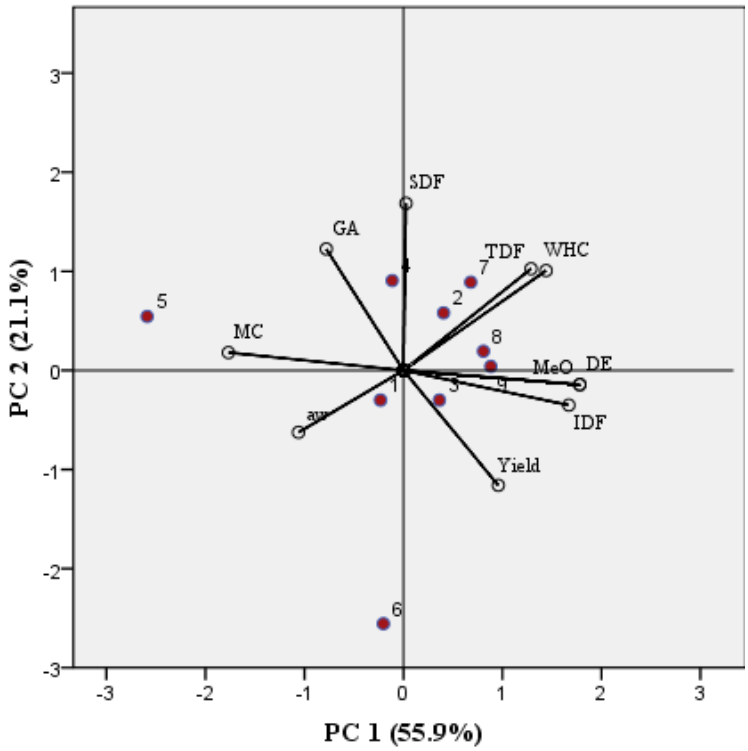

Figure 2. Principal component analysis (PCA) was performed using data related to extracted pectin and its physicochemical : (1) extracted pectin using UAE 10 min at amplitude 20% (2) extracted pectin using UAE 20 min at amplitude 20% (3) extracted pectin using UAE 30 min at amplitude 20% (4) extracted pectin using UAE 10 min at amplitude 30% (5) extracted pectin using UAE 20 min at amplitude 30% (6) extracted pectin using UAE 30 min at amplitude 30% (7) extracted pectin using UAE 10 min at amplitude 40% (8) extracted pectin using UAE 20 min at amplitude 40% (9) extracted pectin using UAE 30 min at amplitude 40%

PC1 was primarily associated with functional and structural parameters, including water holding capacity (WHC), degree of esterification (DE), methoxyl content (MeO), total dietary fiber (TDF), insoluble dietary fiber (IDF), and yield, all of which were positively loaded along this component. This pattern agrees well with the correlation analysis, where WHC showed strong positive correlations with DE and MeO ($r \approx 0.84$), and TDF was highly correlated with IDF ($r = 0.95$) (Figure 3), confirming that structural modification and fiber composition were the dominant contributors to functional performance. In contrast, moisture content (MC) and water activity (aw) were positioned oppositely, consistent with their negative correlations with WHC, DE, and MeO, indicating reduced free water availability as structural binding increased. Notably, samples extracted at 40% amplitude for 10 min (TRT7) were located close to WHC, TDF, SDF, IDF, DE, and MeO vectors, demonstrating a strong association between these response variables and the extraction conditions. This suggests that higher ultrasonic intensity combined with shorter

extraction time promoted molecular disruption and chemical substitution, enhancing water-holding capacity and dietary fiber functionality. Overall, the PCA results strongly support the correlation analysis, highlighting that extraction-induced structural changes govern the functional and compositional properties of pectin.

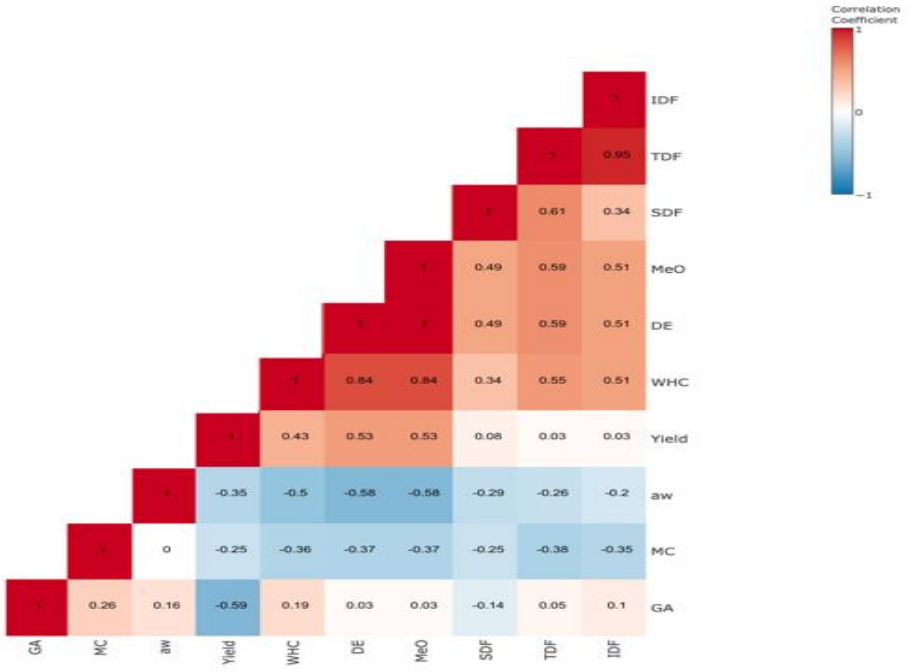

Figure 3. Correlation matrix using heat map analysis demonstrated pearson correlation coefficients within physicochemical properties of extracted pectin from guava pulp.

4. Conclusion

In conclusion, this study demonstrated that ultrasound-assisted extraction (UAE) is an effective and sustainable technique for extracting pectin from guava pulp by-products. Both ultrasound amplitude and extraction time significantly influenced pectin yield and functional properties. The optimal extraction condition was identified at 40% amplitude for 10 min, which produced favorable pectin yield and superior physicochemical characteristics, including high degree of esterification, methoxyl content, and galacturonic acid content. Multivariate analysis using principal component analysis (PCA) further confirmed that this optimal condition was strongly associated with enhanced functional properties such as water holding capacity, total dietary fiber, soluble and insoluble dietary fiber, methoxyl content, and degree of esterification. These results indicate that the extraction parameters directly affect the structural and functional quality of pectin. Overall, the findings highlight the potential of UAE as a green and efficient extraction method for valorizing guava processing by-products. The high-quality pectin obtained under optimized conditions shows promise for application as a functional ingredient in beverage products, while also contributing to waste reduction and improved resource sustainability in the food industry.

5. Acknowledgment

This research was partially supported by Chiang Mai University, Grant number RG1152567000017. The authors would also like to thank the Faculty of Agro-Industry, Chiang Mai University, Thailand, for supporting laboratory facilities and instruments for this research.

6. References

1. Sakkaekaew K, Pasukamonset P, Siriwong N. Effects of Fat Replacement by Pectin from Dragon Fruit Peels on Physicochemical Properties of Salad Dressing.
2. Thongsombat W, Sirichote A, Chanthachum S. The production of guava juice fortified with dietary fiber. Songklanakarin J Sci Technol. 2007;29(Suppl 1):187-96.
3. Palachum W, Choorit W, Manurakchinakorn S, Chisti Y. Guava pulp fermentation and processing to a vitamin B12-enriched product. Journal of Food Processing and Preservation. 2020;44(8):e14566.
4. Wu Y, Eskin N, Cui W, Pokharel B. Emulsifying properties of water soluble yellow mustard mucilage: A comparative study with gum Arabic and citrus pectin. Food Hydrocolloids. 2015;47:191-6.
5. Tsirigotis-Maniecka M, Górska E, Mazurek-Hołys A, Pawlaczyk-Graja I. Unlocking the potential of food waste: a review of multifunctional pectins. Polymers. 2024;16(18):2670.
6. Babaei AB, Dara A, zokaeiyan S, Mallakian S, Beig babaei k. Comparison on efficiency of Bioactive Compound Extraction from Saffron via Ultrasonic-Assisted Extraction and Maceration Methods. Applied Food Research. 2026:101702.
7. Nguyen DQ, Mounir S, Allaf K. Functional Properties of Water Holding Capacity, Oil Holding Capacity, Wettability, and Sedimentation of Swell-Dried Soybean Powder. 2015;3:402-12.
8. Pinheiro EsR, Silva IMDA, Gonzaga LV, Amante ER, Teófilo RF, Ferreira MMC, et al. Optimization of extraction of high-ester pectin from passion fruit peel (Passiflora edulis flavicarpa) with citric acid by using response surface methodology. Bioresource Technology. 2008;99(13):5561-6.
9. AOAC, editor Official methods of analysis. AOAC International; 2020: Association of Official Analytical Chemists.
10. Kamal MM, Akhtaruzzaman M, Sharmin T, Rahman M, Mondal SC. Optimization of extraction parameters for pectin from guava pomace using response surface methodology. Journal of Agriculture and Food Research. 2023;11:100530.
11. AOAC. A, editor Official Methods of Analysis of the AOAC. International; 1990: Association of Official Analytical Chemist International Washington, DC.
12. Mazurek-Hołys A, Górska E, Tsirigotis-Maniecka M, Zoumpanioti M, Bleha R, Pawlaczyk-Graja I. Eco-Friendly Recovery of Homogalacturonan-Rich Pectin from Flaxseed Cake via NADES Extraction. Polymers. 2025;17(18):2532.
13. Chemat F, Rombaut N, Sicaire A-G, Meullemiestre A, Fabiano-Tixier A-S, Abert-Vian M. Ultrasound assisted extraction of food and natural products. Mechanisms, techniques, combinations, protocols and applications. A review. Ultrasonics sonochemistry. 2017;34:540-60.
14. Voragen AG, Coenen G-J, Verhoef RP, Schols HA. Pectin, a versatile polysaccharide present in plant cell walls. Structural chemistry. 2009;20(2):263-75.
15. Xu Y, Zhang L, Bailina Y, Ge Z, Ding T, Ye X, et al. Effects of ultrasound and/or heating on the extraction of pectin from grapefruit peel. Journal of Food Engineering. 2014;126:72-81.
16. Chan S-Y, Choo W-S. Effect of extraction conditions on the yield and chemical properties of pectin from cocoa husks. Food Chemistry. 2013;141(4):3752-8.
17. BeMiller JN. Carbohydrate chemistry for food scientists: Elsevier; 2018.
18. Grassino ANB, Mladen Vikić-Topić, Dražen Roca, Sunčica Dent, Maja Brnčić, Suzana Rimac. Ultrasound assisted extraction and characterization of pectin from tomato waste. Food chemistry. 2016;198:93-100.
19. Stephen AM, Phillips GO. Food polysaccharides and their applications: CRC press; 2016.

20. Gerschenson LN, Fissore EN, Rojas AM, Idrovo Encalada AM, Zukowski EF, Higuera Coelho RA. Pectins obtained by ultrasound from agroindustrial by-products. Food Hydrocolloids. 2021;118:106799.
21. Wang, Cao Y, Li X, Nian Q, You R, Su K, et al. Effect of freezing-induced pectin degradation on the texture stability of strawberry. Food Chemistry. 2025:146406.
22. Singh J, Sandhu HK, Panesar PS. Valorization of Guava Fruit Waste and By-Products. Biorefining Fruit Waste: Technological Advances in a Circular Bioeconomy. 2025:193-227.

P - 190

Analysis of Physicochemical Properties and Functional Properties of Six Banana (*Musa* sp.) Varieties and their Application as Ingredient for Energy Gel

Arriya Tadtan[1], Napatsawan Chaimahawan[1], Gerry Renaldi[1], Natthanicha Banpacha[1], Phatthawin Setthaya[12], Rajnibhas Sukeaw Samakradhamrongthai[1,2]*

[1]*Department of Food Science and Technology, Division of Food Innovation Design and Development, Faculty of Agro-Industry, Chiang Mai University, Chiang Mai 50100 Thailand*
[2]*INterdisciplinary and Food product development for wellness Research Unit (INFRU), Chiang Mai University, Chiang Mai 50200 Thailand*
[3]*Division of Product Development Technology, Faculty of Agro-Industry, Chiang Mai University, Chiang Mai 50100 Thailand*

**Corresponding author E-mail: rajnibhas.s@cmu.ac.th*

Abstract: Banana (*Musa* sp.) is a widely cultivated tropical fruit valued for its nutritional richness and functional potential, but its high perishability limits its applications. Converting bananas into flour extends their shelf life and makes it a versatile ingredient for developing functional foods. Beyond its role as a gluten-free flour substitute, banana flour shows promise in innovative applications such as energy gels. This study analyzed physicochemical and functional properties of flours from six Thai banana varieties: "Kluai Khai (KK)", "Kluai Hak Muk (HM)", "Kluai Leb Mue Nang (LMN)", "Kluai Hin (KH)", "Kluai Hom Thong (HT)", and "Kluai Nam Wa (NW)". The study showed that except the ash content, all measured properties were significant (p <0.05) different between varieties. The moisture content of the flours was ranged from 5.4–7.4%, protein 2.12–5.58%, fat 0.09–0.41%, crude fiber 1.27–4.38%, and total carbohydrates 74.82–85.94%. Functional properties varied, with water absorption capacity of 1.00–1.75 g/g, water solubility index of 0.20–0.40 g/g, and swelling power of 6.89–9.40 g/g. GI ranged from 55.01 - 59.59, glucose digested from 2752.67 - 3572.33 mg/dL, and resistant starch (RS) content from 6.6 - 31.06 g/100 g. The Principal Component Analysis (PCA) showed 69.01% of total variance, exhibited high correlation between KK with the protein content, and the HM with the RS and GI value (42.31% of PC2). The prototype of energy gel from KK and HM flour revealed the necessity to increase the sweetness and mouthfeel from the appropriateness of sensory attributes level using Just-About-Right (JAR) analysis, altogether with the preference rating score in range of like slightly to like moderately (6.4–7.2). Significant variations among varieties indicate that varieties and chemical composition affect flour nutritional value, functionality and digestibility. The findings from this study suggested that KK and HM flours can be used as ingredients for energy gel and demonstrated potentials as carbohydrate sources which capable of conveying and sustained energy release for endurance sports and training.

Keywords: Banana flour; Nutritional properties; Glycemic index; Resistant starch; Energy gel

1. Introduction

Banana (*Musa* sp.), belonging to the genus Musa in the family Musaceae, order Scitamineae, is the fourth most important food crop in the world after rice, wheat, and corn (1, 2). It is cultivated in tropical and subtropical regions across more than 130 countries, with Asia being the largest producer, contributing 54.4% of global production (3). Most edible banana cultivars are allopolyploid triploids with genome constitutions of AAA (dessert bananas), AAB (plantains),

and ABB (cooking bananas). In Thailand, banana production reached 1.36 million tons in 2020 (2).

As a climacteric fruit, bananas have a high respiration rate, making them unsuitable for long-term storage and often leading to substantial post-harvest losses (1). Converting bananas into flour offers an efficient means of extending shelf life while preserving their original flavor and nutritional quality. Banana flour is rich in resistant starch, dietary fiber, and potassium, which enhances its value as a functional food ingredient with wide-ranging applications (4). It also serves as an excellent, cost-effective gluten-free alternative to wheat flour, improving the nutritional and functional attributes of gluten-free products without compromising consumer acceptability (5). Due to these characteristics, banana flour shows great potential for incorporation into various food formulations (5, 6).

Carbohydrate-based energy supplements, such as energy gels, are commonly preferred by athletes and physically active individuals over natural food sources like whole bananas because they are more portable, convenient, and easier to consume during exercise (7). However, integrating banana flour into such products offers a promising strategy to combine functionality with practicality. The presence of resistant starch and slowly digestible carbohydrates can contribute to a sustained energy release, supporting endurance performance while delivering additional nutritional benefits beyond conventional carbohydrate gels.

This study analyzed flours from six Thai banana varieties such as Kluai Khai (KK), Kluai Hak Muk (HM), Kluai Leb Mue Nang (LMN), Kluai Hin (KH), Kluai Hom Thong (HT), and Kluai Nam Wa (NW) to assess their proximate composition, sugar profile, functional properties (water absorption capacity, water solubility index, and swelling power), and in vitro glycemic response. In addition, the chosen flours were utilized further in the production of energy gel prototypes. The results aim to determine the most suitable varieties for use in functional food applications, particularly energy gel.

2. Materials and Methods

2.1 Materials

Six varieties of a stage-6 (a full yellow peel with no brown spots) ripe cooking bananas (*Musa* spp.), namely, Kluai Khai (KK) were obtained from Khlong Khlung district, Kamphaeng Phet, Thailand , Kluai Hak Muk (HM) were obtained from Thayang district, Phetchaburi, Thailand, Kluai Leb Mue Nang (LMN) were obtained from Khlong Luang District, Pathum Thani, Thailand, Kluai Hin (KH) were obtained from Mueang Songkhla district, Songkhla, Thailand, Kluai Hom Thong (HT), and Kluai Nam Wa (NW), were obtained from local market in Chiang Mai, Thailand. The ripe bananas were peeled and sliced into thin slices less than 5 mm thick using a stainless knife. The sliced bananas were freeze dried using a freeze dryer. The dried banana slices were ground 2–3 times by using a grinder and sieved with a 100-mesh sieve. Then, the banana flours were collected, packed in a vacuum aluminum pack, and stored at room temperature for further analysis. All the chemicals used were of reagent grade.

2.2 Polarized light microscopy

The morphology and birefringence of six banana flours were observed using a polarizing optical microscope (Nikon, model Eclipse Ci-POL, Tokyo, Japan) equipped with a digital camera.

2.3 Proximate composition

Proximate composition of the banana flour (moisture, protein, fat, ash, crude fiber, and total carbohydrate) was measured according to the AOAC methods (8). And values were expressed as percentages on a dried basis.

2.4 Functional properties

2.4.1 Water Absorption Capacity (WAC)

The WAC of GBF was determined using the method described by Gadhave et al. (9), with some modifications. Precisely, 1 g flour sample was weighed into 15 mL centrifuge tubes followed

by the addition of 10 mL distilled water. Thereafter, they were centrifuged at 4000 rpm for 15 min at 25 °C. The WAC was expressed as mL of water absorbed per gram of flour.

2.4.2. Water Solubility Index (WSI) and Swelling Power (SP)

The water solubility index and swelling power were determined following the method detailed by Gadhave et al. (9). Banana flour (0.2 g) was mixed with distilled water (5 mL) for 30 s using a vortex. After that, the mixture was heated at 90 °C for 30 min, followed by cooling and centrifugation at 4000 rpm for 15 min. The supernatant was evaporated at 105 °C for 16 h in an oven. The solubility index was calculated as the ratio of the mass of dried supernatant to the mass of the flour expressed in percentage (g/100 g DW). After centrifugation, the filtrate was also weighed to obtain the swelling power.

2.5 Sugar content

The sucrose and total sugar content was done according to the titrimetric method described by Lane and Eynon (10).

2.6 Glycemic index, in vitro starch digestion, and resistant starch

The glycemic index analysis was done based on the modified method of Liang, Tu, Fu, Wang, & Sheng (11). Banana flour (0.25 g) was incubated in 30 mL distilled water at 37 °C for 30 min. The pH was adjusted to 2.5 using 1 M HCl, followed by the addition of 0.8 mL 2% pepsin (≥ 2,500 units/mg). Gastric digestion was simulated with constant stirring (130 rpm) for 30 min. To initiate the intestinal phase, the solution's pH was adjusted to 6.2 with 1 mL 1 M NaHCO3, then 5 mL of a porcine pancreatin and amyloglucosidase (AMG) mixture (v:v = 1:1) was added, reaching a final volume of 55 mL. Aliquots (1.0 mL) were collected at 0, 10, 20, 60, 120, and 180 min, terminated with 4 mL absolute ethanol, and centrifuged at 3000 rpm for 10 min. Glucose content in the supernatant (0.1 mL) was was taken to measure the amount of glucose by a glucose oxidase–peroxidase (GOPOD) kit. A standard reference was created by taking 0.25 g of white bread.

In vitro starch digestion analysis was done based on the modified method of Monro & Mishra (12). was mixed with 30 mL water, 1.0 mL 1 M HCl, and 1 mL 10% pepsin (in 0.05 M HCl-KCl). The intestinal phase was then initiated by adjusting the pH to 6.3 using 2 mL 1 M NaHCO3 and 5 mL 0.2 M Na-maleate buffer, before bringing the total volume to 53 mL with distilled water.Intestinal digestion and carbohydrate monitoring were initiated by adding 0.1 mL amyloglucosidase (Megazyme, E-AMGDF, Megazyme, Wicklow, Ireland) and 1.0 mL 1% pancreatin (Sigma-Aldrich, P-7545, 4 × USP, Merck Life Science, Auckland, New Zealand) in maleate buffer. The mixture was then incubated in digestion pots at 37 °C with constant stirring at 130 rpm. Samples (0.5 mL) were removed to boiling water The mixture was incubated for 3 hrs, during which the glucose concentration in the digesta was measured with Accu-Check Performa glucometer at specific periods (0, 10, 20, 40, 60, 120 and 180 min). during which the glucose concentration in the digesta was measured with Accusure 582 Blood glucometer (13).

Resistant starch content was quantified using a Megazyme RS assay kit (Megazyme International Ireland Ltd., Bray, Ireland) described in Rahaman et al. (14) with minor modifications. Pancreatic α-amylase (10 mg/mL) and amyloglucosidase (3 U/mL) were added to 25 mg of banana flour and incubated at 37 °C for 16 h while shaking at 200 rpm. The reaction stopped with an equal volume of absolute ethanol, and the RS pellet was recovered by centrifugation at 3000 rpm for 10 min. The pellet was washed twice with 50% ethanol (v/v), suspended in 0.5 mL of 2 M KOH, and stirred in an ice bath for 20 min After adding 2 mL of 1.2 M sodium acetate buffer (pH 3.8) and 0.025 mL of amyloglucosidase (300 U/mL), the mixture was vortexed and incubated at 50 °C for 30 min. The supernatant was collected after centrifugation, and 0.025 mL aliquots were mixed with 0.75 mL GOPOD reagent and incubated for 20 min at 50 °C. Absorbance was measured at 510 nm, and the RS content was calculated according to the manufacturer's protocol.

2.7 Formulation of energy gel from banana flour

2.7.1 Preparation of energy gel from banana flour

The prototype of the energy gel from banana flour was made according to Seow et al. (15). A dry mixture was prepared by thoroughly mixing Kluai Khai (KK) flour (45%), Kluai Hak Muk (HM) flour (45%), and maltodextrin (9%), The hydrocolloid blend consisted of gellan gum (0.7%) and xanthan gum (0.3%) was separately prepared and then added to the dry mixture. This combined dry mixture was then gradually dispersed in water under continuous stirring to create a homogeneous slurry with a total solid content of 8 g per 100 mL of water. The prepared slurry was subsequently transferred to a double-jacketed steam kettle (double boiler) and subjected to a controlled heating process (approx. 90−95 °C) for a defined period to induce starch gelatinization of the banana flour and full hydration of the hydrocolloids. Immediately following heating, the hot mixture was hot filled into pre-sterilized packaging (approx. 15g/bag) and hermetically sealed. The final edible gel product was then formed by allowing the sealed packages to cool and gel at room temperature (approx. 25 °C).

2.7.2 Sensory evaluation

The prototype of the energy gel was subjected to Just-About-Right (JAR) analysis and sensory evaluation (n = 120), evaluated by untrained panelists recruited around Chiang Mai municipality, Thailand, with the age range was 15-40 years old that do daily exercise, using a 9-point hedonic scale, ranging from 9 = “like extremely” to 1 = “dislike extremely” (Meilgaard, Civille, & Carr, 2007). The ethical approval approved by the Office of Human Research Ethics Committee, Chiang Mai University (Approval No: CMUREC No 66/046) and conducted following the guidelines provided in the Helsinki Declaration. All participants had to sign a permission form and give written consent before the evaluation. The suitability of 4 sensory attributes (banana aroma, sweetness, mouthfeel, and swallowability) of the energy gel prototype was evaluated with a 5-point JAR scale, ranging from 5 = “much too much” to 1 = “much too little” (16).

2.8 Statistical analysis

All experimental data are presented as mean ± SD. The differences between means and the significance of mean differences were assessed by Duncan’s Multiple Range Test using SPSS version 16.0 (SPSS Inc., Chicago, IL, USA), with $p \leq 0.05$ considered statistically significant. The Principal Component Analysis (PCA) was used to analyze the correlation banana variety and the measured properties.

3. Results & Discussion

3.1 Granular morphology and birefringence

The granular morphology and birefringence patterns of banana flours from the different cultivars observed under normal and polarized light are presented in Figure 1. All samples showed the presence of non-starch components and exhibited characteristic Maltese crosses. This Maltese cross pattern, produced by birefringence, reflects the organized molecular orientation within the starch granules and is associated with their crystalline structure (11, 17). Because granule morphology and hilum position are influenced by botanical origin (18), distinct structural differences were evident among the cultivars.

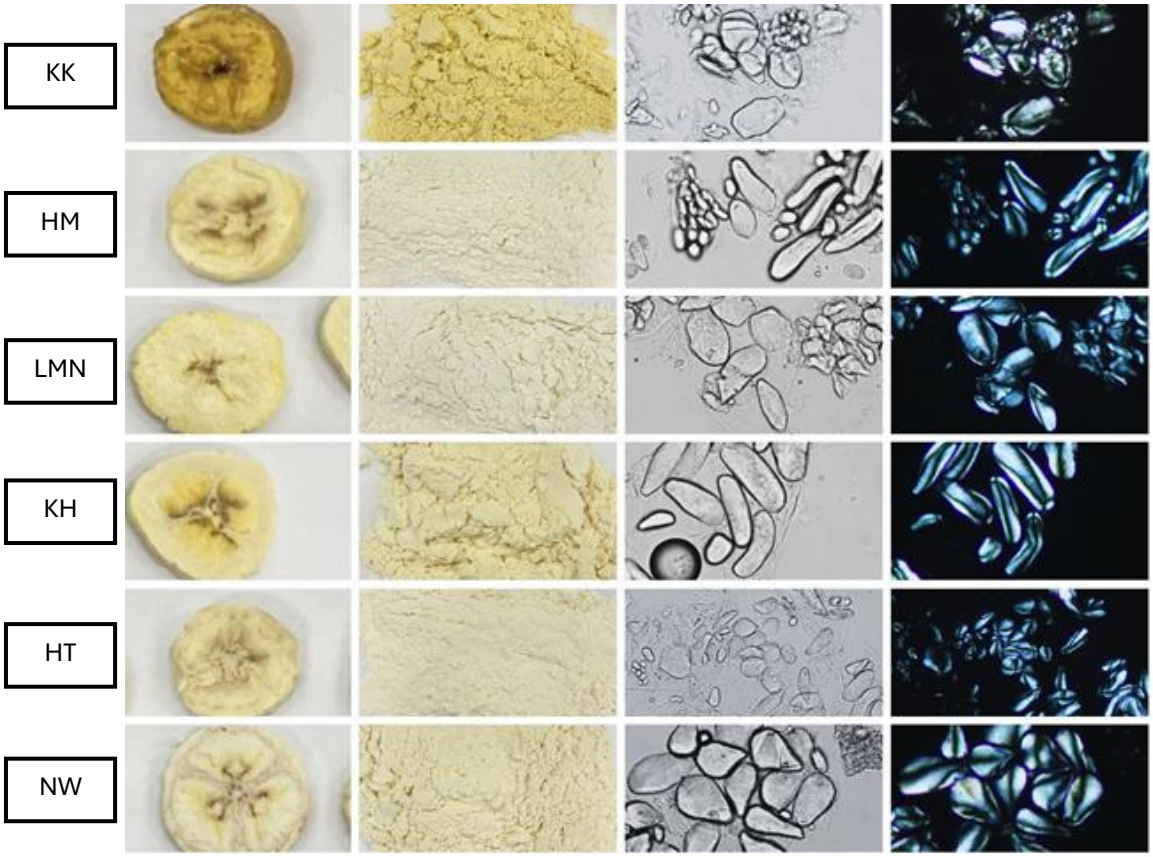

Figure 1. Banana flour from different cultivars and morphology of its granules under normal and polarized light

3.2 Proximate composition

Table 1 showed the proximate composition of banana flour from different varieties. It was shown that all flours exhibited significantly ($p \leq 0.05$) different proximate compositions, except ash content (1.29–3.86%) that was not significantly ($p > 0.05$) different between variety. Proximate composition of the banana flours showed significant differences depending on the cultivar type, similar with the findings of (19).

Moisture content plays a crucial role in determining both the physical and chemical properties of food products, as higher moisture levels can accelerate chemical, biochemical, and textural changes while promoting microbial growth, ultimately reducing shelf life and stability (20). The relatively low moisture content observed in the banana flours of this study suggests good stability and potential for extended shelf life. Fat content was found to be low (0.09–0.41%), which limits starch granule swelling and reduces susceptibility to oxidation, further contributing to prolonged storage stability (21). In addition, the protein content ranged from 2.12–5.58%, crude fiber from 1.27–4.38%, and total carbohydrates from 74.82–85.94%. These variations in chemical composition are largely influenced by factors such as regional climate, agronomic practices, and harvesting conditions (20, 22).

Table 1. Proximate composition of banana flour from different varieties

Variety	Moisture (%)	Protein (%)	Fat (%)	Ash^{ns} (%)	Crude fiber (%)	Total carbohydrate (%)
KK	11.0±0.1^{a}	5.58±0.11^{a}	0.32±0.03^{ab}	3.86±2.14	4.38±0.52^{a}	74.82±2.25^{c}
HM	10.7±0.2^{a}	3.31±0.19^{d}	0.34±0.08^{ab}	2.52±0.07	3.70±1.40^{ab}	79.44±1.53^{b}
LMN	9.3±0.0^{ab}	3.64±0.07^{c}	0.09±0.03^{c}	2.81±0.82	2.59±1.25^{bc}	81.60±0.92^{b}
KH	10.6±3.3^{ab}	3.38±0.10^{cd}	0.12±0.06^{c}	2.55±0.22	3.73±0.20^{ab}	81.58±3.09^{b}
HT	7.1±0.1^{b}	4.38±0.28^{b}	0.41±0.04^{a}	3.62±0.30	1.73±0.26^{c}	82.78±0.48^{b}
NW	9.2±0.1^{ab}	2.12±0.11^{e}	0.23±0.08^{b}	1.29±0.39	1.27±0.17^{c}	85.94±0.59^{a}
p-value	0.042	<0.001*	<0.001*	0.071	0.003	<0.001*

Data was presented as mean ± SD
Different superscript letters within column means significant ($p \leq 0.05$) difference between variety
^{ns} superscript letter means no significant ($p > 0.05$) difference between variety in the same column

3.3 Hydration properties

The water absorption capacity (WAC) of the banana flours ranged from 1.00–1.75 g/g, with the highest value observed in the LMN variety and the lowest in the NW variety. WAC reflects the volume occupied by starch granules after swelling in excess water and is influenced by the degree of disintegration of native starch granules, as well as the presence of dietary fiber and proteins (20, 23). Hydrophilic sites in the starch chains facilitate water interaction through hydrogen bonding, contributing to water retention. A higher WAC suggests suitability for food products requiring thick consistency, such as bakery formulations, while a lower WAC is desirable for products needing a thinner consistency due to its impact on gelatinization behavior (24).

The water solubility index (WSI) of the banana flours ranged from 0.20–0.40 g/g, with the highest value observed in the KK variety and the lowest in the LMN variety. The swelling power (SP) ranged from 6.89–9.40 g/g, with the HM variety showing the highest value and KH the lowest. WSI reflects the number of soluble solids released from the flour, while SP indicates the retention of starch granule integrity under high-temperature cooking conditions (20, 25, 26). Both parameters are influenced by the structural organization within starch granules, including the crystalline (amylose) and amorphous (amylopectin) regions, the degree of branching, and the length of branches. Higher WSI and SP values suggest enhanced starch gelatinization, which is advantageous for applications requiring pre-gelatinized starch. Conversely, low solubility coupled with low swelling power indicates a more ordered and tightly bonded granule structure, often associated with low amylose solubility, restricted swelling, and slight retrogradation (24).

Variations in these parameters among the banana flours in this study may also be attributed to differences in starch granule crystallinity and the distribution of amylose and amylopectin (27).

Table 2. Functional properties of banana flour from different varieties

Variety	Water absorption capacity (WAC) g/g	Water solubility index (WSI) g/g	Swelling power (SP) g/g
KK	1.16±0.1^{bc}	0.4± 0.0^{a}	7.06±0.1^{b}
HM	1.36±0.5^{abc}	0.20±0.1^{b}	9.12±0.5^{a}
LMN	1.75±0.4^{a}	0.20±0.08^{b}	7.48±1.39^{b}
KH	1.33±0.2^{bc}	0.22±0.02^{b}	6.89±0.79^{b}
HT	1.65±0.1^{ab}	0.29±0.06^{b}	7.12±0.93^{b}
NW	1.00±0.1^{c}	0.23±0.0^{b}	9.40±0.2^{a}
p-value	0.048	<0.001*	0.005

Data was presented as mean ± SD
Different superscript letters within column means significant ($p \leq 0.05$) difference between variety

3.4 Sugar content and glycemic characteristics

Sucrose and total sugar contents differed significantly ($p \leq 0.05$) among the banana flour varieties (Table 3). Sucrose ranged from 7.05–13.17 %, with the highest content in the HT variety and the lowest in HM, while total sugar ranged from 12.85–22.28%, with the highest content in KK and the lowest in KH. These findings align with Karaman, Pinar, Ciftci, and Kaplan (19), who reported sucrose as the predominant sugar in banana flour, ranging between 8.97–15.31%. This high sugar content is fundamentally linked to the stage-6 ripening phase (full yellow) of the bananas used in this study. During this specific stage, extensive starch-to-sugar conversion occurs, maximizing the soluble sugars such as sucrose, which subsequently provides the rapid energy-releasing properties required for energy gel products.

Table 3. Sucrose and total sugar of banana flour from different varieties

Variety	Sucrose	Total sugars	Glycemic index^{ns}	Glucose digested (mg/dL)	Resistant starch (g/100 g)
KK	12.81±0.46^{a}	22.28±1.02^{a}	55.39±1.55	3,033.00±31.18^{b}	7.06±0.30^{d}
HM	7.05±2.17^{ab}	15.26±1.55^{bc}	57.17±3.62	3,572.33±110.07^{a}	31.06±1.78^{a}
LMN	10.57±2.04^{ab}	15.71±2.02^{bc}	55.52±1.66	2,752.67±35.92^{d}	11.45±0.26^{c}
KH	7.69±0.42^{b}	12.85±0.48^{c}	56.30±1.38	2,810.00±52.37^{cd}	16.77±2.87^{b}
HT	13.17±4.70^{a}	19.18±4.53^{ab}	55.01±2.56	2,892.33±82.00^{c}	6.62±0.33^{d}
NW	11.39±2.40^{ab}	17.75±2.55^{b}	59.59±2.51	2,905.67±55.90^{c}	15.09±1.27^{b}
p-value	0.046	0.006	0.098	<0.001*	<0.001*

Data was presented as mean ± SD
Different superscript letters within column means significant ($p \leq 0.05$) difference between variety
^{ns} superscript letter means no significant ($p > 0.05$) difference between variety in the same column

Table 3 also showed the glycemic index (GI), *in vitro* starch digestion, and resistant starch (RS) of banana flours from different varieties. The NW variety showed the highest GI value and the lowest in the HT variety. These values fell within the low to medium GI category and were lower than that of D (+)-glucose (94.61 ± 0.01) but comparable to white bread (57.50 ± 1.61). The amount of glucose digested ranged from 2,752.67–3,572.33 mg/dL, with the HM variety showing the highest value and LMN the lowest. The RS content varied widely from 6.62–31.06 g/100 g, with the highest found in the HM variety and the lowest in the KK and HT varieties.

GI and RS are key indicators of starch digestibility, and their levels in banana flours can be influenced by protein and fat content, particle size, and the maturity or ripeness of the fruit (20, 28, 29). In terms of the RS, it acts similarly to dietary fiber by escaping digestion in the small intestine and undergoing fermentation in the colon, thereby promoting the growth of beneficial gut microbiota and supporting gut homeostasis (19, 28). Its presence in banana flour also helps modulate glucose release from starchy foods, potentially reducing the risk of obesity and related metabolic disorders. Given that starch is the primary carbohydrate in banana flour, its digestibility characteristics have significant implications for both health-related benefits and food product development, particularly for the formulation of functional and designer foods (29, 30).

3.5 PCA

PCA is a statistical method for deriving data from variables and explaining sample differentiation (31). Based on the PCA biplot (Fig. 2), the first two principal components accounted for 69.01%, with PC1 and PC2 showed 26.70% and 42.31%, respectively. The figure showed strong correlation between KK with the protein and fiber content, align with the proximate results. The HM was also shown to exhibited high correlation with the GI and RS value, supported by the results on the GI and RS values measurement. Based on the results on the properties

measurement and PCA, the KK and HM were selected as the ingredients in the production of energy gel prototype.

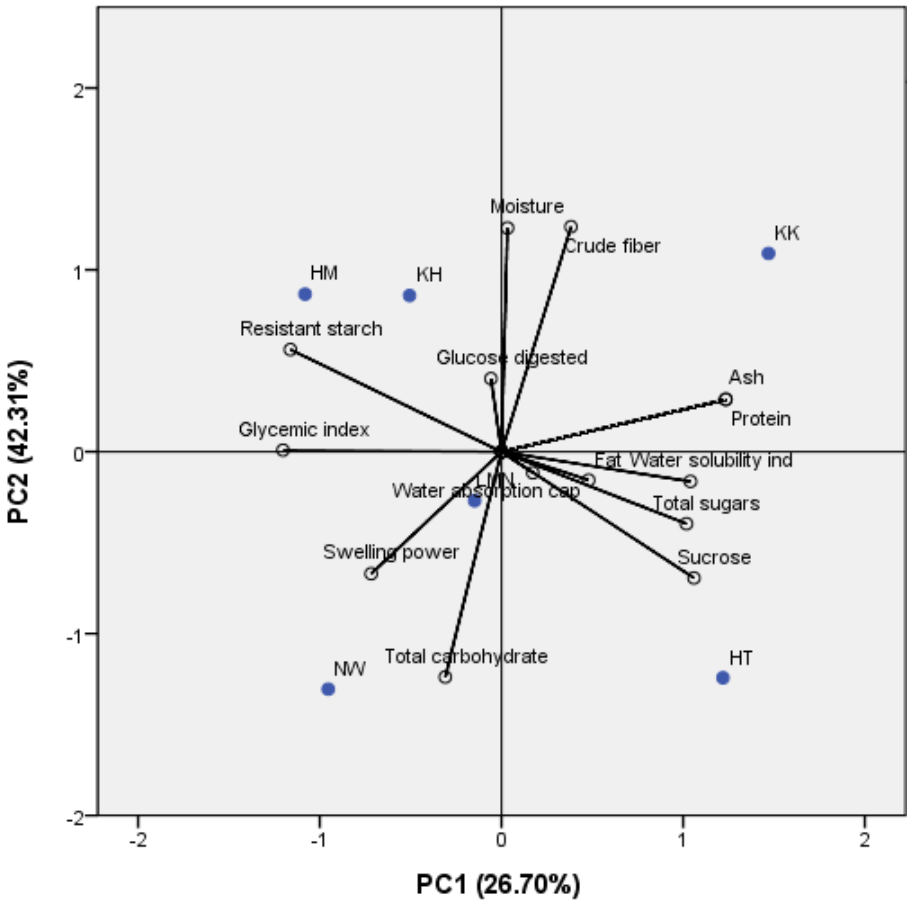

Figure 2. PCA biplot of banana flours, physicochemical, and functional properties

3.6 Sensory evaluation

Sensory evaluation was done to the energy gel prototype (Figure 3). Evaluating the sensory properties of food is important for understanding how it is perceived and whether it is likely to be well-received by consumers (32). The sensory rating score was in the range of like slightly to like moderately (6.4–7.2). To evaluate the sensory properties of the basic formulation of the energy gel the product was subjected to JAR analysis to see the direction of energy gel development. As shown in Figure 4, the JAR results on "swallowability" exceeded 70%, excluding the attribute from penalizations. Furthermore, the due to the net effect value below 20%, the "banana aroma" was also excluded from the penalization. Attributes with JAR value exceeded 70% and net effect value lower than 20% was excluded from penalization (33). The remaining attributes: "sweetness" (39.17%) and "mouthfeel" (23.34%) were subjected into penalization, and the range of ingredients in the formulation for further study was adjusted accordingly.

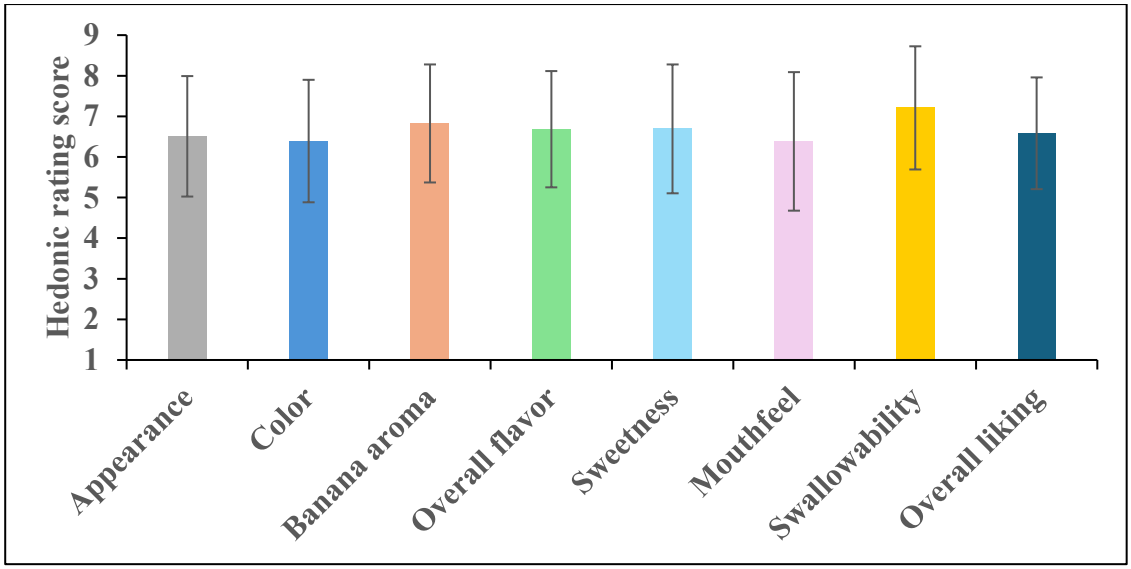

Figure 3. Sensory evaluation of energy gel prototype

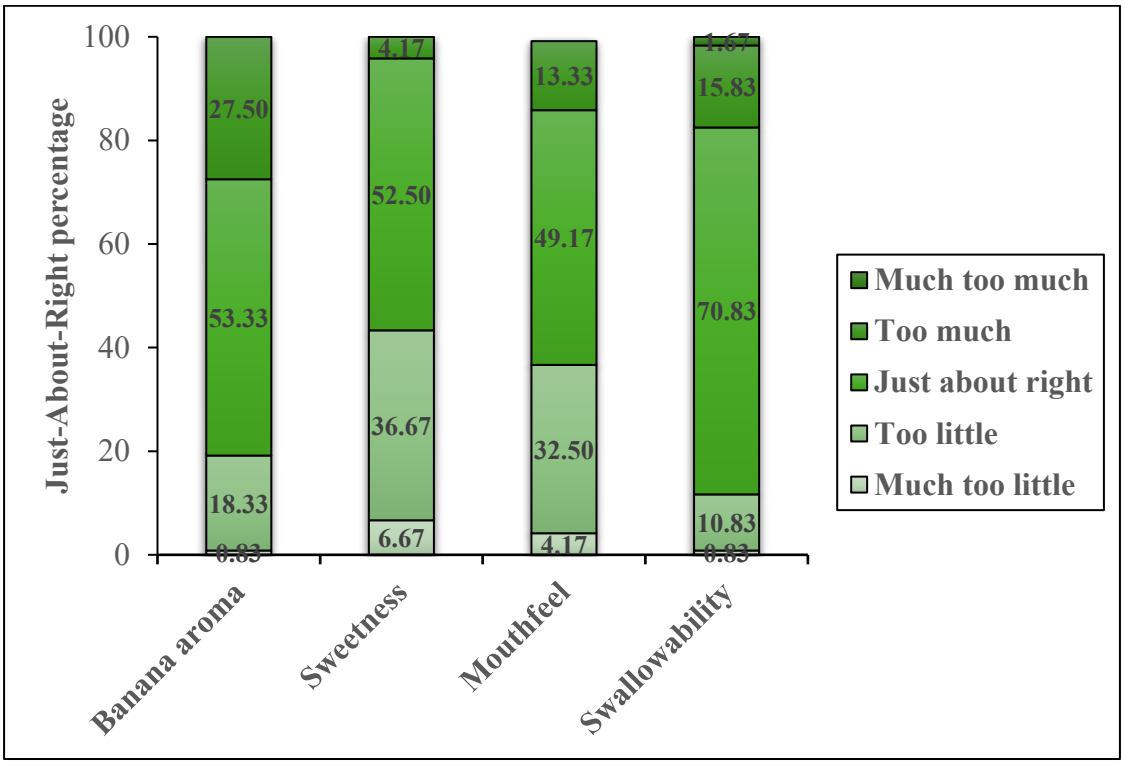

Figure 4. Just-about-right percentage of the energy gel prototype formulation

4. Conclusion

The investigation demonstrated that banana flours derived from six Thai cultivars exhibited significant variations in their proximate compositions and *in vitro* glycemic responses. Notably, Kluai Khai (KK) and Kluai Hak Muk (HM) were selected as the ingredients for the development of energy gel product due to the high total sugar and low to moderate glycemic index of the KK, along with the high glucose digested and resistant starch content of HM. Despite the energy gel prototype energy gel exhibited like slightly to like moderately (6.4–7.2) sensory rating score, Just-About-Right (JAR) analysis revealed the necessity to adjust the attributes of the product, specifically to increase perceived sweetness and mouthfeel of the energy gel. Further study to optimize the formulation of the energy gel product should be done to ensure the balance between the functionalities of the selected ingredients and the achieved the suitable sensory attributes for energy gel product.

Acknowledgements

The author would like to thank the Faculty of Agro-Industry, Chiang Mai University, Thailand, for supporting the study. The author would also like to thank Department of Geological Sciences, Faculty of Sciences, Chiang Mai University, Thailand, for supporting the instrument (Polarized light microscopy).

References

1. Chang L, Yang M, Zhao N, Xie F, Zheng P, Simbo J, et al. Structural, physicochemical, antioxidant and in vitro digestibility properties of banana flours from different banana varieties (Musa spp.). Food Bioscience. 2022;47:101624.
2. Wongwaiwech D, Kamchonemenukool S, Ho C-T, Li S, Thongsook T, Majai N, et al. Nutraceutical Difference between Two Popular Thai Namwa Cultivars Used for Sun Dried Banana Products. Molecules. 2022;27(17):5675.
3. Kidoń M, Uwineza PA. New smoothie products based on pumpkin, banana, and purple carrot as a source of bioactive compounds. Molecules. 2022;27(10):3049.
4. Campuzano A, Rosell CM, Cornejo F. Physicochemical and nutritional characteristics of banana flour during ripening. Food Chemistry. 2018;256:11-7.
5. Radünz M, Camargo TM, Nunes CFP, Pereira EDS, Ribeiro JA, Dos Santos Hackbart HC, et al. Gluten-free green banana flour muffins: chemical, physical, antioxidant, digestibility and sensory analysis. Journal of food science and technology. 2021;58(4):1295-301.
6. Batista A, Silva R, Cappato L, Ferreira M, Nascimento K, Schmiele M, et al. Developing a synbiotic fermented milk using probiotic bacteria and organic green banana flour. Journal of functional foods. 2017;38:242-50.
7. Assis R, Valentim A, Barbosa I, Silva J, Aquino A, Viana J, et al. Development of Fruit-Based Carbohydrate Gel for Endurance Athletes. Processes. 2024;12(10):2304.
8. AOACOfficialMethods. *Official Methods of Analysis of AOAC International.* 21st ed. Gaithersburg, MD: AOAC International 2019.
9. Gadhave R, Kaur R, Prasad K. Effect of acid pretreatment on physicochemical, optical, functional, thermal, and morphological characteristics of unripe plantain and banana flour. Journal of Food Chemistry and Nanotechnology. 2023;9(1):27-35.
10. Lane JH, Eynon L. Determination of reducing sugars by Fehling's solution with methylene blue indicator: N. Rodger; 1934.
11. Liang M, Tu S, Fu J, Wang J, Sheng O. Structural and Physicochemical Characterization of Resistant Starch from Sixteen Banana Cultivars across Three Genome Groups. Foods. 2024;13(20):3277.

12. Monro J, Mishra S. In vitro digestive analysis of digestible and resistant starch fractions, with concurrent glycemic index determination, in whole grain wheat products minimally processed for reduced glycaemic impact. Foods. 2022;11(13):1904.
13. Srikaeo K. Application of a rapid in vitro method based on glucometer for determination of starch digestibility and estimated glycemic index in rice. Starch-Stärke. 2023;75(1-2):2200174.
14. Rahaman S, Awana M, Goswami D, Kumari S, Bollinedi H, Anand A, et al. Predictive model for resistant starch (RS) in rice (Oryza sativa L.) based on digestibility factors. Journal of Plant Biochemistry and Biotechnology. 2025:1-18.
15. Seow E-K, Muthu V, Che Muhamed AM, Ooi CH, Singh R, Mat Easa A, et al. Influence of low-level gelling agents on the dissolution and in-vitro nutrient release study of coconut water-based hydrogel. Journal of Food Science and Technology. 2022;59(2):589-96.
16. Ares G, Varela P. Methods in consumer research, volume 1: new approaches to classic methods: Woodhead Publishing; 2018.
17. Keeratiburana T, Siangwengwang N, Somphunga W, Fu T, Blennow A. Ultrasound-assisted annealing treatment to improve physicochemical and digestive properties of banana flour. Journal of the Science of Food and Agriculture. 2024;104(11):6640-8.
18. Li Z, Guo K, Lin L, He W, Zhang L, Wei C. Comparison of physicochemical properties of starches from flesh and peel of green banana fruit. Molecules. 2018;23(9):2312.
19. Karaman K, Pinar H, Ciftci B, Kaplan M. Effects of Banana Flour on Some Physicochemical, Textural, Bioactive, and Sensory Properties of Gluten-Free Cookie. Food Science & Nutrition. 2025;13(1):e4756.
20. Khoza M, Kayitesi E, Dlamini BC. Physicochemical characteristics, microstructure and health promoting properties of green banana flour. Foods. 2021;10(12):2894.
21. Ye J, Hu X, Luo S, McClements DJ, Liang L, Liu C. Effect of endogenous proteins and lipids on starch digestibility in rice flour. Food Research International. 2018;106:404-9.
22. Khoozani AA, Birch J, Bekhit AE-DA. Production, application and health effects of banana pulp and peel flour in the food industry. Journal of food science and technology. 2019;56(2):548-59.
23. Pereira J, Malairaj S, Brohi SA, Boateng EF, Zhang W. Impact of unripe banana flour on water states, rheological behaviour and structural properties of myofibrillar protein composite gel. Lwt. 2020;125:109276.
24. Khoozani AA, Kebede B, Birch J, Bekhit AE-DA. The effect of bread fortification with whole green banana flour on its physicochemical, nutritional and in vitro digestibility. Foods. 2020;9(2):152.
25. Ahmed J, Thomas L, Khashawi R. Influence of hot-air drying and freeze-drying on functional, rheological, structural and dielectric properties of green banana flour and dispersions. Food Hydrocolloids. 2020;99:105331.
26. Tasnim T, Das PC, Begum AA, Nupur AH, Mazumder MAR. Nutritional, textural and sensory quality of plain cake enriched with rice rinsed water treated banana blossom flour. Journal of Agriculture and Food Research. 2020;2:100071.
27. Cui F, Zi H, Liu H, Zhang S, Yuan B. A study of starch-urea-water mixtures with a combination of molecular dynamics simulation and traditional characterization methods. International Journal of Biological Macromolecules. 2020;148:121-8.
28. Chakravarty A, Tandon M, Attri S, Sharma D, Raigond P, Goel G. Structural characteristics and prebiotic activities of resistant starch from Solanum tuberosum: Kufri Bahar, a popular Indian tuber variety. LWT. 2021;145:111445.
29. Lal MK, Singh B, Sharma S, Singh MP, Kumar A. Glycemic index of starchy crops and factors affecting its digestibility: A review. Trends in Food Science & Technology. 2021;111:741-55.

30. Kumar PS, Saravanan A, Sheeba N, Uma S. Structural, functional characterization and physicochemical properties of green banana flour from dessert and plantain bananas (Musa spp.). Lwt. 2019;116:108524.
31. Samakradhamrongthai RS, Jannu T, Tongboonchu T, Sangpimpa W, Srichan P, Renaldi G, et al. Physicochemical and sensory properties of Southern Thai curry pastes. International Journal of Food Properties. 2025;28(1):2545527.
32. Baroyi SAHM, Yusof YA, Ghazali NSM, Al-Awaadh AM, Kadota K, Mustafa S, et al. Determination of physicochemical, textural, and sensory properties of date-based sports energy gel. Gels. 2023;9(6):487.
33. Kaewpetch K, Yolsuriyan S, Disayathanoowat T, Phokasem P, Jannu T, Renaldi G, et al. Influence of gelatin and Propolis extract on honey gummy jelly properties: Optimization using D-optimal mixture design. Gels. 2024;10(4):282.

P - 191

Phytochemical Composition, Phenolic Profiling, and Bioactive Activities from Ethanolic Extraction of Different Parts of Mulberry (*Morus alba* L.)

Napatsawan Chaimahawan[1,2], Arriya Tadtan[1,2], Gerry Renaldi[1,2], Natthanicha Banpacha[1,2], Rajnibhas Sukeaw Samakradhamrongthai[2,3]*

[1]*Department of Food Science and Technology, Division of Food Innovation Design and Development, Faculty of Agro-Industry, Chiang Mai University, Chiang Mai 50100 Thailand*
[2]*INterdisciplinary and Food product development for wellness Research Unit (INFRU), Chiang Mai University, Chiang Mai 50200 Thailand*
[3]*Division of Product Development Technology, Faculty of Agro-Industry, Chiang Mai University, Chiang Mai 50100 Thailand*

**Corresponding author E-mail: rajnibhas.s@cmu.ac.th*

Abstract: The mulberry (*Morus alba* L.) belongs to the Moraceae family and is cultivated in many Asian countries, including Thailand. There are many uses for all parts of the mulberry plant, which are used in various fields, including food, cosmetics and folk medicine. This study was done to investigate the phytochemical properties, including phenolic compound profiling, quantification of the resveratrol content, and measurement on the SIRT1 activity, of ethanolic extract (60–80%) using three different parts of mulberry plant: fruit, leaf, and branch. It was found that mulberry leaves possessed the highest total phenolic content (45.29±1.66 mg GAE/mL DW) and total flavonoid content (34.84±2.20 mg CE/mL DW), while the branch exhibited the highest resveratrol content (12.06±2.23 µg/mL DW). The extract of mulberry branch also showed the highest SIRT1 activity (274.42±12.30%) compared to other treatments. Regarding the fruit, it contained the highest caffeic acid (2,062.55±10.35 µg/mL DW), epicatechin (172.01±1.36 µg/mL DW), p-coumaric acid (243.12±0.72 µg/mL DW), and myricetin (13,260.99±65.84 µg/mL DW). The Principal Component Analysis (PCA) on the phytochemical properties and phenolic compounds showed total variance of 78.64% and 68.48%, respectively. The PCA showed that mulberry branch extracted with 60% of ethanol (MB 60) exhibited high correlation between with the TPC, DPPH, resveratrol, and SIRT1 activity, along with some phenolic compounds (quercetin, catechin, and rutin). In conclusion, different parts of the mulberry plant extracted under different concentrations of ethanol showed different properties, with the MB 60 was shown to possessed high correlation with the phytochemical properties and phenolic composition. The results suggested that the mulberry plant, especially its branch extracted using 60% of ethanol, can be considered as a valuable source of bioactive compounds for food, nutraceutical, and health applications.

Keywords: Mulberry; Ethanolic extraction; Phenolic compound; Resveratrol; SIRT1

1. Introduction

In recent decades, interest in medicinal herbs has expanded rapidly due to their natural origins and minimal side effects, making them increasingly appealing in both developing and developed countries [1]. This growing attention aligns with the rising focus on plant-derived secondary metabolites, such as phenols, terpenes, anthocyanins, and alkaloids, recognized for their significant health-promoting and nutritional benefits [2]. These bioactive compounds not only protect plants from insects, microorganisms, and herbivores but also serve as valuable sources of nutrients and therapeutic agents for humans. However, determining the optimal solvent concentration for capturing a broad spectrum of these phytochemicals remains a significant

challenge. Preliminary literature reviews of various plant parts and cultivars reveal that the extractability of bioactive compounds and their antioxidant capacities are often inconsistent, as the efficiency is heavily influenced by the structural complexity of the plant matrix and the specific extraction techniques employed [3, 4]. Consequently, a variable range of 60–80% ethanol was selected in this study to systematically optimize the recovery of diverse phytochemicals and account for the non-linear relationship between solvent polarity and bioactive yields [5]. Among plants abundant in these secondary metabolites, mulberry stands out as a particularly rich source.

Mulberry (*Morus alba* L.) is a fast-growing shrub or medium-sized tree characterized by a straight, cylindrical trunk with dark grayish-brown bark marked by longitudinal cracks and a rough surface. The plant exudes a white to yellowish latex and bears simple, alternate, dentate leaves that are often trilobed with three prominent veins at the base. The greenish flowers have four free, scale-like petals and are arranged in catkin-like inflorescences [1]. This distinctive morphology not only supports its adaptability across diverse environments but also contributes to the accumulation of valuable nutrients and bioactive compounds throughout the plant.

Owing to this physiological adaptability, mulberries have developed a rich nutritional profile, making them one of the most nutrient-dense and functionally significant crops. The fruit contains approximately 0.5–1.4% protein and 7.8–9.0% carbohydrates, with a low total fat content. Its carbohydrate fraction includes neutral sugars such as arabinose, galactose, glucose, rhamnose, xylose, and mannose, along with significant amounts of uronic acids, primarily galacturonic and glucuronic acid. Although the total lipid content is low, essential fatty acids including linoleic, oleic, palmitic, and stearic acids account for 69.66–78.02% of total fatty acids. Mulberries are also a rich source of vitamin C, followed by vitamins A and B [1]. Moreover, they contain high-value phytochemicals such as anthocyanins, phenols, and flavonoids, which enhance their potential as functional ingredients in nutraceuticals [6, 7].

Medicinally, all parts of the mulberry plant, including fruits, leaves, and branches, have been utilized in traditional medicine for their therapeutic properties [1]. The phytochemical composition, however, varies considerably depending on the plant part and its developmental stage, influencing both the type and concentration of bioactive compounds [2]. Therefore, this study was conducted to explore the phytochemical properties of different parts of mulberry plants (fruit, leaf, and branch) and profile its phenolic compounds.

2. Materials and Methods

2.1 Raw materials and chemicals

The fruits, leaves, and branches of mulberry (*Morus alba* L. var. Buriram 60) were harvested from a Queen Sirikit Sericulture Center in Chiang Mai, Thailand. Fruits were used at “fully ripe” ripening stages, leaves and branches are harvested on pruning period in September 2024. The samples were dried in a hot air oven (ULM 600, Memmert, Germany) at 40 °C for 2–8 h, or until the moisture content was below 14.00±1.00%. Each mulberry sample was then ground into a fine powder using a grinder mill (PG10, Belt and Bearings, Thailand) and sieved through a 50-mesh screen. The powdered samples were stored in vacuum-sealed plastic bags until extraction. All chemicals used in this study were analytical grade.

2.2 Mulberry extract preparation

Mulberry extract preparation The mulberry extracts were prepared using an ultrasonic-assisted extraction (UAE) method. Based on previous literature regarding the optimal recovery of diverse phytochemicals from different plant matrices [3-5], aqueous ethanol at concentrations of 60%, 70%, and 80% (v/v) was selected as the extraction solvent. A solid-to-solvent ratio of 1:20 was applied for each concentration. The UAE parameters were adapted from Kattil et al. [8] with slight modifications. The extraction was carried out at 500 W and 20 kHz (VCX 500, Sonics & Materials, USA) with a 25% amplitude for 60 min at 30 °C. The resulting extract was then filtered using Whatman No.1 filter paper. The solvent was removed with a rotary evaporator (R-1005,

Greatwall Scientific, China) under reduced pressure. All crude extracts were then stored at 4 °C in an amber bottle protected from light until further analysis. A schematic of the extraction process is shown in Figure 1.

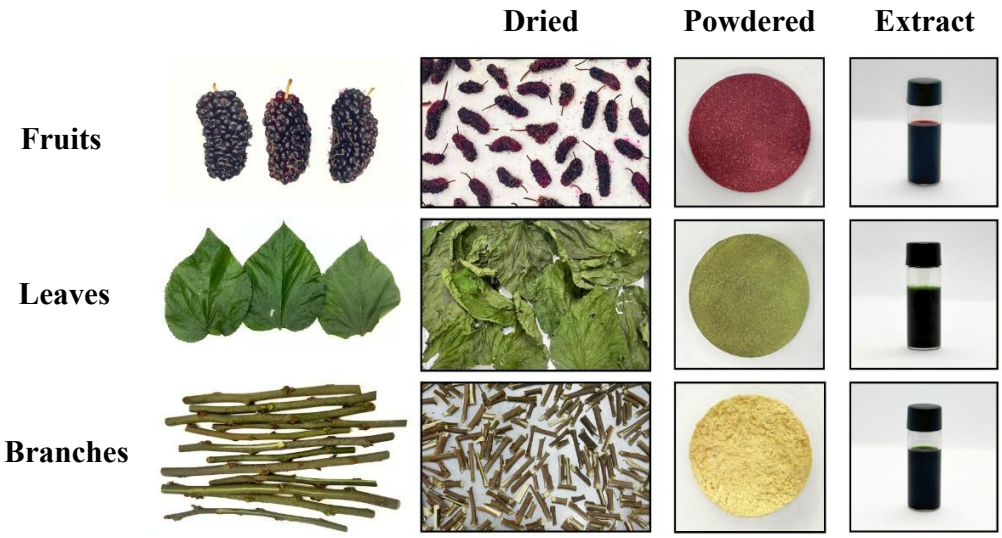

Figure 1. Extraction of different parts of *Morus alba* L.

2.3 Phytochemical properties

2.3.1 Total phenolic content

The total phenolic content (TPC) of the extracts was determined using a modified Folin–Ciocalteu reagent method, adapted from Belew et al. [9]. Briefly, 20 µL of each diluted extract was combined with 100 µL of 10% Folin–Ciocalteu reagent in a 96-well plate. The plate was shaken and then incubated in the dark for 5 min. Subsequently, 80 µL of 7.5% Na_2CO_3 solution was added, and the mixture was left at room temperature for 90 min in the dark. A reagent blank was prepared concurrently with ethanol. The absorbance was measured at 765 nm using a Spark multimode microplate reader (Tecan Ltd., Männedorf, Switzerland). The TPC was calculated from a gallic acid standard curve and is expressed as milligrams of gallic acid equivalents per gram of dry extract weight (mg GAE/g DW).

2.3.2 Total flavonoid content

The total flavonoid content (TFC) in the extracts was measured using a colorimetric method [9]. In this procedure, 120 µL of each sample solution was pipetted into a 96-well plate, followed by the addition of 6 µL of 5% $NaNO_2$. After 5 min of incubation, 12 µL of 10% $AlCl_3$ was added. The mixture was allowed to react for 6 min before adding 40 µL of 1M NaOH and 22 µL of distilled water. The plate was then shaken. The absorbance of the solution was read at 510 nm using a Spark multimode microplate reader (Tecan Ltd., Männedorf, Switzerland). A calibration curve was prepared using catechin as the standard. The total flavonoid content was then expressed as milligrams of catechin equivalent per gram of dry weight (mg CE/g DW).

2.3.3 Antioxidant activities

The DPPH radical-scavenging activity of the extracts was evaluated following the method of Jannat et al. [10]. In a 96-well plate, 5 µL of each sample, prepared at various concentrations in methanol, was combined with 195 µL of 60 µM DPPH in methanol. The plate was shaken and then incubated in the dark at room temperature for 30 min. The absorbance was subsequently measured at 517 nm using a Spark multimode microplate reader (Tecan Ltd., Männedorf, Switzerland). The percentage of DPPH radical scavenging was calculated using the formula:

$$\text{DPPH radical scavenging (\%)} = \{(A_0\text{-}A_1)/A_0\} \times 100$$

where A_0 is the absorbance of the DPPH blank solution in methanol, and A_1 is the absorbance of the extract or standard solution. The median inhibition concentration (IC_{50}) was determined by plotting the percentage of DPPH radical scavenging activity against the sample concentration. The ABTS radical scavenging potential was assessed using a slightly modified method from Sanpinit et al. [11]. First, the ABTS radical cation ($ABTS^{\bullet+}$) was generated by mixing 7 mM ABTS and 2.4 mM potassium persulfate at a 1:1 volume ratio. This mixture was stored in a dark room at room temperature for 16 hours. Ethanol was then added to adjust the absorbance at 734 nm. For the assay, 3 µL of each sample, prepared at various concentrations in ethanol, was added to individual wells of a 96-well plate. Subsequently, 197 µL of the $ABTS^{\bullet+}$ solution was added. After a 6 min incubation in the dark, the absorbance was measured at 734 nm using Spark multimode microplate reader (Tecan Ltd., Männedorf, Switzerland). The ABTS radical scavenging activity was calculated using the following formula:

$$\text{ABTS radical scavenging (\%)} = \{(A_0\text{-}A_1)/A_0\} \times 100$$

where A_0 is the absorbance of the $ABTS^{\bullet+}$ blank solution in ethanol, and A_0 is the absorbance of the extract or standard solution. The median inhibition concentration (IC_{50}) was determined by plotting the percentage of ABTS radical scavenging activity against the sample concentration. The ferric reducing antioxidant power (FRAP) of the extract was determined using a modified method based on the protocol by Aouadi et al. [12]. First, the FRAP reagent was prepared by mixing 300 mM acetate buffer (pH 3.6), 10 mM 2,4,6-tri-2-pyridyl-s-triazine (TPTZ) in 40 mM HCl, and 20 mM $FeCl_3$ in a 10:1:1 (v/v/v) ratio. The mixture was shaken and then incubated for 30 minutes. For the assay, 10 µL of each diluted extract was combined with 190 µL of the FRAP reagent in a 96-well plate. The plate was then incubated at room temperature for 30 min in the dark. The absorbance was measured at 593 nm with a Spark multimode microplate reader (Tecan Ltd., Männedorf, Switzerland). The FRAP activity was calculated from a calibration curve using Trolox standards and is expressed as milligrams of Trolox per gram of dry extract weight (mg GAE/g DW).

2.3.4 Resveratrol

Based on a previous study [13], High-performance liquid chromatography (HPLC) analysis was conducted on an Agilent 1260 series equipped with a diode array detector (DAD) (Agilent Technologies, Santa Clara, CA, USA). The separation was carried out on a Kinetex C18 column (4.6 mm × 250 mm, 5 µm; Phenomenex, USA). The mobile phase, which was degassed before use, consisted of (A) ultrapure water containing 0.05% acetic acid and (B) HPLC-grade acetonitrile. Isocratic elution was performed at a ratio of A:B (70:30) at a flow rate of 1.2 mL/min and a temperature of 30°C for 15 minutes. The chromatogram was recorded at 306 nm. For calibration, a 1 mg/mL stock solution of *trans*-resveratrol was prepared by dissolving 10 mg of the reference standard (Sigma-Aldrich, USA) in 10 mL of HPLC-grade methanol. This stock was then used to create standard solutions with concentrations ranging from 0.0020-0.2500 mg/mL. All samples were filtered through a 0.45 µm membrane before a 10 µL injection volume was used for each analysis.

2.4 Phenolic profile

The analysis of phenolic compounds was performed using an Agilent 1260 Infinity II LC System (Agilent Technologies, Santa Clara, CA, USA) equipped with a G7115A Diode Array Detector (DAD). Separation was achieved on a 250 mm × 4.6 mm, 5 µm particle size Kinetex C18 column (Phenomenex, USA). A gradient elution method, adapted from Chaipoot et al [14]. The mobile phases consisted of (A) 2% acetic acid in water and (B) 100% acetonitrile. The flow rate was maintained at 1 mL/min, and the column temperature was set to 30 °C. The gradient program

for mobile phase B was as follows: 0–5 min, 5–7% B; 5–25 min, 7–8% B; 25–27 min, 8–11% B; 27–32 min, 11–12% B; 32–44 min, 12–15% B; 44–52 min, 15–15% B; 52–53 min, 15–32% B; 53–59 min, 32–32% B; 59–63 min, 32–20% B; 63–69 min, 20–90% B; 69–74 min, 90–90% B; 74–75 min, 90–5% B. The run stopped at 85 min. Before analysis, the extract sample was diluted with absolute acetonitrile at a 1:1 (v/v) ratio in a microcentrifuge tube and filtered through a 0.45 µm membrane. A 10 µL injection volume was used. Ten phenolic standards were identified and quantified by detection at 280 nm: gallic acid, catechin, chlorogenic acid, vanillic acid, caffeic acid, epicatechin, p-coumaric acid, rutin, myricetin, and quercetin.

2.5 SIRT1 activity

Sirtuin-1 (SIRT1) activation was evaluated using the SIRT1 Assay Kit (Sigma-Aldrich, St. Louis, MO, USA) according to the manufacturer's instructions. The extract samples were tested at a concentration of 10 µL/mL, while 10 µM Resveratrol (RES) was used as a positive control and Nicotinamide (NAM) served as an inhibitor. SIRT1 activity was measured using a fluorescent spectrometer microplate reader Spark (Tecan Ltd., Männedorf, Switzerland) with an excitation wavelength of 350 nm and an emission wavelength of 434 nm. The relative SIRT1 activity for each extract was expressed as a percentage relative to the corresponding control, which contained the same volume of extraction solvent.

2.6 Statistical analysis

All experimental were performed in triplicate ($n=3$), and the data are presented as mean ± SD. The differences between means and the significance of mean differences were assessed by Duncan's Multiple Range Test using SPSS version 16.0 (SPSS Inc., Chicago, IL, USA), with p-values < 0.05 considered statistically significant. The Principal Component Analysis (PCA) was used to analyze the correlation banana variety and the measured properties.

3. Results & Discussion

3.1 Phytochemical properties

Based on the measurements presented in Table 1, the phytochemical properties of the different mulberry plant parts differed significantly. The highest total phenolic content (TPC) was observed in ML 70 (37.75±1.38 mg GAE/g DW) and ML 80 (37.61±0.14 mg GAE/g DW), while ML 80 also exhibited the highest total flavonoid content (TFC) (29.03±1.84 mg CE/g DW). Overall, the fruit extracts demonstrated significantly higher TPC and TFC values compared to the leaf and branch extracts. The heterogeneous distribution of phytochemical compounds among plant parts may be attributed to differences in their physiological roles and metabolic specialization [15]. Various parts of the mulberry plant have attracted considerable scientific attention due to their therapeutic potential; however, the fruit remains the most extensively studied component, recognized for its exceptional pharmacological and health-promoting properties [16]. Mulberries possess exemplary nutritional and phytochemical value, which has drawn considerable scientific attention toward analyzing their antioxidant potential [17]. Based on the antioxidant activity measurements, the IC_{50} values for DPPH (1.06–5.18 mg/mL), IC_{50} ABTS (3.04–11.74 mg/mL), and FRAP (8.90–24.85 mg TE/g DW) assays showed significant differences ($p < 0.05$) among the samples. These findings reaffirm the strong antioxidant capacity of mulberry extracts, which are known to effectively scavenge free radicals, inhibit low-density lipoprotein oxidation, and reduce macrophage-induced atherosclerosis [7].

Table 1. Phytochemical properties of mulberry extract

Parts (A)	EtOH % (B)	TPC (mg GAE/ g DW)	TFC (mg CE/ g DW)	IC_{50} DPPH (mg/mL)	IC_{50} ABTS (mg/mL)	FRAP (mg TE/ g DW)	T-RVT (µg/g DW)
Fruit	60	18.41±0.10^{g}	2.28±0.19^{e}	2.87±0.01^{cd}	8.18±0.03^{b}	11.99±0.76^{de}	3.00±0.79^{b}
	70	23.08±0.67^{d}	1.42±0.05^{e}	2.71±0.13^{d}	6.74±0.06^{c}	12.90±0.35^{d}	2.93±0.40^{b}
	80	18.90±0.13^{ef}	1.94±0.14^{e}	3.56±0.11^{b}	6.34±0.01^{d}	8.90±0.27^{f}	3.02±0.27^{b}
Leaf	60	20.59±0.05^{e}	7.80±0.51^{c}	3.00±0.17^{c}	11.74±0.18^{a}	14.40±0.10^{c}	ND
	70	37.75±1.38^{a}	25.66±0.21^{b}	1.27±0.01^{e}	3.04±0.02^{h}	23.74±0.04^{b}	ND
	80	37.61±0.14^{a}	29.03±1.84^{a}	1.06±0.01^{f}	3.06±0.03^{h}	24.85±0.43^{a}	ND
Branch	60	30.90±0.73^{b}	6.03±0.10^{d}	5.12±0.01^{a}	4.80±0.07^{g}	14.25±0.31^{c}	9.21±0.15^{a}
	70	28.86±1.87^{c}	9.30±0.56^{c}	1.09±0.00^{f}	6.05±0.08^{e}	11.84±0.48^{e}	10.05±1.86^{a}
	80	31.25±0.82^{b}	8.09±0.50^{c}	5.18±0.06^{a}	5.08±0.08^{f}	11.39±0.39^{e}	9.78±1.63^{a}
Main effect (A)		<0.001*	<0.001*	<0.001*	<0.001*	<0.001*	<0.001*
Main effect (B)		<0.001*	<0.001*	<0.001*	<0.001*	<0.001*	0.875
Interaction (A×B)		<0.001*	<0.001*	<0.001*	<0.001*	<0.001*	0.949

Remarks: Data was presented as mean±SD; TPC = total phenolic content; TFC = total flavonoid content; T-RVT = resveratrol; GAE = gallic acid equivalent; CE = catechin equivalent; TE = Trolox equivalent; different superscript letter within the same column means significant ($p < 0.05$) difference between samples; ND = not detected

Resveratrol (trans-3,5,4′-trihydroxystilbene; T-RVT) is a polyphenolic compound found in mulberry that has been recognized as a promising functional feed additive and nutraceutical ingredient due to its diverse biological activities, including antioxidant, anti-cancer, anti-inflammatory, and anti-diabetic effects [13, 14]. In the present study, the mulberry branch extract exhibited significantly ($p < 0.05$) higher T-RVT content (9.21–10.05 µg/g DW) than the fruit extract (2.93–3.02 µg/g DW), while T-RVT was undetected in the leaf extract. Similarly, Li et al. [18] reported that different parts of the mulberry plant vary in their T-RVT content, with the branches containing the highest concentrations.

3.2 Phenolic profile

Phenolic compounds exert beneficial effects against various chronic diseases, including diabetes, hypertension, and cancer. Accordingly, higher phenolic content is generally associated with greater potential for health-promoting activity [19]. In the present study, ten phenolic compounds were identified across different parts of the mulberry plant (Table 2): gallic acid (GA), catechin (CAT), chlorogenic acid (CGA), vanillic acid (VA), caffeic acid (CA), epicatechin (EC), p-coumaric acid (p-CA), rutin (RUT), myricetin (MYR), and quercetin (QUE).

These findings are consistent with previous studies reporting GA, VA, CGA, CA, RUT, p-CA, and QUE in mulberry extracts [16, 20]. Different plant parts exhibited distinct phenolic profiles and concentrations. Among the fruit extracts (MF), CA (1,593.83–1,901.89 µg/g DW) and MYR (8,648.03–11,050.83 µg/g DW) were the most abundant compounds. In contrast, VA (10,506.87–23,766.58 µg/g DW) predominated in the leaf extracts (ML), while CAT (124.16–1,028.90 µg/g DW) was the major constituent in the branch extracts (MB). These variations suggest that the biosynthesis and accumulation of phenolic compounds in mulberry are tissue-specific, likely to reflect differences in physiological function and metabolic activity among plant parts [15].

Table 2. Phenolic compounds of mulberry extract

Parts (A)	EtOH% (B)	Phenolic Compounds (µg/g DW)									
		GA	CAT	CGA	VA	CA	EC	p-CA	RUT	MYR	QUE
Fruit	60	175.39 ±1.74^{d}	92.89 ±0.28^{h}	1.46 ±0.02^{h}	510.80 ±2.03^{de}	1,593.83 ±4.75^{c}	8.07 ±0.08^{g}	4.98 ±0.03^{h}	ND	11,050.83 ±54.86^{a}	11.29 ±0.08^{g}
	70	119.54 ±0.24^{g}	385.18 ±1.16^{c}	32.41 ±0.10^{d}	352.82 ±1.41^{f}	1,718.79 ±8.63^{b}	143.34 ±1.14^{a}	202.60 ±0.59^{a}	7.12 ±0.03^{g}	10,059.69 ±10.00^{b}	6.37 ±0.03^{h}
	80	125.45 ±0.50^{f}	57.68 ±0.17^{i}	1.25 ±0.00^{h}	542.33 ±2.16^{d}	1,901.89 ±5.67^{a}	68.60 ±0.27^{c}	12.01 ±0.04^{g}	10.88 ±0.06^{f}	8,648.03 ±25.82^{c}	12.69 ±0.07^{f}
Leaf	60	231.95 ±0.69^{b}	458.27 ±2.27^{b}	48.66 ±0.19^{b}	23,766.58 ±70.50^{a}	70.63 ±0.36^{f}	14.65 ±0.05^{e}	33.46 ±0.34^{d}	22.76 ±0.11^{e}	3,210.71 ±15.99^{f}	38.56 ±0.19^{d}
	70	431.93 ±1.73^{a}	379.96 ±1.14^{d}	75.79 ±0.23^{a}	10,665.30 ±42.53^{b}	238.59 ±1.19^{e}	110.18 ±0.33^{b}	89.21 ±0.27^{b}	61.19 ±0.25^{b}	6,301.31 ±19.75^{d}	31.86 ±0.16^{e}
	80	155.92 ±0.47^{e}	272.07 ±0.82^{f}	7.45 ±0.03^{g}	10,506.87 ±31.40^{c}	291.77 ±1.17^{d}	ND	41.08 ±0.13^{e}	38.88 ±0.11^{d}	5,671.18 ±28.27^{e}	32.49 ±0.16^{e}
Branch	60	229.74 ±0.69^{c}	1,028.90 ±5.13^{a}	22.01 ±0.06^{e}	115.89 ±0.35^{g}	ND	11.66 ±0.04^{f}	33.28 ±0.11^{d}	89.29 ±0.28^{a}	148.42 ±0.45^{g}	154.07 ±0.45^{b}
	70	112.51 ±0.34^{h}	124.16 ±0.49^{g}	43.64 ±0.13^{c}	455.84 ±1.81^{e}	18.98 ±0.05^{g}	68.66 ±0.21^{c}	22.58 ±0.07^{e}	39.57 ±0.11^{c}	56.25 ±0.17^{h}	163.75 ±0.49^{a}
	80	74.53 ±0.15^{i}	339.85 ±1.01^{e}	20.27 ±0.06^{f}	528.98 ±1.58^{d}	10.78 ±0.04^{g}	22.20 ±0.11^{d}	14.17 ±0.07^{f}	ND	116.79 ±0.23^{g}	143.69 ±0.72^{c}
Main effect (A)		<0.001*	<0.001*	<0.001*	<0.001*	<0.001*	<0.001*	<0.001*	<0.001*	<0.001*	<0.001*
Main effect (B)		<0.001*	<0.001*	<0.001*	<0.001*	<0.001*	<0.001*	<0.001*	<0.001*	<0.001*	<0.001*
Interaction (A×B)		<0.001*	<0.001*	<0.001*	<0.001*	<0.001*	<0.001*	<0.001*	<0.001*	<0.001*	<0.001*

Remarks: Data was presented as mean±SD; GA = Gallic acid; CAT = Catechin; CGA = Chlorogenic acid; VA = Vanillic acid; CA = Caffeic acid; EC = Epicatechin; p-CA = *p*-Coumaric acid; RUT = Rutin; MYR = Myricetin; QUE = Quercetin; different superscript letter within the same column means significant ($p < 0.05$) difference between samples; ND = not detected

3.3 SIRT1 activity

Sirtuin 1 (SIRT1), a member of the NAD^+-dependent class III histone deacetylases, plays a vital role in regulating numerous biological processes, including tumor suppression, mitochondrial homeostasis, energy metabolism, cellular aging, and apoptosis [21]. As shown in Figure 2, the branch (MB; 260.32–274.42%) and leaf (ML; 263.43–267.86%) extracts exhibited significantly ($p < 0.05$) higher SIRT1 activity compared to the control (100.00±5.82%) and NAM (68.03±5.73%) treatments, with no significant differences observed between each other or the positive control (257.87±3.29%). In contrast, the fruit (MF) extracts demonstrated significantly ($p < 0.05$) lower SIRT1 activity (183.63–207.88%) than the MB and ML samples. Although nicotinamide (NAM) is a well-recognized SIRT1 inhibitor, our results showed no significant difference compared to the control ($p > 0.05$), which might be due to the experimental concentration or sensitivity of the assay system.

The elevated SIRT1 activity in the MB samples may be attributed to the high resveratrol (T-RVT) content detected in the branches, consistent with the T-RVT quantification results. Resveratrol has been widely reported as a potent SIRT1 activator in both in vitro and in vivo systems [21, 22]. Interestingly, high SIRT1 activity was also observed in ML samples where T-RVT was undetected. This suggests that other phytochemicals may contribute to SIRT1 activation. Vanillic acid (VA), one of the predominant phenolic acids in the ML samples, has been reported to upregulate SIRT1 expression [23]. Therefore, the abundant VA content in ML extracts may partially explain their high SIRT1 activity despite the absence of resveratrol.

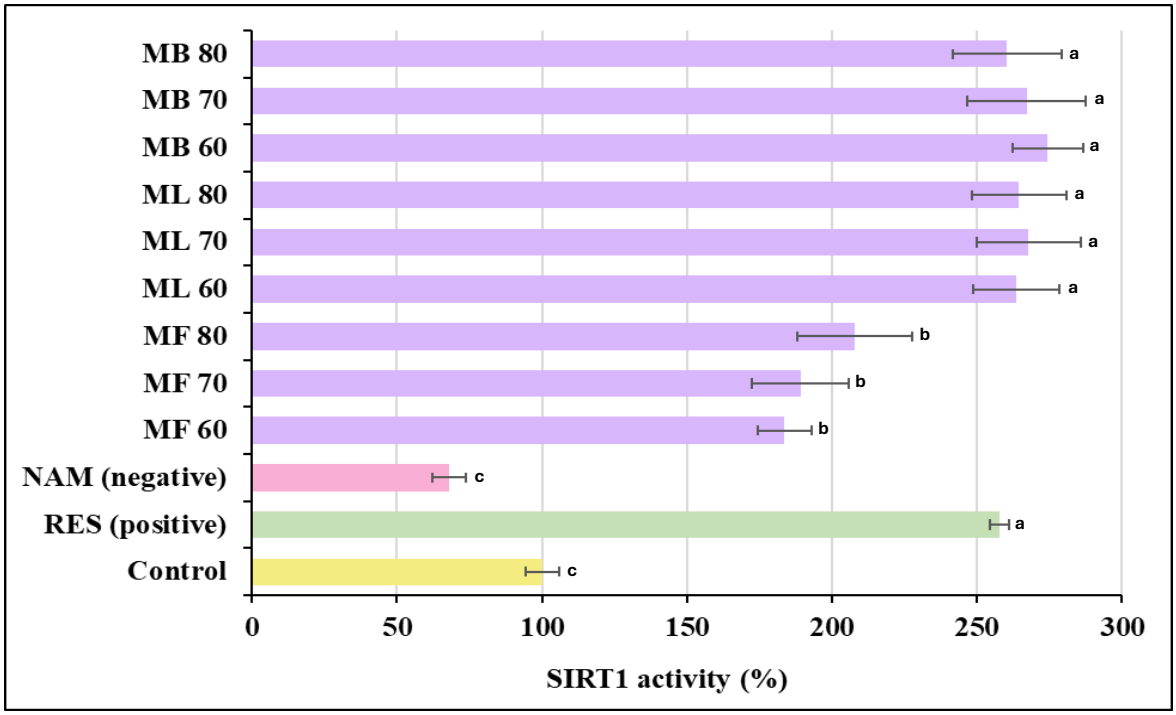

Figure 2. SIRT1 activity of mulberry extracts; different superscript letter means significant ($p < 0.05$) different between samples

3.4 Principal component analysis

The PCA biplot between the samples with their phytochemical properties (Fig. 3a) and phenolic compounds (Fig. 3b) showed total variance of 79.21% (55.79% of PC1 and 23.42% of PC2) and 68.48% (40.32% of PC1 and 28.16% of PC2), respectively. Figure 2a demonstrates a strong positive correlation among branch extracts (MB) with TPC, SIRT1 activity, and T-RVT, suggesting the extracts rich in phenolics and resveratrol are potent SIRT1 activators, that were shown by the MB extracts. Figure 2b differentiates the extracts based on specific phenolic markers. The MB 80 extract is uniquely associated with the highest QUE content, while the fruit extracts are shown to highly correlate with CA and MYR. The results showed different parts of a plant and preparation method of the extract from the same plant part, exhibit distinct phenolic compound profiles and corresponding bioactivities.

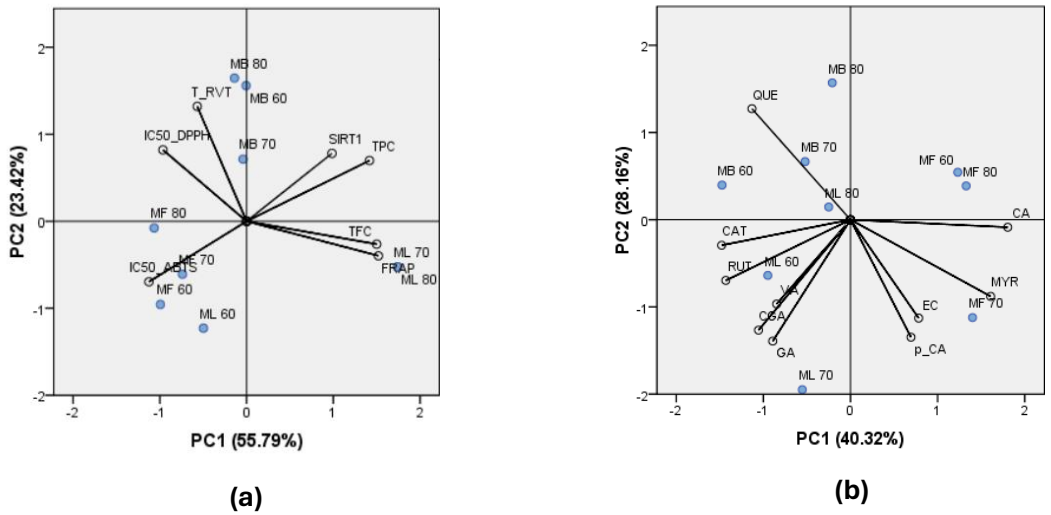

Figure 3. PCA biplot between mulberry extracts and phytochemical properties (a); phenolic compounds (b)

4. Conclusion

Different parts of the mulberry plant displayed distinct phytochemical compositions and bioactivities. While the leaf extracts (ML 70 and ML 80) exhibited the highest total phenolic content and total flavonoid content, the branch extract prepared with 60% ethanol (MB 60) showed the greatest SIRT1 activity (274.42%), comparable to the positive control and significantly higher than other extracts. The elevated SIRT1 activity in MB 60 is likely due to its high resveratrol (T-RVT) content, highlighting its potential as a functional ingredient. These findings suggest that MB 60 extract is a promising candidate for incorporation into functional foods or nutraceuticals aimed at supporting metabolic health and oxidative stress regulation.

Acknowledgements

The author would like to thank the Queen Sirikit Sericulture Center, Chiang Mai, Thailand, for providing the mulberry raw materials for the study, and the Faculty of Agro-Industry, Chiang Mai University, Thailand, for supporting the instrumentation and facilities used in this study.

References

1. Batiha GE, Al-Snafi AE, Thuwaini MM, Teibo JO, Shaheen HM, Akomolafe AP, Teibo TK, Al-Kuraishy HM, Al-Garbeeb AI, Alexiou A, Papadakis M. Morus alba: a comprehensive phytochemical and pharmacological review. Naunyn-schmiedeberg's Archives of Pharmacology. 2023 Jul;396(7):1399-413.
2. Hao J, Na R, Sun L, Jia Y, Han F, Fu Z, Wang Z, Zhao M, Gao C, Ge G. Chemical profile and quantitative comparison of constituents in different medicinal parts of Lactuca indica during varied harvest periods using UPLC-MS/MS method. Food Chemistry: X. 2023 Dec 30;20:101031.
3. Ferreira LR, Abelém BR, Reis JD, Herman CA, Figueiredo PL, Pinto LC, Martins LH, Silva MN, Gomes PW, Silva JK. Optimization of the Extraction of Bioactive Compounds and Metabolomic Profile of Licaria armeniaca. Plants. 2025 Oct 14;14(20):3158.
4. Chen C, Mokhtar RA, Sani MS, Noor NQ. The effect of maturity and extraction solvents on bioactive compounds and antioxidant activity of mulberry (Morus alba) fruits and leaves. Molecules. 2022 Apr 8;27(8):2406.
5. Martín-García B, Aznar-Ramos MJ, Verardo V, Gómez-Caravaca AM. The establishment of ultrasonic-assisted extraction for the recovery of phenolic Compounds and evaluation of their antioxidant activity from Morus alba leaves. Foods. 2022 Jan 24;11(3):314.
6. Wen P, Hu TG, Linhardt RJ, Liao ST, Wu H, Zou YX. Mulberry: A review of bioactive compounds and advanced processing technology. Trends in food science & technology. 2019 Jan 1;83:138-58.
7. Hao J, Gao Y, Xue J, Yang Y, Yin J, Wu T, Zhang M. Phytochemicals, pharmacological effects and molecular mechanisms of mulberry. Foods. 2022 Apr 18;11(8):1170.
8. Kattil A, Dash KK, Shams R, Sharma S. Nutritional composition, phytochemical extraction, and pharmacological potential of mulberry: A comprehensive review. Future Foods. 2024 Jun 1;9:100295.
9. Belew AA, Hanan GG, Meshesha DS, Akele ML. Evaluation of total phenolic, flavonoid contents, antioxidant and antibacterial activity of leaf extracts from Rhus vulgaris. Discover Plants. 2025 May 7;2(1):141.
10. Jannat N, Haque MA, Sharna JF, Fatema K, Rahman M, Sarker MS, Uddin MN, Uddin AR, Patwary MA. Chemical profiling, antioxidant potential, and thrombolytic activity of extracts from entire plant of Nelsonia canescens: An in vitro and chemoinformatic investigation. South African Journal of Botany. 2025 Nov 1;186:497-509.

11. Sanpinit S, Goon JA, Wetchakul P. Characterization of the antioxidant activity, identified free radical-relieving components by LC/QTOF/MS and acute oral toxicity studies of Tri-Tharn-Thip tea. Journal of Agriculture and Food Research. 2024 Jun 1;16:101131.
12. Aouadi A, Saoud DH, Bouafia A, Mohammed HA, Gamal HG, Achouri A, Laouini SE, Abdullah MM, Al-maswari BM, Al-Lohedan HA. Unveiling the antioxidant power: synthesis and characterization of lemon and orange peel-derived carbon quantum dots with exceptional free radical scavenging activity. Biomass Conversion and Biorefinery. 2025 Mar;15(6):9691-704.
13. Xu S, Luo H, Chen H, Guo J, Yu B, Zhang H, Li W, Chen W, Zhou X, Huang L, Liu N. Optimization of extraction of total trans-resveratrol from peanut seeds and its determination by HPLC. Journal of separation science. 2020 Mar;43(6):1024-31.
14. Chaipoot S, Wiriyacharee P, Phongphisutthinant R, Buadoktoom S, Srisuwun A, Somjai C, Srinuanpan S. Changes in physicochemical characteristics and antioxidant activities of dried shiitake mushroom in dry-moist-heat aging process. Foods. 2023 Jul 15;12(14):2714.
15. Gevrenova R, Zheleva-Dimitrova D, Balabanova V, Voynikov Y, Sinan KI, Mahomoodally MF, Zengin G. Integrated phytochemistry, bio-functional potential and multivariate analysis of Tanacetum macrophyllum (Waldst. & Kit.) Sch. Bip. and Telekia speciosa (Schreb.) Baumg.(Asteraceae). Industrial Crops and Products. 2020 Nov 1;155:112817.
16. Ramappa VK, Srivastava D, Singh P, Kumar U, Kumar D, Gosipatala SB, Saha S, Kumar D, Raj R. Mulberries: A promising fruit for phytochemicals, nutraceuticals, and biological activities. International Journal of Fruit Science. 2020 Sep 21;20(sup3):S1254-79.
17. Hosseini AS, Akramian M, Khadivi A, Salehi-Arjmand H. Phenotypic and chemical variation of black mulberry (Morus nigra) genotypes. Industrial Crops and Products. 2018 Jul 1;117:260-71.
18. Li Z, Chen X, Liu G, Li J, Zhang J, Cao Y, Miao J. Antioxidant activity and mechanism of resveratrol and polydatin isolated from mulberry (Morus alba L.). Molecules. 2021 Dec 14;26(24):7574.
19. Wang K, Ren W, Jia X, Xing Y, Wang Y, Wang J, Xu H. Physicochemical properties and phytochemical components of white mulberry (Morus alba L.) fruits with different density at harvest. Journal of Food Composition and Analysis. 2023 Apr 1;117:105113.
20. Skrovankova S, Ercisli S, Ozkan G, Ilhan G, Sagbas HI, Karatas N, Jurikova T, Mlcek J. Diversity of phytochemical and antioxidant characteristics of black mulberry (Morus nigra L.) fruits from Turkey. Antioxidants. 2022 Jul 8;11(7):1339.
21. Yang X, Jiang T, Wang Y, Guo L. The role and mechanism of SIRT1 in resveratrol-regulated osteoblast autophagy in osteoporosis rats. Scientific reports. 2019 Dec 5;9(1):18424.
22. Ciccone L, Piragine E, Brogi S, Camodeca C, Fucci R, Calderone V, Nencetti S, Martelli A, Orlandini E. Resveratrol-like compounds as SIRT1 activators. International Journal of Molecular Sciences. 2022 Dec 1;23(23):15105.
23. Ma WF, Duan XC, Han L, Zhang LL, Meng XM, Li YL, Wang M. Vanillic acid alleviates palmitic acid-induced oxidative stress in human umbilical vein endothelial cells via Adenosine Monophosphate-Activated Protein Kinase signaling pathway. Journal of Food Biochemistry. 2019 Jul;43(7):e12893.

P - 201

Good Manufacturing Practices of Chili Paste Producing Community Enterprises in Songkhla, Thailand: Major Defect Criteria Outlook

Karnjapan Janthawornpong*

Food industry management program, Faculty of Agro-industry, Prince of Songkla University, Thailand

**Corresponding author E-mail: karnjapan.j@psu.ac.th*

Abstract: Community-based enterprises (CBEs) are regarded as a means to mitigate the material poverty of the rural population through their economic development process. The venture aims to leverage local natural resources, cultural assets, and social strengths to enhance community living conditions. Products of a CBE, including food products, are mainly derived from its local assets. In Songkhla province, rural residents effectively utilize chili paste production for both internal consumption and sale. The quality and safety of food products are crucial to the success and sustainability of the business. From a food safety perspective, CBE products are obliged to comply with the Good Manufacturing Practices (GMP) standard. These rural business entities still lack essential features for business success, including technological capabilities, food quality and safety management, and business knowledge. This study, therefore, aims to elucidate the weaknesses and opportunities to improve food safety in accordance with the GMP standard. A convenient sampling was conducted. Thirty-eight chili paste-producing CBEs, located across Songkhla province, participated voluntarily. Socio-economic data were collected through face-to-face interviews with the group leader and key group committee members, using a semi-structured questionnaire. A site visit observation was performed at each facility, using the GMP checklist form issued by the Food and Drug Administration of Thailand. The results indicate that among the seven major defect criteria, three criteria were not met by half of the studied CBEs. The major defect criteria for which about half of CBEs received a need-improvement level were measures to manage the packing area to prevent recontamination (44.7%), regular process control to reduce and eliminate microbial hazards (60.5%), and the provision of annual product quality analysis results (52.6%). Areas for improvement to align with food safety standards were discussed. Strengthening GMP standards not only enhances consumer trust in food safety but also promotes sustainable economic growth and competitiveness in rural communities.

Keywords: Chili paste producer; Community-based enterprises; Good Manufacturing Practices; Local food safety; Major defect criteria

1. Introduction

Creating a community-based enterprise (CBE) is regarded as a means of mitigating material poverty among rural populations through economic development. The venture serves as a way to capitalize on local natural resources as well as cultural and social assets to improve the living conditions of the community. The strength and sustainability of a CBE depend on community involvement in decision-making. Successful endeavors can be transferred to other communities, both within the exact geographical location and to businesses of the same type [1],[2]. In Thailand, CBEs are neighborhood groups that manage assets, such as cultural and natural resources, to generate income, fostering self-reliance and supporting national sustainability [3]. The success of CBE performance in southern Thailand depends largely on creating a competitive advantage. Knowledge management, government support, and supply chain

management practices are parts of this competitive advantage. However, when considering each component, trust in product quality was inadequate, indicating that CBEs in the South produce relatively few high-quality products or services. As such, products or services should be produced in accordance with Thai industrial standards, the Food and Drug Administration, or Halal [4]. Additionally, from a food safety standpoint, food products from small and medium-sized enterprises, including CBEs, must meet mandatory safety standards, such as Good Manufacturing Practices (GMP), to build consumer trust and gain a competitive edge. The critical part that determines whether a food operator passes or fails to meet the GMP standards is defined as the major defect criteria. All food producers seeking GMP certification must meet these criteria.

From a global perspective, small and medium-sized food enterprises (SMEs) face similar challenges in complying with food safety standards. Many SMEs encounter significant obstacles, including limited financial resources, lack of technical expertise, insufficient training, and complex documentation requirements [5]. In a developing country like Pakistan, implementing HACCP, ISO 22000, and GMP helps improve documentation systems, hazard control procedures, and product quality management. Many SMEs struggle to remain compliant due to limited financial capacity, a lack of technical knowledge, and insufficient regulatory guidance [6]. In a developed country like the USA, compliance costs are high for SMEs. Labor and time are major hidden costs. Training programs rarely address financial aspects. Many small food processors believe the costs of implementation will outweigh the benefits [7].

Likewise, in Thailand, according to the Department of Agricultural Extension's 2025 database, there are approximately 250 food-processing CBEs in Songkhla province, but fewer than 10% are GMP-certified. This study, therefore, aims to clarify the challenges and opportunities for enhancing food safety practices in line with GMP standards for CBEs, using chili paste-producing community enterprises in Songkhla province as a case.

2. Materials and Methods

2.1 Population and Sampling

Songkhla province, situated on the Gulf of Thailand, is considered an economic powerhouse in the lower southern region. The city is rich not only in natural resources but also in cultural heritage. This culture is also reflected in the food, which is renowned for its unique spicy southern curry, derived from a variety of chili pastes. Chili pastes are produced locally throughout the province, primarily by CBEs, as they are essential ingredients in most southern cuisines and consumed daily. According to the Department of Agricultural Extension's list, there are currently 48 chili paste-producing CBEs registered by name in Songkhla province. All registered chili paste-producing CBEs were contacted by telephone to request permission, including permission to schedule interviews and site visits. As a result, thirty-eight chili paste CBEs agreed to participate in the survey.

2.2 Data collection

Socio-economic data were collected through face-to-face interviews with the group leader and 2-3 key members of the group committees, using a semi-structured questionnaire. A site visit observation was conducted, and consequently, at each facility, the GMP checklist form issued by the Food and Drug Administration (FDA) of Thailand was used. CBEs' practices were evaluated through observation and by asking some questions, as stated in the FDA's GMP manual, to clarify certain points. Each GMP requirement or sub-requirement was scored based on a decision flowchart (Figure 1). The decision flowchart consists of three questions. For each question, evaluate whether the answer is 'Yes' or 'No.' If the first answer is 'No,' proceed to the second; if the second is 'No,' proceed to the third until all three questions are completed, and a final score will be obtained. There are three score levels: Good, Acceptable, and Needs Improvement, corresponding to 2, 1, and 0 points, respectively. Individual CBE information was kept confidential. It was reported only as a group.

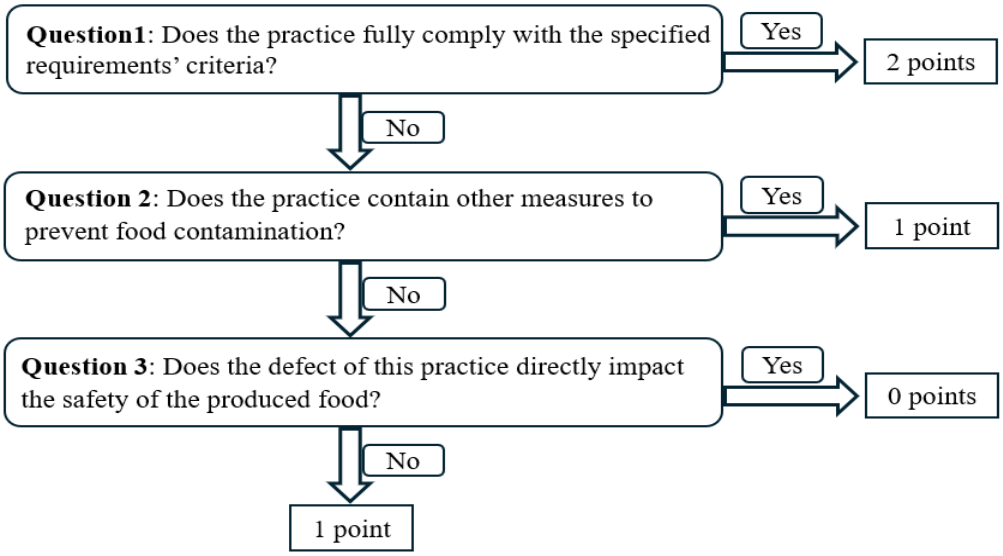

Figure 1. Decision flowchart of questions for GMP requirements scoring

2.3 Data analysis

Socioeconomic and scoring data for CBEs were analyzed using descriptive statistics. The relationship between socioeconomic variables and GMP major defect criteria scores was examined with the Mann-Whitney U test for two independent ordinal groups. The Kruskal-Wallis H test was employed to identify if there were statistically significant differences among three or more independent groups of ordinal data. A p-value of <0.05 was considered significant.

3. Results & Discussion

3.1 Socio-economic characteristics of the studied chili paste-producing community enterprises

Table 1. Socio-demographic profiles of chili paste-producing CBEs

Characteristics	Categories	Frequency (%) N = 38
Years in operation	0-5 years	39.47
	6-10 years	31.58
	more than 10 years	28.95
Number of members	≤ 10	10.53
	11-30	47.37
	31-50	23.68
	more than 50	18.42
Annual production volume (kg.)	less than 5,000	63.16
	5,001 - 20,000	26.32
	more than 20,000	10.53
Possession of a production facility	Yes	68.42
	No	31.58
Business loan	Yes	13.16
	No	86.84
Basic hygienic training	Yes	28.95
	No	63.16

Socio-economic profiles of surveyed chili paste-producing CBEs, including years in operation, number of members, annual production volume, possession of production facilities, loan status, and hygienic training, are presented in Table 1. Years of establishment are distributed quasi equally across three groups: 0-5 years (39.47%), 6-10 years (31.58%), and more than 10 years (28.95%). Half of the studied CBEs have between 11 and 30 members (47.3%). Most CBEs produce less than 5,000 kgs of chili paste annually (63.16%). They have separate production facilities (68.42%). Some of them carry debts (13.16%). A few of the studied CBEs have received basic hygienic training (28.95%) from competent authorities.

3.2 GMP major defect criteria performance of studied CBEs

Food safety practices of chili paste producers in Songkhla province were evaluated against the GMP major defect criteria, as shown in Figure 2. Based on the FDA's GMP standards checklist, 7 sub-requirements are defined as major defect criteria. A description of each sub-requirement is presented in Table 2.

Table 2. Description of GMP sub-requirements defined as major defect criteria

Sub-requirement	Description
Req 1.8	The production building has a packing room and implements measures to prevent re-contamination of the packaging area after the product has been sterilized.
Req 3.3.1	When using food additives, they must be used as prescribed by law, weighed/measured with appropriate equipment, mixed thoroughly, and records of use results must be kept. For processing aids, they must be used in accordance with safety data, and measures must be in place to remove them to safe levels.
Req 3.3.3	Water and ice used as ingredients or in contact with ready-to-eat food must meet the quality standards specified in the Ministry of Public Health announcement, or have analytical test results at least once a year, and must be stored in a manner that prevents contamination.
Req 3.4	The process for reducing and eliminating microbial hazards is controlled to ensure safe consumption levels, with regular monitoring and recording of results.
Req 3.5	For production without microbial reduction/elimination processes—such as mixing dry ingredients or oil-based liquids, portioning dry foods, trimming fresh vegetables/fruits, or packaging fresh foods—contamination must be strictly controlled throughout the entire production process.
Req 3.7	During production, raw materials, ingredients, food additives, and final products are transported in such a way that prevents cross-contamination.
Req 3.9.1	Final products meet the quality or standards specified in relevant Ministry of Public Health announcements, with analytical test results conducted at least once per year.

In Req 1.8, one third (36.8%) of survey CBEs received "Good" scores. Those who received a "Fine" score (18.4%) lacked a designated packing area, although they maintained hygienic packing conditions. Almost half of the survey CBEs (44.7%) failed to meet Req 1.8. They received a zero score or "Need improvement." The major reason was the lack of a distinct building or designated area for packing, which prevents cross-contamination and re-contamination. Some CBEs shared production utensils with other food products. They lacked production equipment specific to chili paste production. Segregating processing zones and providing dedicated clean

areas for handling finished products and packaging are critical. Without separation, pathogens from raw or preparation areas can contaminate ready-to-eat products through equipment, surfaces, or employee movement, leading to product recontamination [8]. Hygienic zoning is essential to prevent contamination and facilitate effective cleaning and sanitation programs. Dividing processing areas into zones based on contamination risk enables better control of personnel movement, environmental monitoring, and sanitation procedures [9]. To overcome this limitation of CBEs, support from competent authorities in layout design would help improve the processing line to comply with GMP.

In southern chili paste production, only basic food additives such as salt were used. All CBEs met this criterion. Most of them (73.7%) received a "Fine" score in Req 3.3.1 for failing to record data after weighing, and some did not use proper weighing utensils. Food containers and other food-contact surfaces in the processing area can serve as vehicles for cross-contamination. Using the correct utensil separately for each product or process should reduce this risk [10].

Water plays a crucial role in food production and processing. Contaminated water can introduce microbiological, chemical, and physical hazards into food products [11], [12]. For Req 3.3.3, water is mainly used to wash raw materials before mixing and grinding to make chili paste. About half of the CBEs that received a "Good" score washed raw materials with tap water and rinsed with filtered water during production (50%). Others with a "Fine" score (47.4%) used tap water. A few CBEs (2.6%) that received a zero score used well water for washing raw materials. Based on these findings, it is highly recommended to educate and encourage CBE workers who received a zero score to use safe water in the chili paste processing. Food safety training is required.

To comply with Req 3.4, the process controls to minimize microbial hazards in chili paste production begin with raw material washing, continue during ingredient mixing and grinding using clean equipment, and extend to chili paste packaging in a designated area, with regular monitoring and record-keeping. In this case, only 10.5% of survey CBEs completed all required actions and received a "Good" score. A few CBEs (28.9%) received a "Fine" score because they did not regularly keep records of good practices. The majority of surveyed CBEs (60.5%) failed to meet this sub-requirement for two main reasons. First, most of them failed to control packaging conditions by using a designated packaging room or area. Second, none of them had a record-keeping system. Inadequate documentation is one of the most common weaknesses in SME food safety systems. Proper record keeping supports traceability, process verification, and compliance with regulatory audits [13]. A digital data recording system, such as a smartphone-based one, could help small food operators keep records more conveniently [14].

For Req 3.5, the part concerning chili paste production focuses on packaging fresh food ingredients. CBEs that maintained hygienic conditions throughout the production process received a "Good" score (44.7%). Others whose chili paste packaging step raised concerns about potential cross-contamination earned a "Fine" score (39.5%). The rest received a "Need improvement" score due to several possible cross-contaminations during chili paste production (15.8%), including raw material washing, ingredient mixing, packaging, and worker hygiene. The main reasons for poor worker hygiene were a lack of hygiene facilities, such as handwashing stations, and unhygienic practices. A study found that food handlers without access to proper hygiene were 4.84 times more likely to engage in unsafe food-handling practices, directly undermining food safety goals [15]. Beyond hygiene facilities, fostering a food safety culture in CBE that views hygiene as a shared value rather than just a rule is vital to the long-term success of the food safety management system [16].

Hygiene and environmental control procedures are key for maintaining product quality and lowering contamination risks [17]. In Req 3.7, transport within chili paste-producing CBEs mainly involves moving washed raw materials and chili paste mixtures. CBEs that kept hygienic conditions during the transfer of washed raw materials and covered the chili paste mixtures during

transport to prevent cross-contamination received a “Good” score (42.1%). Other CBEs that did not cover the chili paste mixtures during transport received a “Fine” score (44.7%). The remaining CBEs (13.2%) failed to show evidence of hygienic control during the transfer of raw materials and semi-finished products. Basic food safety training is required for this latter group.

Finished product testing is part of validation and verification procedures that help ensure the food safety management system works as intended. It emphasizes that food manufacturers should conduct regular reviews to demonstrate that their "finished product quality" remains under control over time, rather than checking each batch individually [18]. The Req 3.9.1 mainly focuses on final product quality. To meet this requirement, CBE must provide analytical test results for the finished chili paste product. Since testing is costly, most CBEs prefer not to allocate funds for it. Only 5.3% of surveyed CBEs have annual test results for finished products and received a “Good” score. For the CBEs that scored “Fine” (42.1%), finished product test results were provided only once. More than half of the surveyed CBEs (52.6%) have never had their finished products undergo analytical testing. Therefore, encouraging CBEs to conduct annual product testing is crucial for achieving GMP certification. A study of Taiwanese food businesses found that the main motivation for SMEs to participate in certification programs, including voluntary quality reviews, is access to export markets [19]. Relevant authorities could use this motivation to increase CBE participation rates.

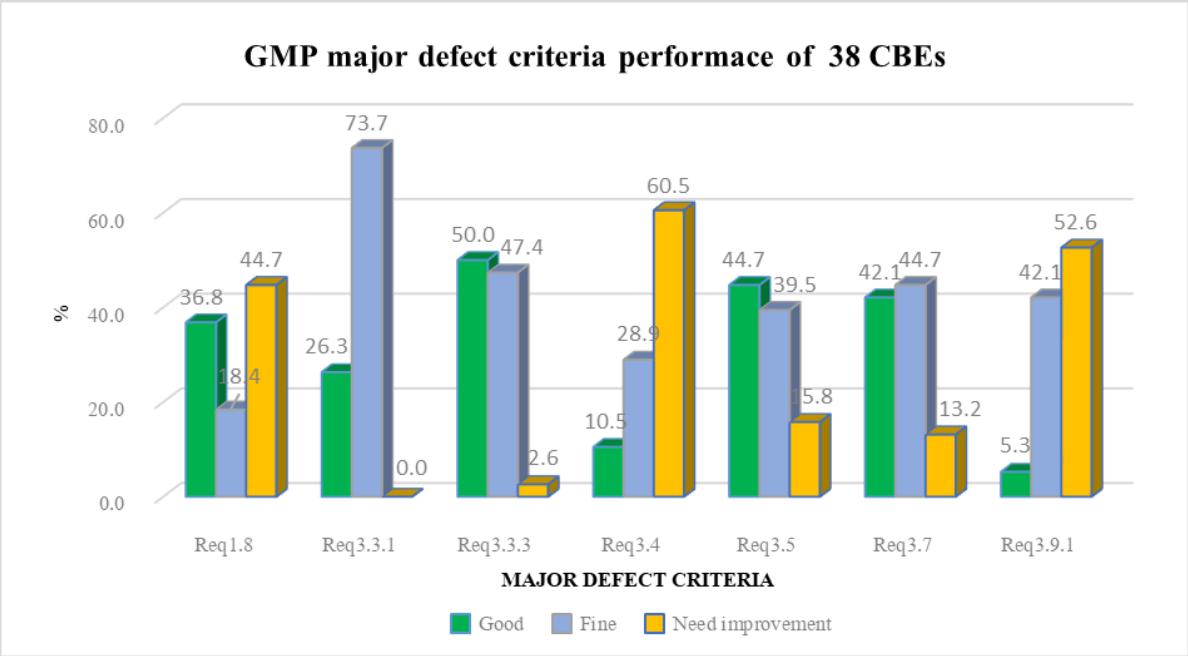

Figure 2. The percentage of CBEs obtained good, fine, and needs improvement scores on the GMP’s major defect criteria

3.3 Association of socio-economic variables with GMP major defect criteria scores

Chili paste-producing CBEs can be grouped according to socioeconomic variables, including annual production volume, the possession of separate production facilities, and completion of basic hygiene training. Based on annual production volume, three groups of chili paste-producing CBEs can be defined: less than 5,000 kgs, 5,001-20,000 kgs, and more than 20,000 kgs. CBEs can be classified by their annual chili paste production volume. The Kruskal-Wallis H test was used to assess whether production volume is associated with the outcome (Table 3).

Table 3. Kruskal-Wallis H test of three groups of CBEs based on annual production volume

Requirements	χ^2	df	p	ε^2	Interpretation
Req1.8	2.185	2	0.335	0.05904	Not significant
Req3.3.1	0.302	2	0.860	0.00815	Not significant
Req3.3.3	1.655	2	0.437	0.04474	Not significant
Req3.4	1.061	2	0.588	0.02868	Not significant
Req3.5	0.280	2	0.869	0.00757	Not significant
Req3.7	2.134	2	0.344	0.05767	Not significant
Req3.9.1	4.660	2	0.097	0.12595	Not significant

Overall, Kruskal–Wallis results indicate no statistically significant differences in GMP major defect criteria scores among the three annual production volume groups ($p > .05$), although data of the sub-requirement 3.9.1 showed a moderate, near-significant trend ($p = 0.097$), suggesting potential group differences that may emerge with a larger dataset. Our result is in line with the study on caterers in Singapore, which found that the scale of operation alone did not determine conformity to hygiene practices. Other factors, such as staff strength and the company's food safety culture, could play a role [20].

When grouping chili paste-producing CBEs according to whether they have separate production facilities or have completed basic hygienic training, there will be two distinct groups: those with and those without. GMP major defect criteria score distributions for these two groups were analyzed to determine whether there is a relationship between the scores and the variable under consideration.

Figure 3 shows seven sets of mean and median GMP scores for the two CBE groups, stratified by the presence of separate production facilities. The distinction between the two mean score lines is noticeable for Req 1.8, Req 3.4, Req 3.7, and Req 3.9.1, indicating pronounced differences in the mean scores. It can be inferred that the presence of a segregated production facility contributes to meeting these requirements.

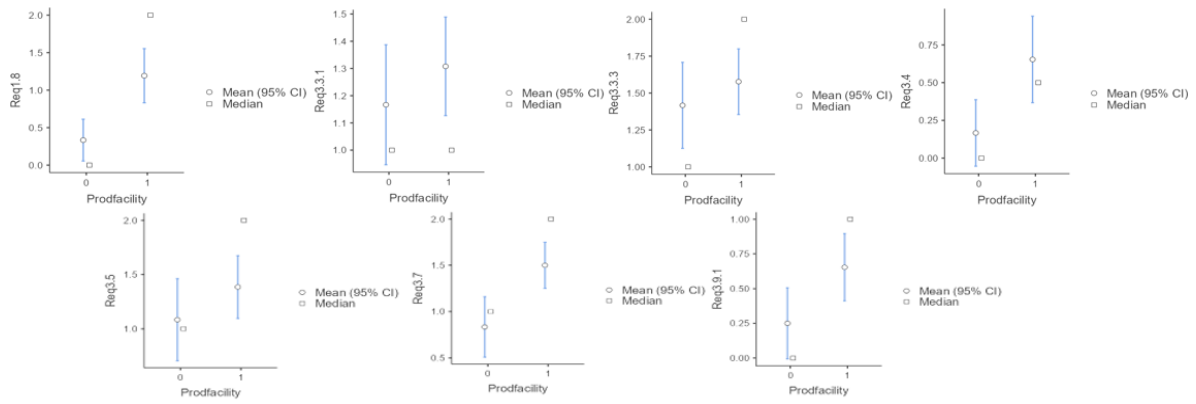

Figure 3. Group mean and median of GMP requirements scores grouped by possession of production facilities status (0 = No, 1 = Yes)

Figure 4 shows seven sets of mean and median GMP scores for the two CBE groups, stratified by attainment of basic hygienic training. The distinction between the two mean score lines is slightly noticeable for Req 3.4 and Req 3.5, indicating that the mean score differences are distinguished in these cases.

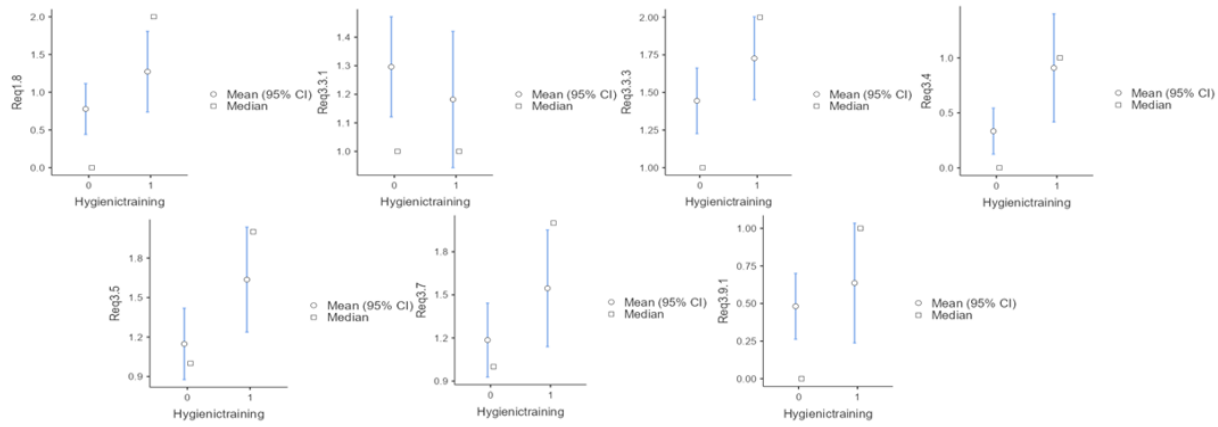

Figure 4. Group mean and median of GMP requirements scores grouped by hygienic training attainment (0 = No, 1 = Yes)

The Mann-Whitney U test was used to compare whether there is a significant difference between the two CBE groups under consideration (Table 3). In the case of owning separate production facilities, a Mann–Whitney U test revealed statistically significant differences ($p < 0.05$) in GMP scores for sub-requirements 1.8, 3.4, and 3.7. The effect size indicates how strongly one group had substantially higher GMP major defect criteria scores than the other. Its value ranges from small (0.1) to large (0.5). In this study, there is a large effect size difference between groups for sub-requirements 1.8 and 3.7, and a medium effect size difference between groups for sub-requirement

3.4. This indicates that having a separate production facility contributed notably to better performance in these sub-requirements.

Additionally, when comparing two CBE groups with and without basic hygienic training, a Mann–Whitney U test revealed statistically significant differences ($p < 0.05$) in GMP scores for sub-requirements 3.4 (medium effect size: 0.397) and 3.5 (medium effect size: 0.384). This suggests that basic hygiene training improves GMP scores for these sub-requirements. The non-significant difference in GMP major defect criteria scores across other sub-requirements indicates that basic hygiene training alone is insufficient to address all issues. It likely results from practical limitations, such as the absence of a designated packing area, access to clean water, appropriate equipment, and testing of finished goods. Nonetheless, providing GMP or other relevant food safety training remains crucial for enhancing food safety practices. Furthermore, regular training programs promote consistent food safety practices [21] and foster positive attitudes toward commitment to food safety standards [22].

Table 3. Mann-Whitney U test of socio-economic variables and GMP requirements scores

Major Defect Requirements	Separate production facility			Hygienic training		
	Mann-Whitney U test	Sig.	Effect size	Mann-Whitney U test	Sig.	Effect size
Req 1.8	78	0.008	0.5	105	0.134	0.293
Req 3.31	134	0.376	0.141	131.5	0.486	-0.114
Req 3.3.3	128.5	0.33	0.176	110.5	0.165	0.256
Req 3.4	100	0.045	0.359	89.5	0.03	0.397
Req 3.5	117	0.189	0.25	91.5	0.048	0.384
Req 3.7	73.5	0.005	0.529	104.5	0.125	0.296
Req 3.9.1	102	0.057	0.346	130.5	0.524	0.121

4. Conclusion

A community- based enterprise (CBE) is a business owned and run by community members. It promotes sustainable development by balancing economic, social, and environmental goals, creating local jobs, reinvesting profits for community benefit, fostering social cohesion through participation, and using local resources sustainably. It also builds community resilience and self-sufficiency through shared ownership, local solutions, and skill development. Chili paste is a common ingredient produced by residents through CBEs in Songkhla province. From a food safety standpoint, products from CBEs must comply with Good Manufacturing Practices (GMP) to earn consumer trust. The key factors that determine whether a food operator passes or fails GMP compliance include seven sub-requirements, known as major defect criteria. Three of these criteria were not met by half of the studied CBEs. The major defect criteria where half of the CBEs received a "Need improvement" score are: 1) having a dedicated packing room and measures to prevent re-contamination after sterilization (44. 7%), 2) regular process control to reduce microbial hazards and keep records (60. 5%), and 3) providing annual product quality analysis results (52. 6%). Addressing these three areas can improve the chances of meeting GMP standards. Analysis of GMP defect scores and socioeconomic variables showed that having separate production facilities greatly helps meet several major defect criteria, including designating a packing area and implementing measures to prevent re-contamination (Req 1.1.8), controlling microbial hazards for safe consumption (Req 3.4.4) and transporting raw materials and work-in-process in ways that prevent cross-contamination (Req 3.7.7). Getting basic hygiene training significantly improves scores on Req 3.3.4 and Req 3.3.5, which concern maintaining hygienic conditions during production. Practices such as the lack of a dedicated packing area, the use of available clean water, and the use of clean equipment need to be effectively addressed and managed by CBEs, with guidance and close supervision from competent authorities, to improve the production layout and enhance safe production. The other support from authorities, such as motivation or financial incentives through market expansion opportunities for CBEs, can encourage them to submit their products for testing. This will help CBEs meet the requirements for providing annual product test results. Lastly, GMP and relevant food safety training, with regular refresher courses, should be implemented to provide knowledge and good practices that foster habits aligned with food safety goals and, ultimately, build a competitive advantage.

Acknowledgements

The author would like to express all appreciation to respondents who voluntarily provided invaluable information for this research.

References

1. Peredo, A.M.; Chrisman, J.J. *The Academy of Management Review* 2006, *31*, 2, 309-328.
2. Khiawnoi, P.; Nakudom, S.; Noobutr, P.; Kaewzang, U. *Sustainability* 2025, *17*, 2, 5483.
3. Mettathamrong, J.; Promket, C.; Vichasilp, K. *International Journal of Operations. and Quantitative Management* 2022, *28*, 1, 121-133.
4. Soonsuwon, K.; Jankingthong, W.; Sangkapan, J. *Migration Letters* 2024, *21*, S2, 450-61.
5. Lee, JC.; Neonaki, M.; Alexopoulos, A.; Varzakas, T. *Foods*, 2023, *12*, 17, 3218.
6. Qamar, T.; Ahmad, RS.; Arshad, MS.; Afzaal, M. *Journal of Food Quality* 2024, *1*, 6110406.
7. Fitzsimmons, JA.; Kinchla, AJ.; Allingham, C. *PLoS ONE* 2024, 19, 9, e0306618.
8. Shimojima, Y.; Kanai, Y.; Moriyama, T.; Arakawa, S.; Tamura, Y.; Okada, Y.; Morita, Y. *Journal of Food Protection* 2023, *86*, 10, 100149.
9. Holah, J. in Hygienic Design of Food Factories; Holah, J.; Lelieveld, HLM.; Moerman, F. Eds. Cambridge: Woodhead Publishing, 2023; pp 221–240.

10. Kirchner, M.; Everhart, S.; Doring, L.; Smits, C.; Faircloth, J.; Duong, M.; Goulter, RM.; Goodson, L.; Shelly, L.; Shumaker, ET.; Cates, S.; Bernstein, C.; Lavallee, A.; Jaykus, LA.; Chapman, B.; Schaffner, D. *Journal of Food Protection* 2022, *85*, 11, 1594–603.
11. Bhagwat, VR. In: Elsevier eBooks 2019, 219–247. Available from: https://doi.org/10.1016/b978-0-12-816333-7.00009-6
12. Khanal, AR.; Timilsina, RH.; Sharma, B.; Pokharel, B.; Aryal, R. *Journal of Food Protection* 2024, *87*, 3, 100228.
13. Dzwolak, W. *Food Control* 2019, *106*, 106716.
14. Lin, K.; Chavalarias, D.; Panahi, M.; Yeh, T.; Takimoto, K.; Mizoguchi, M. *Nature Food* 2020, *1*, 11, 673-679.
15. Negassa, B.; Ashuro, Z.; Soboksa, NE. *Environmental Health Insights* 2022, 16, 11786302221105320.
16. Pai, AS.; Jaiswal, S.; Jaiswal, AK. *Foods* 2024, *13*, 24, 4078.
17. Chandimali, N.; Bae, J.; Hwang, JY.; Bak, SG.; Cheong, SH.; Lee, SJ. *Journal of Food Protection* 2025, *88*, 7, 100547.
18. Awuchi, CG. *Cogent Food & Agriculture* 2023, *9*, 1, 2176280.
19. Chen, SY.; Lien, KW. *Foods* 2025, *14*, 21, 3784.
20. Hartantyo, SHP.; Selvaraj, R.; Ho, J.; Oh, JQ.; Er, JC.; Li, A.; Aung, KT. *Foods* 2023a, *12*, 12, 2376.
21. Tuglo, LS.; Agordoh, PD.; Tekpor, D.; Pan, Z.; Agbanyo, G.; Chu, M. *Environmental Health and Preventive Medicine* 2021, *26*, 1, 54.
22. Alkhaldi, S.; Hod, R.; Isa, ZM.; Idris, IB.; Karim, N. *Current Research in Nutrition and Food Science Journal* 2025, *13*, 2, 541–58.

P - 204

Preparation and Characterization of Mulberry Leaf (*Morus alba* Linn.) Hydrogel Microparticles via Extrusion Microencapsulation

Ploypailin Akanitkul, Sopapim Wattanapoka, Thunnalin Winuprasith*

Institute of Nutrition, Mahidol University, Salaya, Nakhon Pathom 73170, Thailand

**Corresponding author E-mail: thunnalin.win@mahidol.ac.th*

Abstract: This study optimized the preparation of mulberry leaf (*Morus alba* L.) hydrogel microparticles produced by extrusion microencapsulation and characterized their stability and functional properties for food applications. Mulberry leaves of the 'Chiang Mai 60' cultivar were selected and processed using vacuum drying (VD) based on their superior chemical composition and physicochemical characteristics compared with sun drying (SD). The vacuum-dried mulberry leaf powder exhibited a significantly higher water solubility (17.88 ± 0.63%) than the sun-dried powder (15.35 ± 0.46%), indicating improved functional performance. Sodium alginate solutions (1–3% w/v) were combined with varying levels of mulberry leaf powder and cross-linked with 10% (w/v) calcium chloride. The resulting hydrogel beads were evaluated for morphology, size uniformity, and structural integrity under pasteurization-like thermal stress (75 °C/10 min), gastric-mimicking acidity (pH 1.8), and swelling in distilled water. The optimal formulation—3.0% (w/v) alginate with 1.0% (w/v) mulberry leaf—yielded spherical, uniform microparticles that maintained integrity across temperature, pH, and swelling challenges. Furthermore, the small and uniform particle size produced by the BUCHI B-390 encapsulator supports incorporation into food products, such as yogurt and functional beverages. This indicates that the technique is an effective and scalable approach to enhance the stability and delivery of mulberry leaf bioactives within food matrices.

Keywords: Mulberry Leaf; Hydrogel Beads; Microencapsulation; Stability

1. Introduction

In recent years, consumer awareness regarding health and wellness has increased significantly, leading to a growing preference for functional food products that offer health-promoting benefits [1]. This shift in market demand has driven the food industry to explore natural bioactive ingredients. Mulberry leaves (*Morus alba* L.) are recognized as a premium source of such compounds, including phenolics, flavonoids, and alkaloids like 1-deoxynojirimycin (DNJ), which are associated with antioxidant and anti-diabetic activities [2]. However, the application of mulberry leaf powder in food systems is challenging due to its poor stability; these bioactive constituents are sensitive to environmental stressors such as light, oxygen, and temperature, which lead to significant degradation during processing and storage.

To overcome these limitations, microencapsulation technology has been utilized to protect and stabilize these sensitive materials. Among various methods, extrusion microencapsulation via ionic gelation is highly effective for food-grade applications [3]. This technique involves the formation of a hydrogel matrix—typically using sodium alginate—which cross-links with multivalent ions to entrap the target material. The extrusion method is particularly advantageous as it allows for the production of uniform microparticles under mild conditions, ensuring the structural integrity of the encapsulated core.

Nonetheless, the development of mulberry leaf hydrogel beads requires precise optimization of the formulation to ensure maximum stability and performance within food

matrices. Therefore, the objective of this study was to optimize the preparation of mulberry leaf (Morus alba L.) hydrogel microparticles produced by extrusion microencapsulation. Furthermore, the research aimed to characterize the stability of these beads under various environmental conditions and evaluate their physicochemical properties. These findings are intended to establish the optimal parameters for utilizing mulberry leaf hydrogel beads as stable ingredients in diverse food applications, such as functional beverages and dairy products.

2. Materials and Methods

2.1 Materials and Chemicals

Mulberry leaves (*Morus alba Linn.,* c.v. Chiang Mai 60) were freshly harvested from an orchard in Chiang Mai province, Thailand. Citric acid anhydrous was purchased from Krungthepchemi (Bangkok, Thailand). Sodium alginate and calcium chloride were purchased from Sigma Aldrich Corp. (St.Louis, MO, USA). All the chemicals were analytical grade.

2.2 Preparation of mulberry leaf powder (MLP)

The mulberry leaves used in this study were processed into fine powders using two different drying methods: sun drying (SD) and vacuum drying (VD) at 45 °C under a vacuum pressure of 50 mbar for 8 h until constant weight was achieved. Both dried samples underwent subsequent grinding. The vacuum-dried sample was further sieved through a standard 100-mesh sieve. The vacuum-dried mulberry leaf powder (MLP) was prepared and supported by Chiang Mai BioVeggie Co., Ltd., Thailand.

2.3 Chemical composition analysis

MLP samples were analyzed for protein, fat, carbohydrate, total dietary fiber, ash and moisture contents were determined using the methods described in the AOAC (2019). All samples were submitted for analysis to ALS Laboratory Group (Thailand) Co., Ltd., Bangkok, Thailand.

2.4 Physicochemical properties of mulberry leaf powder (MLP)

2.4.1 Particle size determination

Particle size and size distribution of both MLP was measured using a laser particle size distribution analyzer (Mastersizer 3000; Malvern Instruments Ltd., Worcestershire, UK). The results were reported as particle size distribution, surface-weighted mean particle diameter (D_{32}).

2.4.2 Colorimetry

Powder color was characterized with a Hunter Lab Digital Colorimeter (Color Reader CR-20, Konica Minolta, Inc., Goyang-si, Korea) calibrated with a white standard tile. For each sample, 3 g powder was poured in a cup (leading to a powder layer of approximately 2 cm high) and color measurement was performed according to the three colors coordinates L*, a*, b* of CIE L*a*b* system. The L* value represents sample luminosity, varying from black (0) to white (100), the a* value represents the color varying from red (+) to green (−) and the b* value represents the color varying from yellow (+) to blue (−).

2.4.3 Moisture content

The moisture content of the dried powder samples was analyzed using moisture analyzer (MOC36u, shimudzu). About 2.0 g of sample was employed for moisture content analysis according to AOAC (2012). The moisture content was read directly from the equipment.

2.4.4 Water activity (aw)

The water activity of the dried powder samples was measured using a Chilled-Mirror dew point water activity meter (Pawkit, Decagon Devices, Inc., Pullman, Washington, USA).

2.4.5 Water solubility (WS) and Water holding capacity (WHC)

Water solubility (WS) and water holding capacity (WHC) of MLP were determined according to the protocol of Koksel et al. (2008) [4]. One gram of MLP was weighed into a pre-weighed centrifuge tube, added with 10 ml of distilled water, and then vortexed for 15 s every 5 minutes until 40 minutes. After 40 minutes of vortex, the samples were centrifuged using a

centrifuge (model Z 400K; HERMLE Labortechnik GmbH, Wehingen, Germany) at 2100 rpm for 10 minutes at room temperature. The supernatant was dried using hot air oven at 100 °C for 2 hours. The precipitate was weighed and then dried using hot air oven at 100 °C for 2 hours. Water solubility (WS) and water holding capacity (WHC) were calculated as follows:

$$\text{WS (\%)} = \frac{\text{weight of dried supernatant (g)}}{\text{weight of sample (g)}} \text{ X } 100$$

$$\text{WHC (g/g)} = \frac{\text{weight of wet precipitate - weight of dried precipitate}}{\text{weight of sample (g)}} \text{ X } 100$$

2.5 Preparation of Hydrogel Beads

Sodium alginate at concentrations of 1–3% (w/v) was dispersed in 100 mL of distilled water at room temperature using a magnetic stirrer for 30 min to obtain homogeneous mixtures. Subsequently, MLP at concentrations of 0.5, 1.0, and 2.0% (w/v) was added and constant stirring was continued for an additional 30 min. The beads were produced by adding the mixture dropwise into 10% w/v calcium chloride using a 3 ml hand-held transfer pipette. The drops were allowed to form beads for 30 min. The hydrogel beads were removed from the $CaCl_2$ solution and cleaned with distilled water. Finally, the beads were dried at 30 ◦C in a hot air oven.

For the extrusion method, a vibrating-nozzle encapsulator (Model B-390, BÜCHI, Flawil, Switzerland) was used with a 1,000 µm nozzle, a frequency of 1,500 Hz, a pressure of 120 mbar, and an electrode tension of 1,100 V. (Table 4) The size and uniformity of the MLP hydrogel beads were monitored and confirmed by the integrated optical monitoring system of the B-390 encapsulator during the production process. For manually prepared beads, a digital caliper was used to verify the diameter of at least 20 beads per batch to ensure consistency.

2.6 Stability Evaluation of Hydrogel Beads

2.6.1 Temperature Stability

Mulberry leaf hydrogel beads were evaluated for thermal stability by subjecting them to a temperature of 75 °C for 10 min. This condition was selected to simulate heat treatment during pasteurization processes commonly applied to food products. After heating, the beads were allowed to cool to room temperature prior to further observation and analysis.

2.6.2 pH Stability

The pH stability of the mulberry leaf hydrogel beads was assessed under acidic conditions by immersing them in a 5% (w/w) citric acid solution adjusted to pH 1.8 to simulate the gastric environment. While a 2–4 hour period is typical for gastric transit, the samples in this study were maintained under these conditions for 24 h at room temperature. This extended duration was intentionally selected to rigorously evaluate the maximum structural endurance of the alginate-calcium matrix and to ensure its suitability for long-term storage within acidic food matrices, such as yogurt or functional beverages. Following incubation, the beads were collected and evaluated for structural integrity and physical changes.

2.6.3 Swelling Capacity

The swelling capacity of the mulberry leaf hydrogel beads was determined according to the method described by Gong et al. (2011) [5] with minor modifications. Ten beads, which had been pre-dried at 25°C for 2 h, were immersed in distilled water. The samples were removed and weighed at specific time intervals of 30, 60, and 120 min. The swelling capacity (%) was calculated using the following equation:

$$\text{Swelling capacity (\%)} = \frac{Wt - W0}{W0} \times 100$$

where Wt represents the weight of beads at time t and W0 is the initial weight of the beads.

2.7 Statistical analysis

Data were expressed as mean ± standard deviation (SD) of triplicate experiments. An unpaired t-test was used to compare significantly differences between the two data sets. Values were considered significantly different at $p < 0.05$. The statistical analyses were conducted using SPSS software Version 23.0 (SPSS Inc., Chicago, IL, USA).

3. Results & Discussion

3.1 Chemical analyses of MLP

Table 1 presents the proximate chemical composition of MLP as influenced by different drying methods. The results showed that VD led to higher energy, fat, carbohydrate, and total dietary fiber contents than SD. Conversely, higher values for protein, ash, and moisture were recorded in the SD samples. The protein (20.0–20.6%), fat (2.46–4.40%), ash (12.3–15.0%), and moisture (4.39–9.31%) contents obtained in this study are in close agreement with those reported by Srivastava et al. (2006), who documented protein, ash, and moisture contents of 15.31–30.91%, 14.59–17.24%, and 5.11–7.24%, respectively. All of these components in MLP might be important from the nutrition point of view. Therefore, enrichment of different food products with MLP would enhance the nutritional quality of the product better than many food sources.

Table 1. Chemical analysis of MLP using different drying methods.

Compositions	Sun Drying (SD)	Vacuum Drying (VD)
Calories (Include Dietary Fiber) (kcals/100g)	315.00 ± 1.05^{b}	355.00 ± 2.01^{a}
Protein (g/100g)	20.60 ± 0.05	20.00 ± 0.02
Fat (g/100g)	2.46 ± 0.17^{b}	4.40 ± 0.12^{a}
Carbohydrate (Include Dietary Fiber) (g/100g)	52.60 ± 0.05^{b}	58.70 ± 0.02^{a}
Dietary Fiber (Total) (g/100g)	27.70 ± 0.05^{b}	31.20 ± 0.15^{a}
Ash (g/100g)	15.00 ± 0.10^{a}	12.30 ± 0.15^{b}
Moisture (g/100g)	9.31 ± 0.04^{a}	4.39 ± 0.05^{b}

* Values were measured in triplicate and shown as mean ± standard deviation.
* Different lowercase letters (a–b) in the same row result in a significant ($p \leq 0.05$) difference concerning different drying methods.

3.2 Physicochemical Properties of MLP

Color values, moisture content, and water activity of MLP produced by sun drying (SD) and vacuum drying (VD) are presented in Table 2. SD samples exhibited higher L* (lightness) than VD samples, while b* values were comparable, indicating a similar yellowish tone. A distinct difference was observed in a* values; SD powder showed a value of 1.17 (redness), whereas VD powder recorded -3.93 (greenness). Consequently, SD and VD powders appeared brownish-green and yellowish-green, respectively (Figure 1). The superior color retention in VD samples is attributed to the vacuum environment, which lowers the boiling point of water and minimizes thermal degradation of chlorophyll [6]. This controlled condition prevents the loss of heat-sensitive pigments and volatile compounds, unlike the SD process, where substantial chlorophyll

degradation led to a more brownish appearance. Furthermore, significant differences ($p < 0.05$) were observed in moisture content and water activity. The VD samples yielded a lower moisture content (5.11%) and water activity (0.23) compared to the SD samples (10.59% and 0.56, respectively). The higher values in SD samples stem from the unregulated nature of the solar dehydration process. The absence of precise temperature and temporal control often hinders effective moisture evaporation, particularly during extended drying periods [7]. Conversely, the vacuum drying technique provides a controlled environment that enhances mass transfer efficiency. This optimized process ensures more thorough moisture extraction, resulting in the superior stability observed in VD mulberry powder. Photographs showing the appearance of MLP produced by sun drying (SD) and vacuum drying (VD) are presented in Figure 1.

Table 2. Physicochemical Properties of MLP using different drying methods.

Properties/Sample	Sun Drying (SD)	Vacuum Drying (VD)
Color		
L*	49.20 ± 1.05^{a}	39.73 ± 1.27^{b}
a*	1.17 ± 0.06^{b}	-3.93 ± 0.21^{a}
b*	24.37 ± 0.20^{a}	25.00 ± 1.00^{a}
% Moisture content	10.59 ± 0.76^{a}	5.11 ± 0.54^{b}
Water activity (aw)	0.56 ± 0.01^{a}	0.23 ± 0.01^{b}

* Values were measured in triplicate and shown as mean ± standard deviation.
* Different lowercase letters (a–b) in the same row result in a significant ($p \leq 0.05$) difference concerning different drying methods.

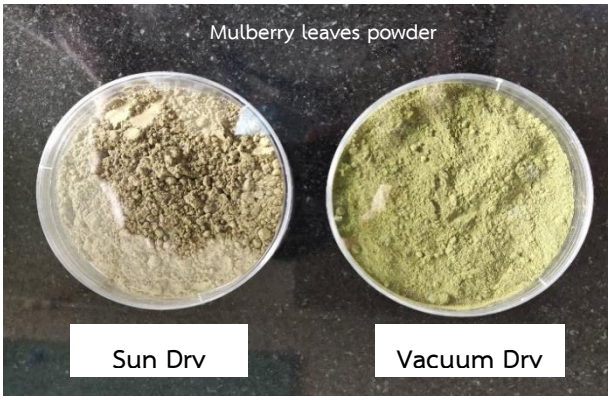

Figure 1. Appearance of MLP produced by sun drying (SD) and vacuum drying (VD)

The water solubility (WS) and water holding capacity (WHC) of MLP are presented in Table 3. The results indicate that VD mulberry powder exhibited significantly higher values for both parameters compared to SD powder ($p \leq 0.05$). This enhancement can be attributed to the VD process, which operates under reduced pressure, leading to a more porous structure that facilitates greater water entrapment within the matrix [8]. According to Elleuch et al. (2011) [8], water-binding properties are directly correlated with the solubility and WHC of dietary fibers, which can fluctuate based on particle size [9]. In this study, VD samples possessed smaller particle sizes (Table 3), resulting in an increased specific surface area and higher porosity, which ultimately enhanced their water holding capacity.

Table 3. Water solubility (WS) and Water holding capacity (WHC) of MLP using different drying methods.

Properties/Sample	Sun Drying (SD)	Vacuum Drying (VD)
% Water Solubility	15.35 ± 0.46[b]	17.88 ± 0.63[a]
Water Holding Capacity (WHC) (g of water/g of sample)	2.98 ± 0.03[b]	3.95 ± 0.08[a]
Particle Size d3,2 (surface-weighted mean diameter) (μm)	705.68 ± 15.72[a]	428.78 ± 29.96[b]

* Values were measured in triplicate and shown as mean ± standard deviation.
* Different lowercase letters (a–b) in the same row result in a significant ($p \leq 0.05$) difference concerning different drying methods.

3.3 Characterization of MLP Hydrogel Beads

Figure 2 shows the product of encapsulation with variation of concentration. The physical appearance of the dry beads was evaluated by visual examination and recorded by a digital camera. The morphology and visual characteristics of the beads, prepared with 1.0% (w/v) sodium alginate and varying concentrations of mulberry leaf powder (0.5–2.0% w/v), initially exhibited irregular, non-uniform shapes with a teardrop-like appearance. Notably, beads containing 0.5% (w/v) mulberry leaf powder displayed a flattened and partially collapsed structure (Figure 2C), indicating insufficient structural integrity. This collapse is likely attributed to the low total solid content and the relatively low alginate concentration, which were inadequate to maintain the bead's spherical geometry during gelation. In contrast, when the sodium alginate concentration was increased to 2.0%–3.0% (w/v), the bead morphology progressively improved toward a more regular and spherical shape. This suggests that higher polymer concentrations enhanced the solution viscosity and reinforced the cross-linked gel network, thereby promoting better shape retention. Such improvements in sphericity align with the formation of a denser 'egg-box' matrix, which facilitates uniform gelation and minimizes deformation upon impact with the hardening bath. In this study the ionic cross-linking agent used is Ca2+ derived from $CaCl_2$. Ca2+ has been selected because it is not toxic and is frequently used as cross-linking of microsphere formation with Na alginate polymer [10]. Alginate can form a formation of egg - box by using ionic cross-linking agents, such as divalent cations (i.e., Ca2+) [11]. The divalent cation binding group or guluronic blocks of alginate chains, as the structure of guluronic blocks that enable high-level coordination from the divalent ions. Guluronic blocks of one polymer then forms a bond with guluronic blocks of other adjacent polymer forming egg-box model of cross-linking, producing a gel structure [10], [11].

The appearance of the alginate beads is expected to be spherical with a smooth surface. In this study, 10% (w/v) $CaCl_2$ was utilized as a high-concentration cross-linking agent to ensure rapid gelation and maintain the structural rigidity of the beads, especially when high levels of MLP are incorporated, which might otherwise interfere with the matrix density. The use of a relatively high $CaCl_2$ concentration ensures an excess of calcium ions to fully saturate the binding sites of the alginate chains, overcoming the potential steric hindrance caused by the solid particles of mulberry leaf powder within the 'egg-box' structure [11]. Although most products showed homogenous size distributions, those prepared with 3% (w/v) alginate and 2% (w/v) mulberry leaf powder exhibited a tailed morphology. This is due to the synergistic effect of the high alginate concentration and powder content, which significantly increased the viscosity of the mixture. Such high viscosity creates substantial viscous drag during extrusion.

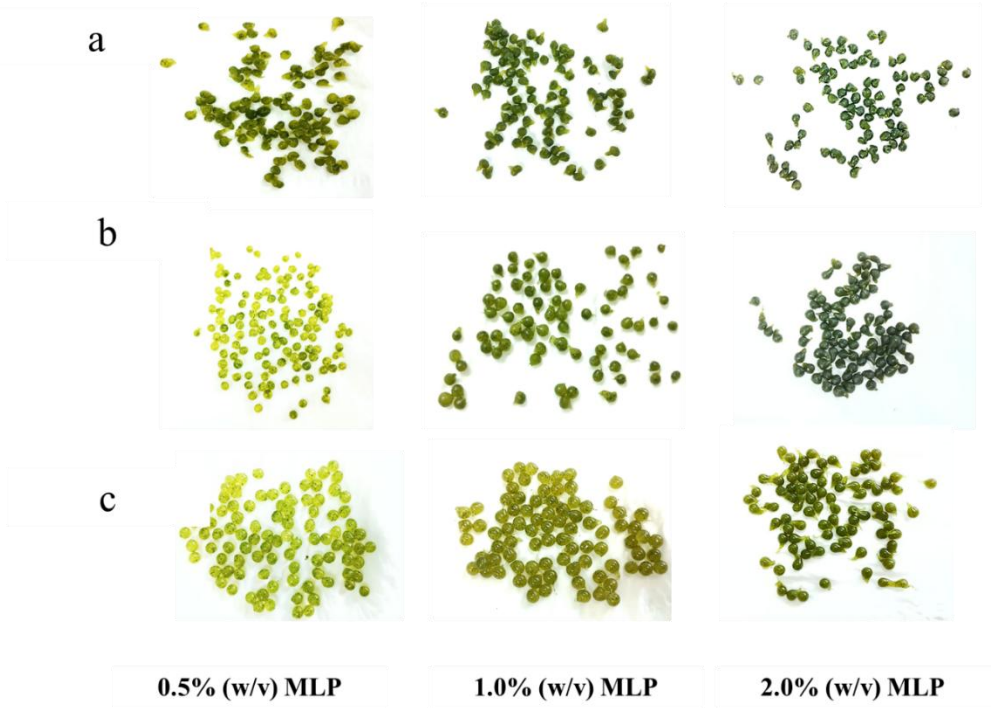

Figure 2. Morphology of MLP hydrogel beads prepared with varying sodium alginate concentrations: 1.0% (a), 2.0% (b), and 3.0% (c) (w/v).

3.4 Thermal Stability of MLP Hydrogel Beads

The thermal stability of mulberry leaf hydrogel beads, prepared with varying concentrations of sodium alginate (1.0%–3.0% w/v) and MLP (0.5%–2.0% w/v), was evaluated at 75 °C for 10 min to simulate pasteurization conditions. Hydrogel beads formulated with 1.0% (w/v) sodium alginate and 0.5% (w/v) MLP exhibited buoyancy after 5 min of heating. A similar phenomenon occurred in beads containing 1.0% (w/v) MLP after 7 min. After thermal treatment, these samples showed significant structural collapse. This instability is likely attributed to the low alginate concentration, which resulted in a thin and fragile encapsulation layer. Under thermal stress, this thin coating underwent structural denaturation, leading to the eventual rupture of the beads [12].

In contrast, hydrogel beads prepared with 2.0% and 3.0% sodium alginate maintained their integrity across all MLP concentrations throughout the 10-min heating period. No discernible morphological changes were observed, and the structural integrity remained intact. The enhanced stability at higher alginate concentrations is ascribed to the formation of a denser hydrogel matrix and increased viscosity provided by the MLP. Furthermore, the presence of cellulose and insoluble dietary fibers within the mulberry leaf [13] functioned as a reinforcing agent for the capsule walls. Such reinforcement acted as a structural support that improved the robustness of the capsule walls, resulting in enhanced stability and resistance to thermal degradation during simulated pasteurization.

3.5 pH Stability of MLP Hydrogel Beads

The pH stability of the mulberry leaf hydrogel beads was evaluated at pH 1.8 to simulate the highly acidic environment of gastric fluid (pH 1.5–3.5). Following a 24-h incubation, macroscopic observations revealed that the structural integrity of the beads remained entirely intact across all experimental groups, comprising sodium alginate concentrations of 1.0%–3.0% (w/v) and MLP contents of 0.5%–2.0% (w/v). Each hydrogel bead successfully maintained its

spherical morphology and structural stability throughout the testing period (Figure 3). These findings highlight the robust capacity of the alginate hydrogel network to preserve its structural form even under extreme acidic stress. Such resilience is primarily attributed to the ionic cross-linking between the alginate polymer chains and calcium ions, which forms a reinforced gel matrix [14]. This structural reinforcement effectively prevents the disintegration and degradation of the beads during simulated gastric transit, ensuring the protection of the encapsulated components within the gastrointestinal environment.

3.6 Swelling Capacity of MLP Hydrogel Beads

The swelling capacity of the mulberry leaf hydrogel beads was tested in distilled water for 30, 60, and 120 min. This parameter is used to indicate the mechanical strength of the beads. Generally, stronger beads show lower swelling because their dense and organized structure limits the space for water to penetrate [15]. As shown in Figure 4, the swelling capacity decreased as the sodium alginate concentration increased. At 120 min, the beads reached their maximum swelling before becoming stable (equilibrium). The highest swelling ratio was 92.11%, found in the 1.0% (w/v) alginate and 0.5% (w/v) mulberry powder formulation. In contrast, beads with 2.0% and 3.0% (w/v) alginate showed much lower swelling. Specifically, the 3.0% (w/v) alginate beads were the most stable, with swelling ratios between 2.50% and 3.45% after 120 min. These results confirm that higher sodium alginate concentrations significantly improve bead strength. The increased alginate creates a more compact matrix with fewer internal gaps, which effectively reduces water diffusion [15]. Additionally, the high fiber content in mulberry leaves helps reinforce the bead walls, providing further structural support and stability.

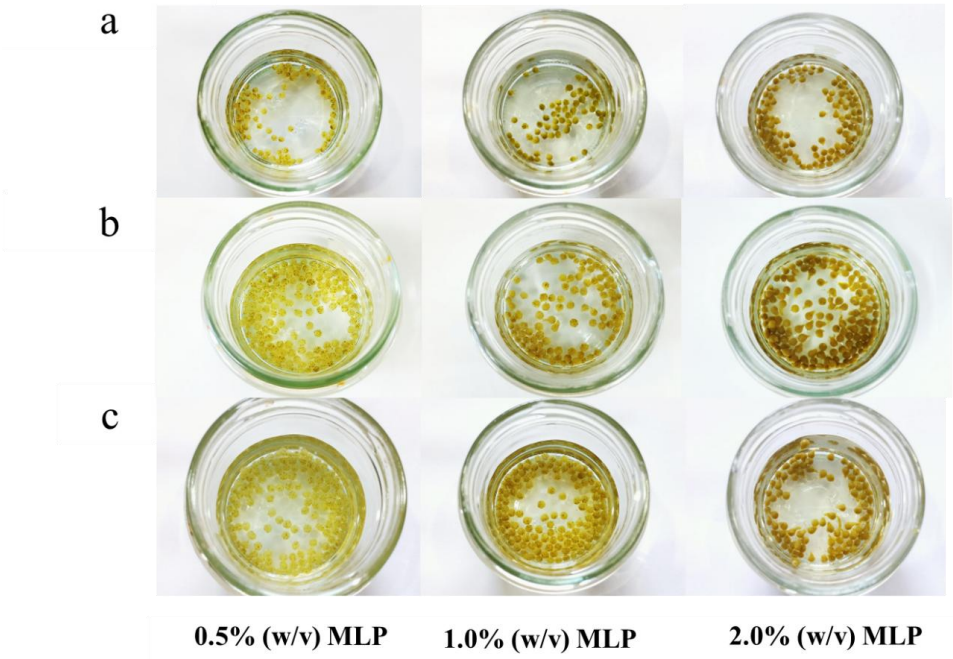

Figure 3. Morphological stability of MLP hydrogel beads at pH 1.8 with varying sodium alginate concentrations: 1.0% (a), 2.0% (b), and 3.0% (c) (w/v).

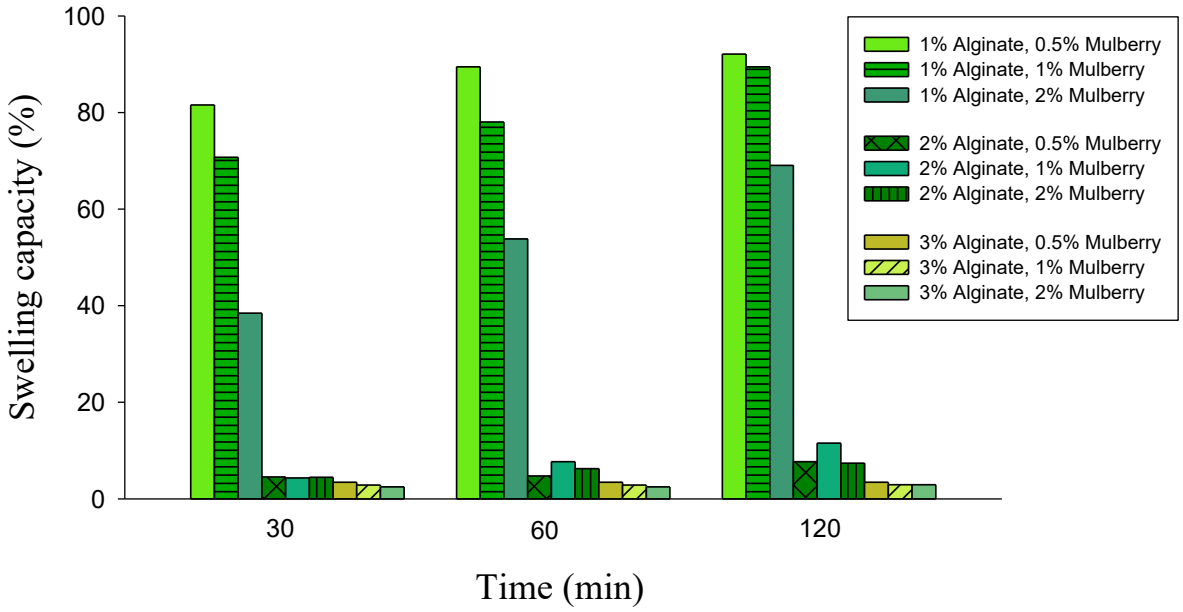

Figure 4. Swelling capacity of MLP hydrogel beads at 30, 60, and 120 min of incubation in distilled water.

Following stability assessments under various conditions, the optimal formulation, comprising 3.0% (w/v) sodium alginate and 1.0% (w/v) mulberry leaf powder, was prepared using an encapsulator (Model B-390, BÜCHI, Flawil, Switzerland). The hydrogel beads were formed via an extrusion method through a 1,000 µm single nozzle. The process parameters, including vibration frequency, amplitude, and electrode tension, are summarized in Table 4.

Table 4. Parameters for the preparation of MLP hydrogel beads using an encapsulator.

Encapsulator parameters				
Nozzle (µm)	Frequency (Hz)	Pressure (mbar)	Electrode (V)	Amplitude
1000	1500	120	1100	5

The MLP hydrogel beads produced by an encapsulator (Model B-390, BÜCHI, Flawil, Switzerland) exhibited a highly spherical shape and excellent size uniformity (Figure 5). These beads appeared as discrete, well-defined spheres characterized by a smooth, non-porous surface and a consistent dark green hue derived from the encapsulated MLP. The homogeneous distribution of the mulberry leaf powder within the transparent alginate matrix resulted in an aesthetically pleasing appearance. The small and uniform particle size ensures seamless incorporation into food products, such as yogurt and functional beverages, without compromising their sensory properties or textural stability. This indicates that the technique is an effective and scalable approach to enhance the stability and delivery of mulberry leaf bioactives within diverse food matrices while maintaining superior product quality.

Figure 5. Appearance of MLP hydrogel beads produced by an encapsulator (Model B-390, BÜCHI, Flawil, Switzerland).

4. Conclusion

This study successfully established the optimal parameters for developing stable mulberry leaf *(Morus alba L.)* hydrogel microparticles using extrusion microencapsulation. The results demonstrate that a formulation of 3.0% (w/v) sodium alginate and 1.0% (w/v) vacuum-dried mulberry leaf powder (MLP), cross-linked with 10% (w/v) calcium chloride, provides the most robust structural integrity. This optimized composition effectively addressed the stability challenges of MLP, maintaining excellent physical form under pasteurization conditions (75 °C for 10 min) and demonstrating high resilience in a simulated gastric environment (pH 1.8). Furthermore, the transition to automated extrusion using a vibrating-nozzle encapsulator (Model B-390) ensured the production of uniform, small-scale beads suitable for seamless integration into food systems. These findings confirm that extrusion microencapsulation via ionic gelation is a highly effective strategy for protecting sensitive mulberry leaf constituents. This research provides a critical foundation for utilizing these stabilized hydrogel beads as functional ingredients in industrial food applications, such as dairy products and functional beverages, ensuring both nutritional value and product stability.

Acknowledgements

The authors are grateful to the Institute of Nutrition, Mahidol University for the research facilities.

References

1. Surini, S.; Diandra, D. M. *Int. J. Appl. Pharm.* 2017, *9 (Suppl 1)*, 68–73.
2. Huang, G. Q.; Zeng, Y. C.; Wei, L.; Yao, Y. Q.; Dai, J.; Liu, G.; Gui, Z. Z. *BMC Plant Biol.* 2020, *20 (1)*, 279.
3. Funfakjit, N.; Kanana, N.; Manopakdee, K.; Charnvanich, D. *Thai J. Pharm. Sci.* 2024, *48*, 2971.
4. Koksel, H.; Masatcioglu, T.; Kahraman, K.; Ozturk, S.; Basman, A. *J. Cereal Sci.* 2008, *47*, 275–282.
5. Gong, R.; Li, C.; Zhu, S.; Zhang, Y.; Du, Y.; Jiang, J. *Carbohydr. Polym.* 2011, *85*, 869–874.
6. Farahmandfar, R.; Tirgarian, B.; Dehghan, B.; Nemat, A. *J. Food Meas. Charact.* 2020, *14*, 862–875.
7. Thamkaew, G.; Sjöholm, I.; Galindo, F. G. Crit. Rev. Food Sci. Nutr. 2021, 61 (11), 1763–1786.

8. Elleuch, M.; Bedigian, D.; Roiseux, O.; Besbes, S.; Blecker, C.; Attia, H. *Food Chem.* 2011, *124 (2)*, 411–421.
9. Kaushal, P.; Kumar, V.; Sharma, H. K. *LWT - Food Sci. Technol.* 2012, *48*, 59–68.
10. Lee, K. Y.; Mooney, D. J. *Prog. Polym. Sci.* 2012, *37*, 106–126.
11. Manjanna, K. M.; Pramod Kumar, T. M.; Shivakumar, B. *Drug Discoveries Ther.* 2010, *4*, 109–122.
12. Shu, X. Z.; Zhu, K. J. *Eur. J. Pharm. Biopharm.* 2002, *53*, 193–201.
13. Iqbal, S.; Younas, U.; Sirajuddin; Chan, K. W.; Sarfraz, R. A.; Uddin, M. K. *Int. J. Mol. Sci.* 2012, *13*, 6651–6664.
14. Lin, Y. H.; Liang, H. F.; Chung, C. K.; Chen, M. C.; Sung, H. W. *Biomaterials* 2005, *26*, 2105–2113.
15. Tsai, F. H.; Chiang, P. Y.; Kitamura, Y.; Kokawa, M.; Islam, M. Z. *Food Hydrocoll.* 2017, *62*, 140–148.

P - 209

Optimization of Protein Hydrolysate Preparation and Nitric Oxide Scavenging Activity from Kam Kung Alga (*Chara corallina*) Using Response Surface Methodology

Papassara Sangtanoo[1], Thanaphorn Mungkhun[2], Wanninee Chankaew[3], Chansawang Ngamphongsai[4], Piroonporn Srimongkol[1], and Aphichart Karnchanatat[1]*

[1]*Institute of Biotechnology and Genetic Engineering, Chulalongkorn University, Bangkok, Thailand*
[2]*Faculty of Science, Khon Kaen University, Khon Kaen, Thailand*
[3]*Faculty of Agriculture, Rajamangala University of Technology Srivijaya, Nakhon Si Thammarat, Thailand*
[4]*National Center for Genetic Engineering and Biotechnology, National Science and Technology Development Agency, Pathumthani, Thailand*

**Corresponding author E-mail: Aphichart.K@chula.ac.th*

Abstract: Kam Kung alga (*Chara corallina*), a freshwater brittlewort (Charophyte), is recognized as an edible alga that is rich in nutrients and comparable to other freshwater macroalgae. It contains high levels of protein, along with various bioactive compounds and antioxidants. This study aimed to optimize the process parameters influencing the nitric oxide (NO) scavenging activity of protein hydrolysate derived from Kam Kung alga using response surface methodology (RSM). Nitric oxide scavenging activity refers to the ability of a sample (such as protein hydrolysates or bioactive extracts) to reduce or suppress nitric oxide production. NO is a signaling molecule that plays important roles in inflammation processes. The NO scavenging activity was evaluated using the Griess assay, in which NO was generated from sodium nitroprusside in aqueous solution and incubated with the sample under controlled conditions. The percentage of NO inhibition was calculated relative to the control without sample. The effects of trypsin concentration (0.66–2.34%), temperature (41.6–58.4°C), and hydrolysis time (38.4–441.6 min) on NO scavenging activity were investigated. Optimization was performed using a Central Composite Design (CCD) combined with RSM. The results showed that the maximum NO scavenging activity of the tryptic hydrolysate was 141.60 µg/mL. The optimal hydrolysis conditions were identified as 1.395% trypsin concentration, 50°C hydrolysis temperature, and 309 min hydrolysis time. The experimentally obtained NO scavenging activity closely matched the predicted value, with a high correlation coefficient (R^2 = 0.9781). RSM analysis indicated that trypsin concentration, temperature, and hydrolysis time were all significant factors affecting NO scavenging activity.

Keywords: Kam Kung alga; Protein hydrolysate; Nitric oxide scavenging activity; Optimization; Response surface methodology

1. Introduction

Protein hydrolysis is defined as a chemical or biological process that breaks down peptide bond in proteins into peptides of different sizes and free amino acids. Modification of protein structure affects the physicochemical and functional properties of proteins [(1)]. Chemical hydrolysis uses acid or alkaline solutions to cleave peptide bonds. Although chemical hydrolysis is less expensive, it involves toxic reagents, limited control of the reaction, and may yield products with lower nutritional quality and functionality[(2)]. In contrast, enzymatic hydrolysis cleaves peptide bonds at specific sites under mild conditions and is considered safer and more environmentally friendly[(3)]. Protein hydrolysates are produced by appropriate enzymes and controlled hydrolysis conditions that depend on various factors such as pH, temperature, the ratio of enzyme to protein,

hydrolysis time, and substrate concentration by enzymatic hydrolysis method [4]. Bioactive peptides usually consist of 2-20 amino acids. They consist of aromatic ring or hydrophobic amino acids such as proline, lysine, tyrosine, and phenylalanine, which play a crucial role in antioxidant activities [5,6].

Enzymatic hydrolysis is strongly preferred for nutritional applications because it is carried out under milder conditions and produces hydrolysates with defined molecular weight distribution, peptide composition, and degree of hydrolysis. Enzymatic hydrolysis can be controlled and optimized to obtain the best response to save cost and time. Optimum enzymatic protein hydrolysis generally depend on the type of proteinase, pH, hydrolysis time, enzyme to substrate concentration and temperature [7]. Trypsin is one of the most commonly used proteolytic enzymes for producing bioactive peptides due to its well-defined cleavage specificity. The enzyme selectively hydrolyzes peptide bonds at the carboxyl side of lysine and arginine residues, leading to the generation of peptides with predictable sequences and suitable molecular sizes. Such peptides are often associated with enhanced biological activities, including antioxidant and anti-inflammatory effects.

Kam Kung alga (*Chara corallina*), commonly found in freshwater ecosystems such as ponds, lakes, and canals in Thailand, is a species of green alga belonging to the Charophyceae class. Previous studies have reported that *Chara* species contain various biologically active constituents such as proteins, polysaccharides, polyphenols, and minerals, which exhibit antioxidant, antimicrobial, and anti- inflammatory activities [8,9]. Kam Kung alga has attracted increasing attention as a potential alternative protein source due to its relatively high protein content and the presence of essential amino acids. Algal proteins are considered promising raw materials for the production of bioactive peptides because they can be easily hydrolyzed to release peptides with diverse biological activities, including antioxidant, anti- inflammatory, and antihypertensive properties. Therefore, Kam Kung alga may serve as a valuable protein source for generating bioactive peptides with potential health-promoting properties. These bioactivities are often associated with amino acid sequences that can scavenge free radicals, inhibit pro- inflammatory mediators, and regulate enzymes involved in oxidative stress and aging processes [10].

Nitric oxide (NO) was selected as the target for inhibition because excessive NO production plays a critical role in inflammatory responses. In activated macrophages, NO is synthesized primarily through the inducible nitric oxide synthase (iNOS) pathway and contributes to the progression of inflammation and tissue damage. Consequently, the inhibition of NO production in stimulated macrophages is widely used as a reliable indicator for evaluating the anti-inflammatory potential of natural compounds and bioactive peptides. Assessing NO inhibition allows researchers to determine the capacity of protein hydrolysates
to modulate inflammatory mediators at the cellular level.

Response surface methodology (RSM) is a collection of mathematical techniques and statistical tools suitable for developing, improving, and optimizing products and processes [11]. This technique studies the relationship between an independent variable and multiple response variables and the complexity of the interactions between the variables will be analyzed until a valid model is obtained [12,13]. The most extensive applications of RSM and the resultant model contains all of the information on the effect of the experimental conditions, can help the user to perform the optimization of the parameters with a minimize the consumption of time, reagents consumption and number of experiments, and the appropriate optimum conditions are determined [14]. Besides, the model can be used to predict future observations within the model ranges.Response Surface Methodology (RSM) is an efficient and widely used tool for optimizing enzymatic hydrolysis conditions and other process conditions to achieve the desired response. The aim of this study was to determine the optimal parameters for trypsin hydrolysis of Kam Kung alga protein to achieve high NO scavenging activity using RSM.

2. Materials and Methods

2.1 Raw material

Kam Kung alga (*Chara corallina*) was obtained from Faculty of Agriculture, Rajamangala University of Technology Srivijaya, Nakhon Si Thammarat, Thailand.

2.2 Chemicals and reagents

Trypsin from porcine pancreas with an activity of 1500U/mg, Bovine serum albumin (BSA), Sodium nitroprusside (SNP), Sulfanilamide, and N-(1-naphthyl)ethylenediamine (NED) were purchased from Sigma-Aldrich Chemical CO. (St. Louis, MO, USA). All chemicals used were all of analytical grade.

2.3 Preparation of the Kam Kung alga

Kam Kung alga was ground into powder using a blender, which was then sieved through a 90 μm mesh. The powder was then filled into polypropylene plastic and stored in a desiccator until required. Proximate analysis of Kam Kung alga was conducted using AOAC standard methods.

2.4 Experimental design for the optimization using response surface methodology (RSM)

Design-Expert software was used to determine the ideal proteolytic parameters of Kam Kung alga to obtain NO scavenging activity (Version 11, stat-Ease, Inc., USA). RSM was applied to investigate the optimize the conditions and to design a model using a central composite design (CCD) with three factors (Independent variables, X) including X_1 (enzyme concentration, % w/v), X_2 (temperature, °C) and X_3 (hydrolysis time, min) were studied to evaluate response (dependent variable, Y) including NO scavenging activity. The complete design matrix consisted of eight factorial points, six axial points and three center points, results in a total of 17 experiments as shown in Equation [1].

$$N = 2^n + 2n + n_c = 2^3 + 2(3) + 3 = 17 \quad [1]$$

Where N is the total number of experiments required, n is the number of independent variables and n_c is the number of center point

The design matrix contains 2^3 factorial design augmented by six axial points code±α and three center point (all factors = zero). The value of α was calculated by Equation [2].

$$\alpha = 2^{n/4} \quad [2]$$

Where n is the number of factors in the design. Therefore, α is equal to $2^{3/4} = 1.68$ according to Equation [2]. The range and levels of all factors in coded and actual values were calculated by Equation [3].

$$x_i = \frac{X_i - X_0}{\Delta X_i} \quad [3]$$

Where, x_i is the independent variable coded value, X_i is the independent variable actual value, X_0 is the independent variable actual value on the center point and ΔX_i is the step change value.

The quadratic polynomial equation was fitted to correlate the relationship between independent variables and response shown in Equation [4].

$$Y = \beta_0 + \Sigma\beta_i X_i + \Sigma\beta ij X_i X_j + \Sigma\beta_i X_i^{\,2} \quad [4]$$

Where Y is the response, X_i and $X_j$are independent variables, β_0 is the intercept, β_i is the linear coefficient, β_{ij} is an interaction coefficient and β_{ii} is a quadratic coefficient. The validity of the model was assessed according to the coefficient of determination (R^2). Optimal values for selected variables were obtained by analyzing response surface and contour plots and the quadratic polynomial equation.

Interactions between independent variables were examined. Three independent variables were examined enzyme concentration (A), temperature (B) and hydrolysis time (C). The effects

of the three independent variables at five levels on NO scavenging activity were examined. The coded and actual values for the experimental design are shown in Table 1.

Table 1. Experimental range and levels of the independent variables

Independent variables	Levels				
	-1.68	**-1**	**0**	**1**	**1.68**
A: Enzyme concentration, %w/v	0.66	1	1.5	2	2.34
B: Temperature, °C	41.6	45	50	55	58.4
C: Hydrolysis time, min	38.4	120	240	360	441.6

2.5 Enzymatic hydrolysis

2.5 g of Kam Kung alga powder was suspended in 50 mL of 20 mM phosphate buffered saline (PBS) at pH 8.0. Then hydrolysis was carried out with trypsin concentration (Table 1) in a shaking incubator at 150 rpm. To complete the reaction, mixture was heated in water bath at a temperature of 90°C for 20 minutes to inactivate the enzyme. In the final step, the Kam Kung alga protein hydrolysate was centrifuged using a Kubota 6500 centrifuge (Shimadzu, Kyoto, Japan) at 10,000 rpm for 20 minutes and a temperature of 4°C. The supernatant was collected and then stored at -20°C until required for analysis.

2.6 Protein content determination

The protein hydrolysates were investigated to determine the protein concentration by the bradford procedure [15]. Bovine serum albumin (BSA) was used as a protein standard. The absorbance at 595 nm (A_{595}) was measured using a microplate reader (multiskan GO; Thermo Fisher Scientific, Waltham, MA, USA).

2.7 Determination of NO scavenging assay

The sample (50 µL) and 50 µL of 10 mM SNP were mixed and incubated for 2.5 hours. Then 200 µL of 0.33% (w/v) sulfanilamide (in 5% (v/ v) phosphoric acid) was added and incubated for 5 minutes. Then, 200 µL of 0.1% (w/ v) NED was added and incubated for 10 minutes. Absorbance at 540 nm (A540) was measured using a microplate reader (Multiskan GO, Thermo Fisher Scientific, Waltham, MA, USA). A control with SNP without the sample was also prepared.

2.8 Calculation of the IC_{50}

The percentage of radical scavenging was calculated from equation 5: as follows

$$\frac{[(\text{Abs control}-\text{Abs blank})-(\text{Abs sample}-\text{Abs background})]\times 100}{(\text{Abs control}-\text{Abs blank})} \quad [5]$$

where Abs control is the A_{540} of the control (no sample), Abs sample is the A_{540} of the sample hydrolysate tested, Abs background is the A_{540} of the sample without the reagents, and Abs blank is the A_{540} of deionized water. The IC_{50} (the concentration of the sample that inhibits 50% of the NO radical scavenging) was calculated using the GraphPad Prism vs. 6.01 for windows software (GraphPad Software Inc., California, USA).

2.9 Statistical analysis

All the experiments were carried out in triplicate. Independent and dependent variables were analyzed using Design Expert Software Version 11 (Stat-Ease, Inc., USA). All measurements were run in independent variables of central composite design (CCD) and data analysis was carried out using oneway analysis of variance (ANOVA). The differences were considered significant at $p < 0.05$. The best solution was selected for optimization and analyzed for validation.

3. Results & Discussion

3.1 Optimization of enzymatic hydrolysis conditions on NO scavenging activity by RSM

This experimental design was based on 2^3 factorial experimental runs according to CCD with three independent variables; enzyme concentration, %w/v (A) temperature, °C (B), and hydrolysis time, min (C) (Table 2). However, to minimize the error, all of the coefficients were considered in the design. Real factors equations can be used to predict the response at certain levels of each factor. The proximate analysis of Kam Kung alga showed a protein content of 16.78±0.33% (w/w).

Table 2. The 17 experimental runs of CCD and NO scavenging activity

Runs	Space type	Independent variables			Responses	
		Enzyme concentration % (w/v), A	Temperature (˚C), B	Hydrolysis time (min),C	Protein content (µg/mL)	NO scavenging activity (IC_{50}; µg/mL)
1	Factoria	2	45	360	287.38	191.93
2	l	1	45	360	264.44	175.93
3		1	45	120	293.65	231.70
4		2	45	120	343.98	292.57
5		2	55	120	218.09	185.63
6		1	55	120	219.17	180.27
7		1	55	360	225.88	184.77
8		2	55	360	246.28	192.43
9	Axial	0.66	50	240	240.51	201.30
10		2.34	50	240	385.06	261.67
11		1.5	41.6	240	336.28	221.27
12		1.5	58.4	240	244.02	164.77
13		1.5	50	441.6	251.74	158.17
14		1.5	50	38.4	318.42	219.23
15	Center	1.5	50	240	264.15	149.00
16		1.5	50	240	286.61	159.20
17		1.5	50	240	275.26	147.47

The equation of the predicted model (based on the actual value) used to estimate NO scavenging activity which represent the response variable (Y) of protein hydrolysate from Kam Kung alga is given below Equation [6].

$$Y = 2153.04-120.62A-62.51B-2.17C-3.19AB-0.08AC+.0.03BC+109.85A^2+0.55B^2+0.0008C^2 \quad [6]$$

Where Y represents predictive values for NO scavenging activity. The letters A, B, and C indicate the enzyme concentration, temperature and hydrolysis time, respectively.

Statistical analysis of the quadratic model and interactions among the three independent variables for NO scavenging activity was shown in Table 4. The model for NO scavenging activity produced an F-values of 34.74, with a very low p-value (p<0.0001) confirming the significance of the model fitness and could be used for the optimization of hydrolysis conditions.

The lack of fit showed a p-value of 0.3271 which was not significant and the experimental data showed a high coefficient of determination ($R^2 = 0.9781$). The value of R^2 indicates that there is good agreement between the experimental values and the values predicted from the model. In general, the p-value determines the significance of each coefficient in the model.

According to Table 4, the ANOVA results indicate a highly significant interaction between temperature (B) and hydrolysis time (C) with a p-value of 0.0003. The significant interaction between temperature and hydrolysis time suggests that the optimal hydrolysis duration tends to decrease as temperature increases, since peptide generation occurs more rapidly under higher thermal conditions. Conversely, at lower temperatures, longer hydrolysis times are typically required to allow sufficient enzymatic cleavage and release of bioactive peptides. This interaction highlights the importance of optimizing both parameters simultaneously to maximize the production of peptides with strong NO scavenging activity.

Table 4. Analysis of variance (ANOVA) for NO scavenging activity

Source	Sum of Squares	df	Mean Square	F-value	p-value	
Model	24789.48	9	2754.39	34.74	< 0.0001	significant
A-Enzyme concentration	2682.35	1	2682.35	33.84	0.0007	
B-Temperature	4361.49	1	4361.49	55.02	0.0001	
C-Time	4496.27	1	4496.27	56.72	0.0001	
AB	509.60	1	509.60	6.43	0.0389	
AC	226.53	1	226.53	2.86	0.1348	
BC	3515.83	1	3515.83	44.35	0.0003	
A^2	8480.04	1	8480.04	106.97	< 0.0001	
B^2	2152.15	1	2152.15	27.15	0.0012	
C^2	1702.32	1	1702.32	21.47	0.0024	
Residual	554.94	7	79.28			
Lack of Fit	473.62	5	94.72	2.33	0.3271	not significant
Pure Error	81.32	2	40.66			
Cor Total	25344.43	16				
$R^2 = 0.9781$, Adjusted $R^2 = 0.9500$, Predicted $R^2 = 0.8334$						

*Significant within a 95% confidence interval

3.2 Response surface and contour plots

Validation of the statistical model and regression equation was performed using the optimal levels of the three factors (trypsin concentration 1.395%, temperature at 50°C, and hydrolysis time 309 min). The experimental data were compared with the predicted values. Under these optimized conditions, the predicted results for NO scavenging activity (IC_{50}; µg/mL) was 144.63 µg/mL. whereas the observed experimental values was 141.60 µg/ mL, respectively (error: 2.10%). These results confirmed the validity of the model and that the experimental designs used in this work were appropriate for predicting the optimized conditions.

The model is significant because the *p*-value is less than 0.05. This result showed that temperature, hydrolysis time and enzyme concentration had a strong effect on NO scavenging activity (Y) (Figure.1). Similar results were reported for the hydrolysis conditions, which also had an effect on the degree of hydrolysis (DH) value and NO inhibitory activity and depended on the characteristic composition and amino acid sequence of the peptides derived [16].

Response Surface Methodology (RSM) was used to improve the NO scavenging activity. The model was validated and found to be statistically reasonable and accurate in predicting the response.

Protein hydrolysates can inhibit nitric oxide (NO) production through several molecular and cellular mechanisms associated with the bioactive peptides released during enzymatic hydrolysis. These peptides often exhibit anti- inflammatory and antioxidant properties that contribute to the suppression of excessive NO production in activated immune cells, particularly macrophages.

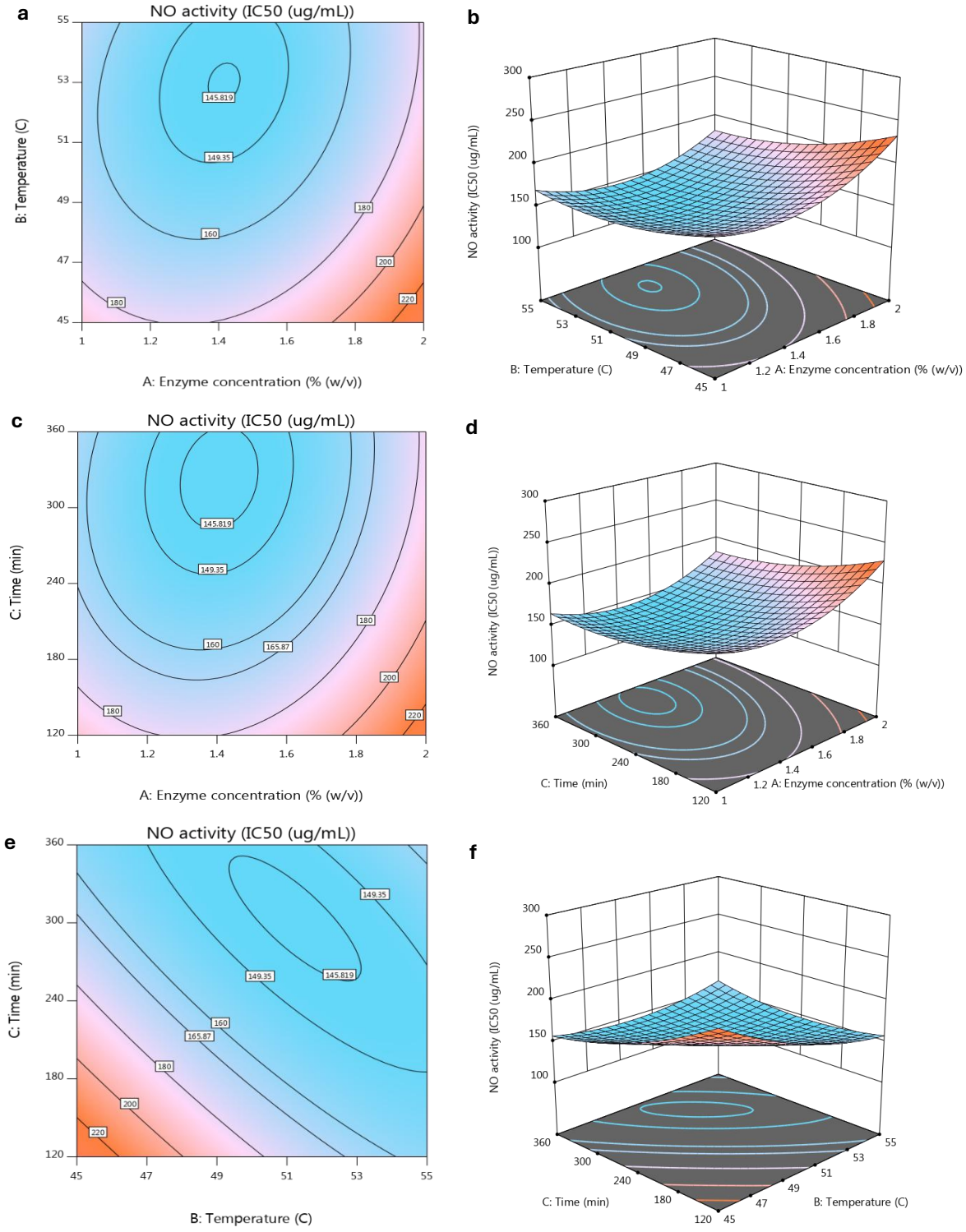

Figure 1. Two-dimensional contour plots and three-dimensional response surface graph of NO scavenging activity (a-f). The interactive effect of enzyme concentration (A), temperature (B) and hydrolysis time (C). The interactive effect of enzyme concentration (A) and temperature (B) (a,b). The interactive effect of enzyme concentration (A) and hydrolysis time (C) (c,d). The interactive effect of temperature (B) and hydrolysis time (C) (e,f).

4. Conclusion

The Kam Kung alga was hydrolyzed by trypsin enzyme. Response surface methodology and central composite design were used to determine the optimal conditions that produced the best results with strong NO scavenging activity (IC_{50} = 141.60 µg/mL). Therefore, Kam Kung alga can be converted into value-added products and could be a good source of bioactive peptides and should be further investigated for applications in food ingredients and food additives.

Acknowledgements

This work was supported by Center of Excellence in Bioconversion and Bioseparation for Platform Chemical Production, Institute of Biotechnology and Genetic Engineering, Chulalongkorn University for their support and providing access to their facilities.

References

1. Severin, S.; Xia, W. S. Enzymatic hydrolysis of whey proteins by two different proteases and their effect on the functional properties of resulting protein hydrolysates. Journal of Food Biochemistry, 2006, 30(1), 77-97.
2. Kristinsson, H. G.; Rasco, B. A. Fish protein hydrolysates: production, biochemical, and functional properties. Critical Reviews in Food Science and Nutrition, 2000, 40(1), 43–81.
3. Akanbi, T. O.; Barrow, C. J. Enzymatic production of antioxidants and their applications. Encyclopedia of Food Chemistry; Elsevier, 2019, 92-96.
4. Adler-Nissen, J. Enzymic hydrolysis of food proteins. Elsevier applied science publishers, 1986. Sarmadi, B. H.; Ismail, A. Antioxidative peptides from food proteins: a review. Peptides, 2010, 31(10), 1949–1956.
5. Wang, W.; De Mejia, E. G. A New Frontier in Soy Bioactive Peptides that May Prevent Age-related Chronic Diseases. Comprehensive Reviews in Food Science and Food Safety, 2005, 4(4), 63–78.
6. Sujith PM.; Hymavathi TV. Recent developments with debittering of protein hydrolysates. As. J. Food Ag-Ind, 2011, 4(06): 365-381.
7. Chankaew W.; Yangthong M.; Sangkaew J. "Evaluation of Antioxidant Activity and Phytochemical from Kamkung (Chara corallina Klein ex C.L.Willdenow)". PNU Journal of Science and Technology, Research & Development.- This article investigates total phenolic, flavonoid, tannin content and antioxidant activity (DPPH, ABTS, metal-chelation) of various solvent extracts of C. corallina. Thai Journal Online, 2020.
8. Khongsai S. " In vitro Antioxidant and Anti- Tyrosinase Activities Along with Phytochemical Constituents of Brittle Wort (Chara corallina) Extracts". Journal of Fisheries Technology & Research. - Reports on antioxidant & anti-tyrosinase activities of
9. C. Coralline aqueous extracts. Thai Journal Online, 2023.
10. Chankaew W., Phetkul U., Srimoon R. "Phytochemicals, α- glucosidase and α- amylase Inhibitory Efficiency of Brittle Wort (Chara corallina) Extract". - Discusses enzyme-inhibition (α-glucosidase, α-amylase) alongside antioxidant assays for C. corallina extracts, 2023.
11. Myers, R. H., Montgomery, D. C., & Anderson- Cook, C. M. Response surface methodology: process and product optimization using designed experiments. John Wiley & Sons, Inc., 2016.
12. Bezerra, M. A.; Santelli, R. E.; Oliveira, E. P.; Villar, L. S.; Escaleira, L. A. Response surface methodology (RSM) as a tool for optimization in analytical chemistry. Talanta, 2008, 76(5): 965-977.
13. Montgomery, D. C. Design and analysis of experiments. John Wiley & Sons, Inc, 2017.

14. Lundstedt, T.; Seifert, E.; Abramo, L.; Thelin, B.; Nyström, Å.; Pettersen, J.; Bergman, R. Experimental design and optimization. Chemometrics and Intelligent Laboratory Systems, 1998, 42(1-2): 3-40.
15. Bradford M. M. A rapid and sensitive method for the quantitation of microgram quantities of protein utilizing the principle of protein-dye binding. Analytical Biochemistry, 1976, 72, 248-254.
16. Chen, H.M., K. Muramoto and F. Yamauchi. Structural analysis of antioxidative peptides from soybean β-conglycinin. Journal of Agricultural and Food Chemistry, 1995, 43: 74-578.

P - 221

Packaging Effects on Freezing Rates and Quality of Roasted Chicken Drumettes

Pasinee Saehong[1], Wiriya Duangsuwan[2], Suttirug Phatcharat[3], Karnjapan Janthawornpong[1]*

[1]*Food industry management program, Faculty of Agro-industry, Prince of Songkla University, Thailand*
[2]*Biotechnology (International) program, Faculty of Agro-industry, Prince of Songkla University, Thailand*
[3]*Faculty of Agro-industry, Prince of Songkla University, Thailand*

**Corresponding author E-mail: karnjapan.j@psu.ac.th*

Abstract: The broiler chicken industry in Thailand is experiencing significant growth in domestic production and consumption, including export value, by 2025. Processed, chilled, and frozen chicken account for approximately 30% of Thailand's chicken product export value. Additionally, modern consumers are increasingly seeking convenient, time-saving meal-preparation options. As a result, ready-to-eat frozen food products have become an attractive choice that meets their needs. Despite the high market potential, the production process must be thoroughly reviewed before commercial investment. Packaging plays a crucial role in protecting product integrity and communicating product quality. However, there is limited information available on the methods and types of packaging that influence freezing efficiency and quality. This study, therefore, aims to investigate how the quality and freezing rate of different packaging types affect the freezing efficiency and post-freezing quality changes in roasted marinated chicken. Chicken drumettes weighing 55 g each were marinated, steamed for 10 min, and roasted at 200°C for 15 min. The yield analysis was based on the cooked product, which weighed 500 g and lost an average of 20.01% of its weight. The samples were then packaged in 3 types of pouches: polyamide/polyethylene (PA/PE), vacuum polyamide/polyethylene (VC), and aluminum (AF). The study used a completely randomized design (CRD), with 3 replicates each. Each packed product was equipped with a thermocouple and frozen in a blast freezer until the sample's core temperature reached -18°C, then thawed in a cold room at 4 ℃ 24 hours before analysis. The experimental results showed that chicken drumettes packed in VC pouches had the highest average freezing rate (0.929 ± 0.336 ℃/min). Furthermore, packaging types did not significantly affect thawing loss, product yield, or changes in product color and texture. Therefore, for production facilities that prioritize freezing speed and production efficiency, it is recommended to use VC pouches.

Keywords: Chicken drumettes; Freezing curves; Freezing rates; Packaging selection; Product quality change; Yield estimation

1. Introduction

Chicken is the most widely consumed poultry product globally due to its low fat, cholesterol, and calorie content, high protein, and lower price compared to other meats. Chicken consumption in Thailand has grown rapidly in recent years. In 2025, broiler chicken consumption reached 2.26 million tons, an increase of 0.02 million tons from 2024 [1]. However, current consumer demand for chicken extends beyond quantity alone. There is an increasing emphasis on the nutritional value and taste of the meat. The freezing process helps extend product shelf life, but if done incorrectly, it can damage the food's microstructure. Freezing can cause various types of damage to the microstructure of food products, especially if not adequately controlled [2]. Freezing technology plays a crucial role and is the most popular and effective method for long-

term preservation. Air-Blast Freezing is a method that uses high-speed cold-air circulation, typically at temperatures between -18 and -34 °C and wind speeds of 1-20 m/s, to enhance heat transfer and accelerate the freezing of food products. This technique is versatile across different product sizes and shapes, making it popular in the food industry for its flexibility and cost-effectiveness. However, improper control of freezing conditions can lead to moisture loss or deterioration in product quality. [3].

Packaging materials are crucial in the food processing industry, enhancing the commercial value of processed foods. Effective packaging attracts consumers while protecting nutritional content and preventing spoilage, thereby extending shelf life. It prevents physicochemical, microbiological, and nutritional deterioration, highlighting that inadequate packaging can compromise the quality of food products [4]. Cooking, along with freezing, has significant impacts on the food matrix, including weight loss due to heating, changes in net yield after cooking, and weight loss from the meat structure during freezing. Changes in product characteristics can be influenced by the type of packaging, which varies in its ability to control heat transfer and water loss [5]

Meat and muscle-based products have a short shelf life. Processing, packing, and freezing processes must work together to protect the product from bacterial growth and prevent chemical degradation during transportation and storage. Poorly packaged frozen foods will lose weight due to sublimation of surface ice. Weight loss is lower at lower temperatures due to the vapor pressure difference between the meat surface and the surrounding air [6]. The dry porous layer that forms in poorly packaged frozen foods alters the product sensory characteristics, leading to quality loss [7]. A sound packaging system is therefore essential for preventing these negative quality changes during frozen storage. Additionally, the freezing rate is a crucial factor influencing the formation of ice crystals within the tissue, which affects structural damage and the amount of water released after thawing. Although several studies have examined the impact of freezing on meat quality, there remains a lack of comparative data on how packaging type affects water-loss behavior and the freezing rate of cooked chicken products, particularly in controlled laboratory studies that clearly isolate the effects of each factor. Among the available packaging options, polyolefins (polyamide/polyethylene pouch, PA/PE) are the most commonly used plastics in the food industry, serving as a practical baseline for comparison. Modifications to this baseline, such as a polyamide/polyethylene vacuum pouch (VC), eliminate residual air to enhance film-to-product contact, increase freezing speed by removing air as an insulator, and minimize oxidative deterioration during frozen storage. Additionally, aluminum foil-based packaging provides an excellent barrier against moisture, air, odours, temperature, light, and microorganisms [8].

The objective of this study was therefore to compare the effects of three packaging types; PA/PE, VC, and Aluminum pouches (AF), on the physical quality changes of frozen roasted chicken drumettes, focusing on freezing rate, thawing loss, product yield and color characteristics, in order to provide evidence-based technical data to support the optimization of freezing process parameters and guide the selection of the most suitable packaging material for commercial production

2. Materials and Methods

2.1 Sample Preparation

The chicken drumettes (approximately 55 g or 10 pieces/kg), manufactured by LPF Meat Frozen Co., Ltd., were sourced from local supermarkets. Raw materials were then stored at 4°C for no longer than 24 hours before use. Chicken drumette samples were washed thoroughly. Each piece was trimmed to approximately 4 x 8 cm and about 2 cm thick. The cooking process began with marinating them in a pickling solution (the recipe is a matter of commercial confidentiality; 15% of the drumette's weight). Samples were then weighed individually, mixed, and hand-

kneaded for 3 min before packing into zip-lock polyethylene (PE) bags containing approximately 500-600 g/bag and stored in a refrigerator at 4 °C for 12 hours.

2.2 Roasting

After marinating at 4 °C for 12 hours, the chicken drumettes were kneaded for another 3 min, then steamed for 10 min, and roasted in an oven at 200 °C for 15 min to ensure they were fully cooked. After roasting, the product was cooled at room temperature with air blown over its surface for 10-15 min until the surface temperature reached approximately 25±5°C, then weighed to calculate cooking loss and product yield.

2.2 Freezing and Thawing Process

The study of the Freezing and Thawing Process used a Completely Randomized Design (CRD). The factors studied were three packaging types: PA/PE, VC, and AF. Each sample was triplicated. Roasted chicken drumettes weighing 500 g were packaged in three types of packaging: PA/PE (polyamide/polyethylene,190 µm of thickness), VC (polyamide/polyethylene vacuum pouch, 190 µm thickness), and AF pouch (aluminum foil laminate, 100 µm of thickness, light and moisture barrier). The PA/PE pouch was designated as the control treatment. The packaged product samples were frozen in a cold-air blast freezer operating at a chamber temperature of -35°C and an air velocity of 1.2–1.6 m/s, with temperature monitored until the product core's temperature reached -18°C. The freezing rate was calculated as the total temperature change from the initial product core temperature to -18°C, divided by the total freezing time. Before the measurement, the samples were stored in a cold room at -18°C for 3 days. The frozen roasted chicken drumette samples were then thawed directly, without packaging, in a microwave oven (Samsung, MS23F300EEK, Malaysia). The selected microwave power was 800 W, and the microwave frequency was 2450 MHz for 10 min. The weight loss of the frozen roasted chicken drumettes during thawing was quantified as the percentage difference between the weight of the drumettes prior to freezing and the final weight of the thawed drumettes. Recorded both the initial and final weights. Yield was determined by dividing the weight of chicken drumettes after defrosting by the weight of the raw material prior to roasting, and expressed as a percentage.

2.3 The effect of packaging type on the quality changes of roasted chicken drumettes.
Color analysis

Surface color of roasted chicken drumettes after thawing was measured using a Hunter Lab Colorimeter (ColorFlex EZ, HunterLab, USA) in the CIE-Lab color space. Samples were cut to 3×3 cm pieces, and measurements were taken at three points per sample. Lightness (*L*),* redness *(a*),* and yellowness *(b*)* values were recorded.

2.4 Texture profile analysis (TPA)

The samples will be thawed in a microwave oven for 10 min, with bones and tendons removed, leaving only the skin and meat, which will then be used for analysis. They were cut into pieces measuring 1.5×3.0×1.0 cm. Texture analysis was conducted at room temperature with a TA-XT Plus. The TPA was performed with a P/50, 50 mm DIA. Cylinder Aluminum probe, with a testing speed of 1.0 mm/s, a pressing time of 5 s, a compression ratio set at 20%, and a trigger force of 0.05 N. Each experimental group was repeated 3 times, with one sample per repetition.

2.5 Statistical analysis

All tests were conducted in triplicate. Data were analyzed using one-way ANOVA by Minitab statistical software (V.21.0, Minitab Inc., State College, PA, USA). The values were expressed as mean ± standard deviation, and $p < 0.05$ was considered significant.

3. Results & Discussion

3.1 Cooking Loss

Cooking loss is the change in the mass of meat after heating, expressed as a percentage of the initial weight. The study found that the average weight loss after cooking (steaming over medium-high heat for 10 min and baking at 200°C for 15 min) was 20.01%. This is consistent with the study of [9], which explained that the heating temperature significantly affects cooking loss. In the study of chicken breast patties, cooking loss was 29% at 40 °C, 7.3% at 50 °C, 8.8% at 60 °C, 8.9% at 70 °C, and 10.3% at 80 °C. Additionally, the study of [10] indicated that cooking loss is more closely related to cooking time than to cooking temperature. The cooking loss value was used as a baseline to calculate weight loss after freezing and thawing and to estimate net yield, ensuring the accuracy of subsequent analyses and their appropriate application in actual production.

3.2 Freezing curve

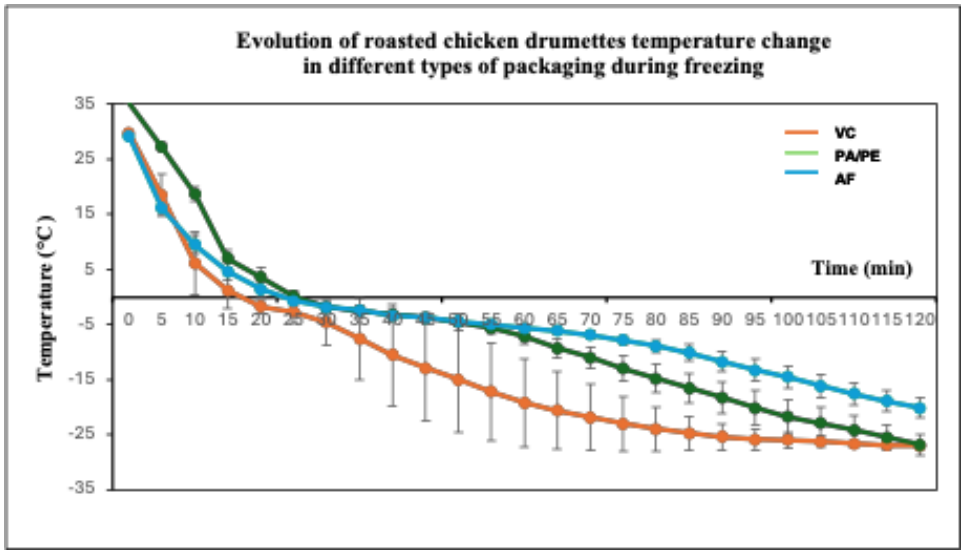

Figure 1. Evolution of roasted chicken drumettes temperature change in different types of packaging during freezing

3.3 Freezing Time and Freezing Rate

Table 1. Freezing time and freezing rate for different packaging types

Packaging	Freezing Time (min)	Freezing Rate (°c/min)
VC	56.1 ± 19.7[a]	0.929 ± 0.336 [a]
AF	111.6 ± 7.1 [b]	0.424 ± 0.027 [b]
PA/PE	107.9± 9.1 [b]	0.446 ± 0.036 [b]

1. Values in the table are presented as mean ± standard deviation.
2. Lower case letters a, b indicate statistically significant differences ($p < 0.05$).

The relationship between time and temperature for frozen roasted chicken packaged in three packaging types, namely VC (orange line), PA/PE (green line), and AF (blue line), is shown in Figure 1. At the beginning of the freezing process, the core temperature of the roasted chicken started at approximately 29.61-29.87°C. During the first 20 min, the temperatures of all three groups decreased rapidly, with the VC group showing the fastest drop. The average temperature of the VC group decreased from 29.77°C to -1.73°C at the 20 min mark, while the PA/PE and AF

groups dropped to 3.07°C and 1.43°C, respectively, at the same time. This difference indicates that vacuum packaging improves heat-transfer efficiency between the product surface and the cold-air medium [11]. This improvement is due to the removal of air from the bag, which allows the film to contact the product surface directly. After the 20-30 min period, the VC group showed a significantly faster rate of temperature reduction than the other groups, with the core temperature dropping below -18°C at around 60 min, which was significantly earlier than in the PA/PE and AF groups. This advantage arises because vacuum packaging enables the packaging film to make close contact with the product surface, reducing the air layer between the product and the packaging and thereby increasing heat transfer efficiency [12]. In contrast, the PA/PE group exhibited the slowest rate of temperature decrease, with the core temperature remaining above -18°C until approximately 110-120 min. This indicates that normal packaging with residual air inside the bag acts as thermal insulation, thereby reducing the freezing rate [13]. The AF group showed a moderate rate of temperature decrease. Although aluminum foil has high thermal conductivity, standard packaging with residual air inside the bag may partially reduce heat-transfer efficiency, which is important for maintaining the desired temperature during freezing processes. This phenomenon highlights the balance between packaging materials and their thermal properties. Understanding these interactions can lead to improved packaging designs that optimize freezing efficiency while preserving food quality. After 60 min, the temperature graphs of all three groups continued to decrease. Toward the end of the experiment (approximately 100-120 min), the temperatures of the three groups approached final values of around -20°C to -27°C. This graph clearly shows that the type of packaging affects the freezing rate of the baked chicken. VC can accelerate the freezing process faster than normal packaging, which is significant for production efficiency and the quality of frozen products. A faster freezing rate helps reduce the formation of large ice crystals that could damage the product's tissue structure [14].

3.4 Thawing Loss and Product Yield (%)

The effects of the packaging type on the thawing loss and product yield of frozen roasted chicken drumettes are presented in Table 2. No statistically significant differences were observed among the three packaging types for either thawing loss or product yield ($p > 0.05$). Mean thawing loss values were 3.08 ± 4.14%, 0.83 ± 0.29%, and 7.74 ± 9.14% for PA/PE, VC, and AF packaging, respectively, while mean product yield values were 78.48 ± 1.80%, 77.62 ± 4.19%, and 83.86 ± 8.96%, respectively. Although no statistically significant differences were detected, the VC packaging showed a numerical trend toward the lowest thawing loss (0.83 ± 0.29%), which may be attributed to the direct film-to-product contact achieved through vacuum sealing, limiting moisture migration at the product surface during frozen storage. The size of ice crystals in meat depends on the cooling rate during freezing, and partial ice crystal formation can increase drip loss during storage [15]. The faster freezing rate achieved by VC packaging, as demonstrated in Table 1, may have contributed to smaller ice crystal formation, thereby reducing cellular damage and subsequent moisture loss upon thawing. The AF packaging showed the highest numerical product yield (83.86 ± 8.96%), which may be attributed to its superior moisture- and light-barrier properties compared to PA/PE and VC. The high variability observed in the present study, particularly in the AF and PA/PE groups, may reflect the limited sample size (n = 3), which reduces statistical power and increases sensitivity to individual-sample variation. Similar high variability in drip loss measurements from frozen poultry products has been reported previously, where coefficients of variation in drip loss among chicken breast samples were found to be considerable, highlighting the inherent variability of water-holding capacity measurements in poultry [16]. The absence of significant differences in product yield among packaging types in the present study may also reflect the relatively short 3-day storage duration, which may have been insufficient to produce measurable differences in moisture migration across packaging types. The volume of drip loss increases proportionally with frozen storage duration, with significant effects

of storage duration on drip loss observed in chicken breast muscles during extended storage [17]. Future studies with longer storage durations and larger sample sizes are recommended to more clearly elucidate the effects of packaging type on thawing loss and product yield in frozen roasted chicken products

3.5 Color of product

The *L*, a*,* and *b** values of roasted chicken drumettes under different packaging conditions are listed in Table 2 and represent lightness, redness, and yellowness, respectively. The results indicated that packaging type had no statistically significant effect on any of the measured color parameters, suggesting it did not influence the product's color quality under the storage conditions examined. Freezing does not usually cause color changes in poultry; dulling of color in frozen products is usually the result of excessive drying due to improper packaging or over-lengthy storage [18]. The absence of color differences across packaging types in this study may be explained by the relatively short storage duration (3 days post-packaging), which may have been insufficient to produce measurable color deterioration regardless of packaging type. Chicken drumettes are cooked at high temperatures, causing myoglobin pigments to lose their color and form cooked metmyoglobin, which is more chemically stable than pigments in fresh meat and is less reactive with residual oxygen in the packaging. Frozen storage is a significant factor in reducing the rate of fat and pigment oxidation [19]. These findings suggest that all three packaging types provided adequate short-term color protection for frozen roasted chicken drumettes.

Table 2 Physical properties of frozen chicken drumettes

Properties	Packaging type		
	PA/PE	VC	AF
*L**	48.84±5.57[a]	55.26±6.43[a]	53.67±4.53[a]
*a**	10.83±2.34[a]	12.36±6.96[a]	9.31±1.65[a]
*b**	27.52±2.44[a]	26.92±3.16[a]	26.18±2.34[a]
%cooking loss	21.52±1.80[a]	22.38±4.19[a]	16.14±8.96[a]
%thawing loss	3.08±4.14[a]	0.83±0.29[a]	7.74±9.14[a]
%product yield	78.48±1.80[a]	77.62±4.19[a]	83.86±8.96[a]
Hardness (g)	22,787±5,798[a]	21,981±3,046[a]	24,379±3,046[a]
Chewiness	9,206±3,137[a]	9,240±2,261[a]	10,830±2,673[a]

Values are expressed as mean±standard deviation (n=3)
Abbreviations: PA/PE = polyamide/polyethylene pouch, VC = polyamide/polyethylene Vacuum pouch, AF= Aluminum pouch
Values with different superscript letters in the same row indicate significantly different ($p<0.05$)

3.6 Texture analysis

The texture characteristics of roasted chicken drumettes were presented in Table 1. Hardness and chewiness values are noticeably higher than those that were reported in the literature [20]. This was because the textural properties of roasted chicken drumettes were significantly hardened by microwave defrosting (800 W, 2450 MHz, 10 min), a typical household method of defrosting food. Texture profile analysis showed high average hardness values of 22,787±5,798 g, 21,981±3,046 g, and 24,379±3,046 g across different samples. Therefore, the chewiness values indicated higher levels, reflecting changes in the internal structure of the meat, consistent with the research of Tian et al. (2025) [20], which found that samples thawed in a microwave oven using 800 W of power had a higher water loss rate from thawing than other methods, approximately 7.65%, and had the highest shear force. This can be explained by the higher drip loss and lower

moisture content. Frozen and thawed meat tends to be tougher and exhibit a higher shear force than fresh meat, which may result from the denaturation of some proteins, shrinkage of fibers, and a reduced ability to retain water or increased drip loss [21], and when compared with the findings of the study on the quality of roasted chicken drumettes that had undergone different freezing durations, measuring the post-cooking values on day 0 revealed that the hardness of fresh wings was 1356.87 g, while the hardness of wings frozen for 12 months was 3651.49 g, showing a continuous increase in hardness with longer freezing durations [22]. Current research indicates that, although the samples underwent rapid heating and freezing (-35°C for 2 hours), the evaluated thawing methods significantly affected the physical, chemical, and structural properties of the meat. Thawing in a microwave at 800 W for 10 min caused damage to the muscle structure. Therefore, future production process improvements should focus more on optimizing upstream processes, such as marinating and roasting, to minimize moisture loss and mitigate texture degradation caused by high-energy microwave thawing. This integrative approach could enhance the texture quality of frozen chicken drumettes, delivering products with a soft, juicy texture after defrosting.

4. Conclusion

The production of high-quality, frozen, ready-to-eat chicken products meets consumers' needs for taste, value, safety, and convenience. As the chicken industry continues to grow, both in Thailand and around the world, it is important to consider the production process, including how to freeze the chicken and what packaging to use to maintain product quality. Many studies have examined how freezing rates affect meat quality, including ice crystal formation and moisture loss. However, there is still insufficient information on how different packaging types and methods affect the quality and freezing efficiency of cooked chicken products, especially when each packaging factor is held constant under controlled conditions. This study fills this gap by systematically comparing the effects of three commonly used packaging types on the freezing rates, thawing loss, yield, color, and texture of frozen roasted chicken drumettes. The goal is to provide evidence-based recommendations for selecting the best packaging for commercial frozen, ready-to-eat production.

This study shows that packaging type affects the freezing efficiency of roasted chicken drumettes. VC has the fastest freezing rate and takes the least time to freeze compared to other packaging types because removing air between the film and the product surface enhances heat transfer during cold-air freezing. In contrast, under normal atmospheric conditions, both PA/PE and AF packaging showed significantly slower, equivalent freezing efficiencies, indicating that the packaging method influences the freezing rate more than the thermal conductivity of the packaging material itself. No statistically significant differences were found among packaging types in drip loss, yield, color quality, and texture. However, AF showed a numerical trend toward higher yield, likely reflecting its superior moisture-barrier properties. The microwave defrosting method at 800 W for 10 min resulted in high hardness and chewiness values across all packaging types, indicating that the defrosting method affects the meat's physical properties and structure, leading to fiber shrinkage and drip loss. These research findings suggest that if the main priorities of a production facility are freezing speed and production efficiency, VC is the more suitable option, whereas AF may offer advantages in moisture retention.

Future research should investigate long-term frozen storage, increase sample sizes, and conduct microstructural analyses, including studies of ice crystal formation and the pathological assessment of muscle tissue integrity, to better understand the protective effects of packaging types on the quality of cooked frozen chicken. Studies on the oxidation of fats and proteins across different packaging types during long-term storage are also recommended, as packaging materials with varying oxygen and moisture permeability have been shown to affect the degradation rates of fats and proteins in frozen chicken products. Future efforts should focus on optimizing

production processes, such as marinating and roasting, that preserve more moisture in the meat, to mitigate texture deterioration caused by high-energy defrosting. This will help understand the impacts of packaging types on the quality of cooked frozen chicken meat.

Acknowledgements

The authors would like to express sincere gratitude to the Food Industry Management Program, Faculty of Agro-Industry, Prince of Songkla University, Thailand, for providing the necessary facilities, laboratory support, and academic guidance throughout this research. The authors would also like to thank the technical staff and laboratory team for their assistance, dedication, and support, which were crucial to the success of this project.

References

1. Sasitorn, K. Industry analysis and outlook: Thai Chicken Product Business trend. https://www.kasikornresearch.com. 2025.
2. Motarjemi, Y.; Moy, GG.; Jooste, PJ.; Anelich, LE. Milk and dairy products. Food safety management. London: Academic Press; 2014. p. 83-117.
3. Saravanan, D. A *International Research Journal of Engineering and Technology* 2016, *3*, 7, 1667.
4. Kan, M.; Miller, SA. *Resources, Conservation and Recycling* 2022, 180.
5. Pires, ISC.; Rosado, GP.; Azeredo, RMC.; Neves, MB.; Miranda, LS. *Revista de Nutrição* 2002, *15*, 2, 163-172.
6. Mulot, V.; Benkhelifa, H.; Pathier, D.; Ndoye, FT.; Flick, D. *Journal of Food Engineering*. 2019, *263,* 13–24.
7. Chu, Y.; Ding, Z.; Xie; J, *Food Research International* 2024, *175*, 113657.
8. Marsh, K.; Bugusu, B. *Journal of Food Science* 2007, *72*, 3, R39-R55.
9. Murphy, RY.; Duncan, LK.; Johnson, ER.; Davis, MD. Vol. 64, *Journal of Food Protection* 2001, *64*, 1549–1555.
10. Barbanti, D.; Pasquini, M. *Food Science and Technology* 2005, *38*, 8, 895–901.
11. Dang, D.S.; Bastarrachea, L.J.; Martini, S.; Matarneh, S.K. *Foods* 2021, *10*, 11, 2707.
12. Wagoner, M.P.; Reyes, T.M.; Zorn, V.E.; Coursen, M.M.; Corbitt, K.E.; Wilborn, BS.; Starkey, C.W.; Brandebourg, TD.; Belk, A.D.; Bonner, T.; Sawyer, J.T. Foods. 2022, 11, 19, 3012.
13. Kiani, H.; Sun, DW. *Trends in Food Science & Technology* 2011, *22*, 8, 407–426.
14. Zhu, Z.; Zhou, Q.; Sun, DW. *Trends in Food Science & Technology* 2019, *90*, 13–25.
15. Jeong, S.K.; Jo, K.; Lee, S.; Jeon, H.; Kim, S.; Han, S.; Woo, M.; Choi, YS.; Jung, S. Food Science of Animal Resources. 2025, 45, 3, 711-726.
16. Zhu, Y.; Zhu, J.; Shi, X.; Fan, M. *Food Science & Nutrition* 2025, *13*, 8, e70774.
17. Scanga, JA. Meat safety: handling, quality assurance & processing. Fort Collins: Colorado State University, Department of Animal Sciences; [cited 2026 Mar 12].
18. U.S. Department of Agriculture, Food Safety and Inspection Service. Freezing and food safety. Washington (DC): USDA; [cited 2026 Mar 12].
19. Pathomyothin, W. *Food Journal* 1992*, 22*, 3, 40. (in Thai).
20. Tian, J.; Yang, Z.; Zhang, Y.; Pu, A.; Feng, Y.; Liu, G et al. *Food Control* 2025, *175*.
21. Xia, X.; Kong, B.; Liu, J.; Diao, X.; Liu, Q. *Food Science and Technology* 2012, *46*, 280-286.
22. Zhang, M.; Li, J.; Ni, Q.; Yu, D.; Yu, P.; Yao, W.; Zhu, K.; Liu, D. *Food Chemistry* 2025, *465*, 1, 141952.

P - 230

Efficiency of Extract from Jackfruit rags to Support Probiotic Growth

Boonsita Ditphoo[1], Pimnibha Hirunsorn[1], Supatra Karnjanapratum[2],
Supawan Thawornchinsombut[1], Kantiya Petsong[1]*

[1]*Department of Food Technology, Faculty of Technology, Khon Kaen University, Khon Kaen, Thailand*
[2]*Division of Marine Product Technology, Faculty of Agro-Industry, Chiang Mai University, Thailand*

**Corresponding author E-mail: kantpe@kku.ac.th*

Abstract: Thailand produces over 95,000 tons of jackfruit (*Artocarpus heterophyllus*) per year. However, up to 60% of jackfruit are agricultural by-products. Jackfruit rags are a major by-product, which are rich in cellulose and represent a potential prebiotic source. This study aimed to evaluate the efficiency of extracts from jackfruit rags to support probiotic growth. Jackfruit rags powder was hydrolyzed by using cellulase (0.5% w/v) at pH 5, 55°C for 30, 60, and 90 minutes (TE30, TE60, and TE90, respectively). The non-reducing sugar contents of TE30, TE60, and TE90 indicated the digestion of jackfruit rags via enzymatic hydrolysis. The growth of five probiotic strains (*Bacillus coagulans, Bifidobacterium animalis* subsp. *lactis, Lactobacillus acidophilus*, *Lactobacillus bulgaricus*, and *Streptococcus thermophilus*) were investigated. After incubation at 37ºC, TE30 showed the outstanding efficiency to support the growth of *L. bulgaricus, L. acidophilus*, and *B. coagulans* more than the control (polydextrose) by 72 h of incubation (4.69, 0.80, and 0.20 log CFU/mL, respectively). TE60 could support the growth of *B. animalis* subsp. *lactis* more than the control up to 1.03 log CFU/mL at 48 h of incubation. While TE90 could support the growth of *S. thermophilus* more than the positive control (polydextrose) up to 1.31 log CFU/mL at 24 h of incubation. Overall, the cellulase-hydrolyzed jackfruit rags extract effectively promoted the growth of selected probiotic strains, confirming their potential as the source of prebiotic ($p < 0.05$). Therefore, this study highlights jackfruit rags as a promising raw material for developing prebiotic ingredients, adding the value to agricultural by-products.

Keywords: Jackfruit rags; Prebiotic; Cellulase; Agricultural waste; Oligosaccharides

1. Introduction

Food waste refers to food or parts of food that are not consumable and generated along the human food supply chain [1]. It has become a critical global and national issue. In 2022, food waste in Thailand was reached to be 9.68 million tons, accounting for 38% of the total 26 million tons of municipal solid waste. On average, each person generates approximately 146 kilograms of food waste per year, consisting of 39% edible and 61% inedible portions [2]. Typical examples include leftover food, by-products from food processing, and inedible parts of fruits and vegetables.

Jackfruit (*Artocarpus heterophyllus*) is one of the important economic fruits in Thailand, with an annual production of approximately 95,000 tons. However, around 50–60% of its biomass is inedible, resulting in nearly 50,000 tons of agricultural residues each year. Among these, jackfruit rags represent a promising agricultural by-product with potential prebiotic properties. Previous studies have reported that jackfruit residues, particularly the peel, contain significant chemical components such as cellulose (27.75%) and pectin (7.52%) [3], which are recognized as potential sources of prebiotics [4]. Of particular interest are cello-oligosaccharides (COS), which are derived from the enzymatic hydrolysis of cellulose into short-chain oligomers with a degree of polymerization (DP) of 2–9, including cellobiose, cellotriose, and cellotetraose [5,6]. These

low-DP oligomers are more readily metabolized by gut microbiota and play a role in modulating the intestinal microbial balance, thereby contributing to host health [6]. This characteristic aligns with the definition of prebiotics, which are substrates that selectively stimulate the growth and activity of beneficial microorganisms in the colon.

The extraction of prebiotics from agricultural residues is therefore a promising approach, as it not only adds value to low-cost biomass and generates income for local farmers, but also contributes to reducing greenhouse gas emissions in line with the zero-waste concept, thereby mitigating global warming. The present study aimed to investigate the efficiency of enzymatic extraction of prebiotic compounds from jackfruit rags, providing a foundation for value-added utilization of agricultural by-products in Thailand and further development of functional food ingredients in the form of prebiotics.

2. Materials and Methods

2.1 Chemical and reagents

Cellulase was purchased from Reach Biotechnology (Pathum Thani, Thailand). Polydextrose as a control was purchased from krungthepchemi (Bankok, Thailand). Chemical for total sugar and reducing sugar analysis including 3, 5 dinitrosalicylic acid (DNS) (Sisco research laboratories Pvt. Ltd., India), potassium sodium tartrate (Kemaus, Australia), sodium hydroxide (Loba chemie PVT. LTD., Indai) glucose powder (Kemaus, Australia), sulfuric acid (QREC, New Zealand), and phenol (DC Fine Chemicals SLU, Spain). Probiotic strains (*Lactobacillus acidophilus* TISTR1338, *Lactobacillu bulgaricus* TISTR451, *Streptococcus thermophilus* TISTR894) were purchased from the TISTR Culture Collection, Thailand Probiotic strains (*Bifidobacterium animalis* subsp. *lactis* BLC1, *Bacillus coagulans* SNZ1969) were purchased from SACCO Srl., Italy. All culture mediums were purchased from HiMedia Laboratories Pvt. Ltd., India.

2.2 Jackfruit rags extraction

Jackfruit rags, the by-product of the peeling process, were obtained from a jackfruit farm in Chon Buri, Thailand. Samples of jackfruit rags were cleaned for 5 times with tap water, then blended by using a grinder (Simplus, China) and washed for 5 times. The samples were pre-treatmented by soaking in clean water at 60 °C for 24 hours and dried in a hot air oven (Vision VS-1202D2N, Korea) at 50°C for 48-72 hours. Jackfruit rags powder was prepared by using an ultra-centrifugal mill (RETSCH ZM200, Germany). Jackfruit rags powder was then extracted by using 0.5% of cellulase (enzyme: solvent, w/v) at 55–57°C pH 5-5.5 for 30, 60, and 90 minutes [7]. The extracted samples were then frozen at -60 °C for 24 hours, before freeze-drying by using a laboratory-scale freeze-dryer (Gamma 2-16LSC, Christ, Germany) for 48-72 hours.

2.3 Total sugar of extracts from jackfruit rags analysis

Total sugar content was determined using the phenol–sulfuric acid method according to Dubois et al. [8] with slight modifications. Jackfruit rag extracts obtained at extraction times of 30, 60, and 90 minutes were used for the analysis. An amount of 1.0 mL from each extract was mixed with a 5% (w/v) phenol solution, followed by the rapid addition of 5.0 mL of concentrated sulfuric acid. The mixture was allowed to stand at room temperature for color development, and the absorbance was measured at 490 nm using a spectrophotometer (Spectramax M3, United States). Total sugar content was quantified using a glucose standard curve and expressed as glucose equivalents.

2.4 Reducing sugar of extracts from jackfruit rags analysis

Reducing sugar content was assessed using the method described by Miller [9]. Jackfruit rag extracts obtained at extraction times of 30, 60, and 90 minutes were used for the analysis. 1.0 mL of each extract was combined with 3.0 mL of DNS reagent, meticulously homogenized, and subsequently heated in a boiling water bath at 100 °C for 5 minutes to facilitate color formation. The mixes were then cooled to the room temperature, and the absorbance was quantified at 540 nm using a spectrophotometer (Spectramax M3, United States). The reducing sugar content was calculated based on a glucose standard curve and expressed as glucose equivalents.

2.5 Non-reducing sugar of extracts from jackfruit rags analysis

Non-reducing sugar content was calculated using an indirect method based on the difference between total sugar content and reducing sugar content, according to the following equation:

$$\text{Non-reducing sugar} = \text{Total sugar} - \text{Reducing sugar}$$

2.6 Bacterial growth conditions

A single colony of *Bacillus coagulans* SNZ196, *Bifidobacterium animalis* subsp. *lactis* BLC1, *Lactobacillus acidophilus* TISTR1338, *Lactobacillus bulgaricus* TISTR451 and *Streptococcus thermophilus* TISTR894, were cultivated in Brain Heart Infusion broth (BHI) (HiMedia Laboratories Pvt. Ltd., India) and incubated at 37 °C for 24-48 hours, under anaerobic conditions.

2.7 Effect of extracts from jackfruit rags to support probiotic growth

The suspensions of *B. coagulans, B. animalis* subsp. *lactis, L. acidophilus, L. bulgaricus* and *S. thermophilus* at 10^3 CFU/mL were prepared. BHI broth was mixed with 1% (w/v) of extracted samples from section 2.2. Positive control samples were prepared by BHI broth mixed with 1% (w/v) polydextrose, whereas negative control samples were prepared by only BHI broth. The mixtures were incubated at 37°C for 72 hours. Probiotic numbers were enumerated at 0, 24, 48 and 72 hours using standard plate count method.

2.8 Statistical analysis

All experiments were performed in three replications. Total sugar, reducing sugar and non-reducing sugar were analyzed using IBM SPSS Statistics 28. Analysis of Variance (ANOVA) was used to compare total sugar, reducing sugar and non-reducing sugar. Comparison of means was declared by Duncan's multiple range tests ($p<0.05$). All Data were processed and presented as mean $\pm$ standard deviation (S.D.).

3. Results & Discussion

3.1 Non-reducing sugar of extracts from jackfruit rags

Table 1 presents the oligosaccharide content based on an evaluation of non-reducing sugars. The research found no significant difference ($p<0.05$) between jackfruit rag extracts digested with cellulase for 30, 60, and 90 minutes (TE30, TE60, and TE90, respectively). These results show that cellulase hydrolysis was able to produce similar quantities of non-reducing sugars across the extraction times tested in this research. The study of non-reducing sugar content is the crucial key for establishing the effectiveness of enzymatic extraction methods because non-reducing sugars, especially oligosaccharides, are the major components involved in prebiotic properties. The measured quantities indicate the preservation of oligosaccharide structures that did not undergo complete breakdown into reducing sugars or monosaccharides. The lack of significant differences in non-reducing sugar content among the different hydrolysis durations indicate that a cellulase hydrolysis time of 30 minutes may be enough to produce oligosaccharides at an appropriate level,

offering advantages in terms of processing efficiency and energy conservation. However, it should be remembered that the measured non-reducing sugar might include both sucrose and oligosaccharides. Further compositional analysis, particularly sucrose profiling, would allow for a more precise calculation of oligosaccharide concentration and give clearer evidence for the involvement of enzyme-extracted non-reducing sugars as substrates promoting probiotic growth [10].

Table 1. Total sugar, reducing sugar, and non-reducing sugar (mg/g sample) of extracts from jackfruit rags.

Sample	Total sugar* (mg/g sample)	Reducing sugar (mg/g sample)	Non-reducing sugar* (mg/g sample)
TE30	20.01±0.25	0.44±0.01^{b}	19.57±0.24
TE60	18.38±1.76	0.44±0.05^{b}	17.93±1.71
TE90	20.44±0.11	0.66±0.04^{a}	19.78±0.06

Lowercase letters as superscript indicate significant difference ($p<0.05$) of non-reducing sugar among various samples. TE30 is the jackfruit rags extracted with cellulase for 30 minutes, TE60 is the jackfruit rags extracted with cellulase for 60 minutes, and TE90 is the jackfruit rags extracted with cellulase for 90 minutes. The symbol (*) indicates non-significant difference ($p>0.05$) of non-reducing sugar among various samples.

3.2 Effect of extracts from jackfruit rags to support probiotic growth

According to the analysis of non-reducing sugar content (Section 3.1), the results indicate that jackfruit rags, an agricultural by-product, possess considerable potential as a raw material to produce functional oligosaccharides. Nevertheless, confirmation of the prebiotic properties of these extracts requires further functional evaluation, particularly their efficiency to support the growth of probiotic microorganisms. This evaluation is essential, as the ability of probiotic strains to utilize specific oligosaccharides as carbon sources varies depending on their metabolic systems. Therefore, the use of jackfruit rag extracts as the sole carbon source for assessing the growth responses of different probiotic strains provides critical information for the future development of effective prebiotics derived from agricultural waste materials.

As shown in Figure 1(a-e), enzyme-hydrolyzed jackfruit rag extracts enhanced the proliferation of various probiotic strains, especially *Lactobacillus bulgaricus* and *Bifidobacterium animalis* subsp. *lactis*, which exhibited superior growth compared to the commercial prebiotic polydextrose. Variations in probiotic growth among strains may be attributed to differences in enzyme specificity within each strain's metabolic system for oligosaccharide utilization. Figure 1b demonstrates that *B. animalis* subsp. *lactis* exhibited superior growth in the jackfruit rag extracts compared to the positive control (polydextrose), with TE60 showing a probiotic count 1.06 log CFU/mL higher than polydextrose after 48 hours. This enhanced growth may be explained by the ability of *B. animalis* subsp. *lactis* to produce β-glucosidase, an enzyme capable of cleaving β-1,4 glycosidic bonds in cellulose to generate short-chain cello-oligosaccharides that can be readily utilized during fermentation [6]. Similarly, Figure 1d, present that *L. bulgaricus* may produce intracellular β-glucosidase, enabling the hydrolysis of oligosaccharides such as cellobiose into monosaccharides for metabolic utilization [11] . In the case of *B. coagulans*, the results indicated that within the first 24 hours, TE30 exhibited a probiotic count comparable to that of polydextrose, while TE60 and TE90 displayed slightly lower counts. After 48 hours, all treatments with jackfruit rag extracts demonstrated higher probiotic counts in comparison to polydextrose. According to Zheng et al. [12], certain *B. coagulans* strains have the ability of metabolizing complex carbohydrates such as cellobiose, one of the primary cello-oligosaccharides

(COS), via an inducible enzyme system. Therefore, the carbohydrates produced from enzyme-hydrolyzed jackfruit rags might need an induction period before effective utilization. This is consistent with the observed growth pattern, in which *B. coagulans* exhibited minimal proliferation during the first 24 hours but showed a pronounced increase after 48 hours. In contrast, *L. acidophilus*, isolated from the intestines of Thai local chickens [13] grew moderately, showing that it might not be able to effectively use the oligosaccharide from jackfruit rag extracts. For TE90, *S. thermophilus* showed the greatest growth, especially in the first 24 hours. This is perhaps the longer hydrolysis that produces more simple sugars, like glucose and nd other small carbohydrates [14,15], which are easily used by strains that are usually found in dairy products and rely on small carbohydrates.

The findings indicate that, compared to other probiotic strains, *L. bulgaricus* and *B. animalis* subsp. *lactis* exhibited outstanding effectiveness in metabolizing oligosaccharides derived from jackfruit rag extracts. The results highlight the potential of jackfruit rag extracts as an alternative prebiotic source for wellness food applications, particularly in synbiotic formulations. Moreover, the value of agricultural by-products in food production aligns with principles of sustainable development and the circular economy, supporting both environmental sustainability and value-added innovation within the food industry.

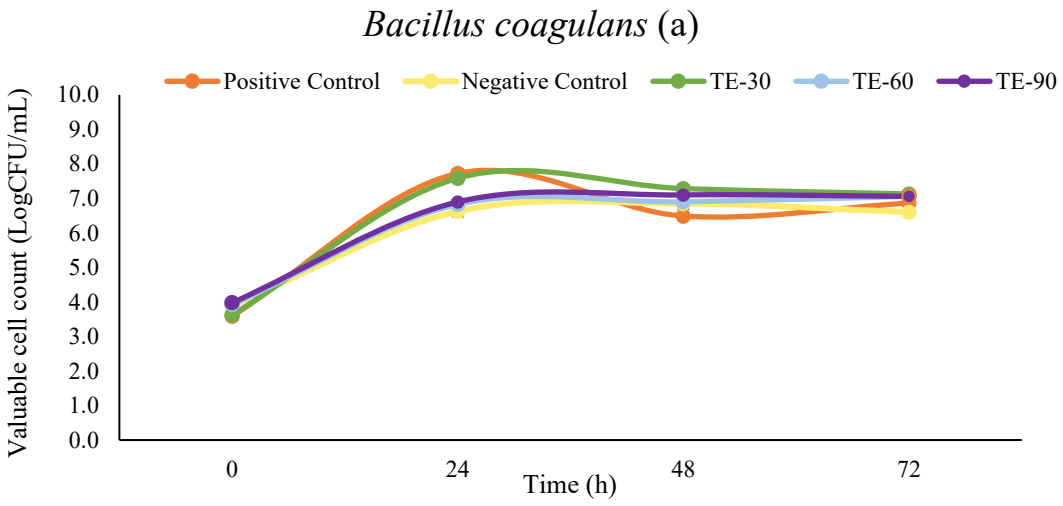

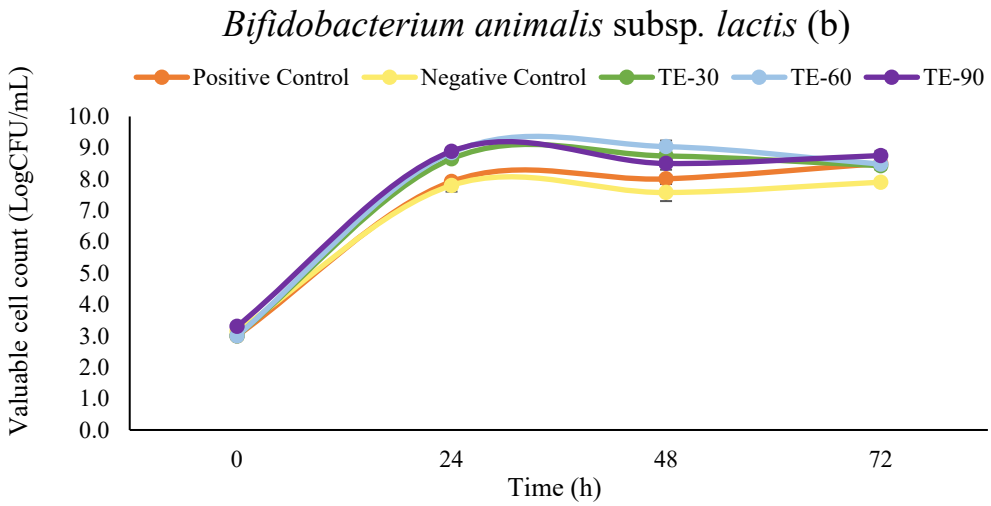

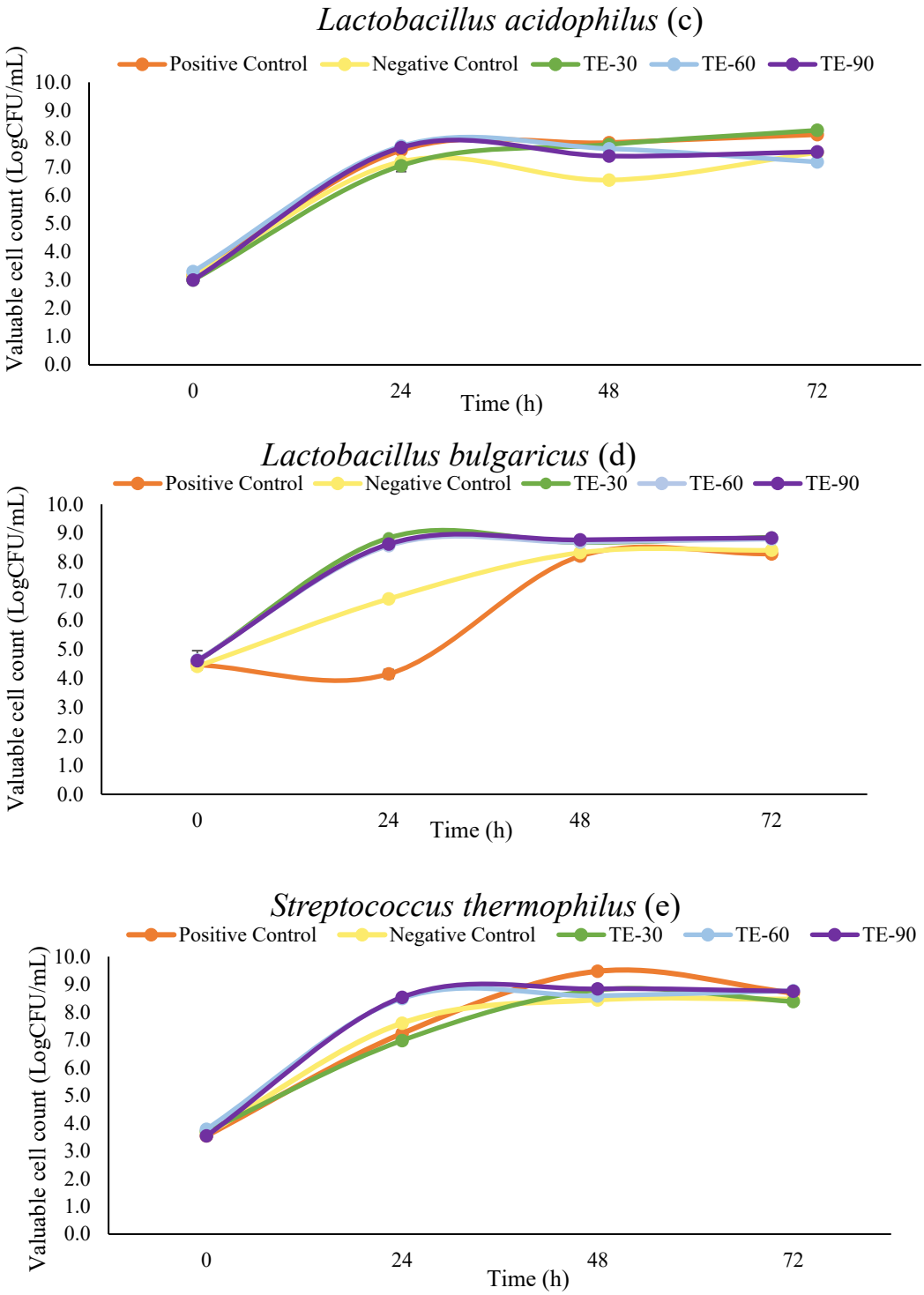

Figure 1. Growth of probiotic strains with addition of extracts from jackfruit rags (TE30, TE60, and TE90) at 1% (w/v) compared with polydextose at 1% (w/v) and BHI alone. Probiotic strains: (a). *B. coagulans*; (b). *B. animalis* subsp. *lactis*; (c). *L. acidophilus*; (d). *L. bulgaricus*; and (e). *S. themophirus.* Probiotic growth was measured and shown as log (CFU/mL). Green line represents TE30, blue line represents TE60, purple line represents TE90, yellow line represents BHI as a negative control and orange represents polydextose as a positive control.

4. Conclusion

This study showed that, compared to commercial polydextrose used as a positive control, jackfruit rags extract significantly promoted the growth of specific probiotic strains, particularly *Bifidobacterium animalis* subsp. *lactis* and *Lactobacillus bulgaricus*. Among the hydrolysis conditions evaluated, enzymatic treatment for 30 minutes provided the most favorable balance between non-reducing sugar content and probiotic growth stimulation, indicating that shorter hydrolysis times might be sufficient to generate functional oligosaccharides while reducing processing time and energy consumption. These findings highlight the potential of jackfruit rags, an abundant agricultural by-product in Thailand, as a valuable and sustainable source of prebiotic ingredients. The cellulase-hydrolyzed extracts could be developed further for application in synbiotic and functional food products. Additionally, utilizing enzymatic hydrolysis provides a scalable and eco-friendly method that is consistent with the circular economy and the value-adding of food waste. This study shows reliable evidence in supporting the discovery of novel prebiotic ingredients from agricultural waste, supporting the growth of health-conscious food industries and sustainable food systems. Future research must additional chromatographic characterisation to identify the specific sugars and to more accurately confirm the prebiotic properties of the extract.

Acknowledgements

This research was funded by the Agricultural Research Development Agency (Public Organization), Thailand (ARDA), under Project Code CRP6805030040.

References

1. United Nations Environment Programme. Food Waste Index Report 2024: Think Eat Save Tracking Progress to Halve Global Food Waste. Nairobi: UNEP; 2024.
2. Pollution Control Department. Patcharawat joins forces with Anutin to manage food waste, aiming to reduce greenhouse gases. Bangkok: Ministry of Natural Resources and Environment, Thailand; 2023.
3. Kalse SB, Swami SB. Recent application of jackfruit waste in food and material engineering: A review. Food Biosci. 2022;48:101808.
4. Hao S, Shan X, Bo W, Yan-Xue C, Ji-Hui L. Waste to wealth: Dynamics and metabolic profiles of the conversion of jackfruit flake into value-added products by different fermentation methods. *Food Chem.* 2024;432:101164.
5. Phirom-on K, Apiraksakorn J. Development of cellulose-based prebiotic fiber from banana peel by enzymatic hydrolysis. *Food Biosci.* 2021;41:101083.
6. Liu X, Hu KKY, Haritos VS. Enzymatic production of cello-oligosaccharides with potential human prebiotic activity and release of polyphenols from grape marc. *Food Chem.* 2024;435:137562.
7. Longern K. Effects of pectinase and cellulase on jackfruit cob extraction for syrup product development [MSc thesis]. Pathum Thani: Rajamangala University of Technology Thanyaburi; 2021.
8. Dubois M, Gilles KA, Hamilton JK, Rebers PA, Smith F. Colorimetric method for determination of sugars and related substances. *Anal Chem.* 1956;28:350–6.
9. Miller GL. Use of dinitrosalicylic acid reagent for determination of reducing sugar. *Anal Chem.* 1959;31:426–8.
10. Ketchulee T. Non-reducing sugar extraction in laboratory and pilot plant scale and evaluation of the resistance to digestion in simulated upper gut condition [MSc thesis]. Songkla: Prince of Songkla University; 2012.
11. Hati S, Ningtyas DW, Khanuja JK, Prakash S. β-Glucosidase from almonds and yoghurt cultures in the biotransformation of isoflavones in soy milk. *Food Biosci.* 2020;34:100542.

12. Zheng Z, Guo W, Zhang K, Liu R, Zheng J, Zhang J. Simultaneous consumption of cellobiose and xylose by engineered *Bacillus coagulans*. *Biotechnol Biofuels.* 2018;11:278.
13. TISTR Culture Collection. Lactobacillus acidophilus TISTR 1338 [Internet]. Pathum Thani: Thailand Institute of Scientific and Technological Research; [cited 2025 Jan 4]. Available from: https://www.tistr.or.th/tistr_culture/cdetail.php?type=b&tno=1338
14. Dong Y, Han M, Fei T, Liu H, Gai Z. Utilization of diverse oligosaccharides for growth by Bifidobacterium and Lactobacillus species and their in vitro co-cultivation characteristics. *Int Microbiol.* 2024;27:941–52.
15. Ghailan AZ, Niamah AK. Streptococcus thermophilus: Metabolic properties, functional features, and useful applications. *Appl Microbiol.* 2025;5:101.

P - 231

Investigation of Functional Carbohydrate Components from Indigenous Plants in Thailand

Boonsita Ditpoo[1], Supatra Karnjanapratum[2], Sasalak Pathapeepat[1], Pojnicha Intawong[1], Areeya Phoolklang[1], Thepparit Pitirit[1], Kantiya Petsong[1]*

[1]*Department of Food Technology, Faculty of Technology, Khon Kaen University, Khon Kaen, Thailand*
[2]*Division of Marine Product Technology, Faculty of Agro-Industry, Chiang Mai University*

**Corresponding author E-mail: kantpe@kku.ac.th*

Abstract: Prebiotics are bioactive compounds that confer various health benefits to the host, with numerous studies highlighting their role in preventing and alleviating symptoms of non-communicable diseases (NCDs). Thailand, located in a tropical region, is rich in biodiversity and originate to a wide variety of indigenous plants, many of which have been reported to contain high levels of prebiotic components. Utilizing these indigenous plants for functional food development offers an opportunity to add value to underutilized raw materials while supporting indigenous agriculture and increasing farmer income. This study aimed to investigate prebiotic composition of various indigenous Thai plants, including jackfruit flesh, jackfruit rag, bracts and immature fruitlets of banana blossoms from two cultivars (Ploek-Bang and Ta-lueng), and ivy gourd leaves. Plant samples were hot-air dried at 60°C for 24 hours and ground into fine powder. Soluble fibers were extracted using two different solvents (distilled water and 50% ethanol) at 70°C for 4 hours. The extracts were filtered, and the supernatants were analyzed for total sugar and reducing sugar contents using phenol-sulfuric acid method and Somogyi–Nelson method, respectively. The amount of non-reducing sugars was then calculated and used as an indicator of potential prebiotic content. The results revealed that extraction with 50% ethanol yielded significantly higher levels of both total sugars and reducing sugars compared to water extraction ($p < 0.05$). Non-reducing sugar analysis indicated that all tested samples potentially contained prebiotic components. Among tested samples, jackfruit rag and Talung banana blossom exhibited the highest non-reducing sugar contents (282.36 ± 6.86 and 292.77 ± 8.90 mg/g sample, respectively), while jackfruit flesh had the lowest content (123.23 ± 32.92 mg/g sample). These findings suggest promising potential for the development of health-promoting food products derived from indigenous Thai plants.

Keywords: Prebiotic; Indigenous plants; Extraction

1. Introduction

In recent years, human health problems have become increasingly prevalent due to environmental changes, sedentary lifestyles, limited time for exercise, and shifts in dietary habits. These factors have contributed to a heightened risk of various diseases, particularly gastrointestinal disorders [1]. As a result, people have become more aware of the importance of maintaining good health. One effective approach to reduce disease risk involves preserving the balance of microorganisms within the human body, especially in the gut. The human gastrointestinal tract hosts two primary types of microorganisms: beneficial microorganisms, such as probiotics, and pathogenic microorganisms. The balance between these groups plays a crucial role in human health [2]. Probiotics, which are predominantly located in the large intestine, rely on specific types of nutrients to thrive. These nutrients are known as prebiotics, non-digestible food components that selectively promote the growth and activity of beneficial gut bacteria [3].

Prebiotics naturally occur in various plant-based foods, particularly fruits and vegetables [4]. Additionally, agricultural byproducts are known to be significant sources of prebiotic substances such oligosaccharides [5,6]. Indigenous plants may serve as valuable sources of prebiotics for the development of health-promoting food products because of their distinct biochemical compositions, environmental tolerance, and significant potential for sustainable use [7,8]. Thailand, located in a tropical region, is rich in biodiversity and home to a wide variety of indigenous plants, many of which have been reported to contain high levels of prebiotic components [9]. However, studies on plant-derived prebiotics in Thailand remain limited, particularly regarding the extraction and characterization of prebiotic compounds from native or underutilized plant species. As most existing research has primarily focused on commonly consumed crops, while agricultural by-products such as jackfruit rags and banana blossom bracts have received comparatively little attention. In addition, comprehensive comparative studies evaluating extraction conditions across diverse plant matrices are still scarce. While solvent type is a critical determinant, extraction efficiency is also influenced by several other key factors, including solvent polarity, extraction temperature, extraction time, solid-to-solvent ratio, and the physicochemical properties of the plant matrix Therefore, this study aims to investigate prebiotic components in selected indigenous plants of Thailand by systematically evaluating the effects of extraction solvents on the recovery of non-reducing sugars, identifying plant species with high prebiotic potential, and examining multiple factors affecting extraction efficiency beyond solvent type. The findings of this study are expected to provide a scientific foundation for the development of functional foods that promote gut health and overall well-being.

2. Materials and Methods

2.1 Chemical and reagents

95% ethanol (RCI Labscan, Thailand), glucose powder (Ajax Finechem, Australian), sulfuric acid (QREC, New Zealand), sodium hydroxide (QREC, New Zealand), copper sulfate pentahydrate (MERCK, Germany), potassium sodium tartrate (Ajax Finechem, Australian), sodium hydroxide (QREC, New Zealand), sodium arsenate dibasic (MERCK, Germany), ammonium molybdate tetrahydrate (BDH Chemicals Limited, England) phenol (MERCK, Germany)

2.2 Preparation of dried samples

The selected indigenous plant samples (jackfruit pulp, jackfruit rag, banana blossom (cultivar Ploek Bang), banana blossom (cultivar Talung varieties), and ivy gourd leaves were purchased from the indigenous market in Khon Kaen Thailand, during June to November 2024. Samples were thoroughly washed with clean water 5 times to remove dirt and sticky plant latex. The samples were then torn or chopped into uniform small pieces, then washed again with clean water 5 times. The samples were blotted to remove excess water and placed in aluminum trays to dry in a hot air oven at 60 °C for 24 hours. The dried samples were ground into fine powder using a grinder and stored in zip-lock bags for further analysis.

2.3 Prebiotic extraction

This study investigated 2 different solvents (ethanol (50%) and distilled water) to extract prebiotics from various indigenous plants. For ethanol, 20 g of dried sample powder were weighed and mixed with 380 mL of 50% ethanol in the beakers. The beakers were covered with aluminum foil to prevent ethanol evaporation. The mixtures were extracted in a water bath at 70 °C for 4 hours. The extracts were filtered using filter cloth. The filtrate was evaporated using a rotary evaporator at 50–60 °C under a pressure of 700 mbar (Rotavapor R-124, BUCHI, Switzerland). The concentrated extracts were stored in amber glass bottles for further analysis. The extraction by distilled water was followed the procedure as ethanol extraction, except the evaporation step.

Each extract's ultimate volume was set to 400 mL. Every extraction was carried out in three separate batches, or triplicate. Based on the normalized extract volume, the concentrations of non-reducing sugars were then computed and expressed as mg per g of dry material.

2.4 Sugar analysis procedures

2.4.1 Total sugar analysis

Phenol-Sulfuric acid method was used to analyze total sugar content in the samples. The analysis was performed according to the method described by Rover et al. [10], with slight modifications. To prepare standard curve, the amount of 0.1 g of glucose was dissolved in distilled water and diluted to 100 mL. The volume of 1 mL of extract or glucose solution was mixed with 0.5 mL of 5% phenol. Then 2.5 mL of conc. sulfuric acid was gradually added to each tubes. The mixtures were left at ambient temperature for 30 minutes and the absorbance was measured at 490 nm by spectrophotometer (UV-1800 Shimadzu, Japan). The experiment was done in triplicate.

2.4.2 Reducing sugar analysis

Somogyi–Nelson method was used to analyze reducing sugar content in the samples. Following Sadeghi et al. [11], with minor modifications. To prepare standard curve, the amount of 0.1 g of glucose was dissolved in distilled water and diluted to 100 mL. The stock solution was serially diluted to obtain concentrations of 0, 20, 40, 60, 80, and 100 mg/L. The volume of 1 mL of extract or glucose solution was transferred to test tubes. The volume 1 mL of Somogyi's alkaline copper reagent was added, and the mixtures were boiled in water for 10 minutes to perform orange precipitate. After cooling, 1 mL of Nelson's reagent was added and mixed to perform a deep blue solution. The mixtures were left for 15 minutes, then 10 mL of distilled water was added and mixed. The absorbance was measured at 540 nm by spectrophotometer (UV-1800 Shimadzu, Japan).

2.4.3 Non-reducing sugar content analysis

Non-reducing sugar content is calculated follow by formulate:

$$\text{Non-reducing sugar content} = \text{Total sugar content} - \text{Reducing sugar content}$$

2.5 Statistical analysis

The experiment was designed using a Completely Randomized Design (CRD) to evaluate differences of non- reducing sugar among 7 different plant samples using the same solvent (distilled water or 50% ethanol). Data were analyzed using one-way ANOVA to compare solvent effects. Paired samples t-test was used to compare non- reducing sugar from each plant sample between two solvents. All statistical analyses were performed at a significance level of $p < 0.05$.

3. Results & Discussion

Table 1. Non-reducing sugar (mg/g sample) extracted from various indigenous Thai plants using distilled water

Sample	Non-reducing sugar (mg/g sample)
Jackfruit flesh	121.73 ± 9.69^{b}
Jackfruit rag	31.63 ± 8.03^{c}
Immature fruitlets of banana blossoms (Ploek-Bang)	42.03 ± 9.06^{c}
Bracts of banana blossoms (Ploek-Bang)	173.63 ± 3.17^{ab}
Immature fruitlets of banana blossoms (Ta-lueng)	181.30 ± 3.82^{a}
Bracts of banana blossoms (Ta-lueng)	200.00 ± 10.96^{a}
Ivy gourd leaves	200.97 ± 6.56^{a}

Lowercase letters as superscript indicate significant difference ($p<0.05$) of non-reducing sugar (mg/g sample) among various samples.

The non-reducing sugar content of materials derived from indigenous Thai plants was utilized as a marker of possible prebiotic chemicals [12]. According to the analysis of non-reducing sugar content extracted with distilled water (Table 1), all seven samples showed statistically significant differences ($p < 0.05$) in their non-reducing sugar levels. Among various samples, immature fruitlets of banana blossoms (Ta-lueng), bracts of banana blossoms (Ta-lueng), and Ivy gourd leaves exhibited the highest. Non-reducing sugar content than others. This may be attributed to the polarity of distilled water, which is likely similar or compatible with the polarity of the sample matrices, thereby enhancing the extraction or solubilization of sugar molecules [13]. But also, to inherent variations in the cell wall structure, carbohydrate profiles, and matrix makeup of plants. Since structural polysaccharides and soluble oligosaccharides, which can be partially solubilized in water during heat extraction, are known to be present in significant quantities in banana flowers, especially immature tissues [14], ivy gourd leaves also contain hydrophilic carbohydrate fractions and soluble dietary fibers that are easily extracted using polar solvents. Faruq et al. [15]. Therefore, the amount of water-soluble oligosaccharides or highly hydrophilic hemicellulosic components may be connected to how well distilled water extracts non-reducing sugars from these samples.

Table 2. Non-reducing sugar (mg/g sample) extracted from various indigenous Thai plants using 50% ethanol

Sample	Non-reducing sugar (mg/g sample)
Jackfruit flesh	123.23 ± 2.92^{d}
Jackfruit rag	282.37 ± 6.87^{a}
Immature fruitlets of banana blossoms (Ploek-Bang)	236.97 ± 7.88^{b}
Bracts of banana blossoms (Ploek-Bang)	214.17 ± 1.02^{bc}
Immature fruitlets of banana blossoms (Ta-lueng)	130.47 ± 7.82^{d}
Bracts of banana blossoms (Ta-lueng)	292.77 ± 8.99^{a}
Ivy gourd leaves	198.33 ± 9.17^{c}

Lowercase letters as superscript indicate significant difference ($p<0.05$) of non-reducing sugar (mg/g sample) among various samples.

According to the analysis of non-reducing sugar content extracted with 50% ethanol (Table 2), all seven samples showed statistically significant differences ($p \leq 0.05$) in their non-reducing sugar levels. Among various samples, jackfruit rag and bracts of banana blossoms (Ta-lueng) exhibited the highest concentrations. This could be attributed to the higher extraction efficiency of 50% ethanol compared to distilled water. The use of 50% ethanol, which has moderate polarity, broad solubility range as a neutral solvent, and low ethanol concentration, has been reported as an effective solvent for extracting oligosaccharides, especially short-chain carbohydrates (Pornsmitikun, V, 2009).

Table 3. Non-reducing sugar (mg/g sample) extracted from various indigenous Thai plants using different solvents (distilled water and 50% ethanol)

Sample	Non-reducing sugar (mg/g)	
	Distilled water	50% ethanol
Jackfruit flesh	121.73 ± 9.69^{b}	123.23 ± 2.92^{a}
Jackfruit rag	31.63 ± 8.03^{b}	282.37 ± 6.87^{a}
Immature fruitlets of banana blossoms (Ploek-Bang)	42.03 ± 9.06^{b}	236.97 ± 7.88^{a}
Bracts of banana blossoms (Ploek-Bang)	173.63 ± 3.17^{b}	214.17 ± 1.02^{a}
Immature fruitlets of banana blossoms (Ta-lueng)	181.30 ± 3.82^{a}	130.47 ± 7.82^{b}
Bracts of banana blossoms (Ta-lueng)	200.00 ± 10.96^{b}	292.77 ± 8.99^{a}
Ivy gourd leaves	200.97 ± 6.56^{a}	198.33 ± 9.17^{b}

Lowercase letters as superscript indicate significant difference ($p<0.05$) of non-reducing sugar (mg/g sample) among various samples.

As shown in Table 3, extraction with 50% ethanol proved to be more efficient in extracting oligosaccharides with prebiotic potential, as indicated by the higher levels of non-reducing sugars obtained from Thai indigenous plant samples compared to distilled water. This phenomenon might be because 50% ethanol is an effective solvent for the extraction of oligosaccharides. Its moderate polarity and low ethanol concentration make it a suitable solvent for the extraction of short-chain carbohydrates [17,18].

4. Conclusion

This study investigated the prebiotic components present in various indigenous plant materials from Thailand, including jackfruit flesh, jackfruit rags, bracts and immature fruitlets of banana blossoms from two cultivars (Ploek Bang and Talueng), as well as ivy gourd leaves. Both distilled water and 50% ethanol were employed as extraction solvents. Among them, 50% ethanol demonstrated significantly higher efficiency in extracting prebiotic components. Notably, jackfruit rags and the bracts of the Talueng banana blossom both which are agricultural by-products exhibited the highest levels of non-reducing sugars, indicating a strong potential as sources of prebiotic compounds. The findings suggest that 50% ethanol offers a simple yet effective method for extracting prebiotics from plant matrices and underscore the potential of indigenously available plant materials in Thailand as promising sources of prebiotic substances. The results also emphasize the potential of locally available Thai plant resources as promising candidates for the development of functional foods and dietary supplements, while contributing to value addition and sustainable utilization of agricultural by-products in the future.

Acknowledgements

The authors would like to express their gratitude to the Department of Food Technology, Faculty of Technology, Khon Kaen University for the facility support.

References

1. Park JH, Moon JH, Kim HJ, Kong MH, Oh YH. Sedentary lifestyle: Overview of updated evidence of potential health risks. *Korean J Fam Med.* 2020;41(6):365-373. doi:10.4082/kjfm.20.0165.
2. Ji J, Jin W, Liu SJ, Jiao Z, Li X. Probiotics, prebiotics, and postbiotics in health and disease. *MedComm (2020).* 2023;4(6):e420. doi:10.1002/mco2.420.
3. Pandey KR, Naik SR, Vakil BV. Probiotics, prebiotics and synbiotics: A review. *J Food Sci Technol.* 2015;52(12):7577–7587. doi:10.1007/s13197-015-1921-1.
4. Chadathong N, Chancha P, Siripornadulsil S, Siripornadulsil W. Prebiotics extracted from fruits and vegetables can be applied to lactic acid bacteria to improve their antioxidant activity. *Food Biosci*. 2025;68:106577.
5. Gonçalves DA, González A, Roupar D, Teixeira JA, Nobre C. How prebiotics have been produced from agro-industrial waste: An overview of the enzymatic technologies applied and the models used to validate their health claims. *Trends Food Sci Technol.* 2023;135:74–92. doi:10.1016/j.tifs.2023.03.016.
6. Guerra L, Romanini D, López S, Castelli V, Clementz A. Upcycling of carrot discards into prebiotics (fructooligosaccharides) as high value food ingredients. *Food Bioprod Process.* 2023;138:172-180. doi:10.1016/j.fbp.2023.01.011.
7. Nabeshima EH, Moro TMA, Campelo PH, Sant'Ana AS, Clerici MTPS. Tubers and roots as a source of prebiotic fibers. In: *Advances in Food and Nutrition Research.* Vol. 94. Academic Press; 2020. p. 267-293. doi:10.1016/bs.afnr.2020.06.005.
8. Tinrat S, Chomnawong MT. Exploring local edible plants as potential prebiotic sources for their synbiotic applications. *LWT.* 2024;213:117063. doi:10.1016/j.lwt.2024.117063.
9. Wichienchot S, Thammarutwasik P, Jongjareonrak A, Chansuwan W, Hmadhlu P, Hongpattarakere T, Itharat A, Ooraikul B. Extraction and analysis of prebiotics from selected plants from southern Thailand. *Songklanakarin J Sci Technol.* 2011;33(5):517–523.
10. Rover MR, Johnston PA, Lamsal BP, Brown RC. Total water-soluble sugars quantification in bio-oil using the phenol–sulfuric acid method. *J Anal Appl Pyrolysis*. 2013;104:194-201. doi:10.1016/j.jaap.2013.08.004
11. Sadeghi R, Fang F, Shao Y, Olsen N, Du B, Lin AHM. Eliminating protein interference when quantifying potato reducing sugars with the miniaturized Somogyi-Nelson assay. *Food Chem*. 2022;373(Pt B):131473. doi:10.1016/j.foodchem.2021.131473
12. Sakr EAE, Massoud MI. Impact of prebiotic potential of stevia sweeteners-sugar used as synbiotic preparation on antimicrobial, antibiofilm, and antioxidant activities. *LWT.* 2021;144:111260. doi:10.1016/j.lwt.2021.111260.
13. Nualla-ong S. Extraction of prebiotics from agricultural plants [master's thesis]. Songkhla: Prince of Songkla University, Faculty of Graduate Studies; 2009.
14. Wang S, Yang Y, Xiao D, Zheng X, Ai B, Zheng L, et al. Polysaccharides from banana (*Musa* spp.) blossoms: Isolation, identification and anti-glycation effects. *Int J Biol Macromol.* 2023;236:123957. doi:10.1016/j.ijbiomac.2023.123957.

15. Faruq AA, Farahnaky A, Torley PJ, Buckow R, Eri R, Majzoobi M. Sustainable approaches to boost soluble dietary fibre in foods: A path to healthier foods. *Food Hydrocoll.* 2025;162:110880. doi:10.1016/j.foodhyd.2024.110880.
16. Pornsmitikun V. Extraction of prebiotics from jackfruit inner rind and seeds using a continuous process [Master's thesis]. Songkhla: Prince of Songkla University, Faculty of Graduate Studies; 2009.
17. Bhornsmithikun V, Chetpattananondh P, Yamsaengsung R, Prasertsit K. Continuous extraction of prebiotics from jackfruit seeds. *Songklanakarin J Sci Technol*. 2010;32(6):635-642.
18. Xiang X, Yang L, Hua S, Li W, Sun Y, Ma H, et al. Determination of oligosaccharide contents in 19 cultivars of chickpea (Cicer arietinum L.) seeds by high performance liquid chromatography. *Food Chem*. 2008;111(1):215-9.

P - 243

Effect of Thermo-Sonication Combined with Essential Oils on Bioactive Compounds and Antioxidant Activity in *Carissa carandas* L. Fruit Juice

Jiratchaya Pengtham[1], Sumethee Songsamoe[1]*

[1]*Food Science and Technology, School of Food Industry, King Mongkut's Institute of Technology Ladkrabang, Bangkok, THAILAND 10520*

**Corresponding author E-mail: sumethee.so@kmitl.ac.th*

Abstract: The development of functional beverages rich in bioactive compounds while maintaining microbial safety is a major challenge in the food industry. *Carissa carandas* L., a tropical fruit abundant in phenolics and vitamin C, was selected as a model juice to investigate the effects of thermo-sonication combined with essential oils on the retention of bioactive compounds and antioxidant activity. Juice samples were inoculated with *Escherichia coli* (6 log CFU/mL) and treated by thermo-sonication at 45, 55, and 65 °C for 10 min in the presence of lemon and orange essential oils (1:1 ratio, 40 µL/mL). Microbial, chemical, and antioxidant properties were monitored for 28 days at 4 °C. The combined treatment at 65 °C achieved > 6 log CFU/mL reduction of *E. coli*, total viable count by > 4 log CFU/mL, and total yeast and mold count by > 4 log CFU/mL, confirming pasteurization-equivalent microbial inactivation. Importantly, this condition effectively retained total phenolic content and vitamin C while enhancing antioxidant activity compared with untreated juice, likely due to the release of the bound phenolics by the cavitation effect of ultrasound. Physicochemical quality attributes during monitoring for 28 days of storage, including pH, total soluble solids (TSS), color, and viscosity, remained stable during storage. These findings demonstrate that thermo-sonication combined with essential oils is a promising and sustainable technique for producing safe, bioactive-rich, and antioxidant-enhanced functional fruit juice.

Keywords: Thermo-sonication; Essential oils; *Carissa carandas* L.; Bioactive compounds; *Escherichia coli*

1. Introduction

The non-alcoholic beverage industry, particularly the fruit juice sector, is projected to grow by 3.5–4.5% in 2025 (1), with the 100% fruit juice market exhibiting a strong expansion trend driven by increasing consumer demand for natural and additive-free products. This growth reflects a broader shift toward health-oriented beverages (2). Modern lifestyles and changing consumption behaviors have contributed to inadequate fruit and vegetable intake, leading to nutritional imbalances and a rising incidence of non-communicable diseases. Consequently, health awareness has increased, supported by government and industry campaigns promoting the consumption of natural fruit and vegetable juices, thereby further stimulating market demand (3). Fruit and vegetable beverages are rich sources of essential nutrients and bioactive compounds, particularly antioxidants, which are valued for their health benefits. Therefore, processing technologies that can preserve nutritional quality are critically important. Conventional thermal pasteurization, while effective for microbial safety, often results in the degradation of heat-sensitive nutrients. Consequently, the development of alternative processing methods that minimize thermal damage is essential to maintain product quality and maximize the health benefits of fruit and vegetable

juices. *Carissa carandas* L. juice is particularly suitable as a model system due to its high acidity, richness in phenolic compounds, and susceptibility to thermal degradation. *Carissa carandas* L. contains several phenolic compounds, including gallic, caffeic, chlorogenic, and ferulic acids, as well as flavonoids such as rutin, quercetin, and kaempferol. Anthocyanins, particularly cyanidin-3-galactoside, have also been reported and contribute to its antioxidant activity [4].

Thermo-sonication is an emerging food processing technology that combines ultrasound waves with moderate temperatures. This technique employs ultrasonic energy at frequencies such as 45 kHz in conjunction with mild heating (typically 45–65°C) to enhance microbial inactivation while better preserving nutritional quality compared to conventional thermal processing [5]. Thermo-sonication induces cavitation phenomena that disrupt microbial cells, inactivate spoilage enzymes, and modify food microstructure. As a result, it can improve food safety, reduce processing time and energy consumption, extend shelf life, and retain flavor, texture, and bioactive compounds more effectively than traditional pasteurization, which relies on higher temperatures and longer treatment durations [6, 7]. In addition to physical processing methods, natural antimicrobial agents such as essential oils have attracted increasing attention in food preservation. Essential oils are widely used as natural preservatives, flavoring agents, and antioxidants due to their ability to disrupt microbial cell membranes and inhibit key metabolic enzymes, thereby enhancing microbial control and extending product shelf life [8]. Previous studies have demonstrated that citrus essential oils exhibit significant antimicrobial activity against various microorganisms due to the presence of bioactive compounds such as limonene and other terpenoids. Yeasmin et al. reported that essential oil extracted from *Citrus limon* contains several bioactive constituents, with *d*-limonene as the major component, and showed strong antimicrobial activity against microorganisms such as *Staphylococcus aureus* and *Candida albicans* [9]. Similarly, orange essential oil has also been reported to inhibit several food-related microorganisms, including *Escherichia coli* and *Salmonella* spp. [10]. These findings demonstrate that citrus essential oils possess promising antimicrobial properties and have potential applications as natural antimicrobial agents in food systems.

Acidic beverages generally inhibit the growth of many foodborne pathogens due to their low pH. However, certain strains of *E. coli* can survive in acidic environments through acid tolerance mechanisms. Therefore, *E. coli* is commonly used as an indicator microorganism to evaluate microbial safety in acidic foods, particularly fruit juice products. In this study, it was selected as a representative pathogenic indicator microorganism to assess the antimicrobial effectiveness of thermo-sonication combined with essential oils in an acidic fruit juice system. Previous studies by Binotti et al. [11,12] and Oteiza et al. [13] have demonstrated that certain strains of *E. coli* can survive in acidic fruit juices due to acid adaptation mechanisms. For example, acid-adapted *E. coli* O157:H7 showed significantly higher survival in orange juice compared with non-adapted cells, and exhibited enhanced resistance to environmental stresses such as low pH and UV exposure. These findings indicate that *E. coli* is a relevant indicator microorganism for evaluating microbial safety in acidic fruit-based products. Moreover, according to the notification of the Ministry of Public Health of Thailand regarding beverages in sealed containers, *E. coli* must not be detected in the final product.

Accordingly, this study aims to investigate the combined application of thermo-sonication and essential oils in fruit juice processing. The objective is to evaluate the combined effects of these technologies on microbial inactivation, as well as their influence on bioactive compounds, antioxidant activity, and overall product quality in a functional fruit juice system. This combined approach represents an environmentally friendly and sustainable food processing strategy, offering a promising industrial alternative to conventional thermal pasteurization while reducing the reliance on synthetic chemical preservatives [14].

2. Materials and Methods

2.1 Preparation of fruit juice and essential oils

2.1.1 Fruit and essential oils

Carissa carandas L. fruits were purchased from Chi Garden, Ratchaburi, Thailand. Food-grade lemon and orange essential oils were obtained from Thai-China Flavours and Fragrances Industry Co., Ltd.

2.1.2 Preparation of *Escherichia coli*

The bacterial strain *Escherichia coli* was obtained from a laboratory culture collection (code 1016). The strain was activated in Tryptic Soy Broth (TSB) and incubated at 37 °C for 18–24 h. The bacterial suspension was adjusted to approximately 10^6 CFU/mL before inoculation into the juice samples.

2.1.3 Preparation of essential oil emulsions and determination of minimum inhibitory concentration (MIC)

Lemon and orange essential oil emulsions were prepared at a total concentration of 40 µL/mL, with lemon and orange essential oils mixed at a 1:1 (v/v) ratio. Tween 80 (food grade, 4 mL) was mixed with distilled water (188 mL) using a magnetic stirrer for 5 min. Subsequently, the essential oil mixture (8 mL) was gradually added to the aqueous phase and mixed for an additional 5 min. The resulting mixture was homogenized using a high-speed homogenizer (IKA T 25 digital ULTRA-TURRAX®) at 9,000 rpm for 3 min, followed by probe-type ultrasonication (SONICS Vibra Cell, 750 W, 20 kHz) at 70% amplitude for a total of 10 min (5 min on / 5 min off). The prepared emulsions were stored at 4 °C until use.

The minimum inhibitory concentration (MIC) of lemon and orange essential oils against *E. coli* was determined using the broth dilution method. Tryptic Soy Broth (TSB, 1 mL) was dispensed into sterile test tubes, followed by serial two-fold dilutions of the essential oil emulsion. The essential oils were tested at concentrations ranging from 40 µL/mL and subsequently diluted by two-fold serial dilution for MIC determination. Each tube was inoculated with *E. coli* (10^6 CFU/mL) and incubated at 37 °C for 18–24 h. The MIC was defined as the lowest concentration showing no visible microbial growth (absence of turbidity).

2.1.4 Fruit Juice Formulation and Determination of Optimal Essential Oil Emulsion Concentration.

Fresh *Carissa carandas* L. fruits were washed and prepared for juice extraction. The juice was obtained by the cold pressing method and filtered through a sieve to obtain a uniform juice matrix. Lemon and orange essential oil emulsions were mixed at a 1:1 ratio and added to the fruit juice at concentrations determined based on the minimum inhibitory concentration (MIC) results described in Section 2.1.3. The prepared juice was then used for subsequent treatments.

2.2 Efficacy of Thermo-Sonication Combined with Essential Oils on Microbial Inhibition

Fruit juice samples containing lemon and orange essential oil emulsions (1:1 ratio) were prepared at a concentration selected based on the minimum inhibitory concentration (MIC) determined in Section 2.1.2. The samples were divided into two groups: inoculated with *Escherichia coli* (approximately 10^6 CFU/mL) and uninoculated controls. Thermo-sonication (TS) treatments were performed using an ultrasonic cleaner (CREST ULTRASONIC, Powersonic Benchtop Cleaner Tank – P1100D-45) operating at a frequency of 45 kHz. Samples were treated at 45, 55, and 65 °C for 10 min. In addition, conventional thermal pasteurization (72 °C for 15 s) was conducted as a reference treatment for comparison. Untreated juice served as the control.

Following processing, all samples were immediately cooled and stored at 4 °C for up to 28 days. Microbiological analyses were conducted on days 0, 7, 14, 21, and 28 of storage. *E. coli* was enumerated on EMB agar incubated at 37 °C for 18–24 h, total viable count (TVC) was determined on Plate Count Agar (PCA) incubated at 37 °C for 48 h, and total yeast and mold (TYM) were enumerated on Malt Extract Agar (MEA) incubated at 25 °C for 48–72 h using the spread plate technique. Microbial counts were expressed as CFU/mL.

2.3 Effects of Thermo-Sonication Combined with Essential Oils on Bioactive and Physicochemical Properties of Fruit Juice

2.3.1 Determination of Total Phenolic Content (TPC)

Total phenolic content was determined using the Folin–Ciocalteu colorimetric method [15]. Juice samples were diluted with distilled water at a ratio of 1:2 (v/v). A 0.5 mL aliquot of sample was mixed with Folin–Ciocalteu reagent and allowed to react at room temperature for 5 min, followed by the addition of sodium carbonate solution. After incubation, absorbance was measured at 765 nm. Results were calculated from a gallic acid standard curve (200–500 µg) and expressed as mg gallic acid equivalents (GAE) per 100 mL of juice.

2.3.2 Determination of Vitamin C Content

Vitamin C content was determined spectrophotometrically following the method described in AOAC [16]. Briefly, 5 mL of juice sample was mixed with 5 mL of potassium permanganate solution. Absorbance was measured immediately at 525 nm using a UV–Vis spectrophotometer. Vitamin C concentration was quantified using a calibration curve constructed with standard ascorbic acid solutions.

2.3.3 Analysis of Antioxidant Activity

Antioxidant activity of the fruit juice was determined using DPPH, ABTS, and FRAP assays with slight modifications from Sun et al. [17].

DPPH radical scavenging assay:

An aliquot of 50 µL of appropriately diluted sample was mixed with 150 µL of 2 mM DPPH solution in a 96-well microplate. The reaction mixture was incubated in the dark at room temperature for 30 min. Absorbance was measured at 517 nm using a multimode microplate reader (EnSight, PerkinElmer). Results were expressed as a percentage of DPPH radical scavenging activity.

$$\%DPPH\ scavenging = \frac{A_{blank} - A_{sample}}{A_{blank}} \times 100$$

ABTS radical scavenging assay:

The ABTS•+ working solution was prepared by reacting 7 mM ABTS with 2.45 mM potassium persulfate and incubating the mixture in the dark at room temperature for 12–16 h. Prior to analysis, the solution was diluted with distilled water to an absorbance of 0.70 ± 0.02 at 734 nm. The sample extract was allowed to react with the ABTS solution for 15 min, and absorbance was measured at 734 nm. Antioxidant activity was calculated using a Trolox standard curve and expressed as %ABTS scavenging activity.

$$\%ABTS\ scavenging = \frac{A_{blank} - A_{sample}}{A_{blank}} \times 100$$

Ferric reducing antioxidant power (FRAP) assay:

A 10 µL aliquot of sample extract was mixed with 200 µL of freshly prepared FRAP reagent (preheated at 37 °C for 10 min). The mixture was incubated at room temperature in the dark for 30 min, and absorbance was recorded at 593 nm. Results were expressed as µmol Trolox equivalents (TE) per gram or milliliter of sample.

$$FRAP\ (\mu mol\frac{TE}{mL}) = \frac{A_{sample} - b}{a} \times DF \times 10^{-3}$$

Calibration curves of gallic acid, vitamin C, and Trolox were prepared for quantitative analysis, and the corresponding curves are presented in Appendix A (Figures A1–A3).

2.3.4 Determination of Total Soluble Solids (TSS)

Total soluble solids were measured using a digital refractometer (PAL-1, ATAGO). A few drops of juice sample were placed on the prism surface, and results were recorded as °Brix.

2.3.5 Determination of pH

The pH of the juice samples was determined using a calibrated benchtop pH meter (SI Analytics Lab 855). Measurements were recorded once the readings stabilized.

2.3.6 Determination of Viscosity

Viscosity was measured using a Brookfield viscometer (Brookfield AMETEK, DV-Next 3T) equipped with a UL adapter. Measurements were conducted using spindle No. 0 at 200 rpm, and viscosity values were recorded when torque values were within the recommended range (85–100%).

2.3.7 Color Measurement

Color parameters (L*, a*, and b*) were measured using a spectrophotometer/colorimeter (HunterLab ColorQuest XE) under the CIELAB color system with illuminant D65 and a 10° observer. Total color difference (ΔE) was calculated using the following standard equations:

$$\Delta E^* = \sqrt{(L_2^* - L_1^*)^2 + (a_2^* - a_1^*)^2 + (b_2^* - b_1^*)^2}$$

2.4 Statistical analysis

Experimental data were expressed as mean ± standard deviation (SD) from three independent replicates (n = 3). Statistical analysis was performed using one-way analysis of variance (ANOVA) followed by Duncan's multiple range test with IBM SPSS Statistics software (version 29.0.1.1; IBM Corp., USA). Differences among means were considered statistically significant at $p < 0.05$. Different superscript letters indicate significant differences among treatments within the same row or column.

3. Results & Discussion

3.1 Antimicrobial Activity (Minimum Inhibitory Concentration, MIC) of Essential Oil Emulsions

The minimum inhibitory concentration (MIC) of the combined lemon and orange essential oil emulsions against *E. coli* was determined using the broth dilution method. Complete inhibition of bacterial growth was observed at a concentration of 40 µL/mL, as indicated by the absence of visible turbidity in the culture medium. This result confirms the strong antimicrobial activity of citrus essential oils and their potential application as natural antimicrobial agents. Similar antimicrobial effects have been reported by Xiao et al. [18], who found that lemon essential oil nanoemulsions inhibited *E. coli* with an MIC of 6.25 mg/mL. Variations in MIC values among studies may be attributed to differences in essential oil composition, emulsion formulation, microbial strains, and experimental conditions. Accordingly, the MIC of 40 µL/mL determined in broth culture was selected as a reference concentration for subsequent application in the fruit juice system.

3.2 Microbiological Stability of Fruit Juice During Storage

The microbiological stability of *Carissa carandas* L. fruit juice treated with thermo-sonication combined with essential oils was evaluated during 28 days of refrigerated storage at 4 °C. Changes in *E. coli*, total viable count (TVC), and total yeast and mold (TYM) are summarized in Tables 1–3. Thermo-sonication combined with essential oils was highly effective in controlling *E. coli* throughout the storage period. All treated samples, regardless of processing temperature (45, 55, and 65 °C), achieved an immediate reduction of approximately 6 log CFU/mL, and *E. coli* remained undetectable during storage. This level of inactivation was comparable to conventional pasteurization (72 °C for 15 s), whereas the untreated control exhibited persistently high microbial

levels (Table 1). These results confirm that the combined application of thermo-sonication and essential oils provides sufficient antimicrobial lethality against *E. coli*, satisfying microbiological safety requirements for fruit juice products.

Although total viable count (TVC) is not specifically regulated under Thai food safety legislation, it is commonly used as an indicator of overall microbiological stability and potential shelf life in fruit juice products. In this study, samples treated at TS 45 °C and 55 °C showed detectable increases in TVC after 14 days of storage, indicating limited microbial stability beyond 7–14 days under refrigerated conditions (Table 2). In contrast, thermo-sonication at 65 °C for 10 min completely suppressed TVC throughout the entire 28-day storage period, demonstrating superior microbial control.

A similar trend was observed for total yeast and mold (TYM). Treatments at 45 °C and 55 °C exhibited detectable yeast and mold growth after 14 days, whereas no yeast or mold was detected in samples treated at 65 °C or in pasteurized samples during storage (Table 3). Importantly, the TS 65 °C treatment complied with the Thai Ministry of Public Health Notification No. 356 (2013), which requires the absence of *E. coli* and limits yeast and mold to less than 100 CFU/g in fruit juice products. The relatively high yeast and mold counts observed in the untreated juice may be attributed to the natural microflora present on the surface of fresh fruits and the high sugar content of the juice, which supports fungal growth during storage, as reported by Snyder et al. [19] has reported that yeast and mold contamination is the most frequent cause of spoilage in fruit and vegetable juice.

Overall, these findings highlight the synergistic antimicrobial effects of thermo-sonication and essential oils, where ultrasonic cavitation, moderate heat, and the bioactive properties of essential oils collectively enhance microbial inactivation and improve shelf-life stability. Among the tested conditions, thermo-sonication at 65 °C for 10 min provided the most effective and consistent microbiological stability during refrigerated storage.

Although *E. coli* was selected in this study as a representative pathogenic indicator microorganism due to its acid tolerance and regulatory relevance in acidic beverage products, the inclusion of additional spoilage microorganisms and other relevant pathogens would provide a more comprehensive validation of the process. Future studies should therefore evaluate the effectiveness of thermo-sonication combined with essential oils against a broader range of microorganisms in *Carissa carandas* juice.

Table 1. Effect of thermo-sonication combined with essential oils on *E. coli* population in *Carissa carandas* L. fruit juice during storage at 4 °C.

Treatments	*E.coli* (log CFU/ml)				
	Day 0	Day 7	Day 14	Day 21	Day 28
TS 45°C 10 min	0.00±0.00^{aA}	0.00±0.00^{aA}	0.00±0.00^{aA}	0.00±0.00^{aA}	0.00±0.00^{aA}
TS 55°C 10 min	0.00±0.00^{aA}	0.00±0.00^{aA}	0.00±0.00^{aA}	0.00±0.00^{aA}	0.00±0.00^{aA}
TS 65°C 10 min	0.00±0.00^{aA}	0.00±0.00^{aA}	0.00±0.00^{aA}	0.00±0.00^{aA}	0.00±0.00^{aA}
Pasteurized (72°C 15 s)	0.00±0.00^{aA}	0.00±0.00^{aA}	0.00±0.00^{aA}	0.00±0.00^{aA}	0.00±0.00^{aA}
Control	6.02±0.01^{bE}	5.84±0.01^{bD}	5.59±0.01^{bC}	5.43±0.02^{bB}	4.42±0.01^{bA}

$^{a-b}$ Different letters in the same column indicate significant differences ($p<0.05$)
$^{A-E}$ Different letters in the same row indicate significant differences ($p<0.05$)

Table 2. Effect of thermo-sonication combined with essential oils on total viable count (TVC) in *Carissa carandas* L. fruit juice during storage at 4 °C.

Treatments	Total Viable Count (log CFU/ml)				
	Day 0	Day 7	Day 14	Day 21	Day 28
TS 45°C 10 min	0.00±0.00^{aA}	0.00±0.00^{aA}	2.00±0.00^{bC}	1.00±1.41^{bB}	3.15±0.02^{cA}
TS 55°C 10 min	0.00±0.00^{aA}	0.00±0.00^{aA}	2.00±0.00^{cC}	1.00±1.41^{bB}	1.00±1.41^{bB}
TS 65°C 10 min	0.00±0.00^{aA}	0.00±0.00^{aA}	0.00±0.00^{aA}	0.00±0.00^{aA}	0.00±0.00^{aA}
Pasteurized (72°C 15 s)	0.00±0.00^{aA}	0.00±0.00^{aA}	0.00±0.00^{aA}	0.00±0.00^{aA}	0.00±0.00^{aA}
Control	6.04±0.01^{bE}	5.92±0.01^{bD}	5.46±0.02^{dC}	5.20±0.01^{cB}	4.70±0.01^{dA}

$^{a-d}$ Different letters in the same column indicate significant differences ($p<0.05$)
$^{A-E}$ Different letters in the same row indicate significant differences ($p<0.05$)

Table 3. Effect of thermo-sonication combined with essential oils on total yeast and mold (TYM) in *Carissa carandas* L. fruit juice during storage at 4 °C.

Treatments	Total Yeast and Mold (log CFU/ml)				
	Day 0	Day 7	Day 14	Day 21	Day 28
TS 45°C 10 min	0.00±0.00^{aA}	0.00±0.00^{aA}	1.00±1.41^{bB}	0.00±0.00^{aA}	0.00±0.00^{aA}
TS 55°C 10 min	0.00±0.00^{aA}	0.00±0.00^{aA}	1.00±1.41^{bB}	0.00±0.00^{aA}	0.00±0.00^{aA}
TS 65°C 10 min	0.00±0.00^{aA}	0.00±0.00^{aA}	0.00±0.00^{aA}	0.00±0.00^{aA}	0.00±0.00^{aA}
Pasteurized (72°C 15 s)	0.00±0.00^{aA}	0.00±0.00^{aA}	0.00±0.00^{aA}	0.00±0.00^{aA}	0.00±0.00^{aA}
Control	5.98±0.01^{bE}	5.74±0.01^{bD}	5.41±0.01^{cC}	4.56±0.06^{bB}	3.15±0.21^{bA}

$^{a-c}$ Different letters in the same column indicate significant differences ($p<0.05$)
$^{A-E}$ Different letters in the same row indicate significant differences ($p<0.05$)

3.3 Bioactive Compounds and Antioxidant Activity

The effects of thermo-sonication at different temperatures (45, 55, and 65 °C for 10 min) and conventional pasteurization (72 °C for 15 s) on total phenolic content (TPC), vitamin C, and antioxidant activity (ABTS, DPPH, and FRAP assays) are presented in Figures 1–3. The results demonstrate that processing conditions significantly influenced both bioactive compound retention and antioxidant capacity ($p < 0.05$).

As shown in Figure 1, total phenolic content ranged from 1709.82 to 1869.40 mg GAE/100 mL. The highest TPC was observed in fruit juice treated by thermo-sonication at 45 °C, followed by treatments at 55 °C and 65 °C. In contrast, pasteurized and untreated control samples exhibited significantly lower TPC values. The enhancement observed under mild thermo-sonication conditions can be attributed to improved extractability of bound phenolic compounds, resulting from partial disruption of plant cell walls and enhanced mass transfer induced by ultrasonic cavitation. Conversely, higher processing temperatures and conventional pasteurization likely promoted thermal degradation, oxidation, or polymerization of phenolic compounds, leading to reduced TPC. These findings are in agreement with Kalsi et al. [(20)], who reported a 10–17% increase in phenolic content in guava juice following thermo-sonication.

Vitamin C content (Figure 2) exhibited a decreasing trend with increasing treatment temperature. The control and TS 45 °C samples retained the highest levels of vitamin C, whereas the pasteurized sample showed the greatest loss. This trend confirms the heat-sensitive nature of ascorbic acid, which is particularly vulnerable to thermal and oxidative degradation during processing. Similar observations were reported by Oladunjoye et al. [(21)], who found that moderate thermo-sonication (40–50 °C) effectively preserved vitamin C in hog plum juice, while higher temperatures resulted in significant losses.

In contrast to vitamin C, antioxidant activities measured by ABTS, DPPH, and FRAP assays increased following moderate thermo-sonication, as shown in Figures 3(a), 3(b), and 3(c). Among all treatments, thermo-sonication at 55 °C consistently produced the highest antioxidant

activities. This enhancement may be attributed to the increased release of phenolic compounds, structural modification of antioxidant molecules, and the possible formation of new antioxidant-active compounds under mild thermal conditions. Comparable results were reported by Sun et al. [17], who demonstrated that ultrasound combined with essential oil nanoemulsions significantly enhanced the antioxidant capacity of kiwifruit juice.

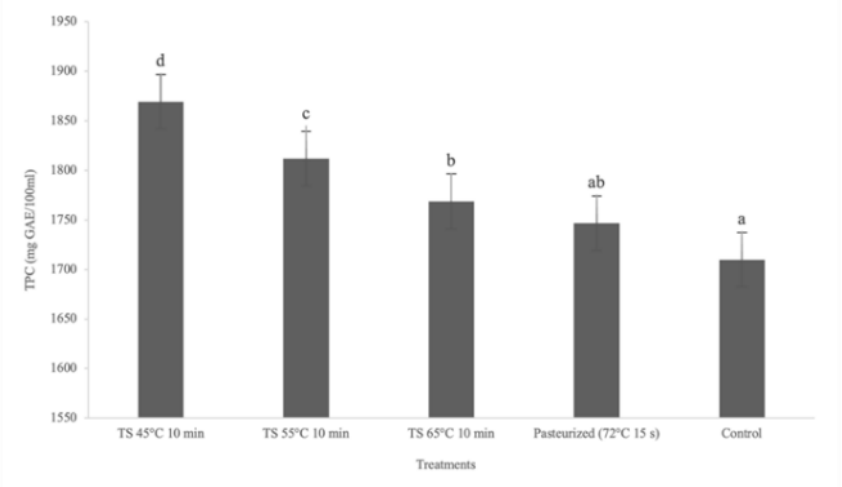

Figure 1. Total phenolic content of *Carissa carandas* L. fruit juice.
Note. Error bars indicate standard deviation (S.D.); $^{a-d}$ different superscripts are significantly different between treatments ($p < 0.05$)

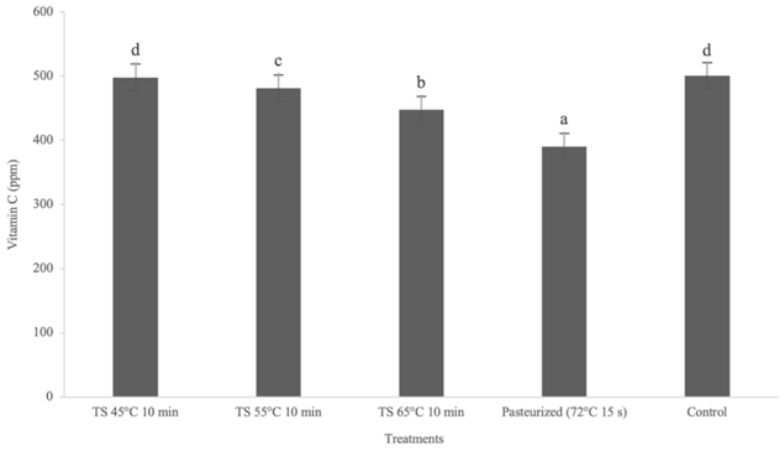

Figure 2. Vitamin C of *Carissa carandas* L. fruit juice.
Note. Error bars indicate standard deviation (S.D.); $^{a-d}$ different superscripts are significantly different between treatments ($p < 0.05$)

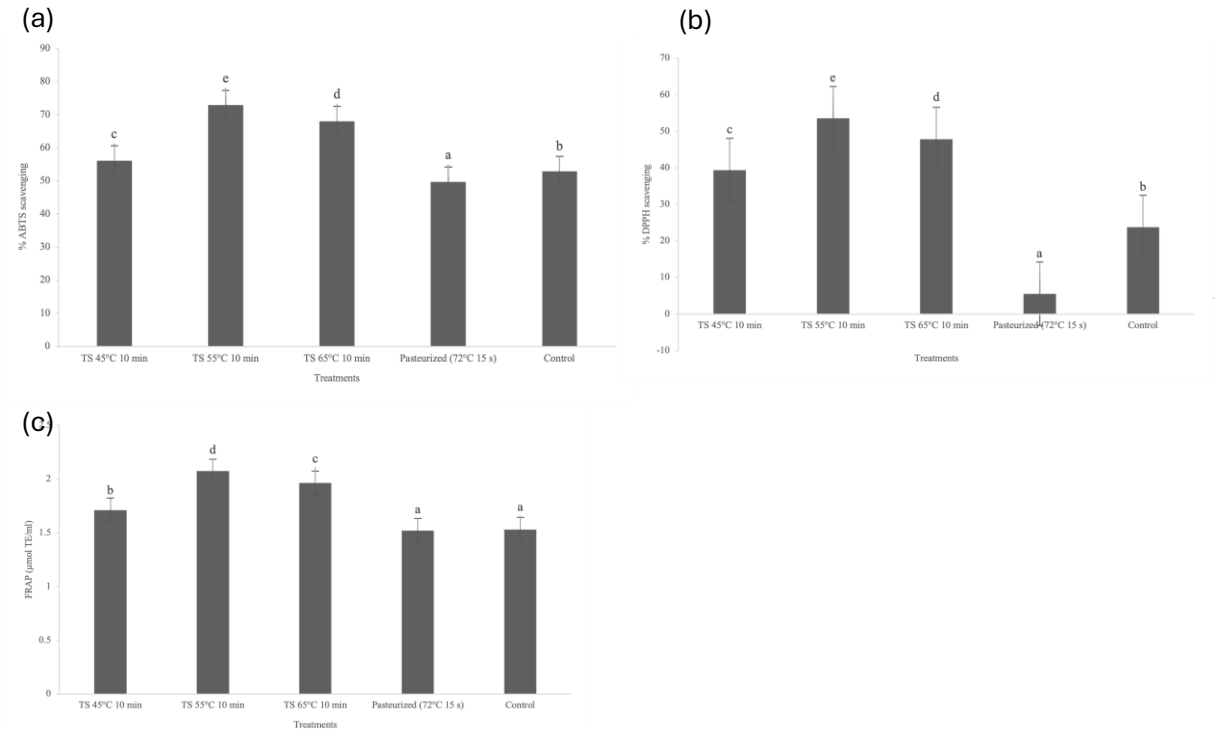

Figure 3. Antioxidant activity of *Carissa carandas* L. fruit juice by different methodologies. ABTS assay (a); DPPH assay (b); FRAP assay (c).
Note. Error bars indicate standard deviation (S.D.); $^{a-e}$ different superscripts are significantly different between treatments ($p < 0.05$)

3.4 Total Soluble Solids (TSS)

Total soluble solids (TSS) values exhibited only minor fluctuations during storage and were not significantly affected by thermo-sonication or pasteurization ($p > 0.05$), as shown in Table 5. These results indicate that thermo-sonication did not alter sugar content or soluble solids in the juice system. Similar findings were reported by Dars et al. [21] for thermo-sonicated mango juice.

Table 4. Total Soluble Solids (TSS) in *Carissa carandas* L. Fruit Juice.

Treatments	Total soluble solids				
	Day 0	Day 7	Day 14	Day 21	Day 28
TS 45°C 10 min	2.90 ± 0.17^{bD}	2.30 ± 0.11^{aA}	2.60 ± 0.10^{aB}	2.60 ± 0.06^{aB}	2.70 ± 0.06^{aC}
TS 55°C 10 min	2.60 ± 0.15^{aC}	2.40 ± 0.34^{aA}	2.50 ± 0.00^{aB}	2.50 ± 0.06^{aB}	2.70 ± 0.06^{aD}
TS 65°C 10 min	2.50 ± 0.06^{aC}	2.10 ± 0.12^{aA}	2.50 ± 0.06^{aC}	2.40 ± 0.06^{aB}	2.60 ± 0.17^{aD}
Pasteurized (72°C 15 s)	2.40 ± 0.06^{aB}	2.30 ± 0.12^{aA}	2.50 ± 0.06^{aC}	2.40 ± 0.06^{aB}	2.60 ± 0.06^{aD}
Control	2.60 ± 0.06^{aC}	2.50 ± 0.12^{aB}	2.50 ± 0.06^{aB}	2.40 ± 0.06^{aA}	2.60 ± 0.17^{aC}

$^{a-b}$ Different letters in the same column indicate significant differences ($p<0.05$)
$^{A-D}$ Different letters in the same row indicate significant differences ($p<0.05$)

3.5 pH Changes During Storage

Post-treatment pH values of fruit juice ranged from 2.66 to 2.92 (Table 5). Although slight fluctuations were observed during storage, thermo-sonication did not significantly affect juice pH. The low pH (<4.5) is advantageous for microbial stability, contributing to extended shelf life. These findings are consistent with Dars et al. [22], who reported minimal pH changes in thermo-sonicated mango juice.

Table 5. pH values of *Carissa carandas* L. Fruit Juice.

Treatments	pH				
	Day 0	Day 7	Day 14	Day 21	Day 28
TS 45°C 10 min	2.81±0.01^{aC}	2.76±0.03^{aB}	2.82±0.06^{aC}	2.68±0.04^{aA}	2.85±0.02^{abC}
TS 55°C 10 min	2.83±0.03^{aB}	2.83±0.06^{aB}	2.91±0.02^{bC}	2.66±0.0 3^{aA}	2.88±0.03^{bBC}
TS 65°C 10 min	2.82±0.01^{aA}	2.80±0.04^{aA}	2.92±0.01^{bB}	2.82±0.09^{bA}	2.88±0.03^{bAB}
Pasteurized (72°C 15 s)	2.85±0.03^{aB}	2.78±0.04^{aA}	2.86±0.07^{abB}	2.74±0.06^{abA}	2.83±0.02^{aB}
Control	2.81±0.03^{aA}	2.81±0.04^{aA}	2.86±0.02^{abA}	2.80±0.06^{bA}	2.87±0.01^{abA}

$^{a-b}$ Different letters in the same column indicate significant differences ($p<0.05$)
$^{A-C}$ Different letters in the same row indicate significant differences ($p<0.05$)

3.6 Viscosity

Viscosity values showed significant changes ($p < 0.05$) throughout storage (Table 6). An initial decrease in viscosity was observed following thermo-sonication, likely due to particle disruption and pectin degradation caused by ultrasonic cavitation. During later storage, viscosity increased, possibly due to molecular reorganization of polysaccharides, proteins, and pectin structures. Similar trends were reported by Paniwnyk et al. [23] for thermo-sonicated fruit juices.

Table 6. Viscosity values of *Carissa carandas* L. Fruit Juice.

Treatments	Viscosity				
	Day 0	Day 7	Day 14	Day 21	Day 28
TS 45°C 10 min	4.93±0.03^{bD}	4.42±0.02^{dB}	4.19±0.02^{aA}	4.61±0.04^{dC}	5.04±0.12^{aE}
TS 55°C 10 min	4.99±0.03^{cD}	3.62±0.00^{aA}	4.72±0.04^{dC}	4.58±0.03^{dB}	5.57±0.13^{bE}
TS 65°C 10 min	5.01±0.02^{cE}	4.71±0.01^{eD}	4.54±0.02^{cC}	4.25±0.02^{bA}	5.49±0.13^{bB}
Pasteurized (72°C 15 s)	5.08±0.03^{dD}	4.39±0.02^{cC}	4.28±0.01^{bB}	3.98±0.02^{aA}	5.49±0.15^{bE}
Control	4.44±0.02^{aD}	4.28±0.02^{bB}	4.20±0.01^{aA}	4.42±0.01^{cC}	5.65±0.13^{bE}

$^{a-e}$ Different letters in the same column indicate significant differences ($p<0.05$)
$^{A-D}$ Different letters in the same row indicate significant differences ($p<0.05$)

3.7 Color Stability

Thermo-sonication influenced juice color stability, as indicated by total color difference (ΔE) values compared to the control at day 0, presented in Table 7. Among heat-treated samples, TS 65 °C exhibited the lowest ΔE over storage, indicating superior color retention, likely due to inhibition of enzymatic and non-enzymatic browning reactions. Although no thermal processing was applied, the control samples also exhibited noticeable color changes during storage. Thermo-sonication at 65 °C achieved a favorable balance between microbial safety and color stability. These findings are consistent with previous studies reporting improved color retention in thermo-sonicated fruit juices [22] and combined ultrasound–essential oil treatments [17].

Table 7. Total color difference (ΔE) in *Carissa carandas* L. Fruit Juice during 28 days of storage.

Treatments	ΔE D-0	ΔE D-7	ΔE D-14	ΔE D-21	ΔE D-28
TS 45°C 10 min	2.97	2.92	1.19	4.97	6.19
TS 55°C 10 min	4.33	1.65	1.49	1.84	2.91
TS 65°C 10 min	3.33	3.57	2.51	1.18	1.24
Pasteurized	5.46	2.54	2.30	1.16	3.30
Control	-	1.47	1.67	1.61	1.80

Although the concentration of essential oils used in this study demonstrated effective antimicrobial activity, sensory evaluation was not included in the present work. Future studies should investigate sensory acceptance and optimize essential oil concentration to ensure both microbial safety and consumer acceptability.

4. Conclusions

This study demonstrates that thermo-sonication combined with lemon and orange essential oil emulsions (1:1 ratio) is an effective alternative to conventional pasteurization for processing *Carissa carandas* L. fruit juice. Treatment temperature played a crucial role in microbial stability and bioactive compound retention. Among the tested conditions, thermo-sonication at 65 °C for 10 min provided the highest level of microbial safety, achieving complete inhibition of *E. coli*, total viable count, and yeast and mold during 28 days of refrigerated storage. In addition to microbial control, thermo-sonication significantly enhanced the functional quality of the juice. Higher total phenolic content and antioxidant activities (ABTS, DPPH, and FRAP) were observed compared to pasteurized samples, likely due to ultrasonic cavitation facilitating the release of bound bioactive compounds. Although vitamin C content decreased with increasing temperature, the losses under thermo-sonication were comparable to or lower than those observed after pasteurization. Furthermore, physicochemical properties, including pH, total soluble solids, and color, remained relatively stable throughout storage. Overall, thermo-sonication combined with essential oils represents a sustainable processing approach for producing microbiologically safe and bioactive-rich functional fruit beverages.

Acknowledgement

The authors gratefully acknowledge the support provided by the School of Food Industry, King Mongkut's Institute of Technology Ladkrabang (KMITL).

References

1. Krungsri Research. Business/Industry Trends 2568-2570: Beverage Industry [Internet]. Bangkok: Krungsri; 2024 [cited 2025 Nov 5]. Available from: https://www.krungsri.com/th/research/industry/industry-outlook/food-beverage/beverage/io/beverage-2025-2027
2. Grand View Research. 100% Juice Market Size, Share & Trends Analysis Report, 2030 [Internet]. San Francisco: Grand View Research; 2023 [cited 2025 Nov 5]. Available from: https://www.grandviewresearch.com/industry-analysis/100-percent-juice-market report
3. Khamwilai M, Papattha C. Marketing mix factors affecting consumers' purchasing decision of organic fruit and vegetable juice in Bangkok. J Liberal Arts (Wang Nang Leng) RMUTP. 2021;1(1). 130. (in Thai). Available from: https://so07.tci-thaijo.org/index.php/LiberalJ/article/view/1311/898
4. Mishra A B, Tomer V, Kumar A. Karonda (Carissa carandas L.): A miracle fruit with multifaceted potential. Journal of Agriculture and Food Research. 2024;18:101417.
5. Mason TJ, Lorimer JP. Sonochemistry and food processing applications. Food Technol J. 2021;35(2):67-80.
6. Pallarés N, Berrada H, Tolosa J, Ferrer E. Effect of high hydrostatic pressure (HPP) and pulsed electric field (PEF) technologies on reduction of aflatoxins in fruit juices. LWT. 2021;142:111000.
7. Knorr D, et al. Ultrasound and heat treatment in food preservation. Int J Food Microbiol. 2020;142(1):9-17.

8. Maleš I, Pedisić S, Zorić Z, Elez-Garofulić I, Repajić M, You L, et al. The medicinal and aromatic plants as ingredients in functional beverage production. Journal of Functional Foods. 2022;96:105210.
9. Yeasmin MS, Uddin MJ, Dey SS, Barmon J, Ema NT, Rana GMM, et al. Optimization of green microwave-assisted extraction of essential oil from lemon (Citrus limon) leaves: Bioactive, antioxidant and antimicrobial potential. Current Research in Green and Sustainable Chemistry. 2024;8:100413.
10. Fisher K, Phillips C. Potential antimicrobial uses of essential oils in food: is citrus the answer? Trends in Food Science & Technology. 2008;19(3):156-64.
11. Bainotti MB, Colás-Medà P, Pié-Amill A, Viñas I, Alegre I. Acid Adaptation Impacts Survival and Pathogenicity of Salmonella Enteritidis and Escherichia coli O157:H7 in Orange Juice. Beverages. 2025;11(3):58.
12. Bainotti MB, Colás-Medà P, Viñas I, Alegre I. Effect of Antimicrobial Compounds on the Survival and Pathogenic Potential of Acid-Adapted Salmonella Enteritidis and Escherichia coli O157:H7 in Orange Juice. Antibiotics. 2025;14(4):335
13. Oteiza JM, Prado-Silva Ld, Caturla MYR, Barril PA, Giannuzzi L, Sant'Ana AS. Variability in the acid adaptation of ten different O157:H7 and non-O157 Escherichia coli strains in orange juice and the impact on UV radiation resistance. Food Microbiology. 2024;124:104610.
14. Assavarachan R. Effect of high pressure processing on microbial and food spoilage eliminating. J Thai Soc Agric Eng. 2016;22(2):41-48. (in Thai).
15. Gao L, Wang S, Oomah BD, Mazza G. Wheat quality: Antioxidant activity of wheat millstreams. AACC International; 2002. p. 219–233.
16. AOAC International. Official methods of analysis of AOAC International. 20th ed. Gaithersburg (MD): AOAC International; 2016.
17. Sun R, Li Y, Su R, Cai X, Kong Y, Jiang T, et al. Antibacterial effect of ultrasound combined with Litsea cubeba essential oil nanoemulsion on Salmonella Typhimurium in kiwifruit juice. International Journal of Food Microbiology. 2025;426:110898.
18. Xiao W, Gao Z, Liu T, Zhong W, Jiang S, He M, et al. Lemon essential oil nanoemulsions: Potential natural inhibitors against Escherichia coli. Food Microbiology. 2024;119:104459.
19. Snyder AB, Worobo RW. The incidence and impact of microbial spoilage in the production of fruit and vegetable juices as reported by juice manufacturers. Food Control. 2018;85:144-50.
20. Kalsi BS, Singh S, Alam MS, Bhatia S. Application of thermosonication for guava juice processing: Impacts on bioactive, microbial, enzymatic and quality attributes. Ultrasonics Sonochemistry. 2023;99:106595.
21. Oladunjoye AO, Adeboyejo FO, Okekunbi TA, Aderibigbe OR. Effect of thermosonication on quality attributes of hog plum (Spondias mombin L.) juice. Ultrasonics Sonochemistry. 2021;70:105316.
22. Dars AG, Hu K, Liu Q, Abbas A, Xie B, Sun Z. Effect of thermo-sonication and ultra-high pressure on the quality and phenolic profile of mango juice. Foods. 2019;8(8):298.
23. Paniwnyk L, Tiwari BK, McHugh TH. The effect of ultrasound on the quality of orange juice. J Food Process Preserv. 2009;33(3):299–310.

Appendix A. Standard calibration curves

Standard calibration curves of gallic acid, vitamin C, and Trolox used for quantitative analysis are shown below.

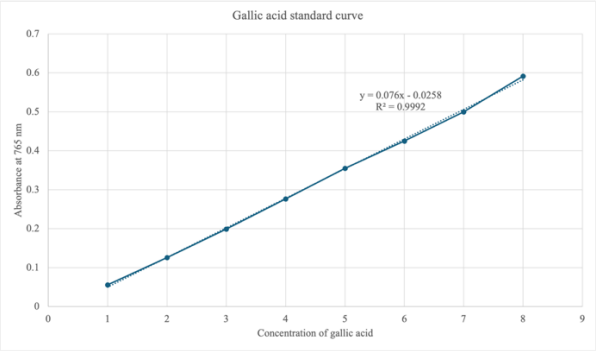

Figure A1. Standard calibration curve of gallic acid for determination of total phenolic content.

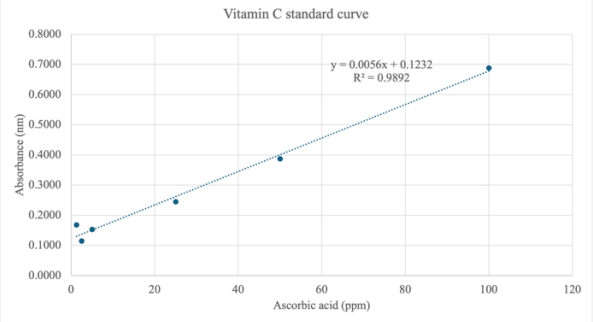

Figure A2. Standard calibration curve of vitamin C.

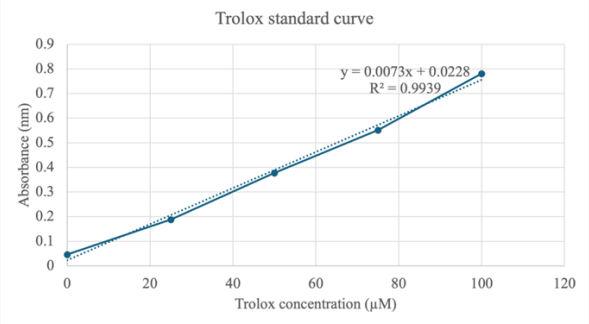

Figure A3. Standard calibration curve of Trolox used for antioxidant activity analysis.

P - 288

Bioactive Compounds and Antioxidant Activities of *Ardisia polycephala* Wall. ex A. DC. Fruit Extract

Phongsadathon Aonmanee, Kanokporn Saenphet, Supap Saenphet, Wararut Buncharoen*

Department of Biology, Faculty of Science, Chiang Mai University, Chiang Mai 52000, Thailand

**Corresponding author E-mail: wararut.bun@cmu.ac.th*

Abstract: *Ardisia polycephala* Wall. Ex A. DC. is a medicinal herb documented in traditional Thai medicine. Its fruits are used as a blood tonic, antipyretic, anti-diarrheal, and hepatoprotective agents. This study aimed to investigate the phytochemicals and antioxidant constituents, and activities of aqueous (APA) and ethanolic (APE) extracts from the fruits of *A. polycephala*. Total phenolic content, total flavonoid content, total antioxidant capacity, 2,2'-azino-bis(3-ethylbenzthiazoline-6-sulphonic acid) (ABTS), 2,2-diphenyl-1-picrylhydrazyl (DPPH) radical scavenging activities and reducing power were determined *in vitro*. Preliminary phytochemical screening revealed the presence of flavonoids, phenolics, coumarins, terpenoids, tannins, reducing sugars, and steroids in both ethanolic and aqueous fruit extracts of *Ardisia polycephala*, with flavonoids being the predominant constituents, while alkaloids were detected only in the aqueous extract. APA contained a higher total phenolic content than APE, with values of 16.91 ± 0.73 and 15.59 ± 2.33 mg gallic acid equivalents (GAE)/g extract, respectively. Similarly, the total flavonoid content was higher in APA (16.11 ± 0.56 mg quercetin equivalents (QE)/g extract) than in APE (14.65 ± 1.34 mg QE/g extract). APA also exhibited greater total antioxidant capacity than APE, with values of 2.58 ± 0.10 and 0.93 ± 0.11 mg ascorbic acid equivalents (AAE)/g extract, respectively. Moreover, APA showed stronger radical scavenging activity against both ABTS and DPPH radicals, with IC_{50} values of 1.59 ± 0.06 and 0.85 ± 0.02 mg/mL, compared to 3.54 ± 0.14 and 1.50 ± 0.19 mg/mL for APE, respectively. Furthermore, the EC_{50} values in the ferric reducing power assay were 0.42 ± 0.06 for APA and 0.63 ± 0.24 mg/mL for APE. These findings indicate that the aqueous extract of *A. polycephala* fruit is a potent natural source of antioxidants.

Keywords: Antioxidants; *Ardisia polycephala*; Extract; Flavonoids; Phenolics

1. Introduction

Free radicals are molecular species characterized by the presence of one or more unpaired electrons, rendering them highly unstable and reactive. These species primarily include reactive oxygen species (ROS) and reactive nitrogen species (RNS), which are continuously generated in biological systems [1]. Endogenous free radicals arise as natural by-products of essential metabolic processes such as mitochondrial respiration, inflammatory responses, and immune cell activation. In contrast, exogenous free radicals originate from environmental exposure, including ultraviolet radiation, air pollution, cigarette smoke, and toxic chemicals [2]. Under normal physiological conditions, cellular redox homeostasis is maintained through the action of endogenous antioxidant defense system [3]. However, excessive free radical production or insufficient antioxidant capacity leads to an imbalance known as oxidative stress [4].

Oxidative stress is a critical pathological condition that induce damage to fundamental cellular macromolecules, including lipids, proteins, and nucleic acids. Lipid peroxidation compromises membrane integrity and alters cellular permeability, while protein oxidation results

in structural modification, enzymatic dysfunction, and accelerated protein degradation. Additionally, oxidative damage to DNA can cause mutation and genomic instability, contributing to disease initiation and progression. Accumulating evidence has demonstrated that oxidative stress plays a central role in the pathogenesis of numerous chronic and degenerative diseases, such as cardiovascular disorders, cancer, diabetes, liver diseases, and neurogenerative conditions [3][5]. Given the limitations of endogenous antioxidant systems under pathological conditions, considerable scientific interest has been directed toward identifying effective exogenous antioxidants capable of mitigating oxidative damage. Plant-derived phytochemicals, particularly phenolic compounds, flavonoids, and related secondary metabolites, have attracted attention due to their strong free radical scavenging activity, metal-chelating properties, and ability to modulate endogenous enzymes. Fruits and medicinal herbs represent important dietary and therapeutic sources of these natural antioxidants and have widely investigated for health-promoting potential [6,7].

In Thailand, *Ardisia polycephala* Wall. Ex A. DC. (Family Myrsinaceae), locally known as "Pilangkasa", is a medicinal traditionally used in local pharmacopoeia. Different parts of the plant are employed for specific therapeutic purposes: the roots are used for the treatment of venereal diseases and as a snakebite antidote; the stems for dermatological conditions; the leaves for liver disorders; cough, and diarrhea; the flowers as antiseptic and anthelmintic agents; and the fruits as blood tonics, antipyretic, anti-diarrheal, and hepatoprotective remedies. In addition, young shoots and immature fruits are consumed as fresh vegetables in certain regions, suggesting a favorable safety profile for human consumption. Among these plant parts, the fruit of *A. polycephala* is of particular interest due to its traditional use as a blood tonic and hepatoprotective agent, which may be closely associated with antioxidant mechanisms. Previous studies have reported that methanolic extracts of *A. polycephala* possess strong antioxidant activity and contain phenolic compounds [8]. Nevertheless, comprehensive information regarding the bioactive constituents of the fruit and their antioxidant potential remains limited. Systemic evaluation of phenolic content and antioxidant activity using standardized analytical approaches is still lacking. Therefore, the present study aims to investigate the bioactive compounds and antioxidant activity of *A. polycephala* hydroethanolic fruit extract. By elucidating its antioxidant properties, this research seeks to provide scientific evidence supporting the traditional medicinal use of this plant and to contributed to the development of high-quality, cost-effective Thai herbal products as potential alternative to imported antioxidant supplements.

2. Materials and Methods

2.1 Plant preparation and extraction

The ripe fruits of *A. polycephala* were collected from cultivation areas in Chiang Mai Province, Thailand. The plant material was taxonomically authenticated by a qualified botanist at the Queen Sirikit Botanic Garden (QBG), Chiang Mai, Thailand, and a voucher specimen (QBG no. 151840) was deposited for future reference. The collected fruits were thoroughly washed with distilled water to remove adhering debris, air-dried at room temperature until a constant weight was achieved, and subsequently pulverized into a fine power using a mechanical grinder. For preparation of the ethanolic extract, 100 g of fruit powder was macerated in 1,000 mL of 70% (v/v) ethanol at room temperature for 24 h with occasional stirring. For the aqueous extract, 100 g of fruit powder was decocted with 1,000 mL of distilled water by boiling for 5 min [9]. After extraction, both extract were filtered through Whatman No. 1 filter paper to remove insoluble residues. The filtrates were concentrated under reduced pressure using a rotary evaporator to remove the extraction solvent. The resulting crude ethanolic extract (*A. polycephala* ethanolic extract, APE) and aqueous extract (*A. polycephala* aqueous extract, APA) were collected, weighed to determine extraction yield, and stored at -20 °C until further analysis. The yield of the APE and APA were 21.13 and 11.84 %, respectively (Table 2).

2.2 Preliminary phytochemical screening

Qualitative phytochemical screening of the APE and APA was performed to detect the presence of major classes of bioactive compounds using standard phytochemical [10,11]. All tests were carried out in triplicate, and the results were recorded based on characteristic color changes or precipitate formation.

2.2.1 Alkaloids: One milliliter of each extract was acidified with 1 mL of 1 % hydrochloric acid, followed by the addition of 1 mL of Hager's solution. The formation of a yellow precipitate indicated the presence of alkaloids.

2.2.2 Cardiac glycosides: One milliliter of each extract was treated with 2 mL of glacial acetic acid containing 1-2 drops of 10 % w/v ferric chloride. Subsequently, 1 mL of concentrated sulfuric acid was carefully added along the side of the test tube. The formation of a brown ring at the interface indicated a positive result for cardiac glycosides.

2.2.3 Coumarins: One milliliter of each extract was mixed with 250 µL of 10 % v/v ammonia solution. The mixture was observed under ultraviolet light, and the appearance of fluorescence indicated the presence of coumarins.

2.2.4 Flavonoids: One milliliter of each extract was mixed with 2 mL of 10 % v/v ammonia solution, followed by the addition of 2-3 drops of concentrated sulfuric acid. The development of a yellow coloration indicated the presence of flavonoids.

2.2.5 Phenols: One milliliter of each extract was treated with 1 mL of 5 % w/v ferric chloride. The formation of a blue, green, or black coloration indicated the presence of phenols.

2.2.6 Phlobatannins: One milliliter of each extract was mixed with 1 mL of 1 % v/v hydrochloric acid and heated to boiling. The appearance of a red precipitate indicated the presence of phlobatannins.

2.2.7 Reducing sugar: One milliliter of each extract was mixed with 2 mL of freshly prepared Fehling's solution (equal volume of Fehling's A and B) and heated for 2 min. The formation of a brick-red precipitate indicated the presence of reducing sugars.

2.2.8 Tannins: One milliliter of each extract was treated with 2-3 drops of 0.1 % w/v ferric chloride. The development of a brownish-green or blue-back coloration indicated a positive result for tannins.

2.2.9 Terpenoids: One milliliter of each extract was mixed with 2 mL of chloroform, followed by the careful addition of 3 mL of concentrated sulfuric acid. The appearance of a reddish-brown coloration at the interface indicated the presence of terpenoids.

2.2.10 Saponins: One milliliter of each extract was vigorously shaken with 1 mL of distilled water. The formation of persistent froth lasting for more than 1 min indicated the presence of saponins.

2.2.11 Steroids: One milliliter of each extract was mixed with 2 mL of chloroform, followed by the addition of 2 mL of concentrated sulfuric acid. The appearance of a red coloration in the chloroform layer indicated the presence of steroids.

2.3 Determination of total phenolic content

Total phenolic content was determined using the Folin-Ciocalteu colorimetric method [12], with minor modifications. Briefly, an aliquot of 100 µL of each extract was mixed with 2 mL of 10 % (w/v) Folin-Ciocalteu reagent. After standing for 5 min at room temperature, 2 mL of 7.5 % (w/v) sodium carbonate solution was added to the mixture. The reaction mixture was thoroughly vortexed and incubated in the dark at room temperature for 20 min. Absorbance was measured at 760 nm using UV-Vis spectrophotometer. Gallic acid was used as a reference standard to construct a calibration curve, and total phenolic content was calculated from the standard curve. The results were expressed as milligrams of gallic acid equivalents per gram of extract (mg GAE/g extract). All measurements were performed in triplicate.

2.4 Determination of total flavonoid content

Total flavonoid content was determined using the aluminum chloride colorimetric method [13], with minor modifications. Briefly, and aliquot of 100 µL of each extract was mixed with 500 µL of 2 % (w/v) aluminum chloride solution. The reaction mixture was vortexed thoroughly and incubated at room temperature for 60 min to allow complex formation. Absorbance was measured at 420 nm using a UV-Vis spectrophotometers. Quercetin was used as a reference standard to generate a calibration curve, and total flavonoid content was calculated accordingly. The results were expressed as milligrams of quercetin equivalents per gram of extract (mg QE/g extract). All measurements were performed in triplicate.

2.5 Determination of vitamin C

Vitamin C content was determined based on its reaction with 2,4-dinitrophenylhydrazine (DNPH) method [14], with minor modifications, Briefly, an aliquot of 100 µL of each extract was mixed with 150 µL of DNPH reagent. Subsequently, 200 µL of 13.3 % (w/v) trichloroacetic acid, 200 µL of distilled water, and 1 mL of 65 % (v/v) sulfuric acid were added sequentially. The reaction mixture was vortexed thoroughly and incubated at 37 °C for 3 h to allow complete color development. After incubation, the absorbance of the resulting solution was measured at 520 nm using a UV-Vis spectrophotometer. Ascorbic acid was used as a reference standard to construct a calibration curve, and the vitamin C content of the extract was calculated accordingly. The results were expressed as milligrams of ascorbic acid equivalents per gram of extract (mg AAE/g extract) All analyses were performed in triplicate.

2.6 Determination of total antioxidant capacity

Total antioxidant capacity (TAC) was determined using the phosphomolybdenum assay [15], with minor modifications. Briefly, an aliquot of 100 µL of each extract was mixed with 2 mL of reagent solution containing 0.6 M sulfuric acid, 28 mM sodium phosphate, and 4 mM ammonium molybdate in a capped test tube. The reaction mixture was incubated in a water bath at 95 °C for 90 min to allow complete reduction of molybdenum (VI) to molybdenum (V). After incubation, the mixture was cooled to room temperature, ant the absorbance was measured at 695 nm using a UV-Vis spectrophotometer. An increase in absorbance indicated higher total antioxidant capacity. Ascorbic acid was used as a reference standard to construct a calibration curve, and TAC values were calculated accordingly. The results were expressed as milligrams of ascorbic acid equivalents per gram of extract (mg AAE/g extract). All measurements were performed in triplicate.

2.7 ABTS radical scavenging activity

The ABTS radical scavenging activity was determined [16], with minor modifications. The ABST radical cation ($ABTS^{\bullet+}$) solution was prepared and diluted with deionized water to obtain and initial absorbance of 0.70 ± 0.02 at 734 nm. For the assay, 1 mL of the diluted $ABTS^{\bullet+}$ was transferred into cuvette, and the absorbance was measured at 734 nm to record the initial absorbance ($A_{initial}$) using a UV-Vis spectrophotometer. Subsequently, 20 µL of the extract at various concentrations was added to the cuvette and mixed thoroughly. After incubation at room temperature for 1 min, the absorbance was measured again at 734 nm to obtain the final absorbance (A_{final}). The percentage of ABTS radical scavenging activity was calculated using following equation:

$$\text{ABTS radical inhibition (\%)} = [(A_{initial} - A_{final}) / A_{initial}] \times 100$$

The percentage inhibition was plotted against the extract concentration to generate a concentration-response curve, from which the half-maximal inhibitory concentration (IC_{50}) value

was calculated using linear regression analysis. Gallic acid was used as a reference standard for comparison. All measurements were performed in triplicate.

2.8 DPPH radical scavenging activity

The DPPH radical scavenging activity was determined [17], with minor modifications. Briefly, a 2 mL aliquot freshly prepared DPPH solution was transferred into a cuvette, and the absorbance was measured at 517 nm to record the initial absorbance ($A_{initial}$) using a UV-Vis spectrophotometer. Subsequently, 100 µL of the extract at various concentrations was added to the cuvette and mixed thoroughly. The reaction mixture was incubated in the dark at room temperature for 30 min to allow complete scavenging of DPPH radical. After incubation, the absorbance was measured again at 517 nm to obtain the final absorbance (A_{final}). The percentage of DPPH radical scavenging activity was calculated using following equation:

$$\text{DPPH radical inhibition (\%)} = [(A_{initial} - A_{final}) / A_{initial}] \times 100$$

The percentage inhibition values were plotted against extract concentrations to generate a concentration-response curve, and the IC_{50} was determined by linear regression analysis. Gallic acid was used as a reference standard for comparison. All experiments were conducted in triplicate.

2.9 Ferric reducing power assay

The ferric reducing power (Fe^{3+} to Fe^{2+} transformation) of the extract was determined [18], with minor modifications. Briefly, 50 µL of the extract at various concentrations was mixed with 400 µL of 0.2 M phosphate buffer (pH 6.6) and 200 µL of 1 % (w/v) potassium ferricyanide in a test tube. The reaction mixture was incubated in a water bath at 50 °C for 20 min to allow reduction of ferric ions. Following incubation, 200 µL of 10 % (w/v) trichloroacetic acid was added to terminate the reaction, and the mixture was vortexed thoroughly. The mixture was then combined with 100 100 µL of 0.1 % (w/v) ferric chloride and 1 mL of distilled water. After incubation at room temperature for 10 min, the formation of Pearl's Prussian blue complex was assessed by measuring the absorbance at 700 nm using a UV-Vis spectrophotometer. An increase in absorbance indicated greater reducing power. Reducing power values were plotted against extract concentrations to generate a concentration-response curve, and the effective concentration required to achieve 50 % of maximal reducing power (EC_{50}) was calculated using linear regression analysis. Ascorbic acid was used as a reference standard for comparison. All measurements were performed in triplicate.

2.10 Data analysis

All graph and data were analyzed using GraphPad Prism version 10 and exhibited as mean ± S.D. The IC_{50} and EC_{50} values were calculated by linear regression.

3. Results & Discussion

3.1 Bioactive compounds

Preliminary phytochemical screening revealed qualitative differences in the bioactive constituents presented in the APE and APA of *A. polycephala* fruits (Table 1). The results demonstrated that both extraction solvents could solubilize several classes of secondary metabolites; however, the abundance and distribution of phytochemicals varied according to solvent polarity. Flavonoids were detected as the predominant phytochemical group in both extracts, with a high presence observed in APE and a moderate presence in APA. This finding suggests that ethanol is more effective than water in extracting flavonoid compounds from *A. polycephala* fruits, likely due to the intermediate polarity of flavonoids, which facilitates their

solubility in hydroethanolic solvents. The higher flavonoid content in APE is consistent with previous reports indicating that ethanolic extraction enhances the recovery of phenolic and flavonoids as potent antioxidants [8,19], their abundance in APE may contribute significantly to the antioxidant activities observed in subsequent assay.

Table 1. Preliminary phytochemical constituents of APE and APA.

Phytochemicals	Extracts	
	APE	APA
Alkaloids	-	+
Cardiac glycosides	-	-
Coumarins	+	++
Flavonoids	+++	++
Phenols	+	+
Phlobatannins	-	-
Reducing sugar	+	+
Tannins	+	+
Terpenoids	+	++
Saponins	-	-
Steroids	+	+

Note: (-) Not detected; (+) low presence; (++) moderate presence; (+++) high presence

Coumarins were detected in both extracts, which a higher presence in APA compared with APE. This suggests that certain coumarin derivatives present in *A. polycephala* fruits may exhibit higher water solubility, allowing more efficient extraction into the aqueous phase. Coumarins are known to possess antioxidant, anti-inflammatory, and hepatoprotective properties [20], which may partially explain the traditional use of *A. polycephala* fruit in liver-related ailments. Phenolic compounds, tannins, reducing sugars, terpenoids were more prominent in APA than in APE, indicating that some polar or glycosylated terpenoid constituents may preferentially partition into aqueous extracts. The presence of tannins and phenolic compounds in both extracts further supports the antioxidant potential of *A. polycephala* fruits, as these compounds are well recognized for their free radical scavenging and metal-chelating activities [7].

Alkaloids were detected only in the APA, whereas they were absent in the APE. This observation suggests that the alkaloids present in *A. polycephala* fruits are likely polar in nature and preferentially extracted by water. In contrast, cardiac glycosides, phlobatannins, and saponins were not detected in either extract, indicating either their absence in the fruit matrix or their presence at concentrations below the detection limit of the qualitative assays employed.

Table 2. Extraction yield of *A. polycephala* fruit extracts

Extracts	Extraction yield (%)
APE	21.13
APA	11.84

The extraction yield and major bioactive compound contents of *A. polycephala* fruits extracts are summarized in Table 2. The APE exhibited a markedly higher extraction yield (21.13 %) than the APA (11.84 %), indicating that 70 % ethanol was more efficient than water in extracting total soluble constituents from the fruit matrix. This observation is consistent with the

ability of hydroethanolic solvents to dissolve a broader range of both polar and moderately nonpolar phytochemicals, indicating phenolics and flavonoids.

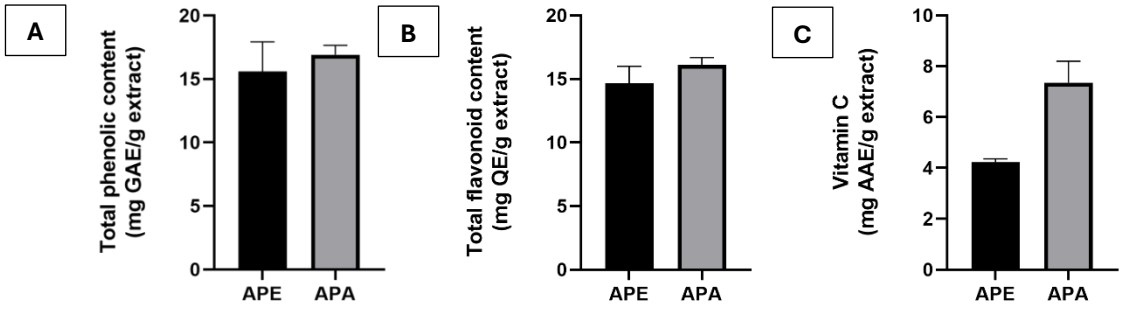

Figure 1. Total phenolic content (A), total flavonoid content (B), and vitamin C (C) content of the APE and APA extract.

Values are represented as mean ± S.D.

Despite the lower extraction yield, APA exhibited higher total phenolic content (16.91 ± 0.73 mg GAE/g extract) and total flavonoid content (16.11 ± 0.56 mg QE/g extract) compared with APE (15.59 ± 2.33 mg GAE/g extract and 14.65 ± 1.34 mg QE/g extract, respectively). This finding suggests that water preferentially extracted phenolic and flavonoid-rich fractions from *A. polycephala* fruits [21], resulting in a more concentrated phenolic and flavonoid profile per gram of extract. These results agree with the preliminary phytochemical screening (Table 1), which demonstrated the presence of multiple polar antioxidant-related compounds, including phenolics, flavonoids, coumarins, and tannins, particularly in the aqueous extract.

Vitamin C content was substantially higher in APA (7.35 ± 0.85 mg AAE/g extract) than in APE (4.23 ± 0.12 mg AAE/g extract). Ascorbic acid is a highly polar, water-soluble antioxidant [22], and its greater abundance in APA is therefore expected. This result further supports the effectiveness of aqueous extraction in recovering hydrophilic antioxidants from *A. polycephala* fruits and provides a plausible explanation for the strong antioxidant potential of APA in assays sensitive to reducing agents and radical scavengers. Taken together, our findings highlight a clear distinction between extraction yield and phytochemical enrichment. While ethanol extraction results in higher overall yield, aqueous extraction produced extracts with higher concentrations of key antioxidant compounds, particularly phenolics, flavonoids, and vitamin C. This inverse relationship between yield and bioactive compound density has been reported in other medicinal plants and fruits and underscores the importance of solvent selection based on the intended biological application.

To confirm the potential of *A. polycephala* fruit extracts, it is crucial to compare their bioactive profile with other well-known antioxidant-rich fruits. Ascorbic acid (vitamin C) is a potent exogenous antioxidant naturally occurring in high quantities in citrus fruits, such as grapefruit, orange, and lemon peels. These plants exhibit a remarkably high vitamin C concentration of approximately 113.3, 110.4 and 58.59 mg/100 g, respectively [23]. In this study, the aqueous extract of *A. polycephala* (APA) demonstrated a substantial vitamin C content of 7.35 ± 0.85 mg AAE/g extract. This high concentration of water-soluble antioxidants underscores the fruit's capability to provide essential nutrients required to neutralize tissue-damaging free radicals, aligning with the well-established benefits of citrus fruits [24].

3.2 Antioxidant activities of *A. polycephala* fruit extracts

As shown in Table 3 and Figure 2-4, both APE and APA extract of *A. polycephala* fruits exhibited concentration-dependent antioxidant activities in all evaluated assays, including total antioxidant capacity, ABTS, DPPH, and reducing power. Notably, APA consistently demonstrated stronger antioxidant activity than APE, as evidence by markedly higher TAC values and lower IC_{50} or EC_{50} values across all assays. The superior antioxidant performance of APA can be closely linked to its phytochemical composition and bioactive compound content. Preliminary phytochemical screening (Table 1) revealed that APA contained moderate-to-high levels of coumarins, terpenoids, flavonoids, phenolics, and alkaloids, while qualitative analysis (Table 2) showed that APA possessed higher total phenolic content, total flavonoid content, and vitamin C levels compared with APE. These classes of compounds are well recognized for their strong antioxidant properties, including free radical scavenging, electron donation, and metal chelation [7].

In the ABTS radical scavenging assay, APA showed markedly lower IC_{50} value than APE, indicating a greater ability to neutralize the $ABTS^{\bullet+}$ radical cation. This assay is particularly sensitive to both hydrophilic and lipophilic antioxidants, suggesting that the enhanced activity of APA may result from its enrichment in water-soluble antioxidants such as phenolic compounds and ascorbic acid. The presence of alkaloids and coumarins, which were more prominent in APA, may further contribute to ABTS radical scavenging through complementary mechanisms. Similarly, the DPPH assay (Figure 3) demonstrated that APA exhibited greater radical scavenging efficacy compared with APE. Since the DPPH radical is reduced mainly through hydrogen atom or electron donation [7], the higher total phenolics and total flavonoids observed in APA likely play a central role in this activity. Phenolic hydroxyl groups and flavonoid structure are particularly effective hydrogen donors [7], supporting the strong concentration-response relationships observed in the aqueous extract.

The ferric reducing power assay (Figure 4) further corroborated these findings, with APA exhibiting a lower EC_{50} value than the APE. The ferric reducing assay reflects the electron-donating capacity of antioxidant to reduce Fe^{3+} to Fe^{2+} [21], a mechanism strongly associated with phenolics and ascorbic acid. The significant higher vitamin C content in APA therefore provides a mechanistic explanation for its superior reduction power. Consistent with these assay-specific results, the TAC assay revealed that APA possessed nearly threefold higher total antioxidant capacity than APE. This integrated measure of antioxidant potential further supports the notion that water extraction preferentially concentrates potent hydrophilic antioxidants, resulting in a more functionally active extract despite its lower overall extraction yield. Taken together, these findings demonstrate that solvent polarity plays a critical role in determining not only extraction yield but also the qualitative and quantitative distribution of bioactive compounds in *A. polycephala* fruit extracts. While ethanolic extraction yields a higher amount of total extract, aqueous extraction enriches key antioxidant compounds, leading to superior antioxidant performance across multiple *in vitro* assays. The strong concordance between phytochemical profiles, bioactive compound contents, and antioxidant activities provide robust evidence supporting the traditional use of *A. polycephala* fruits as a functional food and medicinal resource with antioxidant potential.

Furthermore, the potential of *A. polycephala* can be directly compared to other local Thai fruits that have been widely investigated for their health-promoting properties. For example, previous studies have successfully applied extracts from *Phyllanthus emblica* Linn. as natural preservatives in food systems that exhibits a total phenolic content of 4,220 ± 121.62 µg GAE/mg extract due to their strong antimicrobial and antioxidant activities [8]. The current study revealed that the aqueous extract of *A. polycephala* exhibits highly competitive bioactive compound levels, notably a total phenolic content of 16.91 ± 0.73 mg GAE/g extract which surpasses the levels reported for *P. emblica*. Since plant-derived phytochemicals, particularly phenolics and flavonoids, are strong free radical scavenging and metal-chelating properties, the rich bioactive profile of APA indicates

that it possesses functional efficacies comparable to those of other recognized medicinal fruits [7]. Consequently, these comparisons robustly support the traditional use of *A. polycephala* fruits and strongly highlight the aqueous extract as a highly promising natural antioxidant source for functional food and nutraceutical applications.

Table 3. Antioxidant activities of *A. polycephala* fruit extracts

Extracts	TAC (mg AAE/g extract)	ABTS IC_{50} (mg/mL)	DPPH IC_{50} (mg/mL)	Reducing power EC_{50} (mg/mL)
APE	0.93 ± 0.11	3.54 ± 0.14	1.50 ± 0.19	0.63 ± 0.24
APA	2.58 ± 0.10	1.59 ± 0.06	0.85 ± 0.02	0.42 ± 0.06

Values are represented as mean ± S.D.

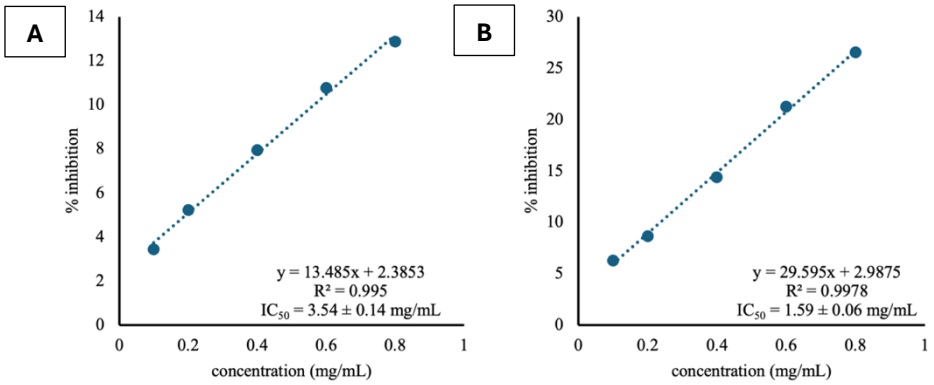

Figure 2. ABTS radical scavenging activity of APE (A) and APA (B).

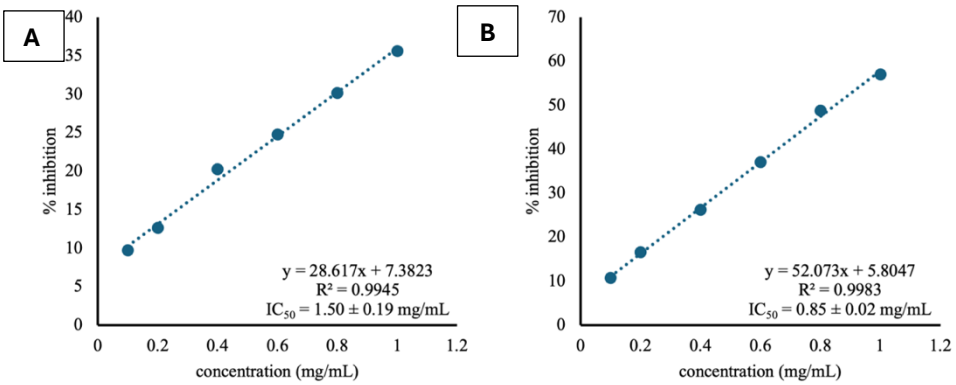

Figure 3. DPPH radical scavenging activity of APE (A) and APA (B).

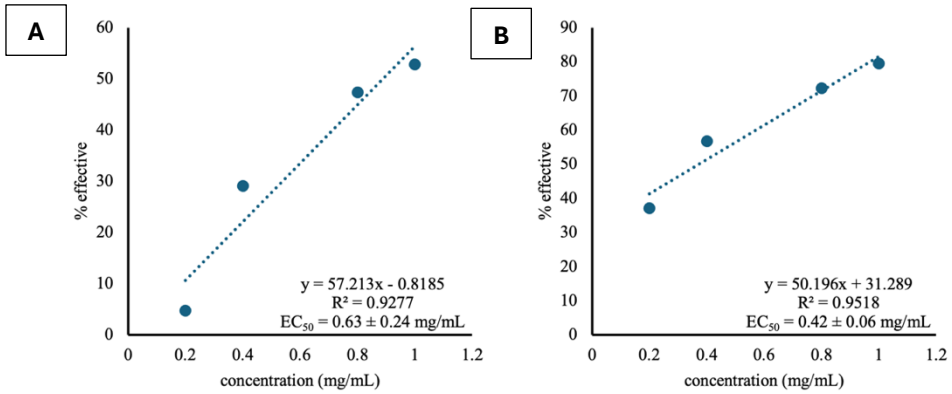

Figure 4. Ferric reducing power of APE (A) and APA (B).

4. Conclusion

In conclusion, *Ardisia polycephala* fruit contains diverse bioactive phytochemical with strong antioxidant potential. The aqueous extract exhibited higher phenolic, flavonoid, and vitamin C contents and consistently greater antioxidant activity than the ethanolic extract across multiple *in vitro* assays. These findings highlight the critical role of extraction solvent in determining phytochemical composition and functional efficacy and support the potential of *A. polycephala* fruit-particulary its aqueous extract-as a promising natural antioxidant source for functional food and nutraceutical applications.

Acknowledgements

The authors would like to thank the Department of Biology, Faculty of Science, Chiang Mai University for providing facilities. This research was partially supported by Chiang Mai University.

References

1. Mironczuk-Chodakowska I, Witkowska AM, Zujko ME. Endogenous non-enzymatic antioxidants in the human body. Adv Med Sci. 2018;63(1):68-78.
2. Divvela, SSK., Gallorini, M., Gellisch, M., Patel, GD., Saso, L. and Brand-Saberi, B.; Navigating redox imbalance: the role of oxidative stress in embryonic development and long-term health outcomes. *Front Cell Dev Biol*. 2025;*13*:1521336.
3. Chandimali N, Bak SG, Park EH, Lee HJ, Wan Y, Kim EK, et al. Natural extracts and compounds in managing free radicals. Cell Mol Biol Lett. 2025;30:2786-806.
4. Burton GJ, Jauniaux E. Oxidative stress. Best Pract Res Clin Obstet Gynaecol. 2011;25(3):287-99.
5. Krumova K, Cosa G. Overview of reactive oxygen species. In: Nonell S, Flors C, editors. Singlet oxygen: applications in biosciences and nanosciences. Cambridge: Royal Society of Chemistry; 2016. p. 5-21.
6. Buachoon N. The study of total phenolic compounds and antioxidant activity of a crude extract from *Ardisia polycephala* leaves. Valaya Alongkorn Rev (Humanit Soc Sci). 2021;16(3):16-24.
7. Tiranakwit T, Puangpun W, Tamprasit K, Wichai N, Siriamornpun S, Srisongkram T, et al. Phytochemical screening on phenolic, flavonoid contents, and antioxidant activities of six indigenous plants used in traditional Thai medicine. Int J Mol Sci. 2023;24(17):13425.
8. Nanasombat S, Khanha K, Phan-im J, Jitaied J, Wannasomboon S, Patradisakorn S, et al. Antimicrobial and antioxidant activities of Thai local fruit extracts: application of a selected fruit extract, *Phyllanthus emblica* Linn. as a natural preservative in raw ground pork during refrigerated storage. Online J Sci Technol. 2012;2(1):1-7.

9. Phrompanya P, Suriyaruean N, Nantarat N, Saenphet S, Tragoolpua Y, Saenphet K. Biological properties of mucus from land snails (*Lissachatina fulica*) and freshwater snails (*Pomacea canaliculata*) and histochemical study of mucous cells in their foot. PeerJ. 2023;11:e15827.
10. Harborne JB. Phytochemical methods: a guide to modern techniques of plant analysis. 3rd ed. London: Chapman and Hall; 1998.
11. Edeoga HO, Okwu DE, Mbaebie BO. Phytochemical constituents of some Nigerian medicinal plants. Afr J Biotechnol. 2005;4(7):685-8.
12. Wolfe K, Wu X, Liu RH. Antioxidant activity of apple peels. J Agric Food Chem. 2003;51:609-14.
13. Ordoñez AAL, Gomez JD, Vattuone MA, Isla MI. Antioxidant activities of *Sechium edule* (Jacq.) Swartz extracts. Food Chem. 2006;97(3):452-8.
14. Khan MMR, Rahman MM, Islam MS, Begum SA. A simple UV-spectrophotometric method for the determination of vitamin C content in various fruits and vegetables at Sylhet area in Bangladesh. J Biol Sci. 2006;6(2):388-92.
15. Umamaheswari M, Chatterjee TK. *In vitro* antioxidant activities of the fractions of *Coccinia grandis* L. leaf extract. Afr J Tradit Complement Altern Med. 2008;5(1):61-73.
16. Miller NJ, Rice-Evans C, Davies MJ, Gopinathan V, Milner A. A novel method for measuring antioxidant capacity and its application to monitoring the antioxidant status in premature neonates. Clin Sci (Lond). 1993;84(4):407-12.
17. Kang HM, Saltveit ME. Antioxidant capacity of lettuce leaf tissue increases after wounding. J Agric Food Chem. 2002;50(26):7536-41.
18. Oyaizu M. Studies on products of browning reactions: antioxidative activities of products of browning reaction prepared from glucosamine. Jpn J Nutr. 1986;44(6):307-15.
19. Subramanian M, Balakrishnan S, Chinnaiyan SK, Sekar VK, Chandu AN. Hepatoprotective effect of leaves of *Morinda tinctoria* Roxb. against paracetamol induced liver damage in rats. Drug Invent Today. 2013;5:223-8.
20. Atmaca M, Bilgin HM, Obay BD, Diken H, Kelle M, Kale E. The hepatoprotective effect of coumarin and coumarin derivates on carbon tetrachloride-induced hepatic injury by antioxidative activities in rats. J Physiol Biochem. 2011;67(4):569-76
21. Prommee N, Saesiw U, Juckmeta T, Thongdeeying P, Yangthaworn K, Dechayont B, et al. *In vitro* investigation of the cytotoxic and antioxidant activities of *Ardisia polycephala*, *Iresine herbstii*, and *Oenanthe javanica* extracts with potential applications in breast cancer therapy. Adv Pharmacol Pharm Sci. 2025;2025:1234439.
22. Li Y, Schellhorn HE. New developments and novel therapeutic perspectives for vitamin C. J Nutr. 2007;137(10):2171-84.
23. Sir Elkhatim KA, Elagib RAA, Hassan AB. Content of phenolic compounds and vitamin C and antioxidant activity in wasted parts of Sudanese citrus fruits. Food Sci Nutr. 2018 Jul;6(5):1214-1219. doi: 10.1002/fsn3.660.
24. Njoku PC, Ayuk AA, Okoye CV. Temperature effects on vitamin C content in citrus fruits. Pak J Nutr. 2011;10(12):1168-9.

P - 299

Comparative Study on Ultrasonic and Pulsed Electric Field Extraction of Phrayawan (*Curcuma phrayawan* Boonma & sansouk) Rhizomes and Evaluation of Bioactive

Phongchai Kanjanamanee[1]*, Surapol Natakankitkul[1], Sukanya Kaewsa-ard[2]

[1]*Graduate School, Cannabis and Medicinal Plants for Local Development, Payap University Chiang Mai, Thailand*
[2]*Faculty of Pharmacy, Payap University, Chiang Mai, Thailand*

**Corresponding author E-mail: 6608020017@payap.ac.th*

Abstract: This study investigated the effects of Ultrasonic-Assisted Extraction (UAE), Pulsed Electric Field (PEF), and their sequential combinations on the extraction efficiency, phytochemical content, and antioxidant activities of *Curcuma phrayawan* Boonma & Saensouk rhizomes. Rhizomes aged 6-8 months were dried, powdered, and extracted using deionized water, 50% ethanol, and 99.7% ethanol under four extraction conditions: UAE, PEF, UAE + PEF, and PEF + UAE. All extractions were performed in triplicate (n=3), and results were expressed as mean ± standard deviation. Extraction yield, total phenolic content (TPC), total flavonoid content (TFC), and antioxidant activities (DPPH, ABTS, and FRAP assays) were evaluated. The UAE + PEF technique using deionized water produced the highest extraction yield (10.32 ± 0.79%), whereas PEF + UAE with 99.7% ethanol achieved the highest TPC (494.69 ± 0.20 mg GAE/g) and TFC (194.51 ± 0.82 mg QE/g). Antioxidant activities correlated positively with TPC and TFC, with PEF + UAE extracts exhibiting the strongest radical scavenging and reducing power (DPPH IC_{50} = 712.53 ± 6.91 µg/mL, ABTS IC_{50} = 651.73 ± 5.22 µg/mL, FRAP IC_{50} = 373.67 ± 3.79 µg/mL). The enhanced performance of the combined UAE and PEF techniques can be attributed to the synergistic effects of acoustic cavitation and electroporation, which improve solvent penetration, cell wall disruption, and mass transfer. These findings demonstrate that integrating UAE and PEF provides a green, efficient, and scalable extraction strategy for producing bioactive-rich *C. phrayawan* extracts with potential applications in functional foods, nutraceuticals, and cosmetics.

Keywords: *Curcuma phrayawan* Boonma & Saensouk; Ultrasonic-Assisted Extraction; Pulsed Electric Field; Antioxidant Activity

1. Introduction

Herbal plants have gained increasing global attention due to their important roles in health promotion and disease prevention. Their rich species diversity, abundance of bioactive compounds, and long-standing traditional knowledge contribute to their recognized therapeutic potential and relative safety, while growing consumer preference for natural-based products continues to expand the global herbal market. Thailand is recognized as one of the most biodiverse countries in terms of medicinal plant resources, with a wide variety of herbal species traditionally used in medicine. To support this sector, the Thai government has implemented national policies promoting herbal production for domestic use and international markets, including the National Master Plan for Thai Herbal Development (2017–2021), which aims to conserve traditional knowledge, improve the quality of herbal raw materials, and encourage the efficient utilization of herbal resources. Despite these efforts, the Thai herbal industry still relies largely on primary processing and the production of raw or minimally processed materials, limiting the development of high-value and innovative herbal products [7].

The Thai herbal market has continued to expand across several product categories, particularly functional beverages, herbal remedies for respiratory symptoms such as coughs and colds, and herbal dietary supplements. Between 2017 and 2019, these product groups experienced an average growth rate of approximately 10.3%, which exceeded the growth rates of major herbal markets in Asia, including China, Japan, and South Korea. This rapid expansion highlights Thailand's strong potential to become a competitive player in the regional herbal economy.

In addition to market growth, botanical exploration and taxonomic research in Thailand have contributed to the discovery of several new medicinal plant species. Researchers from Mahasarakham University, with support from the National Science and Technology Development Agency (NSTDA), reported several new species within the Zingiberaceae family, particularly in the genera Curcuma and Kaempferia. These discoveries reflect the rich biodiversity of medicinal plants in Thailand and highlight the potential for identifying new plant resources with pharmaceutical and nutraceutical value [6].

Among these species, *Curcuma phrayawan* Boonma & Saensouk, commonly known as "Phaya Wan," has attracted increasing attention due to its potential medicinal properties. The plant exhibits morphological characteristics similar to turmeric, including a yellow rhizome, bitter taste, white flowers, a red pseudostem, and a mild aromatic scent. In Thai traditional medicine, *C. phrayawan* is believed to possess various therapeutic properties, including detoxification effects, cardiovascular support, and relief of symptoms associated with the eyes, throat, nose, digestive system, and skin [11].

Despite its ethnomedicinal importance, scientific studies on *C. phrayawan* remain limited. In particular, there is still a lack of information regarding efficient extraction techniques, phytochemical composition, and biological activities such as antioxidant capacity. Therefore, further investigation is necessary to explore its potential as a valuable source of bioactive compounds.

The extraction process plays a crucial role in determining the yield and quality of bioactive compounds obtained from plant materials. Conventional extraction techniques often require long processing times and large volumes of solvents, which may reduce extraction efficiency and increase processing costs. In contrast, modern extraction technologies have been developed to improve extraction efficiency while preserving thermolabile compounds.

Ultrasonic-assisted extraction (UAE) is an emerging technique that utilizes ultrasonic waves to generate acoustic cavitation. This phenomenon disrupts plant cell walls and enhances the release of intracellular compounds into the extraction solvent [12]. Another promising technique is pulsed electric field (PEF) extraction, a non-thermal technology that applies short pulses of high voltage to plant tissues. This process increases cell membrane permeability through electroporation, thereby facilitating the release of bioactive compounds [5].

The integration of UAE and PEF technologies may provide synergistic effects due to their different mechanisms of action. While UAE enhances mass transfer through cavitation-induced cell disruption, PEF promotes the permeabilization of cell membranes. The combination or comparison of these advanced extraction approaches may therefore improve the efficiency of phytochemical recovery from medicinal plants [3].

Therefore, this study aimed to compare ultrasonic-assisted extraction (UAE) and pulsed electric field (PEF) extraction for the recovery of bioactive compounds from *C. phrayawan* rhizomes and to evaluate the antioxidant activities of the resulting extracts. The findings of this research are expected to provide useful insights into efficient extraction techniques for this medicinal plant and contribute to the development of value-added herbal products in the Thai herbal industry.

2. Materials and Methods

2.1 Sample Preparation

Rhizomes of *C. phrayawan* aged 6-8 months were collected from Maha Sarakham Province, Thailand. The rhizomes were thoroughly washed with distilled water to remove soil and other impurities and then sliced into small pieces (approximately 0.2-0.5 cm in thickness). The sliced samples were dried in a hot air oven at 50 °C until a constant weight was obtained, corresponding to a final moisture content of approximately 10%.

The dried rhizomes were subsequently ground into fine powder using a laboratory grinder and passed through a 40-mesh sieve to obtain a uniform particle size. The powdered samples were packed in aluminum foil bags, sealed to prevent moisture absorption, and stored at a temperature below 4 °C until further analysis.

2.2 Materials

Gallic acid, quercetin, aluminum chloride, sodium carbonate, and 2,2-diphenyl-1-picrylhydrazyl (DPPH) were purchased from Sigma-Aldrich (St. Louis, MO, USA). Folin–Ciocalteu reagent was obtained from Merck (Germany). Ethanol and other analytical-grade solvents were purchased from RCI Labscan (Thailand). Deionized water was used throughout the experiments.

2.3 Extraction Process of *C. phrayawan*

The dried rhizome powder of *C. phrayawan* was extracted using three different solvents, namely deionized water (DI), 50% ethanol, and 99.7% ethanol (v/v), at a solid-to-solvent ratio of 1:10 (w/v). The mixtures were subjected to different extraction techniques to evaluate the efficiency of bioactive compound recovery. Ultrasonic-assisted extraction (UAE) was performed using an ultrasonic bath (UC-360D, China) operating at a power of 250 W for 25 min while maintaining the extraction temperature below 40 °C. Pulsed electric field (PEF) treatment was conducted using a custom-built pulsed electric field system developed at Payap University, Chiang Mai, Thailand, where the extraction mixture was treated with an electric field strength of 2 kV/cm with 49 pulses. To compare the efficiency of different extraction approaches, four extraction methods were investigated: UAE, PEF, UAE followed by PEF (UAE + PEF), and PEF followed by UAE (PEF + UAE). Each extraction method was carried out using the three solvents under identical experimental conditions. After extraction, the mixtures were filtered through Whatman No. 1 filter paper, and the resulting extracts were collected and stored at −20°C until further analysis. All experiments were conducted in triplicate [4,12].

2.4 Determination of Total Phenolic Content

The total phenolic content (TPC) of *C. phrayawan* extracts was determined using the Folin–Ciocalteu colorimetric method with slight modifications. Gallic acid was used as the standard and prepared in 95% ethanol. A calibration curve was constructed using gallic acid concentrations ranging from 0–200 µg/mL. The extract samples were also diluted with 95% ethanol prior to analysis. Briefly, 0.3 mL of each standard or sample solution was mixed with 1.5 mL of Folin–Ciocalteu reagent and 1.2 mL of 7.5% Na_2CO_3 solution. The mixture was incubated at room temperature in the dark for 30 min. The absorbance was measured at 725 nm using a UV–Vis spectrophotometer (UV-1800, Shimadzu, Japan). The TPC was calculated from the gallic acid calibration curve and expressed as mg GAE/g extract. All measurements were performed in triplicate [8].

2.5 Determination of Total Flavonoid Content

The total flavonoid content (TFC) was determined using the aluminum chloride colorimetric method [8]. Quercetin was used as the standard to construct a calibration curve with concentrations ranging from 0-100 µg/mL. Briefly, 100 µL of the sample solution (1000 µg/mL) was added into a 96-well microplate, followed by the addition of 100 µL of 2% $AlCl_3$ solution. The mixture was gently mixed and allowed to stand at room temperature for 15 min. The absorbance was measured at 405 nm using a microplate reader (Spark, Tecan, Switzerland). The

TFC was calculated from the quercetin calibration curve and expressed as milligrams of quercetin equivalents per gram of extract (mg QE/g extract). All measurements were performed in triplicate.

2.6 Determining Antioxidant Activity

The antioxidant activity of the extracts was evaluated using three standard assays: DPPH radical scavenging, ABTS radical cation decolorization, and ferric reducing antioxidant power (FRAP) assays. All measurements were performed using a microplate reader.

2.5.1 DPPH Radical Scavenging Assay

The DPPH radical scavenging activity was determined with slight modification from the method of Tanzadehpanah et al. [14]. Briefly, 20 µL of each sample solution was mixed with 180 µL of 0.2 mM DPPH solution prepared in ethanol. The mixture was vortexed for 10 s and incubated at room temperature in the dark for 30 min. The absorbance was measured at 517 nm using a microplate reader.

The percentage of DPPH radical scavenging activity was calculated using the following equation:

$$\%\text{Inhibition} = \frac{\text{Absorbance of control} - \text{Absorbance of sample}}{\text{Absorbance of control}} \times 100$$

The antioxidant activity of the extracts was expressed as IC_{50} values (µg/mL), defined as the concentration required to inhibit 50% of DPPH radicals. The IC_{50} values were calculated from the plotted graph of DPPH inhibition (%) against sample concentration. All measurements were performed in triplicate.

2.5.2 ABTS Radical Cation Decolorization Assay

The ABTS assay was carried out according to the modified method of Re et al. [10]. The ABTS radical cation ($ABTS^{\bullet+}$) was generated by mixing 7 mM ABTS solution with 2.45 mM potassium persulfate in a 1:1 ratio and allowing the mixture to stand in the dark for 12-16 hours at room temperature. A 20 µL aliquot of the sample solution was added to 180 µL of the $ABTS^{\bullet+}$ working solution and mixed by vortexing. The reaction was incubated at 37°C for 6 minutes in the dark, and absorbance was measured at 734 nm. The percentage inhibition was calculated using the same formula as above.

2.5.3 Ferric Reducing Antioxidant Power (FRAP) Assay

The FRAP assay was performed following the method of Benzie and Strain [2] with slight modification. The FRAP reagent was freshly prepared by mixing 300 mM acetate buffer (pH 3.6), 10 mM TPTZ (2,4,6-tripyridyl-s-triazine) in 40 mM HCl, and 20 mM $FeCl_3 \cdot 6H_2O$ in a 10:1:1 ratio (v/v/v). A 10 µL aliquot of the sample was added to 190 µL of FRAP reagent, vortexed briefly, and incubated at 37°C for 30 minutes in the dark. The reducing power was expressed as percentage of antioxidant activity (%). The IC_{50} value, defined as the concentration required to reach 50% reducing activity, was calculated from the dose-response curve.

$$\%\text{Reduction power} = \frac{\text{Absorbance of sample} - \text{Absorbance of blank}}{\text{Absorbance of sample}} \times 100$$

2.7 Determining Antioxidant Activity

All data are expressed as mean ± SD (n=3). Statistical analysis was performed using one-way ANOVA followed by Tukey's post hoc test using SPSS version 17.0 (SPSS Inc., Chicago, IL, USA). IC_{50} values were calculated by nonlinear regression using GraphPad Prism (GraphPad Software Inc., USA). Statistical significance was set at $p < 0.05$.

3. Results & Discussion

3.1 Extraction Yield

The extraction yield of *C. phrayawan* rhizome extracts obtained using four extraction techniques ultrasonic-assisted extraction (UAE), pulsed electric field (PEF), UAE followed by PEF (UAE + PEF), and PEF followed by UAE (PEF + UAE) with three different solvents (99.7% ethanol, 50% ethanol, and deionized water) was evaluated. All extractions were performed in triplicate, and the results are summarized in Table 1. Among all conditions, the highest extraction yield was obtained using the UAE + PEF technique with deionized water as the solvent, yielding 10.32 ± 0.79%, followed by PEF + UAE using 99.7% ethanol (9.93 ± 0.47%). Other techniques produced slightly lower yields, indicating that the sequential combination of ultrasonic and electric field treatments significantly enhances extraction efficiency compared to applying either method alone.

The superior extraction yield observed in UAE + PEF with deionized water can be attributed to the synergistic effect of both techniques. Ultrasonic-assisted extraction (UAE) generates cavitation, which disrupts plant cell walls, while pulsed electric field (PEF) induces electroporation, increasing membrane permeability and facilitating solvent penetration. This dual action enhances mass transfer of intracellular compounds into the solvent, resulting in higher extraction efficiency. Similar synergistic effects of combining UAE and PEF have been reported by Sai Krishna et al. (2023) and Hoang Le-Tan et al. (2022), who found that sequential treatment improved extraction yield and reduced extraction time [4,12].

Additionally, deionized water, being a highly polar solvent, may preferentially extract hydrophilic compounds from *C. phrayawan*, contributing to higher yields under certain conditions compared to ethanol. These results suggest that both solvent polarity and extraction technique play critical roles in maximizing recovery of bioactive compounds.

Table 1. Extraction yield of *C. phrayawan* rhizome extracts under different extraction techniques and solvents.

Extraction Technique	Extraction Yield (%)		
	99.7% ethanol	50% ethanol	Deionized Water
UAE	9.07±1.10^{b}	6.77±0.26^{b}	7.88±0.89^{b}
PEF	9.05±0.87^{b}	5.87±0.08^{c}	9.29±0.71^{ab}
UAE + PEF	9.73±0.97^{ab}	7.17±0.62^{b}	10.32±0.79^{a}
PEF+ UAE	9.93±0.47^{a}	8.22±0.49^{a}	7.59±0.92^{b}

Different superscript letters within each column indicate significant differences ($p < 0.05$).

3.2 Total Phenolic Content (TPC)

The total phenolic content (TPC) of *C. phrayawan* extracts obtained using four extraction techniques ultrasonic-assisted extraction (UAE), pulsed electric field (PEF), UAE followed by PEF (UAE + PEF), and PEF followed by UAE (PEF + UAE) with three solvents (50% ethanol, 99.7% ethanol, and deionized water) was evaluated. All extractions were performed in triplicate (n=3), and results are expressed as mean ± SD (Table 2).

Among all conditions, PEF + UAE using 99.7% ethanol yielded the highest TPC (494.69 ± 0.20 mg GAE/g sample), significantly higher than the other extraction methods ($p < 0.05$). PEF and UAE alone gave comparable yields (476.14 ± 0.07 and 475.67 ± 0.19 mg GAE/g, respectively), while UAE + PEF produced the lowest TPC (457.82 ± 0.17 mg GAE/g). Moderate TPC values were observed with 50% ethanol, whereas deionized water resulted in markedly lower yields (<100 mg GAE/g), indicating that high-concentration ethanol is a more effective solvent for phenolic extraction.

The superior performance of PEF + UAE can be attributed to the synergistic effect of both techniques: PEF induces electroporation, enhancing cell membrane permeability, while UAE generates cavitation that disrupts cell walls, facilitating mass transfer of intracellular phenolics. These findings are consistent with Pitivitayakul et al. (2020) [8], who reported that ethanolic extracts of *Curcuma zedoaria* and *Curcuma comosa* exhibited the highest TPC and strongest antioxidant activities. Overall, sequential PEF + UAE using 99.7% ethanol was the most effective method for extracting phenolic compounds from *C. phrayawan*.

Table 2. Total phenolic contents (TPC) of *C. phrayawan* rhizome extracts under different extraction techniques and solvents.

Extraction Technique	Total Phenolic Compounds (mg GAE/g sample)		
	99.7% ethanol	50% ethanol	Deionized Water
UAE	475.67±0.19^{b}	148.29±0.12^{d}	81.86±0.031^{a}
PEF	476.14±0.07^{b}	386.90±0.17^{a}	41.43±0.03^{c}
UAE + PEF	457.82±0.17^{c}	271.13±0.13^{b}	45.23±0.05^{b}
PEF+ UAE	494.69±0.20^{a}	226.49±0.14^{c}	35.13±0.01^{d}

3.3 Total Flavonoid Content (TFC)

The total flavonoid content (TFC) of *C. phrayawan* rhizome extracts obtained using four extraction techniques ultrasonic-assisted extraction (UAE), pulsed electric field (PEF), UAE followed by PEF (UAE + PEF), and PEF followed by UAE (PEF + UAE) with three solvents (50% ethanol, 99.7% ethanol, and deionized water) was evaluated. All extractions were performed in triplicate (n=3), and results are expressed as mean ± SD.

As shown in Table 3, the TFC followed a trend similar to total phenolic content (TPC). The PEF + UAE technique using 99.7% ethanol produced the highest flavonoid yield (194.51 ± 0.82 mg QE/g sample), followed by UAE (190.14 ± 0.04 mg QE/g) and PEF (184.07 ± 0.11 mg QE/g). UAE + PEF showed the lowest value (179.79 ± 0.72 mg QE/g) within this solvent group. Using 50% ethanol, PEF yielded the highest TFC (168.75 ± 0.78 mg QE/g), while all extractions with deionized water resulted in markedly lower yields, with UAE achieving the highest among them (15.02 ± 0.58 mg QE/g). These results indicate that high-concentration ethanol (99.7%) is a more effective solvent for flavonoid extraction from *C. phrayawan* rhizomes.

The superior performance of PEF + UAE can be explained by the synergistic effect of the two techniques: PEF induces electroporation, increasing cell membrane permeability, and UAE generates cavitation that disrupts cell walls, enhancing flavonoid release and solvent penetration. Lower yields with deionized water are attributed to the poor solubility of flavonoids in highly polar aqueous media. These findings are consistent with previous reports by Pitivitayakul et al. (2020) [8] demonstrating that sequential PEF and UAE treatments improve flavonoid recovery in plant matrices. Overall, PEF + UAE using 99.7% ethanol was the most efficient method for flavonoid extraction from *C. phrayawan* rhizomes.

Table 3. Total flavonoid contents (TFC) of *C. phrayawan* rhizome extracts under different extraction techniques and solvents.

Extraction Technique	Total Flavonoid Contents (mg QE/g sample)		
	99.7% ethanol	50% ethanol	Deionized Water
UAE	190.14±0.04^{a}	58.46±0.53^{c}	15.02±0.58^{a}
PEF	184.07±0.11^{b}	168.75±0.78^{a}	6.68±0.05^{b}
UAE + PEF	179.79±0.72^{c}	95.31±0.51^{b}	8.29±0.05^{b}
PEF+ UAE	194.51±0.82^{a}	83.52±0.59^{b}	6.12±0.02^{b}

Different superscript letters within each column indicate significant differences ($p < 0.05$).

3.4 Selection of the Optimum Extraction Technique for Antioxidant Activity Evaluation

The results revealed that both extraction technique and solvent type significantly influenced the extraction efficiency and bioactive compound content of *C. phrayawan* extracts. Although the UAE + PEF method using deionized water provided the highest extraction yield (10.32 ± 0.79%), it exhibited the lowest total phenolic and flavonoid contents. In contrast, the PEF + UAE extraction using 99.7% ethanol achieved the highest total phenolic content (494.69 ± 0.20 mg GAE/g) and total flavonoid content (194.51 ± 0.82 mg QE/g), indicating superior efficiency in extracting polyphenolic and flavonoid content, which are key contributors to antioxidant activity [1]. Therefore, the PEF + UAE technique with 99.7% ethanol is considered the most appropriate method for evaluating the antioxidant activity of *C. phrayawan* extracts, as it yields the highest concentrations of antioxidant-related compounds, consistent with the findings of Pitivitayakul et al. (2020) [1], who reported that ethanolic extracts of *C. zedoaria* and *C. comosa* with higher phenolic contents exhibited stronger antioxidant capacities than those extracted with other solvents.

3.5 Antioxidant Activity

The antioxidant activities of *C. phrayawan* rhizome extracts obtained using the PEF + UAE (P+U) technique were evaluated using DPPH, ABTS, and FRAP assays. All experiments were performed in triplicate (n=3), and the results are expressed as mean ± standard deviation (SD) (Table 4).

The IC_{50} values of the P+U extract were significantly higher than those of Trolox, a standard antioxidant compound, in all assays ($p < 0.05$), indicating lower radical scavenging and reducing capacities compared with the positive control. Specifically, the IC_{50} value of the extract in the DPPH assay was 712.53 ± 6.91 µg/mL, whereas Trolox exhibited an IC_{50} of 100.25 ± 3.78 µg/mL. In the ABTS assay, the extract showed an IC_{50} value of 651.73 ± 5.22 µg/mL compared with 59.31 ± 1.22 µg/mL for Trolox. Similarly, in the FRAP assay, the extract exhibited an IC_{50} value of 373.67 ± 3.79 µg/mL, while Trolox demonstrated a substantially lower IC_{50} of 25.16 ± 0.64 µg/mL. These findings indicate statistically significant differences in antioxidant activity between the *C. phrayawan* extract and Trolox across all assays, confirming that the extract possesses comparatively lower antioxidant capacity.

The relatively high IC_{50} values observed for the P+U extract may be attributed to the concentration and composition of bioactive compounds present in the rhizome, which are generally less potent on a mass basis than pure antioxidant standards such as Trolox. Nevertheless, the extract still exhibited measurable radical scavenging and reducing activities, suggesting its potential as a natural antioxidant source when applied at appropriate concentrations.

The antioxidant activity detected in the *C. phrayawan* extract may be associated with the presence of bioactive phytochemicals, particularly phenolic compounds and curcuminoids, which are widely reported in *Curcuma* species and contribute to their antioxidant properties [1]. Previous studies have also demonstrated that rhizome extracts of *Curcuma* species obtained using green extraction techniques exhibit detectable antioxidant activities due to these phytochemical constituents [9]. Although plant extracts generally show lower antioxidant activity than pure standards such as Trolox, they can still provide biologically relevant radical scavenging and reducing capacities [15].

Table 4. Antioxidant activities (IC_{50}) of *C. phrayawan* rhizome extracts and Trolox.

Sample	DPPH IC_{50} (µg/mL)	ABTS IC_{50} (µg/mL)	FRAP IC_{50} (µg/mL)
Trolox	100.25 ± 3.78^{b}	59.31 ± 1.22^{b}	25.16 ± 0.64^{b}
PEF+UAE	712.53 ± 6.91^{a}	651.73 ± 5.22^{a}	373.67 ± 3.79^{a}

Values are presented as mean ± SD (n = 3). Different superscript letters within each column indicate significant differences ($p < 0.05$).

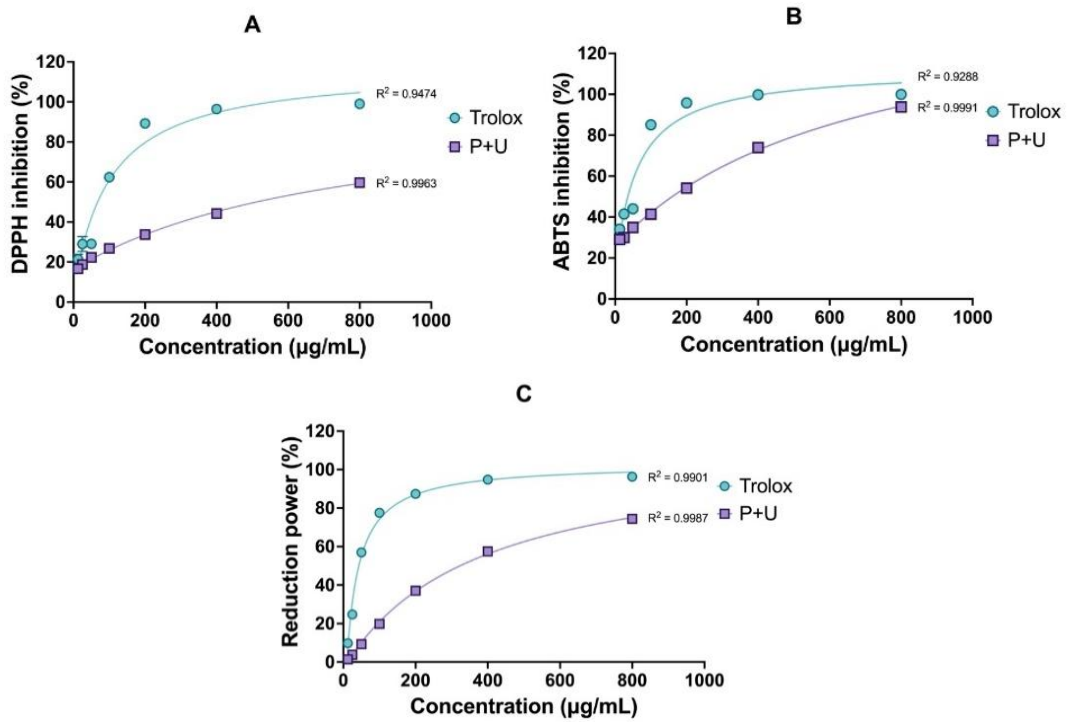

Figure 1. Nonlinear regression curves used for the determination of IC_{50} values of Trolox and *C. phrayawan* extract obtained by pulsed electric field followed by ultrasonic-assisted extraction (P+U). Antioxidant activities were evaluated using (A) DPPH, (B) ABTS, and (C) FRAP assays.

4. Conclusion

This study demonstrates that both extraction technique and solvent type play critical roles in determining the efficiency of bioactive compound recovery from *C. phrayawan* rhizomes. Among the investigated approaches, the sequential application of pulsed electric field followed by ultrasonic-assisted extraction (PEF + UAE) using 99.7% ethanol provided the most effective recovery of phenolic and flavonoid compounds. The enhanced extraction efficiency of this method is likely attributed to the synergistic effects of electroporation and acoustic cavitation, which facilitate cell wall disruption and improve solvent penetration, thereby promoting the release of intracellular phytochemicals.

Although the antioxidant activity of the extract was lower than that of the Trolox standard, the extract still exhibited appreciable radical scavenging and reducing capacities in DPPH, ABTS, and FRAP assays, indicating its potential as a natural antioxidant source. Overall, the PEF + UAE technique using ethanol represents an efficient strategy for enhancing the recovery of antioxidant-related phytochemicals from *C. phrayawan* rhizomes. These findings provide valuable insights for the development of antioxidant-rich herbal extracts with potential applications in nutraceutical and cosmetic industries. Further studies focusing on compound characterization and process optimization may facilitate future industrial applications.

Acknowledgements

The authors sincerely thank the Graduate School, Payap University, for providing excellent research facilities. Special thanks are extended to the staff of the Graduate School, Department of Cannabis and Medicinal Plants for Local Development, for their technical assistance throughout the experiments. The authors also wish to acknowledge colleagues and faculty members for their valuable advice and constructive suggestions during the course of this research.

References

1. Ak T, Gülçin I. Antioxidant and radical scavenging properties of curcumin. Chem Biol Interact. 2008;174(1):27–37.
2. Benzie IFF, Strain JJ. The ferric reducing ability of plasma (FRAP) as a measure of "antioxidant power": The FRAP assay. *Anal Biochem.* 1996;239(1):70–76.
3. Chatzimitakos T, Athanasiadis V, Kalompatsios D, Mantiniotou M, Bozinou E, Lalas SI. Pulsed electric field applications for the extraction of bioactive compounds from food waste and by-products: A critical review. Biomass. 2023;3:367–401.
4. Hoang Le-Tan, Fauster T, Haas K, Jaeger H. Aqueous extraction of curcuminoids from *Curcuma longa*: effect of cell disintegration pre-treatment and extraction condition. *Food Bioprocess Technol*. 2022;15:1359–1373.
5. Muangrat R, Thipsuwan Y. Enhancing bacterial inhibition in beetroot beverages: The potent combination of sappan heartwood extracts via accelerated solvent extraction and pulsed electric field methods. J Agric Food Res. 2024;18:101268.
6. National Archives of Thailand. Thailand Archives B.E. 2564 [Internet]. Bangkok: National Archives of Thailand, Fine Arts Department; 2022. p. 240. Available from: https://www.nat.go.th/Portals/0/ebook/e-book64/files/basic-html/page240.html
7. National Herbal Policy Committee. National Herbal Action Plan, 2nd edition, B.E. 2566–2570 [Internet]. Nonthaburi: Division of Economic Herbs, Department of Thai Traditional and Alternative Medicine, Ministry of Public Health; 2023. 188 p. ISBN 978-616-11-5107-2.
8. Pitivitayakul N, Wajeesing P, Prasomsub T. Senior project, Academic Year 2020: Study of acetylcholinesterase inhibitor and antioxidant activities from *Curcuma zedoaria* Roscoe and *Curcuma comosa* Roxb. [Graduate research project]. Burapha University, Faculty of Pharmaceutical Sciences; 2020. Thai.
9. Priyadarsini KI. The chemistry of curcumin: From extraction to therapeutic agent. Molecules. 2014;19(12):20091–20112.
10. Re R, Pellegrini N, Proteggente A, Pannala A, Yang M, Rice-Evans CA. Antioxidant activity applying an improved ABTS radical cation decolorization assay. *Free Radic Biol Med.* 1999;26(9–10):1231–1237.
11. Saensouk S, Boonma T, Saensouk P. Six new species and a new record of *Curcuma* L. (Zingiberaceae) from Thailand. Biodiversitas: J Biol Divers. 2021;22(4):1658–1685.
12. Sai Krishna G, Sravanya K, Pranuthi P, Thirumdas R. Effect of microwave boiling and ultrasound-assisted extraction on curcumin from the turmeric rhizomes. *Food Sci Eng*. 2023;4(2):237.
13. Senate Committee on Commerce and Industry. Study Report: Adding Value to Herbal Products through Cosmetic/Medicinal-Cosmetic Products [Internet]. Bangkok: Secretariat of the Senate; 2022 Sep 12 [cited 2025 Oct 30]. 266 p. Available from: https://hdl.handle.net/20.500.14156/602362
14. Tanzadehpanah H, Asoodeh A, Chamani J. An antioxidant peptide derived from ostrich (*Struthio camelus*) egg white protein hydrolysates. *Food Res Int.* 2012;49(1):105–111.
15. Thaipong K, Boonprakob U, Crosby K, Cisneros-Zevallos L, Byrne DH. Comparison of ABTS, DPPH, FRAP, and ORAC assays for estimating antioxidant activity from guava fruit extracts. J Food Compos Anal. 2006;19(6–7):669–675.

P - 317

Optimization and Characterization of Soluble Dietary Fiber Extracted from Edamame (*Glycine max L.)* Hulls by Plasma-Activated Water Technology

Malee Pisitchaiwet and Sudarat Jiamyangyuen*

Division of Food Science and Technology, Faculty of Agro-Industry, Chiang Mai University, Chiang Mai, Thailand.

**Corresponding author E-mail: sudarat.j@cmu.ac.th*

Abstract: Edamame (*Glycine max L.*) hulls, an abundant agricultural by-product, are rich in dietary fiber but underutilized. This study investigated the optimization of soluble dietary fiber (SDF) extraction from edamame hulls using plasma-activated water (PAW) as a green, non-thermal technology. A Box–Behnken Design (BBD) was employed to optimize three extraction parameters: solid-to-liquid ratio (1:5-1:15 w/v), treatment time (10–30 min), and gas flow rate (1–5 L/min). The quadratic regression model showed excellent fit ($R^2 = 0.9535$, $p < 0.0001$). Optimal conditions were determined as 1:14.7 w/v ratio, 25.2 min treatment time, and 3.5 L/min gas flow rate, achieving a maximum SDF yield of 7.82%. Fourier-transform infrared spectroscopy (FT-IR) revealed structural modifications in O–H stretching (3400 cm^{-1}), C–H vibration (2921 cm^{-1}), and C=O stretching (1738 cm^{-1}), confirming partial depolymerization of cellulose and hemicellulose into hydrophilic SDF. Scanning electron microscopy (SEM) demonstrated significant morphological changes: PAW-treated fibers exhibited rougher, more porous surfaces with fragmentation compared to the compact, smooth structure of control samples, indicating effective cell wall disruption. These findings demonstrate that PAW pretreatment is an energy-efficient, solvent-free method for enhancing SDF extraction and modifying fiber structure, offering a sustainable approach to valorize agricultural by-products into functional food ingredients

Keywords: Edamame hulls; soluble dietary fiber; plasma-activated water; Box–Behnken Design

1. Introduction

The edamame industry plays a significant role in the global agricultural and food market, with Thailand being one of the major producers and exporters of edamame products. Edamame (*Glycine max (L.)*), also known as green soybean, is not only an important cash crop but also a highly nutritious food source rich in dietary fiber (DF), high-quality plant proteins, vitamins (such as vitamins E and C), and essential minerals including calcium, iron, and zinc [(1)(2)(3)]. Moreover, edamame is considered a complete protein as it contains all nine essential amino acids required by the human body, making it particularly valuable for children, elderly individuals, vegetarians, and people concerned with muscle maintenance and metabolic health [(4)(5)].

Despite its nutritional value, a considerable amount of edamame is discarded during postharvest handling and processing due to cosmetic defects such as irregular size, shape, or color. This results in a large volume of agricultural byproducts, particularly edamame hulls, which are often underutilized or treated as waste. With increasing concerns regarding food loss, sustainability, and circular bioeconomy, there is growing interest in valorizing such byproducts into value-added functional ingredients.

Dietary fiber is one of the most abundant and valuable components in edamame and its byproducts. Fresh edamame beans contain approximately 5.2 g of total dietary fiber (TDF) per 100 g, a level that is generally higher than that of many other vegetables [(6)]. Dietary fiber is a complex carbohydrate polymer composed of ten or more monosaccharide units and is commonly

classified into soluble dietary fiber (SDF) and insoluble dietary fiber (IDF) based on its solubility in water [7][8]. DF exhibits important physicochemical properties, including water-holding capacity, oil-holding capacity, and swelling ability, which contribute to its functional roles in food systems as well as its health benefits, such as cholesterol reduction and bile acid binding [9][10][11].

From a physiological perspective, SDF is particularly important because it can be fermented by gut microbiota in the large intestine to produce short-chain fatty acids (SCFAs), such as acetate, propionate, and butyrate, which play key roles in regulating inflammation, improving gut barrier integrity, and reducing the risk of intestinal diseases [12][13]. In contrast, IDF is poorly soluble in water, tends to precipitate easily, and is less desirable in food applications due to its negative effects on texture, appearance, and sensory quality [14]. Although IDF provides benefits such as enhanced gastrointestinal motility and satiety, excessive IDF content can limit its applicability in functional food formulations [15][16].

Previous studies have attempted to modify dietary fiber structure or convert IDF into SDF using various techniques, including chemical treatments, enzymatic hydrolysis, high-pressure processing, ultrasound-assisted extraction, and thermal methods. These approaches aim to disrupt plant cell wall structures and improve the solubility and functionality of dietary fiber [17]. However, such methods often require harsh chemicals, high temperatures, or long processing times, which may negatively affect the structural integrity of dietary fiber or increase environmental impact. In addition, some conventional treatments may cause partial degradation of polysaccharides or require high energy consumption, which limits their industrial applicability.

Although several agricultural byproducts have been explored as sources of dietary fiber, studies specifically focusing on edamame hulls remain limited. Edamame hulls are typically discarded during processing despite containing substantial amounts of structural polysaccharides such as cellulose, hemicellulose, and lignin, which represent potential sources of dietary fiber. Therefore, exploring efficient and sustainable methods to valorize edamame hulls as a functional dietary fiber source is of significant interest.

In recent years, plasma-activated water (PAW) has emerged as a promising green technology for biomass modification and extraction processes. PAW contains various reactive oxygen and nitrogen species (RONS) capable of disrupting plant cell wall matrices, facilitating the release or transformation of structural polysaccharides without the need for harsh chemicals or high temperatures [18]. Compared with conventional extraction methods, PAW offers several advantages, including milder processing conditions, reduced chemical usage, and improved environmental sustainability.

However, systematic studies on the application of PAW for enhancing soluble dietary fiber extraction from edamame hulls remain scarce. Therefore, the objective of this study is to valorize edamame hulls by optimizing the extraction of soluble dietary fiber using PAW technology. The effects of key processing parameters on SDF yield and structural characteristics are investigated in order to provide a sustainable strategy for converting edamame processing byproducts into value-added functional food ingredients.

2. Materials and Methods

2.1 Preparation of Edamame Hulls

Frozen edamame hulls were dried in a convection oven at 60 °C until a constant weight was obtained. The dried hulls were then ground using a hammer mill equipped with a 0.5 mm sieve to obtain edamame hull powder.

Proteins were removed from the edamame hull powder using a modified method based on Yu et al. [19]. Briefly, enzymatic hydrolysis was performed using Alcalase 2.4 L at an enzyme loading of 0.8% (w/w). The solid loading of the edamame hull suspension was 10% (w/v). The pH of the suspension was adjusted to 7.5 using 4 M NaOH, and the mixture was incubated in a

water bath at 70 °C with shaking at 115 rpm for 4 h. During enzymatic hydrolysis, the pH was monitored every 1 h and maintained at 7.5 by adding 1 M NaOH when necessary. After incubation, the mixture was centrifuged at 5,000 rpm for 10 min. The solid fraction was collected and oven-dried to obtain pretreated edamame hull powder for further experiments.

2.2 Experimental design for optimization and statistical analysis

To find the optimum conditions for the extraction of SDF in Edamame Hulls using the plasma activated water technique, a Response Surface Methodology (RSM) was employed. The Box-Behnken design (BBD) was used with the independent variables Solid-to-liquid ratio (w/v), Treatment Time (min) and Gas flow rate (L/min). The dependent variable was the

SDF yield. The Design-Expert software (Version 13, Stat-Ease, Inc., USA) was used for the optimization process and Table 1 shows the variables and levels.

Table 1. Range of independent variables and their corresponding levels.

Independent variable	Level		
	-1	**0**	**1**
Solid-to-liquid ratio (w/v)	1:5	1:10	1:15
Treatment Time (min)	10	20	30
Gas flow rate (L/min)	1	3	5

2.3. Extraction procedure

2.3.1 Plasma-Activated Water (PAW) Extraction

PAW was prepared by treating distilled water under plasma discharge at different gas flow rates (1–5 L/min) and treatment times (10–30 min), according to the experimental design. The distance between the plasma jet nozzle and the liquid surface was fixed at approximately 10 cm. To avoid excessive heating during plasma treatment, the system temperature was controlled and maintained close to room temperature.

For SDF extraction, dried and ground edamame hull powder was mixed with PAW at solid-to-liquid ratios ranging from 1:5 to 1:15 w/v. The mixtures were treated with PAW under the specified experimental conditions based on the BBD.

2.3.2 Hot Water Extraction (HWE)

In this study, hot water extraction was conducted to compare the efficiency of extraction with the PAW extraction method, using the modified of Barbosa et al. [20] method. Initially, 10 g of dried Edamame hull powder was mixed with 100 mL of distilled water and then extracted using a water bath at 100 ◦C for 3 h, with a solid-to-liquid ratio of 1:10. Subsequently, the mixture was filtered, alcohol precipitated, the supernatant collected, and the following extraction step was performed in accordance with Section 2.4 The obtained sample was then analyzed for SDF yield and stored for further investigations.

2.4 Isolation and determination of yield of SDF

After PAW and HWE treatment, the samples were centrifuged at 5,000 × g for 10 min to separate the insoluble fraction. The supernatant containing SDF was collected and precipitated by adding four volumes of 95% (v/v) ethanol, followed by storage at 4 °C for 12 h. The solution was

then centrifuged again at 4000 rpm for 15 min, washed with ethanol and the precipitate was collected as crude extract.

This was air-dried at 60°C until constant weight All. samples were ground using a mortar and pestle and sieved through a 60-mesh screen to minimize the effect of particle size. and percentage yield was calculated using equation 1.

$$\text{Yield (\%)} = \frac{\text{Weight of dried crude extract (g)}}{\text{Weight of sample (g)}} \times 100 \quad (1)$$

2.5 Structural analysis of SDF

2.5.1. Scanning Electron Microscopy (SEM)

The morphological properties of the SDF samples were observed by SEM. The SDF samples were fixed into a Leica ACE600 Sputter and sputtered with 10 nm Pt/Pd. The SEM images were taken by FEI Quanta 600 FEG (FEI Company, Hillsboro, OR, USA) with an accelerating voltage of 20 kV and an image magnification of 500X and 5,000X [21].

2.5.2 Fourier Transformed Infrared Analysis (FT-IR)

Chemical bonds of different SDF samples were analyzed by FT-IR. The instrument was calibrated through background scanning. Afterward, the samples were directly placed on the Zn Se flat-top plate. The FT-IR spectrum was analyzed using a 400 FT-IR/FT-NIR Spectrometer (PerkinElmer Corp., Shelton, CT, USA) with a wavenumber range of 400−4000 cm^{-1}, resolution of 4 cm^{-1}, and scan of 32 times [21].

2.6 Physicochemical and functional properties of SDF

2.6.1 Water holding capacity (WHC)

The method reported by López-Marcos et al. [22] was used to improve our methodology. The sample (0.25 g) was placed in a 50 mL centrifuge tube, to which 25 mL of deionized water was added. The sample was shaken vigorously at 37 °C for 30 min. Following centrifugation at 5,000×g for 15 min, the supernatant was extracted using a pipette, and the residue was weighed. The WHC of each sample was expressed as the weight of water retained by 1 g of the DF sample. The WHC was calculated as follows; (2)

$$\text{WHC}\left(\frac{\text{g}}{\text{g}}\right) = \frac{(\text{Wet weight(g)} - \text{Dry weight(g)})}{\text{Dry weight(g)}} \quad (2)$$

2.6.2 Oil holding capacity (OHC)

A reference to López-Marcos et al. [22] was made to improve the methodology. The sample (0.25 g) was placed in a 50 mL centrifuge tube, and 20 mL of soybean oil was added. The sample was vigorously shaken at 37 °C for 30 min. Following centrifugation at 5,000×g for 15 min, the supernatant was removed using a pipette, and the residue was weighed. The OHC of each sample was expressed as the weight of oil retained by 1 g of the DF sample and calculated as follows:

$$\text{OHC}\left(\frac{\text{g}}{\text{g}}\right) = \frac{(\text{Wet weight(g)} - \text{Dry weight(g)})}{\text{Dry weight(g)}} \quad (3)$$

2.7. Statistical analysis

All experiments were performed in triplicate and presented by mean ± standard derivation. The experimental data were fitted to the second-order polynomial model (Equation (1)) to obtain the regression coefficients (b) using Design-Expert software version 13 (Stat-Ease Inc., Minneapolis, MN, USA). The generalized second-order polynomial model used in the response surface analysis was the following:

$$Y = \beta_0 + \sum \beta_i X_i + \sum \beta_{ii} X_i^2 + \sum \beta_{ij} X_i X_j \quad (4)$$

where Y is the dependent variable (response variable) to be modelled, β0 is a constant coefficient (intercept); β1, β2, and β3 are the coefficients of the linear, quadratic, and interactive terms, respectively; X1, X2, and X3 are the independent variables. Parametric estimation responses were collected in the form of Yield contents.

3. Results & Discussion

3.1 Optimization of PAW Extraction from SDF

Based on the results derived from the preliminary screening in single factor analysis, the utilization of the Box–Behnken design for three factors confers some advantage in requiring fewer number of runs; it is also particularly useful when the factors have moderate ranges. As shown in Table 1, the Box–Behnken design recommended a total of 15 experimental runs for the optimization of three extraction variables: PAW power (X_1), treatment duration (X_2), and solid-to-liquid ratio (X_3). The optimization process was focused on dependent variables, namely the SDF yield (%)

Table 2. Box–Behnken experimental design and PAW extraction results.

Run	Factors			Response
	solid-to-liquid ratio (w/v) X_1, A	**Treatment time (min) X_2, B**	**Gas flow rate (L/min) X_3, C**	**SDF Yield (%)**
1	1:5	10	3	5.39
2	1:15	10	3	7.45
3	1:5	30	3	4.9
4	1:15	30	3	7.92
5	1:5	20	1	4.34
6	1:15	20	1	7.21
7	1:5	20	5	4.37
8	1:15	20	5	6.19
9	1:10	10	1	6.13
10	1:10	30	1	5.66
11	1:10	10	5	6.53
12	1:10	30	5	6.29
13	1:10	20	3	7.82
14	1:10	20	3	7.54
15	1:10	20	3	7.6
HWE	1:10	0	0	4.92

3.2 Effect of Extraction Variables on Edamame Hull Soluble Dietary Fiber (SDF) Yield

The SDF yield obtained from edamame hulls under the Box–Behnken design (BBD) ranged from **4.31 to 7.92%**. The relationship between the independent variables—solid-to-liquid ratio (X_1), treatment time (X_2), and gas flow rate (X_3)—and SDF yield was described using a reduced quadratic model. To satisfy the regression assumptions of normality and constant variance of residuals, the response variable was subjected to a natural logarithm transformation. The final predictive equation, expressed in terms of actual factors, was as follows:

$$\ln(\text{SDF yield}) = 0.4463 + 0.1725X_1 + 0.0115X_2 + 0.2805X_3 - 0.0007X_1^2 - 0.0003X_2^2 - 0.047X_3^2 \quad (5)$$

Analysis of variance (ANOVA) (Table 3) indicated that the reduced quadratic model was highly significant ($F = 27.35$, $p < 0.0001$), confirming its suitability for predicting SDF yield within the studied factor ranges. The coefficient of determination ($R^2 = 0.9535$) demonstrated that 95.35% of the variation in the response could be explained by the model. In addition, the lack-of-fit test was not significant ($p = 0.0789$), further supporting model adequacy.

Among the investigated parameters, the solid-to-liquid ratio was the most influential factor ($F = 101.20$, $p < 0.0001$). Increasing the ratio enhanced SDF extraction, likely by improving mass transfer due to a higher concentration gradient between the plant matrix and the extracting medium, consistent with Fick's law of diffusion. Moreover, a larger solvent volume may facilitate matrix swelling and reduce apparent viscosity, thereby promoting the release and diffusion of soluble polysaccharides. However, the significant negative quadratic term (X_1^2, $p = 0.0007$) indicates a curvature effect, suggesting that the yield approaches a maximum at higher ratios and may plateau once the system becomes less responsive to further increases in solvent volume.

Gas flow rate exhibited a significant quadratic effect (X_3^2, $p = 0.0003$), indicating the presence of an optimum gas flow for maximizing SDF yield. This may be attributed to improved mixing and enhanced interaction between PAW and the edamame hull matrix, which promotes cell wall disruption and increases solvent accessibility. At excessive flow rates, however, reduced effective interaction time and operational issues may limit extraction efficiency, resulting in the observed antagonistic quadratic behavior. In contrast, treatment time did not significantly affect SDF yield within the investigated range (**$p = 0.3857$**), indicating that SDF solubilization likely reached equilibrium relatively quickly under PAW-assisted extraction conditions.

To further evaluate the predictive capability of the developed model, a confirmation experiment was conducted under the optimized extraction conditions, and the results are presented in **Section 3.2.1**.

Table 3. ANOVA of the effect to the PAW extraction variables on SDF yield

Source	Sum of squares	DF	Mean	F-Value	p-Value
Model	0.5582	6	0.0930	27.35	< 0.0001
A-Ratio	0.3443	1	0.3443	101.20	< 0.0001
B-Time	0.0029	1	0.0029	0.8417	0.3857
C-Gas flow	0.0001	1	0.0001	0.0196	0.8921
A^2	0.0990	1	0.0990	29.09	0.0007
B^2	0.0041	1	0.0041	1.22	0.3023
C^2	0.1278	1	0.1278	37.57	0.0003
Residual	0.0272	8	0.0034		
Lack of Fit	0.0265	6	0.0044	12.00	0.0789
Pure Error	0.0007	2	0.0004		
Cor Total	0.5854	14			
Std. Dev.	0.0583	R^2	0.9535		
Mean	1.83	Adjusted R^2	0.9186		
C.V. %	3.19	Predicted R^2	0.8162		
		Adeq Precision	14.7900		

3.2.1 Optimization and Model Validation

Response surface methodology (RSM) based on the Box–Behnken design was applied to determine the optimal extraction conditions for maximizing SDF yield from edamame hulls using plasma-activated water. The developed quadratic model showed a satisfactory fit to the experimental data, with a coefficient of determination ($R^2 = 0.9535$) and high overall model significance ($p < 0.0001$), indicating that the model was reliable for predicting SDF yield within the investigated factor ranges. Response surface analysis confirmed that the solid-to-liquid ratio was the most influential factor affecting SDF yield, consistent with the ANOVA results discussed in Section 3.2. Increasing solvent availability enhanced the interaction between PAW and the plant matrix, facilitating the release and diffusion of soluble polysaccharides.

Although treatment time was included in the regression model, its linear effect was not statistically significant within the studied range ($p > 0.05$). Therefore, treatment time was not considered a primary factor affecting SDF yield. However, an appropriate treatment duration was still applied during optimization to ensure adequate interaction between the biomass and the reactive oxygen and nitrogen species generated in PAW. Gas flow rate also significantly affected SDF recovery because it governs plasma stability and the generation of reactive species in the PAW system. Appropriate gas flow conditions may promote effective oxidative modification of cell wall polysaccharides, thereby facilitating the conversion of insoluble components into soluble dietary fiber.

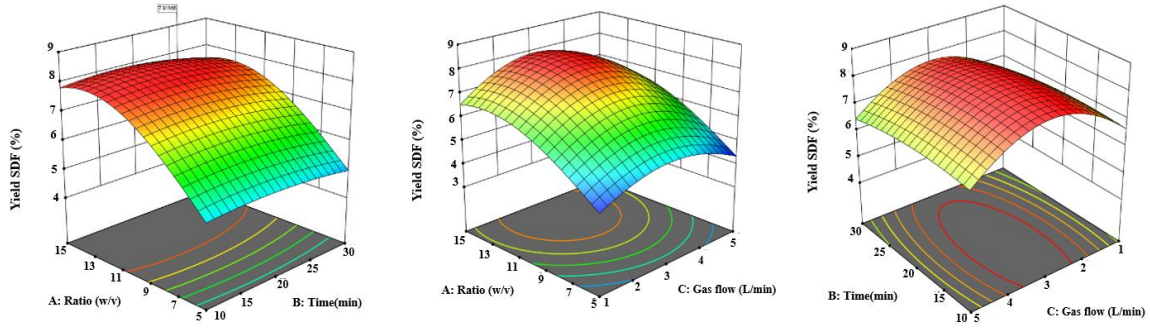

Figure 1. Response surface plot of the SDF yield with the interaction effects of time and solid-to-liquid ratio (left); solid-to-liquid ratio and Gas flow rate (middle); and Time and Gas flow rate (right).

The response surface methodology predicted the optimum extraction conditions as a solid-to-liquid ratio of 1:14.7 w/v, extraction time of 25.2 min and gas flow rate of 3.5 L/min, corresponding to a predicted maximum SDF yield of 7.82%.

For practical implementation, the solid-to-liquid ratio was applied directly at the predicted value, and the extraction experiment was conducted under these optimized conditions to validate the model. All validation experiments were performed in triplicate to ensure the reproducibility of the results. The experimental soluble dietary fiber (SDF) yield obtained under these conditions showed good agreement with the predicted value, confirming the adequacy and reliability of the developed model. The experimental SDF yield obtained under these conditions was 7.91%, which closely agreed with the predicted value. The absolute deviation between predicted and experimental responses was 0.09 percentage points, corresponding to a relative error of 1.15%, indicating good agreement between the predicted and experimental values and confirming the reliability of the developed model.

In addition, the optimized PAW extraction was compared with conventional **hot water extraction (HWE)** under similar conditions. The SDF yield obtained using PAW (**7.91%**) was higher than that obtained using HWE (**4.92%**), representing an improvement of approximately 60**.77%**. This result highlights the potential advantage of PAW as an effective pretreatment strategy for enhancing the extraction of soluble dietary fiber from agricultural byproducts.

The close agreement between predicted and experimental responses suggests that the selected factor combination provides an appropriate extraction severity, where a high solid-to-liquid ratio improves mass transfer while moderate treatment time and gas flow rate ensure effective generation and utilization of reactive species in PAW without causing excessive degradation of polysaccharides.

The extract obtained under the optimized conditions was selected for subsequent characterization, including structural, physicochemical, and functional analyses. Structural morphology was examined using scanning electron microscopy (SEM), while chemical structure was analyzed using Fourier transform infrared spectroscopy (FTIR). Functional properties were evaluated through water-holding capacity (WHC) and oil-holding capacity (OHC).

3.3. Comparison of Different Extraction Techniques on the SDF Yield and the Water holding capacity and Oil holding capacity.

PAW extraction (1:14.7 w/v, 25.2 min, and 3.5 L/min) was replicated in triplicate under the previously optimized conditions. The experimentally obtained SDF yield 7.91% was compared with the value predicted by the model to validate the optimization results. Furthermore, a comparative analysis was conducted with the conventional hot water extraction (HWE) method (90 °C, 3 h, and 1:10 w/v).

The SDF yield obtained from HWE was 4.92%, whereas PAW extraction significantly increased the yield to 7.91 representing approximately a **60.77% improvement** compared with the conventional extraction method. The higher yield suggests that PAW pretreatment enhanced the solubilization of fiber components, likely through disruption of the cell wall matrix and partial depolymerization or oxidative modification of insoluble polysaccharides, thereby facilitating the release of soluble fractions.

In addition to improving yield, PAW-extracted SDF exhibited significantly greater hydration capacity. The WHC increased from **5.58 ± 0.04 g/g** (HWE) to **10.57 ± 0.10 g/g** (PAW) ($p < 0.05$). The markedly higher WHC suggests that PAW treatment promoted structural features favorable for water binding, such as increased porosity and surface roughness, as well as greater exposure of hydrophilic functional groups, thereby enhancing moisture retention.

Similarly, the OHC of PAW-extracted SDF (**16.52 ± 0.45 g/g**) was significantly higher than that of HWE-extracted SDF (**11.73 ± 0.66 g/g**) ($p < 0.05$). The enhanced OHC may be attributed to an increase in surface area and the formation of a more open fiber network capable of physically entrapping oil. Although the increase in hydrophilic functional groups mainly enhances water-holding capacity, the improved oil-holding capacity of PAW-extracted SDF is primarily associated with PAW-induced structural modifications. The formation of a more porous and open fiber network with increased surface area and surface roughness facilitates physical oil entrapment, leading to improved oil retention despite the overall increase in hydrophilicity [24]. These improved functional properties suggest that SDF extracted from edamame hulls could be used as a functional dietary fiber ingredient in food formulations. The enhanced water- and oil-holding capacities are beneficial for improving texture, moisture retention, and stability in products such as bakery items, plant-based foods, and fiber enriched formulations.

Overall, PAW not only improved SDF extraction efficiency but also significantly enhanced key functional properties (WHC and OHC), supporting the potential of PAW as a green processing strategy to valorize edamame hull by-products into functional dietary fiber ingredients.

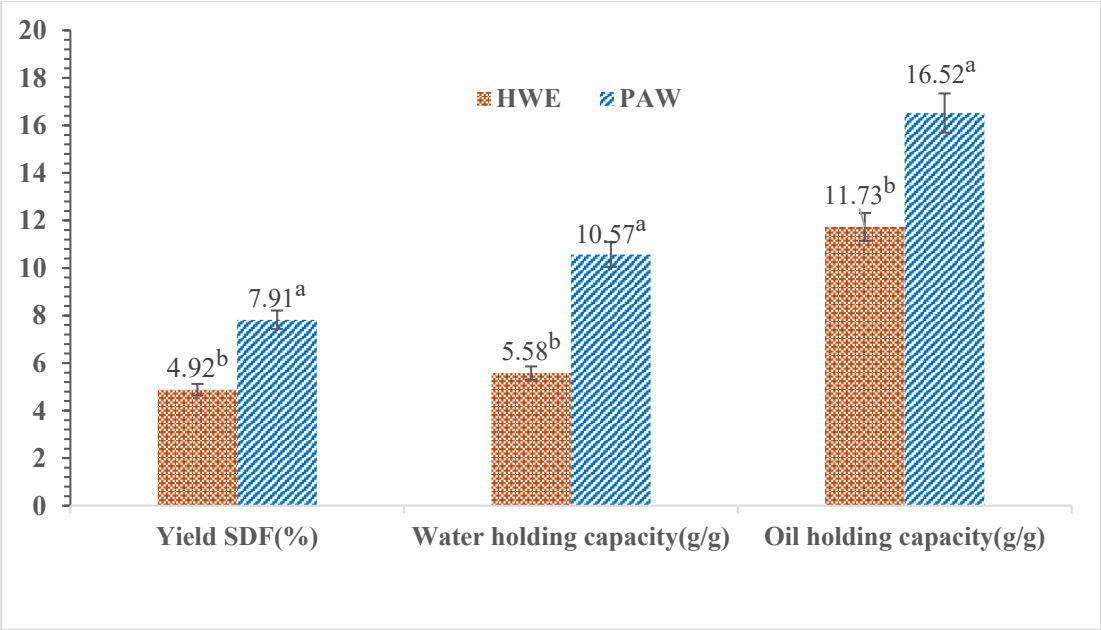

Figure 2. Yield and functional properties of SDF extracted from edamame hulls by HWE and PAW. Values are expressed as mean ± SD (n = 3). Different lowercase letters indicate significant differences (one-way ANOVA, $p < 0.05$).

3.4. Scanning Electron Microscopy

The microstructural characteristics of SDF extracted from edamame hulls using HWE and PAW were examined by SEM at magnifications of 500X and 5000X, as shown in Figure 3. At 500X magnification, the HWE-treated sample exhibited relatively large, compact, and sheet-like structures with smooth surfaces and limited fragmentation. These morphological features suggest that conventional HWE caused minimal disruption to the plant cell wall matrix, resulting in fiber aggregates with lower surface area and fewer exposed functional groups.

In contrast, the PAW-treated sample displayed pronounced fragmentation and particle dispersion at the same magnification [23]. The fiber particles appeared smaller, irregularly shaped, and more loosely aggregated, indicating that PAW treatment effectively disrupted the rigid lignocellulosic structure of edamame hulls. This enhanced disintegration is likely attributed to the reactive oxygen and nitrogen species (RONS) generated in PAW, which can partially cleave glycosidic bonds and weaken hydrogen bonding within cellulose and hemicellulose networks. Consistent findings have been reported in previous studies, where plasma-activated water promoted structural modification and enhanced the extraction efficiency of polysaccharides from biological materials [23].

At higher magnification (5000X), the microstructural differences between the two treatments became more evident. The HWE sample exhibited a relatively dense and continuous surface with limited porosity, characterized by thick fiber walls and fewer void spaces. Such compact morphology may restrict water and oil penetration, thereby limiting the functional properties of the extracted fiber.

Conversely, the PAW-treated sample showed a highly porous, rough, and sponge-like structure with numerous micro-pores distributed across the fiber surface. The increased porosity and surface roughness suggest significant cell wall erosion and internal structural collapse induced by PAW treatment. The formation of a porous structure increases the specific surface area of the fiber matrix, which facilitates greater water and oil entrapment within the porous network. In addition, the rough and irregular surface may enhance capillary retention, thereby improving the ability of the fiber to retain moisture and oil. Such structural modifications have also been reported in dietary fibers subjected to various physical and non-thermal treatments, which can enhance the accessibility of functional groups and improve hydration-related functional properties [26]. These structural modifications enhance the accessibility of hydrophilic functional groups (e.g., hydroxyl and carboxyl groups), which are crucial for improving WHC and OHC.

Overall, the SEM observations provide strong morphological evidence that PAW pretreatment promotes effective cell wall disruption and structural loosening of edamame hull fibers. These changes are consistent with the observed increases in SDF yield and functional properties. From an application perspective, the sponge-like and porous structure of PAW-extracted SDF may be advantageous in food systems, as it can enhance water and oil retention, contributing to improved texture, moisture stability, and fat-binding properties in fiber-enriched food formulations. These findings support the potential of PAW as an efficient and non-thermal pretreatment technique for valorizing agricultural by-products into functional dietary fiber ingredients.

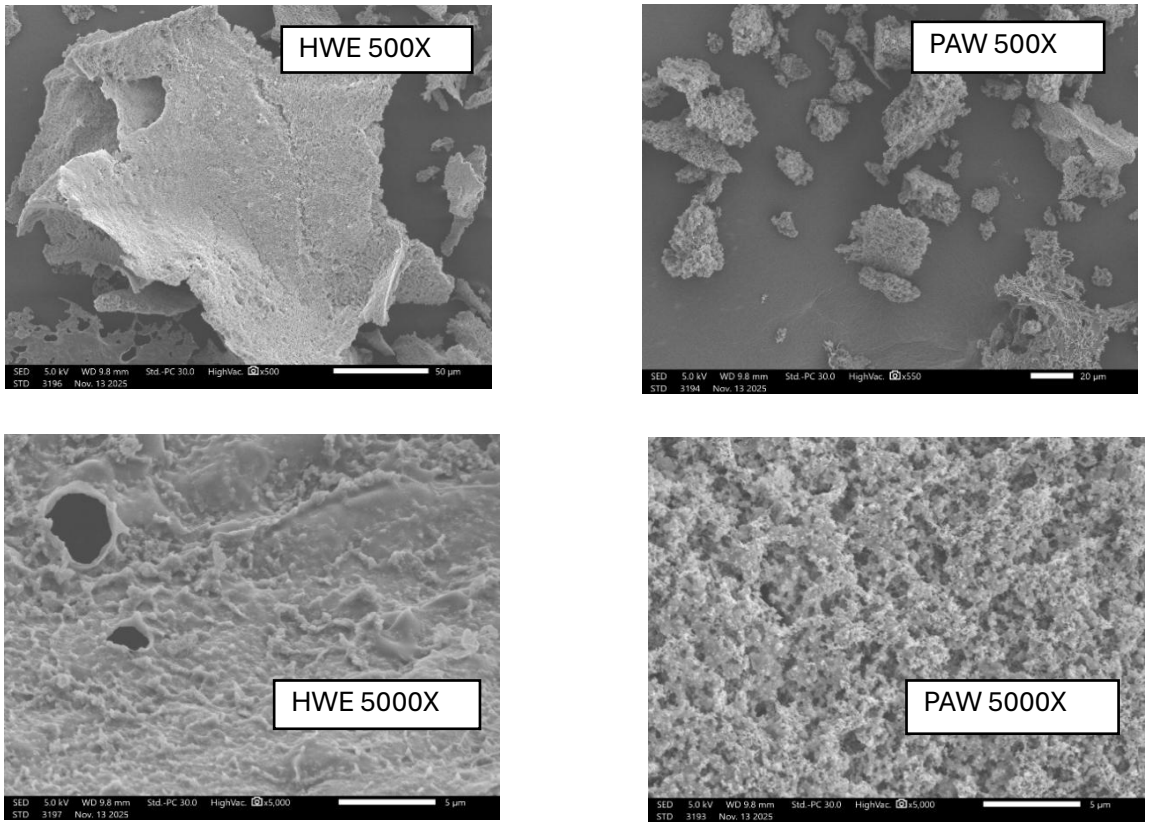

Figure 3. SEM images depicting the powder of hot water extracted SDF (90 ◦C, 3 h, and 1:10 w/v), and the powder of PAW-extracted SDF (1:14.7 w/v, 25 min, and 3.5 L/min). A magnification of 500X and 5,000X was uniformly applied to all samples.

3.5. FT-IR Spectra

FT-IR is used to identify chemical bonds and functional groups on the material's surface, aiding in the characterization of surface modifications upon extraction of SDF. Figure 4 depicts the FT-IR spectra from different samples measured in 4000–400 cm^{-1} region. It is crucial to note that all of the samples' FT-IR spectra exhibited similarity, with no discernible emergence of new peaks after plasma-treated. A broad absorption band observed at approximately 3423 cm^{-1} corresponds to the stretching vibration of hydroxyl (–OH) groups, which are abundant in cellulose, hemicellulose, and pectic substances. The PAW-treated sample exhibited slightly higher transmittance intensity in this region, suggesting enhanced exposure or availability of hydroxyl groups [19]. This phenomenon may result from plasma-induced disruption of intermolecular hydrogen bonding within the fiber matrix, leading to increased accessibility of hydrophilic functional groups.

The absorption band around 2921 cm^{-1} is attributed to C–H stretching vibrations of aliphatic $–CH_2$ and $–CH_3$ groups, commonly present in polysaccharide backbones. No significant shift in this peak was observed between PAW and control samples, indicating that PAW treatment did not cause substantial degradation of the primary carbohydrate backbone.

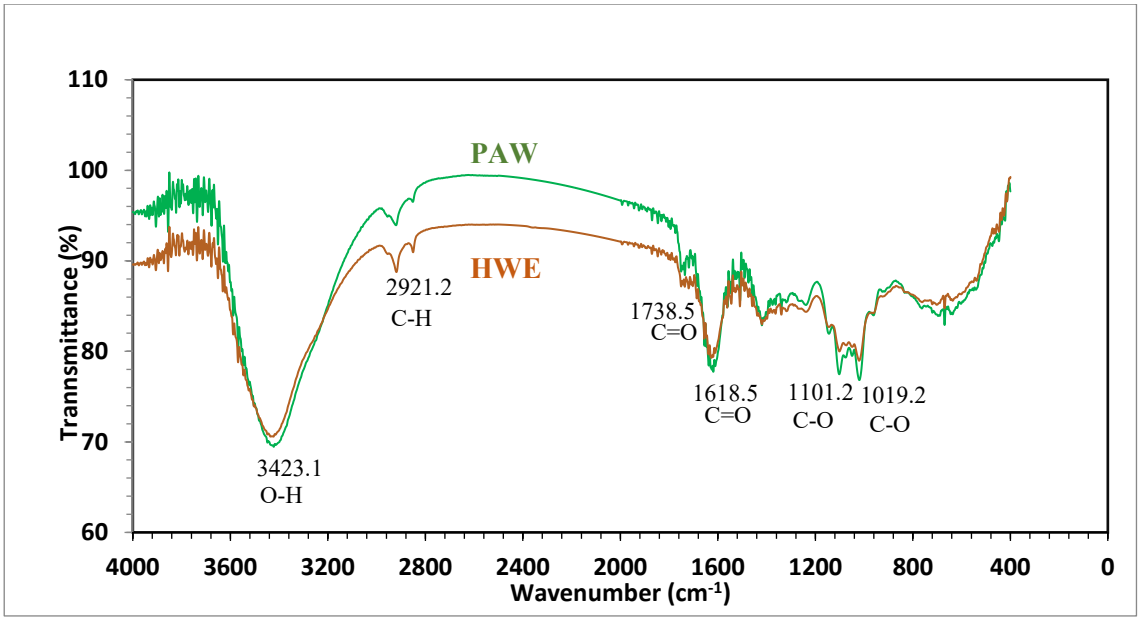

Figure 4. FT-IR spectra of PAW and HWE in the range of 4000 – 400 cm^{-1}

The peak detected at approximately 1738 cm^{-1} corresponds to the stretching vibration of carbonyl (C=O) groups, which are typically associated with esterified carboxyl groups in hemicellulose and pectin. A slight enhancement of this band in the PAW-treated sample suggests partial cleavage of ester linkages or oxidation reactions induced by RONS generated during PAW treatment [25]. Additionally, absorption bands at 1618 cm^{-1} are attributed to asymmetric stretching of carboxylate groups ($–COO^–$), while peaks in the region of 1101–1019 cm^{-1} are characteristic of C–O–C and C–O stretching vibrations associated with glycosidic bonds in polysaccharides. Minor differences in peak intensity between the two samples indicate subtle structural rearrangements rather than chemical decomposition [19].

Overall, the FT-IR results demonstrate that PAW treatment primarily modifies the intermolecular interactions and surface functional group accessibility of SDF without altering its core polysaccharide structure. These structural modifications are consistent with the enhanced functional properties, such as water-holding capacity and oil-holding capacity, observed in PAW-extracted SDF

4. Conclusion

This study confirmed that PAW is an effective non-thermal pretreatment for enhancing SDF extraction from edamame hulls. Optimization using response surface methodology revealed that the solid-to-liquid ratio, treatment time, and gas flow rate significantly affected SDF yield. Under the optimal conditions, the model predicted a maximum SDF yield of 7.82%, while the experimentally validated yield reached 7.91%, confirming the reliability of the developed model. Compared with conventional hot water extraction (HWE), which produced an SDF yield of 4.92%, the PAW-assisted process resulted in an approximately 60.77% increase in SDF yield.

PAW pretreatment also improved the functional properties of SDF, as indicated by increased water- and oil-holding capacities. SEM analysis showed that PAW-treated fibers possessed a more fragmented and porous structure compared to the control, suggesting enhanced cell wall disruption. FT-IR results confirmed increased exposure of hydrophilic functional groups without altering the main polysaccharide backbone. Overall, PAW represents a green and efficient approach for converting edamame hulls into value-added functional dietary fiber ingredients.

References

1. An, N. N., Sun, W. H., Li, B. Z., Wang, Y., Shang, N., Lv, W. Q., Li, D., & Wang, L. J. (2022). Effect of different drying techniques on drying kinetics, nutritional components, antioxidant capacity, physical properties and microstructure of edamame. Food Chemistry, 373, 131412–131423. https://doi.org/10.1016/j. foodchem.2021.131412
2. Islam, M., Zhang, M., & Fan, D. (2019). Ultrasonically enhanced low-temperature microwave-assisted vacuum frying of edamame: Effects on dehydration kinetics and improved quality attributes. Drying Technology, 2087–2104. https://doi.org/ 10.1080/07373937.2018.155823
3. Johnson, D., Wang, S., & Suzuki, A. (2000). Edamame: A vegetable soybean for Colorado. Energy (Kcal), 582, 573–576
4. Kudełka, W., Kowalska, M., & Popis, M. (2021). Quality of soybean products in terms of essential amino acids composition. Molecules, 26(16), 5071–5080. https://doi.org/ 10.3390/molecules2616
5. Church, D. D., Hirsch, K. R., Park, S., Kim, I. Y., Gwin, J. A., Pasiakos, S. M., Wolfe, R. R., & Ferrando, A. A. (2020). Essential amino acids and protein synthesis: Insights into maximizing the muscle and whole-body response to feeding. Nutrients, 12(12), 3717–3731. https://doi.org/10.3390/nu12123717
6. United States Department of Agriculture. (2019). National nutrient database for standard reference release 28. USDA Agric Res Serv.
7. Aleixandre, A., & Miguel, M. (2008). Dietary fiber in the prevention and treatment of metabolic syndrome: A review. Critical Reviews in Food Science and Nutrition, 48(10), 905–912. https://doi.org/10.1080/10408390701761886
8. Bader Ul Ain, H., Saeed, F., Ahmed, A., Asif Khan, M., Niaz, B., & Tufail, T. (2019). Improving the physicochemical properties of partially enhanced soluble dietary fiber through innovative techniques: A coherent review. Journal of Food Processing and Preservation, 43(4), e13917–e13929. https://doi.org/10.1111/jfpp.13917
9. Gunness, P., & Gidley, M. J. (2010). Mechanisms underlying the cholesterol-lowering properties of soluble dietary fibre polysaccharides. Food & Function, 1(2), 149–155. https://doi.org/10.1039/C0FO00080A
10. Xie, F., Wang, Y., Wu, J., & Wang, Z. (2016). Functional properties and morphological characters of soluble dietary fibers in different edible parts of Angelica keiskei. Journal of Food Science, 81(9), C2189–C2198. https://doi.org/10.1111/1750- 3841.13399
11. Xie, F., Li, M., Lan, X., Zhang, W., Gong, S., Wu, J., & Wang, Z. (2017). Modification of dietary fibers from purple-fleshed potatoes (*heimeiren*) with high hydrostatic pressure and high pressure homogenization processing: A comparative study. Innovative Food Science & Emerging Technologies, 42, 157–164. https://doi.org/ 10.1016/j.ifset.2017.05.012
12. P´erez-Lopez, ´ E., Cela, D., Costabile, A., Mateos-Aparicio, I., & Rup´erez, P. (2016). In vitro fermentability and prebiotic potential of soyabean Okara by human faecal microbiota. British Journal of Nutrition, 116(6), 1116–1124. https://doi.org/ 10.1017/S0007114516002816
13. He, Y., Wang, B., Wen, L., Wang, F., Yu, H., Chen, D., Su, X., & Zhang, C. (2022). Effects of dietary fiber on human health. Food Science and Human Wellness, 11(1), 1–10. https://doi.org/10.1016/j.fshw.2021.07.001
14. Robin, F., Schuchmann, H. P., & Palzer, S. (2012). Dietary fiber in extruded cereals: Limitations and opportunities. Trends in Food Science & Technology, 28(1), 23–32. https://doi.org/10.1016/j.tifs.2012.06.008
15. Marlett, J. A., McBurney, M. I., & Slavin, J. L. (2002). Position of the American dietetic association: Health implications of dietary fiber. Journal of the American Dietetic Association, 102(7), 993–1000. https://doi.org/10.1016/S0002-8223(02)90228-2

16. Mudgil, D. (2017). The interaction between insoluble and soluble fiber. In Dietary fiber for the prevention of cardiovascular disease (pp. 35–59). Academic Press. https://doi.org/10.1016/B978-0-12-805130-6.00003-3
17. Figuerola, F., Hurtado, M. L., Est´evez, A. M., Chiffelle, I., & Asenjo, F. (2005). Fibre concentrates from apple pomace and citrus peel as potential fibre sources for food enrichment. Food Chemistry, 91(3), 395–401. https://doi.org/10.1016/j.foodchem.2004.04.036
18. Sojithamporn, P., Leksakul, K., Saikum, C., Jaipinta, S., & Sawangrat, C. (2025). Optimization of pinhole plasma jet for reactive nitrogen species generation in plasma-activated water and its application in microgreen cultivation. Journal of Industrial and Engineering Chemistry, 151, 788–801.
19. Yu, D., Yang, Z., Jin, Q., Wang, H., Duncan, S., Yin, Y., Zhang, B., O'Keefe, S., & Huang, H. (2025). Production and properties of soluble dietary fiber from edamame shell using combined physical and chemical treatments. ACS Food Science & Technology. https://doi.org/10.1021/acsfoodscitech.5c00248
20. Barbosa, J. R., Freitas, M. M. S., Oliveira, L. C., Martins, L. H. S., Almada-Vilhena, A. O., Oliveira, R. M., Pieczarka, J. C., Brasil, D. S. B., & Carvalho Junior, R. N. (2020). Obtaining extracts rich in antioxidant polysaccharides from the edible mushroom *Pleurotus ostreatus* using binary system with hot water and supercritical CO_2. Food Chemistry, 330, 127173. https://doi.org/10.1016/j.foodchem.2020.127173
21. Wang, C.-Y. (2020). A review on the potential reuse of functional polysaccharides extracted from the by-products of mushroom processing. Food and Bioprocess Technology, 13, 217–228. https://doi.org/10.1007/s11947-019-02356-5
22. López-Marcos, M. C., Bailina, C., Viuda-Martos, M., Pérez-Alvarez, J. A., & Fernández-López, J. (2015). Properties of dietary fibers from agroindustrial coproducts as source for fiber-enriched foods. Food and Bioprocess Technology, 8, 2400–2408. https://doi.org/10.1007/s11947-015-1591-z
23. Punthi F, Yudhistira B, Gavahian M, Chang CK, Husnayain N, Hou CY, Yu CC, Hsieh CW. Optimization of plasma-activated water extraction of *Pleurotus ostreatus* polysaccharides on its physiochemical and biological activity using response surface methodology. Foods. 2023;12(23):4347. doi:10.3390/foods12234347.
24. Song Y, Shi Y, Liu Y, Ma Y, Lin C, Nie N, Song X, Yang J. Physicochemical properties of soluble dietary fiber from passion fruit peel based on various extraction methods. Agriculture. 2025;15(1):44. doi:10.3390/agriculture15010044.
25. Rashid, F., Bao, Y., Ahmed, Z., & Huang, J.-Y. (2020). Effect of high voltage atmospheric cold plasma on extraction of fenugreek galactomannan and its physicochemical properties. Food Research International, 138, 109776. https://doi.org/10.1016/j.foodres.2020.109776
26. Jin, T.; Zhou, Z.; Zhou, J.; Ouyang, W.; Wu, Z. The Potential Effects of Dielectric Barrier Discharge Plasma on the Extraction Efficiency of Bioactive Compounds in Radix paeoniae alba. Front. Nutr. 2021, 8, 735742. https://doi.org/10.3389/fnut.2021.735742

P - 327

Comparative Effects of Finasteride and Minoxidil on Sperm Quality and Histological Changes in the Reproductive Organs of Male Mice with Testosterone-Induced Alopecia

Watcharapond Kantarun, Kanokporn Saenphet, Supap Saenphet, Wararut Buncharoen*

Department of Biology, Faculty of Science, Chiang Mai University, Chiang Mai Thailand 50200, Thailand

**Corresponding author E-mail: wararut.bun@cmu.ac.th*

Abstract: **:** Finasteride and minoxidil are widely used as treatment for androgenetic alopecia (AGA), yet their potential adverse effects on the male reproductive system remain a concern. Although these drugs are applied topically, systemic absorption has been reported, which may lead to unintended effects on reproductive endocrine and spermatogenic function. Finasteride inhibits 5α-reductase, reducing androgen conversion and potentially impairing fertility, whereas minoxidil exerts systemic vasodilatory effects. This study compared the effects of finasteride and minoxidil on sperm quality and histopathological changes in male reproductive organs in a testosterone-induced AGA mouse model. Male mice were randomly assigned to four groups (n=6 per group): normal control, AGA model (negative control), finasteride-treated, and minoxidil-treated groups. AGA was induced by subcutaneous injection of 3.5 mg/kg testosterone propionate, while normal control received olive oil. Thirty minutes after induction, finasteride and minoxidil were topically applied to the two treatment groups, and vehicle solution (propylene glycol: ethyl alcohol: water) was applied to control groups for 28 consecutive days. Finasteride significantly reduced (p<0.05) the relative seminal vesicle weight (7.20±1.17 g/100g) compared with both the AGA model (10.30±1.26 g/100g) and normal control (9.54±1.57 g/100g). No significant differences (p>0.05) were observed in testicular and epididymal weights among groups. Both finasteride and minoxidil significantly decreased (p<0.05) sperm concentrations (6.11±1.81 and 6.95±3.80 million cells/mL, respectively), compared with the AGA model (25.14±7.22 million cells/mL) and normal control (29.78±7.90 million cells/mL) groups. Additionally, both drugs increased the percentage of immotile sperm, reduced non-progressive motility, and elevated sperm head abnormalities. However, histopathological analysis revealed no major structural changes in the testes, epididymis, or seminal vesicles; however, finasteride and minoxidil significantly impaired sperm concentration, motility, and morphology. Germ cell exfoliation in seminiferous tubules and epithelial detachment in prostatic acini were observed in treated groups. These findings indicate that finasteride and minoxidil adversely affect sperm quality and induce subtle histopathological alterations in male reproductive organs. These findings enhance understanding of how anti-alopecia medications may influence male reproductive function and suggest potential implications for long-term topical use in humans, warranting further clinical evaluation.

Keywords: Androgenetic alopecia; Finasteride; Minoxidil; Reproductive System; Sperm

1. Introduction

Androgenetic alopecia (AGA) is the most prevalent form of hair loss in men and is primarily driven by genetic predisposition and heightened sensitivity of hair follicles to androgens, particularly dihydrotestosterone (DHT). Elevated DHT levels promote follicle miniaturization and shorten the anagen phase of the hair growth cycle, ultimately leading to progressive hair thinning [1]. Finasteride and minoxidil remain the most widely approved pharmacological treatments for

AGA, owing to their well-documented efficacy in reducing hair loss and stimulating hair regrowth [2,3]. Finasteride exerts its therapeutic effect by inhibiting 5α-reductase, thereby preventing the conversion of testosterone to DHT. While suppression of DHT is beneficial for hair follicles, concerns have emerged regarding finasteride-associated adverse effects on the male reproductive system, including reduced libido, decreased semen volume, and potential fertility impairment in susceptible individuals [4,5]. In contrast, topical minoxidil has been reported to undergo limited systemic absorption (approximately 1.4% of the applied dose) and is metabolized to its active form, minoxidil sulfate, providing a mechanistic basis for possible physiological effects beyond the scalp, although these effects are generally considered minimal [6]. These finding have raised critical questions about the reproductive safety of prolonged finasteride use. Minoxidil, in contrast, is primarily administered as a topical agent and is believed to promote hair growth via vasodilation and enhanced scalp microcirculation, although its precise molecular mechanisms remain incompletely understood [7]. Although generally considered safe, accumulating evidence suggests that topical minoxidil may undergo systemic absorption, potentially eliciting physiological effect beyond the scalp. Previous studies have reported possible alterations in testicular blood flow and sperm quality following minoxidil exposure. Moreover, experimental studies in male rats have demonstrated that prolonged topical application of minoxidil may induce adverse changes in the male reproductive system, including reductions in reproductive organ weights, decreased sperm motility, and histopathological alterations of the seminiferous epithelium, potentially mediated by oxidative stress. Collectively, these findings suggest that, despite its topical route of administration, long-term minoxidil exposure may influence male reproductive function [8]. However, the available data are limited, heterogeneous, and inconclusive [9,10].

Importantly, both finasteride and minoxidil may influence male reproductive function either directly through hormonal modulation or indirectly via vascular, endocrine, or cellular pathways. Despite their widespread and often long-term use, systematic evaluations comparing their reproductive effects under controlled experimental conditions remain scarce. In particular, comprehensive assessments of sperm parameters and histopathological alterations in male reproductive organs are lacking, representing a critical gap in current knowledge. Experimental rodent models provide a well-established and ethically appropriate platform for investigating drug-induced reproductive toxicity, allowing detailed examination of spermatogenesis, reproductive organ integrity, and underlying histopathological changes that cannot be readily assessed in human studies. Data derived from such models are essential for elucidating potential mechanisms of reproductive toxicity and for generating translational insights relevant to human health risk assessment.

Therefore, the present study aimed to systematically evaluate and compare the effects of finasteride and minoxidil on sperm quality and histopathological changes in male reproductive organs using a testosterone-induced AGA mice model. We hypothesized that subchronic exposure to these agents may differentially affect spermatogenic function and reproductive tissue integrity. The findings of this study are expected to provide critical baseline data and mechanistic insight into the reproductive safety profiles of finasteride and minoxidil, thereby supporting informed clinical decision-making and guiding future investigations into the long-term reproductive implications of AGA pharmacotherapy.

2. Materials and Methods

2.1 Animals grouping and Treatment

Six-week-old male C57BL/6NJcL mice were purchased from Nomura Siam International, Bangkok, Thailand, and were acclimatized in the laboratory for one week before start of the experiment. The animals were maintained under standard laboratory conditions with a 12-hour light/dark cycle and a constant temperature of 25 ± 1°C. Mice were allowed ad libitum access to

water and food during the acclimatization period. All experimental procedure were reviewed and approved by the Institutional Animal Care and Use Committee in the Department of Biology, Faculty of Science, Chaing Mai University (ID: Re. 003/24).

2.2 Experimental Design

The mice were randomly divided into four groups, each consisting of six animals: the normal control group, an AGA model (negative control) group, a finasteride-treated group, and a minoxidil-treated groups. The hair on the dorsal skin of all mice was removed over an area of 2 x 2 cm^2. squrecentrimeters. AGA was induced in the experimental groups by subcutaneous injection of testosterone propionate at a dose of 3.5 mg/kg, whereas the normal control group received olive oil subcutaneously. Thirty minutes after induction, mice in the treatment groups were topically treated with finasteride (1 mg/kg) or minoxidil (10 mg/kg) once daily for 28 consecutive days on the shaved dorsal area. The control groups received the vehicle solution (propylene glycol: ethyl alcohol: water).

At the end of the experimental period, the body weights of mice were recorded, and the animals were sacrificed. Reproductive organs including the testes, epididymis, seminal vesicles, and prostate gland, were carefully collected, the surrounding fat and removed, and the organs were weighted. Right epididymis from mice of each group was used to evaluate sperm parameters. All collected reproductive organs were fixed in 10 % neural buffered formalin for histological examination.

2.3 Relative weight of male reproductive organs

The relative weights of the reproductive organs of mice, including testes, epididymis, seminal vesicles and prostate gland, were calculated using the following formula [11]:

$$\text{Relative organ weight (\%)} = \left(\frac{\text{Organ weight (g)}}{\text{Body weight (g)}}\right) \times 100$$

2.4 Sperm collection and sperm quality analysis

Sperm parameters, including concentration, motility, viability, and morphology, were evaluated as previously described, following standard laboratory procedures [12]. In brief, the right cauda epididymis was minced in 10 mL of Krebs–Henseleit solution until a cloudy, whitish fluid was visibly released. The mixture was then thoroughly mixed to obtain a sperm suspension [13]. The suspension was subsequently used to evaluate sperm concentration, viability, motility, and morphology.

2.4.1 Sperm concentration

The number of epididymal sperm was determined according to the WHO manual [12,14]. A 10 µL of the sperm suspension prepared in section 2.4 was transferred to a hemocytometer and counted under a light microscope (Olympus CX31) at 400x magnification. The procedure was performed in duplicate for each mouse in each group, and the concentration of sperm was calculated accordingly, and recorded in million cell per milliliter.

2.4.2 Sperm viability

Trypan blue staining was used to assess sperm viability. In the trypan blue exclusion technique, spermatozoa with intact plasma membranes exclude the dye, whereas nonviable sperm with compromised membranes take up the dye and appear blue [13]. Briefly, an aliquot of the sperm suspension (10 µL) was gently mixed with 0.4 % trypan blue solution at a ration of 1:1 v/v. The

mixture was incubated at room temperature for 3 min to allow adequate staining. A drop of the stained suspension was then placed on a clean glass slide, covered with a coverslip, and examined under a light microscope (Olympus CX31) at 400x magnification. A 200 spermatozoa per sample were counted. Unstained sperm were identified as viable, whereas blue-stained sperm were classified as nonviable. Sperm viability was expressed as the percentage of viable sperm relative to the total number of sperm counted.

2.4.3 Sperm motility

For the assessment of sperm motility, an aliquot of 100 µL of the sperm suspension was placed onto a clean glass slide, covered with a coverslip, and examined under a light microscope (Olympus CX31) at 10× magnification. A total of 200 spermatozoa per sample were evaluated using a cell counter. Sperm motility was expressed as a percentage and classified into progressive, nonprogressive, immotile, and circular movements [15].

2.4.4 Sperm morphology

For sperm morphology analysis, an aliquot of the sperm suspension was pipetted onto a glass slide and smeared evenly over the slide surface. The smeared slide was air-dried, fixed, and stained using Wright-Giemsa staining. A total of 2000 spermatozoa per sample were evaluated for normal and abnormal morphology under a light microscope (Olympus CX31) at 1000x magnification. Abnormal spermatozoa were classified into head defects, tail defects, and combine head and tail defects [15].

2.5 Histopathological examinations

Histological examination of the reproductive organs of mice was performed according to our previous study [16]. The tissues were fixed in 10% neutral buffered formalin for 48 h and routinely processed by dehydration through ascending grades of alcohol, clearing in xylene, and embedding in paraffin (Paraplast®). The embedded tissues were sectioned at a thickness of 6 µm using a rotary microtome. The tissue sections were then deparaffined through an alcohol-xylene series and stained with hematoxylin and eosin (H&E). The stained tissue sections were examined under a light microscope (Olympus BX61) to assess histological alterations.

2.6 Statistical Analysis

The data are expressed as mean ± standard deviation (SD). Statistical analysis was performed using one-way analysis of variance (one-way ANOVA) followed by Duncan's test for post hoc comparisons. All statistical analyses were performed using SPSS for Windows, Version 26, and a p-value < 0.05 was considered statistically significant.

3. Results & Discussion

3.1 Effect of testosterone-induced AGA on relative reproductive organ weights

To assess the effects of topical finasteride and minoxidil on androgen-dependent organs in a testosterone-induced AGA model, the relative weights of four male reproductive organs-testes, epididymis, seminal vesicles, and prostate-were evaluated. Repeated subcutaneous administration of testosterone propionate (3.5 mg/kg) for 28 consecutive days did not significant alter ($p > 0.05$) the relative weights of any reproductive organs when compared with normal control mice (Table 1). These findings indicate that the selected dose and duration of testosterone exposure were sufficient to induce androgen-dependent response in the skin and hair follicle, but not strong enough to elicit measurable changes in reproductive organ mass. AGA is primarily driven by tissue-specific androgen sensitivity rather than systemic androgen overload. Hair follicles express high levels of androgen receptors and 5α-reductase, making them particularly susceptible to DHT, whereas reproductive organs are physiologically adapted to high endogenous androgen

concentrations. Consequently, moderate exogenous androgen exposure over a relative short duration may not disrupt reproductive organ weight homeostasis. Moreover, testicular and epididymal weights are tightly regulated and typically require prolonged or supraphysiological androgen exposure to exhibit measurable changes [17].

Consistent with this interpretation, topical minoxidil treatment did not induced significant changes in the relative weights of testes, epididymis, seminal vesicle, or prostate gland when compared with either the negative control or normal control groups. This observation agrees with the pharmacological profile of minoxidil, which lacks anti-androgenic activity and primarily exerts local vasodilatory and hair follicle-stimulating effects [4]. In contrast, topical finasteride treatment resulted in a significant reduction ($p < 0.05$) in the relative weights of seminal vesicles when compared with both the negative control and normal control groups, whereas the relative weights of testes, epididymis, and prostate gland remained unchanged. Given that seminal vesicles are highly dependent on androgen and DHT signaling, this finding suggests that they particularly sensitive to mild androgen suppression induced by 5α-reductase inhibition, even in the absence of overt changes in other androgen-responsive organs.

The reduction in seminal vesicle weight following finasteride treatment, while prostate weight remained unchanged, may reflect the differential sensitivity of these androgen-dependent organs to dihydrotestosterone (DHT). Seminal vesicles rely strongly on androgen signaling for growth and secretory function [18,19]. Therefore, inhibition of DHT production by finasteride, a 5α-reductase inhibitor, may reduce androgenic trophic support and lead to decreased seminal vesicle weight. In contrast, the prostate may still receive sufficient stimulation from circulating testosterone, which can activate androgen receptors even when DHT levels are reduced. Additionally, morphological or weight changes in the prostate often require longer periods of androgen suppression. Consistent with this, previous studies have reported that androgen deficiency conditions preferentially reduce the weight of accessory reproductive glands, particularly the seminal vesicles [20,21].

Table 1. Relative weights of the reproductive organs of testosterone-induced AGA mice treated with minoxidil and finasteride compared with the control group.

Groups	Relative weight (g/100 g BW)			
	Testes	Epididymis	Seminal vesicle	Prostate gland
Normal control	8.91±0.52^{b}	3.35±0.27^{a}	9.54±1.57^{b}	1.12±0.38^{a}
Negative control	8.40±0.79^{ab}	3.47±0.66^{a}	10.30±1.26^{b}	1.14±0.24^{a}
Minoxidil	8.34±0.52^{ab}	3.46±0.24^{a}	10.91±1.46^{b}	1.27±0.30^{a}
Finasteride	7.77±0.43^{a}	3.35±0.29^{a}	7.20±1.17^{a}	0.90±0.27^{a}

Values are presented as mean ± S.D. of six mice per group. Superscript letters indicate statistically significant differences at $p<0.05$ according to Duncan's test.

3.2 Effects on sperm parameters

Induction of AGA by repeated testosterone propionate administration did not result in significant changes ($p>0.05$) in sperm concentration, viability, motility, or morphology compared with the normal control group (Table 2 and Figure 1). These results indicate that the testosterone-induced AGA model produced localized dermatological effects without impairing spermatogenesis or sperm functional integrity. Spermatogenic processes are maintained by tightly regulated intratesticular androgen levels, and moderate exogenous androgen exposure over 28 days is unlikely to disrupt sperm quality. In contrast, topical treatment with either finasteride or minoxidil significantly reduced ($p<0.05$) sperm concentration in AGA-induced mice compared with the negative control group, while sperm viability remained unchanged. Preservation of sperm

viability suggests that neither treatment exerted direct cytotoxic effects on spermatozoa or compromised plasma membrane integrity. Instead, the reduction in sperm concentration likely reflects subtle effects on sperm production, release, or epididymal transit rather than direct sperm cell damage.

The effect of finasteride on sperm concentration is biologically plausible, as finasteride inhibits 5α-reductase and reduces the conversion of testosterone to DHT-an androgen involved in the maintenance of normal spermatogenesis [6,22]. Although finasteride was applied topically, partial systemic absorption may have occurred, leading to modest reductions in tissue-specific DHT levels and, consequently, reduced sperm output. In contrast, minoxidil dose not possess anti-androgenic activity, and its effect on sperm concentration may be mediated directly through alterations in the testicular or epididymal microenvironment without affecting sperm viability [4].

Notably, only finasteride significantly reduced (p<0.05) the proportion of sperm exhibiting non-progressive motility compared with both negative and normal control groups, while progressive motility and sperm morphology were not affected. This selective on motility pattern may reflect subtle androgen-dependent modulation of sperm maturation or epididymal function rather than structural abnormalities of spermatozoa. The absence of morphological abnormalities across all groups further supports the conclusion that neither testosterone-induced AGA nor topical treatments caused overt spermatogenic toxicity.

The potential effects of minoxidil on the male reproductive system may be related to its vasodilatory properties. The active metabolite, minoxidil sulfate, acts as an ATP-sensitive potassium channel opener that relaxes vascular smooth muscle and increases peripheral blood flow [23]. Such alterations in microcirculation may also occur in the testes and epididymis, potentially influencing the physiological environment required for spermatogenesis and sperm maturation. Because the epididymis plays a critical role in sperm maturation and the acquisition of motility, disturbances in its microenvironment could affect sperm function [24]. Supporting this interpretation, experimental studies in rodents have reported that minoxidil exposure can induce changes in testicular structure and sperm parameters, likely through indirect effects on local tissue regulation rather than through direct anti-androgenic activity [25].

Table 2. Concentration and viability of epididymal sperm of testosterone-induced AGA mice and treated with minoxidil and finasteride compared with the control group.

Groups	Sperm concentration (x10^6 cells/mL)	Viability (%)
Normal control	29.78±7.90^a	50.21±4.00^a
Negative control	25.14±7.22^a	50.92±7.21^a
Minoxidil	6.95±3.80^b	48.58±7.51^a
Finasteride	6.11±1.81^b	51.98±6.98^a

Values are expressed as mean ± S.D. Superscript letters indicate statistically significant differences at p<0.05 according to Duncan's test.

Table 3. Motility of epididymal sperm of testosterone-induced AGA mice and treated with minoxidil and finasteride compared with the control group.

Groups	Sperm motility (%)			
	progressive	non-progressive	immotile	circle
Normal control	2.50±2.92^a	43.70±8.74^b	53.75±10.72^a	0.00±0.0^a
Negative control	0.50±0.87^a	32.67±3.69^{ab}	65.67±5.75^{ab}	1.17±1.61^a
Minoxidil	1.75±2.06^a	24.88±3.94^a	71.25±4.17^{ab}	2.25±1.04^a
Finasteride	2.63±3.20^a	19.63±16.50^a	75.75±20.52^b	1.50±1.91^a

Values are presented as mean ± S.D. Superscript letters indicate statistically significant differences at p<0.05 according to Duncan's test.

Table 4. Morphology of sperm of testosterone-induced AGA mice and treated with minoxidil and finasteride compared with the control group.

Groups	Sperm morphology (%)		
	Normal	Head-abnormality	Tail-abnormality
Normal control	89.17±2.31[a]	2.58±1.31[a]	8.25±1.16[a]
Negative control	88.50±2.07[a]	3.35±0.96[ab]	8.15±3.00[a]
Minoxidil	87.60±1.93[a]	4.60±1.14[b]	7.80±1.27[a]
Finasteride	87.25±2.46[a]	4.75±0.68[b]	8.00±2.09[a]

Values are expressed as mean ± S.D. Superscript letters indicate statistically significant differences at $p<0.05$ according to Duncan's test.

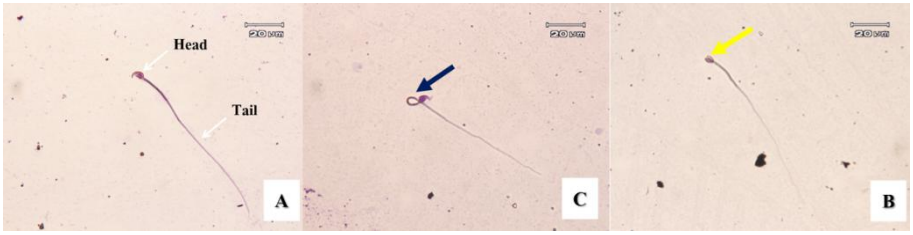

Figure 1. Normal (A) and abnormal sperm (B-C) morphology of testosterone-induced AGA mice and treated with minoxidil and finasteride. H&E stain, 400× magnification
(head-abnormality, tail-abnormality)

3.3 Histological finding of reproductive organs

Histological examinations of reproductive organs are presented in Figure 2-8. Repeated subcutaneous injection of testosterone propionate did not induce detectable histopathological alterations in the testes, epididymis, seminal vesicles, or prostate gland of when compared with normal control mice. Seminiferous tubules exhibited normal germ cell organization, and no evidence of inflammation or structural disruption was observed accessory reproductive organs. These findings are consistent with sperm parameter results, confirming that testosterone-induce AGA alone did not impair male reproductive structure or function. In contrast, topical treatment with finasteride and minoxidil resulted in mild but distinct histopathological changes in the testes and prostate gland. Both treatments were associated with detachment and sloughing of germ cells into the seminiferous tubule lumen (Figure 2-3). Such alterations suggest disruption of seminiferous epithelial integrity and early impairment of Sertoli-germ cell junctions rather than overt germ cell loss or tubular degeneration. These changes are compatible with the observed reduction in sperm concentration, as impaired germ cell adhesion and spermiation efficacy may reduce sperm release without affecting sperm viability or morphology. Previous studies have reported more severe testicular alterations following finasteride or minoxidil exposure, including germ cell depletion and seminiferous tubular degeneration [26].

In the prostate gland, leukocyte accumulation within the prostatic lumen was observed in finasteride- and minoxidil-treated mice (Figure 7-8), indicating a localized inflammatory response. In finasteride-treated mice, inhibition of DHT synthesis may disrupt androgen-dependent homeostasis within the prostate, thereby triggering inflammatory changes [27]. Although minoxidil lack anti-androgenetic activity, prolonged topical exposure may indirectly alter local vascular or tissue microenvironments, resulting in similar inflammatory responses. Notably, these changes did not translate into alterations in sperm viability or morphology during the experimental period.

Notably, no histopathological abnormalities were detected in the epididymis or seminal vesicles in finasteride- and minoxidil-treated mice (Figure 4-6). The absence of histological alterations in these organs suggests that the epididymal and seminal vesicles are less susceptible to the effects of topical finasteride and minoxidil under the experimental conditions employed. This tissue-specific resistance may reflect differences in androgen dependence, local drug bioavailability, or compensatory mechanisms that preserve epididymal function and seminal vesicle integrity. These findings differ from several previous reports. In adult BALB/c mice, treatment with either finasteride or minoxidil has been shown to induce histopathological changes in the epididymis, with finasteride exerting more pronounced effects on epididymal function and sperm transit time than minoxidil [28]. Similarly, morphometric, stereological, and ultrastructural studies in finasteride-treated rats have demonstrated reduced epithelial height and increased ductal lumen diameter, indicative of compromised epididymal integrity and function [29]. Moreover, studies in DHT-deficient models suggest that inhibition of 5α-reductase activity may reduce sperm content within the epididymal lumen, further implicating finasteride in the disruption of epididymal morphology and sperm maturation processes. The absence of epididymal and seminal vesicle pathology in the present study suggests that the dose, route, and duration of topical finasteride and minoxidil administration were insufficient to induce overt structural damage in these tissues. Importantly, sperm viability and morphology remained unchanged in both treatment groups, indicating that the observed reproductive effects were not associated with direct cytotoxic damage to spermatozoa or gross defects in spermatogenesis. Rather, these finding support the notion that finasteride and minoxidil primarily affected sperm output rather than sperm cell quality. Furthermore, preservation of epididymal histoarchitecture across all groups indicate that sperm maturation and storage processes within the epididymis were largely maintained.

Interpretation of these finding is subject to certain limitations. Circulating and intratesticular levels of testosterone, DHT, luteinizing hormone, and follicle-stimulating hormone were not measured. Therefore, direct correlations between hormonal alterations and reproductive outcomes cannot be definitively established. Further studies incorporating comprehensive endocrine profiling, along with molecular markers of Sertoli cell junction integrity and androgen signaling, will be necessary to clarify the mechanisms underlying the subtle reproductive effects observed following topical finasteride and minoxidil treatment.

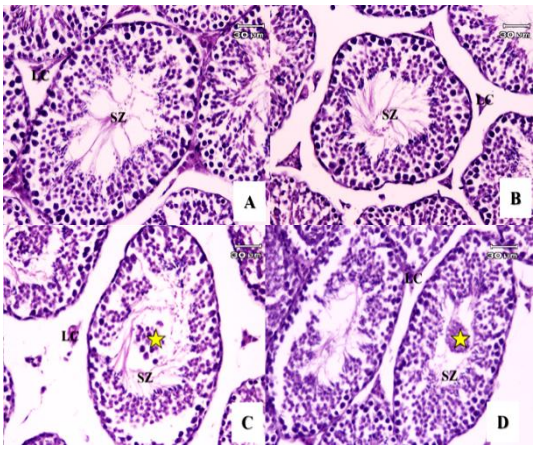

Figure 2 Testicular tissues of testosterone-induced AGA mice (B) treated with finasteride (C) and minoxidil compared (D) with the control groups (A). 100x magnification. H&E stain. LC: Leydig cell, SZ : spermatozoa, ★: sloughing germ cell

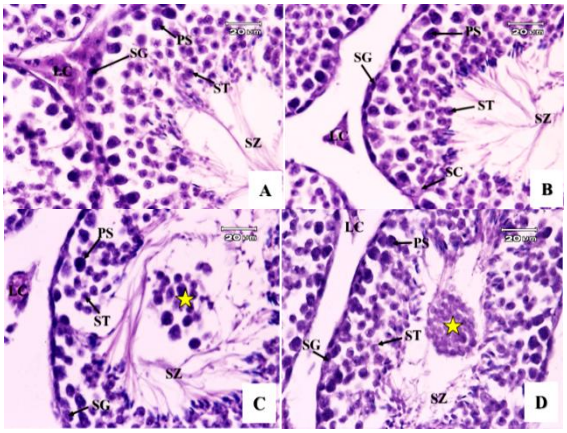

Figure 3. Testicular tissues of testosterone-induced AGA mice (B) treated with finasteride (C) and minoxidil compared (D) with the control groups (A). 400x magnification. H&E stain. LC: Leydig cell, PS: primary spermatocyte, SC: Sertoli cell, SG: spermatogonia, ST: spermatid, SZ: spermatozoa, ★: sloughing germ cell

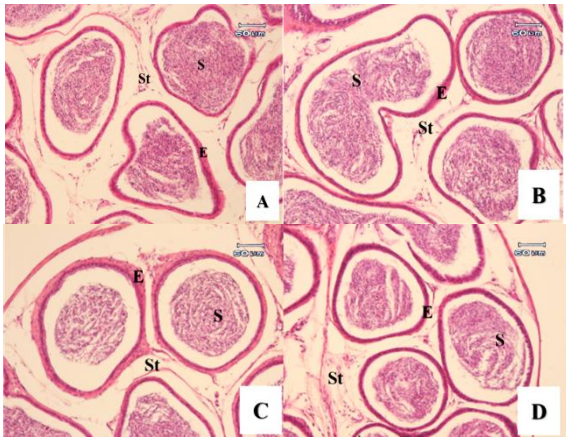

Figure 4. Epididymal tissues of testosterone-induced AGA mice (B) treated with finasteride (C) and minoxidil compared (D) with the control groups (A). 100x magnification. H&E stain. S: epididymal spermatozoa, St: stroma, E: epididymal epithelium

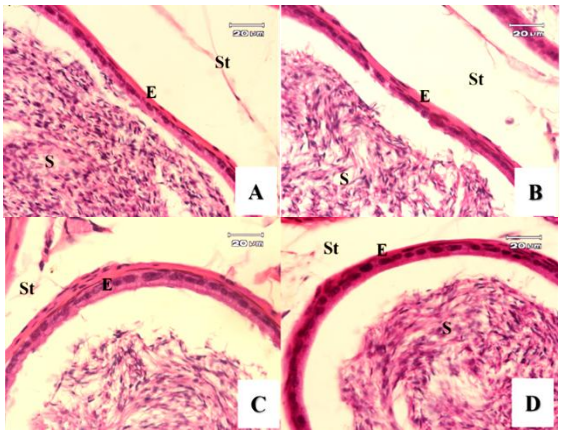

Figure 5. Epididymal tissues of testosterone-induced AGA mice (B) treated with finasteride (C) and minoxidil compared (D) with the control groups (A). 400x magnification. H&E stain. S: epididymal spermatozoa, St: stroma, E: epididymal epithelium

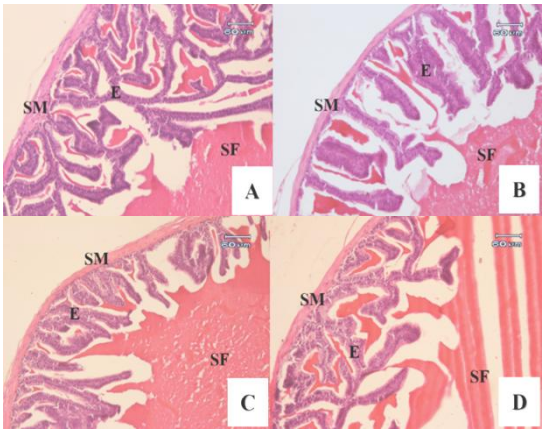

Figure 6. Seminal vesicle tissues of testosterone-induced AGA mice (B) treated with finasteride (C) and minoxidil compared (D) with the control groups (A). 100x magnification. H&E stain. SF: seminal fluid, E: seminal epithelium, SM: smooth muscle

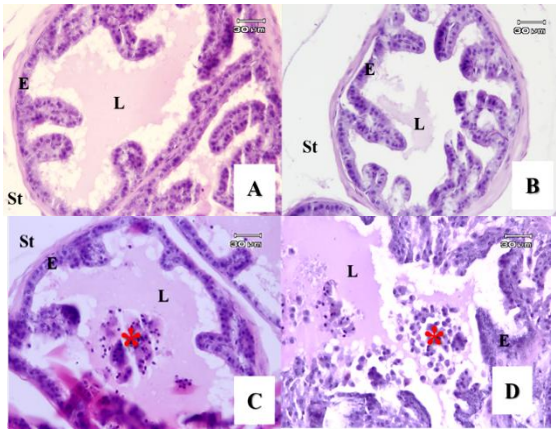

Figure 7. Prostate gland tissues of testosterone-induced AGA mice (B) treated with finasteride (C) and minoxidil compared (D) with the control groups (A). 200x magnification. H&E stain. L: prostatic lumen, St: stroma, E: prostatic epithelium, *: leukocyte infiltration

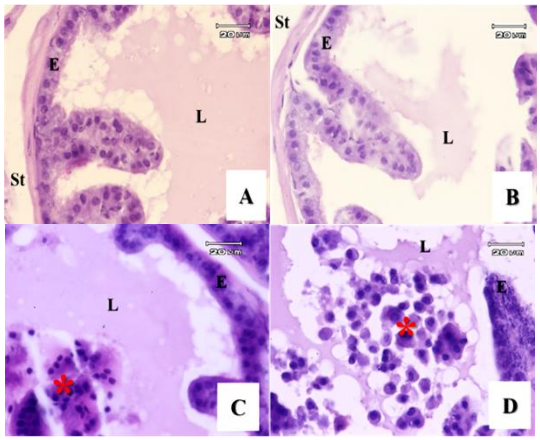

Figure 8. Prostate gland tissues of testosterone-induced AGA mice (B) treated with finasteride (C) and minoxidil compared (D) with the control groups (A). 400x magnification. H&E stain. L: prostatic lumen, St: stroma, E: prostatic epithelium, *: leukocyte infiltration

5. Conclusion

In conclusion, the present findings indicate that topical minoxidil and finasteride exert distinct biological effects on the male reproductive system in testosterone-induced AGA mice. While both treatments reduced sperm concentration and were associated with mild histopathological changes in the testes and prostate gland, finasteride demonstrated greater sensitivity of androgen-dependent endpoints, including a significant reduction in seminal vesicle weight and selective modulation of sperm motility parameters. In contrast, minoxidil produced comparable reductions in sperm concentration without overt-androgenic effects or significant alterations in androgen-dependent organ weights. These differences highlight the divergent mechanisms underlying the reproductive effects of minoxidil and finasteride and underscore the importance of considering tissue-specific androgen regulation when evaluating the reproductive safety of topical anti-alopecia therapies.

Acknowledgements

We would like to thank the Department of Biology, Faculty of Science, Chiang Mai University for supporting facilities. Also thank to Dr. Phornphan Phrompanya and Ms. Panumat Piosinsak for their helps.

References

1. Fu D, Huang J, Li K, Chen Y, He Y, Sun Y, et al. Dihydrotestostrone-induced hair regrowth inhibition by activation androgen receptor in C57BL6 mice simulates androgenetic alopecia. Biomed Pharmacother. 2021;137:111247. 1-12. doi:10.1016/j.biopha.2021.111247.
2. Li Y, Huang Q, Zhou Z, Zhang Y. Comparing minoxidil–finasteride mixed solution with minoxidil solution alone for male androgenetic alopecia: a systematic review and meta-analysis of randomized controlled trials. Front Med. 2025;12:1632139. doi:10.3389/fmed.2025.1632139.
3. Rossi A, Caro G. Efficacy of the association of topical minoxidil and topical finasteride compared to their use in monotherapy in men with androgenetic alopecia: a prospective, randomized, controlled, assessor-blinded, 3-arm, pilot trial. J Cosmet Dermatol. 2024;23(2):502–509. doi:10.1111/jocd.15953.
4. Santana FdFV, Lozi AA, Gonçalves RV, Da Silva J, Da Matta SLP. Comparative effects of finasteride and minoxidil on the male reproductive organs: a systematic review of *in vitro* and *in vivo* evidence. Toxicol Appl Pharmacol. 2023;478:116710. doi:10.1016/j.taap.2023.116710.
5. Pereira AFJR, Coelho TODA. Post-finasteride syndrome. An Bras Dermatol. 2020;95(3):271–277. doi:10.1016/j.abd.2020.02.001.
6. Amory JK, Wang C, Swerdloff RS, Anawalt BD, Matsumoto AM, Bremner WJ, et al. The effect of 5α-reductase inhibition with dutasteride and finasteride on semen parameters and serum hormones in healthy men. J Clin Endocrinol Metab. 2007;92(5):1659–1665. doi:10.1210/jc.2006-2203.
7. Kozicka K, Łukasik A, Pastuszczak M, Dyduch G, Kłosowicz A, Wojas-Pelc A. Scalp vascularization as a marker of topical minoxidil treatment efficacy in patients with androgenetic alopecia. Postepy Dermatol Alergol. 2022;39(2):316–320. doi:10.5114/ada.2021.103301.
8. Turkina V, Chemodurova NY, Grushka OI, Pryzyhley H. Topical effect of minoxidil-containing lotion on morphofunctional indicators of male rats' reproductive system. Ukr J Mod Toxicol Asp. 2020;89(2):27–31. doi:10.33273/2663-4570-2020-89-2-27-31.

9. Santana FdFV. The impact of minoxidil on male reproductive biology: a multi-approach study including systematic review, *in vivo*, and *ex vivo* experiments [thesis]. Universidade Federal de Viçosa. 2025. pp34-38. doi:10.47328/ufvbbt.2025.205
10. Hussein RS, Dayel SB, Abahussein O, El-Sherbiny AA. Applications and efficacy of minoxidil in dermatology. Skin Health Dis. 2024;4(6):e472. doi:10.1002/ski2.472.
11. Thanamool C, Papirom P, Chanlun S, Kupittayanant S. *Talinum paniculatum* (Jacq.) Gertn: a medicinal plant with potential estrogenic activity in ovariectomized rats. In J Pharm Pharm sci. 2013;5(2):478-485.
12. World Health Organization. WHO laboratory manual for the examination and processing of human semen. Geneva: WHO; 2021. pp. 23–63.
13. Laoung-on J, Nuchniyom P, Intui K, Saenphet K, Jaikang C, Sudwan P. Effect of white *Nelumbo nucifera* on Rat sperm motility and Sperm viability. Microsc Microanal Res. 2023;36(1):1–4.
14. Türk G, Sönmez M, Aydin M, Yüce A, Gür S, Yüksel M, et al. Effects of pomegranate juice consumption on sperm quality, spermatogenic cell density, antioxidant activity and testosterone level in male rats. Clin Nutr. 2008;27(2):289–296. doi:10.1016/j.clnu.2007.12.006.
15. Yotarlai S, Chaisuksunt V, Saenphet K, Sudwan P. Effects of *Boesenbergia rotunda* juice on sperm qualities in male rats. J Med Plants Res. 2011;5(16):3861–3867.
16. Sampannang A, Arun S, Burawat J, Sukhorum W, Iamsaard S. Testicular histopathology and phosphorylated protein changes in mice with diabetes induced by multiple-low doses of streptozotocin: an experimental study. Int J Reprod Biomed. 2018;16(4):235–246. PMID: 29942931; PMCID: PMC6004591.
17. Brooks DE. Influence of androgens on the weights of the male accessory reproductive organs and on the activities of mitochondrial enzymes in the epididymis of the rat. J Endocrinol. 1979;82(2):293–303. doi:10.1677/joe.0.0820293.
18. Welsh M, Moffat L, Jack L, McNeilly A, Brownstein D, Saunders PTK, et al. Deletion of androgen receptor in the smooth muscle of the seminal vesicles impairs secretory function and alters its responsiveness to exogenous testosterone and estradiol. Endocrinology. 2010;151(7):3374-85. doi: 10.1210/en.2009-1339. PMID: 20444943; PMCID: PMC3033689.
19. Walker WH, Cooke PS. Functions of steroid hormones in the male reproductive tract as revealed by mouse models. Int J Mol Sci. 2023;24(3):2748. doi:10.3390/ijms24032748. PMID: 36769069; PMCID: PMC9917565.
20. Eriksson ES, Johansson I, Mårtensson AKF, Rodriguez ML, Schilperoort M, Kroon J, et al. Castration of male mice induces metabolic remodeling of the heart. J Endocr Soc. 2022;6(11):bvac132. doi:10.1210/jendso/bvac132. PMID: 36249410; PMCID: PMC9557843.
21. Maekawa K, Sobue A, Komine O, Saito Y, Murayama S, Saido TC, et al. Long-term systemic androgen deprivation partially modulates neuroinflammation in male $App^{NL-G-F/NL-G-F}$ mice. Sci Rep. 2025;15:14702. doi:10.1038/s41598-025-98825-z.
22. Zito PM, Bistas KG, Patel P, et al. Finasteride. StatPearls [Internet]. 2024 [cited 2025 Nov 24] Available from:https://www.ncbi.nlm.nih.gov/books/NBK513329/.
23. Messenger AG, Rundegren J. Minoxidil: mechanisms of action on hair growth. Br J Dermatol. 2004;150(2):186-94. doi: 10.1111/j.1365-2133.2004.05785.x. PMID: 14996087.
24. Robaire B, Hinton BT. The epididymis. In: Plant TM, Zeleznik AJ, editors. *Knobil and Neill's Physiology of Reproduction.* 4th ed. San Diego: Elsevier; 2015. p. 691-771.doi: 10.1016/B978-012515400-0/50027-0

25. Dkhil MA, Zrieq R, Al-Quraishy S, Abdel Moneim AE. Finasteride and minoxidil alter reproductive parameters and testicular histology in male mice. Molecules. 2016;21(1517):479-85. doi:10.3390/molecules21111517.
26. Obaid FN, Jaffat HS. Physiological and histological study of the effect of finasteride drug (Prostacare) on the fertility of albino male rats. Asian J Pharm Clin Res. 2018;11(6):2323–2325. doi:10.5958/0974-360X.2018.00431.6.
27. Gao Y, Wei L, Wang C, Huang Y, Li W, Li T, et al. Chronic prostatitis alters the prostatic microenvironment and accelerates preneoplastic lesions in C57BL/6 mice. Biol Res. 2019;52:30. doi:10.1186/s40659-019-0237-4. PMID: 31088536; PMCID: PMC6518623.
28. Serga CNK. The effect of different doses of finasteride on sperm morphology and motility and reactive oxygen species concentrations in rats. Med J Cairo Univ. 2009;77(1):439–447.
29. Kolasa A, Marchlewicz M, Wenda-Rózewicka L, Wiszniewska B. Morphology of the testis and the epididymis in rats with dihydrotestosterone (DHT) deficiency. Rocz Akad Med Bialymst. 2004;49(Suppl 1):117–119.

P - 330

Production of Alcoholic Beverage from Glutinous Rice

Chatchaya Onumpai[1,2], Matana Bunrueang[2], Sataporn Thongnarin[2], Metinee Maweang[1,2]*

[1]*Indigenous Food Research and Industrial Development Center, Ubon Ratchathani University, Ubon Ratchathani 34190, Thailand*
[2]*Department of Agro-Industry , Faculty of Agriculture, Ubon Ratchathani University, Ubon Ratchathani 34190, Thailand*

**Corresponding author E-mail: metinee.m@ubu.ac.th*

Abstract: A naturally sweet and low-bitterness profile is exhibited by traditional Sato due to its rice-based fermentation system, which limits the incorporation of hop-derived characteristics. To address this limitation, two hop-addition strategies were compared to evaluate their effects on microbial dynamics, biochemical changes, and product quality. Glutinous rice was saccharified using *look-pang* under solid-state fermentation for 3 days, and alcoholic fermentation was carried out with *Saccharomyces cerevisiae*. Hop extract (0.5% w/v) was incorporated by (i) whole-mash fermentation, in which the extract was added to the fermented rice matrix, and (ii) filtered liquid fermentation, in which the extract was mixed into the pressed rice filtrate. Higher populations of yeast and mold, and lactic acid bacteria were observed in whole-mash fermentation, and greater acidification and saccharolytic activity were associated with these increases. Higher ethanol content (10.63±0.05% v/v) was produced in whole-mash fermentation compared with filtered liquid fermentation (8.87±0.04% v/v), and the higher ethanol content observed in whole-mash fermentation may be associated with continued saccharification from residual starch-containing solids and enzymatic activity retained within the mash matrix, although this mechanism was not directly quantified in the present study. Sensory evaluation using a 9-point hedonic scale with 50 untrained consumers indicated higher overall liking for the whole-mash fermented beverage (7.77±1.63) than for the filtered liquid fermented variant (7.16±1.63) ($p < 0.05$). Overall, enhanced ethanol productivity and stronger consumer acceptance were achieved by whole-mash hop-integrated fermentation, while improved process controllability and scalability were offered by filtered liquid fermentation.

Keywords: Sato; Hop extract; Craft alcoholic beverage; Glutinous rice fermentation

1. Introduction

In recent years, a range of innovative rice-derived alcoholic beverages has emerged, including traditional *Sato* and modern variations such as sparkling and flavored *Sato*, as well as rice-based beers. These developments underscore growing interest in rice as a versatile substrate for value-added alcoholic beverage production. Beer is the most widely consumed alcoholic beverage globally, including in Thailand(1), highlighting the potential for hybrid rice–beer products. However, existing literature on rice beer has predominantly focused on rice malting techniques(2-3) or the use of rice malt as an adjunct to barley malt(4) in conventional brewing systems.

In traditional Thai sweet fermented rice production, rice starch is converted into fermentable sugars through the enzymatic activity of mixed microbial consortia in *look-pang*, resulting in *kaomak*. Yeasts can subsequently ferment these sugars into ethanol and a range of flavor-active compounds. Different yeast strains produce distinct profiles and concentrations of volatile and non-volatile metabolites, thereby shaping the sensory characteristics of alcoholic

beverages[5]. The incorporation of ale yeast and hop may further introduce beer-like bitterness and aroma, offering a novel sensory dimension to rice wine and enabling the development of new rice-based alcoholic beverages.

Despite this potential, there is limited comparative evidence regarding the influence of fermentation matrix handling. In particular, the alcoholic fermentation of whole *kaomak* mash (whole-mash fermentation) versus the fermentation of filtered sweet rice liquor (filtered liquid fermentation) may differentially affect (i) chemical composition, (ii) microbial ecology, and (iii) sensory characteristics of the final beverage.

Therefore, the present study compares two fermentation processes—whole mash (whole-mash fermentation) and filtered sweet liquor (filtered liquid fermentation)—in terms of their chemical, microbiological, and sensory profiles. By integrating traditional *look-pang*–based mixed-culture saccharification with commercial yeast and hop additions, this study provides insights into process–flavor design for novel rice-based alcoholic beverages

2. Materials and Methods

2.1 Materials

Glutinous rice (*Oryza sativa* L. var. RD6) was purchased from a local market in Ubon Ratchathani Province, Thailand. A commercial kaomak starter culture (*look-pang*) was obtained from Roi Et Province, Thailand. Dextrose, hop pellets (*Humulus lupulus* L.), and commercial *Saccharomyces cerevisiae* were purchased from Home Brew Co., Ltd. (Thailand).

Hop extract was prepared by boiling dried hop pellets (0.5% w/w) in water for 15 minutes and then filtering the extract through sterile gauze.

2.2 Fermentation processes

Glutinous rice was washed, soaked in water for 3-4 h and steamed for 30 min. After steaming, the cooked rice was cooled to approximately 30 °C before inoculation with the look-pang starter. Saccharification was conducted in a sterile container under ambient laboratory conditions (28–30 °C) for 72 h. Relative humidity was not actively controlled. After incubation, namtoi or the sweet liquid was obtained. Two alcoholic fermentation treatments were conducted in this study as described below.

The first treatment employed whole-mash fermentation. A 0.5% (w/v) hop extract (temperature at 30–35 °C) was directly added to the *kaomak* mash. The total soluble solids of the mixed solution were below 18 °Brix. The second treatment was filtered liquid fermentation. The kaomak was pressed and filtered through gauze. The resulting filtrates were put in the presterile tank and subsequently mixed with boiling hot 0.5% (w/v) hop extract. The total soluble solids of the mixture were adjusted to below 18 °Brix.

For alcoholic fermentation, commercial yeast was inoculated at 2.5 g/L. The alcoholic fermentation was undergone for six days at ambient temperature (25–30°C). Finally, the fermentation broth was filtered through gauze. The last step was carbonation by priming with 0.5% w/v dextrose to the beverage and maturing at 18–24°C for one week. All processes were done under good hygienic conditions.

2.3 Physicochemical and microbial analysis

The namtoi (the sweet liquid fraction formed during *kaomak* fermentation) and the liquid fractions obtained from both whole-mash and filtered liquid alcoholic fermentations were evaluated. The pH was measured using a calibrated digital pH meter. Titratable acidity, expressed as a percentage of lactic acid, was determined according to AOAC (2000) methods. Total soluble solids (TSS) were measured using a hand refractometer. Total sugar concentration was quantified by spectrophotometric methods following AOAC (2000)[6]. Ethanol concentration was determined using an ebulliometer.

The fermentation samples were evaluated for total viable counts, yeast and mold counts, and lactic acid bacteria (LAB) counts. For kaomak and whole-mash fermentation samples, the solid and liquid fractions were analyzed separately. A 25 g or 25 mL portion of each sample was transferred to a sterile container and serially diluted tenfold. Appropriate dilutions were plated on potato dextrose agar for yeast and mold enumeration, de Man–Rogosa–Sharpe (MRS) agar for LAB enumeration, and Plate Count Agar for total viable counts. Results were expressed as log colony-forming units (CFU) per gram or per milliliter.

2.4 Sensory evaluation

The attributes of color, aroma, acidity, sweetness, foam stability, and overall acceptability were evaluated using a 9-point hedonic scale (1 = dislike extremely, 2 = dislike very much, 3 = dislike, 4 = dislike slightly, 5 = neither like nor dislike, 6 = like slightly, 7 = like, 8 = like very much, and 9 = like extremely) by 50 untrained panelists. Samples (20 mL) were served in separate 50 mL tasting cups and labeled with random three-digit codes. The order of sample presentation was randomized among panelists. Panelists were instructed to rinse their mouths with water between samples to cleanse their palates.

2.5 Statistical analysis

All experiments were conducted in triplicate. Data are presented as mean ± standard deviation (SD). Statistical differences between treatments were evaluated using one-way analysis of variance (ANOVA) followed by Tukey's multiple comparison test. Differences were considered statistically significant at $p < 0.05$.

3. Results & Discussion

3.1 Saccharification and fermentation kinetics

Look-pang is a culture of microorganisms that contains yeast (*S. cerevisiae* and *Candida* species), mold (*Aspergillus* species, *Rhizopus* species, *Mucor* species and *Amylomyces rouxii*) and LAB in rice flour and mixed with herbs[7]. During fermentation of kaomak, saccharolytic enzymes from mold hydrolyse starch to oligosaccharide and glucose[7]. At the end of *kaomak* fermentation (3 days), high total soluble solids (31.5±2.9 °Brix) and total sugar concentrations (22.87±5.86 g/100 mL) were detected in the namtoi, indicating efficient enzymatic hydrolysis of rice starch into sugars. Titratable acidity (expressed as lactic acid) was 1.01± 0.78% (w/v), and the pH was 3.62 ± 0.08. Lactic acid bacteria numbers were 7.14 ± 0.09 log CFU/mL with counts almost tenfold higher than those of yeasts and molds. Ethanol concentration was below 1% (v/v). Kaomak had Aroma flavor of alcohol, solvent-like, wine-like, whiskey-like, sweet and fruity aromas[7]. There are efforts to diversify fruity and floral beer aroma[8]. Kaomak could be a good substrate to produce floral fruity rice wine which having characters of beer.

The commercial ale yeast was selected due to ability to do the alcoholic fermentation at relatively warm temperature (20-22°C) when compare to lager. Moreover, ales yeasts have a short fermentation time (2–4 days)[9]. Before starting the alcoholic fermentation, hop extract was directly poured into the kaomak fermentation tank (whole-mash alcoholic fermentation) or mixed with pressed rice filtrate (filtered liquid alcoholic fermentation). The amount of hop extract was at the same ratio based on the mass of glutinous rice used for kaomak production. TSS of liquid fraction in whole-mash and filtered liquid alcoholic fermentation after addition of hop extract were 17.3±0.4 and 15.7±1.5°Brix, respectively. Hop extract also diluted the organic acid concentration and pH increased 0.3-0.4 unit (Table 1). The rice mash matrix may also influence the behavior of hop-derived compounds. Suspended solids can potentially adsorb or modify the perception of hop bitter acids and volatile terpenoids. In contrast, filtered liquid fermentation may allow more direct expression of hop aroma compounds. Further studies using chemical analysis of hop-derived compounds such as iso-α-acids and terpenoids would provide deeper insight into these matrix

effects. The commercial ale yeast was inoculated at final concentration of about 10^6 CFU/mL. A rapid growth of yeast was observed thus more than 1 log increase in viable count in whole-mash fermentation and 0.8 log in filtered liquid fermentation. The ethanol was accumulated and its concentration increased to about 5% within 2 days. After 6 days, the alcoholic content reached 10.6±0.1% (v/v) and 8.9±0.1% (v/v) in whole-mash fermentation treatment and filtered liquid fermentation treatment, respectively.

The microbial ecology of kaomak or pressed rice filtrate was already dominated by mixed *look-pang* culture. At initial phase of alcoholic fermentation, the LAB counts were 6.33 ± 0.01 and 7.71 ± 1.73 log CFU/g in filtered liquid and whole-mash fermentation, respectively (Table 2). The viable count of LAB was higher than yeast and mold. According to limited oxygen supply, filtered liquid and whole-mash fermentation did not support growth of filamentous fungi. The initial pH of substrates was about 3.9 and decreased continuously to about 3.6 which was below the optimum pH for growth of commercial yeast. Nevertheless, the inoculated yeast strain remained active under these acidic conditions. During alcoholic fermentation, yeast populations increased rapidly following inoculation, while lactic acid bacteria also continued to grow. The coexistence of yeast and LAB is typical in traditional rice fermentations and may contribute to flavor complexity through metabolic interactions and acid production. The gradual increase in LAB populations likely contributed to the observed decrease in pH and increase in titratable acidity during fermentation. This suggested that the selected strain could still successfully grow in the acidic condition of kaomak and or pressed rice filtrate. *Saccharomyces cerevisiae* acted as the principal ethanol and also flavor producer. In parallel, LAB species such as *Lactobacillus* and *Pediococcus* contributed to moderate acidification and flavor development. More than 1 log CFU increase in LAB number during alcoholic fermentation was observed. The initial TA were approximately 0.3% w/v and net increase was about 0.3-0.5 % (w/v) in whole-mash fermentation and filtered liquid fermentation, respectively. Organic acids produced by LAB during fermentation may contribute to microbial stability by lowering pH and creating unfavorable conditions for spoilage microorganisms. Although preservation effects were not directly evaluated in this study, the acidic environment generated during fermentation may enhance product stability. de Oliveira Lino et al. (2021) found that yeast–bacteria metabolic cooperation enhanced ethanol productivity through redox interactions and metabolite exchange, while high ethanol levels eventually constrained overall microbial viability[10].

Table 1. Physicochemical properties of fermentation substrate during alcoholic fermentation (mean ± SD, n = 3; P < 0.05)

Day	TSS (°Brix)		pH		%TA		Ethanol (% v/v)	
kaomak	31.50 ± 2.90		3.62 ± 0.08		1.01 ± 0.78		<1	
	L	**S**	**L**	**S**	**L**	**S**	**L**	**S**
1	15.7±1.5^a	17.3±0.4^a	3.89±0.04^a	3.99±0.08^a	0.33±0.12^a	0.36±0.08^a	3.5±0.1^a	3.5±0.2^a
2	15.2±1.4^a	16.6±0.4^a	3.74±0.06^a	3.67±0.15^a	0.48±0.06^a	0.48±0.02^a	4.8±0.1^b	5.3±0.1^a
3	13.3±1.2^a	13.7±1.2^a	3.69±0.0^a	3.60±0.18^a	0.48±0.06^b	0.63±0.05^a	6.3±0.1^a	6.8±0.9^a
4	11.3±1.2^a	11.3±1.2^a	3.59±0.09^a	3.57±0.23^a	0.55±0.08^b	0.70±0.06^a	6.3±0.1^a	7.3±1.8^a
5	9.7±0.6^a	11.3±0.5^a	3.71±0.05^a	3.63±0.22^a	0.55±0.06^b	0.83±0.15^a	7.3±0.9^a	8.9±2.0^a
6	9.0±0.2^a	8.2±0.3^b	3.74±0.07^a	3.64±0.25^a	0.61±0.06^b	0.83±0.05^a	8.9±0.1^b	10.6±0.1^a

TSS: Total Soluble Solids, %TA: Titratable acidity expressed as lactic acid.
L= Filtered liquid fermentation, S= Whole-mash fermentation
Different superscript letters within the same day and parameter indicate significant differences between treatments (p < 0.05).

The inclusion of hop extract imparted a floral aroma that enhanced flavor complexity. During carbonation, *Saccharomyces cerevisiae* fermented dextrose into ethanol and CO_2 under microaerophilic conditions. The beverages had a sweet and sour taste with a character of beer which had foam, fizzy and hop, fruity aroma. According to the ethanol content and tartness, these could be classified as a strong sour beer (5 % − 12 %). The rice based alcoholic beverages fermented by using look-pang and commercial yeast by whole-mash and filtered liquid alcoholic fermentation shared similar chemical profiles. However, some attributes obtained different preference scores (Table 3).

Table 2. Microbial populations during alcoholic fermentation (mean ± SD, n = 3)

	Total viable counts		**Yeast and mold counts**		**LAB counts**	
kaomak	7.18 ± 1.58		6.35 ± 0.21		7.14 ± 0.09	
	During Alcoholic fermentation					
days	**L**	**S**	**L**	**S**	**L**	**S**
0	6.17 ± 1.57	8.13 ± 1.53	6.85 ± 0.71	6.46 ± 0.10	6.33 ± 0.01	7.71 ± 1.73
1	7.84 ± 0.20	8.14 ± 1.39	7.26 ± 0.17	7.73 ± 0.22	7.12 ± 0.61	7.73 ± 1.35
3	8.38 ± 0.91	8.21 ± 0.69	7.67 ± 0.01	7.73 ± 0.49	8.20 ± 1.07	8.58 ± 0.66
6	7.11 ± 0.39	8.50 ± 0.47	7.65 ± 0.32	8.36 ± 0.12	7.11 ± 0.49	8.35 ± 0.44

LAB = Lactic Acid Bacteria
L= Filtered liquid fermentation, S= Whole-mash fermentation

The consumer preference scores for hop aroma attribute were 6.34±1.90 and 6.73±1.68 for whole-mash and filtered liquid fermentation treatments, respectively. Both filtered liquid and whole-mash fermentation treatments also exhibited comparable scores for sweetness, acidity, and colour, with mean values indicating moderate to good consumer acceptance across these attributes (Table 3). Most notably, overall acceptance differed significantly between treatments. The foam stability scores of both beverages were relatively low. However, the whole-mash treatment achieved a significantly higher overall acceptance score (7.77±1.63) than the filtered liquid treatment (7.16±1.63). Although individual sensory attributes did not differ significantly between treatments, the whole-mash fermented beverage obtained a significantly higher overall acceptance score. This suggests that consumer preference may reflect the integrated perception of multiple sensory characteristics rather than any single attribute.

Table 3. Sensory evaluation of glutinous rice–hop fermented beverages (mean ± SD, n = 50; 9-point hedonic scale)

Treatment	Aroma	Sweetness	Acidity	Colour	Foam stability	Overall acceptance
L	6.73±1.68^{a}	5.98±1.91^{a}	4.82±2.51^{a}	6.80±1.86^{a}	4.34±2.50^{a}	7.16±1.63^{b}
S	6.34±1.90^{a}	6.36±2.14^{a}	5.34±2.61^{a}	6.32±2.25^{a}	4.98±2.50^{a}	7.77±1.63^{a}

L= Filtered liquid fermentation, S= Whole-mash fermentation
the same letter in the same column are not significantly different from each other ($p<0.05$)

4. Conclusion

This study demonstrated that integrating *kaomak* fermentation with hop extract successfully produced a rice-based alcoholic beverage that combines traditional Thai mixed-culture fermentation with beer-like aroma and flavor characteristics. The addition of hop (0.5 % w/v) provided moderate bitterness and floral aroma through volatile terpenoids (e.g., myrcene, linalool, humulene). From a process perspective, the results underscore the importance of matrix handling (whole kaomak and pressed rice filtered), hop dosage, and maturation control in achieving both sensory balance and microbial stability. Overall, enhanced ethanol productivity

and stronger consumer acceptance were achieved by whole-mash hop-integrated fermentation, while improved process controllability and scalability were offered by filtered liquid fermentation.

Acknowledgements

The authors would like to express sincere appreciation to the Faculty of Agriculture, Ubon Ratchathani University and the Indigenous Food Research and Industrial Development Center, Ubon Ratchathani University, for research facilities and academic support throughout this project. The authors also gratefully acknowledge institutional funding support from Ubon Ratchathani University that enabled the completion of this research on traditional rice fermentation and product development.

References

1. แนวโน้มธุรกิจ/อุตสาหกรรมปี 2568-2570: อุตสาหกรรมเครื่องดื่ม [Internet]. krungsri.com. [cited 2026 Jan 30]. Available from: https://www.krungsri.com/th/research/industry/industry-outlook/food-beverage/beverage/io/beverage-2025-2027
2. Ceccaroni D, Sileoni V, Marconi O, De Francesco G, Lee EG, Perretti G. Specialty rice malt optimization and improvement of rice malt beer aspect and aroma. Lebenson Wiss Technol [Internet]. 2019;99:299–305. Available from: http://dx.doi.org/10.1016/j.lwt.2018.09.060
3. Guimaraes BP, Schrickel F, Rettberg N, Pinson SRM, McClung AM, Luthra K, et al. Investigating the malting suitability and brewing quality of different rice cultivars. Beverages [Internet]. 2024;10(1):16. Available from: http://dx.doi.org/10.3390/beverages10010016
4. Schubert C, Aitkens M, Maust A, Sen R, Lafontaine S, Kono M. The role of adjunct milled rice, barley malt, and different Koji variations in alcoholic and non-alcoholic beer production. Monatsschrift Brauwiss [Internet]. 2024 [cited 2026 Jan 30];77(9/10):107–17. Available from: https://brewingscience.de/index.php/brewingscience/article/view/105
5. Walker G, Stewart G. Saccharomyces cerevisiae in the Production of Fermented Beverages. Beverages [Internet]. 2016;2(4):30. Available from: http://dx.doi.org/10.3390/beverages2040030
6. Association of Official of Analytical Chemist (AOAC). 2000. Official methods of analysis of AOAC international. Arling, VA, USA: AOAC International.
7. Wongsa J, Rungsardthong V, Yasutomo T. Production and analysis of volatile flavor compounds in sweet fermented rice (Khao Mak). MATEC Web Conf [Internet]. 2018;192:03044. Available from: http://dx.doi.org/10.1051/matecconf/201819203044
8. Holt S, Miks MH, de Carvalho BT, Foulquié-Moreno MR, Thevelein JM. The molecular biology of fruity and floral aromas in beer and other alcoholic beverages. FEMS Microbiol Rev [Internet]. 2019;43(3):193–222. Available from: http://dx.doi.org/10.1093/femsre/fuy041
9. Bonatto D. The diversity of commercially available ale and lager yeast strains and the impact of brewer's preferential yeast choice on the fermentative beer profiles. Food Res Int [Internet]. 2021;141(110125):110125. Available from: http://dx.doi.org/10.1016/j.foodres.2021.110125
10. de Oliveira Lino, F. et al. (2021). Microbial interactions in mixed fermentations enhance ethanol yield. Nat. Commun., 12, 1498. https://doi.org/10.1038/s41467-021-21775-3

P - 338

Effect of Heat Pump Drying Conditions on the Physicochemical Properties of King Oyster Mushroom (*Pleurotus eryngii*) Powder

Sukrit Kamnoi, Soraya Kerdpiboon, Natthaporn Chotigavin*

School of Food Industry, King Mongkut's Institute of Technology Ladkrabang, Bangkok 10520, Thailand

**Corresponding author E-mail: natthaporn.ch@kmitl.ac.th*

Abstract: King oyster mushroom (*Pleurotus eryngii*) is a nutritionally rich edible fungus containing proteins, dietary fiber, vitamins, and bioactive compounds with antioxidant activity. This study investigated the effects of heat pump drying at three temperatures (55, 60, and 65 °C) and two durations (5.0 and 5.5 h) on the physicochemical properties of mushroom powder using a 3×2 factorial completely randomized design. Drying temperature and time significantly influenced color parameters, moisture content, water activity (a_w), and functional properties of the powder. Lower drying temperatures and prolonged drying time tended to result in higher moisture content and a_w, together with reduced lightness (L*), which may be associated with enzymatic browning during slower moisture removal. In contrast, higher drying temperature intensified non-enzymatic browning reactions, particularly at longer drying time, leading to changes in color characteristics and slight reductions in water-holding capacity (WHC) and oil-holding capacity (OHC), reflecting thermal effects on component functionality. Among all conditions, drying at 60 °C for 5.5 h yielded the most desirable balance of quality attributes, producing mushroom powder with acceptable lightness (L* ≈ 69.9), low moisture content (≈ 7.7%), low a_w (≈ 0.33), high WHC (≈ 3.4 g/g), and high OHC (≈ 1.5 g/g). These results provide clear evidence of how temperature–time combinations affect the physicochemical and functional characteristics of *Pleurotus eryngii* powder. These findings demonstrate that controlling drying conditions is essential for optimizing the physicochemical quality of king oyster mushroom powder, providing practical guidance for its application as a functional ingredient in various food products.

Keywords: *Pleurotus eryngii*; Heat pump drying; Physicochemical properties; Water holding capacity; Oil holding capacity

1. Introduction

King oyster mushroom (*Pleurotus eryngii*) has attracted increasing attention as a sustainable and functional ingredient in plant-based food development due to its high nutritional and bioactive content. It contains protein, dietary fiber, essential amino acids, vitamins (B-complex, D), and bioactive compounds such as β-glucans and polysaccharide protein complexes that exhibit antioxidant, immunomodulatory, and cholesterol-lowering effects [1,2]. These attributes support its use as a clean-label, natural alternative to synthetic additives in the formulation of meat analogues [3]. Fresh mushrooms, however, have a high moisture content (85–90%) and are highly perishable. Drying is one of the most effective methods to prolong their shelf life while concentrating nutrients and enhancing versatility in food applications. Converting mushrooms into powder not only improves storage stability but also allows for their incorporation into soups, sauces, seasonings, baked goods, and extruded products [3]. The quality of mushroom powder is highly dependent on the drying method and conditions. Conventional hot-air drying often causes shrinkage, browning, and loss of bioactive compounds due to high temperatures and prolonged drying [5]. Compared to conventional drying techniques, heat pump drying provides several advantages in preserving the quality of mushrooms. Hot-air drying (HAD), while widely

used, often leads to significant color degradation, shrinkage, and loss of bioactive compounds due to high temperatures and uncontrolled humidity. Freeze drying (FD) is excellent in preserving nutritional and structural integrity but is costly, time-consuming, and energy-intensive, making it less feasible for commercial-scale applications. Vacuum drying offers moderate preservation but still requires high energy input and specialized equipment. In contrast, heat pump drying operates at moderate temperatures (typically 40–65°C) and allows better control of drying kinetics and humidity, which helps retain color, reduce non-enzymatic browning, and maintain functional properties such as water-holding and oil-holding capacities [4,5]. This makes heat pump drying a promising, energy-efficient alternative for producing functional mushroom powder. Despite prior mushroom-drying studies using hot-air drying, freeze drying, and vacuum drying, heat-pump drying for *Pleurotus eryngii* has not been systematically optimized in terms of temperature and time, and mechanistic understanding of how these parameters drive powder quality, particularly color development and functional performance (WHC and OHC) remains limited. Therefore, this study aimed to determine the effects of heat pump drying temperature and duration on the physicochemical and functional properties of king oyster mushroom powder. Key indicators such as color, moisture content, water activity, water-holding capacity (WHC), and oil-holding capacity (OHC) were used to identify the most suitable drying condition. These results are expected to facilitate the utilization of king oyster mushroom powder as a functional ingredient in alternative protein formulations, particularly where water- and oil-holding capacities are important.

2. Materials and Methods

2.1 Raw Material Preparation

Fresh king oyster mushrooms (*Pleurotus eryngii*) were sourced from Shenzhen Maoxiong Co., Ltd. (Guangdong, China). Mushrooms were cleaned and sliced into approximately 5mm thick pieces to facilitate uniform drying. Prior to drying, the mushroom slices were immersed in an aqueous ascorbic acid solution (0.5%, w/v) for 5 min and subsequently drained at room temperature. The ascorbic acid pretreatment was applied to inhibit enzymatic browning by reducing quinone compounds formed through polyphenol oxidase activity, thereby preserving color quality and cellular structure during drying. This treatment was used as an alternative to blanching to minimize browning reactions without inducing thermal damage to the mushroom tissue

2.2 Drying Process

Drying was carried out in a laboratory-scale heat pump dryer with controlled temperature and airflow. Drying temperatures were set to 55 °C, 60 °C, and 65 °C. Two drying durations were evaluated: 5 hours and 5.5 hours. These conditions were chosen based on preliminary trials indicating they could reduce moisture to around 10% or lower. Approximately equal quantities of mushroom slices (about 1,000 g) were spread in a single layer on drying trays for each run. The dryer reduced air relative humidity via the heat pump dehumidification cycle, allowing efficient moisture removal at moderate temperatures. The experiment was designed as 3 × 2 factorial designs arranged in a Completely Randomized Design (CRD) with the two factors being temperature and time. Three independent drying runs were performed for each treatment (n = 3).

After drying, the mushroom slices were immediately cooled to room temperature and ground into a fine powder using an Ultra-Centrifugal Mill (RETSCH ZM-200, Germany)**.** The powder was sieved through a 250 μm mesh to obtain a uniform particle size for analysis and to mimic powder preparation for food applications. The powder samples were stored in airtight containers at room temperature prior to analysis**.**

2.3 Physicochemical Analyses

All measurements were conducted in triplicate and results were expressed on either a dry weight or wet weight basis as appropriate.

2.3.1 Color values (L*, a*, b*)

Color values of the mushroom powder were measured using a Chroma Meter (Konica Minolta CR-400, Japan) based on the CIE L*a*b* color system and calibrated with a white standard tile. *L* indicates lightness (0 = black, 100 = white), a indicates redness/greenness (positive = red, negative = green), and b indicates yellowness/blueness (positive = yellow, negative = blue).

2.3.2 Moisture content (% wet basis)

Moisture content was determined by an infrared moisture balance (Mettler Toledo MJ33, Switzerland). Approximately 3 g of mushroom powder was used for each measurement. The instrument heats the sample and records weight loss until constant weight. Results were cross-checked by oven drying at 105°C for accuracy [6].

2.3.3 Water activity (a_w)

Water activity (a_w) of the mushroom powder was determined at 25 °C using a water activity meter (AquaLab 4TEV, Meter Group, USA). The instrument measures the equilibrium relative humidity of the sample in a sealed chamber and converts it to water activity. Water activity reflects the amount of free water available for microbial growth and chemical reactions in food systems.

2.4 Functional Properties

2.4.1 Water holding capacity (WHC) and oil holding capacity (OHC)

Water holding capacity (WHC) and oil holding capacity (OHC) were evaluated using a centrifugation method as described by Sosulski [6]. For WHC determination, an accurately weighed mushroom powder sample (~1.000 g) was placed in a pre-weighed centrifuge tube and mixed with 10 mL of distilled water. The mixture was allowed to stand at room temperature for 30 min and then centrifuged at 4,000 rpm (≈ 2,700 × g) for 20 min using an Eppendorf 5702 centrifuge (Eppendorf AG, Germany). After centrifugation, the supernatant was carefully decanted, and the tube containing the sediment was weighed. Oil holding capacity (OHC) was determined using the same procedure, except that distilled water was replaced with 10 mL of commercial refined soybean oil purchased from a local supermarket. WHC and OHC were expressed as grams of water or oil retained per gram of dry powder.

Water-holding capacity (WHC) and oil-holding capacity (OHC) were calculated based on the difference in weight before and after centrifugation and expressed as grams of water or oil retained per gram of dry sample according to the following equations.

$$\text{WHC(g/g)} = (W2 - W1) / W1, \text{OHC(g/g)} = (W3 - W1) / W1$$

where W_1 is the weight of dry mushroom powder (g), W_2 is the weight of the hydrated sediment after centrifugation (g), and W_3 is the weight of the oil-absorbed sediment after centrifugation (g).

2.4.2 Emulsion capacity (EC)

Emulsion capacity of the mushroom powder was determined using a centrifugation-based method. Mushroom powder (2 g) was first dispersed in 200 mL of distilled water (1:100, w/v) and stirred using a magnetic stirrer to ensure uniform dispersion. The dispersion was allowed to hydrate at room temperature for 30 min. Prior to homogenization, 180 mL of the hydrated mushroom dispersion was mixed with 20 mL of commercial refined soybean oil purchased from a local supermarket. The mixture was

homogenized using a high-speed homogenizer (IKA T25, Germany) at 6,000 rpm for 1 min to form an emulsion. An aliquot (12 mL) of the emulsion was transferred into a 15 mL centrifuge tube and centrifuged at 4,000 rpm (≈ 2,700 × g) for 10 min to separate the emulsified and non-emulsified phases.

Emulsion capacity (EC) was calculated as the ratio of the volume of the emulsified layer to the total volume of the mixture and expressed as a percentage (%) according to the following equation.

$$EC\ (\%) = (V_e\ /\ V_t) \times 100$$

where V_e is the volume of the emulsified layer after centrifugation (mL), and V_t is the total volume of the emulsion (mL). This measurement was used to evaluate the emulsifying ability of the mushroom powder rather than the long-term stability of the emulsion.

2.5 Experimental Design and Statistical Analysis

Data was analyzed using IBM SPSS Statistics (Version 29). Two-way analysis of variance (ANOVA) was used to assess the effects of drying temperature, drying time, and their interaction on the measured responses. When ANOVA indicated a significant effect ($p < 0.05$), Duncan's New Multiple Range Test was applied to compare mean values. Results are reported as mean ± standard deviation. Different lowercase letters indicate significant differences among drying conditions at the 95% confidence level.

3. Results and Discussion

3.1 Color Properties

Table 1. Color values (L*, a*, and b*) of king oyster mushroom powder under different drying temperature–time combinations

Drying condition	L*	a*	b*
55 °C, 5 h	70.82 ± 0.31^{b}	5.31 ± 0.09^{b}	23.16 ± 0.12^{d}
55 °C, 5.5 h	68.63 ± 0.10^{d}	5.31 ± 0.05^{b}	24.68 ± 0.19^{b}
60 °C, 5 h	64.58 ± 0.19^{e}	5.69 ± 0.06^{a}	23.82 ± 0.25^{c}
60 °C, 5.5 h	69.86 ± 0.20^{c}	4.86 ± 0.08^{c}	23.85 ± 0.08^{c}
65 °C, 5 h	71.21 ± 0.18^{a}	5.79 ± 0.11^{a}	23.06 ± 0.18^{d}
65 °C, 5.5 h	68.56 ± 0.26^{d}	5.31 ± 0.09^{b}	25.12 ± 0.06^{a}

Note: Mean ± SD (n = 3). Different superscript letters within the same column indicate significant differences according to Duncan's multiple range test ($p < 0.05$).

Drying temperature and drying time significantly affected the color parameters (L*, a*, and b*) of king oyster mushroom powder ($p < 0.05$), as shown in Table 1. At a drying time of 5.0 h, L* values differed significantly among all temperatures, with the highest lightness observed at 65 °C, followed by 55 °C, while drying at 60 °C resulted in markedly lower L* values, indicating

pronounced darkening under this condition. At 5.5 h, samples dried at 55 °C and 65 °C exhibited comparable L* values, whereas drying at 60 °C produced significantly higher lightness, suggesting a less severe darkening effect at this intermediate temperature. In addition to changes in lightness, variations in redness (a*) and yellowness (b*) were also observed. For a*, samples dried at 5.0 h showed higher redness at 60 °C and 65 °C compared with 55 °C. At 5.5 h, the lowest a* value was observed at 60 °C, while samples dried at 55 °C and 65 °C exhibited comparable redness. The relatively higher redness observed at lower drying temperatures may be attributed to enhanced enzymatic browning due to slower moisture removal and prolonged exposure time [3]. Regarding b*, yellowness increased with both temperature and drying time. At 5.0 h, b* values differed significantly among all temperatures, whereas at 5.5 h, b* increased progressively with temperature in the order of 65 °C > 55 °C > 60 °C. The pronounced increase in b* at higher temperature and longer drying time may be associated with non-enzymatic browning reactions, such as Maillard reactions, which commonly occur during thermal processing of mushrooms [5]. Overall, although a* and b* exhibited temperature-dependent variations, the magnitude of these changes was smaller than that observed for L*, indicating that color deterioration was primarily manifested as overall darkening rather than pronounced chromatic shifts. Similar color changes during drying have been reported in previous studies on *Pleurotus eryngii* and other edible mushrooms, where increasing drying temperature intensified browning reactions and resulted in lower L* values due to thermal degradation and Maillard reactions [1]. These results demonstrate a clear temperature–time interaction effect on the color characteristics of mushroom powder, highlighting the importance of controlling both parameters to preserve color quality during drying.

3.2 Moisture Content and Water Activity (a_w)

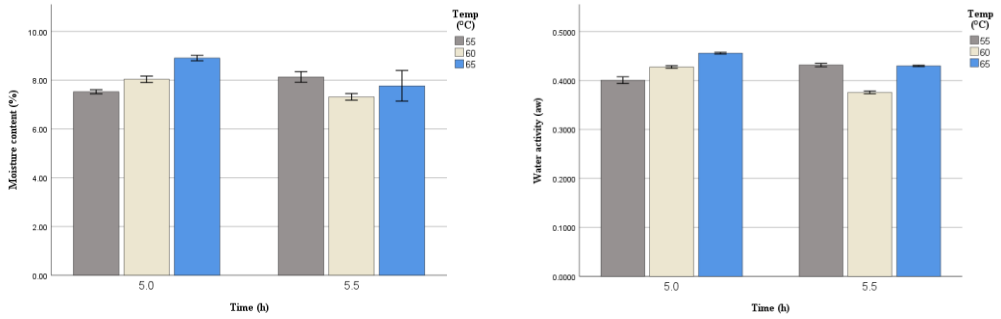

(a) (b)

Figure 1. Interaction effects of drying temperature and drying time on **(a)** moisture content (%) and **(b)** water activity (a_w) of king oyster mushroom powder (mean values, $n = 3$).

Drying temperature and drying time significantly influenced the moisture content and water activity (aw) of king oyster mushroom powder ($p < 0.05$), as illustrated in Figure 1. A clear temperature–time interaction effect was observed for both parameters. For moisture content Figure 1(a), different trends were observed between drying times. At 5.0 h, moisture content increased with increasing temperature. This phenomenon may be related to case hardening during drying. At higher drying temperatures, rapid moisture evaporation at the surface may form a hardened outer layer that restricts internal moisture diffusion, thereby limiting moisture removal from the interior of the material [5]. In contrast, at 5.5 h, the lowest moisture content was obtained at 60 °C. A similar interaction effect was observed for water activity Figure 1(b). At 5.5 h, drying at 60 °C resulted in the lowest aw, indicating reduced free water availability. Overall, drying at 60 °C for 5.5 h provided the most favorable moisture-related properties, which are important for improving storage stability of mushroom powder.

3.3 Water Holding Capacity (WHC) and Oil Holding Capacity (OHC)

Table 2. Water holding capacity (WHC) and oil holding capacity (OHC) of King Oyster mushroom powder under different drying conditions

Drying condition (trt)	WHC (g/g)	OHC (g/g)
55 °C, 5 h	3.20 ± 0.19^{b}	1.54 ± 0.03^{b}
55 °C, 5.5 h	3.59 ± 0.18^{a}	1.45 ± 0.03^{c}
60 °C, 5 h	3.45 ± 0.17^{ab}	1.12 ± 0.02^{d}
60 °C, 5.5 h	3.26 ± 0.26^{ab}	1.47 ± 0.04^{c}
65 °C, 5 h	3.23 ± 0.22^{b}	1.59 ± 0.02^{a}
65 °C, 5.5 h	2.78 ± 0.04^{c}	1.16 ± 0.01^{d}

Note: Mean ± SD (n = 3). Different superscript letters within the same column indicate significant differences according to Duncan's multiple range test ($p < 0.05$).

Drying temperature and drying time significantly affected both water-holding capacity (WHC) and oil-holding capacity (OHC) of king oyster mushroom powder ($p < 0.05$), with a clear temperature–time interaction (Table 2). For WHC, higher values were generally observed at a longer drying time (5.5 h), particularly at 55°C and 60°C, whereas a marked decrease was observed at 65°C for 5.5 h, suggesting possible structural collapse or reduced water-binding sites. In contrast, OHC exhibited the highest value at 65°C for 5.0 h, while prolonged drying (5.5 h) tended to reduce OHC across temperatures. Overall, drying at 60°C provided a favorable balance between WHC and OHC, making it a suitable condition for food formulation applications.

3.4 Emulsion Capacity (EC)

Based on physicochemical and functional screening results, three representative drying conditions were selected for emulsion capacity (EC) evaluation. These conditions corresponded to the samples exhibiting relatively high water-holding capacity (WHC) and oil-holding capacity (OHC), as well as moderate moisture content and low water activity, which are desirable attributes for emulsifying ingredients. Specifically, the selected samples were dried at 55 °C for 5.5 h, 60 °C for 5.5 h, and 65 °C for 5.0 h, representing low-, medium-, and high-temperature drying conditions with differing drying intensities. The sample dried at 55 °C for 5.5 h was selected due to its relatively high WHC, indicating strong water-binding ability, whereas the sample dried at 65 °C for 5.0 h exhibited higher OHC, suggesting enhanced affinity for lipid phases. The intermediate condition at 60 °C for 5.5 h demonstrated a balanced combination of WHC, OHC, and moisture-related properties and was therefore used as a reference condition. The selected samples represented different temperature–time combinations to capture the effects of drying severity on emulsifying performance. Evaluating EC under these representative conditions allows for a clearer assessment of the suitability of heat pump–dried mushroom powder as a functional ingredient for stabilizing oil–water systems in plant-based food formulations [3]. Mushroom-derived powders can contribute to emulsion formation due to the presence of proteins and polysaccharides that interact with both aqueous and lipid phases, thereby stabilizing oil–water interfaces [4].

Table 3. Emulsion capacity (EC) of selected king oyster mushroom powder samples dried under different heat pump drying conditions

Drying condition	Mean EC ± SD (%)
55°C, 5.5 h	25.21 ± 2.30
60°C, 5.5 h	34.72 ± 2.41
65°C, 5.0 h	26.39 ± 2.41

Note: EC was calculated as the percentage of the emulsified layer volume relative to the total sample volume (12 mL). Values are expressed as Mean ± SD (n = 3).

The emulsion capacity (EC) of the selected mushroom powder samples varied among the evaluated drying conditions. The sample dried at 60°C for 5.5 h showed the highest EC (34.72 ± 2.41%), while lower EC values were observed for samples dried at 55°C for 5.5 h (25.21 ± 2.30%) and 65°C for 5.0 h (26.39 ± 2.41%). The EC results were consistent with the trends observed for water holding capacity (WHC) and oil holding capacity (OHC), which are important functional properties influencing emulsifying behavior in food powders [9]. The higher EC obtained at 60°C for 5.5 h corresponded to relatively higher WHC and OHC, indicating improved interactions between mushroom components and both aqueous and oil phases, which is related to the presence of mushroom proteins and polysaccharides capable of stabilizing oil–water interfaces [7,8]. In contrast, lower EC values at 55°C and 65°C may be associated with insufficient structural modification at lower temperature and aggregation or partial denaturation of functional components at higher temperature, which may reduce the ability of these components to stabilize emulsions [7]. Overall, EC was used as supportive functional evidence to complement WHC and OHC results rather than as a primary quantitative parameter.

4. Conclusion

This study demonstrated that drying temperature and drying time during heat pump drying significantly influenced the physicochemical and functional properties of king oyster mushroom (*Pleurotus eryngii*) powder. The drying conditions affected color characteristics, moisture content, water activity, and functional properties including water-holding capacity (WHC), oil-holding capacity (OHC), and emulsion capacity (EC). Among the evaluated conditions, drying at 60 °C for 5.5 h provided the most favorable overall quality, producing mushroom powder with acceptable color, relatively low moisture content and water activity, and balanced functional properties. These results indicate that appropriate control of temperature–time combinations during heat pump drying is important for optimizing the quality and functionality of mushroom powder. The findings also suggest that heat pump drying is a promising technique for producing mushroom powder suitable for use as a functional ingredient in plant-based and emulsion-based food products. Future research should further investigate the application of this mushroom powder in food formulations and evaluate its effects on product stability, texture, and sensory properties.

References

1. Chang ST, Miles PG. Mushrooms: cultivation, nutritional value, medicinal effect, and environmental impact. 2nd ed. Boca Raton (FL): CRC Press; 2004.
2. Wasser SP. Medicinal mushrooms as a source of antitumor and immunomodulating polysaccharides. Appl Microbiol Biotechnol. 2002;60(3):258–274.

3. Das AK, Nanda PK, Madane P, Biswas S, Das A, Zhang W, et al. A comprehensive review on mushroom powders: nutritional profile, functional properties, and food applications. Food Rev Int. 2020;36(5):1-24. doi:10.1080/87559129.2020.1720016.
4. Liu Z, Zhang M, Mujumdar AS. Comparison of three heat pump drying modes for drying of Pleurotus eryngii slices. Drying Technol. 2014;32(13):1642-1650.
5. Chua LYW, Chua BL, Figiel A, Chong CH, Wojdyło A. Drying of edible mushrooms: recent developments and future research trends. Trends Food Sci Technol. 2019;88:1-12.
6. Sosulski FW. The centrifuge method for determining flour absorption in hard red spring wheats. Cereal Chem. 1962;39:344-350.
7. Popa M, Tăușan I, Drăghici O, Soare A, Oancea S. Influence of convective and vacuum-type drying on quality, microstructural, antioxidant and thermal properties of pretreated *Boletus edulis* mushrooms. Molecules. 2022;27(13):4063.
8. Kalač P. A review of chemical composition and nutritional value of wild-growing and cultivated mushrooms. J Sci Food Agric. 2013;93(2):209–218.
9. Pasban A, Mohebbi M, Shahidi F. Effects of drying methods on physicochemical and functional properties of mushroom powder. J Food Process Preserv. 2020;44:e14384.

P - 352

Growth Stimulation of *Lachancea thermotolerans* and *Saccharomyces cerevisiae* Using Pulsed Electric Field

Nuttapong Kunma and Wannaporn Klangpetch*

Division of Food Science and Technology, Faculty of Agro-Industry, Chiang Mai University, Chiang Mai, 50100

**Corresponding author E-mail: wannaporn.u@cmu.ac.th*

Abstract: Fermentation relies on microorganisms, which convert sugars into key metabolites that determine product quality. Enhancing yeast growth and nutrient uptake is therefore critical. Pulsed electric field (PEF) technology has emerged as a promising approach to improve fermentation efficiency by increasing cell membrane permeability and facilitating mass transfer. This study evaluated the growth stimulatory effects of PEF on two yeast species, including *Lachancea thermotolerans* JCM 19085 and *Saccharomyces cerevisiae* K901, cultured in YPD medium. PEF electric field strength (0.5 and 3.0 kV/cm) and treatment duration (30 and 90 s) were varied, and cell growth was measured via OD_{660} over 36 h of incubation. The optimal condition for electro permeabilization of *L. thermotolerans* was determined to be 0.5 kV/cm for 30 s. This treatment significantly increased the specific growth rate (μ) from 0.154 ± 0.002 h^{-1} to 0.205 ± 0.005 h^{-1}. However, the lag time also substantially increased from 9.065 ± 0.495 h to 11.385 ± 0.050 h. In contrast, the optimal condition for *S. cerevisiae*, considering both μ and lag time, was 0.5 kV/cm for 90 s. Under this condition, μ slightly increased from 0.171 ± 0.008 h^{-1} to 0.191 ± 0.006 h^{-1}, while the lag time was substantially reduced from 13.376 ± 1.322 h to 8.321 ± 0.410 h. Ethanol production was quantified by HPLC analysis, revealing that PEF treatment enhanced ethanol concentration by *L. thermotolerans* from 3.28 ± 0.09 g/L (control) to 4.21 ± 0.07 g/L, corresponding to an increase of approximately 28.4%. In contrast, ethanol concentration produced by S. *cerevisiae* decreased from 7.29 ± 0.15 g/L (control) to 6.77 ± 0.27 g/L after PEF treatment, representing a decrease of approximately 7.1%. Overall, the results highlight the potential of PEF as a controllable non-thermal tool for enhancing fermentation performance in a species-dependent manner.

Keywords: Pulsed Electric Field; Stimulation; Yeast; Specific growth rate; Lag time

1. Introduction

Fermentation is a food processing method used to preserve food for an extended time. It's used worldwide and can be found in many cultures and regions. This process demands microorganisms such as bacteria, yeast, and mold to convert carbohydrates or sugars into alcohols or acids, which helps extend the shelf life and improve the taste, texture, and nutritional value of food products [1]. Fermentation processes have many types depending on the microorganism and raw material used in production. Alcoholic fermentation is commonly used in beverage production, such as beer, wine, and spirits, where yeasts convert sugars into alcohol and carbon dioxide and could create beneficial aromas and flavors. Many types of non-Saccharomyces yeasts have been found in natural fermentation processes, including *Candida*, *Pichia*, and *Lachancea* species. These yeasts contribute to the complexity of flavors and aromas in alcoholic beverages by producing enzymes and metabolites that enhance the sensory properties of the final product. [3].

Lachancea species, such as *Lachancea thermotolerans*, are interesting yeasts for producing wine, beer, and fruit wine. Their notable characteristics include the ability to produce

lactic acid, which increases the acidity of beverages and improves flavor and stability; the production of various compounds such as esters, higher alcohols, and terpenes, which are crucial for the sensory characteristics of the final product and its ethanol tolerance; and the production of enzymes like β-glucosidase, which can release aromatic compounds in grape must [4]. Despite its potential benefits, several limitations remain, particularly the prolonged fermentation duration, which frequently necessitates co-fermentation with *S. cerevisiae* to ensure process efficiency. Furthermore, microbial contamination poses a significant challenge to fermentation performance and product quality; lactic acid bacteria (LAB), for example, can outcompete yeast for nutrients and generate undesirable metabolites, resulting in fermentation inhibition and decreased ethanol yields [5].

Additionally, stress tolerance is a factor; non-Saccharomyces yeasts have lower stress tolerance and may die during fermentation, resulting in the loss of desired compounds [6]. Stimulating growth and reducing fermentation time are intriguing possibilities to improve production efficiency. Pulsed Electric Fields (PEF) are a method for enhanced fermentation, biomass growth, and improved extraction of bioactive compounds. The mechanisms by which PEF enhances yeast activity are electroporation and increased permeability. PEF stimulates electroporation, creating pores in the yeast cell membrane to increase the permeability of external substances. This procedure can increase nutrient consumption, resulting in a faster fermentation rate, helping to reduce fermentation time and increase product concentration, which is beneficial in the fermentation process [7]. Studies have been conducted on the use of PEF to stimulate yeast growth and various activities, such as stimulating *S. cerevisiae* yeast with PEF at an electric field intensity of 0–1.5 kV/cm, which resulted in an increased growth rate, reaching its peak at an electric field intensity of 0.85 kV/cm [8]. Research on the growth rate of *Hanseniaspora* sp. by using PEF showed that the yeast could achieve maximum growth at an electric field intensity of 285 V/cm during the lag and exponential phases, resulting in faster glucose consumption and increased biomass concentration [7]. This data suggests moderate PEF intensity can be beneficial for yeast growth. This study aimed to evaluate the effect of pulsed electric field (PEF) treatment on the growth kinetics and ethanol production of *L. thermotolerans* and *S. cerevisiae* during fermentation.

2. Materials and Methods

2.1 Preparation of Yeast cells

Lachancea thermotolerans JCM 19085 and *Saccharomyces cerevisiae* K901 were cultured on PDA and incubated at 25°C for 48 h. Then it was subculture in Yeast Extract Peptone Dextrose Medium and incubated at 25°C for 48 h. Thereafter, the cell suspension was harvested by centrifugation at 6000 rpm for 10 min at 4°C (Dynamica Velocity 18R Pro, UK), and the supernatant was replaced by distilled water three times. For further experiments, the final yeasts cell concentration was adjusted to 10^9 CFU/mL [9].

2.2 PEF apparatus

A PEF apparatus was kindly provided by Innovative Drying Technology Co., Ltd. (Chiang Mai, Thailand) was used in this study, as shown in Figure 1. The system consisted of a high-voltage power supply (0–2.5 kV), an energy storage capacitor, and a solid-state high-voltage switch controlled by a Variable Voltage Transformer (3kVA-TDGC2, Yueqing Tianze Elec. Co., Ltd., China) The generated rectangular pulses were applied to the PEF chamber with an electrode gap of 0.5 cm and a total capacity of 20 mL. The amplitude, frequency, and pulse width were controlled and monitored by an oscilloscope (DSO2D10, Qingdao Hantek Electronic Co., Ltd., China) and Function Signal Generator (FY3200S, FeelTech Technology Co., Ltd., China). The treatment parameters were varied according to the experimental design.

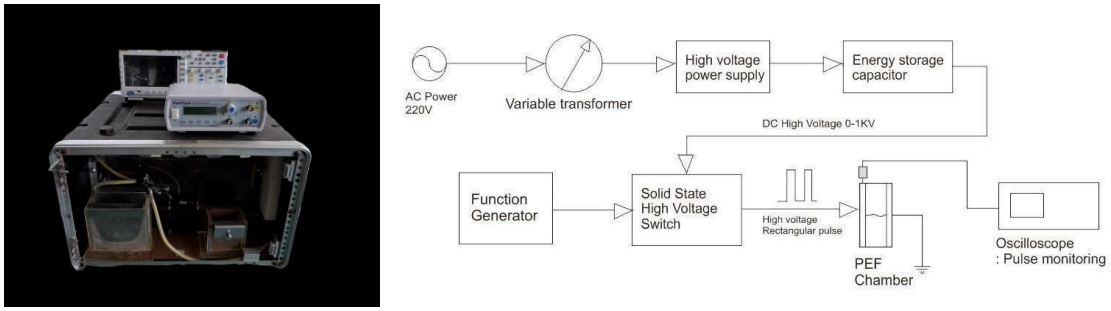

Figure 1. Schematic diagram of PEF system by Innovative Drying Technology Co., Ltd.

2.3 Microbial stimulation by PEF processing

The PEF process parameters for yeast stimulation include electric field strength, time, frequency, pulse width, pulse current, and monopolar rectangular. The yeast was inoculated into the stimulated YPD medium to achieve a final cell count of approximately 10^6 CFU/mL. After that, the inoculated sample was subjected to PEF treatment under the conditions shown in Table 1. After treatment, the yeasts were examined and compared to the untreated PEF sample as a control. PEF-treated samples were collected aseptically in three sterile microtubes and then quickly chilled in an ice bath.

Table 1. PEF process parameters for yeast stimulation

Parameters	Values/ Detail
Electric field strength (kV/cm)	0.5, 3.0
Time (s)	30, 90
Frequency (Hz)	10
Pulse width (μs)	30
Pulse current **(**Amp**)**	5
Pulse shape	Monopolar rectangular

2.4 Determination of yeast growth by optical density

The samples were measured for absorbance at a wavelength of 660 nm every 30 min using a temperature-controlled microplate reader (Infinite 200 PRO, Tecan Trading AG, Switzerland) for 36 h at 25°C, modified according to the method of Soro et al. [10]. After obtaining the absorbance OD_{660} values at each time point, the values were plotted on a graph with the X-axis representing time (hours) and the Y-axis representing the $\ln OD_{660}$ value to analyze the characteristics of the growth period.

2.4.1 Specific growth rate (μ) was determined from the slope of the ln (OD_{660}) versus cultivation time curve during the exponential growth phase. The linear portion of the ln (OD_{660})–time plot corresponding to the exponential growth phase was identified according to the method of Wood et al. [11]. The specific growth rate was calculated using the following equation:

$$\mu = \frac{(\ln OD_2 - \ln OD_1)}{(t_2 - t_1)}$$

When

OD_1 and OD_2 represent the optical density at t_1 and t_2, respectively. In this study, μ represents the highest specific growth rate obtained from the steepest slope of the ln (OD660) versus time curve during the exponential growth phase.

2.4.2 Lag Time (λ) from the graph of $\ln OD_{660}$ with time, the lag time (λ) is the period microorganisms take to adjust before entering exponential growth. The lag time can be calculated according to the method of Baranyi & Pin [12].

$$\lambda = t_2 - \frac{\ln\left(\frac{OD_2}{OD_0}\right)}{\mu}$$

When
OD_0 is the OD value at the starting point before entering the exponential phase.
t_2 is the time during the exponential phase.
μ is the specific growth rate.

2.5 Determination of ethanol concentrations by HPLC

Yeast samples stimulated under the condition yielding the highest μ value were used to study sugar and ethanol concentrations. Fermentation was conducted in 30 mL. Sterile plastic containers containing 15 mL of YPD medium with an initial glucose concentration of 2% (w/v). The yeast inoculum was added to obtain an initial concentration of 10^6 CFU/mL. The cultures were incubated at 25 °C under static conditions for 14 days, and samples were collected at the end of fermentation for ethanol analysis. The concentrations of ethanol were analyzed using a modified method based on Chaiyaso et al. [1 3]. A high-performance liquid chromatograph (HPLC; Chromaster, Hitachi, Japan), equipped with a refractive index detector (RID; VWR Hitachi Chromaster 5450) and an Aminex HPX-87H column (300 mm × 7.8 mm; Bio-Rad, Hercules, CA, USA), was utilized. Both samples and standards were filtered through a 0.22 μm nylon filter and eluted with a mobile phase of 5.0 mmol/L H_2SO_4 at an elution rate of 0.75 mL/min, with the column maintained at 55°C and the detector at 40°C.

3. Results & Discussion

3.1 Growth kinetics of PEF-treated yeasts during fermentation

The stimulation characteristics of *L. thermotolerans* and S. *cerevisiae* in YPD medium under PEF processing are shown in Figure 2. Growth kinetics were evaluated based on the linear region of the $\ln OD_{660}$–time profiles. Figure 2A shows how *L. thermotolerans* grow in different PEF conditions. The untreated control group started earlier in the exponential phase than the low-intensity PEF treatment group (0.5 kV/cm, 30–90 s), which means that the dormancy period was longer. But growth started again, these treatments displayed steeper growth curves, which meant that the specific growth rate was higher. When examined, treatment with 0.5 kV/cm for 90 s led to the most biomass produced (maximum $\ln OD_{660}$ = 2.452 ± 0.05). In contrast, treatment with a higher PEF intensity (3.0 kV/cm, 90 s) resulted in an earlier initiation of the exponential growth phase, with a significantly lower maximum $\ln OD_{660}$ (1.213 ± 0.02) than the untreated control (2.403 ± 0.08), indicating inhibition of later growth.

Furthermore, the absence of a clear resting phase for treatment with 3.0 kV/cm for 30 s suggests that excessive electric field strength interferes with normal cell adjusting, preventing the transition from resting to a stable exponential growth phase. Figure 2B shows the growth behavior of *S. cerevisiae* under PEF treatment. Compared to *L. thermotolerans*, *S. cerevisiae* showed significant stimulation under low-intensity PEF conditions, particularly at 0.5 kV/cm for 90 s, resulting in a higher final $\ln OD_{660}$ (2.409 ± 0.03) compared to the untreated control (2.142 ± 0.04).

On the other hand, the moderate growth promotion was observed at 0.5 kV/cm in 30 s. Conversely, high-intensity PEF treatment (3.0 kV/cm, 30–90 s) resulted in significantly reduced exponential growth and biomass accumulation, as reflected in the significantly lower final $\ln OD_{660}$ (≤ 1.667), indicating an inhibitory effect under these conditions. The distinct growth responses

observed between *L. thermotolerans,* and *S. cerevisiae* highlight the strain-dependent nature of yeast response to PEF processing. Low-intensity electrical stimulation appears to enhance yeast growth, whereas increasing electric field strength results in growth suppression. To quantitatively confirm these observations, key kinetic parameters, including the maximum specific growth rate (μ) and lag phase duration, were subsequently calculated and are presented in Figure 3 and Figure 4.

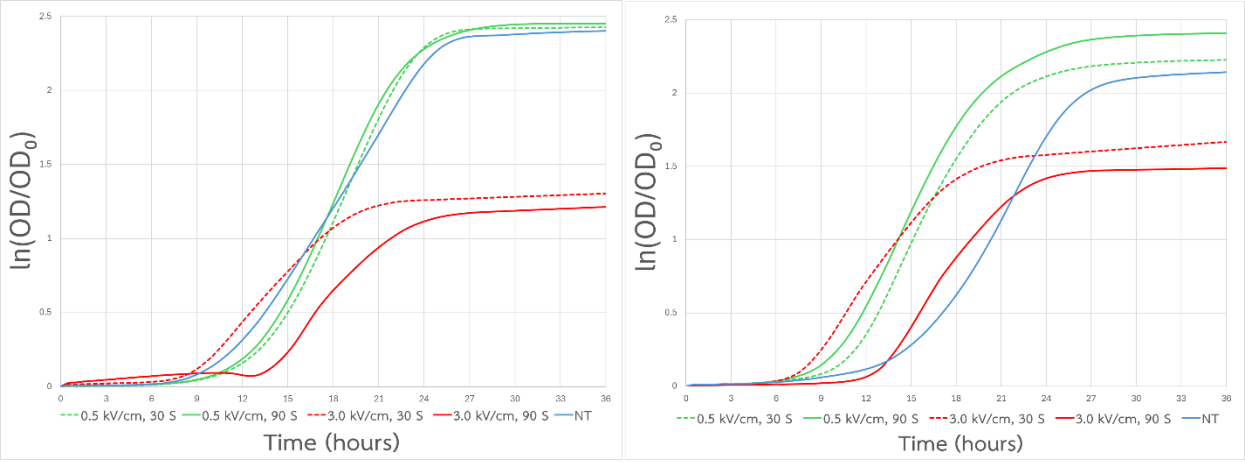

Figure 2. Growth curves of yeast expressed as ln (OD/OD_0) under different PEF treatment conditions. *L. thermotolerans* (A) and *S. cerevisiae* (B)

3.2 Effect of PEF treatment on growth kinetic parameters.

The impact of PEF treatment on the growth kinetic parameters of *L. thermotolerans* and *S. cerevisiae* during fermentation is summarized in Figure 3 (μ) and Figure 4 (Lag time). The assessed parameters were μ and lag time, in comparison to the untreated group. Low-intensity PEF treatment at 0.5 kV/cm increased μ but extended the lag phase of *L. thermotolerans* compared to the untreated group ($p < 0.05$). At an electric field of 0.5 kV/cm for durations of 30 s and 90 s, the μ values were 0.205 ± 0.005 and 0.199 ± 0.003, respectively, reflecting increases of 33.37% and 29.76%. In addition, the lag time was significantly prolonged to 11.385 ± 0.050 h and 10.831 ± 0.147 h, representing increases of 25.59% and 19.47% compared with the untreated group. In contrast, higher electric field strength at 3.0 kV/cm resulted in a significant reduction of μ ($p < 0.05$) at 3.0 kV/cm for 30 s and 90 s; the μ values were 0.106 ± 0.001 and 0.108 ± 0.004, respectively, reflecting decreases of 30.84% and 29.86%, respectively. Similarly, the lag time was significantly prolonged at 3.0 kV/cm for 90 s to 12.373 ± 0.028 (36.48%), but treatment at 3.0 kV/cm for 30 s was significantly shortened to 7.434 ± 0.0087 (−17.99%). The extended lag phase observed in *L. thermotolerans* following PEF treatment may be a result of sublethal membrane disruption caused by electroporation [14]. Previous studies have shown that (σ/σ_i) to values above 1.1–1.3, signifying temporary membrane permeabilization and ionic leakage under non-lethal conditions. This ionic imbalance demands more metabolic energy and time for membrane repair and the recovery of homeostasis, which might result in a longer lag phase preceding the initiation of exponential growth.

A similar trend was observed in *S. cerevisiae*. PEF treatment at 0.5 kV/cm for 90 s resulted in a modest statistically significant increase in μ to 11.99% ($p < 0.05$) in comparison to the control group. However, treatment at 0.5 kV/cm for 30 s resulted in only a slight increase in μ (6.20%), which was not statistically significant ($p > 0.05$). Concurrently, the lag time was markedly reduced under low-intensity PEF treatment, decreasing by 29.29% and 37.79% at 0.5 kV/cm for 30 s and

90 s, respectively. This suggests that yeast cells adapted more rapidly under low PEF intensity conditions. Exposure to higher electric field strength of 3.0 kV/cm reduction in μ of 22.53% and 20.51% for durations of 30 s and 90 s, respectively ($p < 0.05$). At 3.0 kV/cm for 30 s, lag time was significantly reduced by 53.09% ($p < 0.05$) in comparison to the control group. However, treatment at 3.0 kV/cm for 90 s resulted in only a slight reduction in lag time (15.35%), which was not statistically significant ($p > 0.05$). Previous research on PEF-treated yeast cells has shown that low electric field intensity can help maintain cell viability and form colonies under bipolar pulse treatment. Under bipolar pulsed treatment, an optimal electric field of approximately 0.85 kV/cm achieved the highest plating efficiency, more than 100% higher than that observed at the lowest field intensity [8]. This confirms the concept that low-intensity PEF induces reversible electroporation, enhancing the metabolic activity of yeast cells.

The results demonstrated that *S. cerevisiae* exhibited higher μ values and a shorter lag time under low pulsed electric field intensity (0.5 kV/cm), whereas higher electric field intensity (3.0 kV/cm) adversely affected its growth kinetics. This suggests that low-intensity PEF treatment (0.5 kV/cm) stimulated microbial growth kinetics, but higher electric field strength (3.0 kV/cm) inhibited the growth of both *L. thermotolerans* and *S. cerevisiae*. These results indicate that the intensity of PEF is a key factor in determining whether the treatment stimulates or negatively affects growth kinetics.

Consistent with these findings, previous studies have reported intensity-dependent electroporation effects on microbial cells. For example, the growth of *lactobacilli* treated at 7.5 kV/cm for 4 ms increased from 0.89 to 1.96 log CFU/mL after fermentation at 37°C for 20 h. This improvement has been linked to temporary membrane permeabilization and increased cell aggregation. In addition, a significant increase in cholesterol uptake, reaching up to 127.2%, was observed in cells electroporate at 7.5 kV/cm for 3.5 ms compared with those treated at a lower field strength of 2.5 kV/cm [19]. Moreover, nsPEF treatment applied during the exponential growth phase has been shown to stimulate microbial metabolism, significantly enhancing organic acid production by *Lactobacillus plantarum* in a voltage-dependent manner without compromising cell viability [20].

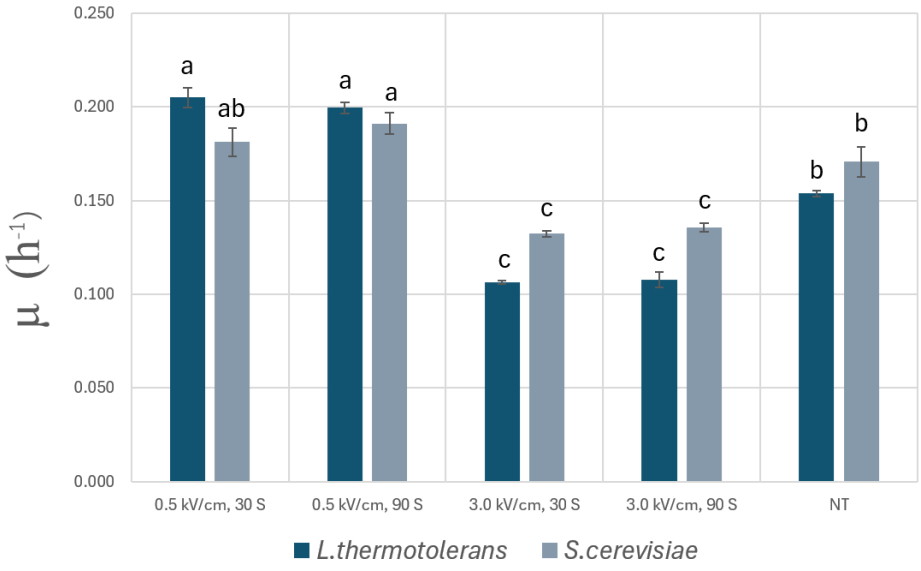

Figure 3. Effect of PEF treatments on the specific growth rate (μ) of *L. thermotolerans* and *S. cerevisiae* during fermentation. Data are presented as mean ± SD (n = 3). Different superscript letters (a–d) indicate significant differences among treatments within the same species ($p < 0.05$). NT: not treated (control).

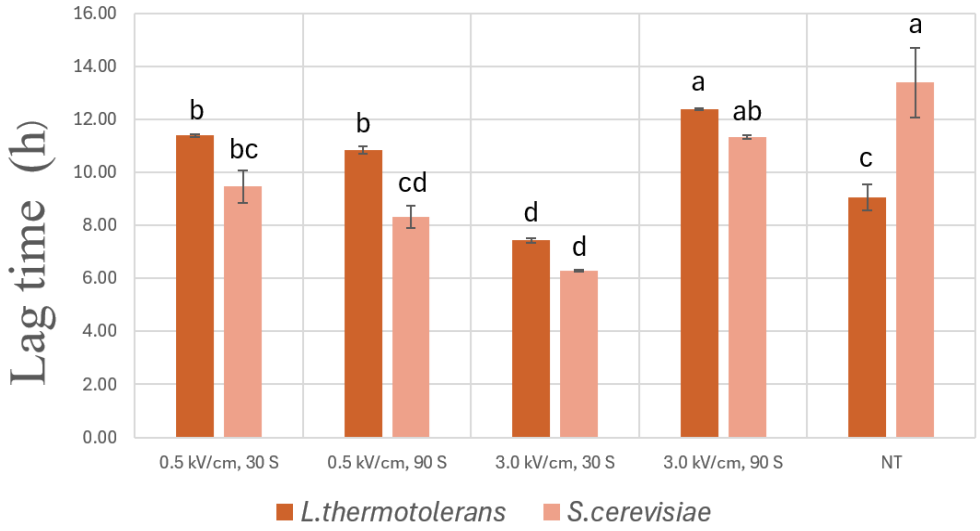

Figure 4. Effect of PEF treatments on the lag time of *L. thermotolerans* and *S. cerevisiae* during fermentation. Data are presented as mean ± SD (n = 3). Different superscript letters (a–d) indicate significant differences among treatments within the same species ($p < 0.05$).
NT: not treated (control).

3.3 Ethanol production during fermentation by PEF processing

The PEF treatment condition of 0.5 kV/cm for 90 s was selected for ethanol concentration analysis by HPLC (Table 2). In *L. thermotolerans*, PEF treatment significantly increased ethanol concentration from 3.28 ± 0.09 to 4.21 ± 0.07 g/L, corresponding to +28.4% compared with the untreated control ($p < 0.05$). A similar trend was reported by McCabe et al. [15], who observed an approximately 40% increase in ethanol production in *Kluyveromyces marxianus* IMB3 following exposure to an electric field of 0.25 kV for 10 ms, relative to non-treated cells. In contrast, ethanol production by *S. cerevisiae* showed a slight, non-significant decrease following PEF treatment, declining from 7.29 ± 0.15 to 6.77 ± 0.27 g/L, corresponding to an approximate reduction of 7.1% compared with the untreated control ($p > 0.05$). The changes in ethanol production may be associated with differences in yeast growth kinetics, showing that PEF treatments may affect fermentation metabolism by changing the substrate used and the metabolic rate. Previous studies have shown that PEF can induce similar metabolic changes in the metabolism of *S. cerevisiae*. Mild PEF treatment enhanced glucose uptake, fermentation efficiency, and ethanol production, suggesting that PEF affects glycolytic and fermentation pathways [16].

The stimulation of *S. cerevisiae* with pulsed electric fields has been shown to enhance substrate consumption in the early stages of fermentation, also supporting the role of PEF in changing yeast metabolic activity [17]. Further investigations into non-Saccharomyces yeasts (*Hanseniaspora* sp.) have revealed substantial decreases in ethanol yield after moderate PEF treatment, confirming the strain-dependent characteristics of PEF-related physiological responses [18]. These findings collectively suggest the impact of PEF on ethanol production is significantly strain-specific, possibly because of differences in membrane composition, stress tolerance capabilities, and regulatory mechanisms controlling fermentative metabolism.

Table 2. Effect of PEF treatment on ethanol concentration determined by HPLC

Treatments	Ethanol concentration	
	L. thermotolerans	*S. cerevisiae*
Control (g/L)	3.28 ± 0.09^{b}	7.29 ± 0.15^{ns}
After PEF (g/L)	4.21 ± 0.07^{a}	6.77 ± 0.27^{ns}

Values are presented as mean ± SD. Different superscript letters (a, b) indicate significant differences ($p < 0.05$); ns indicates not significant.

4. Conclusion

The optimal PEF conditions for *L. thermotolerans* and *S. cerevisiae* in YPD medium were evaluated in this study. Low-intensity PEF treatment at 0.5 kV/cm for 30 s and 90 s stimulated yeast growth kinetics. In *L. thermotolerans*, these treatments increased the specific growth rate (μ), although a longer lag phase was observed before reaching the exponential phase. In contrast, *S. cerevisiae* exhibited a shorter lag time under low PEF intensity, while the increase in μ was significant, only at 0.5 kV/cm for 90 s. Ethanol concentration analysis by HPLC showed that PEF treatment significantly increased ethanol production in *L. thermotolerans* compared with the untreated control. However, ethanol concentration in *S. cerevisiae* showed no significant difference following PEF treatment. These findings indicate that the effects of PEF on yeast growth and ethanol production are strain dependent. Overall, low-intensity PEF treatment may serve as a potential approach to enhance fermentation performance depending on the yeast species.

Acknowledgements

The authors gratefully acknowledge Innovative Drying Technology Co., Ltd. for providing the pulsed electric field (PEF) equipment used in this study.

References

1. Hui YH, Evranuz EÖ, editors. Handbook of plant-based fermented food and beverage technology. 2nd ed. Boca Raton: CRC Press; 2012.
2. Nout MJR. Food Technologies: Fermentation. In: Motarjemi Y, editor. Encyclopedia of food safety. Vol. 3. Amsterdam: Elsevier; 2014. p. 168-177.
3. Tolosa JJM, Prieto SM. Non-Saccharomyces Yeasts: An Enzymatic Unexplored World to be Exploited. In: Kuddus M, editor. Enzymes in food biotechnology: production, applications, and future prospects. London: Academic Press; 2019. p. 433-450.
4. Lei X, Chen Y, Gao B, Zhang T, Dang G, Cheng C, et al. Fermentative performance of indigenous Lachancea thermotolerans in high-sugar and low-acid wine production: Insights from volatomics and metabolomics. Food Res Int. 2025;116411. doi: 10.1016/j.foodres.2025.116411
5. Reis VR, Bassi APG, Cerri BC, et al. Effects of feedstock and co-culture of Lactobacillus fermentum and wild Saccharomyces cerevisiae strain during fuel ethanol fermentation by the industrial yeast strain PE-2. AMB Expr. 2018;8:23. doi: 10.1186/s13568-018-0556-9
6. Lee PR, Li X, Yu B, Curran P, Liu SQ. Non-Saccharomyces yeasts and wine. In: Volkov V, editor. Wine: types, production and health. New York: Nova Science Publishers; 2012. p. 1-42.
7. Al Daccache M, Koubaa M, Maroun RG, Salameh D, Louka N, Vorobiev E. Pulsed electric field-assisted fermentation of Hanseniaspora sp. yeast isolated from Lebanese apples. Food Res Int. 2020;129:108840. doi: 10.1016/j.foodres.2019.108840
8. Fologea D, Vassu-Dimov T, Stoica I, Csutak O, Radu M. Increase of Saccharomyces cerevisiae plating efficiency after treatment with bipolar electric pulses. Bioelectrochemistry and Bioenergetics. 1998 Oct;46(2):285-287. doi: 10.1016/S0302-4598(98)00139-1

9. Sharma P, Wichaphon J, Klangpetch W. Antimicrobial and antioxidant activities of defatted Moringa oleifera seed meal extract obtained by ultrasound-assisted extraction and application as a natural antimicrobial coating for raw chicken sausages. Int J Food Microbiol. 2020;332:108770. doi:10.1016/j.ijfoodmicro.2020.108770
10. Soro AB, Oliveira M, O'Donnell CP, Tiwari BK. Ultrasound assisted modulation of yeast growth and inactivation kinetics. Ultrason Sonochem. 2021;80:105819. doi: 10.1016/j.ultsonch.2021.105819
11. Wood JL, Osman A, Wade SA. An efficient, cost-effective method for determining the growth rate of sulfate-reducing bacteria using spectrophotometry. MethodsX. 2019;6:2248–2257. doi:10.1016/j.mex.2019.09.036
12. Baranyi J, Pin C. Estimating bacterial growth parameters by means of detection times. Appl Environ Microbiol. 1999;65(2):732–736. doi:10.1128/AEM.65.2.732-736.1999
13. Chaiyaso T, Manowattana A, Techapun C, Watanabe M. Efficient bioconversion of enzymatic corncob hydrolysate into biomass and lipids by oleaginous yeast Rhodosporidium paludigenum KM281510. Prep Biochem Biotechnol. 2019;49(6):545–556. doi:10.1080/10826068.2019.1591985
14. Mattar JR, Turk MF, Nonus M, Lebovka NI, El Zakhem H, Vorobiev E. *S. cerevisiae* fermentation activity after moderate pulsed electric field pre-treatments. *Bioelectrochemistry*. 2015;103:92–97. doi:10.1016/j.bioelechem.2014.08.016
15. McCabe A, Barron N, McHale L, et al. Increased efficiency of substrate utilization by exposure of the thermotolerant yeast strain Kluyveromyces marxianus IMB3 to electric-field stimulation. Biotechnol Tech. 1995;9:133–136. doi:10.1007/BF00224412
16. Ying N, Liu W, Fan C, Mo Q, Li S, Zhu L. Moderate pulsed electric field enhances fermentation capacity and induces stress responses in *Saccharomyces cerevisiae*. *Int J Agric Biol*. 2021;25(1):160–164. doi:10.17957/IJAB/15.1651
17. Mattar JR, Turk MF, Nonus M, et al. Stimulation of Saccharomyces cerevisiae cultures by pulsed electric fields. Food Bioprocess Technol. 2014;7:3328–3335. doi:10.1007/s11947-014-1336-4
18. Al Daccache M, Koubaa M, Salameh D, Vorobiev E, Maroun RG, Louka N. Control of the sugar/ethanol conversion rate during moderate pulsed electric field-assisted fermentation of a Hanseniaspora sp. strain to produce low-alcohol cider. Innov Food Sci Emerg Technol. 2020;59:102258. doi:10.1016/j.ifset.2019.102258
19. Lye HS, Karim AA, Rusul G, Liong MT. Electroporation enhances the ability of lactobacilli to remove cholesterol. J Dairy Sci. 2011;94(10):4820-30. doi: 10.3168/jds.2011-4426
20. Kanafusa S, Uhlig E, Uemura K, Galindo FG, Håkansson Å. The effect of nanosecond pulsed electric field on the production of metabolites from lactic acid bacteria in fermented watermelon juice. Innov Food Sci Emerg Technol. 2021;72:102749. doi: 10.1016/j.ifset.2021.102749

P - 374

Development of composite film using chitosan from Mantis shrimp shell and gelatin as bioactive carrier for active packaging

Pimonpan Kaewprachu, Khemmika Jaisunthon, Pannapat Wattanakulsuwan, Supatra Karnjanapratum*

Division of Marine Product Technology, Faculty of Agro-Industry, Chiang Mai University, Chiang Mai 50200, Thailand

**Corresponding author E-mail: suphat.phongthai@cmu.ac.th*

Abstract: Mantis shrimp (*Harpiosquilla raphidea*) shells, a waste material from seafood processing, were utilized as a raw material for chitosan (CS) extraction and subsequent preparation of composite films with gelatin (GE). This study aimed to extract CS from mantis shrimp shells and to develop CS–GE composite films. The CS–GE composite film was prepared by mixing 2% (w/v) CS and 2% (w/v) GE solutions at a 1:1 ratio (v/v). The CS–GE films exhibited significantly higher tensile strength and elongation at break compared with the CS film alone. However, the CS film showed lower water vapor permeability and water solubility than the composite films ($P < 0.05$). When ethanolic extract of propolis (EEP) was incorporated into the CS–GE composite films at various concentrations (0, 1, 2.5, and 5% w/w), tensile strength and elongation at break decreased, while water vapor permeability significantly increased at the highest EEP concentration (5%) ($P < 0.05$). The color of EEP influenced the appearance of the films and enhanced their light barrier properties, particularly in the visible light region. The incorporation of EEP improved the release of bioactive compounds in an aqueous system in a dose-dependent manner, whereas a lower release was observed in a solvent system (95% ethanol). Although an increase in total soluble matter of the composite films containing EEP was observed, a decrease in released phenolic compounds was detected. This suggests that phenolic compounds from EEP may have been present in a bound form and were gradually liberated from the composite film matrix, affecting the availability of bioactive compounds. Overall, chitosan extracted from mantis shrimp shells demonstrated strong potential for the preparation of composite films with gelatin. Moreover, the incorporation of EEP highlighted the effectiveness of CS–GE composite films as carriers for the controlled release of bioactive compounds.

Keywords: Mantis shrimp shells; Chitosan; Composite film; Bioactive carrier; Propolis.

1. Introduction

Large quantities of by-products are generated from small and medium-sized enterprises (SMEs) in the seafood industry, particularly waste derived from the processing of shell-bearing aquatic animals such as mantis shrimp. These residues can be effectively valorized, especially through the extraction of bio-based polymers with high potential for the development of active packaging materials.

Chitin and chitosan (CS) are natural polymers commonly found in the shells of crustaceans, including shrimp, crab, and mantis shrimp. Chitosan is obtained through the deacetylation of chitin and exhibits outstanding properties such as biocompatibility and biodegradability [12]. In addition, chitosan is capable of forming films with good flexibility, mechanical strength, and barrier properties, including low water vapor permeability, making it

suitable for functional packaging applications. Its properties can be further enhanced by modification or blending with other polymers, such as gelatin [9]. Composite films based on chitosan and gelatin have been reported to exhibit improved mechanical and physicochemical properties compared to films prepared from a single component [18].

Gelatin is a protein derived from by-products of the animal processing industry and is known for its excellent film-forming ability, good flexibility, and effective oxygen and gas barrier properties. However, gelatin films tend to exhibit high water sensitivity due to the presence of hydrophilic amino groups, resulting in reduced mechanical properties and stability under high-humidity conditions [13]. Therefore, the fabrication of chitosan–gelatin composite films represents a promising strategy to enhance mechanical performance and barrier properties compared with single-component films.

To achieve the concept of active packaging, packaging materials must possess antioxidant properties to extend the shelf life of food products. Although chitosan exhibits intrinsic antioxidant activity, it is often insufficient to effectively inhibit food oxidation processes [8]. Consequently, the incorporation of bioactive compounds, particularly propolis extract, has been explored. Propolis is a natural resinous substance produced by bees and is rich in phenolic compounds with strong antioxidant activity [8]. The incorporation of propolis extract into composite films enhances their ability to retard food deterioration and increases their potential for industrial packaging applications.

Therefore, the utilization of mantis shrimp shells from seafood SMEs as a raw material for chitosan extraction and the subsequent production of chitosan–gelatin composite films incorporated with propolis extract represents a value-added approach for waste utilization. This strategy not only reduces environmental impacts but also supports the development of safe, sustainable, and high-performance food packaging materials suitable for active packaging applications.

2. Materials and Methods

Raw Materials and Chemicals

Mantis shrimp shell waste was obtained from food processing and mantis shrimp trimming enterprises in Samut Sakhon Province, Thailand. Porcine gelatin was used. Hydrochloric acid (HCl), sodium hydroxide (NaOH), and ethyl alcohol (AR grade) were purchased from RCL Labscan Ltd., Ireland. DL-malic acid (food additive grade) was obtained from Bangkok Chemical Co., Ltd., Thailand. Propolis extract was purchased from the Zippysoap shop via the Lazada online platform, Thailand. All chemicals used in this study were of analytical grade.

2.1 Preparation of Raw Materials

The mantis shrimp shells were thoroughly washed and then dried in a hot-air oven at 60 °C for 24 h. After drying, the shells were ground using a laboratory sample mill and subsequently sieved through a 10-mesh screen. The shell powder was packed in laminated foil bag and stored at 4 °C until used for chitosan extraction.

2.2 Extraction of Chitosan from Mantis Shrimp Shells

Chitosan was extracted from ground mantis shrimp shells using a modified method [21]. The extraction process began with demineralization, in which 200 g of the ground mantis shrimp shells were treated with 3 M hydrochloric acid at a solid-to-liquid ratio of 1:10 (w/v) and heated at 70 °C for 2 h. After the treatment, the samples were washed with water until neutral pH was achieved, drained on a sieve, and subsequently dried in a hot-air oven at 70 °C for 12 h.

Following demineralization, deproteinization was carried out by treating the shells with 10% sodium hydroxide solution at a solid-to-liquid ratio of 1:10 (w/v). The mixture was heated at 80 °C for 2 h to remove proteins. The resulting material was then washed with distilled water until

neutral pH, drained on a sieve, and dried at 80 °C for 24 h. The product obtained at this stage was chitin.

In the final step, deacetylation of chitin was performed by immersing the chitin in 50% sodium hydroxide solution at a solid-to-liquid ratio of 1:20 (w/v) and heating the mixture at 100 °C for 3 h. After completion of the reaction, the samples were washed with water until neutral pH, drained on a sieve, and dried in a hot-air oven at 80 °C for 24 h. The final product obtained from this process was chitosan.

2.3 Characterization of chitosan

2.3.1 Deacetylation Degree (%DD)

Chitosan samples were analyzed using Fourier transform infrared (FTIR) spectroscopy. The spectra were recorded in the range of 4000 to 400 cm^{-1} at room temperature. The degree of deacetylation (DD) was calculated according to the following equation.

$$\%DD = 100\% - \left(\frac{A_{1320}}{A_{1420}} - 0.3822\right) \times \frac{1}{0.0313} \qquad (1)$$

2.3.2 Nitrogen Content

The analysis was performed using the Kjeldahl method (Kjeltec, FOSS, Denmark). Chitosan powder (0.5–1.0 g) was placed in a digestion tube, and 20 mL of sulfuric acid (H_2SO_4) was added. The sample was digested for 2 h to decompose organic nitrogen. Subsequently, nitrogen was distilled using a semi-automatic distillation unit. The distillate was titrated with 0.1 M hydrochloric acid (HCl) until a pale pink endpoint was reached. The volume of titrant consumed was recorded and used to calculate the nitrogen content (%) according to the following equations.

$$Nitrogen\ Content\ (\%) = \frac{(A-B)\times N\times 1.4007}{W} \qquad (2)$$

where A is the volume (mL) of HCl used to titrate the sample, B is the volume (mL) of HCl used to titrate the blank, W is the sample weight (g), N is the molarity of the solution, and 1.4007 is the nitrogen content expressed as percentage by weight.

2.3.3 Moisture Content

Moisture content was determined according to AOAC (2020) (Association of Official Analytical Chemists). Aluminum moisture dishes were first dried in a hot-air oven at 105 °C for 24 h. Approximately 5.xxxx g of the sample was then weighed into the aluminum dish, and the exact weight was recorded. The samples were dried in a hot-air oven (Binder, FD260, Germany) at 105 °C for 3 h. After drying, the samples were transferred to a desiccator and allowed to cool to room temperature. The dishes were reweighed, the weights were recorded, and the moisture content (%) was calculated.

$$Moisture\ Content\ (\%) = \frac{W_1 - W_2}{W_1} \times 100 \qquad (3)$$

where w_1 is the initial weight of chitosan and w_2 is the final weight of chitosan.

2.3.4 Ash Content

Ash content was determined by first drying porcelain crucibles with lids in a hot-air oven at 105 °C for 24 h. Approximately 0.5xxx g of the sample was accurately weighed into the porcelain crucible with lid, and the exact weight was recorded. The samples were then incinerated

in a muffle furnace at 550 °C until white ash was obtained. After incineration, the crucibles were transferred to a desiccator and allowed to cool to room temperature. The crucibles were reweighed, the weights were recorded, and the ash content (%) was calculated.

$$\text{Ash content (\%)} = (W_3 - W_1) / W_2 \times 100 \qquad (4)$$

where W_1 is the weight of the porcelain crucible with lid, W_2 is the weight of the sample, and W_3 is the weight of the porcelain crucible with lid and ash.

2.3.5 Color

Color of the samples was measured using a colorimeter (HunterLab, ColorFlex EZ, USA). Color values were expressed in terms of *L** (lightness), *a** (redness/greenness), and *b** (yellowness/blueness).

2.4 Preparation of Composite Films from Mantis Shrimp Shell Chitosan and Gelatin

The composite films were prepared by blending mantis shrimp shell chitosan (CS) and gelatin (GE) solutions. Chitosan solution (2%, w/v) was prepared by dissolving chitosan in 1% (v/v) malic acid solution with continuous stirring for 2 h. Gelatin solution (2%, w/v) was prepared by dissolving gelatin in distilled water and stirring for 30 min at 60 °C. The CS and GE solutions were mixed at weight ratios of 0:2, 1:1, and 2:0. Glycerol was added as a plasticizer at 30% (w/w), and the mixture was stirred for 30 min at 35 °C.

For film formation, the film-forming solutions were cast onto silicone resin plates (15 × 15 cm). The films were dried in a hot-air oven (Binder, FD260, Germany) at 40 °C overnight. Subsequently, the dried films were conditioned in a temperature- and humidity-controlled chamber (Binder, KMF115, Germany) at 25 °C and 50 ± 5% relative humidity for 24 h. The films were then peeled off from the casting plates and subjected to film property analyses.

2.5 Film Characterization

2.5.1 Mechanical Properties

Mechanical properties of the films were determined using a texture analyzer (Stable Micro Systems, TA.XT plus Extended Height, England) equipped with a 0.049 N load cell and tensile grips under tension mode. The pre-test speed was set at 1.00 mm/s, the test speed at 8.00 mm/s, and the post-test speed at 10.00 mm/s, with a grip separation distance of 20 mm.

Film samples (2 × 5 cm) were prepared, with a total of 10 specimens per formulation. Prior to testing, the films were conditioned at 50 ± 5% relative humidity in a humidity-controlled chamber. Tensile strength (TS) and elongation at break (%EAB) were calculated as the average values from 10 replicates.

2.5.2 Thickness

Film thickness was measured using a digital thickness gauge (Mitutoyo, Japan). Six random positions were measured for each film, with a total of 10 films per formulation.

2.5.3 Appearance and Color

Photographs of the films were taken using a smartphone camera (iPhone 15, Apple Inc., Cupertino, CA, USA). Film samples (2 × 2 cm) were analyzed for color using a colorimeter (HunterLab, ColorFlex EZ, USA). Color values were expressed as *L** (lightness), *a** (redness/greenness), and *b** (yellowness/blueness).

2.5.4 Light Transmittance and Transparency

Light transmittance of the films was measured using a spectrophotometer (Biochrome, Libra S60, England). Film samples (1.4 × 4.5 cm) were scanned over a wavelength range of 200–800 nm. The transparency value was calculated to evaluate the transparency and opacity of the films using the following equation:

$$\text{Transparency} = -\log(T600)/\text{Thickness (mm)} \quad (5)$$

where T600 is the light transmittance at 600 nm.

2.5.5 Water Vapor Permeability (WVP)

Dried silica gel was placed into the water vapor permeability test cups. Film samples (8 × 8 cm) were mounted over the cups and sealed with paraffin wax. The test cups were placed in a temperature- and humidity-controlled chamber (Binder, KMF115, Germany) at 25 °C and 75% relative humidity. The weight of the cups was recorded every hour for 8 h.

$$\text{WVTR } (g/m^2 \cdot s) = \frac{\text{Slope}}{A} \text{ x I} \quad (6)$$

$$\text{WVP } (g \cdot m/m^2 \cdot s \cdot P) = \left(\frac{\text{WVTR}}{\Delta P}\right)/3600 \quad (7)$$

where Slope is the slope of the weight change curve, A is the surface area of the film (πr^2), I is the film thickness (m), and ΔP is the partial pressure difference $(RH_{out} - RH_{in})/100 (RH_{out} - RH_{in})/100$.

2.5.6 Total Soluble Matter (TSM)

Film samples (2 × 2 cm) were weighed to obtain the initial weight and placed in pre-dried centrifuge tubes. The samples were immersed in distilled water and 95% ethanol and shaken at 250 rpm using a horizontal shaker (GFL, Model 3017, Germany) for 24 h. The remaining solids were dried at 105 °C for 24 h, cooled in a desiccator, and weighed to obtain the final weight. Total soluble matter was calculated as follows:

$$\text{Total Soluble Matter (\%)} = [((W_1 - W_2)/ W_1) \times 100] \quad (8)$$

where W_1 is the initial weight of the film and W_2 is the final weight of the film.

2.6 Preparation of Chitosan–Gelatin Composite Films Incorporated with Propolis

Propolis was first dissolved in 95% ethanol (w/w). The propolis extract was then added to the chitosan–gelatin composite film-forming solutions at concentrations of 0, 1, 2.5, and 5% (w/w). Air bubbles were removed using an ultrasonic cleaner (GT SONIC, D20, China). The film-forming solutions were cast onto silicone resin plates (15 × 15 cm) and dried in a hot-air oven (Binder, FD260, Germany) at 40 °C overnight.

The films were conditioned in a temperature- and humidity-controlled chamber (Binder, KMF115, Germany) at 25 °C and 50 ± 5% relative humidity for 24 h. The obtained films were then subjected to film property analyses as described in Section 2.5

2.7 Total Phenolic Content (TPC) of Chitosan–Gelatin–Propolis Composite Films

Total phenolic content was determined using the Folin–Ciocalteu method with slight modifications [5]. Film samples (2 × 2 inches) were dissolved in malic acid and shaken at room temperature for 24 h. Subsequently,1 mL of sample was mixed with 0.2 mL of Folin–Ciocalteu reagent and allowed to stand at room temperature for 3 min. Then, 3 mL of 2% (w/v) sodium

carbonate solution was added, and the mixture was incubated at room temperature for 40 min. Absorbance was measured at 760 nm using a single-beam UV–Vis spectrophotometer (Mapada, model P1). A gallic acid standard curve (0–40 µg/mL) was prepared in advance. All analyses were performed in triplicate, and the results were expressed as total phenolic content.

2.8. DPPH Radical Scavenging Activity

DPPH radical scavenging activity was determined following a modified method [15]. A sample solution (100 µL) dissolved in ethanol was mixed with 100 µL of DPPH solution. The mixture was incubated in the dark at room temperature for 30 min. Absorbance was measured at 517 nm using a microplate reader (Varioskan Lux).

DPPH solution without sample was used as the control, and 70% ethanol was used as the blank. The DPPH radical scavenging activity was calculated using the following equation:

$$\text{DPPH scavenging activity (\%)} = \frac{A_{control} - A_{sample}}{A_{control}} \times 100 \qquad (9)$$

where $A_{control}$ is the absorbance of the control and A_{sample} is the absorbance of the sample.

2.9 Characterization of composite film from Mantis shrimp shell chitosan and gelatin as bioactive carrier

2.9.1 Total Soluble Matter (TSM)

Film samples (2 × 2 cm) were immersed in distilled water and 95% ethanol and shaken at 250 rpm using a horizontal shaker (GFL, Model 3017, Germany) for 24 h. The remaining solids were dried at 105 °C for 24 h and then weighed again to obtain the final weight, according to the procedure described in Section 2.5.6.

2.9.2 Releasing of Phenolic Compound

The release of total phenolic compounds was expressed as a percentage of the total phenolic content present in the film samples (2 × 2 inches). The films were dissolved in distilled water and 95% ethanol and shaken at room temperature for 24 h, after which the released phenolic compounds were analyzed.

The total phenolic content (TPC) of the samples was determined using the method described [5]. with slight modifications, as described in Section 2.7.1.

2.10 Statistical Analysis

All data were analyzed using analysis of variance (ANOVA). Differences among mean values were determined using Duncan's multiple range test. Statistical analysis was performed using the Statistical Package for the Social Sciences (IBM SPSS Statistics, IBM, New York, USA).

3 Results & Discussion

3.1 Chemical composition of chitosan extracted from mantis shrimp shells

The chitosan extracted from mantis shrimp shells was evaluated for its degree of deacetylation and chemical composition. The results are summarized in Table 1. The degree of deacetylation was 93.30%, while the protein content was 5.01 ± 0.69% and the ash content was 0.54 ± 0.05%. These values are consistent with those reported [1]. In terms of color parameters, the chitosan exhibited an L* value of 85.06 ± 0.05, an a* value of 3.94, and a b* value of 12.63 ± 0.04. The moisture content was 9.65 ± 0.14%. These results are in agreement with previous studies, which reported L*, a*, and b* values of 79.79 ± 0.48, 3.03 ± 0.30, and 14.68 ± 0.68, respectively, along with a moisture content of 6.54 ± 0.34% [21].

Table 1. Chemical and physical properties of chitosan extracted from mantis shrimp shells

Properties	Chitosan from Mantis shrimp shell
Degree of Deacetylation (%)	93.30
Nitrogen content (%)	5.01 ± 0.69
Ash content (%)	0.54 ± 0.05
Color	
*L**(Lightness)	85.06 ± 0.05
*a** (redness)	3.94 ± 0.03
*b** (yellowness)	12.63 ± 0.04
Moisture content (%)	9.65 ± 0.14

Values are given as mean±SD, n = 3.

3.2 Properties and characteristics of the developed films

3.2.1 Mechanical properties, thickness, and water vapor permeability of the developed films

The experimental results presented in Table 2 show that the chitosan film (CS) exhibited lower tensile strength than the gelatin film (GE). This can be attributed to the molecular structure of gelatin, which consists of more orderly arranged polymer chains and a higher density of intermolecular interactions, resulting in greater film strength [14]. Previous studies reported that mammalian gelatin films exhibited tensile strength (TS) values in the range of 2.40–63.25 MPa for porcine skin gelatin films, which is comparable to the findings [3]. who reported that gelatin films without glycerol exhibited a high tensile strength of up to 69.53 MPa but a low elongation at break of only 3.2%. This indicates that gelatin films are strong but brittle and prone to fracture under tensile stress.

In contrast, the CS–GE composite film exhibited moderate tensile strength, suggesting that blending chitosan with gelatin improves the compatibility between the two polymers while slightly reducing the rigidity of the gelatin network.

Regarding elongation at break, the CS–GE composite film showed the highest elongation compared to the CS and GE films, indicating enhanced flexibility resulting from the combination of chitosan and gelatin. Said and Sarbon (2022) reported that single-component gelatin films derived from bovine and porcine sources exhibited elongation values in the ranges of 0.78–30.83% and 4.40–90.55%, respectively. In general, gelatin films are more flexible and softer than chitosan films due to their amorphous structure, whereas chitosan exhibits a semi-crystalline structure that contributes to higher rigidity and strength [18].

In terms of film thickness, the CS film exhibited the highest thickness, while the GE film showed the lowest thickness. The CS–GE composite film presented an intermediate thickness. These differences are associated with polymer structure, as gelatin films possess a more ordered molecular arrangement. When blended with chitosan, this ordered structure contributes to a more compact composite film matrix [18], resulting in reduced thickness compared to the CS film alone.

For water vapor permeability (WVP), the CS film exhibited the lowest WVP, indicating superior resistance to water vapor diffusion compared to the GE film. This behavior is due to the hydrophilic nature of gelatin, which facilitates the absorption and transmission of water vapor through the film. The CS–GE composite film showed an intermediate WVP value because the 1:1 (v/v) ratio of chitosan to gelatin allowed the less hydrophilic chitosan to partially suppress the hydrophilic characteristics of gelatin, thereby reducing water vapor transmission relative to the GE film. This observation is consistent with previous findings [2]. who reported that composite films with a CH75:GE25 ratio exhibited approximately a 31% reduction in WVP ($p < 0.05$). The reduction was attributed to enhanced crosslinking between chitosan and gelatin, which decreased free volume within the polymer matrix and limited water molecule diffusion. Water vapor

permeability is influenced by film properties such as molecular weight, degree of deacetylation, and chitosan content [6].

Overall, the developed composite films exhibited sufficient mechanical strength, enhanced flexibility, and appropriate resistance to water vapor transmission, indicating strong potential for application as biodegradable packaging materials that require both mechanical durability and effective moisture barrier properties.

Table 2. Mechanical properties, thickness, and water vapor permeability of the developed Films.

Films	Tensile strength (MPa)	Elongation at break (%)	Thickness (mm)	Water vapor permeability ($g \cdot m/m^2 \cdot s \cdot Pa$)
CS	31.54±0.89 ^{a}	13.14±1.39 ^{b}	0.068±0.003 ^{b}	1.48±0.11 x 10^{-10} ^{b}
GE	62.87±4.19 ^{c}	4.68±0.69 ^{a}	0.036±0.007 ^{a}	2.81±0.14 x 10^{-10} ^{a}
CS-GE	36.78±2.70 ^{b}	31.43±4.18 ^{c}	0.058±0.005^{b}	2.45±0.61 x 10^{-10} ^{a}

Values are given as mean±SD, n = 5 for mechanical properties determination, n = 6 for thickness determination and n = 3 for water vapor permeability determination. Different superscripts in each column indicate significant difference ($p < 0.05$). CS: chitosan-based films; GE: gelatin-based films; CS-GE: chitosan/gelatin composite film

3.2.2 Light transmittance

Optical properties are important factors determining the suitability of films or coatings for food surface applications, as they directly influence product appearance and perceived quality. The light transmittance of the films in the wavelength range of 200–800 nm is shown in Figure 1. In the ultraviolet (UV) region (200–300 nm), all films effectively blocked light transmission. Among them, the CS film exhibited the highest UV-blocking efficiency, while the GE film showed higher light transmittance. The CS–GE composite film also demonstrated good light-barrier properties, which can be attributed to the incorporation of chitosan, resulting in a slightly yellowish film that enhanced light absorption and reduced light transmission. [2]. reported that CH75:GE25 composite films exhibited low light transmittance in the range of 200–380 nm, indicating effective UV protection. This behavior was attributed to the presence of aromatic amino acids, such as phenylalanine and tyrosine, which are capable of efficiently absorbing UV radiation. In the visible light region (400–800 nm), the GE film exhibited the highest light transmittance, whereas the CS film showed the lowest values, indicating superior light-barrier performance. The incorporation of chitosan into the GE film reduced light transmittance, further confirming the ability of chitosan to enhance UV-blocking properties. The reduction in light transmission is associated with the hydroxyl auxochrome groups of chitosan, which contribute to increased light absorption [7].

Figure1. Light transmittance of the developed films CS: chitosan-based films; GE: gelatin-based films; CS–GE: chitosan/gelatin composite film.

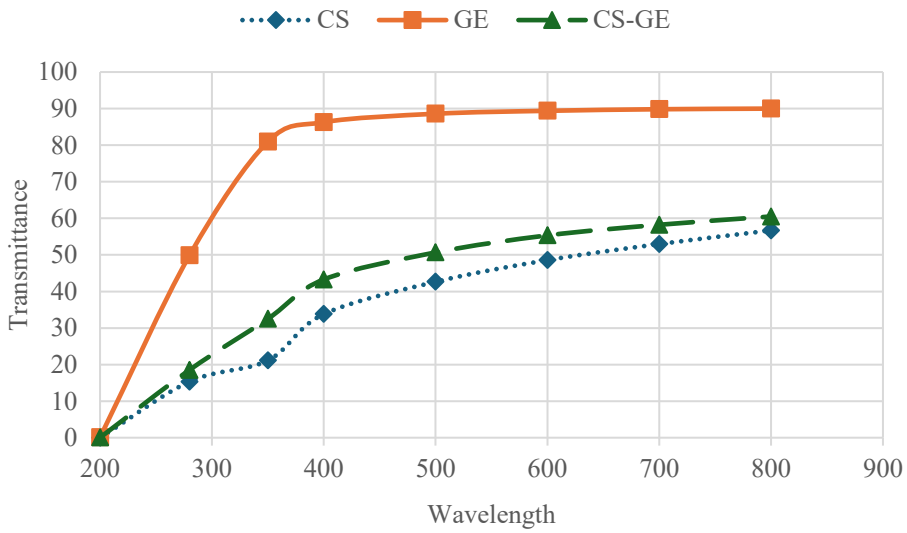

3.2.3 Appearance, color, transparency and total soluble matter

Photographs of the GE, CS, and CS–GE films are shown in Figure 2. The GE film appeared transparent, while the CS film was also transparent but exhibited a more pronounced yellow hue. The CS–GE composite film showed a slight yellow tint, which is consistent with the observed decrease in the L* value upon blending chitosan with gelatin. The a* value, indicating redness, was lower in the composite film compared to the CS and GE films. The positive b* value reflects the yellow coloration of the films.

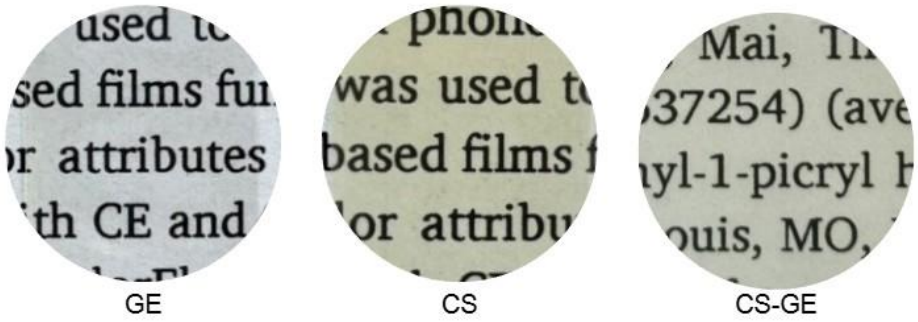

Figure 2. Photographs of the prepared films: gelatin-based film (GE), chitosan-based film (CS), and chitosan/gelatin composite film (CS–GE).

The lightness (L^*) value was highest for the CS film, followed by the CS–GE composite film, and lowest for the GE film. This indicates that the addition of chitosan increases the brightness of the films. Chitosan, being a semi-crystalline polysaccharide with high transparency, efficiently reflects and scatters light, resulting in higher L^* values. In contrast, gelatin films exhibited lower L^* values due to the naturally light-yellow color of gelatin.

For redness (a^*), all films exhibited negative values, with the CS–GE composite film showing the most negative value (-1.69 ± 0.10). Regarding yellowness (b^*), the CS and CS–GE films had significantly higher values than the GE film, with CS at 5.79 ± 0.20 and CS–GE at 5.20 ± 1.11, compared to GE at 0.52 ± 0.04. This yellowish hue is attributed to the natural pale-yellow color of chitosan.

Regarding transparency, as shown in Table 3, lower transparency values indicate higher film transparency. It has been reported that higher transparency values are correlated with decreased lightness (L*) values, as lower lightness results in reduced optical clarity [18].

The solubility of the films in water and ethanol is summarized in Table 3. The CS film showed the lowest solubility in water (30.05%) due to its hydrophobic nature, whereas the GE film exhibited higher solubility (40.90%) because gelatin is hydrophilic. The CS–GE composite film had intermediate solubility (53.74%), as the hydrophilic gelatin allows water molecules to penetrate more easily, while the hydrophobic chitosan contributes to water resistance by limiting electrostatic interactions and hydrogen bonding with water molecules [18].

Regarding ethanol solubility, the CS film had the lowest value (1.59%), followed by the CS–GE composite film (5.01%) and the GE film (7.94%). According [11]. immersion of the CS–GE composite film in 96% ethanol resulted in higher solubility, as dehydration of gelatin caused the internal structure of the film to become more compact, helping maintain the film's shape and properties.

Table 3. Color properties, transparency and total soluble matter of the developed films.

Properties	CS	GE	CS-GE
Color			
*L**(Lightness)	91.37 ± 0.14^{b}	90.61 ± 0.05^{a}	91.20 ± 0.44^{b}
*a** (redness)	-1.57 ± 0.03^{b}	-1.63 ± 0.02^{b}	-1.69 ± 0.11^{a}
*b** (yellowness)	5.79 ± 0.19^{b}	0.52 ± 0.03^{a}	5.20 ± 1.22^{b}
Transparency	4.64 ±0.15 ^{b}	1.34 ±0.04 ^{a}	4.46 ±0.72 ^{b}
Total soluble matter (%)			
Distilled water	30.05 ± 4.43^{b}	40.90 ± 2.66^{b}	53.74 ± 8.45^{a}
Ethanol	1.59 ± 0.86^{c}	7.94 ± 2.34^{a}	5.01 ± 0.93^{b}

Values are given as mean±SD, n = 3 for color properties determination and n = 3 for total soluble matter determination determination. Different superscripts in row indicate significant difference ($p < 0.05$). CS: chitosan-based films; GE: gelatin-based films; CS-GE: chitosan/gelatin composite film.

3.3 Properties and characteristics of chitosan–gelatin composite films incorporated with propolis extract

3.3.1 Mechanical properties, thickness, and water vapor permeability of chitosan–gelatin films with propolis extract

Table 4. presents the mechanical and physical properties of the chitosan–gelatin films containing different concentrations of ethanolic extract of propolis (EEP). The tensile strength (TS) was highest at 36.78 ± 2.70 MPa for films without EEP (0%) and decreased significantly with increasing EEP concentration, reaching the lowest value of 8.98 ± 2.48 MPa for films containing 5% EEP. This reduction in tensile strength indicates that higher EEP concentrations alter the interactions between chitosan and gelatin, likely due to the increased presence of phenolic and hydrophobic compounds in the film matrix, which reduces intermolecular interactions ([4]; [10]). Similar observations have been reported, showing that higher propolis content tends to decrease the mechanical strength of the films.

The elongation at break (EAB) decreased from 31.43% for the control (0% EEP) to 11.19%, 19.24%, and 26.02% for 1%, 2.5%, and 5% EEP, respectively, indicating that EEP affects the film's flexibility. Previous studies have similarly reported that propolis can influence the elasticity of polymer films depending on its concentration ([4]; [10]).

Film thickness increased from 0.058 mm (0% EEP) to 0.060, 0.074, and 0.106 mm for 1%, 2.5%, and 5% EEP, respectively, showing a significant increase ($p < 0.05$) with higher EEP concentrations.

Water vapor permeability (WVP) decreased upon the addition of EEP, with the lowest WVP observed at 2.5% EEP, indicating effective control of active compound release from propolis. However, at 5% EEP, WVP increased due to structural changes in the film caused by high EEP content. This observation aligns [19]. who reported that lower WVP values result from denser polymer networks with enhanced hydrogen bonding and crosslinking. At higher EEP concentrations, WVP tends to increase due to the formation of voids or pores in the film structure as EEP molecules insert between polymer chains. Similar trends were described by [17]. who explained that high filler concentrations can lead to aggregation and uneven distribution of particles, creating voids within the film. [16]. further noted that the propolis-to-chitosan ratio and sample preparation conditions influence these structural changes.

These results suggest that moderate levels of EEP incorporation can effectively reduce water vapor permeability while higher concentrations may compromise the barrier properties of the films.

Table 4. Mechanical properties, thickness, and water vapor permeability of chitosan/gelatin composite films incorporated with propolis extract at different concentrations.

EEP content (%, w/w)	Tensile strength (MPa)	Elongation at break (%)	Thickness (mm)	Water vapor permeability (g·m/m²·s·Pa)
0	36.78±2.70 ^{a}	31.43±4.18 ^{a}	0.058±0.004 ^{b}	2.45±0.61 x 10^{-10} ^{b}
1	26.50±1.80 ^{b}	11.19±3.03 ^{c}	0.060±0.009 ^{b}	2.41±0.44 x 10^{-10} ^{b}
2.5	21.36±1.64 ^{c}	19.24±6.25 ^{b}	0.074±0.002 ^{b}	2.12±0.19 x 10^{-10} ^{b}
5	8.98±2.48 ^{d}	26.02±8.28 ^{ab}	0.106±0.033 ^{a}	4.53±0.37 x 10^{-10} ^{a}

Values are given as mean±SD, n = 5 for mechanical properties determination, n= 6 for thickness determination and n= 3 for water vapor permeability determination. Different superscripts in each column indicate significant difference (p<0.05). EEP: propolis extract.

3.3.2 Light transmittance

The transparency of packaging films is important for consumer acceptance and for visual inspection of products during storage. The light transmittance of the chitosan–gelatin films incorporated with different concentrations of ethanolic extract of propolis (EEP) was measured using a spectrophotometer in the wavelength range of 200–800 nm, as shown in Figure 3 and summarized in Table 5. The results indicate that the addition of EEP reduced both light transmittance and transparency as its concentration increased. EEP dispersed within the film matrix caused light scattering, reducing the amount of transmitted light and increasing film opacity. This demonstrates that the films exhibit effective UV-blocking properties. These observations align [4]. who reported that films containing propolis exhibit higher opacity compared to films without propolis. The differences in transparency can be attributed to film thickness, molecular structure, and internal arrangement. The current films are considered low-opacity films, allowing clear visibility of the packaged product. However, more opaque films are also desirable in specific applications, such as protecting products sensitive to oxidative reactions.

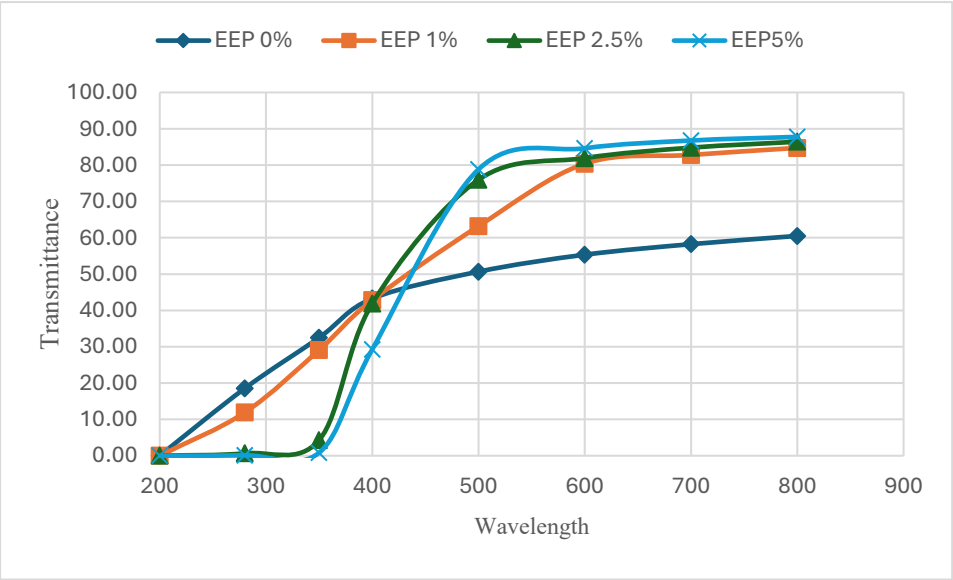

Figure 3. Light transmittance of chitosan/gelatin composite films incorporated with different concentrations of ethanolic extract of propolis (CS-GE/EEP). The numbers (0, 1, 2.5, and 5%) indicate the concentration of propolis extract incorporated into the film formulation.

3.3.3 Appearance, color, transparency of chitosan/gelatin composite films incorporated with propolis extract

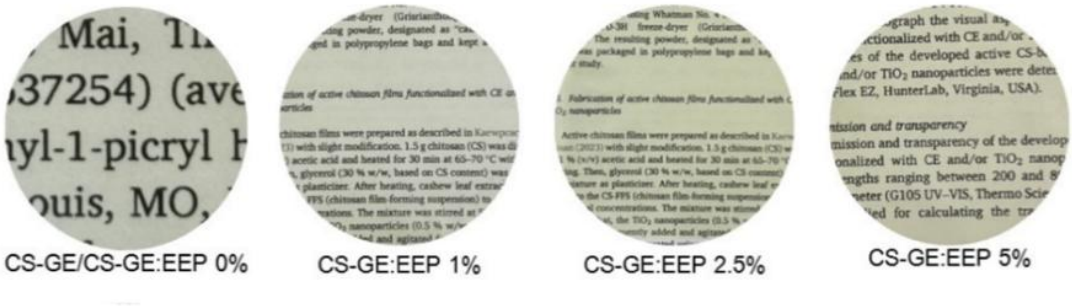

Figure 4. Photographs of chitosan/gelatin composite films incorporated with different concentrations of ethanolic extract of propolis (CS-GE/EEP). The numbers (0, 1, 2.5, and 5%) indicate the concentration of propolis extract incorporated into the film formulation.

From Table 5, the addition of propolis extract (EEP) affected the L^*, a^*, and b^* values. The lightness (L^*) of the films decreased with increasing EEP concentration. The film without EEP (0%) had the highest L^* value (91.20), indicating greater transparency and brightness, whereas the film with 5% EEP had the lowest L^* value (88.03), reflecting a darker color as EEP concentration increased. This trend corresponded with increasingly negative a^* values and higher b^* values, consistent [8]. At 5% EEP, the films tended to exhibit a greenish-yellow hue, characteristic of the dark-colored phenolic compounds in propolis.

Table 5. Color properties and transparency of chitosan/gelatin composite films incorporated with different concentrations of propolis extract (EEP).

Characteristics	EEP content (%, w/w)			
	0	1	2.5	5
Color				
L*(Lightness)	91.20 ± 0.52^{a}	90.09 ± 0.12^{b}	89.96 ± 0.34^{b}	88.03 ± 0.71^{c}
a* (redness)	-1.69 ± 0.10^{a}	-1.95 ± 0.02^{b}	-2.24 ± 0.05^{c}	-2.79 ± 0.11^{d}
b* (yellowness)	5.20 ± 1.11^{c}	4.76 ± 0.40^{c}	8.91 ± 0.58^{b}	13.06 ± 2.14^{a}
Transparency	4.46±0.72 ^{a}	1.57±0.06 ^{b}	1.17±0.03 ^{bc}	0.68±0.04 ^{c}

Values are given as mean±SD, n = 3 for color properties determination and n= 3 for total soluble matter determination .Different superscripts in row indicate significant difference ($p<0.05$). EEP: propolis extract.

3.4 Total Phenolic Content and DPPH Radical Scavenging Activity of Chitosan/Gelatin Composite Films Incorporated with Propolis Extract

As shown in Table 6, The total phenolic content (TPC) and DPPH radical scavenging activity of the chitosan/gelatin films increased significantly ($p < 0.05$) with increasing concentrations of ethanolic propolis extract (EEP). Films without EEP (0%) exhibited the lowest TPC (76.83 ± 5.99 mg gallic acid/g sample) and showed no antioxidant activity (0%). In contrast, the addition of EEP at 1%, 2.5%, and 5% resulted in a continuous increase in TPC, with the highest value observed at 5% EEP (529.23 ± 10.64 mg gallic acid/g sample). This trend is consistent with the findings [8]. indicating that the high phenolic compound content in EEP effectively reflects its antioxidant properties.

Furthermore, DPPH radical scavenging activity increased with increasing EEP concentration, reaching the highest value (61.31 ± 0.50%) at 5% EEP. The phenolic compounds present in EEP play a significant role in enhancing the antioxidant capacity of the films ($p < 0.05$). These results are in agreement with the report [8]. who explained that DPPH antioxidant activity increased by 49.8%, 94.0%, and 94.5% in films containing 5%, 10%, and 20% propolis, respectively.

Table 6. Total phenolic content and DPPH radical scavenging activity of chitosan/gelatin composite films incorporated with different concentrations of propolis extract (EEP).

EEP content (%, w/w)	0	1	2.5	5
Total phenolic content (%)	7.68 ± 0.60^{d}	15.68 ± 0.72^{c}	32.46 ± 0.70^{b}	52.92 ± 1.06^{a}
DPPH scavenging activity (%)	0.00 ± 0.00^{d}	34.09 ± 5.46^{c}	48.69 ± 4.12^{b}	61.31 ± 0.50^{a}

Values are given as mean±SD, n = 3 for total phenolic content determination and n= 3 for DPPH scavenging activity determination. Different superscripts in row indicate significant difference ($p<0.05$). EEP: propolis extract

3.5 Potential of chitosan/gelatin composite films incorporated with propolis extract on releasing of bioactive compound

As show in Figure 5 (a), The total soluble matter (TSM) analysis showed that films dissolved more readily in distilled water than in ethanol. The film without EEP (0%) had the lowest water solubility (53.74%), which increased with higher EEP concentrations, reaching 69.94% at 5% EEP. This aligns [20]. who reported that phenolic compounds enhance water solubility due to their hydrophilic nature and their ability to disrupt the original film structure. In contrast,

solubility in 95% ethanol decreased with increasing EEP concentration, ranging only from 1.43–1.54% for films containing 2.5–5% EEP. The reduced solubility in ethanol, which mimics fatty food matrices, is attributed to gelatin dehydration in ethanol, which also contributes to a more ordered internal film structure [11].

From figure 5 (b), The total phenolic content (TPC) released from the films in distilled water and ethanol decreased significantly as EEP concentration increased. Films without EEP (0%) showed the highest phenolic release in water at 0.28 ± 0.02%, which progressively decreased to 0.21 ± 0.00, 0.11 ± 0.02, and 0.07 ± 0.01% for films containing 1%, 2.5%, and 5% EEP, respectively. This reduction is due to phenolic compounds in EEP interacting more strongly with the polymer matrix, limiting their solubility in water.

Similarly, phenolic content released in ethanol decreased from 0.22 ± 0.04% in the 0% EEP film to 0.19 ± 0.65, 0.07 ± 0.00, and 0.05 ± 0.00% in films with 1%, 2.5%, and 5% EEP, respectively. The reduced release with higher polyphenol concentrations may result from hydrogen bonding and complex formation between polyphenols and polymer chains, where polyphenols act as crosslinking agents, densifying the film structure and restricting the diffusion of active compounds. This aligns with reports [11,22].

From figure 5 (b), The total phenolic content (TPC) released from the films into both distilled water and ethanol significantly decreased with increasing EEP concentration. The film without EEP (0%) exhibited the highest phenolic release in distilled water (0.28 ± 0.02%). As the EEP concentration increased to 1%, 2.5%, and 5%, the amount of phenolics released into distilled water continuously decreased to 0.21 ± 0.00, 0.11 ± 0.02, and 0.07 ± 0.01%, respectively. For ethanol, the film containing 0% EEP showed a released TPC value of 0.22 ± 0.04%, which decreased to 0.19 ± 0.65, 0.07 ± 0.00, and 0.05 ± 0.00% in films containing 1%, 2.5%, and 5% EEP, respectively. These results indicate that the films exhibited higher solubility in distilled water than in ethanol, which is a less polar solvent. This can be attributed to the ability of water to more effectively penetrate the hydrophilic polymer matrix. The findings are consistent with the report [11]. who stated that hydrophilic biopolymer films tend to dissolve and release active compounds more effectively in highly polar solvents. Moreover, EEP concentration significantly influenced film solubility. Increasing EEP content from 0% to 1%, 2.5%, and 5% resulted in a continuous reduction in film solubility in both distilled water and ethanol, as reflected by the decreasing TPC values released from the films. This reduction can be explained by the interaction between phenolic compounds in EEP and polymer chains through hydrogen bonding and complex formation, which increases the density of the film structure. As a result, phenolic compounds become entrapped within the polymer matrix and are less able to dissolve or diffuse into the surrounding solvent. In addition, film solubility was directly correlated with the amount of phenolic compounds released. Films with higher solubility exhibited higher phenolic release, whereas films with lower solubility released lower amounts of phenolics, particularly at higher EEP concentrations. This phenomenon is mainly due to the role of phenolic compounds as crosslinking agents, which enhance the strength and compactness of the polymer network, thereby limiting the diffusion of active compounds from the film into the solvent. Furthermore, the denser film structure reduces solvent uptake, resulting in lower film solubility and reduced phenolic release, in agreement with the findings reported [22].

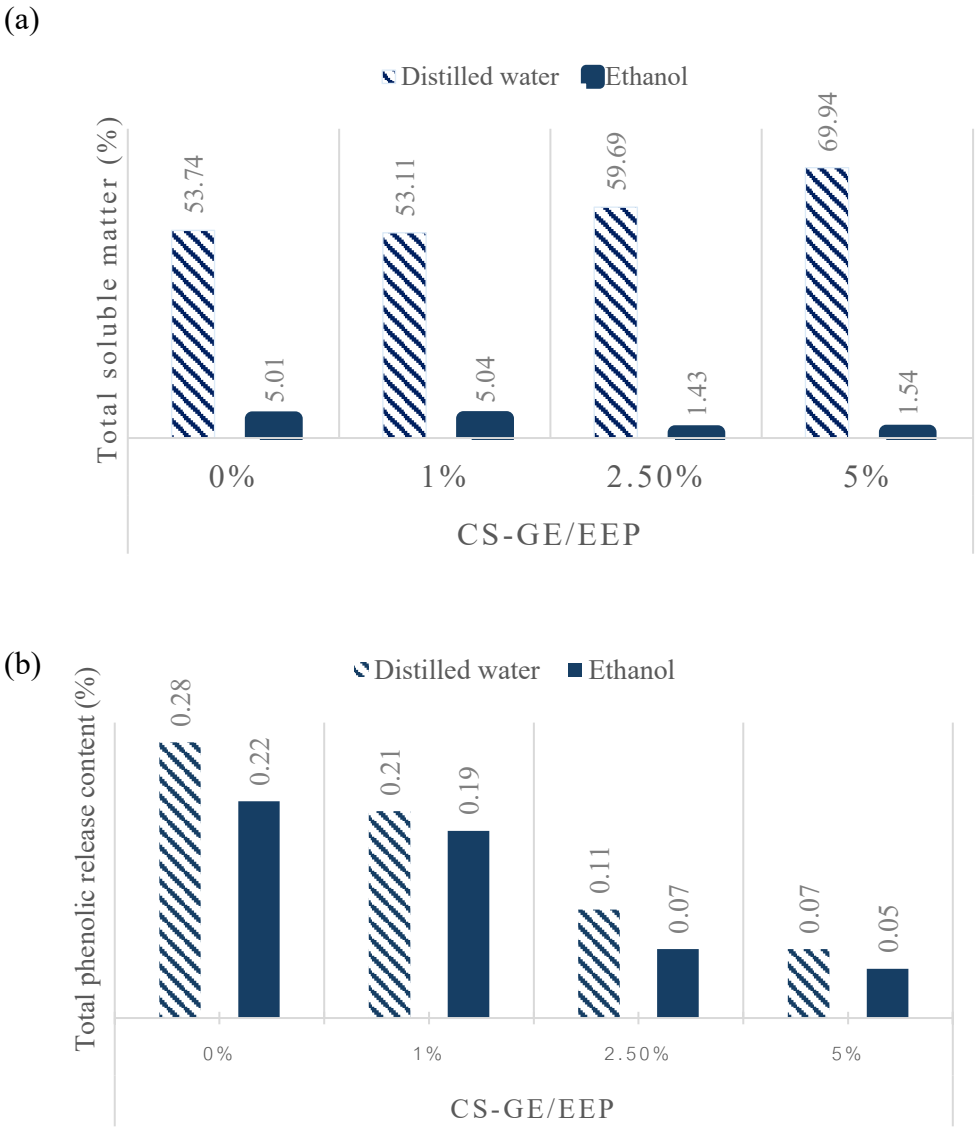

Figure 5. Total soluble matter of chitosan/gelatin composite films incorporated with different concentrations of ethanolic extract of propolis (CS-GE/EEP**).** The numbers (0, 1, 2.5, and 5%) indicate the concentration of propolis extract incorporated into the film formulation.

4. Conclusion

The development of composite films combining chitosan extracted from mantis shrimp shells, a by-product of seafood processing, with gelatin aimed to serve as an active carrier for bioactive compounds in packaging was investigated. The effect of blending chitosan and gelatin on mechanical properties, thickness, water vapor permeability, and the release of active compounds was studied. The CS-GE composite film exhibited greater flexibility than the chitosan-only film and showed better resistance to water vapor transmission than the gelatin-only film. The interaction between chitosan and gelatin enhanced hydrogen bonding between the polymers, resulting in a denser film structure capable of retaining bioactive compounds. When propolis extract (EEP) was incorporated, the film properties changed according to the EEP concentration: tensile strength decreased, while flexibility, thickness, and antioxidant activity increased. The films became darker, less transparent, and demonstrated effective UV protection. These results clearly indicate that the CS–GE composite film functions effectively as a carrier for bioactive compounds, as the polymer–polymer and polymer–phenolic interactions enable the entrapment and controlled retention of active substances within the film matrix. Furthermore,

the incorporation of EEP at different concentrations significantly influenced the release behavior of bioactive compounds. Increasing EEP content led to a reduction in the release of phenolic compounds, which can be attributed to the formation of hydrogen bonds and complexes between polyphenols and the polymer chains. In this context, polyphenols acted as natural crosslinking agents, increasing the density of the composite film structure and restricting the diffusion of active compounds. As a result, the composite films exhibited a concentration-dependent controlled release profile rather than a rapid release. Therefore, the utilization of chitosan extracted from mantis shrimp shells in the fabrication of CS–GE composite films represent an alternative and promising strategy for the development of active packaging materials. In addition to food packaging applications, the tunable mechanical properties, antioxidant activity, UV-blocking ability, and controlled release behavior of EEP-loaded composite films also highlight their potential for biomedical and medical-related applications, such as wound dressings or drug delivery systems, where sustained release and bioactivity are desirable.

5. Acknowledgements

The authors would like to sincerely thank Associate Professor Dr. Supatra Kanchanapratum and Assistant Professor Dr. Pimolpan Kaewpraju, our research advisors, for their guidance, valuable suggestions, and continuous support throughout the research project. We also extend our gratitude to the staff of the Faculty of Agro-Industry, Department of Seafood Technology, Chiang Mai University, for their kind assistance and facilitation during the study and the implementation of this research project.

References

1. Ahmed, H., Noyon, M. A. R., Uddin, M. E., Rafid, M. M., Hosen, M. S., & Layek, R. K. (2025). Development and characterization of chitosan-based antimicrobial films: A sustainable alternative to plastic packaging. Cleaner Chemical Engineering, 11, 100157.
2. Aliabbasi, N., Emam-Djomeh, Z., & Rezaeinia, H. (2025). The development and analysis of modified chitosan-gelatin composite films using ultrasound treatment followed by enzymatic crosslinking. Journal of Polymers and the Environment, 1-18.
3. Azmi, N. S., Basha, R. K., Othman, S. H., Mohammed, M. A. P., Wakisaka, M., Ariffin, S. H., & Salim, N. H. (2025). Development of fish gelatin film for anti-fogging mushroom packaging. Journal of Food Engineering, 387, 112306.
4. Biratu, G., Woldemariam, H. W., & Gonfa, G. (2024). Development of active edible films from coffee pulp pectin, propolis, and honey with improved mechanical, functional, antioxidant, and antimicrobial properties. Carbohydrate Polymer Technologies and Applications, 8, 100557.
5. Carvalho, D. G., Ranzan, L., Jacques, R. A., Trierweiler, L. F., & Trierweiler, J. O. (2021). Analysis of total phenolic compounds and caffeine in teas using variable selection approach with two-dimensional fluorescence and infrared spectroscopy. Microchemical Journal, 169, 106570.
6. Cazón, P., & Vázquez, M. (2020). Mechanical and barrier properties of chitosan combined with other components as food packaging film. Environmental chemistry letters, 18(2), 257-267.
7. Chen, H., Lan, X., Guan, X., Luo, R., Zhang, Q., Ren, H., Xu, Z., & Tang, J. (2024). Comparative study on the effects of chitosan, carrageenan, and sodium alginate on the film-forming properties of fish skin gelatin. Lwt, 199, 116111.
8. De Carli, C., Aylanc, V., Mouffok, K. M., Santamaria-Echart, A., Barreiro, F., Tomás, A., Pereira, C., Rodrigues, P., Vilas-Boas, M., & Falcão, S. I. (2022). Production of chitosan-based biodegradable active films using bio-waste enriched with polyphenol propolis extract

envisaging food packaging applications. International journal of biological macromolecules, 213, 486-497.
9. Hosseini, S. F., Rezaei, M., Zandi, M., & Ghavi, F. F. (2013). Preparation and functional properties of fish gelatin–chitosan blend edible films. Food chemistry, 136(3-4), 1490-1495.
10. Júnior, L. M., de Ávila Gonçalves, S., da Silva, R. G., Martins, J. T., Vicente, A. A., Alves, R. M. V., & Vieira, R. P. (2022). Effect of green propolis extract on functional properties of active pectin-based films. Food Hydrocolloids, 131, 107746.
11. Kurek, M., Ščetar, M., Nuskol, M., Janči, T., Tanksoić, M., Klepac, D., Čakić Semenčić, M., & Galić, K. (2024). Assessment of chitosan/gelatin blend enriched with natural antioxidants for antioxidant packaging of fish oil. Antioxidants, 13(6), 707.
12. Leceta, I., Guerrero, P., & De La Caba, v. K. (2013). Functional properties of chitosan-based films. Carbohydrate polymers, 93(1), 339-346.
13. Murugan, G., Nilsuwan, K., Prodpran, T., Ponnusamy, A., Rhim, J.-W., Kim, J. T., & Benjakul, S. (2024). Active fish gelatin/chitosan blend film incorporated with guava leaf powder carbon dots: properties, release and antioxidant activity. Gels, 10(4), 281.
14. Said, N. S., & Sarbon, N. M. (2022). Physical and mechanical characteristics of gelatin-based films as a potential food packaging material: A review. Membranes, 12(5), 442.
15. Saiwong, S., Autsavapromporn, N., Siriwoharn, T., Techapun, C., & Wangtueai, S. (2023). Enzymatic hydrolysis optimization for preparation of sea cucumber (Holothuria scabra) hydrolysate with an antiproliferative effect on the HepG2 liver cancer cell line and antioxidant properties. International Journal of Molecular Sciences, 24(11), 9491.
16. Stefanowska, K., Bucher, M., Reichert, C. L., Sip, A., Woźniak, M., Schmid, M., Dobrucka, R., & Ratajczak, I. (2024). Chitosan-based films with nanocellulose and propolis as active packaging materials. Industrial Crops and Products, 219, 119112.
17. Tabassum, Z., Girdhar, M., Malik, T., Kumar, A., & Mohan, A. (2024). Advancing sustainability: a novel biopolymer-based degradable nanoclay composite film for next-generation packaging. Materials Advances, 5(20), 8060-8073.
18. Tagrida, M., Nilsuwan, K., Gulzar, S., Prodpran, T., & Benjakul, S. (2023). Fish gelatin/chitosan blend films incorporated with betel (Piper betle L.) leaf ethanolic extracts: Characteristics, antioxidant and antimicrobial properties. Food Hydrocolloids, 137, 108316.
19. Wang, Z.-Q., Chen, H.-X., Zhang, Y.-C., & Zheng, Y.-Z. (2025). Tailoring functional chitosan films using deep eutectic solvents extracts of propolis for active food packaging. Food Hydrocolloids, 111822.
20. Yang, J., Fei, T., Zhang, W., & Cong, X. (2023). Tannic Acid and Ca(2+) Double-Crosslinked Alginate Films for Passion Fruit Preservation. Foods, 12(21). https://doi.org/10.3390/foods12213936
21. Yarnpakdee, S., Kaewprachu, P., Jaisan, C., Senphan, T., Nagarajan, M., & Wangtueai, S. (2022). Extraction and physico–chemical characterization of chitosan from mantis shrimp (Oratosquilla nepa) shell and the development of bio-composite film with agarose. Polymers, 14(19), 3983.
22. Yi, F., Chen, X., Hou, F., Song, L., Zhan, S., Wang, X., Zhang, R., Yang, Q., Wang, X., & Liu, Z. (2024). Chitosan/zein-based sustained-release composite films: Fabrication, physicochemical properties and release kinetics of tea polyphenols from polymer matrix. International journal of biological macromolecules, 269, 131970.

P - 403

Effect of Tween 20 and Tween 80 on Characteristics of the Water-in-Oil-in-Water Emulsion of *Centella asiatica* Beads

Sirapassorn Chansong, Jiraporn Sirison*

School of Food Industry, King Mongkut's Institute of Technology Ladkrabang, Bangkok, 10520, Thailand

**Corresponding author E-mail: jiraporn.si@kmitl.ac.th*

Abstract: Most bioactive compounds in extracted *Centella asiatica* are heat-sensitive during food processing. Spherification can help preserve both water- and oil-soluble compounds, while surfactants are needed to form stable emulsions. This study investigated the effects of polysorbates (Tween 20 and Tween 80) on the characteristics of *Centella asiatica* beads. Water-in-oil (W/O) emulsions of extracts obtained by 95% ethanol were prepared with Tween 20, Tween 80, or a mixture of Tween 20 and Tween 80. The ratio of extract to surfactant was 2:1. These W/O emulsions were then dispersed in a gum arabic (0.5% w/v) and alginate (1.5% w/v) solution to form water-in-oil-in-water (W/O/W) emulsions before bead formation using an encapsulation machine. The beads were evaluated for yield, size, swelling capacity at pH 4 and pH 7, texture, and polyphenol content. The production yield of the beads was 42.59 ± 0.15%. The beads were generally spherical. The largest bead diameters (3.38 mm) were obtained when the core W/O emulsions were made using Tween 80. The mixture of Tween 20 and Tween 80 produced beads with the lowest swelling capacity in both acidic (pH 4; citric and acetic acid) and neutral (pH 7; phosphate buffer) conditions with swelling values of 145.96%, 25.48%, and 189.27% in citric acid, acetic acid and neutral conditions, respectively. All bead samples exhibited higher swelling at pH 7 and the lowest swelling in acetic acid (pH 4). Springiness, cohesiveness, and chewiness did not differ among treatments, while hardness and gumminess were highest in beads produced with the Tween 20 and Tween 80 mixture. Polyphenol contents in all bead samples were low ranging from 0.61 to 0.64 mg GAE/100 g beads. In conclusion, *Centella asiatica* beads produced using a Tween 20 and Tween 80 mixture in the core (W/O emulsion), with gum arabic and alginate as the outer wall (W/O/W emulsion), are suitable for acidic foods. Beads prepared with the mixture of Tween 20 and Tween 80 exhibited the lowest swelling, suggesting a lower release of bioactive compounds, and show potential for use as functional ingredients in food products such as beverages and dairy products (e.g., yogurt).

Keywords: *Centella asiatica*; Spherification; *Centella asiatica* bead; W/O/W emulsion

1. Introduction

Centella asiatica is a medicinal herb with numerous therapeutic benefits. Its bioactive constituents include triterpenoids and phenolic compounds, particularly flavonoids, which exhibit antioxidant and anti-inflammatory activities, provide protection against wound formation, promote natural wound healing processes, and enhance cognitive function[1, 2]. Research on the benefits of *Centella asiatica* includes using extracts to treat Ulcerative Colitis[3]. However *Centella asiatica* extract has limited use in food production due to its poor solubility in aqueous media, poor stability, and degradation of the functionality of its bioactive compounds during food processing[4, 5]. Encapsulation technique, considered as an effective approach to enhancing the feasibility of incorporating bioactive compounds into food products, could help increase the

utilization of *Centella asiatica* extract in food processing. This technique further enhances the stability of the final product and facilitates the controlled release of food ingredients[6].

The encapsulation substance being encapsulated is called the core material, while the material used for encapsulation is known as the wall material. The role of the wall material is to help protect the core material from various environmental factors. Sodium alginate is a wall material from brown algae, commonly used to crosslink hydrogels with divalent cations such as calcium. However, alginate exhibits elevated porosity, leading to the premature release of significant compounds throughout the process. Therefore, gum arabic is used to help improve the efficiency of encapsulation[7].

Tweens are commonly used surfactants and are generally recognized as safe. Tweens are typical amphiphilic small molecules with similar hydrophilic heads consisting of sorbitan ring connecting up to polyoxymethylene chains with variable lengths, and the fourth chain esterified with different hydrophobic fatty acid moieties[8]. Tween 20 and 80 are approved food additives, Tween 20 could increase the stability of dodecane-loaded alginate-based dispersions and increase the solubility. Tween 80 in calcium alginate is a complete release[9]. The application of Tween as a surfactant facilitates the formation of a water-in-oil-in-water (W/O/W) emulsion system. Accordingly, this study investigated the effects of polysorbates (Tween 20 and Tween 80) on the characteristics of *Centella asiatica* beads encapsulated with sodium alginate and gum arabic.

Centella asiatica beads produced by encapsulation can enhance the utilization of the extracts by masking undesirable sensory attributes and protecting bioactive compounds during food processing, demonstrating strong potential as a functional ingredient in various food products to improve health benefits.

2. Materials and Methods

2.1 Materials

Centella asiatica (leaves and stems) was purchased from a farm certified by the Department of Agriculture, Ministry of Agriculture and Cooperatives, in Nakhon Pathom, Thailand. Sodium alginate, gum arabic, calcium chloride, and ethanol which were food grade were obtained from Bangkok Chemical Co., Ltd. (Bangkok, Thailand), and Liquor Distillery Organization (Chachoengsao, Thailand), respectively. Tween 20 and 80 (food grade) were obtained from RR Cosmetics & Food ingredients Co., Ltd. (Samut Prakan). Reagents which were used for all analysis were of analytical grade. Deionized (DI) water was used in all experiments.

2.2 Extraction of *Centella asiatica* extracts

Extractions of *Centella asiatica* were carried out according to the method of Wong and Ramli[2] with some modification. Briefly, fresh *Centella asiatica* (leaves and stems) were washed with clean water and cut into approximately 1 X 1 inches. They were dried in a hot air oven (Patch/663, Thailand) at 50°C overnight. Dried samples were ground into powders using a pin mill (Retsch ZM1000, Germany) and sieved through a 160-micron sieve. *Centella asiatica* powders (100 g) were mixed with 95% ethanol in the ratio of 1:4 (w/v) in a glass bottle. The bottles were covered with aluminum foil and stored in the dark at room temperature for 7 days. After storage, the mixture of *Centella asiatica* powders and ethanol were filtered through a Whatman No. 1 filter paper. The filtrate was evaporated using a rotary evaporator (BUCHI Rotavapor R-300, Switzerland) at 50°C with a speed of 150 revolutions per minute (rpm) for 1 hour. Crude extracts were stored in brown glass bottles in a refrigerator for further use.

2.2 Preparation of *Centella asiatica* beads

Spherification of *Centella asiatica* extracts was carried out according to the method of Mariadi et al. (11) with slight modifications. Briefly, the extracts were first mixed with Tween 20, Tween 80, or a mixture of Tween 20 and Tween 80 using a magnetic stirrer at an extract-to-Tween ratio of 2:1 (w/w); for the combined treatment, Tween 20 and Tween 80 were used at a ratio of 1:1 (w/w). The resulting mixtures were slowly added to a wall material solution containing 0.5%

(w/v) gum arabic and 1.5% (w/v) sodium alginate and stirred for 1 h at room temperature until homogeneous. The mixtures were then fed into an encapsulator B-390 (Büchi, Germany) equipped with a concentric nozzle (1000 µm diameter). Beads were formed at 700 mbar pressure and 700 Hz vibration frequency, and subsequently dropped into 1% (w/v) calcium chloride solution and allowed to harden for 30 min. The beads were washed twice with distilled water and stored under refrigeration for further analysis.

2.3 Yield

Yields of produced *Centella asiatica* beads was calculated using following equation[10]

$$\text{Yield (\%)} = (Y/Y_0) \times 100$$

Where Y is the total mass of *Centella asiatica* beads and Y_0 is the total mass of the mixture A *(Centella asiatica* extracts and Tween) and the mixture B (gum arabic and sodium alginate).

2.4 Size

Sizes of ten *Centella asiatica* beads which were randomly selected from each replicate were measured by using a vernier caliper (Mitutoyo, Japan).

2.5 Color

Colors of *Centella asiatica* beads were analyzed by using a chroma meter (Konica Minolta, cr 400, Japan). The standard color scale used was CIELAB with parameter L^* (lightness/darkness), a^* (+a = redness, -a = greenness), b^* (+b = yellowness, -b = blueness), and ΔE is the measurement of color difference[11].

$$\Delta E = [(\Delta L)^2 + (\Delta a)^2 + (\Delta b)^2]^{1/2}$$

2.6 Swelling capacity

Swelling capacity was determined according to the method of Li et al.[12] with some modification. *Centella asiatica* beads were immersed in acetic acid (pH 4), citric acid (pH 4) and phosphate buffer (pH 7) for 8 hours at room temperature. Swollen beads were removed from the solutions and immediately weighed. Swelling capacity was calculated using the following equation.

$$\text{Swelling (\%)} = ((W_t - W_0)/ W_0) \times 100$$

where W_t is the weight of swollen beads at time, and W_0 is the initial weight of the beads.

2.7 Texture properties

Texture profiles of *Centella asiatica* beads which were hardness, springiness, cohesiveness, gumminess and chewiness were analyzed by using a texture analyzer (Stable Micro Systems, TA. XT Plus, England). A P36/R cylindrical probe was used and attached to a 5-kg load cell. Compression forces were set at 75% of the original height with a trigger force of 5 g. The pre-test speed, test speed, and post-test speed were set at 1, 5, and 5 mm/sec, respectively[13].

2.8 Total phenolic content (TPC)

Centella asiatica beads were dissolved in a 5% (w/v) sodium citrate solution and centrifuged at 7,500 rpm for 30 min at a temperature of 25°C[7]. Clear supernatants were collected and analyzed for total phenolic content (TPC) using the Folin–Ciocalteu method as described by Aksornsri and Peanparkdee[10], with some modifications. Briefly, 200 µL of the samples was mixed with 1 mL of Folin–Ciocalteu reagent and allowed to stand for 5 min. Then, 3 mL of 7.5% (w/v) sodium carbonate solution was added, vortexed and stored in a dark place at room temperature for 30 min. The absorbances of the solutions were measured using a spectrophotometer (Shimadzu, uv1900i, Japan) at a wavelength of 765 nm. The total phenolic content was expressed as mg gallic acid equivalents (GAE) per 100 g of *Centella asiatica* beads.

A Gallic acid standard curve was developed using concentrations of 0, 25, 50 125, 250 and 500 ppm. The linear regression of the standard curve used in TPC calculation was not less than 0.99.

2.8 Statistical analysis

Experiments were conducted using a Completely Randomized Design (CRD). Mean comparisons were performed using Duncan's New Multiple Range Test (DMRT). Statistical analysis was carried out at a 95% confidence level using SPSS statistical software.

3. Results & Discussion

3.1 Yield and Size

Yields of *Centella asiatica* beads produced with Tween 20, Tween 80 and their mixture are presented in Table 1. No significant differences ($p > 0.05$) in production yields were observed among the Tween types. The average production yields of BT20, BT80, and BT20,80 were 42.59% ± 0.15. Smaller bead sizes were observed in BT20, BT80, and BT20,80 compared to the control, suggesting enhanced gel compaction upon the addition of Tween 20 and Tween 80, which are amphiphilic low-molecular-weight surfactants. The size of *Centella asiatica* beads using Tween 80 exhibited higher longest dimension and shortest dimension, whereas beads using Tween 20 and 80 showed the lowest longest dimension. Beads using Tween 20 and the mixture of Tween 20 and 80 had the lowest shortest dimensions, with no significant difference ($p > 0.05$) between them. However, the incorporation of Tween surfactants did not significantly affect bead size, consistent with the findings of Zheng et al. (2023), although Tween 80 tended to increase bead dimensions. This effect may be attributed to its higher molecular weight (1310 g/mol) compared to Tween 20 (1228 g/mol)[14], which could influence the structural arrangement of the gel matrix.

Table 1. Yield, size, and color of *Centella asiatica* beads

Bead	Yield (%)	Size		Color			
		Longest dimension (diameter) [mm]	Shortest dimension (height) [mm]	L*	a*	b*	ΔE
BC	43.18±0.40^{a}	3.44±0.13^{a}	3.29±0.18^{a}	32.42±0.39^{a}	-0.25±0.03^{a}	-0.16±0.02^{a}	31.11±0.39^{b}
BT20	42.49±0.53^{a}	3.19±0.27^{bc}	2.88±0.15^{c}	31.91±0.30^{ab}	-0.29±0.05^{a}	-0.59±0.02^{b}	31.67±0.30^{ab}
BT80	42.52±0.83^{a}	3.38±0.22^{ab}	3.10±0.09^{b}	32.03±0.16^{a}	-0.22±0.03^{a}	-0.46±0.04^{ab}	31.54±0.16^{ab}
BT20,80	42.77±0.91^{a}	3.11±0.30^{c}	2.87±0.18^{c}	31.23±0.61^{b}	-0.22±0.04^{a}	-0.59±0.32^{b}	32.32±0.61^{a}

Data are means ± standard deviation. Means within columns not sharing a common letter are significantly different at $p \leq 0.05$
BC: *Centella asiatica* beads of control
BT20: *Centella asiatica* beads of Tween 20
BT80: *Centella asiatica* beads of Tween 80
BT20,80: *Centella asiatica* beads of Tween 20 and Tween 80

3.2 Color

The average color values (L*, a*, b*, and ΔE) of *Centella asiatica* beads are presented in Table 1. Overall, the L* value and ΔE of the beads decreased with the addition of Tween 20 and Tween 80, likely due to the blending of the dark green color of the extracts with the inherent yellow hue of the surfactants. The L* value of the sample containing Tween 80 (BT80) is significantly higher, while the sample containing both Tween 20 and Tween 80 (BT20,80) showed the lowest. No significant difference ($p < 0.05$) in L* values was observed between the samples containing Tween 20 (BT20) and Tween 20 combined with Tween 80 (BT20,80). The a* value

shows greenness, and no significant difference ($p > 0.05$) was observed among treatments. The b* value of Tween 20 (BT20) and Tween 20,80 (BT20,80) were not significantly different ($p > 0.05$). The sample containing Tween 80 (BT80) showed a slightly higher b* value and was not significantly different ($p > 0.05$) from the other treatments. The ΔE values of *Centella asiatica* beads with different Tweens was not significantly different ($p > 0.05$).

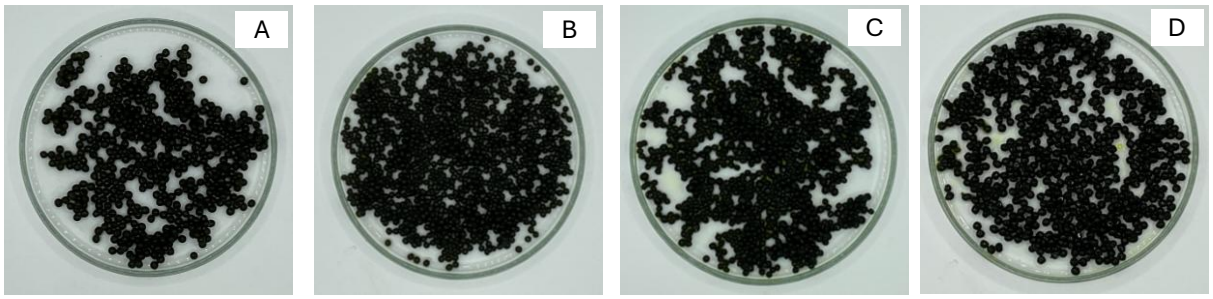

Figure 1 Appearances of *Centella asiatica* beads. A: Control, B: Beads with Tween 20, C: Beads with Tween 80, D: Beads with Tween 20 and Tween 80.

3.3 Swelling capacity

The swelling capacity of *Centella asiatica* beads was evaluated in different buffer systems, including pH 4 (acetic acid and citric acid) and pH 7 (phosphate buffer), as shown in Figure 2. The highest swelling capacity was observed in phosphate buffer (pH 7), followed by citric acid and acetic acid solutions, respectively. At pH 4, the swelling behavior after 1 h of immersion varied depending on the type of surfactant used. Beads containing Tween 20 exhibited maximum swelling capacities of 21.19% and 92.89% in acetic acid and citric acid buffers, respectively. No significant differences ($p > 0.05$) were observed between beads containing Tween 80 and those containing a combination of Tween 20 and Tween 80 in citric acid and phosphate buffers.

With increasing immersion time, the swelling capacity of the beads generally increased. In acetic acid buffer (pH 4), beads containing Tween 80 and the Tween 20/80 mixture showed a significant increase in swelling after 4 h compared to 1 h, while Tween 20 beads exhibited a marked increase to 36.10% after 8 h. However, no significant change ($p > 0.05$) was observed for beads containing the Tween 20/80 mixture between 4 and 8 h. In citric acid buffer, a slight but significant increase in swelling capacity was observed for all bead formulations after 4 and 8 h of immersion. In phosphate buffer (pH 7), beads containing Tween 20 showed the highest swelling capacity (53.46%) after 1 h, and all formulations exhibited a rapid increase in swelling after 4 h of immersion.

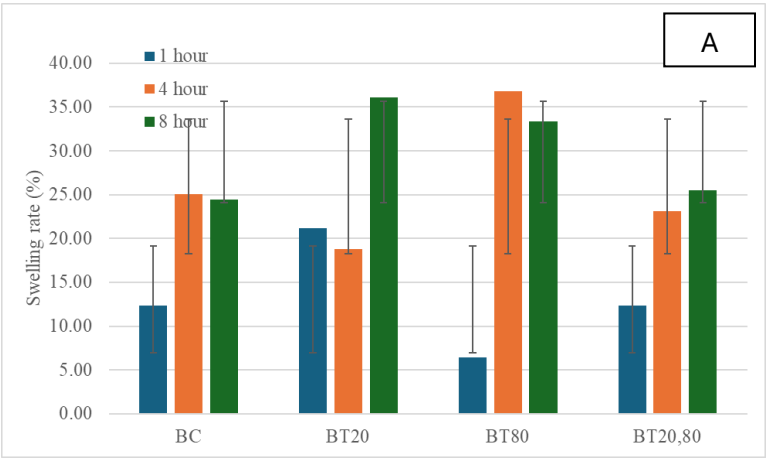

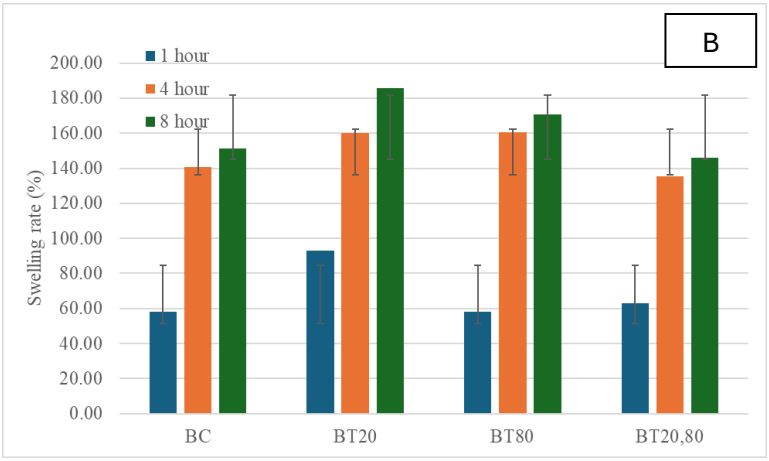

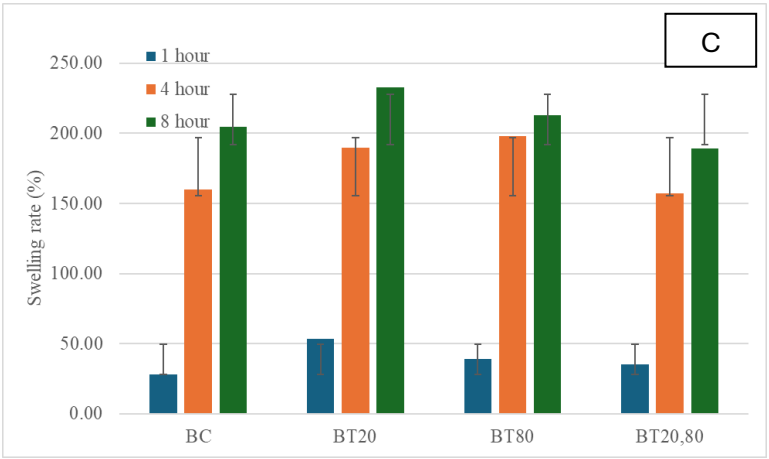

Figure 2 Swelling capacity of *Centella asiatica* beads was evaluated in different buffer solutions, including pH 4 (acetic acid and citric acid) and pH 7 (phosphate buffer) for 1, 4, 8 hour. A: Acetic acid (pH4), B: Citric acid (pH4), C: Neutral condition (pH7), BC: *Centella asiatica* beads of control, BT20: *Centella asiatica* beads of Tween 20, BT80: *Centella asiatica* beads of Tween 80, BT20,80: *Centella asiatica* beads of Tween 20 and Tween 80

The swelling behavior of the beads, characterized by high water uptake, was attributed to increased internal water absorption and ion diffusion, which vary depending on the buffer system used. The incorporation of hydrophilic or hydrophobic group of alginate significantly affected the hydrophilicity of the beads[15]. Alginate beads are polymers containing carboxyl groups (–COOH). In acetic acid and citric acid (pH 4), the carboxylate ions are protonated from acids, and hydrogen bonding between groups is enhanced. The inter-polymer interactions may be stronger than the interactions between the polymer and water during the swelling process, resulting in lower swelling of the beads. In phosphate buffer (pH 7), the carboxyl groups of alginate dissociate into carboxylate ions ($–COO^-$), leading to an increased charge density and disruption of hydrogen bonding between groups. The electrostatic repulsion between polymer chains causes them to expand, and hydrogen bonds between the water and anionic forms of saccharides can easily be formed, leading to water absorption by the hydrogels and resulting in higher swelling of the beads. This contributes to increased swelling of *Centella asiatica* beads[16, 17].

The swelling of alginate beads was influenced by the type of Tween used. Tween 20, with a shorter fatty acid chain and higher HLB (16.7), facilitated the greatest water uptake. Tween 80 lower HLB (15.0), with a longer unsaturated tail, reduced swelling due to increased hydrophobic interactions with the polymer network. The combination of Tween 20 and Tween 80 further decreased swelling, likely due to enhanced network stabilization from mixed hydrophobic interactions[8, 18].

3.4 Texture properties

The texture properties of *Centella asiatica* beads swollen in pH 4 (acetic acid and citric acid) and pH 7 (phosphate buffer) for 1, 4, and 8 h are presented in Table 2. The hardness of *Centella asiatica* beads varied with swelling medium and time. Beads containing mixed of Tween 20 and Tween 80 exhibited the highest hardness values when immersed in acetic acid and citric acid at all time points. Under pH 7 conditions, beads containing Tween 20 showed the highest hardness at 1 h; however, after 8 h of swelling, no significant differences ($p > 0.05$) in hardness were observed among the bead formulations.

For gumminess, no significant differences ($p > 0.05$) were observed among beads immersed in acetic acid at 1 h. At 4 and 8 h, beads containing Tween 20 and Tween 80 showed the highest gumminess values. In citric acid, beads containing Tween 20 and Tween 80 exhibited the highest gumminess values at 1, 4, and 8 h. Under pH 7 conditions, beads containing Tween 20 showed the highest gumminess at 1 h, while no significant differences ($p > 0.05$) were observed at 4 h. At 8 h, beads containing Tween 20 and Tween 80 exhibited the highest gumminess values.

Springiness values of *Centella asiatica* beads swollen immersed in pH 4 (acetic acid and citric acid) and pH 7 (phosphate buffer) for 1, 4, and 8 h showed no significant differences ($p > 0.05$) among the samples. In contrast, cohesiveness values of beads immersed in acetic acid and citric acid were higher than those of beads immersed in phosphate buffer at pH 7.

Chewiness showed a similar trend to gumminess and hardness. Beads containing Tween 20 and Tween 80 exhibited the highest chewiness values at all immersion times, particularly in acetic acid.

Table 2. Texture properties of *Centella asiatica* beads

Time	Beads	Hardness			Springiness			Cohesiveness			Gumminess			Chewiness		
		Acetic acid	Citric acid	pH 7	Acetic acid	Citric acid	pH 7	Acetic acid	Citric acid	pH 7	Acetic acid	Citric acid	pH 7	Acetic acid	Citric acid	pH 7
1	BC	867.62 ±10.37^{c}	418.62 ±30.87^{c}	203.77 ±74.13^{bc}	0.42 ±0.01^{a}	0.67 ±0.07^{a}	0.68 ±0.10^{a}	0.44 ±0.02^{b}	0.29 ±0.03^{b}	0.29 ±0.06^{b}	383.04 ±16.18^{b}	123.09 ±20.64^{b}	60.20 ±28.47^{bc}	160.33 ±10.49^{b}	82.94 ±20.05^{b}	40.82 ±20.03^{ab}
	BT20	997.25 ±30.53^{b}	505.82 ±40.16^{b}	324.05 ±117.75^{a}	0.40 ±0.04^{a}	0.65 ±0.06^{a}	0.62 ±0.13^{a}	0.55 ±0.02^{a}	0.31 ±0.06^{b}	0.35 ±0.06^{a}	550.93 ±24.76^{a}	155.91 ±38.26^{b}	118.33 ±58.71^{a}	218.69 ±29.87^{a}	102.28 ±30.29^{b}	79.26 ±52.31^{a}
	BT80	1009.93 ±39.76^{b}	544.38 ±17.30^{ab}	261.97 ±47.59^{ab}	0.42 ±0.02^{a}	0.69 ±0.03^{a}	0.64 ±0.10^{a}	0.53 ±0.03^{a}	0.40 ±0.05^{a}	0.37 ±0.02^{a}	540.25 ±44.67^{a}	218.12 ±34.51^{a}	96.84 ±15.16^{ab}	226.20 ±23.44^{a}	150.31 ±27.04^{a}	62.38 ±16.21^{a}
	BT20, 80	1049.13 ±19.57^{a}	567.76 ±39.76^{a}	113.78 ±17.33^{c}	0.41 ±0.02^{a}	0.65 ±0.02^{a}	0.59 ±0.08^{a}	0.52 ±0.03^{a}	0.45 ±0.04^{a}	0.28 ±0.03^{b}	547.58 ±34.13^{a}	258.92 ±38.49^{a}	32.21 ±7.64^{c}	224.17 ±19.11^{a}	169.07 ±27.14^{a}	18.63 ±2.60^{b}
4	BC	746.92 ±30.82^{c}	238.40 ±15.92^{b}	3.22 ±0.10^{b}	0.46 ±0.01^{a}	0.66 ±0.10^{a}	0.73 ±0.04^{a}	0.52 ±0.03^{a}	0.21 ±0.02^{a}	0.31 ±0.03^{a}	385.89 ±9.51^{c}	51.01 ±5.93^{b}	1.00 ±0.07^{a}	178.50 ±3.29^{b}	34.08 ±7.99^{b}	0.73 ±0.08^{a}
	BT20	837.13 ±45.39^{b}	254.48 ±28.68^{b}	3.41 ±0.49^{ab}	0.42 ±0.02^{b}	0.57 ±0.06^{a}	0.73 ±0.13^{a}	0.45 ±0.01^{b}	0.21 ±0.01^{a}	0.30 ±0.06^{a}	372.77 ±25.17^{c}	54.13 ±6.42^{b}	6.51 ±12.29^{a}	156.10 ±13.11^{b}	30.79 ±6.08^{b}	5.93 ±11.75^{a}
	BT80	848.12 ±12.81^{b}	254.77 ±12.34^{b}	3.69 ±0.13^{a}	0.41 ±0.03^{b}	0.60 ±0.10^{a}	0.62 ±0.11^{a}	0.50 ±0.04^{a}	0.28 ±0.11^{a}	0.27 ±0.05^{a}	426.12 ±32.37^{b}	69.60 ±24.09^{ab}	1.00 ±0.19^{a}	177.31 ±24.93^{b}	40.28 ±9.19^{ab}	0.61 ±0.11^{a}
	BT20, 80	1047.35 ±21.58^{a}	358.94 ±21.58^{a}	3.31 ±0.34^{ab}	0.42 ±0.03^{b}	0.63 ±0.07^{a}	0.63 ±0.02^{a}	0.48 ±0.03^{ab}	0.21 ±0.03^{a}	0.25 ±0.05^{a}	507.33 ±22.02^{a}	76.85 ±11.90^{a}	0.84 ±0.24^{a}	212.85 ±22.47^{a}	49.18 ±13.10^{a}	0.53 ±0.15^{a}
8	BC	743.89 ±48.74^{c}	246.24 ±21.31^{b}	2.94 ±0.70^{a}	0.43 ±0.05^{a}	0.54 ±0.04^{b}	0.65 ±0.23^{a}	0.53 ±0.01^{a}	0.22 ±0.03^{a}	0.32 ±0.04^{a}	390.95 ±22.88^{a}	53.31 ±10.90^{a}	0.94 ±0.32^{b}	168.90 ±24.11^{a}	28.86 ±7.55^{b}	0.57 ±0.12^{b}
	BT20	716.19 ±10.29^{c}	139.32 ±25.79^{d}	2.75 ±0.41^{a}	0.40 ±0.04^{a}	0.60 ±0.12^{ab}	0.66 ±0.22^{a}	0.45 ±0.06^{b}	0.17 ±0.02^{a}	0.27 ±0.02^{ab}	323.67 ±44.82^{b}	24.53 ±8.03^{b}	0.76 ±0.14^{b}	129.13 ±26.52^{b}	14.17 ±3.23^{c}	0.51 ±0.24^{b}
	BT80	829.10 ±50.55^{b}	178.36 ±18.10^{c}	3.38 ±0.25^{a}	0.41 ±0.02^{a}	0.60 ±0.09^{ab}	0.58 ±0.09^{a}	0.48 ±0.03^{ab}	0.17 ±0.04^{a}	0.25 ±0.02^{b}	399.12 ±26.81^{a}	30.94 ±10.21^{b}	0.85 ±0.14^{b}	162.29 ±12.52^{a}	18.14 ±4.88^{c}	0.49 ±0.12^{b}
	BT20, 80	975.64 ±11.16^{a}	331.67 ±11.16^{a}	3.09 ±0.70^{a}	0.41 ±0.01^{a}	0.66 ±0.05^{a}	0.65 ±0.06^{a}	0.45 ±0.05^{b}	0.20 ±0.03^{a}	0.30 ±0.02^{a}	435.78 ±52.26^{a}	64.92 ±9.87^{a}	8.64 ±10.57^{a}	179.18 ±19.21^{a}	43.26 ±8.67^{a}	5.77 ±7.11^{a}

Data are means ± standard deviation. Means within columns not sharing a common letter are significantly different at $p \leq 0.05$
BC: *Centella asiatica* beads of control
BT20: *Centella asiatica* beads of Tween 20
BT80: *Centella asiatica* beads of Tween 80
BT20,80: *Centella asiatica* beads of Tween 20 and Tween 80

The differences in textural properties of *Centella asiatica* beads can be attributed to pH-dependent alginate gelation and surfactant–polymer interactions. At pH 7, alginate is highly ionized, promoting strong Ca^{2+} mediated crosslinking and formation of a stable gel network; under these conditions, Tween 20, due to its higher hydrophilicity, enhances network uniformity and polymer–water interactions, resulting in greater hardness, gumminess, chewiness, and cohesiveness. In contrast, at pH 4, protonation of alginate reduces electrostatic interactions and weakens the gel structure; therefore, the combination of Tween 20 and Tween 80 provides a synergistic effect, where Tween 20 improves dispersion and Tween 80 contributes hydrophobic interactions, helping to reinforce the weakened matrix and enhance textural properties. These findings are consistent with previous studies on alginate gel behavior and surfactant–biopolymer interactions.(19)

3.5 Total phenolic content

Table 3 showed that total phenolic content (TPC) in *Centella asiatica* beads was relatively low, ranging from 0.61 to 0.64 mg GAE/100 g beads. The TPC of BT20, BT80 and BT20, 80 were not different from the control. However, the highest TPC was observed in beads containing both Tween 20 and Tween 80 whereas the lowest TPC was found in the control suggesting more phenolic can be more protected by the mixture of Tween 20 and Tween 80.

Table 3. Total phenolic content of *Centella asiatica* beads

Centella asiatica beads	TPC (mg GAE/ 100 g bead)
BC	0.57±0.00 [a]
BT20	0.63±0.00 [a]
BT80	0.61±0.00 [a]
BT20,80	0.64±0.00 [a]

Data are means ± standard deviation. Means within columns not sharing a common letter are significantly different at $p \leq 0.05$
BC: *Centella asiatica* beads of control
BT20: *Centella asiatica* beads of Tween 20
BT80: *Centella asiatica* beads of Tween 80
BT20,80: *Centella asiatica* beads of Tween 20 and Tween 80

3.6. Potential application of *Centella asiatica* beads in food industry

As explained above, *Centella asiatica* beads produced by using the mixture of sodium alginate and gum arabic as wall materials in this study presented approximately 50% of production yield with 3.38 mm for an average diameter. Using of Tween 20 and 80 improved their swelling capacity and increased hardness and gumminess of the beads. Additionally, the encapsulation technique in this study can mask unpleasant odors and flavors of *Centella asiatica* extracts and might protect *Centella asiatica* extracts from severe conditions in food processing for example heating, cooling and acidic conditions. The *Centella asiatica* beads might have a high potential to apply for using in food products in an industrial level such as non-alcoholic and alcoholic beverages, carbonated beverage and dairy products. The utilization of *Centella asiatica* beads which contain bioactive compounds from *Centella asiatica* known as a Thai herb can improve health benefits of those products.

4. Conclusion

This study investigated the effects of polysorbates (Tween 20 and Tween 80) on the characteristics of *Centella asiatica* beads. The results showed that the incorporation of different Tween types caused slight differences in bead size and color values. The findings also indicated that beads containing both Tween 20 and Tween 80 exhibited lower swelling behavior compared with beads prepared with either Tween 20 or Tween 80, only. In addition, *Centella asiatica* beads demonstrated potential applicability in acetic food systems. Furthermore, the incorporation of Tween improved the compatibility and solubility of *Centella asiatica* extract.

Acknowledgements

This work was supported by King Mongkut's Institute of Technology Ladkrabang (KREF226806).

References

1. Vasantharuba S, Banumathi P, Premalatha MR, Sundaram SP, Thangaiah A. Functional properties of Centella asiatica (L.): A review. International Journal of Pharmacy and Pharmaceutical Sciences 2012;4:8–14.
2. Wong JX, Ramli S. Antimicrobial activity of different types of Centella asiatica extracts against foodborne pathogens and food spoilage microorganisms. LWT 2021;142:111026.
3. Guo X, Suzuki H, Sawafuji T, Fukuda S, Yamada T, Kobayashi M, et al. A Clinical Trial to Evaluate the Safety and Efficacy of Centella asiatica for Ulcerative Colitis. JGH Open 2025;9:e70258.
4. Hong SS, Kim JH, Li H, Shim CK. Advanced formulation and pharmacological activity of hydrogel of the titrated extract of C. asiatica. Arch Pharm Res 2005;28:502–8.
5. Tripathy S, Srivastav PP. Encapsulation of Centella asiatica leaf extract in liposome: Study on structural stability, degradation kinetics and fate of bioactive compounds during storage. Food Chemistry Advances 2023;2:100202.
6. Xu Y, Yan X, Zheng H, Li J, Wu X, Xu J, et al. The application of encapsulation technology in the food Industry: Classifications, recent Advances, and perspectives. Food Chemistry: X 2024;21:101240.
7. Fuangchoom V, Narkprasom N, Jaturonglumlert S, Varith J, Narkprasom K. Energy-efficient extraction and environmental impact of the kinetic release of total phenolic compounds from longan extract beads. Maejo International Journal of Energy and Environmental Communication 2023;5:35–42.
8. Zheng Y, Zi Y, Shi C, Gong H, Zhang H, Wang X, et al. Tween emulsifiers improved alginate-based dispersions and ionic crosslinked milli-sized capsules. NPJ Sci Food 2023;7:33.
9. Petchsomrit A, Sermkaew N, Wiwattanapatapee R. Effect of Alginate and Surfactant on Physical Properties of Oil Entrapped Alginate Bead Formulation of Curcumin. International Journal of Medical, Pharmaceutical Science and Engineering 2013;7:479–83.
10. Aksornsri T, Peanparkdee M. Alginate beads loaded with rambutan extract: characterization and stability during in vitro gastrointestinal digestion. J Sci Food Agric 2024;104:5712–23.
11. Papia EM, Kondi A. Quantifying subtle color transitions in Mark Rothko's abstract paintings through K-means clustering and Delta E analysis. Journal of Cultural Heritage 2025;72:194–204.
12. Li W, Chen W, Wang Z, Chen W, Zhang M, Zhong Q, et al. Preparation and Characterization of Beads of Sodium Alginate/Carboxymethyl Chitosan/Cellulose Nanofiber Containing Porous Starch Embedded with Gallic Acid: An In Vitro Simulation Delivery Study. Foods 2022;11.

13. Bubin SFA, Mat Ali S, Shukri R, Wan Ibadullah WZ, Ramli NS, Mustapha NA, et al. Characterization and stability of pitaya pearls from hydrocolloids by reverse spherification. International Journal of Food Properties 2019;22:1353–64.
14. Mehta SK, Kaur G, Bhasin KK. Tween-embedded microemulsions--physicochemical and spectroscopic analysis for antitubercular drugs. AAPS PharmSciTech 2010;11:143–53.
15. Song S, Wang Z, Qian Y, Zhang L, Luo E. The Release Rate of Curcumin from Calcium Alginate Beads Regulated by Food Emulsifiers. Journal of Agricultural and Food Chemistry 2012;60:4388–95.
16. Postolović KS, Antonijević MD, Ljujić B, Miletić Kovačević M, Gazdić Janković M, Stanić ZD. pH-Responsive Hydrogel Beads Based on Alginate, κ-Carrageenan and Poloxamer for Enhanced Curcumin, Natural Bioactive Compound, Encapsulation and Controlled Release Efficiency. Molecules 2022;27.
17. Lu T, Xiang T, Huang X-L, Li C, Zhao W-F, Zhang Q, et al. Post-crosslinking towards stimuli-responsive sodium alginate beads for the removal of dye and heavy metals. Carbohydrate Polymers 2015;133:587–95.
18. Bąk A, Podgórska W. Interfacial and surface tensions of toluene/water and air/water systems with nonionic surfactants Tween 20 and Tween 80. Colloids and Surfaces A: Physicochemical and Engineering Aspects 2016;504:414–25.
19. McClements D. Food Emulsions: Principles, Practices, and Techniques, Third Edition2015.

P - 405

Development of Soy Protein-Based Meat Substitute using Freezing Process Combined with Transglutaminase and Alginate

Nidchanya Sawedveeraphat, Saban Thongkong, Parichat Paksin,
Pitchaporn Phannarai, and Suphat Phongthai*

Division of Food Science and Technology, Faculty of Agro-Industry, Chiang Mai University, Chiang Mai

**Corresponding author E-mail: suphat.phongthai@cmu.ac.th*

Abstract: This study aimed to optimize the structuring conditions of a soy protein–based meat analogue using a freezing process in combination with transglutaminase and alginate to improve textural, physicochemical, and nutritional properties. Response Surface Methodology (RSM) with a Box–Behnken Design was applied to investigate the effects of three independent variables: number of freezes–thaw cycles (1–3 cycles at −10 °C), alginate concentration (3–9%, w/w), and transglutaminase concentration (0–1%, w/w). Degrees of texturization and chewiness were selected as the main response variables for optimization.

The quadratic models developed for both responses were statistically significant ($p < 0.05$), with high coefficients of determination ($R^2 > 0.88$) and non-significant lack-of-fit, indicating good agreement between predicted and experimental values. Interaction effects, particularly between freeze–thaw cycles and alginate concentration, contributed positively to fiber structure formation and textural development. The optimal condition predicted and confirmed by the model consisted of two freeze–thaw cycles, 9% alginate, and 1% transglutaminase. Under this condition, the experimental values of degree of texturization and chewiness were in close agreement with the predicted values, with percentage errors below 5%.

Physicochemical analysis showed that the optimized plant-based meat substitute had higher moisture content, dietary fiber, and in vitro protein digestibility, and lower fat content and energy value than commercial chicken nuggets. Although the plant-based product was slightly less chewy than the commercial product, it remained within an acceptable range and indicated successful formation of a fibrous protein network.

Overall, the results indicated that the combination of controlled freeze–thaw processing, alginate gelation, and enzymatic cross-linking with transglutaminase can effectively improve the structural and nutritional characteristics of soy protein–based meat substitute. This approach offers a promising, low-cost alternative for developing plant-based meat products with properties comparable to those of conventional meat products.

Keywords: Soybean; Freezing; Alginate; Transglutaminase enzyme; Meat Substitute.

1. Introduction

The United Nations projected that the global population will continue to increase, reaching approximately 8.6 billion in 2030 and 9.8 billion in 2050 [8]. This population growth is expected to lead to a corresponding increase in global food demand. Therefore, the development and production of food to meet future consumer needs is essential, particularly protein-rich foods, which are major nutrients required for human health. As a result, global demand for meat consumption has continuously increased. This trend has contributed to several environmental problems, including greenhouse gas emissions and excessive use of water and land resources [20].

In addition, meat production is associated with risks of zoonotic diseases, such as avian influenza and swine influenza. There are also health concerns related to high meat consumption, especially red meat and processed meat, which may increase the risk of non-communicable diseases, including cardiovascular diseases and certain types of cancer [5]. Although consumers have become increasingly aware of the environmental and health impacts associated with meat consumption, only a portion of the global population has adopted vegetarian diets or consumed plant-based meat products c This is partly because meat is still perceived as having high nutritional value [17,24].

Consequently, various technologies have been developed to help reduce meat consumption among consumers. At the same time, limited natural resources may lead to shortages of food and raw materials for meat production, which may not be sufficient to meet the increasing global demand. Therefore, alternative protein sources have gained increasing attention from both consumers and food producers, as they can provide sustainable nutritional solutions while reducing environmental and health impacts. These factors have contributed to changes in protein consumption behavior, with consumers placing greater emphasis on plant-based proteins.

A report in 2020 indicated that the market value of plant-based protein foods was approximately 390 billion THB and is expected to grow to approximately 1 trillion THB by 2027 In addition, individuals with allergies to meat, milk, or other animal-derived products have increasingly turned into plant-based protein sources. Common plant protein sources used in the food industry include cereals such as quinoa, oats, wheat, wheat germ, and chia seeds, as well as various legumes that are rich in protein. These materials serve as major raw ingredients for meat substitute products. Commonly used legumes include soybean, red bean, edamame, and pea, each of which provides different nutritional benefits [12].

Soybean (*Glycine max* (L.) Merrill) is one of the most widely used plant protein sources due to its high protein content, ranging from approximately 35–40%, and its content of essential amino acids [10]. Owing to its nutritional value and functional properties, soybean has been extensively used in the food industry. Soy protein exhibits high *in vitro* digestibility, with reported values of 95–98%, which are comparable to those of animal proteins and dairy products As a result, soy-based products have gained increasing popularity due to growing consumer awareness of health benefits. Currently, soybeans are processed into a wide range of products, including soymilk, soy powder, tofu, soy sauce, soy flour, fermented soybean products, tempeh, and soybean oil. In addition, soybeans can be further developed into plant-based meat products to meet the needs of health-conscious consumers [10].

Although plant-based meat products have been increasingly developed, their texture remains a major limitation for replacing animal meat. However, ongoing research and development efforts have aimed to improve the nutritional value and texture of plant-based meat substitutes to more closely resemble animal protein. As a result, the production and market trends of plant-based meat products have continued to grow [26]. Strategies to mimic meat texture vary depending on the type of product and can be classified into three main categories: ground meat products, processed meat products (e.g., sausages, nuggets, and ham), and whole meat substitutes [7].

Several commercial plant-based meat products have been developed, such as beef Substitute by Memphis Meats and Aleph Farms, chicken Substitute by JUST Incorporated, and fish Substitute by Finless Foods. However, these products generally require relatively high production costs and rely on complex and advanced technologies, including high-moisture extrusion, shear cell technology, and three-dimensional food printing. In contrast, low-cost processing methods, such as freezing, represent an alternative approach for mimicking fibrous meat-like structures. Freezing can lead to the formation of small ice crystals, which, upon thawing, generate porous microstructures with elongated cavities aligned in one direction. These structures

resemble the orientation of muscle fibers in animal meat and can contribute to juiciness and a meat-like texture [6, 7, 25].

In addition, transglutaminase is an enzyme that catalyzes the formation of covalent cross-links between protein molecules via isopeptide bonds. This cross-linking reaction enhances protein network stability and can be used to improve firmness, viscosity, and elasticity of protein-rich food products [12]. Transglutaminase has therefore been recognized as a promising enzyme for improving the quality of meat substitute products without negatively affecting flavor or nutritional value. Furthermore, hydrocolloids such as alginate are often incorporated to improve texture and reduce water loss during heat processing, thereby enhancing chewiness and overall textural quality [9, 22].

Therefore, the objective of this study was to determine the optimal conditions for structuring a soy protein–based meat substitute using freeze–thaw processing in combination with transglutaminase and alginate. In addition, the developed plant-based meat substitute was compared with a commercial product in terms of final product quality, including physicochemical properties, in vitro protein digestibility, and nutritional value.

2.Materials and Methods

2.1 Selection of Soy Protein Coagulants

Soybeans (500 g) were soaked in excess water for 4 h. The soaked soybeans were then ground with water at a ratio of 1 L of water per 150 g of soybeans until a smooth slurry was obtained. The slurry was filtered through a single layer of cheesecloth, and the liquid fraction was separated from the okara by squeezing.

The obtained soymilk was heated in boiling water for 15 min. After heating, the soymilk was allowed to cool naturally until the temperature reached approximately 70 °C. Protein coagulation was then performed using 4 different coagulants: calcium sulfate ($CaSO_4$), magnesium sulfate ($MgSO_4$), calcium chloride ($CaCl_2$), and acetic acid (CH_3COOH). Each coagulant was added at concentrations of 2.0, 2.5, and 3.0% (w/w, based on dry soybean weight). The mixture was allowed to stand for approximately 10 min to allow protein precipitation.

The protein curds were transferred onto double-layered cheesecloth placed on a mold. The curds were then dewatered using a centrifugal separator for approximately 20 min to remove excess water. The obtained concentrated protein curd was weighed, and protein yield was calculated according to Equation (1). The coagulant and concentration that provided the highest protein yield were selected for use in subsequent experiments.

$$\text{Protein yield (\%)} = \frac{\text{Weight of protein curd}}{\text{Weight of soaked soybeans}} \times 100 \qquad (1)$$

2.2 Optimization of Structuring Conditions for Plant-Based Meat Substitute

Response Surface Methodology (RSM) with a Box–Behnken Design (BBD) was used to determine the optimal conditions for structuring the plant-based meat Substitute. Three independent variables were investigated: number of freezes–thaw cycles at −10 °C (1–3 cycles), transglutaminase concentration (0.0–1.0 w/w), and alginate concentration (3–9%, w/w). Each factor was evaluated at three levels. A total of 17 experimental runs were generated, as shown in Table 3.

The concentrated protein curd obtained from Section 1 was mixed with transglutaminase and alginate at concentrations specified by the experimental design. The mixtures were poured into molds with dimensions of 5 × 6 cm. The samples were frozen at −10 °C for 12 h and then immersed in 3% (w/v) calcium chloride ($CaCl_2$) solution for 4 h. This procedure was defined as one freeze–thaw cycle. The process was repeated according to the assigned number of freeze–thaw cycles.

Two response variables were evaluated: degree of texturization and chewiness. Textural properties were measured using a texture analyzer (Brookfield, India). Uncooked commercial chicken nuggets were used as a reference sample for comparison.

Table 1 Independent variables and their levels used in the Box–Behnken design

Factor	Symbol	values of Factor		
		-1	0	1
Number of freeze–thaw cycles at −10 °C (12 h per cycle)	A	1	2	3
Transglutaminase concentration (%, w/w)	B	0.0	0.5	1.0
Alginate concentration (%)	C	3	6	9

2.2.1 Degree of Texturization

Degree of texturization (DT) was determined using a single-blade cutting probe (TA7). Cutting force was measured in both transverse and longitudinal directions. The DT value was calculated using Equation (2) and used as an indicator of fiber structure formation. A DT value greater than 1 was considered indicative of fiber-like structure.

$$\text{Degree of texturization (DT)} = \frac{\text{Transverse cutting force}}{\text{Longitudinal cutting force}} \qquad (2)$$

2.2.2 Chewiness

Chewiness was measured using a TA25/1000 probe. Samples were compressed to 50% of their original thickness at a speed of 1 mm s^{-1} for the first compression, followed by a recovery period of more than 5 s. A second compression was then applied at 1 mm s^{-1} to 50% of the first compression distance. The parameters measured included hardness (N), springiness (m), and cohesiveness (N·s). Chewiness was calculated using Equation (3).

$$\text{Chewiness} = \text{Hardness} \times \text{Springiness} \times \text{Cohesiveness} \qquad (3)$$

The experimental responses obtained from the Box–Behnken design were fitted to a second-order polynomial model to describe the relationship between the independent variables and the response variables. Regression analysis was performed to estimate the coefficients of the model. Analysis of variance (ANOVA) was conducted to evaluate the significance of the model terms and their interactions at a confidence level of 95% ($p < 0.05$). The adequacy of the developed models was assessed using the coefficient of determination (R^2) and lack-of-fit tests.

Response surface methodology was applied to generate three-dimensional surface plots and contour plots for visualising the effects of process variables. The optimal processing conditions were determined using a desirability function approach. The predicted optimal conditions were subsequently validated by conducting additional experiments, and the experimental values were compared with the predicted values to assess the reliability of the models.

2.3. Physicochemical Analyses of Products

Plant-based meat Substitute samples and uncooked commercial chicken nuggets were prepared by cutting into cubes (2 × 2 × 2 cm). The samples were cooked by steaming at 72–82 °C for 15–20 min prior to physicochemical analysis.

2.3.1 Proximate Composition

Moisture, ash, crude fiber, protein, and fat contents were determined according to AOAC (2000) methods (Methods 927.05, 942.05, and 920.39, respectively). Protein content was calculated from total nitrogen determined by the Kjeldahl method (Method 984.13) using a conversion factor of 6.25.

2.3.2 Texture Profile Analysis

Texture profile analysis was performed using a Texture Analyzer (CT3, Brookfield, India). Samples were placed centrally under the probe on the platform. A TA25/1000 probe was used with the following settings: pre-test speed 5 mm s^{-1}, test speed 1 mm s^{-1}, post-test speed 1 mm s^{-1}, distance 75% strain, trigger type Auto-5 g, time 35 s, and data acquisition rate 10 pps. Each formulation was analyzed in triplicate. Hardness, adhesiveness, gumminess, cohesiveness, and springiness

2.3.3 Color Measurement

Color values (L*, a*, and b*) were measured using a Hunter Lab digital color difference meter. L* represents lightness, a* represents redness (+) to greenness (−), and b* represents yellowness (+) to blueness (−). Measurements were performed in triplicate at 25 ± 1 °C.

2.3.4 In Vitro Protein Digestibility

In vitro protein digestibility was determined following the method of Phongthai [14]. Samples were ground, and 1 g of sample was mixed with 100 mL of distilled water. The pH was adjusted to 1.5 using 1 M HCl, and the mixture was incubated at 37 °C for 5 min. Pepsin was added at an enzyme-to-protein ratio of 1:100 (g enzyme per g protein), and the mixture was incubated at 37 °C for 120 min. The pH was then adjusted to 7.0 using 1 M NaOH. Trypsin was added at an enzyme-to-protein ratio of 1:100 (g enzyme per g protein), followed by incubation at 37 °C for an additional 120 min. Enzyme activity was terminated by heating at 90 °C. The mixture was centrifuged at 6000 rpm for 15 min to separate the protein precipitate. The remaining protein was determined using the Dumas method (conversion factor = 6.25). Protein digestibility was calculated using Equation (4).

$$\text{Protein digestibility (\%)} = \frac{(I-F)}{I} \times 100 \qquad (4)$$

where I = protein content before digestion,
F = protein content after digestion.

2.3.5 Calorific Value

Calorific value was determined using a bomb calorimeter (Parr 6400, Parr Instrument Company, USA) following ASTM standard procedures. Results were expressed as kcal g^{-1}.

2.4 Statistical Analysis

All experiments were conducted in triplicate. Results were expressed as mean ± standard deviation. Statistical analysis was performed using SPSS Statistics version 17.0. Mean comparisons were carried out using Duncan's Multiple Range Test (DMRT) at a 95% confidence level ($p < 0.05$).

3. Results and Discussion

3.1 Selection of Soy Protein Coagulants

The effects of different coagulants on soy protein precipitation and protein yield are presented in Table 2. The results indicated that both the type and concentration of coagulant significantly influenced the efficiency of protein recovery ($p < 0.05$). Among the tested coagulants, calcium sulfate ($CaSO_4$) at a concentration of 3% provided the highest protein yield (70.05 ±

14.40). This was followed by acetic acid (CH_3COOH), calcium chloride ($CaCl_2$), and magnesium sulfate ($MgSO_4$), respectively.

The superior performance of $CaSO_4$ can be attributed to the role of Ca^{2+} ions in promoting protein aggregation and gel network formation. Calcium ions reduce electrostatic repulsion between protein molecules, facilitating their association and precipitation. This observation is consistent with the findings of Kao [11], who reported that $CaSO_4$ improved protein recovery and produced a more uniform tofu microstructure compared with other coagulants. The effect of coagulant concentration further indicated the presence of an optimal level for each coagulant. For $CaSO_4$, protein yield increased with concentration and reached a maximum at 3%. In contrast, $CaCl_2$ and $MgSO_4$ showed maximum yields at 2.5%, followed by a significant decrease at higher concentrations.

Protein precipitation by salt-type coagulants is governed by changes in the hydration shell and surface charge of protein molecules. At relatively low salt concentrations, protein solubility may increase (salting-in effect). However, when salt concentration exceeds a critical level, protein–protein interactions become dominant, leading to aggregation and precipitation (salting-out effect) [8]. Calcium ions can further promote protein aggregation and gel network formation by reducing electrostatic repulsion between protein molecules [11].

In contrast, acetic acid induced protein precipitation primarily by lowering the pH of soymilk toward the isoelectric point of soy proteins. This mechanism enhanced protein aggregation and increased yield at higher acid concentrations. However, excessive acid addition may negatively affect curd uniformity and sensory quality, particularly sour odor and taste [15].

Overall, considering both protein yield and practical applicability, calcium sulfate ($CaSO_4$) at 3% was identified as the most suitable coagulant for soy protein precipitation in this study. This observation was consistent with previous findings demonstrating that $CaSO_4$ improves protein recovery and contributes to the formation of a more uniform protein network [2].

Table 2 Protein yield (%) obtained from different coagulants

Protein Coagulants	Protein yield (%)		
	2%	2.5%	3%
Magnesium sulfate ($MgSO_4$)	23.84±3.02 ^{d}	54.86±0.85 ^{b}	40.16±1.20 ^{c}
Calcium sulfate ($CaSO_4$)	47.85±5.62 ^{bc}	44.34±5.13 ^{bc}	70.05±14.40 ^{a}
Calcium chloride ($CaCl_2$)	55.72±0.84 ^{b}	56.13±0.55 ^{b}	51.34±2.99 ^{bc}
Acetic acid (CH_3COOH)	39.98±4.62 ^{c}	40.96±3.63 ^{c}	55.26±0.54 ^{b}

* Values are expressed as mean ± standard deviation from triplicate experiments (n = 3).
* Different superscript letters (a–d) within the same column indicate significant differences among treatments ($p < 0.05$).

3.2 Optimal Conditions for Fibrous Structure Formation using Transglutaminase, Alginate, and Freeze–Thaw processing

3.2.1 Model Adequacy Analysis

The experimental design based on the Box–Behnken Design (BBD) consisted of 17 experimental runs, as shown in Table 3. Three independent variables were evaluated: number of freeze–thaw cycles (A), alginate concentration (B), and transglutaminase concentration (C), each investigated at three levels. Three center-point replicates were included to estimate experimental error. The experimental design and data analysis were performed using Design-Expert software (version 6.0.2).

Analysis of variance (ANOVA) indicated that the quadratic models developed for both response variables were statistically significant ($p < 0.05$). In addition, the lack-of-fit for both models was not statistically significant ($p \geq 0.05$), indicating that the models were adequate to describe the relationships between the independent variables and the response values.

The coefficients of determination (R^2) for the fitted models ranged from 0.88 to 0.91 for degree of texturization and chewiness, respectively, while the adjusted R^2 values were within a comparable range. These results indicated that more than 88% of the variability in the experimental data was explained by the models. Similar model adequacy and predictive performance have been reported in previous studies applying Response Surface Methodology to optimize food processing systems [1]. The high R^2 values together with the non-significant lack-of-fit confirmed that the developed models provided a reliable basis for response prediction and optimization.

The statistical significance of the models further confirmed that freeze–thaw cycles, alginate concentration, and transglutaminase concentration exert significant effects on the structural and textural properties of the soy protein–based meat substitute.

Table 3 Degree of texturization and chewiness of samples obtained from the 17 experimental runs

Experimental run	Variables			Degree of texturization		Chewiness (N)	
	Number of freeze–thaw (cycles)	Alginate concentration (%)	Transglutaminase concentration (%, w/w)	Experimental value	Predicted value	Experimental value	Predicted value
1	2	6	0.5	1.35	0.97	2513.07	2109.26
2	2	6	0.5	0.33	0.33	196.13	338.51
3	3	6	0.0	0.32	0.33	138.97	342.34
4	1	6	1.0	0.59	0.97	336.67	740.48
5	2	6	0.5	0.72	0.40	618.30	1002.40
6	3	9	0.5	0.29	0.40	490.50	328.40
7	2	6	0.5	0.37	0.40	515.10	677.20
8	1	6	0.0	0.24	0.40	708.43	328.40
9	2	9	0.0	0.85	0.73	1791.00	677.20
10	1	3	0.5	0.77	0.73	894.37	324.33
11	2	3	0.0	0.72	0.73	1101.67	1810.71
12	2	3	1.0	0.56	0.73	810.43	652.66
13	2	6	0.5	1.72	1.91	2057.93	1343.38
14	3	3	0.5	1.75	1.91	2735.80	790.72
15	1	9	0.5	2.49	1.91	2076.70	2437.05
16	3	6	1.0	1.98	1.91	2445.80	2437.05
17	2	9	1.0	1.62	1.91	2869.00	2437.05

3.2.2 Analysis of Variance and Response Surface Analysis

Response Surface Methodology was applied to evaluate the individual and interactive effects of freeze–thaw cycles (A), alginate concentration (B), and transglutaminase concentration (C) on degree of texturization and chewiness. The regression equations describing the fitted quadratic models were presented in Equations (5) and (6).

$$\text{Degree of texturization} = 1.91 - 0.79A^2 - 0.47B^2 - 0.71C^2 + 0.32AB \quad (5)$$

$$\text{Chewiness} = 2437.05 - 256.71A - 427.68B - 82.32C - 1103.56A^2 - 537.28B^2 - 750.40C^2 + 628.66AB + 80.28AC + 151.35BC \quad (6)$$

When A, B, and C represented freeze–thaw cycles, alginate concentration, and transglutaminase concentration, respectively

Table 4 Analysis of variance (ANOVA) for the quadratic response surface model

Response variable	Regression coefficients of the model	Sum of squares	Degree of freedom	Mean square	F-value	p-value
Fibrous protein structure formation	A^2	2.64	1	2.64	32.98	< 0.0001
	B^2	0.94	1	0.94	11.72	0.0051
	C^2	2.15	1	2.15	26.84	0.0002
	AB	0.42	1	0.42	5.19	0.0418
	Residual	0.96	12	0.080		
	Lack of Fit	0.47	8	0.059	0.49	0.8205
	Pure Error	0.49	4	0.12		
	Cor Total	7.75	16			
Chewiness	A	5.272E+005	1	5.272E+005	2.67	0.1462
	B	1.463E+006	1	1.463E+006	7.41	0.0296
	C	54209.37	1	54209.37	0.27	0.6164
	A^2	5.128E+006	1	5.128E+006	25.98	0.0014
	B^2	1.215E+006	1	1.215E+006	6.16	0.0421
	C^2	2.371E+006	1	2.371E+006	12.01	0.0105
	AB	1.581E+006	1	1.581E+006	8.01	0.0254
	AC	25781.12	1	25781.12	0.13	0.7284
	BC	91624.26	1	91624.26	0.46	0.5175
	Residual	1.381E+006	7	1.973E+005		
	Lack of Fit	8.319E+005	3	2.773E+005	2.02	0.2538
	Pure Error	5.495E+005	4	1.374E+005		
	Cor Total	1.475E+007	16			

Table 4 presents the analysis of variance (ANOVA) for the quadratic models describing the degree of texturization and chewiness. The results indicate that several quadratic and interaction terms were statistically significant ($p < 0.05$), demonstrating that the selected independent variables contributed to the observed variation in the experimental data. The positive coefficients associated with the interaction terms AB and AC indicated that combined effects between freeze–thaw cycles, alginate, and transglutaminase contributed positively to fibrous structure development and chewiness within appropriate ranges.

For fibrous structure formation, the absence of significant linear effects (A, B, and C) suggested that the individual factors did not exert a direct linear influence on the response. However, the quadratic terms of A^2, B^2, and C^2 were statistically significant ($p < 0.05$), indicating that non-linear effects of freeze–thaw cycles, alginate concentration, and transglutaminase concentration played a dominant role in fiber structure development. The significant interaction term of AB ($p < 0.05$) suggested an interaction effect between freeze–thaw processing and alginate addition.

For chewiness, a significant linear effect of factor B (alginate concentration) was observed ($p < 0.05$), indicating that alginate directly influenced textural properties. In contrast, factors A (freeze–thaw cycles) and C (transglutaminase concentration) did not show significant linear effects ($p > 0.05$). Significant quadratic effects of A^2, B^2, and C^2 ($p < 0.05$) were also observed, suggesting the presence of curvature and the existence of optimum levels within the studied range. The interaction term AB (freeze–thaw cycles x alginate concentration) was significant ($p < 0.05$), while BC (alginate concentration x transglutaminase concentration) and AC (freeze–thaw cycles x transglutaminase concentration) were not significant ($p > 0.05$), indicating that not all factor combinations contributed equally to chewiness.

The lack-of-fit tests for both response variables were not significant ($p > 0.05$), confirming that the quadratic models were adequate for describing the experimental data.

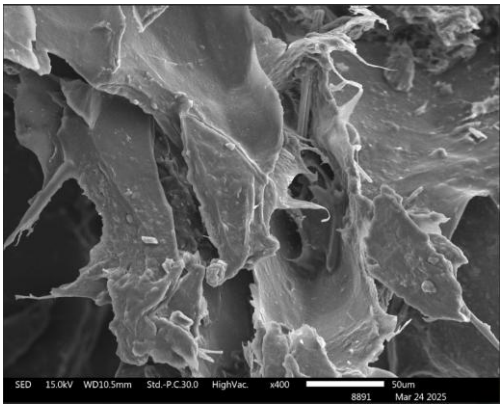

Figure 1 Microstructural analysis of the sample from experimental run 15 at 400× magnification (1 freeze–thaw cycle, 9% alginate, and 0.5% transglutaminase).

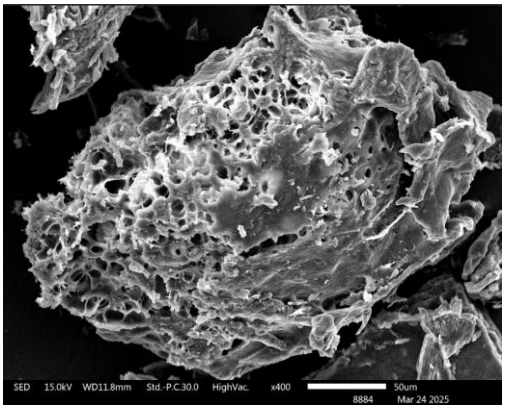

Figure 2 Microstructural analysis of the sample from experimental run 17 at 400× magnification (2 freeze–thaw cycles, 9% alginate, and 1% transglutaminase).

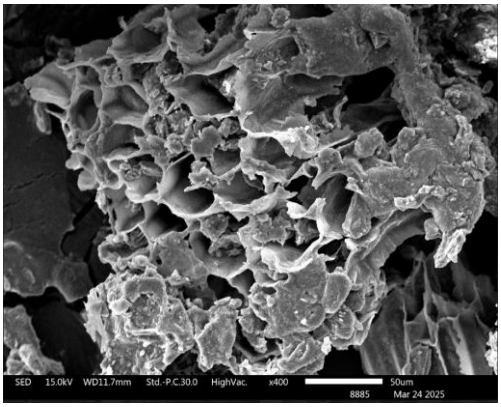

Figure 3 Microstructural analysis of the sample from optimal condition at 400× magnification (2 freeze–thaw cycles, 9% alginate, and 1% transglutaminase).

Microstructural images obtained at 400× magnification provided physical evidence supporting statistical results. As shown in Figure 1, the sample subjected to one freeze–thaw cycle with 9% alginate and 0.5% transglutaminase exhibited a relatively heterogeneous protein network with limited fiber alignment, indicating insufficient structural reorganization.

In contrast, Figure 2 showed a more continuous and aligned fibrous structure after two freeze–thaw cycles with 9% alginate and 1% transglutaminase. The presence of elongated pores and a more coherent protein matrix suggested enhanced protein alignment and enzymatic cross-linking.

Figure 3 represented the structure of the sample obtained from the optimal condition identified by the response surface model (two freeze–thaw cycles, 9% alginate, and 1% transglutaminase). The microstructure under this condition exhibited the most uniform and well-aligned fibrous morphology among the examined samples. The elongated and interconnected pore structures and continuous protein network were consistent with the highest degree of texturization and favorable chewiness obtained in this study.

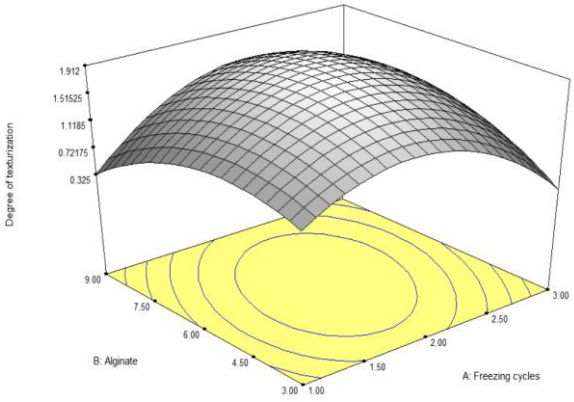

Figure 4 Three-dimensional response surface plot showing the effects of freeze–thaw cycles (A) and alginate concentration (B) on the degree of texturization of the plant-based meat substitute.

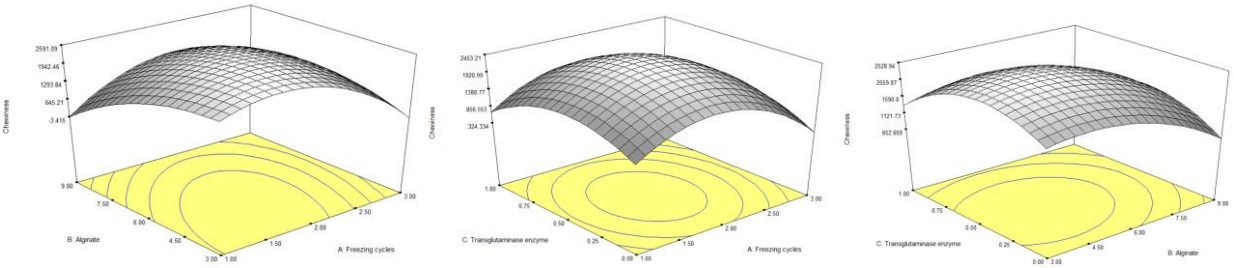

Figure 5 Three-dimensional response surface plot showing the effects of freeze–thaw cycles (A), alginate concentration (B), and transglutaminase concentration (C) on the chewiness of the plant-based meat substitute.

The three-dimensional response surface plots illustrated the combined effects of processing variables. As shown in Figure 4, degree of texturization increased as freeze–thaw cycles increased from one to two, followed by a decline at three cycles, indicating the presence of an optimal intermediate level for freeze–thaw processing. A similar trend was observed for alginate concentration, with improvements at intermediate levels and a reduction at higher concentrations.

Figure 5 presented the response surface for chewiness as a function of freeze–thaw cycles, alginate concentration, and transglutaminase concentration. Chewiness increased from one to two freeze–thaw cycles and decreased at three cycles. Alginate concentration also exhibited an optimal range, while transglutaminase contributed positively at moderate levels. At higher levels, excessive enzymatic cross-linking likely promoted over-crosslinking, resulting in reduced elasticity and chewiness.

The visual trends in Figures 4 and 5 were consistent with the ANOVA results in Table 4 and the regression coefficients in Equations (5) and (6), confirming that all three variables must be balanced to achieve optimal fibrous structure.

3.2.3 Model Validation and Determination of Optimal Conditions

Model validation was performed using confirmation experiments to evaluate the accuracy of the developed quadratic regression models. The optimal processing condition predicted by the response surface methodology consisted of two freeze–thaw cycles, 9% alginate, and 1% transglutaminase.

Under this optimal condition, the experimentally obtained degree of texturization was 0.69, which was close to the predicted value of 0.72. This corresponded to a percentage error of 4.44%, indicating good agreement between experimental and predicted values. Similarly, the experimentally measured chewiness was 561.30, compared with the predicted value of 579.85, resulting in a percentage error of 3.20%.

The small deviations between predicted and experimental values confirmed the reliability and predictive capability of the quadratic models within the studied factor ranges. These results indicated that the response surface models can be used to accurately estimate processing conditions that balance fibrous structure formation and textural performance.

The validated optimal condition reflected a balance between freeze–thaw-induced structural reorganization, alginate gelation, and enzymatic protein cross-linking by transglutaminase. Two freeze–thaw cycles appear to be sufficient to promote directional pore formation and protein alignment, while avoiding the structural degradation observed at higher numbers of cycles. The use of 9% alginate provided effective ionic gelation and water retention, whereas 1% transglutaminase promoted covalent cross-linking of protein chains without inducing excessive rigidity.

Overall, the model validation results confirmed that the selected optimal condition provided a suitable combination of processing variables for producing a soy protein–based meat substitute with improved fibrous structure and acceptable chewiness. This condition was therefore selected for subsequent physicochemical and nutritional analyses.

Table 5 Model validation and determination of optimal conditions

Variables			Degree of texturization			Chewiness		
A	**B**	**C**	**Experimental value**	**Predicted value**	**% Error**	**Experimental value**	**Predicted value**	**% Error**
2.00	9.00	1.00	0.69	0.72	4.44	561.30	579.85	3.20

Figure 6 Plant-based meat substitute containing 9% alginate and 1% transglutaminase subjected to two freeze–thaw cycles.

3.3 Physicochemical Properties of the Plant-based Meat Substitute

The physicochemical properties of the optimized plant-based meat substitute, produced using two freeze–thaw cycles in combination with transglutaminase and alginate, were comparable with those of a commercial chicken nugget. The results are summarized in Table 6 and demonstrate several notable differences in both nutritional composition and physical quality attributes.

In terms of proximate composition, the plant-based meat substitute exhibited significantly higher moisture content (78.58 ± 1.28%, wet basis) compared with the commercial chicken nugget (69.18 ± 0.69%, wet basis) ($p < 0.05$). This high moisture content can be attributed to the combined effects of alginate gel formation and freeze–thaw processing, which enhanced the water-holding capacity of the protein matrix through the formation of a porous hydrocolloid–protein network. Similar findings have been reported in previous studies demonstrating that alginate incorporation can improve water retention and enhance the structural stability of plant-based protein systems [3,9].

The protein content of the plant-based meat substitute (12.51 ± 0.37%, dry basis) was significantly lower than that of the commercial chicken nugget (15.29 ± 0.24%, dry basis) ($p < 0.05$). This reduction may be associated with the incorporation of non-protein ingredients, particularly alginate, which diluted the relative protein concentration within the dry matter of the formulation. Similar observations have been reported in previous studies on plant-based meat analogues, which demonstrated that incorporation of structuring agents and hydrocolloids may reduce the relative protein concentration unless supplemented with concentrated protein ingredients such as soy protein isolate or wheat gluten [7 ,21]. Nevertheless, the developed product still provided plant-derived protein together with dietary fiber.

With respect to lipid content, the plant-based meat substitute contained significantly lower fat content (12.64 ± 0.87%, dry basis) than the commercial chicken nugget (19.59 ± 0.93%, dry basis) ($p < 0.05$). This lower lipid level may be advantageous for consumers seeking reduced-fat or lower-energy food products. Similar findings were reported by Zhang [26] who demonstrated that plant-based protein products could reduce dietary fat intake without substantially compromising texture characteristics.

Regarding textural properties, the plant-based meat substitute exhibited a slightly lower degree of texturization (6.85 ± 0.06) and chewiness (564.24 ± 2.92) compared with the commercial chicken nugget (7.23 ± 0.15 and 600.18 ± 0.38, respectively) ($p < 0.05$). Nevertheless, the values remained within an acceptable range, indicating successful development of a fibrous and cohesive protein structure. The improved textural characteristics can be attributed to protein cross-linking mediated by transglutaminase, which forms ε-(γ-glutamyl) lysine isopeptide bonds through catalyzing an acyl transfer reaction between the γ-carboxamide group of glutamine residues and the ε-amino group of lysine residues, thereby enhancing network strength and elasticity. Similar findings have been reported in previous studies demonstrating that transglutaminase improves the structural integrity and mechanical properties of plant-based meat analogues [12, 21].

Color measurements in the CIELAB system revealed that the plant-based meat substitute had a significantly lower lightness value ($L^* = 68.80 \pm 0.33$) compared with the commercial chicken nugget (71.58 ± 1.03) ($p < 0.05$), indicating a darker appearance. In addition, the b^* value, representing yellowness, was significantly lower in the plant-based product (13.31 ± 0.07) than in the commercial chicken nugget (17.25 ± 0.31) ($p < 0.05$), whereas the a^* value (red–green axis) did not differ significantly ($p \geq 0.05$). Similar observations have been reported in previous studies showing that plant protein–based products often exhibit darker color development due to the presence of phenolic compounds and Maillard reaction products formed during thermal processing [Chen,Phongthai].

The *in vitro* protein digestibility of the plant-based meat substitute (73.88 ± 0.31%) was significantly higher than that of the commercial chicken nugget (62.41 ± 0.06%) ($p < 0.05$). This enhanced digestibility may be attributed to structural modifications induced by freeze–thaw processing and enzymatic cross-linking, which can increase enzyme accessibility to peptide bonds. Similar effects have been reported in previous studies demonstrating that controlled protein network modification can improve enzymatic hydrolysis and protein bioaccessibility [4,27].

Finally, the Calorific value of the plant-based meat substitute was substantially lower (2.28 ± 0.03 kcal/g) than that of the commercial chicken nugget (6.05 ± 0.02 kcal/g) ($p < 0.05$). This significant reduction in caloric value reflected the combined effects of lower fat content and higher moisture content, highlighting the strong potential of the developed product as a low-energy, health-oriented meat alternative.

Overall, these results indicated that the soy protein-based meat substitute developed in this study exhibited favorable physicochemical and nutritional characteristics, including lower fat and energy content, higher dietary fiber, and improved protein digestibility, while maintaining textural properties comparable to those of a commercial chicken nugget. These attributes supported the potential of the developed product for further optimization and commercialization, particularly for health-conscious consumers

Table 6 Comparison of physicochemical properties between commercial chicken nuggets and the plant-based meat substitute.

Parameter	Plant-based Meat Substitute	Commercial Chicken Nuggets
Proximate composition (%)		
- Moisture	78.58±1.28[a]	69.18±0.69[b]
- Protein	15.51±0.37[b]	50.29±0.24[a]
- Fat	12.64±0.87[b]	19.59±0.93[a]
- Crude fiber	2.36±0.01[a]	0.35±0.14[b]
- Ash	0.08±0.00[ns]	0.05±0.00[ns]
Degree of texturization	6.85±0.06[b]	7.23±0.15[a]
Chewiness	564.24±2.92[b]	600.18±0.38[a]
Color values		
- L*	68.80±0.33[b]	71.58±1.03[a]
- a*	1.17±0.05[ns]	1.25±0.03[ns]
- b*	13.31±0.07[b]	17.25±0.31[a]
In vitro protein digestibility (%)	73.88±0.31[a]	62.41±0.06[b]
Energy (kcal/g)	2.28±0.03[b]	6.05±0.02 [a]

* Three repeated experiments are presented as the mean ± standard deviation.
* The letters (a, b, c, d) that are different in the same row indicate a significant difference (*p*-value).

4. Conclusion

This study successfully developed a soy protein-based meat substitute using a freeze–thaw process in combination with transglutaminase and alginate to improve fibrous structure formation, textural properties, and nutritional quality. The selection of calcium sulfate ($CaSO_4$) at 3% as the protein coagulant provided the highest protein yield and produced a uniform protein matrix suitable for subsequent structuring.

The optimal condition for fibrous structuring was identified as two freeze–thaw cycles, 9% alginate, and 1% (w/w) transglutaminase. These results confirmed that the combined effects of freeze–thaw-induced microstructural modification, enzymatic protein cross-linking, and alginate–

Ca^{2+} gel formation contributed synergistically to the development of a stable and fibrous protein network.

The optimized plant-based meat substitute exhibited favorable physicochemical and nutritional characteristics, including low fat and calorific value, high dietary fiber, and *in vitro* protein digestibility, while maintaining textural properties within an acceptable range. Although the protein content of the developed product was lower than that of the commercial product, this limitation could be addressed in future studies through formulation strategies such as supplementation with soy protein isolate or wheat gluten.

Overall, the findings of this study demonstrated that freeze–thaw processing combined with transglutaminase and alginate was an effective and relatively low-cost approach for structuring soy protein into a meat-like fibrous matrix. This approach showed strong potential for further development and scale-up in the production of healthier plant-based meat alternatives.

Acknowledgements

This research was financially supported by the master's Thesis Research Grant (Fiscal Year 2024) from the Faculty of Agro-Industry, Chiang Mai University.

References

1 Bezerra MA, Santelli RE, Oliveira EP, Villar LS, Escaleira LA. Response surface methodology (RSM) as a tool for optimization in analytical chemistry. Talanta. 2008;76(5):965–977. doi:10.1016/j.talanta.2008.05.019

2 Boye J, Zare F, Pletch A. Pulse proteins: Processing, characterization, functional properties and applications in food and feed. Food Res Int. 2010;43(2):414–431.

3 Chen, Q., et al. (2022). Protein–amylose/amylopectin molecular interactions during high moisture extruded texturization toward plant-based meat substitutes applications. *Food Hydrocolloids, 127*, 107559.

4 Cheng Y, Ye A, Singh H. Characterization of emulsion gels formed with whey and soy protein mixtures and their protein digestion under *in vitro* gastric conditions. Curr Res Food Sci. 2024;8:100674.

5 Clark MA, Stewart GB, Panzone LA, Kyriazakis I, Frewer LJ. A systematic review of public attitudes, perceptions and behaviours towards production diseases associated with farm animal welfare. J Agric Environ Ethics. 2017;30:455–478.

6 Consolacion, F., & Jelen, P. (1986). Freeze texturization of proteins: Effect of alkali, acid, and freezing treatments on texture formation. *Food Microstructure, 5*(1), 33–39.

7 Dekkers, B. L., Boom, R. M., & van der Goot, A. J. (2018). Structuring processes for meat analogue. *Trends in Food Science & Technology, 81*, 25–36. https://doi.org/10.1016/j.tifs.2018.08.011

8 Food and Agriculture Organization of the United Nations (FAO). (2023). The state of food and agriculture 2023: Revealing the true cost of food to transform agrifood systems. FAO. https://doi.org/10.4060/cc7724en

9 Goh, K. K. T., Haisman, D. R., & Singh, H. (2022). Protein–polysaccharide interactions in food systems: Recent advances and future perspectives. Current Opinion in Food Science, 45, 100830. https://doi.org/10.1016/j.cofs.2022.100830.

10 Jooyandeh, H. (2011). Soy products as healthy and functional foods. *Middle-East Journal of Scientific Research, 7*(1), 71–80.

11 Kao, F.-J., Su, N.-W., & Lee, M.-H. (2003). Effect of calcium sulfate concentration in soymilk on the microstructure of firm tofu and protein constituents in tofu whey. *Journal of Agricultural and Food Chemistry, 51*(21), 6211–6216.

12 Kieliszek, M., & Misiewicz, A. (2020). Microbial transglutaminase and its application in the food industry: A review. Folia Microbiologica, 65, 59–74. https://doi.org/10.1007/s12223-019-00730-7
13 Nardi, M., Marti, A., & Bonomi, F. (2021). Digestibility and nutritional quality of plant proteins in meat analogue. Foods, 10 (11), 2760. https://doi.org/10.3390/foods10112760
14 Phongthai, S., Homthawornchoo, W., & Rawdkuen, S. (2017). Preparation, properties, and application of rice bran protein: A review. *International Food Research Journal, 24*(1).
15 Prabhakaran MP, Perera CO, Valiyaveettil S. Effect of different coagulants on isoflavone levels and physical properties of firm tofu. Food Chem. 2006;99(3):492–499.
16 Rizzo, G., & Baroni, L. (2020). Soy, soy foods and their role in vegetarian diets. Nutrients, 12 (11), 3495. https://doi.org/10.3390/nu12113495
17 Schösler H, de Boer J, Boersema JJ. Can we cut out the meat of the dish? Constructing consumer-oriented pathways towards meat substitution. Appetite. 2012;58(1):39–47.
18 Shi, Y. G., Yang, Y., Piekoszewski, W., Zeng, J. H., Guan, H. N., Wang, B., et al. (2022). Influence of four different coagulants on the physicochemical properties, textural characteristics and flavour of tofu. International journal of food science & technology, 55(3), 1218-1229.
19 Sijtsema SJ, Linnemann AR, van Gaasbeek T, Dagevos H, Jongen WMF. Variables influencing food perception reviewed for consumer-oriented product development. Crit Rev Food Sci Nutr. 2002;42(6):565–581.
20 Steinfeld H, Gerber P, Wassenaar T, Castel V, de Haan C. Livestock's long shadow: Environmental issues and options. Rome: Food and Agriculture Organization of the United Nations; 2006.
21 Sun, X., Chi, Y., Tang, C., & Li, Y. (2019). Effect of microbial transglutaminase on textural and structural properties of plant-based meat analogs. *Food Hydrocolloids, 94*, 132–139
22 Thu, H. E., Zulfakar, M. H., & Ng, S. F. (2012). Alginate based bilayer hydrocolloid films as potential slow-release modern wound dressing. International journal of pharmaceutics, 434(1-2), 375-383.
23 United Nations. World population prospects: The 2017 revision. New York: United Nations; 2017.
24 Verbeke W, Pérez-Cueto FJA, de Barcellos MD, Krystallis A, Grunert KG. European citizen and consumer attitudes and preferences regarding beef and pork. Meat Sci. 2010;84(2):284–292.
25 Yuliarti, O., Yi, N. J., & Ismail, I. (2021). Freeze–thaw induced structural modification of plant protein gels: Mechanism and applications. Food Hydrocolloids, 118, 106791. https://doi.org/10.1016/j.foodhyd.2021.106791
26 Zhang, J., Liu, L., Jiang, Y., & Shah, B. R. (2020). Application of transglutaminase in the food industry: A review. *Food Research International, 137*, 109361.
27 Zhou X, et al. Protein network modification and enzymatic digestibility in plant protein systems. Food Chem. 2021;344:128694.

P - 407

Comparative Nutritional and Functional Attributes of Thai Underutilized Legumes

Abubakar Ibrahim Garba[1,2], Pilairuk Intipunya[1]*

[1]*Faculty of Agro-Industry, Chiang Mai University, Chiang Mai, 50100, Thailand*
[2]*Institute for Agricultural Research, Ahmadu Bello University, 1044, Nigeria*

**Corresponding author E-mail: pilairuk.intipunya@cmu.ac.th*

Abstract: Thailand's underutilized legumes have been reported to be the future of protein supply and climate remediation in Asia and beyond; however, their utilization has been limited due to a lack of scientific evidence of usability. This study investigated the proximate composition and techno-functional properties of four potential Thai legumes: *Vigna radiata* (Mung bean), *Psophocarpus tetragonolobus* (Winged bean), *Acacia concinna* (Sompoi), and *Vigna unguiculata subsp. Sesquipedalis* (Yardlong bean) and compared them with mainstream soybeans. The protein and fat contents of the Thai legumes ranged from 5.87% to 27.66% and 0.21% to 1.38%, respectively, with yardlong bean having the highest protein content and Sompoi mix having the highest fat content. The protein and fat contents of the underutilized legumes represent up to 66.04% and 8.2% of those found in soybeans. The functional properties of the flour varied among the varieties, with water absorption capacity ranging from 1.15 mL/g in winged bean to 3.8 mL/g in *Acacia concinna* seed, and oil absorption capacity ranging from 1.0 mL/g in Sompoi mix pulp to 2.60 mL/g in soy, respectively. The mixed Sompoi flour has the highest solubility of 40.5 %, while Sompoi pulp has the least solubility. The highest swelling power of 12.21 g/g was found in the Sompoi pulp sample. All varieties have acidic flour, with a pH ranging from 3.20 to 6.02, and a titratable acidity of 0.08% to 0.45%, respectively. The findings of this research have practical applications in mainstream food product development, particularly in high-protein food products, such as meat analogues. This research underscores the potential of Thai legumes as high-protein food sources and their role in addressing pressing food and nutritional insecurity in Thailand and beyond.

Keywords: Functionality; High-protein; Protein; Underutilized legumes

1. Introduction

The agricultural landscape of Thailand is rich in untapped high-protein legume species with a potential for usage as food extending far beyond mainstream high-protein grains such as wheat, peas and soybean. These underutilized legumes present a significant potential in improving household food security, enriching traditional cuisines, and bolstering low-input farming systems. However, despite their undeniable potential, many of these legumes remain underexplored, especially in advanced food product development such as plant and dairy alternatives, even though they present high nutrition and sustainability potential [1]. Recently, underutilized high-protein legumes have been studied as climate-friendly alternatives to mainstream legumes. Moving rapidly from marginalized research perspective to the mainstream of food system solutions [2]. With the rise in concern for climate change, supply-chain issues, and persistent micronutrient deficiencies in conventional legume staples, underexplored legumes such as *Vigna radiata* (Mung bean), *Psophocarpus tetragonolobus* (Winged bean), *Acacia concinna* (Sompoi), and *Vigna unguiculata subsp. Sesquipedalis* (Yardlong bean) bring a compelling advantage of high nutrient

density, low agricultural input requirements, sensory diversity, and ecological and climate resilience [3].

Additionally, research shows that while conventional sources like soy and wheat dominate plant-based protein markets, emerging options like chickpeas, lentils, and various regional pulses are being spotlighted for their low allergenicity and impressive nutritional profiles [4]. For example, chickpea flour exhibits impressive emulsifying properties and can contribute significantly to textural improvements in food products, as demonstrated in recent analyses [5]. Such findings suggest that underutilized legumes have the potential to play vital roles in enhancing dietary quality while promoting local agricultural biodiversity. Mung bean is an indigenous crop of Southeast Asia, including Thailand; however, despite its long history in the region, nutritional composition and climate resilience, Mung bean remains underutilized in the mainstream food production industries. Recently, the Thai Bio-circular Green (BCG) economy failed to capture relevant high-potential legumes such as mung bean in its national agricultural framework, indicating policy neglect. Various studies have reported a wide range of nutrients in mung beans, including 4.95 – 5.22 % fiber, 1.3-2.91 % fat, 44.29-64.4 % carbohydrate and 19.25-34.99 % protein [2,6]. Other nutrients include a significant amount of calcium, phosphorus, potassium, sodium, zinc, iron, and magnesium [2]. Beyond their good nutrition, mung beans have also been reported to have excellent functional properties, including solubility, water retention, emulsification, gelation, foaming, and foam stability, making them attractive for food product development [2]. Moreover, mung beans contain bioactive compounds with diverse physiological effects, including antioxidant properties, both in their raw and processed forms [2,7].

However, for adequate utilization of the nutrients in underutilized legumes, for the development of legume-based products, there is a need for the adequate evaluation and documentation of their nutritional, processing and functional properties considering regional differences and varietal variation. It is on this basis that this research was carried out to evaluate Thai underutilize legumes as potential raw material for the emerging consumer-based development of plant-based diets relevant to the Thai regional cuisine. This study aimed to explore the nutritional and functional attributes of selected Thai underutilized legumes, interlinking their potential with evidence-based macronutrient composition and key functional properties. This study also aims to identify the varietal differences that could influence their application in food technologies. The findings of this research are helpful for the appropriate utilization of these under-explored legumes in a healthier and more diverse diet for consumers, paving the way for sustainable agricultural practices that bolster food security in Thailand and beyond.

2. Materials and Methods

2.1 Material Collection

The seeds used in this study were sourced from a local producer (Thanya Farm, Chiang Mai, Thailand) and retailed by Makro Ltd., Thailand. The seeds initially sorted by the producer were cleaned and stored in a hygienic environment at room temperature before the experiments. All reagents used in this research are of analytical grade, while all equipment was calibrated and certified for use by the Department of Food Science and Technology, Chiang Mai University, Thailand.

2.2 Sample preparation and flour production

The cleaned, dried seeds were milled using a hammer mill (SK-300, Retsch, Thailand) equipped with a 1 mm sieve. The powder is then sieved (AS-200, Retsch, Thailand) through a 250 µm sieve. The flour was packed in a clean opaque Ziplock bag and stored at room temperature (27±2^{o}C) until used.

2.3 Determination of proximate composition

The proximate composition of the flour was determined using the procedure described by AOAC [8]. Moisture content, ash, fiber and lipid contents were evaluated using method 925.26,

940.26, 991.43 and 933.05, respectively. The protein content was evaluated using the micro Kjeldahl method 920.87. Determination of carbohydrates was done by difference as described in Equation 1.

$$Total\ carbohydrate\ =\ 100\ -\ (\%\ Moisture\ +\ \%\ Ash\ +\ \%\ Fat\ +\ \%\ Protein) \quad (1)$$

2.4 Determination of color

The color properties of the legume flour were determined using a colorimeter (CR-300, Konica Minolta, Japan). The color indices corresponding to the CIE-Lab system (Commission Internationale de l'Eclairage) were determined by reflectance in L*, a*, and b* color coordinates. Three measurements were done for each sample and were recorded as color indices and used to calculate hue indices, ΔE and whiteness index using Equations 2 and 3.

$$\Delta E\ =\ \sqrt{(\Delta L\ *)^2 + (\Delta a\ *)^2 + (\Delta b\ *)^2} \quad (2)$$

$$C_0 = 100 - \sqrt{(a\ *)^2 + (b\ *)^2} \quad (3)$$

2.5 Functional properties

2.5.1 Water and oil absorption capacity

The water absorption capacity (WAC) and oil absorption capacity (OAC) of the protein concentrate were determined using the method described by Badjona et al. [9] and expressed as the amount of water/oil held by a gram of the concentrate. About 1.0 g of isolated protein flour will be dispersed in 40 mL of distilled water or sunflower oil for water and oil absorption, respectively. The mixture was vortexed for 1 minute, and allowed to stand for 6 hours at 20-30°C. After that, the mixture was centrifuged at 3000*g* and 20°C for 30 minutes. The oil and water holding capacity were then calculated using Equations 4 and 5.

$$WAC(mL) = \frac{V_0\ - V_1}{W_2} \quad (4)$$

$$OAC(mL) = \frac{V_0\ - V_1}{W_2} \quad (5)$$

Where V_o is the initial volume of water or oil used, and V_1 is the final volume of water or oil used, W_2 is the initial weight of the sample.

2.5.2 Determination of solubility and swelling power

The solubility of the flour was determined as the amount of the flour that dissolved in water at 85°C, while the swelling power was expressed as the increase in weight following centrifugation using the procedure described in Osei et al. [10]. About 1 g of the flour was dissolved in 40 mL of water, and the suspension was stirred well, allowed to dissolve at room temperature for 30 minutes and heated in a closed container in a water bath at 85°C for 30 minutes with continuous shaking. The samples are then removed, cooled to room temperature (24.5 ± 0.53 °C) and centrifuged for 15 minutes at 2200 rpm. The supernatant is then decanted and dried in a hot air oven until constant weighs. The solubility and swelling power are calculated using Equations 6 and 7.

$$Solubility\ (\%) = \frac{Weight\ of\ dried\ supernatant}{Weight\ of\ the\ sample\ used} x100 \quad (6)$$

$$Swelling\ capacity\ (g/g)\ = \frac{Weight\ of\ wet\ flour}{Weight\ of\ dry\ flour} \quad (7)$$

2.5.3 Determination of pH

The pH of the flour was determined as the acidity level of the flour, which affects its usability in food product development and was determined using the procedure described in Osei et al. [10]. Approximately 10% suspension of the flour was prepared, and the pH was measured using an automatic pH meter (Mettler Toledo S220, USA), initially calibrated to 7.0 using standard buffer.

2.5.4 Determination of Titratable Acidity

The procedure described by Obike et al. [11] was used to determine the titratable acidity as the flour's minimum acidity. The suspension from the pH experiment (10% suspension) was used to titrate against 0.1 M NaOH using phenolphthalein as an indicator until the pink endpoint. The volume of NaOH added was read from the burette and multiplied by 0.09 to obtain the % titratable acidity as lactic acid (being the predominant acid).

2.6 Rheological properties of the flours

The rheological properties of the flours were evaluated using a modular compact rheometer (Anton Paar, USA) equipped with PP50 parallel plate geometry through amplitude and frequency sweep. A 20% dispersion of the flour was prepared and evaluated for a linear viscoelasticity test at 25°C and 1 Hz frequency. Storage modulus (G') and Loss modulus (G") were analysed at a shear strain range of 0.01 to 100 % and constant strain [12].

2.7 Statistical analysis

All experiments were carried out in duplicate. Before statistical analysis, the data were collected on Microsoft Excel and exported to the data interface of SPSS V21. The data was further analysed using One-Way ANOVA, and means were separated using Duncan Multiple Range Test to determine the significant difference.

3 Results & Discussion

3.1 Proximate composition of Thai legumes

The proximate composition of Thai underutilized legumes is presented in Table 1. The result shows a high protein potential up to 67.5%, comparable to mainstream soybeans. Winged beans have the highest protein with 27.66%, while Sompoi has the least protein of 5.87 %. The protein contents of the varieties varied significantly, $p<0.05$ and are within the 20-45% protein range reported for high-protein crops suitable for advanced food product development, such as meat analogue [13]. Additionally, the protein and fiber content reported in this research for Sompoi (5.87-18.58 % and 9.86-48.61 %, respectively) is higher than 6.73% and 9.15% reported by Ganogpichayagrai & Suksaard [14] in Sompoi from Thailand, indicating varietal variation across the species produced in the same climatic and topographical conditions. The protein content of all the legumes is higher than 13.6% protein content of the cowpea variety reported by Makeri et al. [15]. High protein content indicates the potential of the legumes in maintaining bone health, reducing the risk of kidney stones and supporting child development [16]. The fat content ranges from 0.21-1.38%, which is lower than 15.11% found in soybeans. Low fat indicates the suitability of these crops in low-fat food formulation, especially those targeting non-communicable disease control, such as hyperlipidemia [17]. Additionally, the fat content reported in this research is lower than 9.16% and 10.66% reported for velvet and yam bean, respectively [11].

Table 1: Proximate composition of Thai underutilized legumes

Sample	Moisture (%)	Ash (%)	Fat (%)	Fiber (%)	Protein (%)	Carbohydrate (%)
Soybean	7.10±0.813^{b}	6.02±0.967^{ab}	15.11±0.951^{a}	10.86±0.144^{c}	41.88±0.129^{a}	19.04±0.844^{d}
Mung bean	8.39±0.021^{b}	3.64±0.103^{b}	1.23±0.661^{b}	4.78±0.127^{d}	21.52±1.783^{bc}	60.44±2.399^{a}
Winged bean	10.06±0.255^{a}	5.75±0.056^{ab}	0.71±0.020^{b}	9.34±1.775^{c}	26.36±0.423^{bc}	47.78±1.643^{b}
Yardlong bean	8.46±0.177^{b}	5.89±1.920^{ab}	0.96±0.154^{b}	26.23±2.556^{b}	27.66±4.254^{b}	30.79±0.109^{c}
Sampoi Pulp	10.33±0.455^{a}	7.86±0.898^{a}	0.21±0.061^{b}	26.80±0.895^{b}	5.87±1.337^{d}	48.94±0.955^{b}
Sampoi Seed	5.92±0.368^{ab}	3.05±0.154^{b}	0.21±0.020^{b}	9.86±0.273^{c}	18.58±2.719^{c}	62.39±2.987^{a}
Sampoi Mix	5.16±0.276^{a}	4.90±0.088^{ab}	1.38±0.027^{b}	48.61±0.535^{a}	9.44±2.835^{d}	30.51±3.208^{c}

Note: Samples with the same superscript on the same column did not differ significantly at $p<0.05$. Data were presented as means of duplicate results ± standard deviation.

3.2 Functional attributes of Thai legumes

The functional attributes of Thai underutilized legumes are presented in Table 2. The results show an oil absorption capacity ranging from 1.0 ml/g in Sompoi seed and pulp flour to 2.60 ml/g in soybean. Soybean has the highest oil absorption capacity, followed by winged bean with 2.45 ml/g. Oil absorption capacity has been described as the ability of a food ingredient to hold oil and is linked to flavor retention Badjona et al. [9]. It is also associated with mouth-rich products such as sausages or baked snacks. The variation in oil absorption capacity among different legume plants was documented earlier among pea, moringa seed, lentil, and chickpea whole flour [11]. The water absorption capacity ranges from 1.15 ml/g in winged bean to 3.77 ml/g in Sompoi seed flour. Mung bean exhibits moderate WAC while Sompoi and winged bean exhibited a very low WAC between 2.5 and 1.15 ml/g, suggesting their matrix may trap more water due to structural differences, such as higher fiber or protein–carbohydrate interactions. According to [11], flour with WHC between 1.49 and 4.72 g/g is suited for moisture-sensitive products such as baked goods and meat substitutes.

The solubility and swelling power of the flour are associated with the dissolution behavior and increase in flour volume as they absorb water at a specified temperature condition. The solubility and the swelling power of the flour range from 18.52 % in Sompoi pulp to 49.10% in soybean, and 0.66g/g in soybean to 12.21 in Sompoi pulp, respectively. The swelling power in this study is comparative (2.18-2.83%), while the solubility is higher (31.04-46.19%) than those reported for velvet bean and African yam bean [11]. High swelling power suggests a greater ability of flour to absorb water and expand, which is a valuable property required in baking and meat extenders. Additionally, the ability of plant flour to swell is linked to starch composition, particularly the amylose-to-amylopectin ratio, as well as the extent of protein-starch interactions [11]. A higher content of long chains in amylopectin has been associated with enhanced starch swelling [18]. Comparatively, the lower swelling power of soybean compared to other legumes such as winged bean (11.968/g) is linked to comparatively lower amylose and amylopectin content of 19-22.5 % and, 68-71% and, 21-29% and 71-79% in winged bean as indicated in previous study [18].

The pH and titratable acidity of the flours range from 3.20 to 6.02 in Sompoi pulp and seed flour and mung bean, 0.095 to 0.450 in mung bean and Sompoi pulp, respectively. This variation in acidity and pH is common to legume flour and has been reported in previous research. Osei [10] reported a pH and titratable acidity of 6.4 and 0.5, which are relatively higher than the values reported in this research. The lower pH in this is important for legume packaging and storage, as lower pH has been associated with longer shelf stability (inhibiting microbial growth) as well as better conditions for enzymes to break down proteins [16]. Additionally, the titratable acidity in this research indicates a potential for improved flavor and aroma, because lower titratable acidity <0.4 has been reported for better sourdough flavor and aroma development and is required for bread and beverage production [10, 11]. It also shows potential for a continued rise as more acid

(due to lactic acid production) is produced, resulting in a much more sour-tasting bread and other food products.

Table 2: Techno-functional properties of Thai potential legumes

Sample	Oil Absorption Capacity (mL/g)	Water Absorption Capacity (mL/g)	Solubility (%)	Swelling Power (g/g)	TTA (%)	pH
Soybean	2.60±0.141^{a}	2.40±0.566^{ac}	49.10±0.765^{a}	0.66±0.262^{a}	0.08±0.000^{a}	5.91±0.021^{a}
Mung bean	2.04±0.549^{ab}	3.00±0.316^{a}	24.21±2.552^{b}	3.82±0.042^{b}	0.095±0.032^{a}	6.02±0.021^{a}
Winged bean	2.53±0.122^{a}	1.15±0.212^{b}	28.64±1.868^{b}	11.96±0.735^{c}	0.392±0.045^{bc}	4.86±0.014^{d}
Yardlong	2.45±0.156^{a}	3.57±0.111^{a}	34.19±0.346^{c}	7.30±2.369^{d}	0.338±0.096^{b}	5.07±0.021^{c}
Sampoi Pulp	1.17±0.031^{b}	1.50±0.163^{bc}	18.52±1.501^{d}	12.21±1.167^{c}	0.450±0.064^{c}	5.30±0.141^{b}
Sampoi Seed	1.49±0.152^{b}	3.77±0.406^{a}	26.55±8.213^{b}	4.06±0.396^{b}	0.099±.013^{d}	5.18±0.014^{bc}
Sampoi mix	1.00±0.140^{b}	2.66±0.078^{ac}	40.50±2.591^{a}	1.00±0.000^{a}	0.234±0.076^{e}	3.20±0.028^{e}

Note: Samples with the same superscript on the same column did not differ significantly at $p<0.05$. Data were presented as means of duplicate results ± standard deviation.

The colorimetric CEILAC chroma of the Thai legumes is presented in Table 3. Soybean consistently exhibited high lightness (82.63), yellowness (24.54), and chroma (24.54), supporting its suitability as a neutral-colored base ingredient. Comparatively, the Sampoi seed flour showed a significantly lower lightness (41.19) and chroma (8.9) with a pronounced red hue (42.02). This color index may have arisen from its high phenolic compounds and seed coat pigments [19]. Sampoi seed and pulp exhibit a high chromatic variation, highlighting the importance of fraction selection when targeting specific color attributes in formulated products. Mung bean exhibits almost similar color behavior with soybean, with a lightness score of 85.57 and chroma index of 12.66, indicating potential as a soybean replacement in terms of color. These findings are particularly relevant for meat analogue development, where color uniformity and consumer acceptance are critical [20]. Collectively, the colorimetric results demonstrate significant differences among the legume materials, reflecting variations in pigment composition, seed fractionation, and biochemical constituents.

Table 3: Color properties of Thai underutilized legumes

Sample	**L***	**a***	**b***	**ΔE**	**C_0**
Soybean	82.63±0.1626^{a}	-0.10±0.0707^{a}	24.54±0.0778^{a}	86.19±0.1339^{a}	24.54±0.0775^{a}
Mung Bean	85.57±0.0071^{a}	-1.94±0.0071^{b}	12.51±0.0000^{b}	86.50±0.0068^{a}	12.66±0.0011^{b}
Wing Bean	63.83±0.0071^{b}	-1.36±0.0141^{c}	17.29±0.0354^{c}	66.14±0.0027^{b}	17.34±0.0364^{c}
Yardlong Bean	58.79±0.0071^{b}	-1.39±0.0071^{c}	17.68±0.0071^{c}	61.40±0.0049^{b}	17.73±0.0065^{c}
Sampoi Pulp	71.21±0.0701^{c}	-4.74±0.3465^{d}	22.39±0.0071^{a}	74.80±0.0433^{c}	22.88±0.0786^{a}
Sampoi Seed	41.09±0.0071^{d}	4.46±0.0212^{d}	7.71±0.1061^{d}	42.04±0.0148^{d}	8.90±0.1024^{d}
Sampoi mix	75.92±0.0000^{c}	-0.36±0.0071^{a}	11.00±0.0141^{b}	76.71±0.0020^{c}	11.01±0.0139^{b}

Note: Samples with the same superscript on the same column did not differ significantly at $p<0.05$. Data were presented as means of duplicate results ± standard deviation.

3.3 Rheological properties of Thai legumes

The rheological properties of Thai underutilized legumes are presented in Figure 1. The amplitude sweep results in Frame A show that all the varieties exhibit higher G' at low strain, indicating a predominantly elastic behavior and formation of structured, solid-like networks within the linear viscoelastic region. Yardlong and winged bean show the highest modulus between 104 and 105 Pa at low strain, exhibiting a highly interconnected and rigid protein-polysaccharide

structure. This behavior indicates that Yardlong and winged flour can be used in a food production process where sustainable deformation capability is required without structural breakdown. It also suggests that their compositional matrix is capable of resisting shear-induced structural disruption [21] and requires further treatment or refining for use in food processes such as extrusion, where structure melting is needed [22].

Comparatively, Soybean and Sampoi seed flours exhibited intermediate viscoelastic behaviour, characterized by moderate G′ values between 10^1-10^2 Pa at low strains, indicating an elastic-dominated rheology. The earlier decline in both G′ and G″ with increasing strain suggests a comparatively weaker network that undergoes progressive structural rearrangement under deformation [23]. However, at a higher temperature, they also show crossover-like behaviour, possibly indicating partial breakdown of the gel matrix and increased viscous dissipation. This shows suitability for a production where low viscous behavior under shear strain is required, such as in protein shakes. Mung bean, however, exhibited the lowest moduli across the entire strain range, with G′ and G″ remaining below 1 Pa. Its narrow linear viscoelastic region (LVR) and early reduction in moduli indicate a loosely associated structure with limited elastic reinforcement. This behavior suggests insufficient network formation, likely due to lower protein-protein interactions or reduced capacity for entanglement and aggregation under the tested conditions [23].

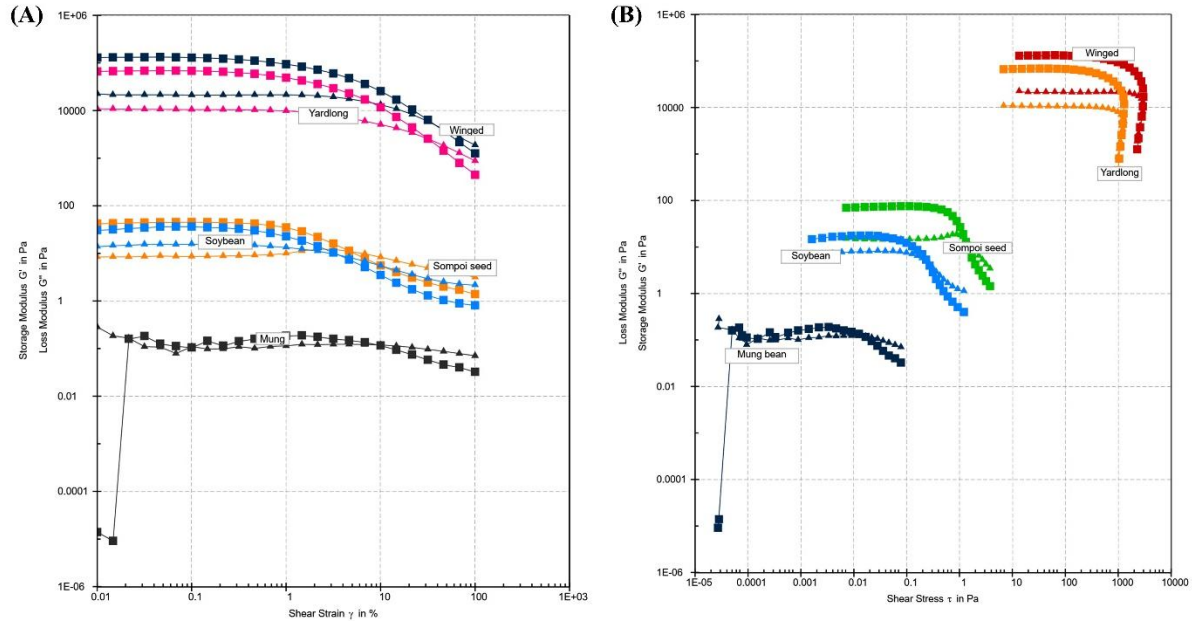

Figure 1: Rheological behavior of Thai underutilized legumes. From the graphs, the storage modulus (G') in Pascal is presented in the graph with trend lines with rectangular dots (⊡) while the Loss modulus (G") is indicated with triangular dots (Δ). Sample names were indicated on each trend line and indicate the actual rheological properties from the measurement interface.

Figure 1 shows the relationship between shear stress, shear strain and storage and loss modulus. Frame (A) shows the relationship between shear strain and loss and storage modulus, while Frame (B) shows the relationship between stress, loss and storage modulus. The amplitude sweep results in both figures present the mechanical stability of the flours under shear stress and strain. Figure 1(A) shows that Thai legume flours exhibited a linear viscoelastic region at low shear stress, followed by a pronounced decrease in both storage and loss moduli. This behavior indicates stress-induced structural breakdown. Among the legumes, winged bean and yardlong displayed the highest storage modulus and widest linear viscoelastic region, reflecting strong, well-connected protein networks with a high resistance to deformation similar to the behavior

indicated in Figure 1B. Sampoi seed and soybean showed intermediate behavior, suggesting less cohesive structures that are more susceptible to stress-induced disruption. Mung bean exhibited the lowest moduli and an absence of a well-defined linear viscoelastic region, indicative of weak or discontinuous network formation.

The result of the frequency sweep showing the relationship between complex viscosity and frequency is presented in Figure 2. The results show that all the legume flour shows decrease in complex viscosity with an increase in angular frequency. This trend confirms the shear-thinning behavior previously described in Figure 1. This agrees with previous research, where legume protein exhibited shear-thinning behavior [23], and has been suggested as an important rheological property required in food product development [12], such as in bread and cake [24]. In this study, yardlong and winged beans show the highest complex viscosity, which correlates with the presence of highly entangled and elastic protein networks that resist deformation previously highlighted in the amplitude sweep. They also exhibited similar decay slopes, suggesting a comparable relaxation mechanism governed by protein–protein interactions and network disentanglement [12]. Additionally, Sompoi seed and soybean presented a higher frequency sensitivity and an intermediate viscosity, indicative of less cohesive or partially particulate structures. The lowest complex viscosity was found in the Mung bean, suggesting limited gelation and weak network formation in mung bean proteins. Such differences in frequency-dependent viscoelastic behavior are critical for high-shear processing operations, as materials with higher low-frequency viscosity and sustained shear-thinning behavior are more capable of developing anisotropic and fibrous structures during extrusion [21].

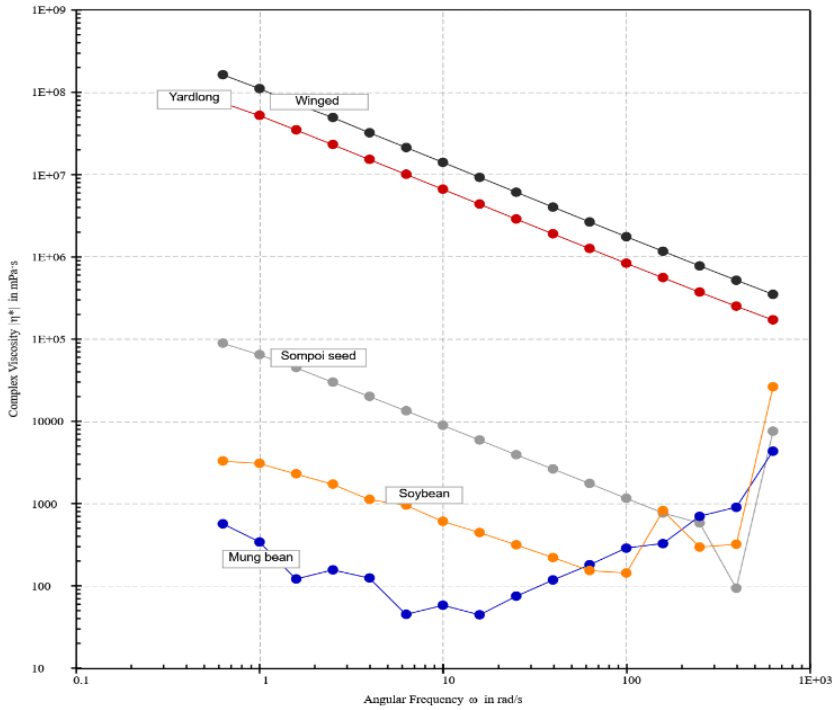

Figure 2: Complex viscosity of Thai underutilized legumes

The shear thinning behavior exhibited by Thai legumes is linked to their swelling properties, which are associated with the amylose and amylopectin content earlier highlighted in the previous section. The ability of the flour to swell upon heating indicates an important attribute linked to its macronutrient composition. Specifically, Thai legumes such as mung beans have a high carbohydrate (consisting of amylose and amylopectin) and protein (factor of deformation), which inherently affects the rheological flow behavior [11, 16]. Compared to carbohydrate (19.0%) and protein (41.88 %) contents of soybean, the lower content of protein (5.87-26.36%)

and higher carbohydrate content in Thai legumes further explain the moderate to weak rheological properties. Overall, the impact of rheology is also manifested in oral perception and digestion, resulting from the effects on the flow characteristics of mechanical and chemical processes [25] in food. The structural breakdown during food mastication is associated with textural sensation, and rheological measurements may, thus, be employed to control other quality attributes such as flavor or nutrient release at specific conditions [26].

4. Conclusion

This study explored the potential of four Thai underutilized legumes as raw material for advanced food product development. The result of the evaluation revealed a significant variability, including high protein content up to 62% of mainstream soybean and a significantly very low fat content. Their rheological profiles demonstrate viscoelastic strength and structural resilience under shear. Yardlong, winged bean and Sompoi exhibited strong rheological properties with higher initial moduli and broader LVRs, indicating superior processability and textural integrity during high-shear operations such as extrusion or mixing, whereas mung bean shows weaker structural networks that are susceptible to structural collapse under mechanical stress. The large variation in the color spectrum shows potential sensory diversity and is linked to phytochemical constituents, including flavonoids. Overall, Thai underutilized legumes present an untapped potential for diverse food product development. Further research is recommended to extract and characterized protein from these legumes.

Acknowledgements

The authors gratefully acknowledge the support received from Chiang Mai University, Chiang Mai, Thailand, through the Presidential Scholarship granted to the first author, Mr AI Garba.

References

1. Shevkani K, Shivani B, Dhaka SS, Patil C. Cowpeas for sustainable agriculture and nutrition security: an overview of their nutritional quality and agroeconomic advantages. Discover Food 2025;5:109. https://doi.org/10.1007/s44187-025-00382-x.
2. Kemal M, Teka TA, Dibaba K, Urugo MM. Effects of processing methods on nutrient and antinutrient composition, techno-functional and antioxidant properties of mungbean (Vigna radiata (L.) R. Wilczek) varieties. LWT 2025;222:117663. https://doi.org/10.1016/j.lwt.2025.117663.
3. Knez M, Ranić M, Gurinović M. Underutilized plants increase biodiversity, improve food and nutrition security, reduce malnutrition, and enhance human health and well-being. Let's put them back on the plate! Nutr Rev 2024;82:1111–24. https://doi.org/10.1093/nutrit/nuad103.
4. Samal I, Bhoi TK, Raj MN, Majhi PK, Murmu S, Pradhan AK, Kumar D, Paschapur AU, Joshi DC, Guru PN. Underutilized legumes: nutrient status and advanced breeding approaches for qualitative and quantitative enhancement. Front Nutr 2023;10. https://doi.org/10.3389/fnut.2023.1110750.
5. Moussaoui D, Chaya C, Badia-Olmos C, Rizo A, Tarrega A. Effect of pH and Calcium on the Techno Functional Properties of Different Pulse Flours, Pastes, and Gels. Food Bioproc Tech 2024;17:2292–303. https://doi.org/10.1007/s11947-023-03264-1.
6. Brishti FH, Zarei M, Muhammad SKS, Ismail-Fitry MR, Shukri R, Saari N. Evaluation of the functional properties of mung bean protein isolate for development of textured vegetable protein. Int Food Res J 2017;24:1595–605.

7. Hou D, Yousaf L, Xue Y, Hu J, Wu J, Hu X, Feng N, Shen Q. Mung Bean (Vigna radiata L.): Bioactive Polyphenols, Polysaccharides, Peptides, and Health Benefits. Nutrients 2019;11:1238. https://doi.org/10.3390/nu11061238.
8. AOAC. Official Methods of Analysis of the Association of Official Analytical Chemists. vol. 21. 21st Edition. AOAC: Washington DC; 2019.
9. Badjona A, Bradshaw R, Millman C, Howarth M, Dubey B. Response surface methodology guided approach for optimization of protein isolate from Faba bean. Part 1/2. Ultrason Sonochem 2024;109:107012. https://doi.org/10.1016/j.ultsonch.2024.107012.
10. Osei Tutu C, Amissah JGN, Amissah JN, Akonor PT, Budu AS, Saalia FK. Physical, chemical, and rheological properties of flour from accessions of Frafra potato (Solenostemon rotundifolius). J Agric Food Res 2024;15:100974. https://doi.org/10.1016/j.jafr.2024.100974.
11. Obike CA, Anyiam PN, Emelike CU, Uhuo EN, Igbazenda SF. Composition, Techno-Functional Properties, and Biological Potential of Velvet and African Yam Beans as Plant Protein Sources. Sustainable Food Proteins 2026;4. https://doi.org/10.1002/sfp2.70050.
12. Kaur S, Ubeyitogullari A. The impact of supercritical carbon dioxide processing on the aroma and physicochemical properties of soybean flour. Future Foods 2024;10:100476. https://doi.org/10.1016/j.fufo.2024.100476.
13. Sowdhanya D, Singh J, Rasane P, Kaur S, Kaur J, Ercisli S, Verma H. Nutritional significance of velvet bean (Mucuna pruriens) and opportunities for its processing into value-added products. J Agric Food Res 2024;15:100921. https://doi.org/10.1016/j.jafr.2023.100921.
14. Ganogpichayagrai A, Suksaard C. Evaluation of proximate composition and biological activities of sompoi (Acacia concinna) leaves in Thailand. J Adv Pharm Technol Res 2022;13:317–21. https://doi.org/10.4103/japtr.japtr_443_22.
15. Makeri MU, Baidu A, Garba AI, Aliyu AA, Abubakar F. Nutrient, anti nutrient and invitro protein digestibility of maruca vitrata resistant cowpea cultivar (Sampea 20T) compared to a local cultiver (Dan-Misra) . In: Bolanle A, Badejo A, Babarinde G, Awoyale W, Adejoke A, Olatoye K, editors. 49th NIFST conference-Isokan 2025, Kwara: Nigerian Institute of Food Science and Technology; 2025, p. 391–4.
16. Sogunle KA, Garba AI, Aliyu AA, Marke IG,. Underutilized Legumes and Cereals Can Replace Wheat in Biscuit: Production and Quality Evaluation of Biscuit from Wheat (Triticum estivum), Bambara Nut (Vigna subterranean) and Sprouted Fonio (Digitaria exillis) Composite. Journal of Underutilized Legumes 2025;7:55–65.
17. Godbharle S, Jeyakumar A, Kesa H. Food away from home and the risk of non-communicable diseases among young working adults in Pune, India: a smartphone-based dietary assessment. BMC Nutr 2025;11:202. https://doi.org/10.1186/s40795-025-01180-5.
18. Sogunle KA, Aliyu AA, Garba AI, Adaobi TF, Okafor AM, ., Puorizaa T,, Ezeoma CC. Smart Food Innovation: Boosting Nutrition through Crafted Breakfast Cereal from Underutilized Crops, Fonio Millet (ACHA) (Digitaria exilis) Bambara Nut (Vigna subterranean) and Soybean (Glycine max). Direct Research Journal of Agriculture and Food Science 2025;13:180–91.
19. Chaovanalikit A, Nudnim P, Mingyai S, Ketjarut S, Potaros T, Prempiyakit W. The effect of heating method on phenolic and flavonoid content and antioxidant activity of velvet bean. Journal of Food Technology, Siam University 2024;19:77–86.
20. Godschalk-Broers L, Sala G, Scholten E. Meat Analogues: Relating Structure to Texture and Sensory Perception. Foods 2022;11:2227. https://doi.org/10.3390/foods11152227.
21. Brito-Oliveira TC, Cavini ACM, Ferreira LS, Moraes ICF, Pinho SC. Microstructural and rheological characterization of NaCl-induced gels of soy protein isolate and the effects of

incorporating different galactomannans. Food Structure 2020;26:100158. https://doi.org/10.1016/j.foostr.2020.100158.
22. Dekkers BL, Boom RM, van der Goot AJ. Structuring processes for meat analogues. Trends Food Sci Technol 2018;81:25–36. https://doi.org/10.1016/j.tifs.2018.08.011.
23. Qi X, Li Y, Xiao J, Zhang Q, Huang Z, Xie J. Modulating the functional properties of pea protein isolate: The impact of gellan gum and sodium chloride. Food Chem X 2025;30:102898. https://doi.org/10.1016/j.fochx.2025.102898.
24. Basak S, Singhal RS. Supercritical carbon dioxide treatment improves the functional properties of pea protein: Application in eggless cakes. Food Chem 2025;475:143224. https://doi.org/10.1016/j.foodchem.2025.143224.
25. Faustino C, Pinheiro L. Analytical Rheology of Honey: A State-of-the-Art Review. Foods 2021;10. https://doi.org/10.3390/foods10081709.
26. Fischer P, Windhab EJ. Rheology of food materials. Curr Opin Colloid Interface Sci 2011;16:36–40. https://doi.org/10.1016/j.cocis.2010.07.003.

P - 419

Efficiency of Pectin Extracted from Nam Wa Banana Peels in Encapsulation of *Centella asiatica* Extracts

Tanawin Rinsinjoy, Jiraporn Sirison, Nitjaree Maneerat*

School of Food Industry, King Mongkut's Institute of Technology Ladkrabang, Bangkok, 10520, Thailand

**Corresponding author E-mail: nitjaree.ma@kmitl.ac.th*

Abstract: Even though *Centella asiatica* (*C. asiatica*) contains potent bioactive compounds, its instability restricts its application in food products. This study aimed to evaluate the potential of pectin extracted from Nam Wa banana (*Musa* (ABB group)) peels as a wall material for encapsulating *C. asiatica* extracts. Pectin was extracted from Nam Wa banana peels using hydrochloric acid (pH 2), citric acid (pH 2), and deionized water (pH 6-6.5). While hydrochloric acid provided the highest yield (7.14 ± 0.21%), citric acid was selected for its safety profile (a pectin yield of 4.81 ± 0.25%, 8.5 ± 0.09% moisture content, 0.44 ± 0.01 water activity). The *C. asiatica* extract was prepared by mixing dried *C. asiatica* with 95% ethanol at a 1:4 (w/v) ratio for 7 days, and refined via oil treatment to remove chlorophyll before encapsulation, resulting in a yellow extract with a yield of 5.24 ± 0.18%. Encapsulation of *C. asiatica* extract (core material) was performed using a maltodextrin-banana pectin mixture (wall materials) via spray drying. The ratio of the extracts to maltodextrin and banana pectin was 1:10:0.5. The resulting encapsulated powder achieved a yield of 41.43% with a moisture content of 6.70 ± 0.19% and a water activity of 0.35 ± 0.02. These results indicate that banana pectin can be effectively utilized as a wall material for encapsulation, providing favorable moisture and water activity values. This demonstrates its potential for applications in functional food products.

Keywords: Pectin; *Centella asiatica*; Nam-Wa banana peel; Encapsulation

1. Introduction

Bananas (*Musa* spp., family *Musaceae*) are one of the most widely cultivated fruit crops worldwide as they are commonly grown across tropical and subtropical regions in over 130 countries, particularly in Southeast Asia. Among the various cultivars, *Musa* (ABB group) or Nam Wa Banana, a hybrid derived from two wild banana species, *Musa acuminata* (AA genome) and *Musa balbisiana* (BB genome), is one of the most important varieties and is extensively cultivated and consumed across many regions of Thailand, making it an important banana variety for both household use and food processing [1,2]. Banana peels are commonly treated as waste after bananas are processed into various food products. Although a portion of this by-product is utilized as animal feed or organic fertilizer, large amounts are still discarded, leading to an increasing burden on by-product waste management. In major banana-producing countries, converting banana peel waste into value-added products could provide economic benefits while also helping to reduce environmental pollution [3]. Banana peels have been widely studied for pectin extraction [4] and are recognized as an abundant and sustainable source of pectin for food applications.

Pectin is a carbohydrate-based polysaccharide composed of repeating monosaccharide subunits and can exist in various structural forms. Pectin molecules are generally classified into three major chain types, with the backbone mainly consisting of methylated D-galacturonic acid residues. The final structure and characteristics of pectin can vary depending on factors such as extraction conditions, as well as the storage and processing of the plant materials prior to isolation

[5]. It is water-soluble and serves as a major structural polysaccharide in the cell walls of higher plants. Due to its functional properties, pectin is widely used in food and beverage products as a thickening and gelling agent, as well as a colloidal stabilizer, texturizing agent, and emulsifier in products such as jams and jellies, fruit juices, yogurt, confectionery, and encapsulation [3, 6, 7].

Encapsulation refers to the entrapment of a core material within a protective wall material. It can be performed using either hot techniques (e.g., solvent evaporation and spray drying) or cold techniques (e.g., spray chilling and freeze drying), with spray drying being the most prevalent industrial method for producing nanoparticles (≈10–1000 nm) or microcapsules (≈3–800 μm) [8]. In recent years, encapsulation technology has advanced rapidly through the use of diverse core and wall materials, expanding its applications in the food industry. It is mainly used to solve three key issues: improving the stability of sensitive ingredients (e.g., preventing oxidation and degradation), enabling controlled release for sustained and targeted delivery of additives and probiotics, and enhancing sensory quality by masking or reducing undesirable tastes and odors [9]. Pectin has been used as an encapsulating agent (wall material) for entrapping bioactive compounds from plant extracts. Previous studies have reported that pectin-based encapsulation can enhance the stability of environmentally sensitive compounds and improve encapsulation efficiency compared with formulations without pectin [7].

Centella asiatica (*C. asiatica*), commonly known as Gotu kola (Asiatic pennywort), is a tropical medicinal plant in the Apiaceae family, native to Southeast Asia and also found in parts of Africa [10]. It is a medicinal herb widely used in traditional medicine and has attracted growing scientific interest due to its broad pharmacological activities, including wound healing, anti-inflammatory, and neuroprotective effects. These benefits are mainly attributed to its bioactive constituents, particularly triterpenoids and saponins, along with flavonoids. Among the most frequently studied compounds are asiaticoside, madecassoside, and asiatic acid, which are commonly used as key markers for evaluating the biological potential of *C. asiatica* extracts [11]. However, *C. asiatica* extract still has an important limitation regarding the stability of its bioactive compounds. Previous studies have reported a reduction in key chemical markers and total phenolic content (TPC) compared with the control, along with decreased biological activities such as antioxidant activity and acetylcholinesterase (AChE) inhibitory activity during storage. In addition, asiatic acid has been found to significantly degrade over time [12]. Therefore, it is necessary to develop strategies to enhance stability and extend the shelf life of *C. asiatica* extract for practical applications in food and health-related products.

To address these stability issues, this study aimed to evaluate pectin extracted from Nam Wa banana peels under different extraction conditions as a natural wall material for encapsulating *C. asiatica* extracts. This alternative pectin source was applied to enhance the stability of bioactive compounds for functional food applications while valorizing banana peel waste as a sustainable, value-added resource. Additionally, the study highlights the novelty of using pectin from Nam wa banana peel as a potential encapsulating agent for *C. asiatica* extract, which has rarely been explored in previous studies.

2. Materials and Methods

2.1 Materials

Nam Wa banana peels were obtained from a banana shop located in a local market in Bangkok, Thailand. Fresh *C. asiatica* (leaves and stems) were purchased from an agricultural farm certified by the Department of Agriculture, Ministry of Agriculture and Cooperatives, in Nakhon Pathom, Thailand.

The chemical reagents for pectin extraction included hydrochloric acid (HCl) obtained from RCI Labscan Limited, citric acid ($C_6H_8O_7$) (food grade) purchased from Bangkok Chemical Co., Ltd., Thailand, and 95% ethanol (C_2H_5OH) purchased from the Liquor Distillery

Organization, Excise Department, Thailand. All chemicals and solvents used in this study were of analytical grade, and deionized (DI) water was used in all experiments.

2.2 Preparation and extraction of pectin from Nam Wa banana peels

The Nam Wa banana peels were washed thoroughly with water and boiled for 5 min. After boiling, the peels were then immediately immersed in cold water. After cooling, the banana peels were cut into approximately 1 × 1 cm pieces, packed in low-density polyethylene (LDPE) bag, and stored at −20°C until further use.

Pectin extraction was conducted using a peel-to-extraction reagents ratio of 1:3 (w/v). Three extraction reagents were studied: DI water (pH 6-6.5), HCl (pH 2), and citric acid (pH 2). The extraction was performed at 90°C for 60 min with continuous stirring using a hot plate stirrer. After extraction, the solid residue was separated by filtration through muslin cloth. The filtrate was precipitated using 95% ethanol at a ratio of 1:2 (w/v) and allowed to stand at room temperature for 12–24 hours. The precipitated pectin was filtered, washed with 95% ethanol, and dried in a hot-air oven at 50°C for 24 hours or until completely dry. The dried pectin was ground into powder, packed in LDPE bag, and stored in a desiccator at room temperature. [13].

2.3 Preparation and extraction of *C. asiatica* extract

The plant material was washed, cut into 1.5 × 1.5 cm pieces, dried in a hot-air oven at 50°C for 12 hours, and ground into powder using a pin mill. Dried *C. asiatica* was mixed with 95% ethanol in the ratio of 1:4 (w/v) for 7 days. The extract was filtered using filter paper and a vacuum filtration system. The solvent was removed under reduced pressure using a rotary evaporator (R-300, Büchi Labortechnik AG, Switzerland) to obtain a concentrated extract [14]. The extract was then partitioned with 50% ethanol and subsequently washed with palm oil to remove chlorophyll at a ratio of 2:3 (ethanol: palm oil). The mixture was gently shaken and centrifuged at 5000 rpm for 10 min using a centrifuge (5804R, Eppendorf, Hamburg, Germany). The supernatant was collected, and the process was repeated. The combined supernatants were filtered, and the solvent was removed under reduced pressure using a rotary evaporator, yielding a dechlorophyllated (yellow) extract [15]. The extract was stored in an amber vial at 4°C until further analysis.

2.4 Encapsulation of *C. asiatica* extract

Encapsulation was carried out using a laboratory-scale mini spray dryer (S-300, Büchi Labortechnik AG, Switzerland). The feed solution utilized *C. asiatica* extract as the core material and a mixture of maltodextrin and banana pectin as wall materials. The ratio of extract to maltodextrin and banana pectin was 1:10:0.5 (w/w) [16]. This formulation was used as the prototype for the encapsulation experiments. Maltodextrin was first dissolved in distilled water under continuous stirring. Subsequently, banana pectin was gradually added and dissolved until a homogeneous solution was obtained. Finally, the *C. asiatica* extract was incorporated into the mixture and stirred thoroughly to ensure complete dispersion. The spray-drying conditions were set as follows: inlet temperature 120°C, outlet temperature 70°C, feed flow rate 5 mL/min, nozzle diameter 0.5 mm, and air pressure 6 bar [16]. The resulting encapsulated powder was collected, packed in aluminum foil pouches and stored in a desiccator at room temperature.

2.5 Characteristics of pectin extracted from banana peel

2.5.1 Yield and appearance of pectin

Pectin yield was determined based on the mass of dried banana peel powder prior to extraction and the mass of the obtained pectin powder. The yield was calculated using Eq. (1). The appearance of the extracted pectin was visually evaluated based on its color and physical form.

$$\text{Pectin Yield (\%)} = [(\text{Mass of Extracted Pectin (g)}) / (\text{Initial Mass of dried banana peel(g)})] \times 100 \quad \textbf{(1)}$$

2.5.2 Water activity and moisture content of pectin

Water activity (a_w) was measured using a Water Activity Meter (4TE, Aqualab) by placing the powdered sample into a sample cup and allowing the reading to stabilize. Moisture content was determined with the AOAC method by using the hot-air oven. The fresh weight of the pectin was recorded, followed by drying at 105°C until a constant weight was achieved. Moisture content was calculated as a percentage using Eq. (2).

$$\text{Moisture content (\%)} = [(\text{Mass of sample before drying (g)} - \text{Mass of sample after drying (g)})/(\text{Mass of sample before drying})] \times 100 \quad \textbf{(2)}$$

2.6 Characteristics of *C. asiatica* extract

2.6.1 Yield and appearance of *C. asiatica* extract

C. asiatica extract (green extract) yield was determined based on the mass of the extract obtained after solvent evaporation and the mass of dried *C. asiatica* used for extraction, then calculated using Eq. (3). The yield of the *C. asiatica* extract (yellow extract) was calculated based on the mass of the extract obtained after evaporation and the mass of the green extract used for washing with vegetable oil, as shown in Eq. (4). The appearance of the extracted was visually evaluated based on its color and physical form.

$$\text{Green extract Yield (\%)} = [(\text{Mass of dried extract (g)}) / (\text{Initial Mass of dried } \textit{C. asiatica} \text{ (g)})] \times 100 \quad \textbf{(3)}$$

$$\text{Yellow extract Yield (\%)} = [(\text{Mass of yellow extract after evaporation (g)})/(\text{Mass of green extract used (g)})] \times 100 \quad \textbf{(4)}$$

2.7 Characteristics of *C. asiatica* encapsulated powder

2.7.1 Yield and appearance of *C. asiatica* encapsulated powder

The yield of spray-dried *C. asiatica* encapsulated powder was determined based on the mass of total solids in the feed and the mass of the dry encapsulated powder collected at the end of the spray-drying process. The yield was calculated using Eq. (5).

$$\text{Encapsulated Yield (\%)} = [(\text{Mass of encapsulated powder (g)})/(\text{Initial Mass of total solids in the feed (g)})] \times 100 \quad \textbf{(5)}$$

2.7.2 Water activity and moisture content of *C. asiatica* encapsulated powder

Water activity (a_w) was measured using a Water Activity Meter (AQUALAB 4TE, METER Group, Inc., USA) by placing the powdered sample into a sample cup and allowing the reading to stabilize. Moisture content was determined with the AOAC method by using the hot-air oven. The weight of *C. asiatica* encapsulated powder was recorded, followed by drying at 105°C until a constant weight was achieved. Moisture content was calculated as a percentage using Eq. (2).

2.8 Statistical analysis

All experiments were performed in triplicate. Data were reported as mean values with standard deviations (SD). One-way analysis of variance (ANOVA) was used to compare the

effects of different extraction conditions. Duncan's multiple range test was used to assess significant differences between means at a 95% significance level. Statistical analyses were conducted using IBM SPSS Statistics 29 (SPSS Inc., USA).

3. Results and discussion

3.1. Yield and physical properties of pectin extracted from Nam Wa banana peels

The yield (%) of pectin extracted from Nam Wa banana peels and its physical properties, including water activity (a_w) and moisture content, are shown in Table 1. The results showed that pectin extracted using HCl exhibited the highest yield, with a value of 7.14 ± 0.21%, which was significantly higher than that obtained using citric acid and DI water ($p < 0.05$). This observation aligns with previously reported trends, which show that acid extraction yields 7-11%. [14], indicating that strong mineral acids are more effective at enhancing cell wall disruption and increasing pectin release.

Despite the superior yield of the HCl extraction, its application in food-grade systems is limited by safety concerns and the potential for corrosive residues, particularly for products requiring strict food safety standards. Conversely, citric acid extraction yielded a lower, yet substantial, pectin recovery of 4.81 ± 0.25%. This treatment demonstrated more advantages in terms of safety and reduced risk of chemical residues with a moisture content of 8.5 ± 0.09% and an a_w of 0.44 ± 0.01%. Although slightly higher than previously reported values (moisture 6–7% and a_w 0.22–0.31) [20], these results still indicate relatively low water availability, which is beneficial for storage stability by inhibiting microbial growth and enzymatic degradation. Citric acid is generally preferred for functional food applications due to its Generally Recognized as Safe (GRAS) status and reduced risk of hazardous chemical carryover, resulting in a lower risk of chemical residues compared to strong mineral acids [17]. Consequently, citric acid-extracted pectin was selected for the subsequent experiments involving the encapsulation of *C. asiatica* extract. Although extraction using DI water represents the safest method, it resulted in the lowest pectin yield and exhibited higher water activity and moisture content compared to the other extraction methods, which could compromise the shelf stability of the final encapsulated product.

Table 1 Yield and physical properties of pectin extracted from Nam Wa banana peels using hydrochloric acid (HCl), citric acid, and deionized (DI) water

Extraction solvents	Yield (%)	Water activity (a_w)	Moisture (%)
HCl	7.14 ± 0.21^a	0.38 ± 0.01^c	7.29 ± 0.08^c
Citric acid	4.81 ± 0.25^b	0.44 ± 0.01^b	8.50 ± 0.09^b
DI water	2.82 ± 0.29^c	0.62 ± 0.01^a	9.37 ± 0.08^a

Values are means ± standard deviation of a minimum of three determinations. Mean values in the same column having different superscripts are significantly different ($p \leq 0.05$).

In addition, the morphology of the pectin powders obtained from each extraction method is illustrated in Figure 1. The pectin powders extracted using different reagents exhibited color variations ranging from light brown to dark brown. Notably, pectin extracted with HCl showed the lightest color compared with those obtained using citric acid and DI water. Similar findings have been reported in previous studies, where pectin extracted under different reagent conditions exhibited noticeable color variations, suggesting that extraction conditions, including the extraction method and type of acid used, can influence the color of banana peel pectin due to the co-extraction or degradation of pigments and phenolic compounds.[18,19]

Figure 1 Morphology of pectin powders extracted using hydrochloric acid (a), citric acid (b), and deionized water (c).

3.2 Extraction yield and characteristics of *C. asiatica* extract

The extraction of *C. asiatica* resulted in a yield of 5.46 ± 0.34%, which is comparatively lower than the yield reported in previous studies (14.7%) [14]. This variance may be attributed to differences in plant maturity, geographical origin, or specific extraction parameters. Despite this, the obtained yield was deemed sufficient for subsequent analysis and encapsulation.

During the preliminary evaluation, the *C. asiatica* extract exhibited the formation of green fibrous materials upon aqueous reconstitution, which could potentially compromise the uniformity of the encapsulation matrix. To mitigate this issue, a phase-separation technique utilizing vegetable oil was employed to remove chlorophyll from the extract [15]. This treatment resulted in a yield of 64.44 ± 7.07% (calculated against the green extract) and produced a visually distinct yellow extract devoid of fibrous particulates, as shown in Figure 2. While a more exhaustive characterization of the *C. asiatica* constituents is planned for future investigation, the dechlorophyllated extract exhibited suitable physicochemical properties for the spray-drying process employed in the encapsulation.

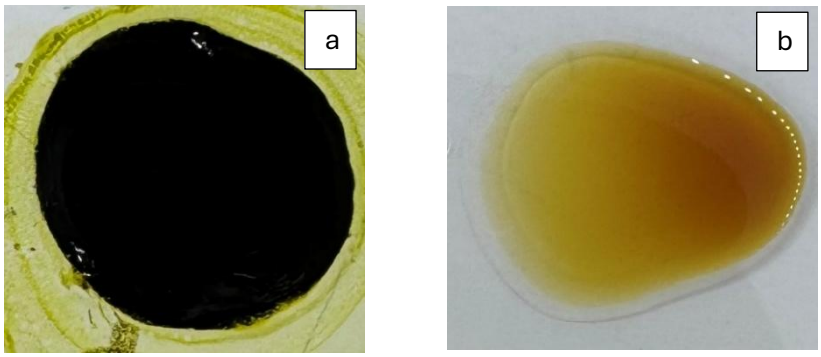

Figure 2 Appearance of *C. asiatica* extracts: (a) green-colored extract before chlorophyll removal and (b) yellow-colored extract after chlorophyll removal

3.3 Encapsulation of *C. asiatica* extract using Nam Wa banana peel pectin and maltodextrin

The encapsulation of *C. asiatica* extract using a composite material of maltodextrin and Nam Wa banana peel pectin was successfully achieved via spray drying. The process resulted in a product yield of 41.43%, with a moisture content of 6.70 ± 0.19%, and an a_w of 0.35 ± 0.02. The morphological characteristics of the encapsulated powder are illustrated in Figure 3. In this preliminary evaluation, the encapsulation efficiency (EE) was 56.69%. Previous studies on spray-dried *C. asiatica* nanoparticles using maltodextrin and β-cyclodextrin reported that the remaining

active compounds after the drying process ranged from approximately 49–54%, indicating that spray drying may lead to a reduction in the stability of bioactive compounds [21]. Therefore, the EE obtained in this study suggests that the developed encapsulation system was able to retain a considerable proportion of the active compounds.

These yield and physicochemical parameters are consistent with the requirements for spray-dried encapsulated powders. Specifically, an a_w below 0.6 is generally considered effective for inhibiting microbial growth and minimizing the rate of degradative chemical reactions, thereby enhancing the shelf stability of the bioactive core, indicating good stability and potential for further application.

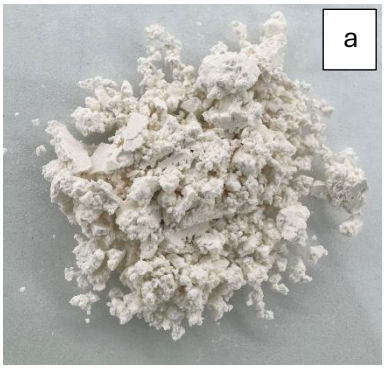

Figure 3. Morphological of spray-dried *C. asiatica* encapsulated powder produced using maltodextrin and Nam Wa banana peel pectin (a)

4. Conclusion

This study demonstrated the potential of pectin extracted from Nam Wa banana peels as a natural wall material for the encapsulation of *C. asiatica* extract. Among the extraction methods evaluated, citric acid was identified as the most suitable solvent due to its food-grade safety and its ability to produce pectin with favorable moisture content and water activity (a_w). The combination of banana peel pectin with maltodextrin successfully enabled spray-dry encapsulation, improving the stability and handling properties of the extract. These findings highlight the potential application of banana peel pectin as an alternative wall material for encapsulation in food systems. Moreover, the utilization of banana peel waste provides a sustainable approach for converting agricultural by-products into value-added ingredients for functional food development. Nevertheless, further studies are recommended to optimize the encapsulation conditions and formulation parameters. The use of advanced analytical techniques and instrumentation may provide more comprehensive results and contribute to improving the encapsulation efficiency and stability of the bioactive compounds.

Acknowledgements

This work was supported by King Mongkut's Institute of Technology Ladkrabang (Grand No. RE-KRIS/FF68/79)

References

1. Wongwaiwech D, Kamchonemenukool S, Ho CT, Li S, Thongsook T, Majai N, et al. Nutraceutical Difference between Two Popular Thai Namwa Cultivars Used for Sun Dried Banana Products. *Molecules*. 2022;27(17).
2. Jaiturong P, Laosirisathian N, Sirithunyalug B, Eitssayeam S, Sirilun S, Chaiyana W, et al. Physicochemical and prebiotic properties of resistant starch from *Musa sapientum Linn*., ABB group, cv. Kluai Namwa Luang. *Heliyon*. 2020;6(12):e05789.

3. Phaiphan A, Churat S, Doungta T, Wichalin P, Khanchai W, Penjumras P. Effects of microwave and ultrasound on the extraction of pectin and its chemical characterisation of banana (*Musa sapientum L.*) peels. *Food Research*. 2020;4:2030-6.
4. Qiu L-p, Zhao G-l, Wu H, Jiang L, Li X-f, Liu J-j. Investigation of combined effects of independent variables on extraction of pectin from banana peel using response surface methodology. *Carbohydrate Polymers*. 2010;80(2):326-31.
5. Chandel V, Biswas D, Roy S, Vaidya D, Verma A, Gupta A. Current Advancements in Pectin: Extraction, Properties and Multifunctional Applications. *Foods*. 2022;11(17):2683.
6. Martău GA, Mihai M, Vodnar DC. The use of chitosan, alginate, and pectin in the biomedical and food sector—biocompatibility, bioadhesiveness, and biodegradability. *Polymers (Basel)*. 2019;11(11):1837.
7. Žugić A, Krgović N, Mudrić J, Kostov MT, Tomović M, Medarević D, et al. Pectin as the carrier for the spray drying of green tea extracts: Tailoring microencapsulation to obtain a prospective nutraceutical. *International Journal of Biological Macromolecules*. 2025;306:141514.
8. Díaz-Montes E. Wall Materials for Encapsulating Bioactive Compounds via Spray-Drying: A Review. *Polymers*. 2023;15(12):2659.
9. Xu Y, Yan X, Zheng H, Li J, Wu X, Xu J, et al. The application of encapsulation technology in the food Industry: Classifications, recent Advances, and perspectives. *Food Chemistry*: X. 2024;21:101240.
10. Orhan IE. *Centella asiatica* (L.) Urban: From Traditional Medicine to Modern Medicine with Neuroprotective Potential. *Evidence-Based Complementary and Alternative Medicine*. 2012;2012:946259.
11. Hein ZM, Gopalakrishna PK, Kanuri AK, Thomas W, Hussan F, Naik VR, et al. *Centella asiatica*: Advances in Extraction Technologies, Phytochemistry, and Therapeutic Applications. *Life*. 2025;15(7):1081.
12. Kaur I, Suthar N, Kaur J, Bansal Y, Bansal G. Accelerated Stability Studies on Dried Extracts of *Centella asiatica* Through Chemical, HPLC, HPTLC, and Biological Activity Analyses. *Journal of Evidence-Based Complementary and Alternative Medicine.* 2016;21(4):Np127-37.
13. Maneerat N, Tangsuphoom N, Nitithamyong A. Effect of extraction condition on properties of pectin from banana peels and its function as fat replacer in salad cream. *Journal of Food Science and Technology*. 2017;54(2):386-97.
14. Wong JX, Ramli S. Antimicrobial activity of different types of *Centella asiatica* extracts against foodborne pathogens and food spoilage microorganisms. *LWT*. 2021;142:111026.
15. Haryanti S, Budiarti M, Farida S, Dewi APK, Supriyati N, Jokopriyambodo W, et al. The palm oil-based chlorophyll removal and the evaluation of antiaging properties on *Centella asiatica* ethanolic extract. IOP Conference Series: *Earth and Environmental Science*. 2024;1312(1):012041.
16. Sansone F, Mencherini T, Picerno P, d'Amore M, Aquino RP, Lauro MR. Maltodextrin/pectin microparticles by spray drying as carrier for nutraceutical extracts. *Journal of Food Engineering*. 2011;105(3):468-76.
17. Oliveira TÍS, Rosa MF, Cavalcante FL, Pereira PHF, Moates GK, Wellner N, et al. Optimization of pectin extraction from banana peels with citric acid by using response surface methodology. *Food Chemistry*. 2016;198:113-8.
18. Estribillo AGM, Rivadeneira J, Gaban PJ, Israel KA. Comparative Study on Chemical and Emulsion Properties of 'Saba' Banana [*Musa acuminata* x *balbisiana* (BBB Group) 'Saba'] Peel Pectin from Different Extraction Methods. *Food Research*. 2022;6:83-92.

19. Mansor MH, Williamson L, Ludwikowski D, Howard F, Muthana M. Pectin Extraction from Citrus Waste: Structural Quality and Yield with Mineral and Organic Acids. *Physchem*. 2025;5(3):32.
20. Khamsucharit P, Laohaphatanalert K, Gavinlertvatana P, Sriroth K, Sangseethong K. Characterization of pectin extracted from banana peels of different varieties. Food Sci Biotechnol. 2018;27(3):623-629. doi:10.1007/s10068-017-0302-0.
21. Pradana AT, Nawatila R, Alkindi F, Darmayani NP, Susanti E. The effect of spray-drying temperature on *Centella asiatica* extract–β-cyclodextrin–maltodextrin nanoparticle characteristics and stability. Pharmaciana. 2021;11(3):394-405.

P - 431

Determination of Co-Flocculation Ability Between Distinct Cyanobacterial Genera and the Fungal Penicillium under the Antibiotic Stress by Erythromycin

Bunyaporn Khiawchaoum, Tanakarn Monshupanee*

Department of Biochemistry, Faculty of Science, Chulalongkorn University, Bangkok, Thailand

**Corresponding author E-mail: Tanakarn.M@chula.ac.th*

Abstract: Co-flocculation between cyanobacteria and the fungal Penicillium has been recently reported and emerged as a promising and sustainable strategy for biomass harvesting and environmental biotechnology applications; however, the influence of antibiotic stress on this process with distinct cyanobacterial genera remains insufficiently explored. In this study, fifteen cyanobacterial genera were screened for their co-flocculation performance with the fungal Penicillium under the antibiotic erythromycin exposure. The results demonstrated clear strain-dependent flocculation behaviors. Complete flocculation was observed in only three cyanobacterial strains, namely *Synechocystis*, *Synechococcus*, and *Spirulina*, with total co-floc biomass yield of 0.44, 0.47, and 0.50 $g.L^{-1}$, respectively. Partial flocculation was detected in *Calothrix, Fischerella*, *Microcystis*, *Cylindrospermum*, *Phormidium*, *Hapalosiphon*, *Myxosarcina*, *Nostoc*, and Fischerella, whereas *Anabaena, Oscillatoria*, *Stigonema*, and *Chroococcus* exhibited no flocculation under the tested conditions. Notably, cyanobacteria–fungal co-flocculation in the presence of erythromycin showed no correlation with cyanobacterial cell morphology or nitrogen-fixation capability. These findings indicate that co-flocculation efficiency under antibiotic stress is governed by strain-specific factors rather than general physiological traits. Future research will focus on elucidating the expression of genes associated with flocculation-related mechanisms to provide deeper insight into the molecular basis of cyanobacteria–fungal interactions. This co-floc technology might be applied to produce protein-rich biomass for animal feed.

Keywords: Cyanobacteria; Fungi; Antibiotic; Flocculation; Biomass

1. Introduction

Cyanobacteria are prokaryotic, oxygenic phototrophic microorganisms that inhabit almost all environments on Earth. They exhibit diverse morphologies, including unicellular and filamentous forms [1]. Cyanobacteria play a crucial role in global carbon fixation and are considered promising biotechnological platforms due to their high biomass productivity and minimal nutritional requirements. Additionally, they hold significant potential for renewable energy production, including biodiesel, biohydrogen, and biogas [2]. However, a critical bottleneck in the utilization of cyanobacteria such as Synechocystis for biotechnological applications is the efficient harvesting of cells from the liquid growth medium [3]. Traditional harvesting methods, including sedimentation, filtration and centrifugation are commonly used, but they suffer from high operational costs and excessive energy consumption [4].

Flocculation is widely regarded as one of the most cost-effective and convenient methods for harvesting microbial biomass, as it promotes cell aggregation through mechanisms such as charge neutralization and polymer bridging, thereby simplifying separation from the liquid phase [5]. In cyanobacteria, flocculation can be induced chemically using agents like aluminum sulfate

[6], ferric chloride, and polyacrylamide. However, the use of chemical coagulants often leads to high operational costs and may leave residual contaminants that compromise the safety and quality of downstream applications. Alternatively, auto-flocculation, or self-flocculation, occurs naturally in some cyanobacteria through the production of extracellular polymeric substances (EPS). This process can be triggered by environmental factors such as high pH [7], increased salinity, or intense light exposure [8]. Despite its chemical-free advantage, auto-flocculation is often unpredictable and highly dependent on cultivation conditions. The mechanisms behind flocculation involve several biological and chemical processes. In addition to biological and chemical factors, environmental stressors may also influence cyanobacterial flocculation behavior. In aquatic systems, cyanobacteria are frequently exposed to abiotic stresses such as metal ions, which can alter cell surface properties and microbial interactions. Copper sulfate ($CuSO_4$), a commonly used algicide, represents a relevant model metal stressor and is therefore considered in this study as a preliminary factor to assess its potential impact on cyanobacteria–fungal co-flocculation. EPS plays a key role by facilitating cell adhesion and trapping oxygen bubbles generated during photosynthesis, which helps the flocs float [9]. Chemical coagulants like aluminum sulfate reduce the negative surface charge of cyanobacterial cells, enhancing aggregation through charge neutralization and bridging effects [10]. Furthermore, certain cyanobacteria exhibit light-induced flocculation through cyclic di-GMP signaling pathways that promote cell clustering under blue light exposure [11]. Natural biopolymers such as chitosan have also been investigated for their flocculation potential, although their effectiveness is influenced by factors like pH and water chemistry [12]. These combined mechanisms are essential for improving the efficiency of biomass harvesting.

Recently, bio-flocculation has gained increasing attention as a sustainable, eco-friendly alternative. This approach involves the co-cultivation of cyanobacteria with flocculating microorganisms such as fungi (e.g., Aspergillus niger, Rhizopus spp.) or bacteria. This approach not only reduces reliance on synthetic chemicals but also improves overall harvesting efficiency. Previous studies have demonstrated successful co-flocculation systems, including Synechocystis–Aspergillus oryzae [13], Nostoc–Aspergillus sp. [14], and Synecho- cystis–Aspergillus fumigatus [15]. However, these systems often require the addition of external carbon sources or large fungal inoculum volumes, which may limit their economic feasibility.

A recent study has shown that co-flocculation between Synechocystis and fungal strains can be successfully induced without organic carbon supplementation. Using erythromycin at a concentration of 10 μM, biomass flocculation efficiency reached 44% within 14 days. Fungal association not only enhanced flocculation but also mitigated chlorosis in Synechocystis under antibiotic stress. Transcriptomic analysis indicates that co-flocculation results from coordinated regulation of genes related to cell surface structures and stress responses. Specifically, this includes down-regulation of minor pilin genes and up-regulation of genes encoding pilin-regulating chaperones, S-layer proteins, exopolysaccharide polymerization enzymes, and signaling proteins involved in cell adhesion and abiotic stress responses [16].

Therefore, this study aims to (i)screen cyanobacterial strains capable of co-flocculating with filamentous fungi under erythromycin treatment, (ii) optimize cultivation parameters including erythromycin concentration, and fungal inoculum amount to maximize flocculation efficiency (iii) preliminarily assess the effect of $CuSO_4$-induced abiotic stress on cyanobacteria–fungal co-flocculation efficiency.

2. Materials and Methods

2.1 Screening and cultivation of cyanobacteria

2.1.1 Pre-cultivation of cyanobacteria and fungi

Fifteen cyanobacterial strains representing 15 genera were obtained from the Thailand Institute of Scientific and Technological Research (TISTR) and cultivated in BG11 medium under

photoautotrophic conditions at 28 ± 2 °C with continuous white, fluorescent light (50 µmol. $m^{-2}.s^{-1}$) and shaking at 160 rpm for 20 days to obtain sufficient biomass. A fungal strain previously isolated in our laboratory was grown on BG11 agar at 37 °C in the dark for 2–3 days, and 5 mg/100 mL of fresh fungal biomass was used for co-flocculation with cyanobacteria.

2.1.2 Co-cultivation of 15 strains of Cyanobacterium and fungi, and cell harvesting.

All cultivations were performed in 100 mL BG11 liquid medium with an initial cyanobacterial cell density (OD_{730}) of 0.4. Erythromycin (5 µM) was added to the medium following the method described by [18] and fungal pellets (5 mg) were added to the medium. For co-cultivation, biomass from 15 cyanobacterial strains was harvested, mixed, and cultivated with fungi for 3 days. Flocculated biomass was collected by gravitational filtration using an aluminum filter (0.05 mm pore size), while the remaining suspended biomass was recovered by centrifugation. Attached biomass remaining on the inner surface of the culture flask was gently scraped and collected. All biomass fractions were dried at 60 °C until constant weight.

After screening 15 cyanobacterial strains for fungal co-flocculation, the strains were classified into three categories based on flocculation performance: complete flocculation, partial flocculation, and no flocculation. The screened strains were further grouped according to cyanobacterial structural characteristics, nitrogen fixation ability, and genus to evaluate potential factors influencing fungal co-flocculation efficiency.

2.2 Optimization of cultivation parameters

Based on the screening results, the most efficient strain was selected for further parameter optimization.

2.2.1 Optimization of fungal inoculum

Fungal pellet weights of 1, 2.5 and 5 mg per 100 mL culture were evaluated. The inoculum levels were selected according to the previously reported conditions [16]. (The fungal biomass was directly added to cyanobacterial cultures, and the optimal biomass was selected and fixed for subsequent experiments.

2.2.2 Optimization of Erythromycin concentration

Erythromycin was added to each experimental group at final concentrations of 1, 2.5 and 5 µM following the method described previously [18], after dissolution in ethanol. The optimal concentration was selected and fixed for subsequent experiments.

2.3 Abiotic stress

Co-cultures of cyanobacteria and fungi were prepared under previously optimized conditions. Copper stress was applied by adding $CuSO_4$ at final concentrations of 2, 4, and 8 µM, replacing erythromycin used in earlier experiments. These concentrations were selected to represent moderate copper stress level that can influence cyanobacterial physiology without causing rapid cell death [19]. Flocculated biomass was harvested and quantified as dry weight to evaluate the effect of Cu^{2+} on flocculation efficiency.

3. Results & Discussion

3.1 Screening of cyanobacterial strains for fungal Co-flocculation efficiency

Fifteen cyanobacterial strains were screened for their co-flocculation efficiency with the fungus Penicillium under erythromycin exposure, based on the heatmap distribution of biomass among flocculated and suspended fractions of the 11 genera (Figure 1).

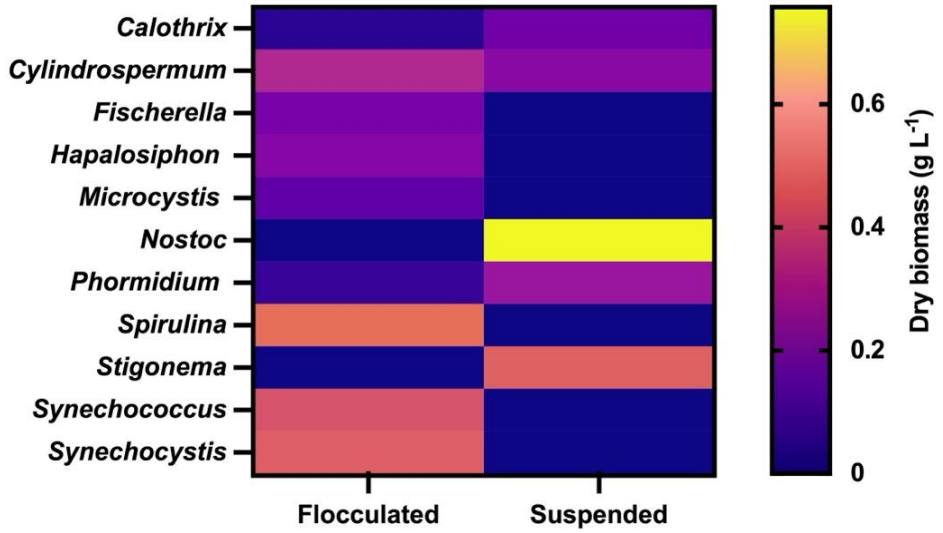

Figure 1. Heatmap showing the distribution of cyanobacterial biomass among flocculated, suspended, and attached fractions. All experiments were performed in triplicate, and values shown represent mean biomass.

A total of 15 cyanobacterial strains were initially screened for flocculation ability. However, only 11 strains were included in the heatmap because these strains showed either complete or partial flocculation with measurable biomass in the flocculated and suspended fractions. The remaining strains were excluded due to cell death or insufficient biomass under the tested conditions, which prevented reliable biomass quantification.

Among the screened strains, *Synechococcus* was selected for further optimization due to its promising flocculation behavior and its potential as a less-explored strain in this context. Although *Synechocystis* also showed flocculation, it has already been extensively studied in previous reports. In contrast, Spirulina cultures were not further pursued due to instability during cultivation under the tested conditions.

The results demonstrated clear strain-dependent co-flocculation behavior (Figure 1). Complete flocculation was observed in *Synechocystis*, *Synechococcus*, and *Spirulina*, with total co-flocculated biomass yields of 0.44, 0.47, and 0.50 $g.L^{-1}$, respectively. Partial flocculation was detected in *Calothrix*, *Fischerella*, *Microcystis*, *Cylindrospermum*, *Phormidium*, and *Hapalosiphon*, whereas *Anabaena*, *Oscillatoria*, *Stigonema*, and *Chroococcus* showed no flocculation under the tested conditions. Compared with previously reported *Synechococcus elongatus–Penicillium* systems (~1.94 $g.L^{-1}$) [17] and *Synechocystis*–fungi systems (~2.0 $g.L^{-1}$) under comparable cultivation conditions [18], the lower co-flocculated biomass obtained in this study highlights the strong strain-dependent nature of fungal-induced co-flocculation.

3.2 Effect of fungal inoculum on co-flocculated biomass

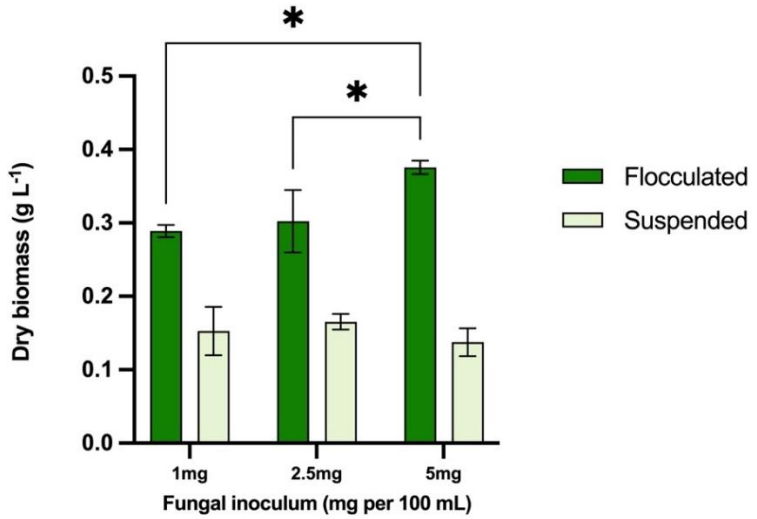

Figure 2. Effect of fungal inoculum on co-flocculated biomass of Synechococcus. Values represent mean ± SD of triplicate experiments. Statistical differences were determined using two-way ANOVA followed by Tukey's multiple comparisons test. * Indicates significant differences between treatments (*p < 0.05). (leave a blank line between main sections)

The effect of fungal inoculum on co-flocculated biomass was evaluated by varying the fungal concentration from 1 to 5 mg per 100 mL. Co-flocculated biomass increased with increasing fungal inoculum, reaching a maximum of approximately 0.37 $g.L^{-1}$ at 5 mg. Statical analysis revealed that the biomass obtained with 5 mg fungal inoculum was significantly higher than with 1 mg and 2.5 mg ($p < 0.05$). This condition also exhibited the most consistent flocculation performance. The observed trend suggests that an adequate amount of fungal biomass is required to facilitate effective physical interactions and aggregation with cyanobacterial cells. Therefore, 5 mg of fungal inoculum was selected as the optimal condition for subsequent experiments.

3.3 Effect of erythromycin concentration on co-flocculation biomass

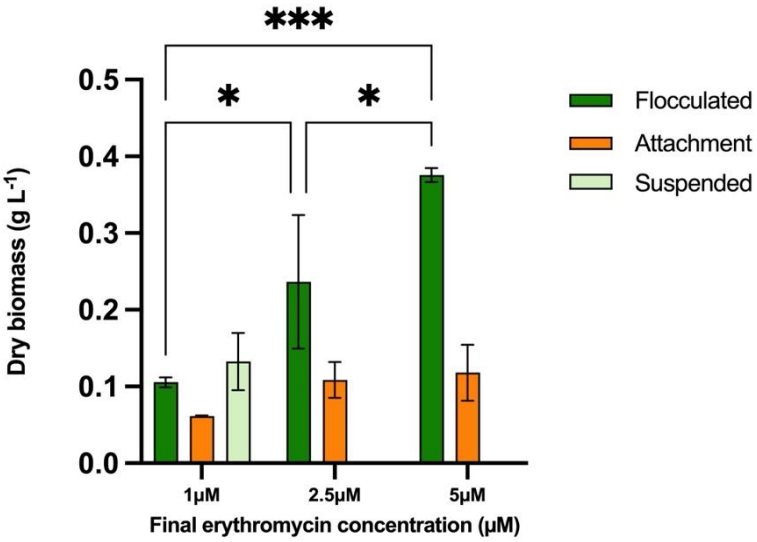

Figure 3. Effect of erythromycin concentration on co-flocculation biomass of Synechococcus. Values represent mean ± SD of triplicate experiments. Statistical significance was determined using two-way ANOVA followed by Tukey's multiple comparison test (*p < 0.05, ***p < 0.001).

The effect of erythromycin concentration on co-flocculation biomass was evaluated at final concentrations of 1, 2.5, and 5 µM (Figure 3). Co-flocculation efficiency increased significantly with erythromycin concentration. Although near-complete flocculation was achieved at 2.5 µM, flocculation process proceeded more slowly than at 5 µM, which yielded the highest and most consistent flocculated biomass. Previous studies have reported erythromycin-mediated co-flocculation in several cyanobacteria, including *Synechocystis*, *Synechococcus elongatus*, and *Oscillatoria jasorvensis*, as well as the eukaryotic green alga Chlorella vulgaris, when co-cultured with Penicillium [17]. In particular, erythromycin-mediated co-flocculation between Synechocystis and Penicillium was shown to preserve normal cell morphology, indicating a protective effect of fungal association under erythromycin stress, The previous studies have suggested that erythromycin-induce co-flocculation may be associated with changes in cell surface properties, including the expression of pilin genes, S-layer proteins, and exopolysaccharide (EPS) production, as well as stress responses to antibiotics. However, the underlying signaling pathways and cell surface interactions remain unclear [16]. As a macrolide antibiotic, erythromycin acts as a bacteriostatic agent that inhibits protein synthesis by binding to the 50S ribosomal subunit [20]. Exposure to sub-inhibitory antibiotic concentrations may alter cell surface properties and stimulate extracellular polymeric substances (EPS) production, thereby promoting cell aggregation and flocculation [21]. The erythromycin concentrations used in this study were relatively low and applied under controlled experimental conditions, and the short-term exposure was intended only to evaluate its role in inducing co-flocculation [22]. Under these conditions, the likelihood of selecting for antibiotic resistant populations is expected to be minimal.

3.4 Effect of $CuSO_4$ concentration on co-flocculation biomass

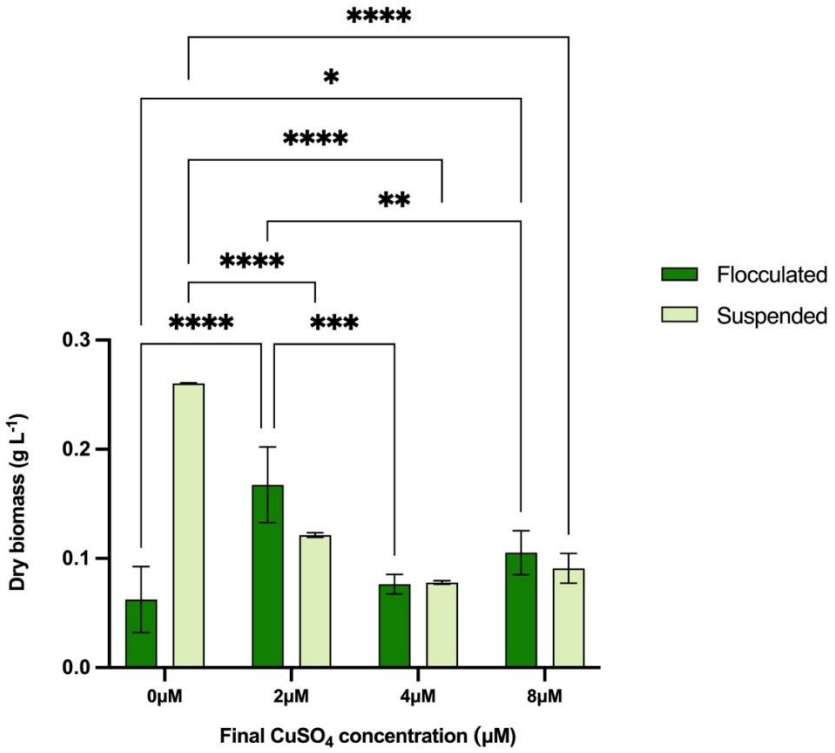

Figure 4. Effect of $CuSO_4$ concentration on co-flocculation biomass of Synechococcus.
Values represent mean ± SD of triplicate experiments. Statistical significance was determined using two-way ANOVA followed by Tukey's multiple comparison test (*$p < 0.05$, **$p < 0.01$, ***$p < 0.001$, ****$p < 0.0001$).

Co-flocculation efficiency was highest at 2 μM $CuSO_4$, whereas higher concentrations resulted in reduced flocculated biomass (Figure 4). This suggests that $CuSO_4$ primarily imposes physiological stress rather than promoting aggregation, consistent with previous reports on copper-induced toxicity and oxidative stress in algae [23].

Previous studies have shown that co-flocculation of microalgae with microbes can produce protein-rich biomass. For example, co-flocculation of Chlorella pyrenoid- osa with Saccharomyces cerevisiae and co-cultivation with Aspergillus oryzae yielded biomass containing approximately 35.5 % and 54.3 % protein (dry weight), respectively [24, 25], which is comparable to or higher than protein levels in typical feeds for farmed fish and poultry (16–35 % dry weight) [26]. While residual erythromycin (EM) may raise environmental concerns in future feed applications, the ability of Aspergillus sydowii W1 to remediate EM [27] suggests that fungi-based co-flocculation systems may offer a promising and sustainable approach to protein production and antibiotic residue mitigation.

4. Conclusion

This study demonstrated strain-dependent fungal–cyanobacterial co-flocculation under antibiotic exposure. Among fifteen screened strains, Synechococcus showed stable and complete flocculation with Penicillium and was selected for further optimization. Erythromycin effectively enhanced co-flocculation, whereas $CuSO_4$ primarily induced cellular stress and reduced biomass recovery, limiting its suitability for co-flocculation-based harvesting.

Acknowledgement

The authors acknowledge the Department of Biochemistry, Faculty of Science, Chulalongkorn University, for financial support and the Development and Promotion of Science and Technology Talents Project (DPST) for scholarship support.

References

1. Castenholz, R.W.; Wilmotte, A.; Herdman, M.; Rippka, R.; Waterbury, J.B.; Iteman, I.; et al. *Phylum BX. Cyanobacteria.*In: *Bergey's Manual of Systematic Bacteriology*; Springer: New York, 2001; pp 473–599.
2. Cheng, J.; Sun, J.; Huang, Y.; Zhou, J. *Cyanobacteria as a biocatalyst for sustainable production of biofuels and chemicals. Energies* 2019, 12, 408.
3. Cui, Y.; Wang, X.; Li, J.; Zhang, Y. *Debottlenecking thermophilic cyanobacteria cultivation and harvesting through the application of inner light photobioreactor and chitosan. Plants* 2023, 10, 1540.
4. Wan, C.; Alam, M.A.; Zhao, X.Q.; Zhang, X.Y.; Guo, S.L.; Ho, S.H.; et al. *Current progress and future prospect of microalgal biomass harvest using various flocculation technologies. Bioresour Technol.* 2015, 184, 251–257.
5. Vandamme, D.; Pontes, S.C.V.; Goiris, K.; Foubert, I.; Pinoy, L.J.J.; Muylaert, K. *Evaluation of electro-coagulation-flocculation for harvesting marine and freshwater microalgae. Biotechnol Bioeng.* 2011, 108, 2320–2329.
6. Zhang, B.; Jiang, D.; Guo, X.; He, Y.; Ong, C.N.; Xu, Y.; et al. *Removal of Microcystis aeruginosa using nano-Fe_3O_4 particles as a coagulant aid. Environ Sci Pollut Res.* 2015, 22, 18731–18740.
7. Mota, R.; Flores, C.; Tamagnini, P. *Cyanobacterial extracellular polymeric substances (EPS).* In: *Polysaccharides of microbial origin: biomedical applications*; Springer International Publishing: Cham, 2022; pp 139–165.
8. Babiak**,** W.**;** Krzemińska, **I.** Extracellular polymeric substances (EPS) as microalgal bioproducts: a review of factors affecting EPS synthesis and application in flocculation processes. Energies 2021, 14, 4007**.**

9. Madsen, M.A.; Semerdzhiev, S.; Twigg, J.D.; Moss, C.; Bavington, C.D.; Amtmann, A. *Environmental modulation of exopolysaccharide production in the cyanobacterium Synechocystis 6803. Appl Microbiol Biotechnol.* 2023, 107, 6121–6134.
10. Şengül, A.B.; Tüfekçi, N.; Aktan, S. *The use of alum as coagulant for removing cyanobacterial cells in drinking water.Desalin Water Treat.* 2016, 57, 25610–25616.
11. Enomoto, G.; Wallner, T.; Wilde, A. *Control of light-dependent behaviour in cyanobacteria by the second messenger cyclic di-GMP. MicroLife* 2023, 4.
12. Renault, F.; Sancey, B.; Badot, P.M.; Crini, G. *Chitosan for coagulation/flocculation processes—an eco-friendly approach. Eur Polym J.* 2009, 45, 1337–1348.
13. Choi, Y.N.; Cho, H.U.; Utomo, J.C.; Shin, D.Y.; Kim, H.K.; Park, J.M. *Efficient harvesting of Synechocystis sp. PCC 6803 with filamentous fungal pellets. J Appl Phycol.* 2016, 28, 2225–2231.
14. Jiang, L.; Li, T.; Jenkins, J.; Hu, Y.; Brueck, C.L.; Pei, H.; et al. *Evidence for a mutualistic relationship between the cyanobacteria Nostoc and fungi Aspergilli in different environments. Appl Microbiol Biotechnol.* 2020, 104, 6413–6426.
15. Miranda, A.F.; Taha, M.; Wrede, D.; Morrison, P.; Ball, A.S.; Stevenson, T.; et al. *Lipid production in association of filamentous fungi with genetically modified cyanobacterial cells. Biotechnol Biofuels* 2015, 8, 1–18.
16. Pichaiyotinkul, P.; Leksingto, J.; Sukkasam, N.; In-Na, P.; Incharoensakdi, A.; Monshupanee, T. *Erythromycin mediates co-flocculation between cyanobacterium Synechocystis sp. PCC 6803 and filamentous fungi in liquid cultivation without organic compounds. Sci Rep.* 2024, 14, 9640.
17. Kaewbai-ngam, J.; Leksingto, J.; Kasemcholathan, S.; Pichaiyotinkul, P.; Sirikantaramas, S.; Monshupanee, T. *Complete co-flocculation of microalgae and Penicillium induced by sub-inhibitory erythromycin: boosting biomass, CO_2 capture, and protein yield in organic-free cultivation. Plant Stress* 2025, 101030.
18. Leksingto, J.; Pichaiyotinkul, P.; Boorachokwiwat, K.; Kaewbai-Ngam, J.; Kanoksinwuttipong, N.; Sukkasam, N.; Monshupanee, T. *Cyanobacterium–Penicillium co-flocculation under erythromycin treatment: increased CO_2 capture and biomass production in an organic compound-free co-cultivation. Biotechnol Rep.* 2025, e00943.
19. Lopez-Maury, L.; Giner-Lamia, J.; Florencio, F.J. *Redox control of copper homeostasis in cyanobacteria. Plant Signal Behav.* 2012, 7, 1712–1714.
20. Wilson, D.N. *Ribosome-targeting antibiotics and mechanisms of bacterial resistance. Nat Rev Microbiol.* 2014, 12, 35–48.
21. Kaplan, J.B. *Antibiotic-induced biofilm formation. Int J Artif Organs* 2011, 34, 737–751.
22. Andersson, D.I.; Hughes, D. *Microbiological effects of sublethal levels of antibiotics. Nat Rev Microbiol.* 2014, 12, 465–478.
23. Pinto, E.; Sigaud-Kutner, T.C.S.; Leitão, M.A.S.; Okamoto, O.K.; Morse, D.; Colepicolo, P. *Heavy metal-induced oxidative stress in algae. J Phycol.* 2003, 39, 1008–1018.
24. Mathur, M.; Kumar, A.; Ariyadasa, T.U.; Malik, A. *Yeast-assisted algal flocculation for enhancing nutraceutical potential of Chlorella pyrenoidosa. Bioresour Technol.* 2021, 340, 125670.
25. Wang, S.K.; Yang, K.X.; Zhu, Y.R.; Zhu, X.Y.; Nie, D.F.; Jiao, N.; Angelidaki, I. *One-step co-cultivation and flocculation of microalgae with filamentous fungi to valorize starch wastewater into high-value biomass. Bioresour Technol.* 2022, 361, 127625.
26. Rajaguru, R.W.A.S.B.; Vohra, P.; Kratzer, F.H. *The effects of feeding high protein diets to chickens. Poult Sci.* 1966, 45, 1339–1345.
27. Ren, J.; Lai, B.; Niu, D.; Wang, Z.; Hardie, W.J.; Zhi, J.; et al. *Characterization of erythromycin-degrading strain Aspergillus sydowii W1 revealed by transcriptome analyses. Int Biodeterior Biodegrad.* 2023, 178, 105545.

P - 433

Bioactive Compounds and Antioxidant Activity of Germinated Thai Indigenous Upland and Lowland Rice

Jirawat Julsumroun, Sumethee Songsamoe*

Food Science and Technology, School of Food Industry, King Mongkut's Institute of Technology Ladkrabang, Bangkok 10520, Thailand

**Corresponding author E-mail: sumethee.so@kmitl.ac.th*

Abstract: Cultivation environment plays an important role in determining the functional quality of germinated rice. Upland and lowland rice are exposed to distinct growing conditions, which may influence the accumulation of bioactive compounds during the germination process. This study aimed to compare the bioactive compound content and antioxidant activity of germinated Thai indigenous rice cultivated in upland and lowland areas. Six Thai indigenous rice varieties were investigated, including lowland rice Hom Mali (white), Thapthim Chumphae (red), and Mali Nil Surin (black), and upland rice Dok Phayom (white), Hom Bon (red), and Med Fai (black). Brown rice samples were germinated for 24 h prior to analysis. Bioactive compounds were determined in terms of γ-aminobutyric acid (GABA) content and total phenolic content, while antioxidant activity was evaluated using DPPH, ABTS, and FRAP assays. The results demonstrated clear differences between germinated upland and lowland rice. Germinated upland rice, particularly pigmented varieties, exhibited significantly higher levels of bioactive compounds and stronger antioxidant activity than germinated lowland rice ($p < 0.05$). Germinated Hom Bon rice (upland, red) showed the highest GABA content (81.88 mg/100 g), total phenolic content, DPPH, and ABTS antioxidant values, which were significantly higher than lowland rice varieties ($p < 0.05$), whereas germinated Med Fai rice (upland, black) exhibited the highest FRAP antioxidant activity, also significantly surpassing lowland varieties ($p < 0.05$). Changes in total phenolic content following germination were dependent on both rice variety and cultivation environment. These findings indicate that pigmented upland germinated rice represents a valuable ingredient for functional food and beverage development.

Keywords: Germinated rice; GABA; Bioactive compounds; Thai indigenous rice; Upland and lowland rice

1. Introduction

Rice (*Oryza sativa* L.) is a major staple crop worldwide and has recently attracted increasing interest as a functional food due to its bioactive compounds, which can be enhanced through germination. Germinated brown rice has been reported to exhibit improved nutritional and functional properties resulting from biochemical and physiological changes occurring during the germination process. Among these changes, the accumulation of GABA and phenolic compounds has been widely recognized, as these constituents are associated with various health-promoting effects [1, 2]. The improvement in functional quality of germinated rice is closely related to the activation of endogenous enzymes and metabolic pathways, which alter the chemical composition of the grain.

Germination induces metabolic processes that promote GABA synthesis, primarily through the decarboxylation of glutamic acid catalyzed by glutamate decarboxylase. The accumulation of GABA in germinated brown rice has been reported to vary significantly

depending on rice variety and cultivation environment. Stress-related factors, including temperature fluctuations, oxygen availability, and moisture conditions during cultivation and germination, have been shown to influence GABA metabolism in rice grains [3]. These factors may affect enzyme activity and substrate availability, thereby determining the extent of GABA accumulation. Consequently, cultivation environment is considered an important determinant of GABA content in germinated rice.

Phenolic compounds constitute another major group of bioactive constituents in rice and are closely associated with antioxidant capacity. Pigmented rice varieties, such as red and purple rice, are known to contain higher levels of phenolic compounds compared to white rice, primarily due to the presence of phenolic acids, flavonoids, and anthocyanins in the bran layer. Previous studies have reported significant differences in total phenolic content and antioxidant activity among rice varieties with different grain colors [4]. In addition, germination has been shown to increase extractable phenolic compounds through the activation of hydrolytic enzymes, which release bound phenolics from the cell wall matrix, further enhancing antioxidant potential [5].

Cultivation environment also plays an important role in the accumulation of phenolic compounds and antioxidant-related metabolites in rice. Upland and lowland rice are exposed to distinct growing conditions, particularly with respect to water availability and abiotic stress. Upland cultivation is generally associated with greater environmental stress, which has been reported to stimulate the biosynthesis of phenolic compounds as part of plant defense mechanisms [6]. These environmental differences may lead to variations in both phenolic content and antioxidant capacity in germinated rice.

Antioxidant capacity of germinated brown rice is commonly evaluated using DPPH radical scavenging activity, ABTS radical cation decolorization, and ferric reducing antioxidant power (FRAP) assays, which collectively reflect the ability of bioactive compounds to neutralize free radicals and donate electrons [7, 8]. Therefore, this study aimed to investigate the effects of cultivation area (lowland and upland) and grain color (white, red, and purple) on GABA content, total phenolic content, and antioxidant capacity of germinated brown rice from six rice varieties. The findings are expected to clarify the combined influence of cultivation environment and varietal characteristics on the functional quality of germinated brown rice and to support the utilization of germinated rice as a functional food ingredient.

2. Materials and Methods

2.1 Preparation of germinated brown rice

Six Thai indigenous rice varieties were investigated and categorized according to their cultivation environment. The lowland rice varieties included Hom Mali (white), Thapthim Chumphae (red), and Mali Nil Surin (black), while the upland rice varieties comprised Dok Phayom (white), Hom Bon (red), and Med Fai (black). Each variety was soaked in water for 8 h. Following soaking, the grains were drained and distributed onto a cotton cloth within a basket. To induce germination, the samples were covered with a moist cotton cloth and allowed to germinate at 30 ± 2 °C for 24 h. Subsequently, the germinated grains were washed with water and dried using a hot-air oven at 50 °C for 1 h. The dried samples were stored at 4 °C prior to analysis.

2.2 Preparation of extracts

Brown rice samples were ground into a powder and passed through a 100-mesh sieve. One gram of the resulting flour was extracted with 80% ethanol at a solid-to-solvent ratio of 1:10 (w/v). The mixture was thoroughly mixed and subjected to ultrasonic-assisted extraction at 40 ± 2 °C for 1 h. The extract was centrifuged at 4,000 rpm for 15 min. The supernatant was filtered through Whatman No. 1 filter paper, and the filtrate was collected for further analysis. This extraction procedure was adapted from the method described by Tabaraki and Nateghi (2011) [9].

2.3 Determination of GABA content

The extraction and quantification of GABA in germinated brown rice (GBR) were performed following the method described by Songsamoe and Khunjan (2021) [10]. Initially, 1 g of dried GBR sample was homogenized with 5 mL of deionized water and extracted for 1 h. The resulting mixture was centrifuged at 15,000×g for 10 min at 4 °C, after which the supernatant was filtered through Whatman No. 1 paper (90 mm diameter). For the colorimetric assay, a reaction mixture was prepared by combining 0.5 mL of the filtrate with 0.2 mL of 0.2 mol/L borate buffer (pH 9.0), 1 mL of 6% phenol, and 0.4 mL of 9% sodium hypochlorite. This solution was heated for 10 min and subsequently allowed to cool for 20 min until a distinct blue color developed. Finally, 2 mL of 60% ethanol was added to the mixture, and the absorbance was measured at 645 nm using an EnSight Multimode Plate Reader (PerkinElmer, USA). The GABA concentration in the samples was calculated by comparing absorbance values against a standard calibration curve.

2.4 Determination of total phenolic content (TPC)

The total phenolic content was determined using the Folin–Ciocalteu colorimetric assay, following the protocol established by Wisetkomolmat and Arjin (2023) [11]. Briefly, a 100 µL aliquot of the ethanolic extract was combined with 100 µL of 10% Folin-Ciocalteu reagent. The mixture was allowed to react for 6 min, after which 1 mL of 6% $NaHCO_3$ was added. The solution was then incubated in the dark at room temperature for 90 min. Absorbance was then measured at 725 nm using an EnSight Multimode Plate Reader (PerkinElmer, USA). The results were calculated and expressed in terms of mg GAE g^{-1} of sample.

2.5 Determination of antioxidant activity of germinated brown rice

2.5.1 Determination of DPPH free radical scavenging activity

The free radical scavenging activity of the extracts was evaluated using the DPPH assay, modified from the method described by Wisetkomolmat and Arjin (2023) [11]. The assay was performed in a 96-well plate by mixing 50 µL of the sample extract or Trolox standard (0.02–0.4 mg/mL) with 150 µL of freshly prepared 0.1 mmol/L DPPH solution. The reaction mixture was incubated in the dark at room temperature for 30 min, and the absorbance was measured at 515 nm using an EnSight Multimode Plate Reader (PerkinElmer, USA). The results were expressed as mg Trolox Equivalents (TE)/100 g dry weight (DW).

2.5.2 Determination of ABTS free radical scavenging activity

ABTS radical scavenging activity was determined based on a modification of the method described by Wisetkomolmat and Arjin (2023) [11]. The $ABTS^{\cdot+}$ working solution was prepared by reacting 7 mmol/L ABTS with 2.45 mmol/L potassium persulfate at a volumetric ratio of 2:3 and incubating the mixture in the dark at room temperature for 16 h. Prior to analysis, the $ABTS^{\cdot+}$ solution was diluted with phosphate buffer (2.4 mmol/L, pH 7.4) to obtain an absorbance of 0.70 ± 0.02 at 734 nm. The absorbance was measured using an EnSight Multimode Plate Reader (PerkinElmer, USA), and the antioxidant activity was expressed as mg Trolox equivalents (TE) per 100 g dry weight (DW).

2.5.3 Determination of Ferric-reducing antioxidant power assay

The ferric reducing antioxidant power (FRAP) assay was performed according to a modified protocol described by Ti and Zhang (2014) [12]. The FRAP working reagent was prepared by mixing 25 mL of 300 mM acetate buffer (pH 3.6), 2.5 mL of 10 mM TPTZ solution (dissolved in 40 mM HCl), and 2.5 mL of 20 mM $FeCl_3 \cdot 6H_2O$ solution. This mixture was incubated at 37 °C prior to analysis. The assay was conducted in a 96-well microplate by mixing 10 µL of the sample extract with 200 µL of the pre-warmed FRAP reagent. Following incubation in the dark at room temperature for 30 min, the absorbance was measured at 593 nm using an EnSight Multimode Plate Reader (PerkinElmer, USA). Trolox served as the reference standard, and the results were expressed as mg Trolox Equivalents (TE)/100 g dry weight (DW).

2.6 Statistical analysis

All the results were expressed as mean ± standard deviation, and one-way ANOVA and Duncan's post hoc tests were employed in statistical analysis using SPSS 29.0 (SPSS Inc., IBM Corp., IL, USA), with $p < 0.05$ considered statistically significant. Pearson correlation analysis was also performed to evaluate the relationships among GABA content, total phenolic content, and antioxidant activities (DPPH, ABTS, and FRAP).

3. Results & Discussion

Figure 1 presents the visual appearance of germinated brown rice samples after 24 h of germination. All rice varieties exhibited visible germination, confirming that the germination conditions were appropriate and that the samples were suitable for subsequent biochemical analyses. Differences in grain color and cultivation environment between upland and lowland rice were apparent, which may be associated with variations in metabolic responses during germination.

Figure 1. Six varieties of germinated brown rice (GBR) from different cultivation environments: (A) Hom Mali, (B) Thapthim Chumphae, and (C) Mali Nil Surin represent lowland cultivars; (D) Dok Phayom, (E) Hom Bon, and (F) Med Fai represent upland cultivars.

3.1 GABA content

The GABA content of germinated brown rice cultivated under different growing areas and grain colors is shown in Figure 2. Significant differences in GABA accumulation were observed among the rice samples ($p < 0.05$), indicating the influence of both cultivation environment and varietal characteristics. Rice cultivated in lowland areas exhibited relatively low GABA contents, ranging from 26.75 to 41.96 mg/100 g. Among these varieties, Hom Mali rice showed the highest GABA content (41.96 ± 0.95 mg/100 g), whereas Mali Nil Surin rice exhibited the lowest value (26.75 ± 0.56 mg/100 g). In contrast, germinated rice cultivated in upland areas generally accumulated higher levels of GABA. The highest GABA content was observed in the upland red

rice variety Hom Bon (81.88 ± 2.61 mg/100 g), followed by the upland black rice variety Med Fai (48.73 ± 3.48 mg/100 g). Dok Phayom rice showed a moderate GABA level (32.83 ± 1.22 mg/100 g). These results clearly demonstrate that cultivation environment plays a critical role in GABA accumulation during germination.

In addition to cultivation environment, the chemical composition of rice grains, particularly the amino acid profile, may also influence GABA accumulation. GABA is synthesized from L-glutamic acid through the action of glutamate decarboxylase (GAD), and therefore the availability of glutamic acid as a precursor plays an important role in GABA formation during germination [2,13]. Differences in protein and amino acid composition among rice cultivars may partly explain the variation in GABA content observed in this study.

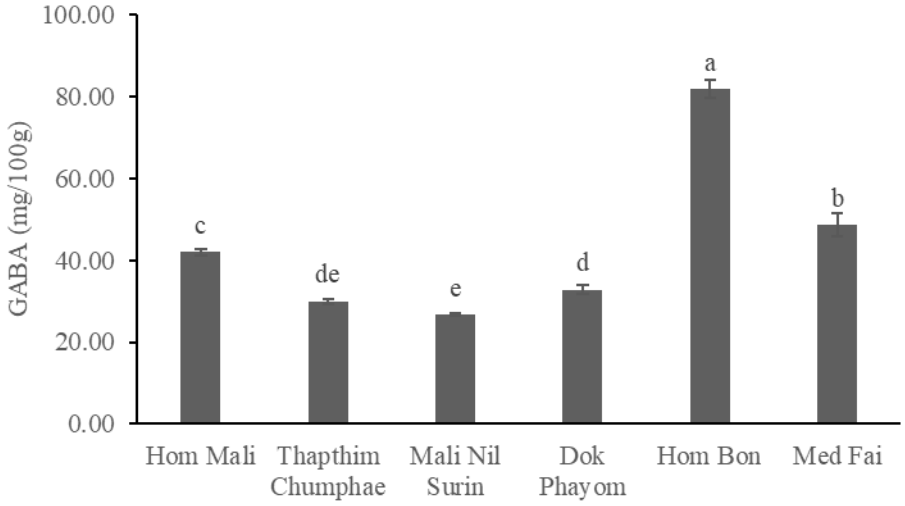

Figure 2. γ-Aminobutyric Acid (GABA) content of six rice varieties cultivated in different cultivation environment. The values are expressed as mean ± SD (n=3) and different letters on bars indicate the difference between rice varieties ($p < 0.05$).

Upland growing conditions are commonly associated with greater exposure to abiotic stresses, such as fluctuations in temperature and water availability, which have been reported to enhance the activity of glutamate decarboxylase, the key enzyme involved in GABA biosynthesis in plants [13]. In addition, stress-related factors such as hypoxic conditions during soaking and germination have been shown to stimulate GABA production in rice grains [14]. When grain color was compared within the same cultivation environment, lowland-grown white rice (Hom Mali) exhibited higher GABA content than red and purple rice varieties. This finding suggests that grain color alone does not necessarily promote GABA accumulation under lowland conditions and supports previous reports indicating that cultivation environment exerts a more dominant influence on GABA synthesis than grain pigmentation [3].

3.2 Total phenolic content (TPC)

The total phenolic content (TPC) of germinated brown rice cultivated in different growing areas and grain colors is presented in Figure 3. Significant differences in TPC were observed among the rice samples ($p < 0.05$), indicating that both cultivation area and grain color influenced phenolic accumulation during germination. In general, germinated rice grown in upland areas exhibited significantly higher TPC than that grown in lowland areas. The TPC of lowland-grown rice ranged from 53.31 to 121.08 mg GAE/100 g, whereas upland-grown rice showed higher values, ranging from 55.14 to 139.57 mg GAE/100 g. Among all samples, the upland red rice variety Hom Bon exhibited the highest TPC (139.57 ± 4.00 mg GAE/100 g), followed by the

upland black rice variety Med Fai (128.16 ± 0.29 mg GAE/100 g). In contrast to the pattern observed for GABA, phenolic content showed a clear association with grain pigmentation. Colored rice varieties consistently exhibited higher TPC than white rice in both lowland and upland environments ($p < 0.05$). The elevated phenolic content observed in upland-grown rice may be attributed to environmental stress conditions, such as lower temperatures, increased ultraviolet radiation, and greater diurnal temperature fluctuations, which are known to stimulate the biosynthesis of phenolic compounds as part of plant defense mechanisms against oxidative and abiotic stress [15].

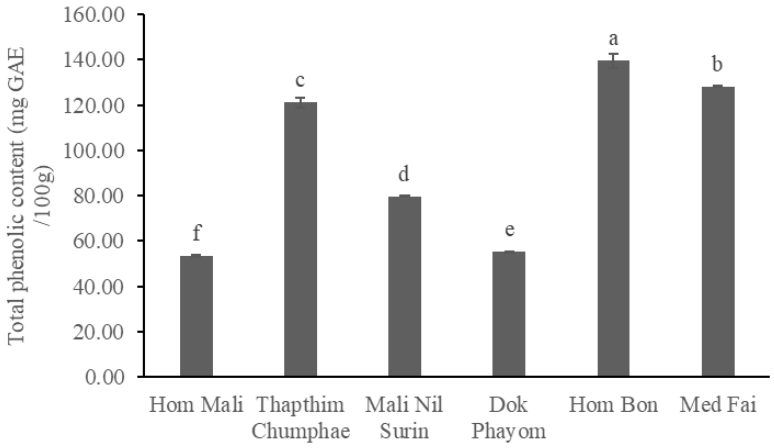

Figure 3. Total Phenolic content of six rice varieties cultivated in different cultivation environment. The values are expressed as mean ± SD (n=3) and different letters on bars indicate the difference between rice varieties ($p < 0.05$).

When comparing grain color within the same cultivation area, colored rice varieties consistently exhibited higher TPC than white rice in both lowland and upland environments ($p < 0.05$). This finding is in agreement with previous studies reporting that colored rice contains higher levels of phenolic acids, flavonoids, and anthocyanins, which are predominantly located in the bran layer [4, 16]. Red rice is particularly rich in proanthocyanidins, while purple rice contains high levels of anthocyanins, both of which substantially contribute to total phenolic content [17, 18]. In addition, germination has been shown to further enhance phenolic levels by activating hydrolytic enzymes that release bound phenolic compounds from the cell wall matrix, thereby increasing their extractable forms [15].

3.3 Antioxidant activity of germinated brown rice

Antioxidant activity of germinated brown rice was evaluated using DPPH, ABTS, and FRAP assays to provide a comprehensive assessment of antioxidant capacity based on different reaction mechanisms. Although each assay is based on distinct principles, consistent trends were observed across all methods.

3.3.1 DPPH free radical scavenging activity

DPPH radical scavenging activity differed significantly among germinated rice samples ($p < 0.05$), as shown in Figure 4. Germinated upland rice exhibited higher DPPH scavenging activity than lowland rice, with a pronounced effect observed in pigmented varieties. Germinated upland red rice (Hom Bon) showed the highest DPPH activity (155.13 ± 10.06 mg TE/100 g), followed by upland black rice (Med Fai) (148.82 ± 9.13 mg TE/100 g). These values were markedly higher than those of lowland white rice (Hom Mali) (38.51 ± 2.53 mg TE/100 g) and upland white rice (Dok Phayom) (43.41 ± 1.15 mg TE/100 g).

DPPH scavenging activity reflects the hydrogen-donating ability of antioxidant compounds, particularly phenolic constituents, which reduce the stable DPPH radical to its non-radical form [7, 19]. The enhanced scavenging activity observed in pigmented upland rice is consistent with their higher phenolic contents, suggesting a strong relationship between TPC and DPPH antioxidant capacity.

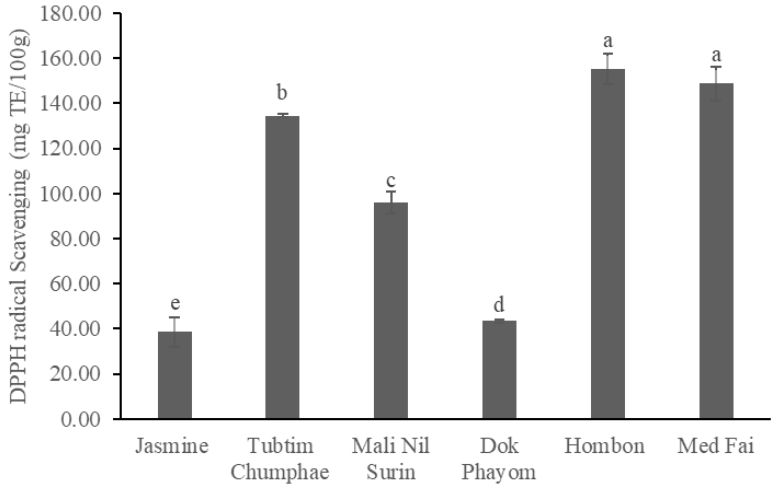

Figure 4. DPPH free radical scavenging of six rice varieties cultivated in different cultivation environments. The values are expressed as mean ± SD (n=3) and different letters on bars indicate the difference between rice varieties ($p < 0.05$).

3.3.2 ABTS free radical scavenging activity

ABTS radical scavenging activity also varied significantly among rice samples ($p < 0.05$), as illustrated in Figure 5. Germinated upland rice exhibited markedly higher ABTS activity than lowland rice, particularly in pigmented varieties. The highest ABTS value was observed in upland red rice (Hom Bon) (482.29 ± 8.77 mg TE/100 g), followed by upland black rice (Med Fai) (454.50 ± 5.82 mg TE/100 g). In contrast, lowland rice varieties, including Hom Mali rice, showed substantially lower ABTS activity (83.21 ± 6.08 mg TE/100 g). The ABTS assay measures the ability of both hydrophilic and lipophilic antioxidants to quench the $ABTS^{\bullet+}$ radical cation and is therefore suitable for evaluating total antioxidant capacity in complex plant matrices [20, 21]. The consistency between ABTS activity and TPC further supports the contribution of phenolic compounds to the antioxidant potential of germinated rice.

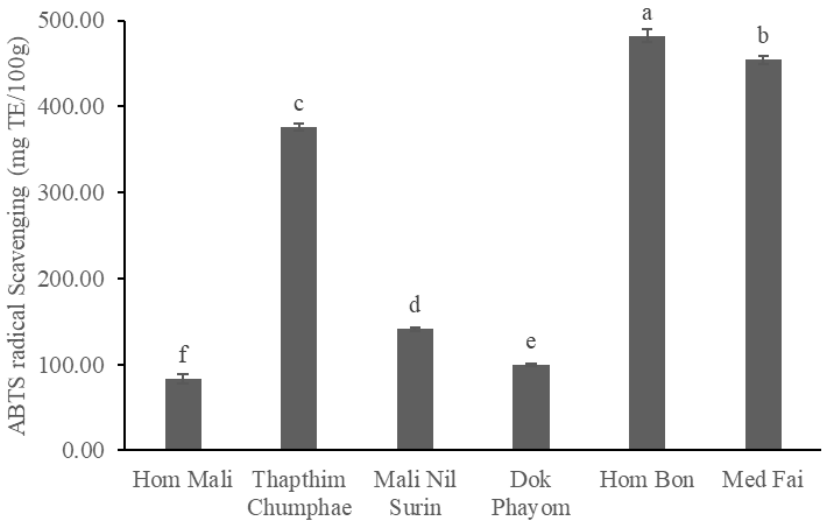

Figure 5. ABTS free radical scavenging of six rice varieties cultivated in different cultivation environments. The values are expressed as mean ± SD (n=3) and different letters on bars indicate the difference between rice varieties ($p < 0.05$).

3.3.3 Ferric-reducing antioxidant power activity

Similar trends were observed in the FRAP assay (Figure 6), where significant differences in ferric-reducing capacity were detected among germinated rice samples ($p < 0.05$). Germinated upland black rice (Med Fai) exhibited the highest FRAP value (244.23 ± 7.66 mg TE/100 g), followed by upland red rice (Hom Bon) (233.69 ± 7.71 mg TE/100 g DW). In contrast, lowland rice varieties, particularly Hom Mali rice, showed considerably lower FRAP values (53.72 ± 2.83 mg TE/100 g).

The FRAP assay evaluates the electron-donating capacity of antioxidants by measuring the reduction of Fe^{3+}–TPTZ to Fe^{2+}–TPTZ under acidic conditions [22]. The elevated FRAP values observed in pigmented upland rice indicate higher concentrations of reducing compounds, such as phenolics, which are influenced by both varietal characteristics and cultivation environment.

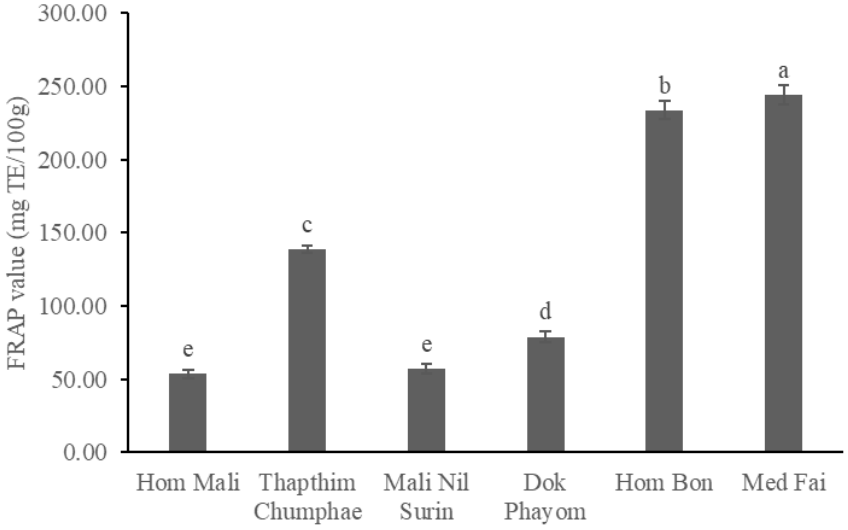

Figure 6. Ferric-reducing antioxidant power of six rice varieties cultivated in different cultivation environments. The values are expressed as mean ± SD (n=3) and different letters on bars indicate the difference between rice varieties ($p < 0.05$).

Taken together, the results from the DPPH, ABTS, and FRAP assays consistently demonstrate that germinated upland rice, particularly pigmented varieties, possesses superior antioxidant capacity compared to lowland rice. This enhanced antioxidant activity is closely associated with higher phenolic content and environmental stress conditions during cultivation, which collectively influence metabolic responses during germination.

3.4 Correlation analysis among bioactive compounds and antioxidant activities

Pearson correlation analysis was performed to further clarify the relationships among GABA content, total phenolic content (TPC), and antioxidant activities of germinated brown rice. The analysis revealed positive correlations between total phenolic content (TPC) and antioxidant activities measured by DPPH, ABTS, and FRAP, suggesting that phenolic compounds contribute significantly to the antioxidant capacity of germinated brown rice. In addition, strong correlations were observed among the antioxidant assays themselves, indicating that these analytical methods consistently reflect the antioxidant properties of the samples.

In contrast, GABA content showed weak correlations with phenolic content and antioxidant activities, suggesting that GABA accumulation occurs through a different metabolic pathway. Specifically, GABA is produced through the GABA shunt pathway, whereas phenolic compounds are synthesized through the phenylpropanoid pathway.

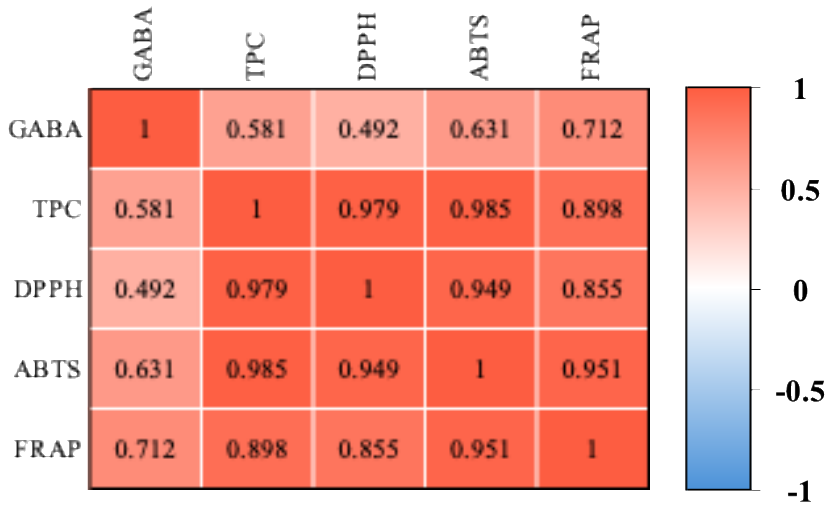

Figure 7. Pearson correlation matrix showing the relationships among GABA content, total phenolic content (TPC), and antioxidant activities (DPPH, ABTS, and FRAP) of germinated brown rice.

4. Conclusion

This study demonstrates that cultivation environment plays a significant role in the accumulation of bioactive compounds and antioxidant activity in germinated Thai indigenous rice. Germinated upland rice exhibited superior functional quality compared to lowland rice, particularly in pigmented varieties. Among the samples, germinated upland red rice (Hom Bon) showed the highest GABA content, total phenolic content, DPPH and ABTS antioxidant activity, while germinated upland black rice (Med Fai) exhibited the strongest FRAP antioxidant activity. Variations in total phenolic content after germination were influenced by both rice variety and cultivation environment. Overall, pigmented upland germinated rice demonstrates high potential as a functional ingredient for food and beverage applications.

Acknowledgements

This work was financially supported by King Mongkut's Institute of Technology Ladkrabang [2567-02-07-001].

References

1. Moongngarm A, Saetung N. Comparison of chemical compositions and bioactive compounds of germinated rough rice and brown rice. Food Chemistry. 2010;122(3):782–8.
2. Cho D-H, Lim S-T. Germinated brown rice and its bio-functional compounds. Food Chemistry. 2016;196:259–71.
3. Komatsuzaki N, Tsukahara K, Toyoshima H, Suzuki T, Shimizu N, Kimura T. Effect of soaking and gaseous treatment on GABA content in germinated brown rice. Journal of Food Engineering. 2007;78:556–60.
4. Sompong R, Siebenhandl-Ehn S, Linsberger-Martin G, Berghofer E. Physicochemical and antioxidative properties of red and black rice varieties from Thailand, China and Sri Lanka. Food Chemistry. 2011;124(1):132–40.
5. Tiozon RJN, Sreenivasulu N, Alseekh S, Sartagoda KJD, Usadel B, Fernie AR. Metabolomics and machine learning technique revealed that germination enhances the multi-nutritional properties of pigmented rice. Communications Biology. 2023;6(1):1000.
6. Shao Y, Xu F, Sun X, Bao J, Beta T. Phenolic acids, anthocyanins, and antioxidant capacity in rice (Oryza sativa L.) grains at four stages of development after flowering. Food Chemistry. 2014;143:90–6.
7. Brand-Williams W, Cuvelier ME, Berset C. Use of a free radical method to evaluate antioxidant activity. LWT - Food Science and Technology. 1995;28(1):25–30.
8. Hung PV, Maeda T, Yamamoto S, Morita N. Effects of germination on nutritional composition of waxy wheat. Journal of the Science of Food and Agriculture. 2012;92(3):667–72.
9. Tabaraki R, Nateghi A. Optimization of ultrasonic-assisted extraction of natural antioxidants from rice bran using response surface methodology. Ultrasonics Sonochemistry. 2011;18(6):1279–86.
10. Songsamoe S, Khunjan K, Matan N. The application and mechanism of action of Michelia alba oil vapour in GABA enhancement and microbial growth control of germinated brown rice. Food Control. 2021;130:108401.
11. Wisetkomolmat J, Arjin C, Hongsibsong S, Ruksiriwanich W, Niwat C, Tiyayon P, et al. Antioxidant Activities and Characterization of Polyphenols from Selected Northern Thai Rice Husks: Relation with Seed Attributes. Rice Science. 2023;30(2):148–59.
12. Ti H, Zhang R, Zhang M, Li Q, Wei Z, Zhang Y, et al. Dynamic changes in the free and bound phenolic compounds and antioxidant activity of brown rice at different germination stages. Food Chemistry. 2014;161:337–44.
13. Bown AW, Shelp BJ. Plant GABA: Not Just a Metabolite. Trends in Plant Science. 2016;21(10):811–3.
14. Saikusa T, Horino T, Mori Y. Accumulation of γ-Aminobutyric Acid (Gaba) in the Rice Germ during Water Soaking. Bioscience, Biotechnology, and Biochemistry. 1994;58(12):2291–2.
15. Goufo P, Trindade H. Rice antioxidants: phenolic acids, flavonoids, anthocyanins, proanthocyanidins, tocopherols, tocotrienols, γ-oryzanol, and phytic acid. Food Sci Nutr. 2014;2(2):75–104.
16. Yawadio R, Tanimori S, Morita N. Identification of phenolic compounds isolated from pigmented rices and their aldose reductase inhibitory activities. Food Chemistry. 2007;101(4):1616–25.
17. Abdel-Aal E-SM, Young JC, Rabalski I. Anthocyanin Composition in Black, Blue, Pink, Purple, and Red Cereal Grains. Journal of Agricultural and Food Chemistry. 2006;54(13):4696–704.
18. Finocchiaro F, Ferrari B, Gianinetti A, Dall'Asta C, Galaverna G, Scazzina F, et al. Characterization of antioxidant compounds of red and white rice and changes in total antioxidant capacity during processing. Molecular Nutrition & Food Research. 2007;51(8):1006–19.
19. Molyneux P. The use of the stable radical Diphenylpicrylhydrazyl (DPPH) for estimating antioxidant activity. Songklanakarin Journal of Science and Technology. 2003;26.

20. Re R, Pellegrini N, Proteggente A, Pannala A, Yang M, Rice-Evans C. Antioxidant activity applying an improved ABTS radical cation decolorization assay. Free Radical Biology and Medicine. 1999;26(9):1231–7.
21. Prior RL, Wu X, Schaich K. Standardized Methods for the Determination of Antioxidant Capacity and Phenolics in Foods and Dietary Supplements. Journal of Agricultural and Food Chemistry. 2005;53(10):4290–302.
22. Benzie IFF, Strain JJ. The Ferric Reducing Ability of Plasma (FRAP) as a Measure of "Antioxidant Power": The FRAP Assay. Analytical Biochemistry. 1996;239(1):70–6.

P - 439

Preliminary Study on the Development of a High-Fiber Wolffia-Enriched Snack Using Pineapple Pomace

Mercy Maina, Phunsiri Suthiluk*

School of Agro-Industry, Mae Fah Luang University, Chiang Rai 57100, Thailand

**Corresponding author E-mail: phunsiri.s@mfu.ac.th*

Abstract: The global food system faces increasing pressure to improve sustainability, reduce waste, and meet rising nutritional demands. This study aimed to develop a high-fiber, protein-rich sheet snack by valorizing Phulae pineapple pomace (PP) and fresh *Wolffia globosa* using twin drum drying technology. A Simplex Lattice Mixture Design was applied to generate seven formulations, with PP and *W. globosa* ranging from 20% to 80% (w/w), while other ingredients were held constant. All formulations exhibited low water activity (0.27–0.33), indicating microbiological stability. Instrumental hardness increased with PP content (2.62–9.94 N), attributed to sugar plasticization and fiber–starch matrix densification during drying. Crude protein ranged from 5.40 to 11.51 g/100 g, confirming *W. globosa* as the primary protein source. Color variation was strongly influenced by ingredient composition, with higher PP producing lighter and more yellow products due to carotenoids, while higher *W. globosa* resulted in darker, greener products associated with chlorophyll content. Based on mixture design optimization, formulations containing 35–50% PP and 50–65% *W. globosa* were identified as optimal, providing a balanced combination of protein content (>8 g/100 g), desirable crispness (2.86–3.51 N), and acceptable color attributes. All samples met Thai community product standards for microbiological quality. This study demonstrates the potential of combining fruit processing by-products with alternative plant protein sources to develop sustainable functional snack products. Future studies should incorporate sensory evaluation to assess consumer acceptability.

Keywords: Pineapple pomace; Wolffia globosa; High-fiber snack; Plant-based protein; Twin drum drying

1. Introduction

The global food system faces a growing challenge in ensuring food security, reducing waste, and meeting nutritional demands amid rising population pressure and environmental constraints. As the world strives for sustainable development, innovative approaches that valorize agri-food by-products are gaining traction as viable solutions (1) . Fruit processing industries generate considerable amounts of waste which, if unmanaged, contribute to environmental degradation; however, many of these by-products possess untapped nutritional and functional value, offering opportunities for the development of functional foods and sustainable dietary alternatives (2).

Pineapple (*Ananas comosus*), a widely cultivated tropical fruit, generates significant volumes of pomace during juice extraction. Approximately 30–35% of the fruit's mass is produced as pomace after juice extraction from peeled pineapples (3). Pineapple pomace is particularly rich in dietary fiber, especially the insoluble fraction, which supports digestive health. Nutrient composition studies show variability due to cultivar, maturity, and processing methods. Selani et al. (4) reported freeze-dried pineapple pomace containing 45.22% total dietary fiber, 4.71% protein, and 0.61% fat, while Nguyen et al. (5) reported a higher total dietary fiber content of

55.4% and carbohydrate content of 90.8% in similarly processed pomace. Beyond fiber, pineapple pomace contains bioactive phenolic compounds with antioxidant activity (6) Its high fiber content presents an opportunity to enhance the nutritional quality and textural characteristics of food products, particularly snacks, which are increasingly popular across age groups.

In northern Thailand, the 'Phulae' pineapple — a dwarf cultivar of *Ananas comosus* native to Chiang Rai — is recognized as a Geographical Indication (GI) product due to its distinctive sweetness, fragrance, and small core size. Thailand is among the world's top producers and exporters of canned and juiced pineapple, and processing of the 'Phulae' variety generates substantial quantities of pomace. These by-products are largely discarded, contributing to food waste and environmental pollution. Valorization of 'Phulae' pineapple pomace therefore offers a promising opportunity for the development of fiber-rich, health-promoting snack products while contributing to circular economy and regional sustainability efforts.

At the same time, there is growing interest in underutilized aquatic plants such as *W. globosa* (duckweed), which contains up to 41% protein by dry weight, including all nine essential amino acids. Studies report a Digestible Indispensable Amino Acid Score (DIAAS) of approximately 0.75, comparable to egg and soy proteins (7). Furthermore, over 70% of *W. globosa's* fatty acid profile comprises unsaturated fats, including essential omega-3 and omega-6 fatty acids. The plant's characteristic green color arises from its chlorophyll content, which also contributes to its antioxidant profile. *W. globosa* thrives in aquatic systems with minimal inputs, making it a sustainable alternative to conventional protein crops (8,9). The potential synergy between pineapple pomace and *W. globosa* for the development of high-fiber, protein-enriched snacks presents a compelling case for functional product development. When optimally blended and processed using twin drum drying, these ingredients can yield a crispy, nutritious snack with extended shelf stability (10,11) .

This study aims to develop a sustainable, high-fiber, protein-rich sheet snack by optimizing the formulation of pineapple pomace and *W. globosa* using a Simplex Lattice Mixture Design and twin drum drying technology. The study evaluates key physicochemical and nutritional attributes — including water activity, color, textural hardness, proximate composition, and microbiological quality — across seven formulations, with the goal of identifying the optimal ingredient ratio.

2. Materials and Methods

2.1 Raw Materials

Phulae pineapple pomace (PP) was obtained as a by-product from local pineapple juice processing activities within the Mae Fah Luang University food science laboratory. The pineapple pomace was dewatered using a hydraulic press, portioned into 2 kg lots, labelled, vacuum-sealed, and stored at −20 °C to prevent microbial growth and enzymatic degradation prior to use (12). Fresh *W. globosa* was sourced from Mecheeva Community Enterprise in Wiang Chai District, Chiang Rai, Thailand. Fresh *W. globosa* was cleaned to remove impurities and frozen at −20 °C prior to sample preparation. Tapioca starch, xanthan gum, sugar, mushroom seasoning powder, and white pepper were procured from Iplus Supplies, a reputable food-grade ingredient supplier in Thailand, and stored in airtight containers at ambient temperature in a cool, dry laboratory storage facility until use.

2.2 Experimental Design by Simplex Lattice Mixture Design

A Simplex Lattice Mixture Design was employed to optimize formulations for a high-fiber, protein-rich snack. Design-Expert software (Version 13, Stat-Ease Inc., Minneapolis, USA) was used to generate experimental runs. Two ingredients were selected as mixture components: pineapple pomace (Component A) and *W. globosa* (Component B), each ranging from 20% to 80% (w/w), with the sum constrained to 100%. Seven formulation runs were generated, including

two replicated extreme-ratio points (80:20 and 20:80) to enable estimation of pure experimental error within the mixture model. The experimental design layout is presented in Table 1.

Table 1. Experimental design layout generated by Simplex Lattice Mixture Design.

Standard Order	Run	Component A: Pineapple Pomace (%)	Component B: Fresh W. globosa (%)
5	1	35	65
3	2	50	50
1	3	80	20
6	4	80	20
2	5	20	80
7	6	20	80
4	7	65	35

Runs 3/4 (80:20) and Runs 5/6 (20:80) represent replicated runs used for estimating experimental error within the mixture model.

2.3 Sample Preparation

The basic formulation concept was modified from Suthiluk et al. (12). Frozen pineapple pomace was thawed and chopped in a food processor, then set aside for weighing. Frozen *W. globosa* was thawed and set aside for weighing. The proportions of pineapple pomace and *W. globosa* were varied between 20% and 80% as per Table 1, with the total constrained to 100%. Both components were mixed with reverse osmosis (RO) water at a 1:1 (w/w) ratio and blended using a Philips HR2223/00 jug blender. Fixed binding and flavoring ingredients were added at constant ratios based on total mixture weight: tapioca starch 1%, xanthan gum 0.1%, mushroom seasoning powder 2%, white pepper 0.17%, and sugar 1.5%.

All ingredients were blended thoroughly to form a homogenous slurry, which was then processed into crispy sheets using a twin drum dryer (Model TDD-3030, Euro Best Technology Co., Ltd., Thailand). Drying conditions were set at 135 °C drum surface temperature, 414 Hz drum rotation frequency, a drum gap of approximately 0.15mm, a feed rate of ~150 mL/min, and a residence time of approximately 3–5 s, as determined from preliminary experiments.

The resulting sheets were cut into pieces measuring 9 cm × 6 cm and cooled on a rack for 25–40 minutes. Cooled sheets were placed individually into aluminum foil bags with a moisture-absorber sachet, flushed with nitrogen gas, and heat-sealed. Packed samples were stored at −20 °C until analysis.

2.4 Determination of Physical Properties

Snack samples from all seven formulations were evaluated for: (i) water activity (a_w) using a water activity meter (model LabMaster-aw neo, Novasina AG, Lachen, Switzerland) in triplicate at 25 °C; (ii) color using a UltraScan VIS Spectrophotometer (HunterLab, Reston, VA, USA), recorded as L* (lightness), a* (red–green chromaticity), and b* (yellow–blue chromaticity), in triplicate; and (iii) textural hardness (crispness) using a texture analyzer TA-XT Plus (Stable Micro Systems, Godalming, Surrey, UK) fitted with a crisp fracture rig (HDP/CFS), with pre-test speed 1.0 mm/s, test speed 1.0 mm/s, post-test speed 10.0 mm/s, and a test height of 3 mm. Eight replicates (n = 8) were performed per sample with a 25 kg load cell; maximum peak force (N) was recorded as a measure of hardness. This method was adapted from Keeratipibul et al. (13).

2.5 Determination of Nutritional Properties

Proximate composition of all seven formulations was determined for moisture content, crude fat, ash, crude protein, and crude fiber following the Association of Official Analytical Chemists (AOAC) Official Methods of Analysis (21st edition) (14). Total carbohydrate content (dry weight basis) was calculated by difference: 100 − (moisture + protein + fat + ash + crude fiber).

2.6 Determination of Microbiological Quality

Microbiological quality was assessed by enumerating total aerobic microorganisms and yeasts and molds using the 3M™ Petrifilm™ method. Sample homogenates were prepared by aseptically diluting 10 g of sample in 90 mL sterile 0.1% peptone water (1:10 dilution). Serial dilutions were prepared and inoculated onto 3M™ Petrifilm™ Aerobic Count Plates and Yeast and Mold Count Plates. Aerobic count plates were incubated at 35 °C for 48 h; yeast and mold plates at 25 °C for 120 h. Results were expressed as colony-forming units per gram (CFU/g) and compared against the Thai Community Product Standard for crispy snacks (total plate count < 1×10^6 CFU/g; yeast and mold count < 100 CFU/g).

2.7 Statistical Analysis

Mixture regression models were fitted using Design-Expert software (Version 13, Stat-Ease Inc.) to assess the effect of ingredient proportions on all responses. Model adequacy was evaluated using analysis of variance (ANOVA), R^2 values, and lack-of-fit tests. One-way multivariate analysis of variance (MANOVA) with post-hoc Tukey's HSD test was used to identify differences between formulations across multiple responses (protein, crude fiber, water activity, and color). One-way ANOVA was conducted for crispness using SPSS Version 18 (IBM Corp., Chicago, IL, USA). All experiments were conducted in triplicate (n = 3), except crispness measurements (n = 8). Data are reported as mean ± standard deviation (SD). Statistical significance was set at $p < 0.05$.

3. Results & Discussion

3.1 Effect of Ingredient Ratios on Physical Properties of the Snacks

The physical properties of the seven pineapple pomace–*W. globosa* snack formulations, including water activity (a_w), color (L*, a*, b*), and textural hardness, are presented in Table 2.

Table 2. Physical properties of seven developed pineapple pomace–*W. globosa* snacks including water activity (aw), color, and textural hardness.

Run	PP (%)	W.g (%)	aw	L*	a*	b*	Hardness (N)
1	35	65	0.28 ± 0.00	39.61 ± 3.96	1.15 ± 0.48	6.93 ± 2.03	2.86 ± 1.15
2	50	50	0.27 ± 0.00	40.66 ± 2.32	0.80 ± 0.55	4.03 ± 3.04	3.51 ± 1.12
3	80	20	0.33 ± 0.00	47.05 ± 1.51	2.55 ± 0.94	11.45 ± 1.55	9.94 ± 3.45
4	80	20	0.30 ± 0.00	44.04 ± 0.82	2.80 ± 0.43	8.03 ± 0.78	9.26 ± 2.93
5	20	80	0.28 ± 0.00	35.78 ± 0.83	0.34 ± 0.02	0.57 ± 0.25	2.62 ± 0.75
6	20	80	0.30 ± 0.00	36.26 ± 0.25	0.73 ± 0.21	0.84 ± 0.31	5.61 ± 2.06
7	65	35	0.32 ± 0.00	42.16 ± 0.79	1.92 ± 0.42	5.05 ± 0.71	4.75 ± 0.84

All data are shown as mean ± SD. aw, L*, a*, b*: n = 3; Hardness (N): n = 8.
PP = pineapple pomace; W.g = *W. globosa*.

All snack samples exhibited a_w values ranging from 0.27 to 0.33, well below the critical threshold of 0.60 above which osmophilic yeasts, xerophilic molds, and pathogenic bacteria can proliferate (15). Formulations with higher pineapple pomace content (Runs 3 and 4, 80% PP)

exhibited slightly higher a_w (0.30–0.33) compared to *W. globosa*-dominant formulations (Runs 5 and 6, 80% *W. globosa*: a_w = 0.28–0.30). This slight elevation can be attributed to the hygroscopic nature of simple sugars and fruit fibers in pineapple pomace, which retain residual moisture in the dried matrix (4). All values remained within the safe zone for dried foods, confirming that twin drum drying effectively removed free water across all formulations (16,17).

Color measurements showed statistically significant differences across formulations ($p < 0.05$). L* values ranged from 35.78 (Run 5, 20% PP) to 47.05 (Run 3, 80% PP), indicating that higher pineapple pomace content produced a significantly lighter product. The b* (yellowness) values ranged from 0.57 to 11.45, with high-pomace formulations notably more yellow, attributable to carotenoid pigments naturally present in pineapple tissue (4,6). In contrast, formulations with higher *W. globosa* content produced darker, greener products (lower L*, near-zero b* values), a direct consequence of the chlorophyll content of *W. globosa*, which imparts characteristic green pigmentation to the dried product (7,18). As noted by Pathare et al. (19), L* values are a critical determinant of consumer acceptance in snack products, and the lighter, more uniform appearance of moderate-to-high pineapple pomace formulations may confer a commercial advantage.

One-way ANOVA revealed a highly significant effect of formulation on textural hardness ($F = 15.31$, $p < 0.0001$, Table 5). Maximum peak force values ranged from 2.62 N (Run 5, 20% PP) to 9.94 N (Run 3, 80% PP), with hardness increasing in direct proportion to pineapple pomace content. While instrumental hardness in thin sheet snacks is often associated with crispness, excessively high force values (as in Runs 3 and 4) are more indicative of a tough, compact texture than a desirable light, brittle fracture (20).

Two primary mechanisms explain this relationship. First, sugar plasticization: pineapple pomace is rich in simple sugars that act as plasticizers within the starch–protein matrix formed during drum drying, lowering the glass transition temperature (T_g) of the dried matrix. This causes the product to shift from a brittle, glassy state to a rubbery, tough state that absorbs more force before fracturing (21). Second, fiber–starch matrix interference: the insoluble dietary fiber fraction of pineapple pomace can disrupt the continuous starch network that normally enables thin, porous cell wall formation during drying. High fiber loading therefore creates dense, thick walls requiring greater force to fracture but lacking the rapid, brittle fracture characteristic of crispy products (20). Together, these mechanisms indicate that an 80% pineapple pomace inclusion rate exceeds the optimal threshold for crispness. A moderate inclusion of 35–50% pineapple pomace appears preferable, yielding force values of 2.86–3.51 N (Runs 1 and 2), consistent with desirable snack crispness.

3.2 Effect of Ingredient Ratios on Nutritional Properties of the Snacks

The proximate composition results (per 100 g dry weight) are presented in Table 3. Nutritional values differed significantly across formulations ($p < 0.05$) for protein and ash, while crude fiber remained relatively stable.

Table 3. Proximate compositions of seven developed pineapple pomace–W. globosa snacks (g/100 g dry weight).

Run	PP (%)	W.g (%)	Moisture (g/100 g)	Protein (g/100 g)	Ash (g/100 g)	Fat (g/100 g)	Crude Fiber (g/100 g)	Total CHO (g/100 g)
1	35	65	7.90 ± 0.15	9.03 ± 0.16	12.99 ± 0.32	0.02 ± 0.00	5.33 ± 0.52	77.97 ± 0.19
2	50	50	7.17 ± 0.39	8.42 ± 0.11	11.11 ± 0.23	0.01 ± 0.01	5.41 ± 0.53	79.60 ± 0.21
3	80	20	9.57 ± 0.16	6.22 ± 0.06	9.11 ± 0.17	0.01 ± 0.00	5.65 ± 0.46	84.66 ± 0.14
4	80	20	9.28 ± 0.14	5.40 ± 0.10	8.97 ± 0.03	0.02 ± 0.01	5.52 ± 0.22	85.61 ± 0.09
5	20	80	7.02 ± 0.04	11.51 ± 0.11	15.49 ± 0.13	0.02 ± 0.01	5.04 ± 0.42	72.97 ± 0.21
6	20	80	6.98 ± 0.10	10.94 ± 0.11	14.95 ± 0.33	0.03 ± 0.02	4.51 ± 0.31	74.08 ± 0.20
7	65	35	9.37 ± 0.09	6.63 ± 0.06	10.38 ± 0.32	0.01 ± 0.00	5.93 ± 0.15	82.98 ± 0.37

All data are shown as mean ± SD (n = 3).
PP = pineapple pomace; W.g = *W. globosa*; CHO = carbohydrates (calculated by difference).

Crude protein content showed a clear and statistically significant inverse relationship with pineapple pomace concentration ($p < 0.05$). Runs 5 and 6 (20% pineapple pomace: 80% *W. globosa*) exhibited the highest protein content, averaging 11.23 g/100 g, while Runs 3 and 4 (80% pineapple pomace: 20% *W. globosa*) exhibited the lowest, averaging 5.81 g/100 g. This confirms that *W. globosa* is the primary protein contributor in the matrix, consistent with its well-documented high protein concentration (up to 41% by dry weight) and complete amino acid profile (7,18). Formulations containing ≥50% *W. globosa* (Runs 1 and 2) exceeded the 8 g/100 g protein level, a nutritionally significant threshold for a snack product.

Crude fiber content ranged from 4.51 to 5.93 g/100 g and did not differ significantly across formulations ($p > 0.05$). Despite pineapple pomace being a well-established dietary fiber source (4), the absence of significant variation across the tested ratios suggests that *W. globosa* provides a comparable fiber contribution within this matrix, effectively buffering total fiber levels regardless of pineapple pomace proportion. It should be noted that the AOAC 962.09 acid–alkali crude fiber method systematically underestimates true total dietary fiber; future studies should employ the enzymatic-gravimetric AOAC 991.43 method for values aligned with food labeling requirements.

Total carbohydrate content (by difference) ranged from 72.97 to 85.61 g/100 g, increasing with higher pineapple pomace proportions, reflecting the lower protein and ash content of pomace-dominant formulations. All formulations were extremely low in fat (0.01–0.03 g/100 g). Ash content ranged from 8.97 to 15.49 g/100 g and was significantly higher in *W. globosa*-dominant formulations, reflecting the higher mineral content of this aquatic plant compared to pineapple pomace.

3.3 Microbiological Quality

Microbiological analysis of all seven formulations showed that total aerobic plate counts, and yeast and mold counts (YMC) were below the maximum permissible limits of the Thai community product standard for crispy snacks (total plate count < 1×10^6 CFU/g; YMC < 100 CFU/g). These results are consistent with the low a_w values recorded across all formulations (0.27–0.33), which limit available free water for microbial growth. The twin drum drying process at 135 °C effectively inactivated microbial populations in the fresh ingredients, and nitrogen-flushed hermetically sealed packaging further prevented post-process contamination, confirming the microbiological safety and shelf stability of all developed formulations.

3.4 Mixture Design

The application of the Simplex Lattice Mixture Design enabled a systematic evaluation of the interactive effects between pineapple pomace (PP) and *Wolffia globosa* (W.g) on the physicochemical and nutritional properties of the developed snack. In contrast to conventional factorial designs, mixture design accounts for the constraint that component proportions must sum to unity, allowing a more realistic representation of formulation systems. The fitted mixture regression models demonstrated that ingredient proportions exerted significant linear effects on key responses, particularly protein content and color parameters ($p < 0.05$), with *W. globosa* contributing positively to protein enrichment while PP predominantly influenced color attributes and textural behavior.

Contour plot visualization and response surface analysis further revealed a distinct optimal formulation region rather than a single optimum point, highlighting the trade-offs inherent in multi-response optimization. Specifically, increasing PP content enhanced lightness (L*) and yellowness (b*) due to carotenoid pigments but simultaneously increased textural hardness through sugar plasticization and fiber–matrix densification. In contrast, higher proportions of *W. globosa* improved protein content and contributed to greener coloration associated with chlorophyll but resulted in darker product appearance.

Multi-response optimization indicated that formulations containing approximately 35–50% PP and 50–65% *W. globosa* provided the most favorable balance among protein content, textural crispness, and color acceptability. The presence of replicated extreme design points (80:20 and 20:80) enabled reliable estimation of pure experimental error and improved model robustness. Overall, the mixture design approach proved to be an effective tool for guiding formulation development and identifying optimal regions in complex food systems involving competing functional attributes.

3.5 Statistical Analysis

MANOVA revealed an overall statistically significant difference among formulations across the combined dependent variables of protein content, crude fiber, water activity, and color (Wilks' $\Lambda = 0.0001$, $F = 21{,}386.48$, $p < 0.0001$, Table 4). This confirms that manipulating the pineapple pomace-to-*W. globosa* ratio significantly and jointly affects the physicochemical and nutritional profile of the product.

Table 4. MANOVA results for the effect of formulation on combined responses.

Test Statistic	Value	F-value	p-value
Wilks' Lambda	0.0001	21,386.48	< 0.0001*

*Significant at $p < 0.05$.

Mixture regression models fitted in Design-Expert confirmed significant linear effects of ingredient proportion on protein content and color parameters ($p < 0.05$). The fitted linear mixture model for protein content is:

$$Protein\ (g/100\ g) = 5.81 \times A + 11.23 \times B$$

where A and B represent the proportions of pineapple pomace and *W. globosa*, respectively. The positive coefficient for B confirms the dominant protein contribution of *W. globosa*. Model adequacy was confirmed by a high R^2 value and non-significant lack-of-fit ($p > 0.05$).

Table 5. One-way ANOVA results for the effect of formulation on textural hardness.

Source	F-value	p-value
Formulation	15.31	< 0.0001*

*Significant at $p < 0.05$.

Post-hoc Tukey's HSD analysis confirmed that crude fiber content did not differ significantly across most formulation pairs ($p > 0.05$). Water activity showed small but statistically significant differences ($p < 0.05$), with Run 3 (0.33) significantly higher than Run 2 (0.27). Color parameters L* and b* were highly discriminatory across formulations ($p < 0.05$), confirming the dominant role of ingredient composition in product appearance.

3.6 Limitations and Future Directions

The current study did not include sensory evaluation, which is an acknowledged limitation. Instrumental measurements of color, hardness, and water activity cannot fully predict consumer acceptability of a novel snack product. Future studies should incorporate hedonic evaluation by a consumer panel (minimum 30–35 untrained panelists per ISO 11136:2014) to assess overall acceptability. Total dietary fiber analysis by the enzymatic-gravimetric AOAC 991.43 method and antioxidant capacity measurements are also recommended to fully characterize the functional potential of this snack. Scale-up and shelf-life studies under commercial packaging conditions would further support translation toward commercial application.

4. Conclusion

This study demonstrates the technical feasibility of developing a high-fiber, protein-rich sheet snack from Phulae pineapple pomace and *W. globosa* by twin drum drying, using a Simplex Lattice Mixture Design across seven formulations (20–80% pineapple pomace and 20–80% *W. globosa*). All formulations met the Thai community product standard for microbial quality and achieved a_w values well below the critical safety threshold of 0.60, confirming microbiological safety and ambient shelf stability.

The results reveal clear compositional trade-offs. Maximizing *W. globosa* content (80%) produces the highest protein (>10 g/100 g) but results in darker, greener products attributable to chlorophyll pigmentation. Maximizing pineapple pomace (80%) yields the lightest, most yellow product through carotenoid contribution, but at the cost of lower protein and excessive textural hardness (>9 N) arising from sugar plasticization and insoluble fiber–starch matrix densification. Formulations containing 35–50% pineapple pomace represent the most promising candidates, balancing protein content >8 g/100 g, moderate hardness consistent with crispness (2.86–3.51 N), and appealing color. Future work should incorporate sensory evaluation to confirm consumer acceptability of the identified optimal range.

Acknowledgements

The authors would like to thank Mae Fah Luang University, Chiang Rai, Thailand, for providing research facilities and resources, and the Thailand International Cooperation Agency (TICA) for provision of scholarship funds.

Reference

1. Barral-Martinez M, Fraga-Corral M, Garcia-Perez P, Simal-Gandara J, Prieto MA. Almond by-products: Valorization for sustainability and competitiveness of the industry. Foods. MDPI AG; 2021. doi:10.3390/foods10081793

2. Erinle TJ, Adewole DI. Fruit pomaces—their nutrient and bioactive components, effects on growth and health of poultry species, and possible optimization techniques. Animal Nutrition. KeAi Communications Co.; 2022. p. 357–77. doi:10.1016/j.aninu.2021.11.011
3. Hemung BO, Sompholkrang M, Wongchai A, Chanshotikul N, Ueasin N. study of the potential of by-products from pineapple processing in Thailand. Int J Health Sci (Qassim). 2022 Aug 25;12605–15. doi:10.53730/ijhs.v6ns4.12131
4. Selani MM, Brazaca SGC, Dos Santos Dias CT, Ratnayake WS, Flores RA, Bianchini A. Characterisation and potential application of pineapple pomace in an extruded product for fibre enhancement. Food Chem. 2014 Nov 15;163:23–30. doi:10.1016/j.foodchem.2014.04.076 PubMed PMID: 24912691.
5. Nguyen TTA, Nguyen HH, Ton NMN, Tran TTT, Le VVM. Enzymatic treatment of pineapple pomace and its application into fiber-rich biscuit making. J Agric Food Res. 2024 Mar 1;15. doi:10.1016/j.jafr.2023.100936
6. Sengar AS, Sunil CK, Rawson A, Venkatachalapathy N. Identification of volatile compounds, physicochemical and techno-functional properties of pineapple processing waste (PPW). Journal of Food Measurement and Characterization. 2022 Apr 1;16(2):1146–58. doi:10.1007/s11694-021-01243-8
7. Boonarsa P, Bunyatratchata A, Chumroenphat T, Thammapat P, Chaikwang T, Siripan T, et al. Nutritional Quality, Functional Properties, and Biological Characterization of Watermeal (Wolffia globosa). Horticulturae. 2024 Nov 1;10(11). doi:10.3390/horticulturae10111171
8. Kaplan A, Zelicha H, Isaban G, Meir YA, Rinnot E, Kovsan J, et al. Protein bioavailability of Wolffia globosa duckweed, a novel aquatic plant – A randomized controlled trial. Clinical Nutrition. 2019;38(6):2576–82.
9. Sulaiman NS, Mohd Zaini H, Wan Ishak WR, Matanjun P, George R, Mantihal S, et al. Duckweed protein: Extraction, modification, and potential application. Food Chemistry. Elsevier Ltd; 2025. doi:10.1016/j.foodchem.2024.141544 PubMed PMID: 39388881.
10. Kakade RH, Das H, Ali S. Performance evaluation of a double drum dryer for potato flake production. J Food Sci Technol. 2011 Aug;48(4):432–9. doi:10.1007/s13197-010-0184-0
11. Galaz P, Valdenegro M, Ramírez C, Nuñez H, Almonacid S, Simpson R. Effect of drum drying temperature on drying kinetic and polyphenol contents in pomegranate peel. J Food Eng. 2017 Sep 1;208:19–27. doi:10.1016/j.jfoodeng.2017.04.002
12. Suthiluk P, Naradisorn M, Setha S. Assessing the impact of drum drying on the nutritional properties of pineapple pomace-fortified crispy mushroom sheets. Front Sustain Food Syst. 2023;7. doi:10.3389/fsufs.2023.1253597
13. Keeratipibul S, Luangsakul N, Lertsatchayarn T. The effect of Thai glutinous rice cultivars, grain length and cultivating locations on the quality of rice cracker (arare). LWT - Food Science and Technology. 2008;41:1934–43.
14. AOAC INTERNATIONAL. Official Methods of Analysis of AOAC International. 21st ed. Rockville, MD, USA: AOAC International; 2019.
15. Tapia S, M, Alzamora M, S, Chirife J. Water Activity in Foods Fundamentals and Applications. First Edition. Barbosa-Cánovas V, G, Jr. FJ, A, Schmidt J, S, Labuza P, T, editors. Blackwell Publishing; 2007. 239–272 p.
16. R. L, B. Microbial stability as affected by water activity. Cereal Foods World. 1981;26(7):345–9.
17. Mathlouthi M. Water content, water activity, water structure and the stability of foodstu□s [Internet]. Report. Available from: www.elsevier.com/locate/foodcont
18. Appenroth KJ, Sowjanya Sree K, Bog M, Ecker J, Seeliger C, Böhm V, et al. Nutritional value of the duckweed species of the Genus Wolffia (Lemnaceae) as human food. Front Chem. 2018 Oct 1;6(OCT). doi:10.3389/fchem.2018.00483

19. Pathare P, Opara U, Al Said F. Colour Measurement and Analysis in Fresh and Processed Foods: A Review. Food and Bioprocess Technology. 2013 Jan;6(1):36–60.
20. Nuchsai T, Sakphisutthikul C. Correlation between physical properties and sensory evaluation of extruded Phyto-snack. Open Access: e-Journal. Report.
21. Katz EE, Labuza TP. Effect of Water Activity on the Sensory Crispness and Mechanical Deformation of Snack Food Products. Report.

Sponsors

Vitafoods™ Asia

2-4 September 2026
Hall 1-3 & Hall 5-7
QSNCC, Bangkok, Thailand

Asia's leading event
for functional ingredients & dietary supplement products and solutions.

Explore 4 key sectors

What you can expect at Vitafoods Asia 2026

650 exhibiting companies
38 participating countries
16,000 attendees
9 international pavilions
30,000 sq.m. exhibit space
50 conference topics

Fi Asia

SCAN HERE!
Postshow report

Fi Vietnam
Register now!

Fi Vietnam
13-15 May 2026
SECC, HCMC, Vietnam

Your gateway opens to Vietnam's F&B ingredients world!

9,000+ Expected attendees
300+ Expected exhibitors
40+ Countries

Fi Asia Indonesia
16-18 September 2026
JIExpo, Jakarta, Indonesia

A world of taste and opportunity

Celebrate 30 years of Fi Asia in Indonesia! Join us for a landmark edition showcasing innovation, global connections, and growth in Asia's thriving food and beverage industry.

24,000+ Expected attendees
700+ Expected companies
100+ Countries

Fi Asia Thailand
1-3 September 2027
QSNCC, Bangkok, Thailand

Bringing the Asian F&B industry together

Asia's leading food and beverage showcase returns to Thailand in 2027, offering unmatched opportunities to connect, innovate, and drive growth in R&D, trade, functional food, and natural ingredients.

23,000+ Expected attendees
750+ Expected companies
70+ Countries
60+ Insightful sessions

Food ingredients - Fi Asia
Food ingredients – Fi Vietnam

Organised by:
informa

บริษัท ซีจี ไซแอนติฟิค จำกัด
CG SCIENTIFIC CO., LTD.

An ISO 9001:2015 Certified Company

02 185 4289
info@cg-sci.com
@cgscientific
cg scientific
www.cg-sci.com

บริษัท ซีจี ไซแอนติฟิค จำกัด

นำเข้าเครื่องมือ เครื่องใช้ และอุปกรณ์วิทยาศาสตร์ สำหรับการ วิเคราะห์ วิจัย และทดสอบคุณภาพสินค้า สำหรับอุตสาหกรรมทุกประเภท เช่น อุตสาหกรรม อาหารและเครื่องดื่ม เครื่องสำอาง เคมีภัณฑ์ ปิโตรเคมี และอื่นๆ ด้วยทีมงานฝ่ายขาย และฝ่ายบริการหลังการขาย รวมทั้งทีมงานวิศวกร ที่มีความสามารถความชำนาญ และเชี่ยวชาญ พร้อมบริการกับลูกค้าด้วยประสบการณ์กว่า 20 ปี ด้วยใจบริการที่มุ่งมั่นที่จะสร้างความพึงพอใจ และความประทับใจให้กับลูกค้าที่เข้ามาใช้บริการ อีกทั้งเราจะไม่หยุดการพัฒนางานบริการให้ดียิ่งขึ้น

Gerhardt Analytical Systems Protein, Fat, Fiber Analysis Hotplate, Shaker	SARTORIUS Laboratory Balance, Moisture Analyzer Water Purication System	BROOKFIELD AMETEK Viscometer, Rheometer Texture Analyzer	SI Analytics a xylem brand pH/Conductivity Meter Titration System, Capillary Viscometer
mp Amino Acid Analyzer, Water Purification Systems	Bellingham + Stanley a xylem brand Laboratory Refractometers, Polarimeters	Nabertherm Furnace, Oven, High Temp Furnace, Tube Furnace	BINDER Ovens, Vacuum Oven, Incubators, Climate Chambers, Growth Chambers
ebro a xylem brand Temperature Data Logger Thermometer, Carbon Dioxide Meter	GIORGIO BORMAC ARGO LAB Ultrasonic Bath, Heating Block	GIORGIO BORMAC XS pH meter / Conductivity Meter Multiparameter	POWTEQ Milling & Sieving for Sample Preparation
μ2 Double Beam UV Vis Spectrophotometer	EMCLAB Double Beam UV Vis Spectrophotometer	WELCH by Gardner Denver Vacuum Pump	Labo Water Baths Refrigerated, Heating Circulator
LABWIT Water Bath, Water Bath Shaker, Shaker	Herolab High-Speed Table Top Floor Standing Centrifuges	HP LABORTECHNIK Autoclave, Steam Sterilizers Disinfection Device	ICAIR Laminar Air flow, Ductless Fume Hood Class II Bio Safety Cabinet
SHINVA Lab Washer Disinfector Class II Bio Safety Cabinet	VESTFROST SOLUTIONS Laboratory Freezers, Refrigerator 20°C to -86°C	LabTech Rotary Evaporator, Centrifuge	Lanon Recirculating Chiller Melting Point Apparatus DiaphragmVacuum Pumps
KPM Discrete Analyzer, Continuous Flow Analysis	MIKROMEISTER MASTERING LIQUIDS Bottle Top Dispenser	YSI a xylem brand Biochemistry Analyzers Clinical Chemistry Analyzers	ZIRBUS Freeze Dry
ONiLAB Hotplate, Overhead Stirrers Vortex Mixer, Pipette	FUNKE GERBER Milk Analyzer	bluelab pH, Conductivity portable meter , Controller	KNAUER HPLC, Compact HPLC UHPLC, FPLC, GPC

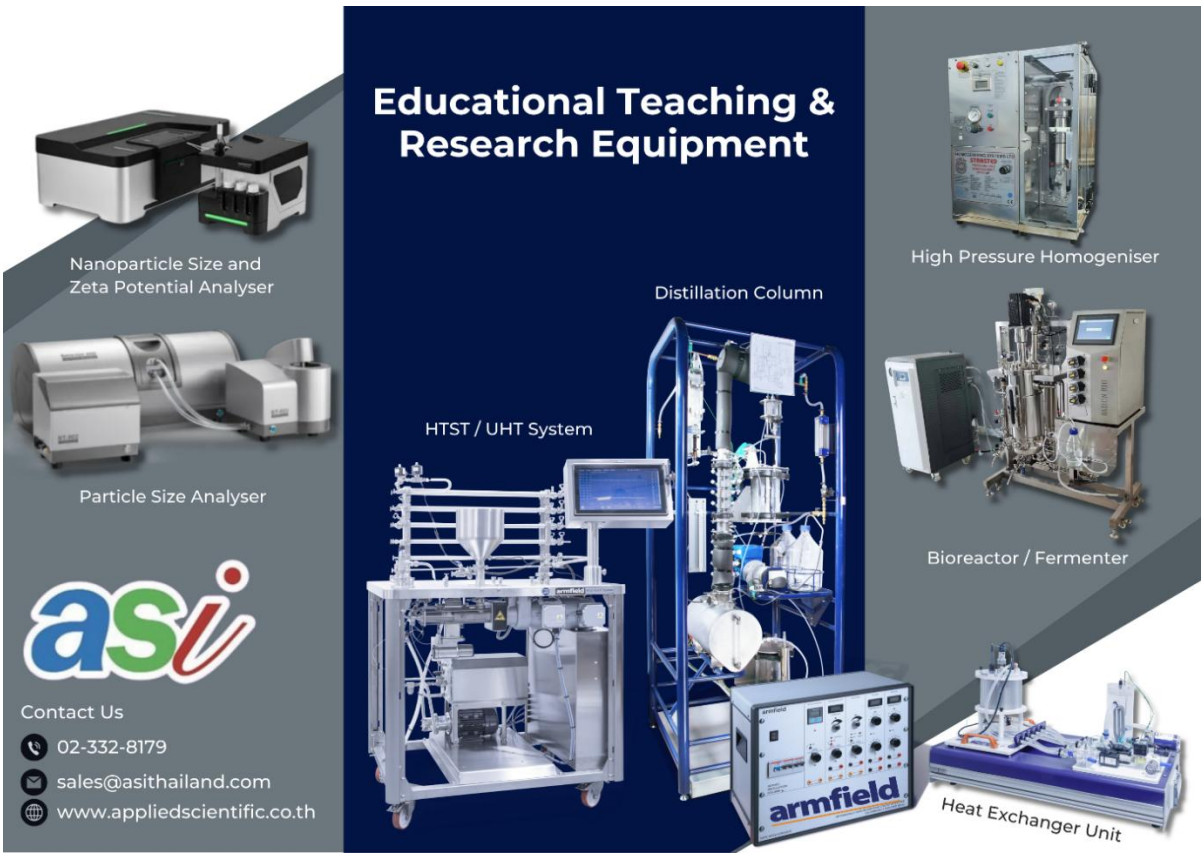

MARVALIC HEALTH
บริษัท มาร์วาลิค เฮลท์ จำกัด
ให้บริการ รับผลิตอาหารเสริมและเครื่องสำอาง แบบครบวงจร (OEM/ODM)
มีบริการตั้งแต่ขั้นตอนการพัฒนาสูตร ผลิตสินค้า การควบคุมคุณภาพ และการขึ้นทะเบียนผลิตภัณฑ์
มีทีมงาน R&D, marketing, และออกแบบเพื่อช่วยคุณสร้างแบรนด์ได้ง่ายขึ้น
• Health Supplement
• Skin Supplement
• Men Supplement
• Women Supplement
• Cream
• Serum
• Soap
• Shampoo & Treatment
• Sunscreen
• Body Lotion
CONTACT US
Tel. 063-6516415 / 094-5141632
www.marvalichealth.com
@marvalio

OUR PRODUCT DIVISION
S.A. CHIANGMAI
Environmental & Industrial Hygiene
General Laboratory Equipment
Agri / Food / Feed
Chemical / Material Testing
Life Science & Medical Technology
Pharmaceutical Clinical / Medical Lab
SITHIPORN associates
Tel. 02-433-8331 Center@sithiphorn.com
S.A. CHIANGMAI
S.A. KHONKAEN
S.A. BANGKOK
S.A. MAP TA PHUT

DRY
Extraordinary Drying Technology
Transform your drying processes
to the latest generation.
> Quality > Clean > Eff Green >icient
Pulse Combustion Spray
Dryer Technology (PCS)
- Dramatically increase product quality
- For Bioactive compound protein , enzyme
- Handle thick ,high viscous product
- Extream short drying time in millisec
Optional : Pulsed Electric Field (PEF)
Pre-treatment
PCS- Pilot P-5
for Pilot plant
Contact Us : Innovative Drying Technology Co.,Ltd.
Tel : (+66)0891911786
FB : Refractance Window Drying Thailand

SYNTECH
INNOVATION CO.,LTD.

Syntech Innovation Co., Ltd. provides high quality scientific instruments with full services including installation, maintenance, repair, and laboratory solutions & supporting customer success at every step

FT-IR SPECTROSCOPY

NMR

TD-NMR

XRF & XRD

CHROMATOGRAPHY

AA & ICP

WWW.SYNTECHINNOVATION.COM / EMAIL : INFO@SYNTECHINNOVATION.COM / TEL: 0 2363 8585

TCEB
THAILAND CONVENTION
& EXHIBITION BUREAU

FACULTY OF AGRO-INDUSTRY

CHIANG MAI UNIVERSITY

Mae-Hia, Muang, Chiang Mai 50100, Thailand

fabc.cmu@gmail.com